

Topics in Organometallic Chemistry 60

Yoshiaki Nishibayashi *Editor*

# Nitrogen Fixation

 Springer

**Editorial Board**

M. Beller, Rostock, Germany  
P.H. Dixneuf, Rennes CX, France  
J. Dupont, Porto Alegre, Brazil  
A. Fürstner, Mülheim, Germany  
F. Glorius, Münster, Germany  
L.J. Gooßen, Kaiserslautern, Germany  
T. Ikariya, Tokyo, Japan  
S.P. Nolan, Ghent, Belgium  
J. Okuda, Aachen, Germany  
L.A. Oro, Zaragoza, Spain  
M. Willis, Oxford, United Kingdom  
Q.-L. Zhou, Tianjin, China

## Aims and Scope

The series *Topics in Organometallic Chemistry* presents critical overviews of research results in organometallic chemistry. As our understanding of organometallic structure, properties and mechanisms increases, new ways are opened for the design of organometallic compounds and reactions tailored to the needs of such diverse areas as organic synthesis, medical research, biology and materials science. Thus the scope of coverage includes a broad range of topics of pure and applied organometallic chemistry, where new breakthroughs are being achieved that are of significance to a larger scientific audience.

The individual volumes of *Topics in Organometallic Chemistry* are thematic. Review articles are generally invited by the volume editors. All chapters from *Topics in Organometallic Chemistry* are published OnlineFirst with an individual DOI. In references, *Topics in Organometallic Chemistry* is abbreviated as *Top Organomet Chem* and cited as a journal.

More information about this series at <http://www.springer.com/series/3418>

Yoshiaki Nishibayashi  
Editor

# Nitrogen Fixation

With contributions by

M.J. Bezdek · P.J. Chirik · A. Eizawa · K. Grund ·  
P.L. Holland · Z. Hou · Y. Ishida · H. Kawaguchi ·  
A. Kindjajev · I. Klopsch · S. Kuriyama · Y. Nishibayashi ·  
I. Pappas · M. Pfeil · S. Schneider · T. Shima ·  
A.L. Speelman · N. Stucke · H. Tanaka · F. Tucek ·  
T. Weyrich · K. Yoshizawa · E.Y. Yuzik-Klimova



Springer

*Editor*

Yoshiaki Nishibayashi  
The University of Tokyo  
Department of Systems Innovation, School of Engineering  
Hongo, Tokyo  
Japan

ISSN 1436-6002                      ISSN 1616-8534 (electronic)  
Topics in Organometallic Chemistry  
ISBN 978-3-319-57713-5              ISBN 978-3-319-57714-2 (eBook)  
DOI 10.1007/978-3-319-57714-2

Library of Congress Control Number: 2017939687

© Springer International Publishing AG 2017

This work is subject to copyright. All rights are reserved by the Publisher, whether the whole or part of the material is concerned, specifically the rights of translation, reprinting, reuse of illustrations, recitation, broadcasting, reproduction on microfilms or in any other physical way, and transmission or information storage and retrieval, electronic adaptation, computer software, or by similar or dissimilar methodology now known or hereafter developed.

The use of general descriptive names, registered names, trademarks, service marks, etc. in this publication does not imply, even in the absence of a specific statement, that such names are exempt from the relevant protective laws and regulations and therefore free for general use.

The publisher, the authors and the editors are safe to assume that the advice and information in this book are believed to be true and accurate at the date of publication. Neither the publisher nor the authors or the editors give a warranty, express or implied, with respect to the material contained herein or for any errors or omissions that may have been made. The publisher remains neutral with regard to jurisdictional claims in published maps and institutional affiliations.

Printed on acid-free paper

This Springer imprint is published by Springer Nature  
The registered company is Springer International Publishing AG  
The registered company address is: Gewerbestrasse 11, 6330 Cham, Switzerland

# Preface

Detailed studies of the preparation of various transition metal–dinitrogen complexes and their reactivity have been achieved in the past 50 years. This volume is not intended to provide a comprehensive view of Nitrogen Fixation by using transition metal–dinitrogen complexes but to focus on recent advances of the explosive field in the last decade. Although many research groups have already reported their excellent results, the authors representing the field have introduced their latest achievements in this volume.

I believe that this volume will be helpful to researchers, teachers, and students who are interested in innovative and sustainable chemistry. I would like to thank all the contributors for their participation in this project and their enthusiastic efforts to present recent advances of Nitrogen Fixation by using transition metal–dinitrogen complexes. I anticipate that their contributions will stimulate further study in Nitrogen Fixation. I would like also to offer my warm thanks to the Springer Nature team for their continuous support. Finally, I deeply appreciate the staff and students in my research group for their valuable assistance.

Tokyo, Japan  
December 2016

Yoshiaki Nishibayashi

# Contents

<b>Determining and Understanding N-H Bond Strengths in Synthetic Nitrogen Fixation Cycles . . . . .</b>	<b>1</b>
Máté J. Bezdek, Iraklis Pappas, and Paul J. Chirik	
<b>Dinitrogen Fixation by Transition Metal Hydride Complexes . . . . .</b>	<b>23</b>
Takanori Shima and Zhaomin Hou	
<b>Reactivity of Group 5 Element Dinitrogen Complexes and N<sub>2</sub>-Derived Nitrides . . . . .</b>	<b>45</b>
Yutaka Ishida and Hiroyuki Kawaguchi	
<b>Functionalization of N<sub>2</sub> by Mid to Late Transition Metals via N–N Bond Cleavage . . . . .</b>	<b>71</b>
Isabel Klopsch, Ekaterina Yu Yuzik-Klimova, and Sven Schneider	
<b>Synthetic Nitrogen Fixation with Mononuclear Molybdenum(0) Phosphine Complexes: Occupying the <i>trans</i>-Position of Coordinated N<sub>2</sub> . . . . .</b>	<b>113</b>
Nadja Stucke, Thomas Weyrich, Mareike Pfeil, Katharina Grund, Andrei Kindjajev, and Felix Tuczek	
<b>Catalytic Nitrogen Fixation Using Molybdenum–Dinitrogen Complexes as Catalysts . . . . .</b>	<b>153</b>
Aya Eizawa and Yoshiaki Nishibayashi	
<b>Computational Approach to Nitrogen Fixation on Molybdenum–Dinitrogen Complexes . . . . .</b>	<b>171</b>
Hiromasa Tanaka and Kazunari Yoshizawa	
<b>Sulfur-Supported Iron Complexes for Understanding N<sub>2</sub> Reduction . . .</b>	<b>197</b>
Amy L. Speelman and Patrick L. Holland	

<b>Catalytic Transformations of Molecular Dinitrogen by Iron and Cobalt–Dinitrogen Complexes as Catalysts</b> . . . . .	215
Shogo Kuriyama and Yoshiaki Nishibayashi	

<b>Index</b> . . . . .	235
------------------------	-----



# Determining and Understanding N-H Bond Strengths in Synthetic Nitrogen Fixation Cycles

Máté J. Bezdek, Iraklis Pappas, and Paul J. Chirik

**Abstract** The fixation of atmospheric dinitrogen to ammonia using molecular catalysts has been a long-standing challenge in homogeneous catalysis and synthetic chemistry. New approaches to this problem may offer more energy-efficient and carbon-neutral routes to this important industrial compound. Despite the ubiquity of ammine, amide, imide and diazenide ligands in coordination chemistry, little thermodynamic data is available for understanding N-H bond strengths in molecules bearing these nitrogenous fragments. This article presents an overview of both computational and experimental approaches for the determination of N-H bond dissociation free energies in a variety of compounds relevant to nitrogen fixation to ammonia. The influence of metal oxidation state, ancillary ligand and identity of the nitrogen donor are highlighted. Implications for future design of molecular systems for the reduction of dinitrogen are discussed.

**Keywords** Ammonia • Bond dissociation free energy • Nitrogen fixation

## Contents

1	Introduction .....	2
2	Proton Coupled Electron Transfer in Synthetic Dinitrogen Reduction Schemes .....	5
3	Determination of N-H Bond Dissociation Free Energies in Transition Metal Complexes .....	7
3.1	Thermochemical Considerations .....	7
3.2	Diazenides (M-N=NH) .....	9
3.3	Hydrazides (M-N-NH <sub>2</sub> ) .....	9
3.4	Imides (M=NH) .....	12
3.5	Amides (M-NH <sub>2</sub> ) .....	14
3.6	Ammine (M-NH <sub>3</sub> ) .....	15

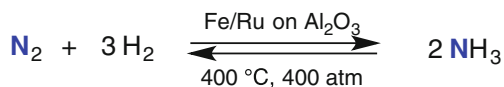
4	Conclusions and Outlook .....	19
	References .....	20

## 1 Introduction

The synthesis of ammonia from its elements is one of the most important transformations in synthetic chemistry owing to the reliance of global food production on  $\text{NH}_3$  and its derivatives as fertilizer [1]. One of the most significant technological achievements of the twentieth century is the Haber–Bosch ammonia synthesis whereby  $\text{NH}_3$  is produced over an iron or ruthenium catalyst from  $\text{N}_2$  and  $\text{H}_2$  [2–6]. Optimized catalysts are known that produce 1–10 tons of ammonia per minute! The high temperature and pressure conditions used for optimal and economic ammonia production are often classified as “harsh.” Sources often cite consumption of 1–2% of the world’s energy supply as motivation for finding “more efficient” versions of the Haber–Bosch reaction [7]. How accurate are such claims and if there are motivations for alternatives to the Haber–Bosch process, what are they?

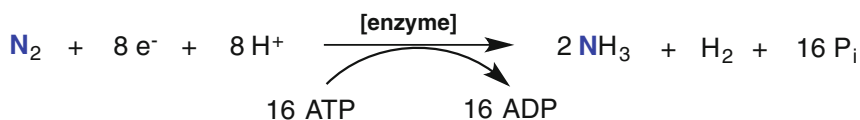
It is instructive to compare the energetics of the Haber–Bosch reaction to biological ammonia synthesis catalyzed by the nitrogenase family of enzymes (Fig. 1). Because the latter process occurs at ambient temperature and pressure, it may seem as if the biological reaction is more energy efficient. Simply comparing the stoichiometry of the two reactions suggests otherwise: the requirement of the enzymatic reaction for 16 equivalents of ATP coupled with the formation of one equivalent of dihydrogen per turnover of ammonia [8] generates a chemical overpotential of approximately 117 kcal/mol [9]. By comparison, the Haber–Bosch ammonia synthesis has been determined to operate with 75% efficiency,

### *Haber-Bosch Ammonia Synthesis*



*Overpotential = 14 kcal/mol*

### *Nitrogenase Enzymes*



*Overpotential = 117 kcal/mol*

**Fig. 1** Comparison of the energetics of industrial (*top*) versus biological (*bottom*) ammonia synthesis

corresponding to a chemical overpotential of approximately 14 kcal/mol. If the Haber–Bosch process is relatively energy efficient, why then search for alternatives?

In addition to a fundamental challenge in chemical synthesis, solution methods for the fixation of molecular nitrogen to ammonia could also have practical benefit. The hydrogen used for the Haber–Bosch ammonia synthesis is almost exclusively fossil fuel derived [10], linking the world's largest chemical process and hence global food production to a carbon footprint [11]. This is particularly troubling as the hydrogenation of nitrogen to ammonia does not involve carbon! While it is possible that hydrogen generated from renewable sources would obviate this pollution, current Haber–Bosch technology requires a continuous flow of ultrapure hydrogen that renders it inherently incompatible with the discontinuous H<sub>2</sub> output of alternative fuels. Given that disruption of the renewable energy source could result in destruction of the catalyst [12], ammonia synthesis technologies that operate in batch and are therefore compatible with intermittent energy sources are attractive.

Although the first transition metal dinitrogen complex was reported in 1965 [13] and extensive effort has been devoted to the synthesis of NH<sub>3</sub> from coordinated N<sub>2</sub>, typically from protonolysis (the so-called Chatt cycle) [14, 15], molecular catalysts for NH<sub>3</sub> generation are rare [16]. Pickett explored addition of an external source of electrons by coupling protonolysis of tungsten dinitrogen complexes to a mercury pool electrode although turnover was not observed [17, 18]. Shilov later reported Ti(OH)<sub>3</sub>, phosphine-phospholipid mixtures in the presence of catalytic Mo(III) that were effective for the catalytic synthesis of ammonia and hydrazine at 150 atm of N<sub>2</sub> [19, 20]. Ashley and coworkers have recently reported iron phosphine complexes that promote the catalytic formation of hydrazine upon addition of protons and electrons [21].

In 2003, Yandulov and Schrock's landmark paper demonstrated that a well-defined molybdenum(III)tris(amido)amine complex was effective for the synthesis of eight equivalents of ammonia per metal center upon addition of decamethylchromocene and a lutidinium salt as electron and proton sources, respectively [22]. Following this report, Nishibayashi revitalized the area with the demonstration that pincer-ligated molybdenum(0) complexes were effective pre-catalysts for catalytic ammonia synthesis, again using strong acid-reductant combinations as the sources of protons and electrons, respectively [23–25]. Peters [26–28] and later Nishibayashi [29] have extended the approach to iron catalysts, demonstrating that molecular catalysts for ammonia synthesis may be available with metals from across the transition series (Fig. 2).

All of the molecular catalysts reported to date operate at ambient temperature or below with 1 atm of dinitrogen. Are these conditions mild and how do the energetics compare to the industrial Haber–Bosch ammonia synthesis? Analysis of the thermodynamics of ammonia synthesis using strong acids and reductants tells a different story and reveals that the introduction of each reagent pair results in a tremendous chemical overpotential when compared to optimal dinitrogen reduction using H<sub>2</sub> (Table 1) [31]. As a result, alternative pathways for ammonia synthesis using H<sub>2</sub> as the thermodynamically ideal reductant are of interest.

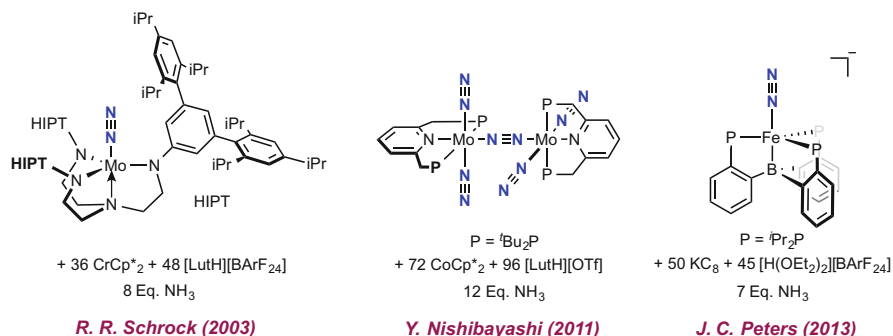


**Fig. 2** Molecular catalyst precursors for catalytic ammonia synthesis

**Table 1** Calculated chemical overpotentials for  $\text{NH}_3$  formation using various acid/reductant pairs

Acid	Reductant	Chemical overpotential <sup>a</sup> (kcal/mol)
$[\text{LutH}][\text{OTf}]$	$\text{Cp}_2\text{Co}$	26.4
$[\text{LutH}][\text{BARF}_{24}]$	$\text{Cp}^*_2\text{Cr}$	44.4
$[\text{H}(\text{OEt}_2)_2][\text{BARF}_{24}]$	$\text{KC}_8$	291.6

<sup>a</sup>Refers to excess thermodynamic driving force using the acid/reductant pair in comparison to ammonia synthesis from dihydrogen [30]

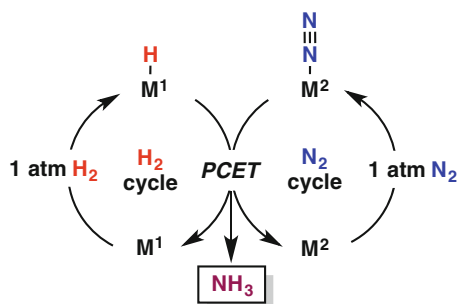


**Fig. 3** Dual catalytic cycle for the synthesis of ammonia via PCET

Our laboratory has been exploring the possibility of a dual catalytic strategy where one metal activates and cleaves  $\text{H}_2$  while the other activates  $\text{N}_2$  and the key N-H bond forming steps occur by proton coupled electron transfer (PCET, Fig. 3) [30, 32]. In the idealized dual catalytic scheme presented in Fig. 3, it is assumed that N-H bond formation is largely governed by the thermodynamics associated with M-H bonds broken and N-H bonds formed. As a consequence, understanding N-H bond dissociation free energies of coordinated nitrogen ligands such as diazenides, hydrazides, imides, and amides bound to a variety of transition metal complexes are at the core of our efforts. Somewhat surprisingly, these values are

by and large absent from the literature (For an example of a detailed thermodynamic analysis of electrocatalytic dinitrogen reduction to diazene, hydrazine and ammonia in an organic solvent, see: [33]). Here we highlight the role of proton coupled electron transfer in both N-H bond formation and cleavage and summarize the state of the art in understanding N-H bond dissociation free energies relevant to  $N_2$  fixation.

## 2 Proton Coupled Electron Transfer in Synthetic Dinitrogen Reduction Schemes

The favorable thermodynamics associated with  $N_2$  hydrogenation to ammonia demonstrates that the challenge with nitrogen fixation is principally kinetic in origin. The pathways typically associated with both PCET or hydrogen atom transfer (HAT) often avoid high-energy intermediates and therefore may facilitate smooth N-H bond formation and ultimately release of free ammonia, offering a potential advantage over conventional dinitrogen reduction strategies [31]. It is important to note that the homogeneous ammonia synthesis catalysts reported by Schrock and Nishibayashi *could* operate by PCET or HAT [34, 35], as the combination of strong pyridinium acids and metallocene reductants can, in principle, lead to the *in situ* formation of pyridinyl radical species with exceedingly weak N-H bonds ( $BDFE_{N-H} \sim 35$  kcal/mol) (For the determination of the N-H BDFEs in related Hantzsch ester derivatives, see: [36]). It is feasible that pyridinyl radicals are thermodynamically poised to deliver hydrogen atom equivalents to the nitrogen-containing ligands during the catalytic cycle, ultimately leading to ammonia formation (Fig. 4). It is also possible that PCET/HAT steps are operative for some steps while others operate by discrete protonation and reduction sequences.

To evaluate the thermodynamic feasibility of PCET or HAT mechanisms with a known molecular ammonia synthesis catalyst, we have conducted thermochemical DFT calculations on diazenido, hydrazido, nitrido, imido amido, and ammine intermediates in the Schrock cycle. While previous studies have examined the thermodynamics associated with stepwise protonation-reduction events using

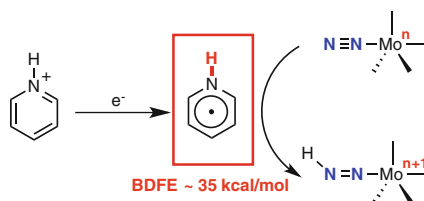


**Fig. 4** Delivery of a hydrogen atom equivalent to a bound dinitrogen fragment by a pyridinyl radical species

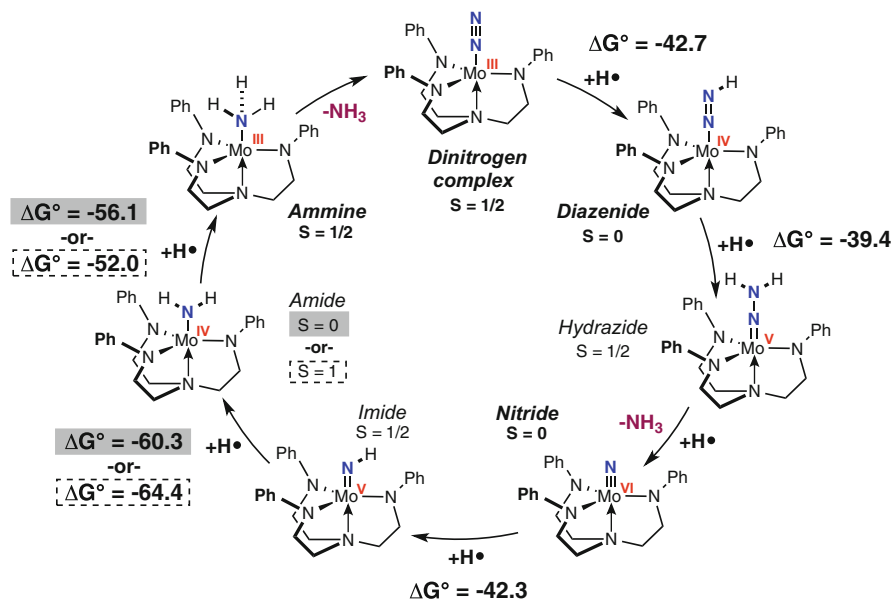


**Fig. 5** DFT-computed thermodynamics of N-H bond formation in model Schrock-type complexes. Numbers are reported in kcal/mol. The 3,5-(2,4,6-*i*-Pr<sub>3</sub>C<sub>6</sub>H<sub>2</sub>)<sub>2</sub>C<sub>6</sub>H<sub>3</sub> substituents were truncated to C<sub>6</sub>H<sub>5</sub> groups for computational expediency. Bolded spin states refer to isolated intermediates. Where multiple spin states were possible with no isolated complex for reference, both high and low spin possibilities were examined

specific acid/reductant pairs for the Schrock cycle [37], we aimed to computationally study the strengths of N-H bonds en route to ammonia formation. Such information allows for determination of the feasibility of PCET pathways with this particular catalyst. As shown in Fig. 5, the thermodynamics of each of the N-H bond forming steps have been computed and range from 39.4 to 64.4 kcal/mol, where some ambiguity arises in the values of two steps due to the possibility of two different spin states of a molybdenum amido intermediate (M. J. Bezdek and P. J. Chirik, Unpublished data). Importantly, these results demonstrate that if pyridinyl radicals do indeed form under the catalytic conditions reported for the Schrock catalyst, the elementary N-H bond forming events leading to the intermediates in Fig. 5 are thermodynamically feasible to be formed by PCET or HAT ( $\text{BDFE}_{\text{N-H}} \sim 35$  kcal/mol, vide supra). It should be noted that no experimental evidence has been presented to support or refute these pathways—the calculations presented in Fig. 5 simply demonstrate that, from a thermodynamic perspective, such mechanisms should be considered.

The computational results in Fig. 5 raise an intriguing possibility for evaluation of ammonia synthesis catalysts—with the knowledge about the thermochemical requirements for N-H bond formation, is it possible to design reaction conditions to effect the desired N-H bond forming reactivity without incurring large chemical

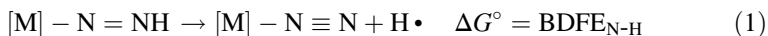
overpotentials in the process? Can hydrogen be used in place of strong acid-reductant combinations that reduce the energetic efficiency of ammonia synthesis? To answer these questions, a thorough and systematic understanding of the thermochemical requirements for N-H bond formation in various transition metal-ligand platforms is needed. Despite the long-standing role of ammonia and other nitrogen-containing ligands in coordination chemistry, few experimental studies to determine these values have been conducted. The lessons learned from these studies will likely have application in the development of new ammonia synthesis catalysts that operate under truly mild reaction conditions.

### 3 Determination of N-H Bond Dissociation Free Energies in Transition Metal Complexes

#### 3.1 Thermochemical Considerations

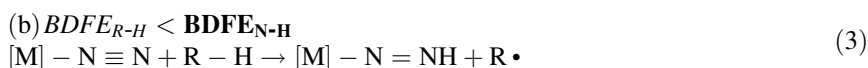
The experimental determination of N-H bond dissociation free energies (BDFEs) in coordinated nitrogen ligands provides the foundation for understanding transformations relevant to ammonia synthesis. While the thermochemical background associated with a broad range of organic and inorganic proton-coupled electron transfer reagents has been extensively reviewed [31], a brief introduction is provided here specifically in the context of N-H bond strengths in transition metal complexes.

The strength—the bond dissociation free energy—of an N-H bond in a transition metal complex is described by the Gibbs free energy change ( $\Delta G^\circ$ ) associated with its homolytic cleavage (Eq. 1). It is important to note that the interchangeable use of bond dissociation *enthalpies* (BDEs) and bond dissociation *free* energies (BDFEs) is not appropriate. When working with transition metals, BDFEs are necessary to account for the often significant entropic contributions that accompany changes in spin state. The calculations on the Schrock cycle in Fig. 5 reinforce this concept as differences of approximately 4 kcal/mol were obtained for various spin states within the same intermediate. In addition, large vibrational entropic changes have been reported for iron(II) complexes undergoing high-spin to low-spin transitions during the course of hydrogen atom abstraction reactions, giving rise to large non-zero entropy terms in the net free energy change of the reaction [38, 39]. As a consequence, BDFE values will be presented and used exclusively throughout.



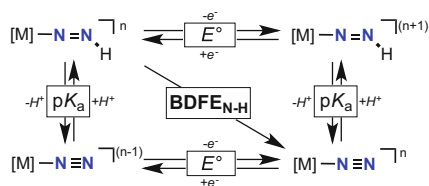
In the following sections, two primary approaches are used to obtain N-H bond dissociation free energies. The first and often the most rapid way to obtain such values experimentally is “chemical bracketing”—a method that relies on addition of hydrogen atom abstracting reagents forming R-H (R=C, N, O) bonds with

known BDFE values. In this case, the hydrogen atom transfer (HAT) reaction of the transition metal complex containing the N-H bond of interest with such reagents will be governed by the relative thermodynamics of bonds broken and bonds formed. Assuming no significant kinetic barrier to a HAT event, one can determine upper and lower bounds for a metal-bound N-H BDFE based on the radical abstracting reagents that lead to productive chemistry or promote no reaction (Eqs. 2 and 3). While this approach is straightforward operationally, bracketing experiments are by definition limited to BDFE bounds set by the availability of hydrogen atom abstracting reagents, which have been extensively reviewed by Mayer et al. [31]



A second, more accurate but time-consuming method for the determination of an N-H bond strength in a transition metal complex relies on the notion that a homolytic N-H bond dissociation (or bond forming) event can be represented by a closed thermochemical square scheme. According to this view, the net abstraction of a hydrogen atom is deconstructed into constituent proton and electron transfer steps (Fig. 6). Following the analysis of Bordwell and Tilset (Eq. 4), BDFEs are commonly derived from experimentally determined values of  $\text{p}K_{\text{a}}$  and  $E^{\circ}$  lying on adjacent sides of the square scheme [40, 41]. Typically,  $\text{p}K_{\text{a}}$  values are determined by acid-base titrations against standards of known reference values, while  $E^{\circ}$  is obtained from cyclic voltammetry. It is important to note that an accurate electrochemical determination of  $E^{\circ}$  is critical for reliable BDFE determinations, typically taken as the  $E_{1/2}$  value between the anodic and cathodic peaks of a reversible wave in a cyclic voltammogram. As can be inferred from the relative weights of the  $\text{p}K_{\text{a}}$  and  $E^{\circ}$  terms in Eq. 4, uncertainty in  $E^{\circ}$  results in a much more pronounced range of BDFE values than an inaccurate  $\text{p}K_{\text{a}}$  determination. The inclusion of the constant  $C_G$  is necessary when determining solution BDFEs in order to satisfy Hess' Law for a closed thermochemical cycle and denotes the  $\text{H}^+/\text{H}\cdot$  reduction potential that is specific to the solvent medium. The value used for  $C_G$  is solvent dependent and is ideally selected for consistency with the conditions used for  $\text{p}K_{\text{a}}$  and  $E^{\circ}$  measurements [42]. While the Bordwell equation can be used to determine exact values for

**Fig. 6** Thermochemical square scheme for measuring the bond dissociation free energy (BDFE) of a transition metal-bound N-H fragment





N-H BDFEs, it is predicated upon the stability of either (1) both the starting material and product of the hydrogen atom abstraction event or (2) one of the two intermediate complexes in the stepwise protonation-reduction (or vice versa) paths (top right and bottom left in Fig. 6). Without access to either set of these compounds, a reliable determination of  $pK_a$  and  $E^\circ$  is not possible using the thermochemical square scheme approach.

$$\text{BDFE}_{\text{N-H}} = 1.37(pK_a) + 23.06(E^\circ) + C_G \quad (4)$$

### 3.2 Diazenides ( $M\text{-N=NH}$ )

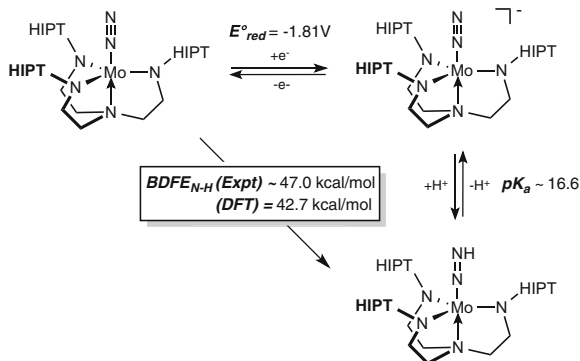
The first N-H bond-forming step in a hypothetical dinitrogen reduction cycle generates a transition metal diazenido ligand,  $M\text{-N=NH}$ . The direct measure of N-H BDFEs associated with diazenides has been hampered by the paucity of these compounds in the literature. While numerous substituted diazenides,  $M\text{-N=N-E}$  have been prepared with boryl [43], silyl [44], benzyl [45], phenyl [46, 47], and alkyl [48] substituents, the only structurally characterized “parent” ( $E\text{=H}$ ) example is Schrock’s  $[\text{N}_3\text{N}^{\text{HIPT}}]\text{Mo-N=NH}$  complex  $(\text{N}_3\text{N}^{\text{HIPT}}=[(\text{HIPTNCH}_2\text{CH}_2)_3\text{N}]^{3-})$ , where  $\text{HIPT} = 3,5\text{-}(2,4,6\text{-}^i\text{Pr}_3\text{C}_6\text{H}_2)_2\text{C}_6\text{H}_3$  [49].

While the N-H BDFE of  $[\text{N}_3\text{N}^{\text{HIPT}}]\text{Mo-N=NH}$  has not been explicitly presented in the literature, the physical data are available to estimate its value. The cyclic voltammogram of  $[\text{N}_3\text{N}^{\text{HIPT}}]\text{Mo-N}_2$  has been obtained and a Mo(III)-Mo(II) couple of  $-1.81$  V (vs.  $\text{Fc}/\text{Fc}^+$ ) has been reported in THF [49]. Additionally, qualitative deprotonation experiments using DBU (DBU = 1,8-Diazabicycloundec-7-ene) have also been conducted demonstrating that the  $pK_a$  of  $[\text{N}_3\text{N}^{\text{HIPT}}]\text{Mo-N=NH}$  can be approximated as 16.6, the value of  $\text{DBUH}^+$  [50]. Application of these values in the Bordwell equation resulted in an experimentally determined N-H BDFE of 47.0 kcal/mol in  $[\text{N}_3\text{N}^{\text{HIPT}}]\text{Mo-N=N-H}$ , comparing favorably to our DFT computed value of 42.3 kcal/mol. The slight discrepancy between these values may be a consequence of the model complex used in the calculations or the use of an unoptimized acid-base combination for the experimental  $pK_a$  determination in  $[\text{N}_3\text{N}^{\text{HIPT}}]\text{Mo-N=N-H}$  (Fig. 7).

### 3.3 Hydrazides ( $M\text{-N-NH}_2$ )

The next N-H bond forming event in a Chatt-type ammonia synthesis cycle is formation of a metal hydrazide,  $M\text{=N-NH}_2$  from the corresponding diazenide. In this case the “distal” mechanism of ammonia synthesis is invoked, where N-H bond formation and subsequent ammonia release occur first at the distal nitrogen as opposed to an “alternating” path in which hydrogen atoms add alternately to both

**Fig. 7** Thermodynamic square scheme for the estimation of the N-H bond strength in  $[\text{N}_3\text{N}^{\text{HIPT}}]\text{Mo-N}=\text{N-H}$ .  $E_{\text{red}}^\circ$  and  $\text{p}K_{\text{a}}$  values cited in THF solution. DFT-calculated N-H BDFE value in kcal/mol for the gas-phase reaction  $[\text{N}_3\text{N}^{\text{Ph}}]\text{Mo-N}=\text{NH} \rightarrow [\text{N}_3\text{N}^{\text{Ph}}]\text{Mo-N}=\text{N} + \text{H}\cdot$  where  $[\text{N}_3\text{N}^{\text{Ph}}] = [(\text{PhNCH}_2\text{CH}_2)_3\text{N}]^{3-}$



nitrogen atoms [51]. Unlike diazenides, numerous examples of transition metal complexes with parent hydrazido ligands have been synthesized [52]. The early examples are the well-known bis(diphosphine) molybdenum and tungsten compounds that are of interest due to their intermediacy in the Chatt cycle for ammonia synthesis from coordinated dinitrogen. Despite their ubiquity and long-standing role in  $\text{N}_2$  fixation chemistry, little is known about the bond dissociation free energies of the N-H linkage in transition metal hydrazides.

Our laboratory recently reported a study that examined the strengths of N-H bonds in bis(diphosphine) molybdenum compounds bearing cyclohexyl-substituted hydrazide ligands [53]. The cyclohexyl rather than parent examples were selected due to their isolability and ability to conduct reliable acidity and electrochemical measurements. The target molybdenum(IV) alkyl hydrazido complexes were synthesized according to the sequence presented in Fig. 8. Alkylation of the molybdenum(0) dinitrogen complex,  $(\text{dppe})_2\text{Mo}(\text{N}_2)_2$  ( $\text{dppe} = \text{Ph}_2\text{PCH}_2\text{CH}_2\text{PPh}_2$ ) with cyclohexyl iodide yielded the molybdenum(II) diazenido complex  $(\text{dppe})_2\text{Mo}(\text{NNCy})(\text{I})$  as previously described [54]. Treatment of this product with the strong acid,  $[\text{H}(\text{OEt}_2)_2][\text{BArF}^{24}]$  ( $\text{ArF}^{24} = (\text{C}_6\text{H}_3-3,5-(\text{CF}_3)_2)_4$ ) afforded the cationic molybdenum(IV) hydrazide,  $[(\text{dppe})_2\text{Mo}(\text{NNHCy})(\text{I})]^+$ . Halide abstraction with  $\text{Na}[\text{BArF}^{24}]$  in the presence of neutral donors such as  $\text{CH}_3\text{CN}$  or  $3,5-(\text{CF}_3)_2\text{C}_6\text{H}_3\text{CN}$  provided the cationic diazenides,  $[(\text{dppe})_2(\text{CH}_3\text{CN})\text{Mo}(\text{NNCy})]^+$  and  $[(\text{dppe})_2(3,5-(\text{CF}_3)_2\text{C}_6\text{H}_3\text{CN})\text{Mo}(\text{NNCy})]^+$ . The corresponding dicationic hydrazides were also synthesized with the goal of determining the influence of the *trans* ligand on the N-H BDFE (Fig. 8).

Titration experiments on this family of compounds demonstrated that more electron withdrawing ligands resulted in more acidic N-H bonds with  $\text{p}K_{\text{a}}$  values between 9.3 ( $\text{L} = \text{I}$ ) and  $<2.6$  ( $\text{L} = 3,5-(\text{CF}_3)_2\text{C}_6\text{H}_3\text{CN}$ ). Likewise, electron withdrawing *trans* ligands also produced less reducing reduction potentials and hence resulted in stronger N-H BDFEs. The experimental measurements were corroborated by DFT calculations, where the N-H BDFE trend as a function of *trans* ligand was confirmed by frequency calculations (Fig. 9).

Despite the marginal increase in BDFE observed with more electron withdrawing *trans* ligands, values between 30 and 35 kcal/mol for the putative Chatt-type

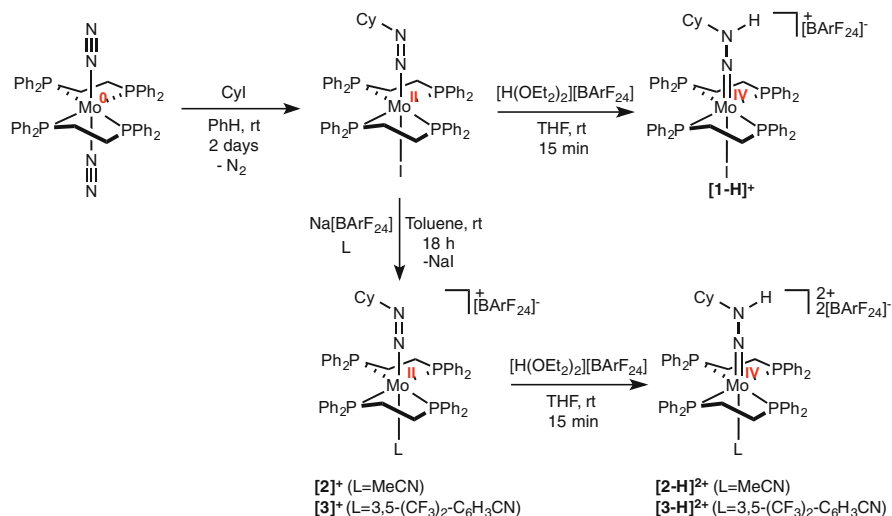


**Fig. 8** Synthesis of bis(phosphine) molybdenum diazenides and the corresponding hydrazides with varying ligands in the coordination site *trans* to the dinitrogen-derived fragment

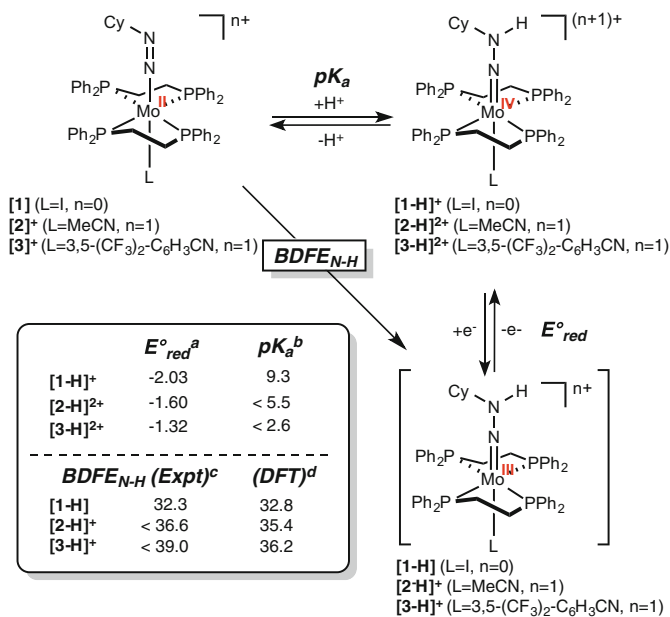


**Fig. 9** Thermochemical square scheme for the determination of N-H bond strengths ( $BDFE_{N-H}$ ) in bis(phosphine) molybdenum complexes. <sup>a</sup>Peak cathodic potentials (for **[1-H]<sup>+</sup>** and **[2-H]<sup>2+</sup>**) and  $E_{1/2}$  (for **[3-H]<sup>2+</sup>**) reported in V relative to Fc/Fc<sup>+</sup> in THF solution. <sup>b</sup>Acidity determined by titration against standards in THF. <sup>c</sup>Calculated value (kcal/mol) in THF from the Bordwell equation for the reaction  $[\text{Mo}-\text{NNHR}]^{n+} \rightarrow [\text{Mo}-\text{NNR}]^{n+} + \text{H}\cdot$  assuming  $C_G(\text{THF}) = 66$  kcal/mol. <sup>d</sup>DFT-calculated value in kcal/mol for the reaction  $[\text{Mo}-\text{NNHR}]^{n+} \rightarrow [\text{Mo}-\text{NNR}]^{n+} + \text{H}\cdot$ .

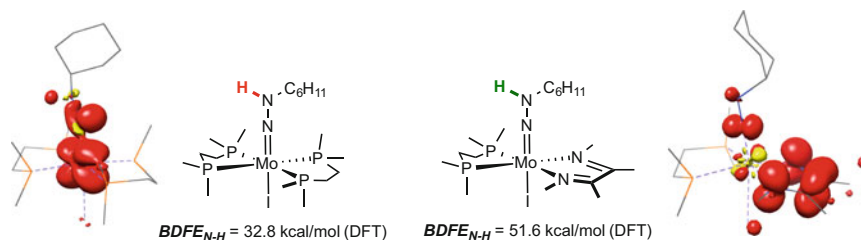


**Fig. 10** Comparison of DFT-computed N-H BDFEs and corresponding spin density plots for  $(dmpe)_2Mo(NNHCCy)(I)$  (left) and  $(dmpe)^{(McDI)}Mo(NNHCCy)(I)$  (right)

molybdenum(III) complexes are very low and are therefore unstable to  $H_2$  loss ( $\Delta G_{H_2} = 48.6 \text{ kcal/mol}$ ). The low BDFEs are driven, principally, by the reducing Mo(IV)-Mo(III) redox couple also presenting obstacles for isolation. Such low N-H BDFE values also imply a thermodynamic difficulty associated with their formation, necessitating the use of strong acid/strong reductant combinations that are often employed in catalytic ammonia synthesis methods. A possible strategy for strengthening such low N-H BDFEs is outlined in Fig. 10. DFT frequency calculations revealed that a simple substitution of a strong field phosphine ligand for a potentially redox non-innocent  $\alpha$ -diimine ( $^{Mc}DI=[CH_3N=C(CH_3)]_2$ ) chelate in  $(dmpe)_2Mo(NNHCCy)(I)$  ( $dmpe=1,2\text{-bis(dimethylphosphino)ethane}$ ;  $Cy = \text{cyclohexyl}$ ) resulted in a significant increase in the N-H BDFE by nearly 20 kcal/mol (M. J. Bezdek and P. J. Chirik, Unpublished data). Examining the DFT-computed spin density plots of the respective hydrazido complexes suggests an explanation: in the case of  $(dmpe)_2Mo(NNHCCy)(I)$ , the spin density resides principally on molybdenum while in  $(dmpe)(DI)Mo(NNHCCy)(I)$ , the spin density is localized on the redox non-innocent DI chelate. Participation of the redox active chelate in the electronic structure of the compound likely results in an energetically accessible redox couple, thus resulting in a net stronger bond as implied by the Bordwell equation.

### 3.4 Imides ( $M=NH$ )

Following  $NH_3$  release and cleavage of the N-N bond to generate a terminal metal-nitride,  $M\equiv N$ , the subsequent N-H bond formation generates the corresponding transition metal imido derivative,  $M=N-H$ . While the synthesis and reaction chemistry of substituted transition metal imido complexes ( $M=N-R$ ) has been well studied for early (For selected reviews on the synthesis and reactivity of early transition metal imides, see: [55–58]) as well as late (For selected reviews on the synthesis and reactivity late transition metal imides, see: [59, 60]) transition metals with a variety of substituents on the nitrogen atom, parent imido complexes,  $M=N-$

H, are typically difficult to access and often extremely reactive, rendering the associated thermochemical studies challenging.

Although the paucity of parent imido transition metal complexes limits systematic thermochemical measurements of the N-H bonds, chemical bracketing studies using hydrogen atom donors and acceptors with isolable metal nitrides have enabled the approximate definition of upper and lower bounds. Seminal work by Smith and coworkers have described stoichiometric ammonia synthesis from a terminal iron(IV) nitrido complex by reaction with the hydrogen atom donor TEMPO-H (TEMPO = 2,2,6,6-tetramethylpiperidine 1-oxyl, Fig. 11) [61]. As part of these studies, the strength of the putative iron(III) imido N-H bond was bracketed between 67.5 kcal/mol (TEMPO-H, DMSO) and 73.3 kcal/mol (xanthene, DMSO) given that productive N-H bond forming chemistry was not observed with weaker H-atom donors. The results unequivocally demonstrate that an N-H bond forming strategy involving concerted hydrogen atom transfer steps (as opposed to stepwise protonation-reduction with strong acids and reductants) is viable for ammonia synthesis.

Schneider and coworkers have also examined the N-H bond strengths of parent imides with mononuclear iridium complexes relevant to the reverse of dinitrogen reduction—the oxidation of ammonia to N<sub>2</sub> [62]. Although detailed thermochemical studies were hampered by rapid disproportionation of the iridium imido species to the corresponding amido and bridging dinitrogen complexes (Fig. 12), bracketing experiments with various hydrogen atom donors have established an

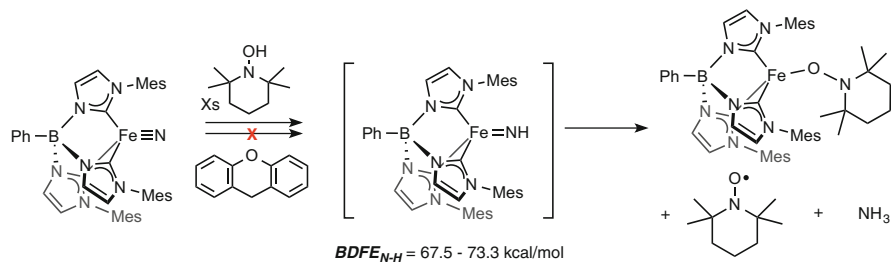


**Fig. 11** Ammonia synthesis by hydrogen atom transfer from TEMPO-H to an Fe(IV) nitride supported by a tris(carbene) borate ligand. BDFE reference values cited in DMSO solution [31]

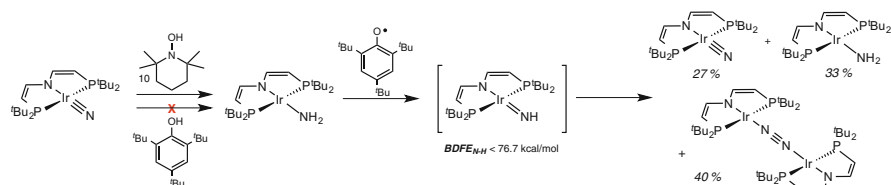


**Fig. 12** Synthesis of a terminal imido complex supported by a PNP-pincer ligand by hydrogen atom abstraction and subsequent disproportionation chemistry. BDFE reference value cited in benzene solution [31]

approximate upper bound for the N-H BDFE in the putative iridium imido complex as that of the O-H bond strength of  $t\text{Bu}_3\text{PhOH}$  (76.7 kcal/mol, benzene) [31]. These results were supported by DFT calculations and provide rare thermochemical insight into the thermodynamics of N-H bond formation in late transition metal nitrides to generate the corresponding parent imido ligand. While such thermochemical information is highly valuable, we note that N-H BDFE measurements in transition metal imido complexes derived from atmospheric dinitrogen are absent from the literature.

### 3.5 Amides ( $M\text{-NH}_2$ )

Transition metal amido ( $M\text{-NH}_2$ ) complexes are generated by N-H bond formation from the corresponding imido complex. As with metal imides, substituted transition metal amide complexes of the type  $M\text{-NRH}$  are ubiquitous in the literature and selected approximate N-H bond strengths have been reported [63–66]. An especially well-defined report was provided by Smith and coworkers establishing an N-H BDFE of 88 kcal/mol in the tetrahedral Fe(III) complex,  $[(\text{LMes})\text{Fe}(\text{HNAd})]^+$  (LMes = phenyltris(1-mesitylimidazol-2-ylidene)borate) [67].

As part of a research program studying potentially redox-active ligands in early transition metal chemistry with the goal of lowering the barriers to  $M\text{-NH}_2$  hydrogenolysis [68], our research group has examined the influence of ligand redox-activity on N-H BDFEs in bis(imino)pyridine complexes of vanadium [69]. Complexes featuring phenyl-substituted bis(imido), imido/anilido and bis(anilido) ligands were synthesized, providing a rare opportunity for studying model amido N-H bond strengths in the series of related complexes featuring an electronically responsive ligand.

As shown in Fig. 13, the redox-active bis(imino) pyridine ligand ( $i\text{Pr}^{\text{B}}\text{PDI} = 2,6\text{-}(2,6\text{-}i\text{Pr}_2\text{-C}_6\text{H}_3\text{N}=\text{CPh})_2\text{C}_3\text{H}_3\text{N}$ ) adjusts to the electronic demands of the transition metal center and can store and release reducing equivalents throughout a series of

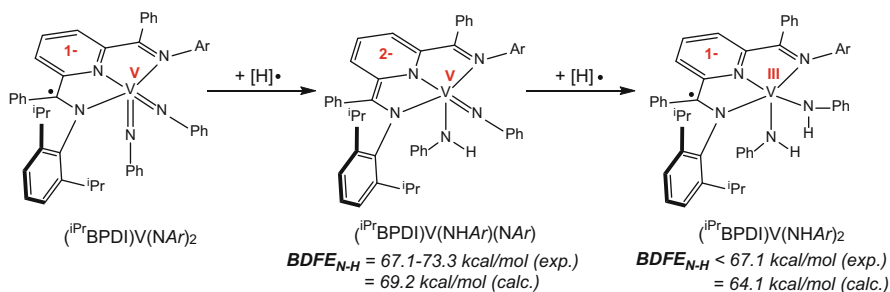


**Fig. 13** Summary of hydrogen atom transfer events and associated N-H bond dissociation free energies in bis(imino) pyridine complexes of vanadium

hydrogen atom transfer events, each a formally one-electron transformation. In the substituted bis(imido) complex ( $i^{\text{Pr}}\text{BPDI}V(\text{NAr})_2$ ), two strongly  $\pi$ -donating imido ( $=\text{NAr}$ ) ligands dominate the ligand field and generate a high oxidation state vanadium compound ( $V(V+)$ ,  $d^0$ ) with the additional reducing equivalent stored in the  $[i^{\text{Pr}}\text{BPDI}]^-$  chelate. When a hydrogen atom is transferred to the apical imido ligand and forms the mixed imido/anilido complex ( $i^{\text{Pr}}\text{BPDI}V(\text{NHAr})(\text{NAr})$ ), the incoming electron is relayed to the redox-active ligand to form doubly reduced  $[i^{\text{Pr}}\text{BPDI}]^{2-}$ , with the vanadium metal center maintaining the +5 oxidation state. Again, the  $\pi$ -donating imido/anilido ligands likely dominate the bonding and hence the highest metal oxidation state is observed. When the second hydrogen-atom is added to form the vanadium bis(anilido) complex ( $i^{\text{Pr}}\text{BPDI}V(\text{NHAr})_2$ ), the disruption of the second  $V=\text{NAr}$   $\pi$ -interaction results in a highly electropositive metal thereby necessitating a primarily metal-based one-electron reduction that is accompanied by the transfer for an additional electron from the redox active chelate. The vanadium bis(anilido) complex is best described as  $V(\text{III}+)$  with a singly reduced  $[i^{\text{Pr}}\text{BPDI}]^-$  chelate (Fig. 13).

The series of vanadium bis(imido), imido-anilido, and bis(anilido) complexes provided a rare opportunity to study N-H BDFEs within a family of related compounds separated by H-atom transfer events. Hydrogen atom donors such as TEMPO-H ( $\text{BDFE}_{\text{O-H}} = 67.5$  kcal/mol, DMSO) or 1,2-diphenylhydrazine ( $\text{BDFE}_{\text{N-H}} = 67.1$  kcal/mol, DMSO) were effective in facilitating the conversion from ( $i^{\text{Pr}}\text{BPDI}V(\text{NAr})_2$ ) to ( $i^{\text{Pr}}\text{BPDI}V(\text{NHAr})(\text{NAr})$ ), while weaker donors with stronger E-H bonds such as xanthene ( $\text{BDFE}_{\text{C-H}} = 73.3$  kcal/mol, DMSO) and 9,10-dihydroanthracene ( $\text{BDFE}_{\text{C-H}} = 76.0$  kcal/mol, DMSO) were unreactive. This set of experiments bracket the N-H BDFE of ( $i^{\text{Pr}}\text{BPDI}V(\text{NHAr})(\text{NAr})$ ) to be in the range of 67.1–73.3 kcal/mol, confirmed by DFT frequency calculations (69.2 kcal/mol, gas phase). A similar set of experiments established an upper bound for the N-H BDFE in ( $i^{\text{Pr}}\text{BPDI}V(\text{NHAr})_2$ ) to be  $<67$  kcal/mol, as the compound proved unreactive toward TEMPO-H. A value of 64.1 kcal/mol (gas phase) was obtained from DFT computations, thus supporting the experimental results. Interestingly, unlike in the case of group(IV) metallocene amido complexes lacking electronically responsive ligands (vide infra), the thermodynamics of N-H bond formation do not change significantly as a function of the net redox state of the molecule and result in notably weaker bonds in comparison to late metal examples.

### 3.6 Ammines ( $M\text{-NH}_3$ )

The final N-H bond-forming step in a dinitrogen reduction cycle generates a transition metal-bound ammonia molecule that is ideally displaced by a dinitrogen ligand to regenerate the starting transition metal dinitrogen complex. Despite the ubiquity and historical significance of ammine ligands in coordination chemistry (For historically significant ammine complexes, see: [70–72]), little thermochemical information exists regarding how the N-H bond strength of ammonia is

influenced upon coordination to a transition metal center. Consequently, the associated thermochemical requirements for forming N-H bonds by the transfer of a hydrogen atom to transition metal amido complexes are generally not well understood.

As part of our investigations into ammonia synthesis by hydrogenolysis of strong titanium-nitrogen bonds using proton coupled electron transfer, the N-H bond dissociation free energies of  $\text{NH}_3$  coordinated bis(cyclopentadienyl) Ti(II), Ti(III) and Zr(III) compounds were measured (Fig. 14). The thermochemical results presented in Fig. 14 established two trends in the observed N-H BDFEs of ammine complexes of these group(IV) metallocenes: reduction from Ti(III) to Ti(II) results in lower N-H BDFEs while substitution of the titanium(III) metal center to the more reducing zirconium(III) has a similar effect. The  $pK_a$ s among the ammine compounds in this series vary little, consistent with the same overall charge in each metallocene. It should be noted that although absolute BDFE values for the complexes **1-(Cl)NH<sub>3</sub>**, **2-(Cl)NH<sub>3</sub>** and **1-NH<sub>3</sub>** could not be determined experimentally due to the observed irreversibility in electrochemical behavior of the corresponding cations, computational studies were used to support the BDFE trend in the series of compounds. While the complex **1-(Cl)NH<sub>3</sub>** features the strongest ammine N-H BDFE in the series (61 kcal/mol), the more reducing Ti (II) and Zr(III) analogues, **1-NH<sub>3</sub>** and **2-(Cl)NH<sub>3</sub>** have markedly lower N-H BDFEs of 42 and 41 kcal/mol. These complexes were not isolated; the exceedingly weak

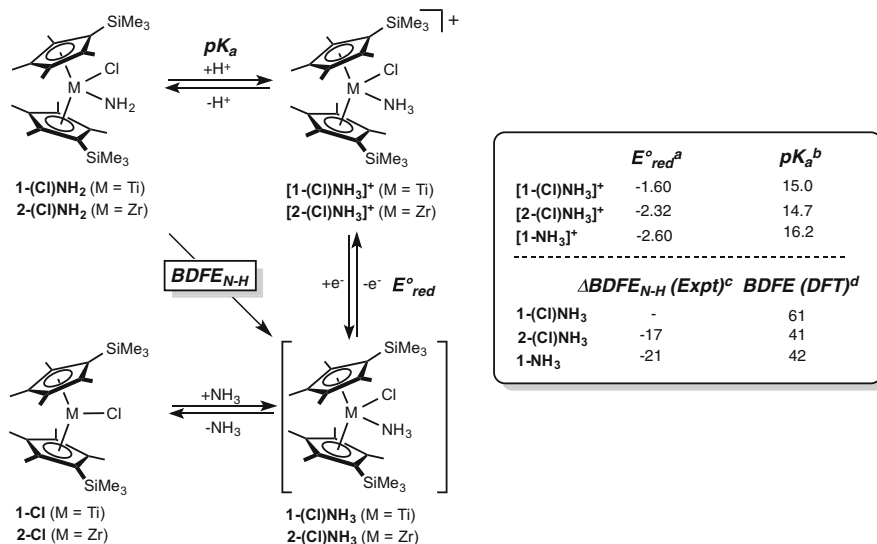


**Fig. 14** Thermochemical square scheme for the determination of N-H bond strengths in Group (IV) metallocenes. <sup>a</sup>Peak cathodic potential reported relative to  $\text{Fc}/\text{Fc}^+$  in Me–THF solution. <sup>b</sup>Acidity determined by UV/vis titration against standards in Me–THF. <sup>c</sup>Defined as  $BDFE(2-(Cl)NH_3) - BDFE(1-(Cl)NH_3)$  and  $BDFE(1-NH_3) - BDFE(1-(Cl)NH_3)$ . <sup>d</sup>DFT-calculated free energy change for the reaction of  $[\text{M}]NH_2-H \rightarrow [\text{M}]NH_2 + H$ .



N-H BDFEs likely contribute to their instability and suggested that **1-(Cl)NH<sub>2</sub>** was the most promising for ammonia liberation by PCET.

Because of the favorable thermodynamics of N-H bond formation in **1-(Cl)NH<sub>2</sub>**, this compound was selected for ammonia synthesis studies by PCET. It should be noted that breaking strong early transition metal-nitrogen bonds with dihydrogen is rare likely due to unfavorable kinetics. Knowledge about the N-H BDFE of the corresponding ammine complex **1-(Cl)NH<sub>3</sub>** led to rational selection of ( $\eta^5\text{-C}_5\text{Me}_5$ )(py-Ph)RhH (**Rh-H**; py-Ph = 2-pyridylphenyl) as the hydrogen atom transfer reagent. With a homolytic Rh-H BDFE of 52.3 kcal/mol [73], hydrogen atom transfer from **Rh-H** to **1-(Cl)NH<sub>2</sub>** should be thermodynamically favorable to generate **1-(Cl)NH<sub>3</sub>** (BDFE<sub>N-H</sub> = 61 kcal/mol) accompanied by ammonia release. Additionally, upon transferring a hydrogen atom, the rhodium complex **Rh-H** can be regenerated under an atmosphere of dihydrogen, potentially enabling a catalytic PCET method with respect to the hydrogen atom donor. With these design principles in hand, a method was developed for the liberation of ammonia from the coordination sphere of an early transition metal complex, where dihydrogen was the stoichiometric hydrogen atom source (Fig. 15). Notably, these results demonstrate that application of PCET to ammonia synthesis offers considerable promise for a method for N-H bond formation with low chemical overpotential.

The advantage of obtaining a thorough and systematic understanding of N-H bond strengths in ammine complexes of transition metals is multifold. Such knowledge could be used to form typically strong ammine N-H bonds bound to metal centers that ultimately facilitate ammonia release using a PCET strategy. On the other hand, coordination of ammonia to a transition metal can induce “bond weakening by coordination”—a phenomenon whereby the redox potential and *pK<sub>a</sub>* of the metal lower the BDFE of ammonia from its gas phase value. This effect can be significant and BDFEs reduced by over 50 kcal/mol have been observed [74]. Recognition and systematic understanding of this effect could in principle enable a new activation mode for small molecules containing typically inert E-H bonds (E = N, O) bonds. To better understand and explore the effect of coordination induced bond weakening, our laboratory initiated a research program studying the reactivity of ammonia with molybdenum phosphine complexes supported by redox active terpyridine ligands (Fig. 16).

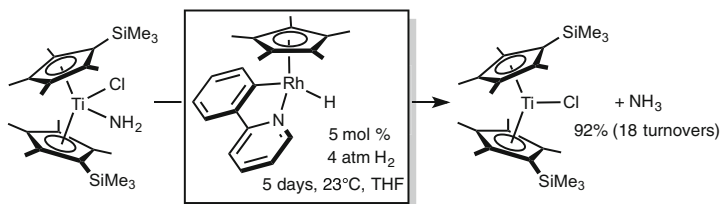


**Fig. 15** Catalytic hydrogenolysis of **1-(Cl)NH<sub>2</sub>** using 5 mol% of **Rh-H** for the generation of ammonia

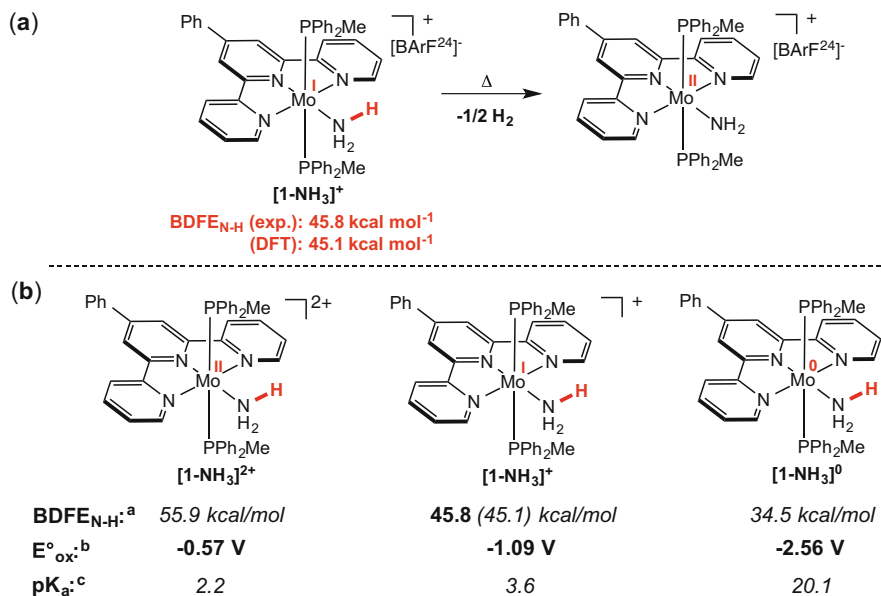


**Fig. 16** (a) Thermolysis of a “non-classical” ammine complex to furnish the corresponding amido complex and liberating dihydrogen. (b) Thermochemical N-H bond strength studies on a series of Mo(II), Mo(I), and Mo(0) ammine complexes. <sup>a</sup>Values obtained from gas-phase DFT calculations, bolded value determined experimentally. <sup>b</sup>Oxidation potentials reported relative to  $\text{Fc}/\text{Fc}^+$  in THF solution. <sup>c</sup>Calculated value in THF from the Bordwell equation for the reaction  $[\text{Mo}^{(m+1)}\text{-NH}_3]^{(m+1)+} \rightarrow [\text{Mo}^{(m+1)}\text{-NH}_2]^{m+}$ , assuming the corresponding DFT-calculated N-H BDFE value and  $C_G(\text{THF}) = 66 \text{ kcal/mol}$

As shown in Fig. 16a, the complex  $[(\text{Ph}^{\text{Tpy}})(\text{PPh}_2\text{Me})_2\text{Mo}(\text{NH}_3)]^+$  ( $[\mathbf{1-NH}_3]^+$ ;  $\text{Ph}^{\text{Tpy}} = 4'\text{-Ph-2,2',6',2''-terpyridine}$ ) is an example of a so-called non-classical ammine complex in that it features as unusually weak N-H bond. The term non-classical refers to a compound where the N-H BDFE of the molecule is  $<49 \text{ kcal/mol}$  and is therefore thermodynamically unstable toward  $\text{H}_2$  loss. Analysis of the constituent thermodynamic parameters (Fig. 16b) revealed a remarkably weak ammine N-H bond of  $45.8 \text{ kcal/mol}$  (THF) as supported by computational studies ( $\text{BDFE}_{\text{N-H}} = 45.1 \text{ kcal/mol}$ , gas phase). The individual  $E^{\circ}_{\text{ox}}$  and  $\text{pK}_a$  values suggested that the exceptionally weak N-H bond in  $[\mathbf{1-NH}_3]^+$  arises from both a reducing Mo(I/II) couple ( $E_{\text{ox}} = -1.09 \text{ V}$ , THF) and a very acidic N-H bond in the corresponding dicationic complex  $[\mathbf{1-NH}_3]^{2+}$  ( $\text{pK}_a = 3.6$ , THF), likely a result of the overall charge of the molecule. The analogous values in the one-electron oxidized and one-electron reduced complexes  $[\mathbf{1-NH}_3]^{2+}$  and  $[\mathbf{1-NH}_3]^0$  were examined to understand the coordination-induced bond weakening phenomenon in a redox series. There is a marked weakening of N-H bonds across the series with the most reduced  $[\mathbf{1-NH}_3]^0$  complex featuring the weakest N-H bond, driven largely by the highly reducing Mo(I)/Mo(0) couple of ( $-2.56 \text{ V}$ , THF). On the other

hand, the N-H bond weakening in the oxidized, dicationic complex  $[\mathbf{1-NH_3}]^{2+}$  is influenced by the acidic nature of the N-H bond ( $pK_a = 2.2$ ), likely a consequence of the dicationic overall charge of the molecule.

These studies are also valuable beyond the context of ammonia activation. Given that many transition metal catalysts contain ligands with N-H bonds, particularly those involved in metal-ligand cooperative reductions, avoiding “bond weakening by coordination” is critical for catalyst stability. Defining and parameterizing the criteria for this phenomenon will contribute to enabling rational catalyst design for ammonia synthesis or small molecule activation chemistry.

## 4 Conclusions and Outlook

Understanding the thermodynamics of N-H bond formation and its microscopic reverse, N-H bond homolysis, is critical for both ammonia synthesis and oxidation chemistry. Despite the maturity of coordination chemistry with nitrogen-containing ligands, until recently little was known about the strengths of the N-H bonds in compounds relevant to dinitrogen reduction and oxidation schemes. Throughout, we have highlighted studies that examine how factors such as ligand environment, identity of the transition metal as well as metal oxidation state affect the thermodynamics of N-H bond formation in a range of model compounds and ammonia synthesis catalysts. Although considerable progress has been made, many challenges remain. It is important to point out that in the latter part of a hypothetical dinitrogen reduction cycle following the formation of a transition metal nitride, all model compounds reported to date where thermochemical data are available are not derived from  $N_2$ . Related studies on dinitrogen derived imido, amide, and ammine complexes are completely absent from the literature. This is likely a consequence of a recurring challenge and dichotomy in the field of dinitrogen reduction chemistry: metals that promote the activation and cleavage of molecular dinitrogen tend to generate inert nitrido complexes with strong  $M\equiv N$  bonds that tend not to undergo further N-H bond forming chemistry. Future efforts in this area should focus on compounds more relevant to  $N_2$ -derived ammonia synthesis as well as understanding molecular catalysts in more detail. One of the primary advantages of approaching ammonia synthesis using a PCET strategy is that, assuming minimal kinetic barriers to a HAT event, the reactivities of the compounds in question are entirely predictable based on thermodynamics. In this regard, computational studies will be valuable in predicting the thermochemical requirements of N-H bond formation in transition metal systems with nitrogen-containing ligands derived from dinitrogen.

## References

1. Smil V (2001) *Enriching the earth: Fritz Haber, Carl Bosch, and the transformation of world food production*. MIT Press, Cambridge, MA
2. Smil V (1999) *Nature* 400:415
3. Haber F, van Oordt G (1905) *Z Anorg Chem* 43:111
4. Haber F, van Oordt G (1905) *Z Anorg Chem* 44:341
5. Haber F, van Oordt G (1905) *Anorg Chem* 47:42
6. Tamaru K (1991) In: Jennings JR (ed) *Catalytic ammonia synthesis*, Plenum Press, New York, NY
7. Worrell E, Phylipsen D, Einstein D, Martin N (2000) *Energy use and energy intensity of the U.S. Chemical Industry*, E. O. Lawrence Berkeley National Laboratory, Publication number LBNL-44313
8. Hoffman B, Lukoyanov D, Dean DR, Seefeldt LC (2013) *Acc Chem Res* 46:587
9. van der Ham CJM, Koper MTM, Hettterscheid DGH (2014) *Chem Soc Rev* 43:5183
10. Appl M (2011) In: Bellussi G et al (eds) *Ullmann's encyclopedia of industrial chemistry*. 7th edn, vol 3. Wiley-VCH, Weinheim, p 139
11. Chagas AP (2007) *Quim Nova* 30:240
12. Shlögl R (2003) *Angew Chem Int Ed* 42:2004
13. Allen AD, Senoff CV (1965) *Chem Commun* 621
14. Chatt J, Dilworth JR, Richards RL (1978) *Chem Rev* 78:589
15. Chatt J, Richards RL (1982) *J Organomet Chem* 239:65
16. Schrock RR (2005) *Acc Chem Res* 38:955
17. Pickett CJ, Ryder KS, Talarmin J (1986) *J Chem Soc Dalton Trans* 1453
18. Pickett CJ, Talarmin J (1985) *Nature* 317:652
19. Shilov AE (2003) *Russ Chem Bull* 52:2555
20. Bazhenova TA, Shilov AE (1995) *Coord Chem Rev* 144:69
21. Hill PJ, Doyle LR, Crawford AD, Myers WK, Ashley AE (2016) *J Am Chem Soc* 138:13521
22. Yandulov D, Schrock RR (2003) *Science* 301:76
23. Arashiba K, Miyake Y, Nishibayashi Y (2011) *Nat Chem* 3:120
24. Kuriyama S, Arashiba K, Nakajima K, Tanaka H, Kamaru N, Yoshizawa K, Nishibayashi Y (2014) *J Am Chem Soc* 136:9719
25. Kuriyama S, Arashiba K, Nakajima K, Tanaka H, Yoshizawa K, Nishibayashi Y (2015) *Chem Sci* 6:3940
26. Ung G, Peters JC (2015) *Angew Chem Int Ed* 54:532
27. Creutz SE, Peters JC (2014) *J Am Chem Soc* 136:1105
28. Anderson JS, Rittle J, Peters JC (2013) *Nature* 501:84
29. Kuriyama S, Arashiba K, Nakajima K, Matsuo Y, Tanaka H, Ishii K, Yoshizawa K, Nishibayashi Y (2016) *Nat Commun* 7:12181
30. Pappas I, Chirik PJ (2016) *J Am Chem Soc* 138:13379
31. Warren JJ, Tronic TA, Mayer JM (2010) *Chem Rev* 110:6961
32. Pappas I, Chirik PJ (2015) *J Am Chem Soc* 137:3498
33. Lindley BM, Appel AM, Krogh-Jespersen K, Mayer JM, Miller AJM (2016) *ACS Energy Lett* 1:698
34. Munisamy T, Schrock RR (2012) *Dalton Trans* 41:130
35. Nishibayashi Y (2015) *Inorg Chem* 54:9234
36. Cheng JP, Lu Y, Zhu XQ, Sun Y, Bi F, He J (2000) *J Org Chem* 65:3853
37. Thimm W, Gradert C, Broda H, Wennmohs F, Neese F, Tucek F (2015) *Inorg Chem* 54:9248
38. Mader EA, Davidson ER, Mayer JM (2007) *J Am Chem Soc* 129:5153
39. Sorai M, Seki S (1974) *J Phys Chem Solids* 35:555
40. Bordwell F, Chang JP, Harrelson JA (1988) *J Am Chem Soc* 110:1229
41. Tilset M (2001) In: Balzani V (ed) *Electron transfer in chemistry*. Wiley-VCH, Weinheim, p 677

42. Parker VD (1992) *J Am Chem Soc* 114:7458
43. Takahashi T, Mizobe Y, Sato M, Uchida Y, Hidai M (1980) *J Am Chem Soc* 102:7461
44. O'Donoghue MB, Davis WM, Schrock RR (1998) *Inorg Chem* 37:5149
45. Chew KC, Clegg W, Coles MP, Elsegood MRJ, Gibson VC, White AJP, Williams DJ (1999) *J Chem Soc Dalton Trans* 2633
46. Hsieh TC, Gebreyes K, Zubieta J (1984) *J Chem Soc Chem Commun* 1172
47. Hsieh TC, Nicholson T, Zubieta J (1988) *Inorg Chem* 27:241
48. Bossard GE, Busby DC, Chang M, George TA, Iske Jr SDA (1980) *J Am Chem Soc* 102:1001
49. Yandulov DV, Schrock RR (2005) *Inorg Chem* 44:1103
50. Rodima T, Kaljurand I, Pihl A, Mäemets V, Leito I, Koppel IA (2002) *J Org Chem* 67:1873
51. Hoffmann BM, Dean DR, Seefeldt LC (2009) *Acc Chem Res* 42:609
52. Hidai M, Mizobe Y (1995) *Chem Rev* 95:1115
53. Bezdek MJ, Chirik PJ (2016) *Dalton Trans* 45:15922
54. Busby DC, George TA, Iske SDA, Wagner SD (1981) *Inorg Chem* 20:22
55. Schrock RR (1990) *Acc Chem Res* 23:158
56. Duncan AP, Bergman RG (2002) *Chem Rec* 2:431
57. Hazari N, Mountford P (2005) *Acc Chem Res* 38:839
58. Mindiola DJ (2006) *Acc Chem Res* 39:813
59. Sharp PR (1999) *Comments Inorg Chem* 21:85
60. Berry JF (2009) *Comments Inorg Chem* 30:28
61. Scepaniak JJ, Young JA, Bontchev RP, Smith JM (2009) *Angew Chem Int Ed* 48:3158
62. Scheibel MG, Abbenseth J, Kinauer M, Heinemann FW, Würtele C, de Bruin B, Schneider S (2015) *Inorg Chem* 54:9290
63. Cowley RE, Holland PL (2012) *Inorg Chem* 51:8352
64. Iluc VM, Miller AJM, Anderson JS, Monreal MJ, Mehn MP, Hillhouse GL (2011) *J Am Chem Soc* 133:13055
65. Iluc VM, Hillhouse GL (2010) *J Am Chem Soc* 132:15148
66. Cowley RE, Bontchev RP, Sorrell J, Sarracino O, Feng Y, Wang H, Smith JM (2007) *J Am Chem Soc* 129:2424
67. Nieto I, Ding F, Bontchev RP, Wang H, Smith JM (2008) *J Am Chem Soc* 130:2716
68. Bart SC, Lobkovsky E, Bill E, Chirik PJ (2006) *J Am Chem Soc* 128:5302
69. Milsman C, Semproni SP, Chirik PJ (2014) *J Am Chem Soc* 136:12099
70. Werner A (1893) *Z Anorg Chem* 3:267
71. Peyrone M (1844) *Ann Chem Pharm* 51:1
72. Ford PC, Rudd DFP, Gaunder R, Taube H (1968) *J Am Chem Soc* 90:1187
73. Hu Y, Norton JR (2014) *J Am Chem Soc* 136:5938
74. Bezdek MJ, Guo S, Chirik PJ (2016) *Science* 354:730

# Dinitrogen Fixation by Transition Metal Hydride Complexes

Takanori Shima and Zhaomin Hou

**Abstract** This chapter describes the activation of dinitrogen by various transition metal hydride complexes. A number of mononuclear transition metal hydride complexes can incorporate dinitrogen, but they are usually difficult to induce N–N bond cleavage. In contrast, multimetallic hydride complexes can split and hydrogenate dinitrogen through cooperation of the multiple metal hydrides. In this transformation, the hydride ligands serve as the source of both electron and proton, thus enabling the cleavage and hydrogenation of dinitrogen without extra reducing agents and proton sources. Generally, the reactivity of the metal hydride complexes is significantly influenced by their composition (nuclearity) and metal/ligand combination.

**Keywords** Dinitrogen cleavage • Hydride • Hydrogenation • Multimetallic • Nitride

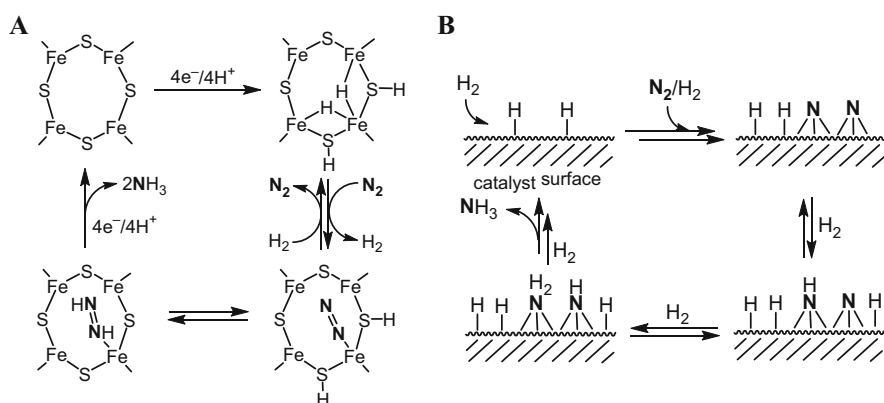
## Contents

1	Introduction .....	24
2	Dinitrogen Complexes Derived from Mononuclear Transition Metal Hydride Complexes .....	25
2.1	Group 9 Transition Metal Hydrides .....	25
2.2	Group 8 Transition Metal Hydrides .....	26
2.3	Group 7 Transition Metal Hydrides .....	28
2.4	Group 6 Transition Metal Hydrides .....	29
2.5	Group 4 Transition Metal Hydrides .....	31
3	Activation and Functionalization of Dinitrogen by Binuclear Transition Metal Hydride Complexes .....	32

4	Activation and Functionalization of Dinitrogen by Tri- and Tetranuclear Transition Metal Hydride Complexes .....	37
5	Concluding Remarks and Outlook .....	39
	References .....	39

## 1 Introduction

Dinitrogen ( $N_2$ ) is an abundant and easily accessible resource, which occupies about 78% of Earth's atmosphere. However,  $N_2$  molecule is chemically inert under ordinary conditions due to its strong N–N triple bond ( $944.84 \pm 0.10$  kJ/mol) [1], large HOMO-LUMO energy gap (10.82 eV) [2], and nonpolarity. Certain microbial organisms can reduce  $N_2$  to  $NH_3$  by using nitrogenase enzymes at ambient temperature and pressure. This process consumes eight protons ( $H^+$ ) and eight electrons ( $e^-$ ) to convert one molecule of  $N_2$  to two molecules of  $NH_3$  with release of one molecule of  $H_2$ . Recent studies revealed that the multiple metal centers having two hydrides and two sulfur-bound protons in the iron–molybdenum cofactor play a key role to promote  $H_2$  release and  $N_2$  reduction (Scheme 1a) [3–6]. However, the biological ammonia synthesis is not yet well understood and is difficult to mimic artificially. Industrially, ammonia is produced from  $N_2$  and  $H_2$  by the Haber–Bosch process under relatively harsh conditions ( $350\sim 550^\circ C$ ,  $150\sim 350$  atm) to activate  $N_2$  on the solid catalyst surface. It was proposed that the reaction is initiated by dissociative absorption of  $N_2$  and  $H_2$  on low valent multiple iron metal sites to form metal hydrides and nitrides, followed by reversible hydrogenation of the nitride species to provide  $NH_3$  (Scheme 1b) [7–11]. Both the biological and the Haber–Bosch processes are thought to take place through the cooperation of multiple metal sites bearing hydride ligands.



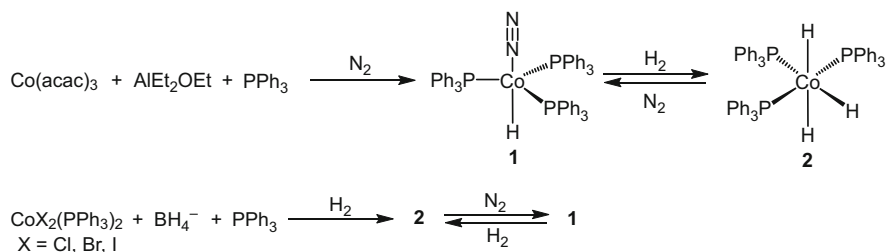
**Scheme 1** Proposed pathways for catalytic ammonia formation by (a) nitrogenase enzyme (only the core structure is shown) and (b) the Haber–Bosch process (only part of the catalyst surface is shown)

In order to further explore the mechanism of  $N_2$  reduction at the molecular level and thereby develop milder chemical processes for ammonia synthesis, extensive studies on the activation of  $N_2$  with organometallic complexes have been carried out over the past decades [12]. As model reactions of the enzyme process, the use of strong metal reducing agents as an electron source in combination with transition metal complexes has been extensively studied, and the catalytic transformation of  $N_2$  to ammonia has been achieved at ambient temperature and pressure by using carefully designed proton sources [13–15]. An alternative approach is the activation of  $N_2$  by transition metal hydrides without the use of extra reducing agents or proton sources [16]. This approach is of particular interest, in view of the fact that both the biological and the industrial Haber–Bosch processes may involve metal hydrides as true active catalyst species. This chapter focuses on the activation and functionalization of  $N_2$  by transition metal hydride complexes.

## 2 Dinitrogen Complexes Derived from Mononuclear Transition Metal Hydride Complexes

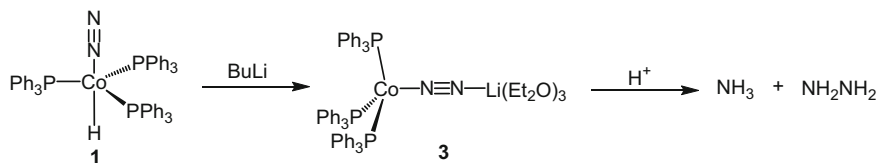
### 2.1 Group 9 Transition Metal Hydrides

The first dinitrogen complex  $[(NH_3)_5Ru(N_2)]^{2+}$  was obtained serendipitously from the reaction of a ruthenium trichloride with hydrazine hydrate in 1965 [17]. Shortly after this discovery, the  $N_2$ -derived end-on coordinated cobalt dinitrogen complex  $[(Ph_3P)_3Co(N_2)H]$  (**1**) was synthesized from the reaction of a cobalt acetylacetonate, diethylaluminium monoethoxide, and triphenylphosphine ligands in the presence of  $N_2$  gas (Scheme 2) [18]. When **1** was kept under an atmosphere of  $H_2$ , the coordinated  $N_2$  ligand was displaced by  $H_2$  to afford the cobalt hydride complex  $[(Ph_3P)_3CoH_3]$  (**2**) [19]. Complex **2** could also be prepared by the reaction of  $[CoX_2(PPh_3)_2]$  ( $X = Cl, Br, I$ ) with borohydride in the presence of  $H_2$  and free  $PPh_3$ , and the reaction of **2** with  $N_2$  easily took place to give **1** (Scheme 2) [20]. Thus, the hydrogenation/dinitrogen coordination reactions are reversible.

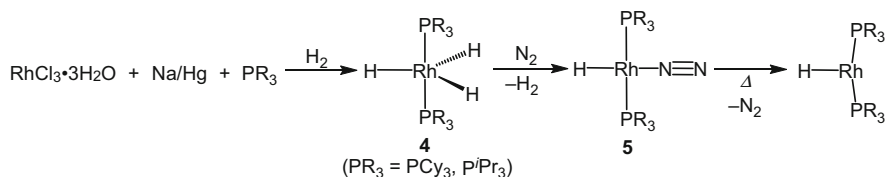


**Scheme 2** Synthesis and reversible hydrogenation of the cobalt dinitrogen complex **1**





**Scheme 3** Protonation of the cobalt dinitrogen complex **1**



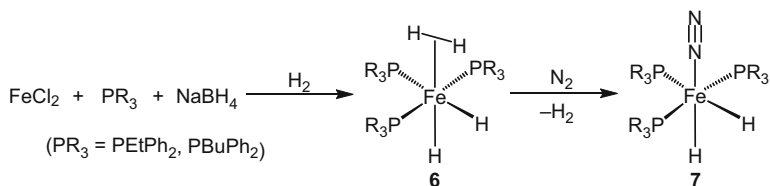
**Scheme 4** Synthesis of the rhodium dinitrogen complex **5**

The reaction of **1** with  $\text{MgEt}_2$ ,  $\text{BuLi}$ , or  $\text{Na}$  metal afforded the  $\text{N}_2$ -bridged heterobimetallic complex,  $[\{(\text{Ph}_3\text{P})_3\text{Co}(\mu\text{-N}_2)\}_2\text{Mg}(\text{THF})_4]$ ,  $[(\text{Ph}_3\text{P})_3\text{Co}(\mu\text{-N}_2)\text{Li}(\text{Et}_2\text{O})_3]$  (**3**), or  $[(\text{Ph}_3\text{P})_3\text{Co}(\mu\text{-N}_2)\text{Na}(\text{THF})_3]$ , respectively [21]. While the coordinated  $\text{N}_2$  ligand in **1** is unable to react with protic acids, the coordinated  $\text{N}_2$  ligand in the electron-rich heterobimetallic complexes such as **3** gives 20–30% of hydrazine and ammonia by addition of  $\text{H}_2\text{SO}_4$  or  $\text{HCl}$  (Scheme 3). However, reaction of the  $\text{Co-N}_2\text{-Li}$  complex **3** with  $\text{H}_2$  afforded an analogous hydrogen complex  $\text{Co-H}_2\text{-Li}$ , with quantitative evolution of  $\text{N}_2$ . Upon exposure to an  $\text{N}_2$  atmosphere, the hydrogen complex  $\text{Co-H}_2\text{-Li}$  released  $\text{H}_2$ , and regenerated **3**, demonstrating the reversibility of the coordination of  $\text{H}_2$  and  $\text{N}_2$  to the  $\text{Ph}_3\text{P-Co-Li}$  moiety.

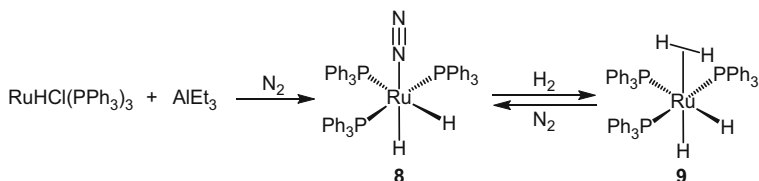
With regard to other group 9 metals, the reduction of  $\text{RhCl}_3 \cdot 3\text{H}_2\text{O}$  with  $\text{Na/Hg}$  in the presence of sterically demanding phosphines and  $\text{H}_2$  afforded the hydride complexes  $[(\text{R}_3\text{P})_2\text{RhH}_3]$  (**4**) ( $\text{R} = \text{Cy}, \text{Pr}$ ), which upon reaction with  $\text{N}_2$  gave the end-on coordinated dinitrogen/hydride complexes  $[(\text{R}_3\text{P})\text{RhH}(\text{N}_2)]$  (**5**) (Scheme 4) [22, 23]. The dinitrogen ligands in these compounds were weakly activated and could readily be released by gentle heating.

## 2.2 Group 8 Transition Metal Hydrides

The iron hydride complexes  $[\text{FeH}_2(\text{H}_2)(\text{PR}_3)_3]$  (**6**,  $\text{PR}_3 = \text{PEtPh}_2, \text{PBuPh}_2$ ), which were prepared by treating  $\text{FeCl}_2$  with  $\text{PR}_3$  and  $\text{NaBH}_4$  under an  $\text{H}_2$  atmosphere, could incorporate atmospheric nitrogen to give the end-on coordinated dinitrogen complexes  $[\text{FeH}_2(\text{N}_2)(\text{PR}_3)_3]$  (**7**) in an irreversible way (Scheme 5) [24–27]. Complex **7** released  $\text{N}_2$  when heated under vacuum or upon addition of  $\text{I}_2$ ,  $\text{HCl}$ , or  $\text{CO}$ .



**Scheme 5** Synthesis and dinitrogen coordination of the iron hydride complex **6**

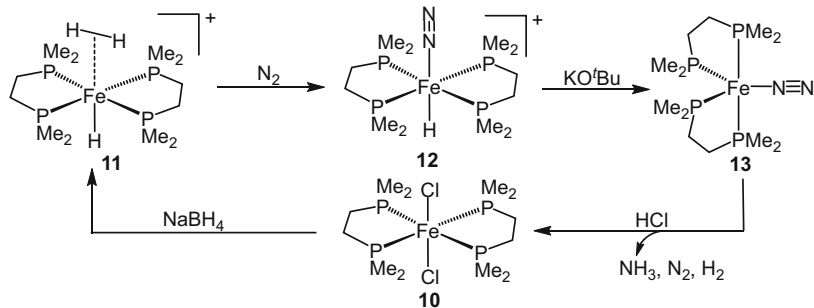


**Scheme 6** Synthesis and hydrogenation of the ruthenium dinitrogen complex **8**

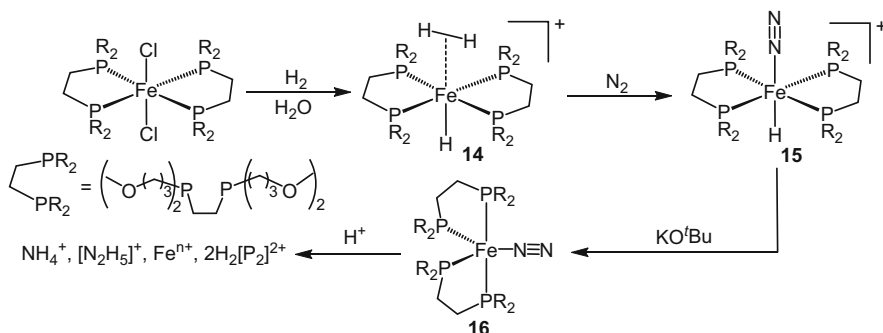
The ruthenium dinitrogen compound  $[\text{RuH}_2(\text{N}_2)(\text{PPh}_3)_3]$  (**8**) was obtained from the reaction of  $[\text{RuHCl}(\text{PPh}_3)_3]$  [**28**] with  $\text{AlEt}_3$  under an  $\text{N}_2$  atmosphere (Scheme 6) [29]. Treatment of **8** with  $\text{H}_2$  gave the corresponding dihydride/dihydrogen complex  $[\text{RuH}_2(\text{H}_2)(\text{PPh}_3)_3]$  (**9**). This conversion was readily reversed by exposing **9** to  $\text{N}_2$ . It is worth noting that the reactions of  $[\text{RuH}_2(\text{PPh}_3)_4]$  with  $\text{N}_2$  and  $\text{H}_2$  did not afford isolable **8** and **9** due to the presence of the dissociated free  $\text{PPh}_3$  ligand [30]. The ruthenium dinitrogen complexes bearing sterically demanding phosphines [31], [PNP] pincer ligand [32], and tris(pyrazolyl)borate ligand [33], were also synthesized from the corresponding hydrogen complexes with  $\text{N}_2$ .

The reaction of  $[\text{FeCl}_2(\text{dmpe})_2]$  (**10**) bearing the bidentate dmpe (bis(dimethylphosphino)ethane) ligand with sodium borohydride ( $\text{NaBH}_4$ ) afforded the hydride complex  $[\text{FeH}(\text{H}_2)(\text{dmpe})_2]^+$  (**11**) in high yield (Scheme 7) [34]. Complex **11** reacted with  $\text{N}_2$  to give an end-on coordinated dinitrogen complex  $[\text{FeH}(\text{N}_2)(\text{dmpe})_2]^+$  (**12**). Deprotonation of **12** by  $\text{KO}^t\text{Bu}$  provided an unstable iron (0) complex  $[\text{Fe}(\text{N}_2)(\text{dmpe})_2]$  (**13**). Treatment of **13** with  $\text{HCl}$  yielded ammonia (12%) and the chloride complex **10** (80%) with release of  $\text{N}_2$  and  $\text{H}_2$  [35–37]. The dichloride complex **10** could serve as a precursor to the hydride complex, and therefore, a synthetic cycle for the transformation of  $\text{N}_2$  to ammonia could be realized.

Hydrogenolysis of an iron chloride complex bearing the bidentate 1,2-bis(bis(methoxypropyl)phosphino)ethane ligands with  $\text{H}_2$  gave the corresponding hydride/dihydrogen complex **14** (Scheme 8) [38]. The  $\text{H}_2$  ligand in **14** could be substituted by  $\text{N}_2$ , quantitatively affording the dinitrogen complex **15**. The reaction with  $\text{KO}^t\text{Bu}$  yielded a neutral  $\text{Fe}(0)$  complex **16**. Protonation of **16** with triflic acid produced  $\text{NH}_4^+$  (15%) and trace  $\text{N}_2\text{H}_5^+$  (2%), but did not give a characterizable iron complex [39].



**Scheme 7** A synthetic cycle for transformation of dinitrogen to ammonia by the iron complexes 10–13

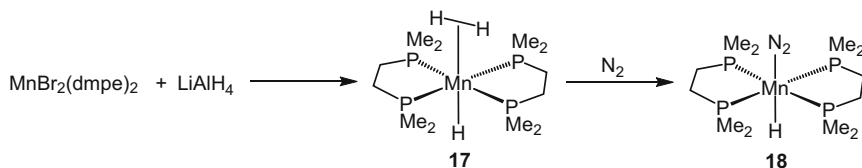


**Scheme 8** Dinitrogen activation by the iron hydride complex 14

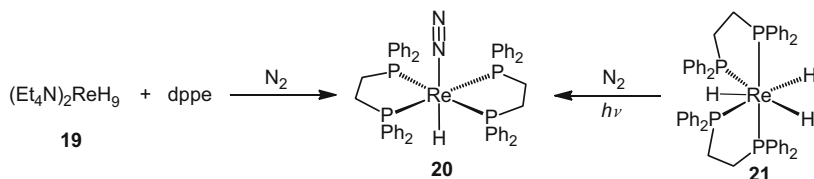
### 2.3 Group 7 Transition Metal Hydrides

Addition of  $\text{LiAlH}_4$  to a suspension of  $[\text{MnBr}_2(\text{dmpe})_2]$  followed by hydrolysis with water afforded the hydride complex  $[\text{MnH}(\text{H}_2)(\text{dmpe})_2]$  (**17**) (Scheme 9) [40]. Complex **17** readily reacted with  $\text{N}_2$  to give the corresponding end-on coordinated dinitrogen complex  $[\text{MnH}(\text{N}_2)(\text{dmpe})_2]$  (**18**) [41]. Half-sandwich manganese dihydride complex  $[(\text{C}_5\text{H}_5)\text{MnH}_2(\text{dfepe})]$  ( $\text{dfepe}$  = diperfluoroethylphosphinoethane) with  $\text{N}_2$  afforded a binuclear end-on coordinated dinitrogen complex  $[(\text{C}_5\text{H}_5)\text{Mn}(\text{dfepe})_2(\text{N}_2)]$  via the formation of a mononuclear dinitrogen complex  $[(\text{C}_5\text{H}_5)\text{Mn}(\text{N}_2)(\text{dfepe})]$  [42].

The rhenium dinitrogen complex  $[\text{ReH}(\text{N}_2)(\text{dmpe})_2]$  (**20**) was obtained from the reaction of the nonahydride complex  $[\text{NEt}_4][\text{ReH}_9]$  (**19**) [43] with  $\text{dppe}$  ( $\text{dppe}$  = 1,2-bis(diphenylphosphino)ethane) under an  $\text{N}_2$  atmosphere (Scheme 10) [44]. In contrast, the reactions of monodentate tertiary phosphines with **19** in an  $\text{N}_2$  atmosphere gave only the hydride complexes. The dinitrogen complex **20** was readily protonated at the metal center by  $\text{HBF}_4$  to form the cationic dihydro dinitrogen rhenium complex  $[\text{ReH}_2(\text{N}_2)(\text{dmpe})_2]\text{BF}_4$ , while protonation at the  $\text{N}_2$  ligand was not observed.



**Scheme 9** Synthesis of the manganese hydride complex **17** and its reaction with  $\text{N}_2$



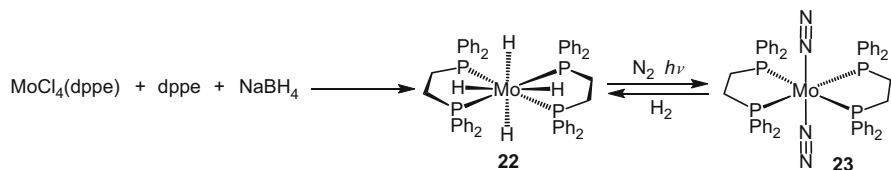
**Scheme 10** Synthesis of the rhenium dinitrogen complex **19** from the reactions of rhenium hydride complexes with  $\text{N}_2$

Synthesis of the dinitrogen complex **20** by photolysis of the trihydride complex  $[\text{ReH}_3(\text{dmpe})_2]$  (**21**) with UV light in an  $\text{N}_2$  atmosphere was also reported [45].

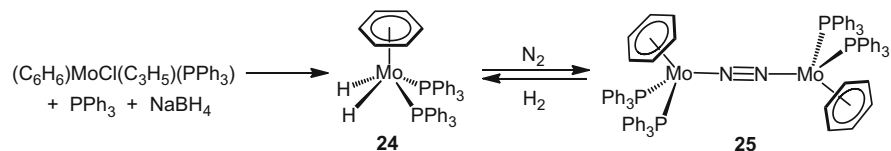
## 2.4 Group 6 Transition Metal Hydrides

The molybdenum and tungsten hydride complexes having bidentate phosphine ligands  $[\text{MH}_4(\text{dppe})_2]$  ( $\text{M} = \text{Mo}$  (**22**),  $\text{W}$ ) were obtained from the reactions of the chloride precursors  $[\text{MCl}_4(\text{dppe})]$  and excess of dppe ligand with  $\text{NaBH}_4$  [46, 47]. Photolysis of  $[\text{MoH}_4(\text{dppe})_2]$  (**22**) with UV light gave an end-on coordinated dinitrogen complex  $[\text{Mo}(\text{N}_2)_2(\text{dppe})_2]$  (**23**) in high yield (Scheme 11) [48], while irradiation of  $[\text{MH}_4(\text{dppe})_2]$  ( $\text{M} = \text{Mo}, \text{W}$ ) with  $\gamma$ -ray gave the dinitrogen complexes  $[\text{M}(\text{N}_2)_2(\text{dppe})_2]$  together with ammonia and hydrazine [49–51]. Hydrogenolysis of  $[\text{Mo}(\text{N}_2)_2(\text{dppe})_2]$  (**23**) with  $\text{H}_2$  regenerated the tetrahydride complex  $[\text{MoH}_4(\text{dppe})_2]$  (**22**) [52, 53]. The reaction of a  $\text{C}_6\text{H}_6$ -coordinated half-sandwich molybdenum dihydride complex  $[(\text{C}_6\text{H}_6)\text{MoH}_2(\text{PPh}_3)_2]$  (**24**) with  $\text{N}_2$  afforded a binuclear end-on coordinated dinitrogen complex  $[(\text{C}_6\text{H}_6)\text{Mo}(\text{PPh}_3)_2]_2(\text{N}_2)$  (**25**) in quantitative yield with release of  $\text{H}_2$  in a reversible fashion (Scheme 12) [54].

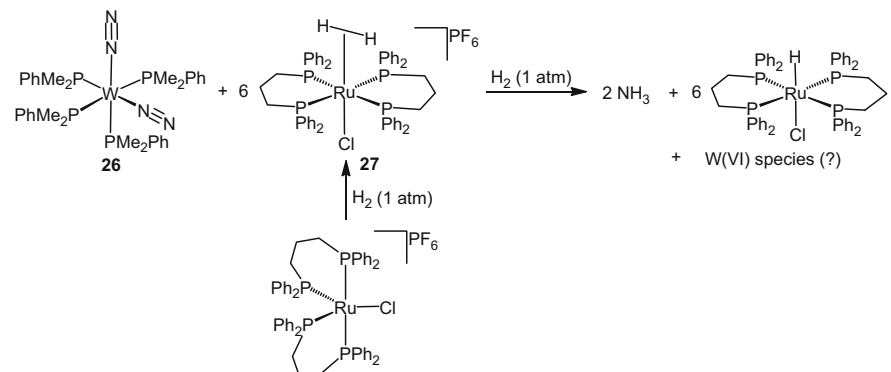
The reaction of the dinitrogen tungsten complex  $[\text{W}(\text{N}_2)_2(\text{PMe}_2\text{Ph})_4]$  (**26**) with the dihydrogen ruthenium complex  $[\text{RuCl}(\text{H}_2)(\text{dppp})_2]$  (**27**) in the presence of  $\text{H}_2$  generated  $\text{NH}_3$  (55%) (Scheme 13) [55]. In this reaction, one H atom of the  $\text{H}_2$  unit in **27** worked as a proton source, which protonated the coordinated  $\text{N}_2$  in **26** to form initially a hydrazido ( $\text{W}\equiv\text{N}-\text{NH}_2$ ) species, and the other H atom remained at the Ru atom as a hydride. Further protonation of the hydrazido units with **27** resulted in the formation of  $\text{NH}_3$ . Although the reaction allowed the formation of  $\text{NH}_3$  from  $\text{N}_2$  in



**Scheme 11** Synthesis of the molybdenum hydride complex **22** and its reaction with  $\text{N}_2$  under UV irradiation



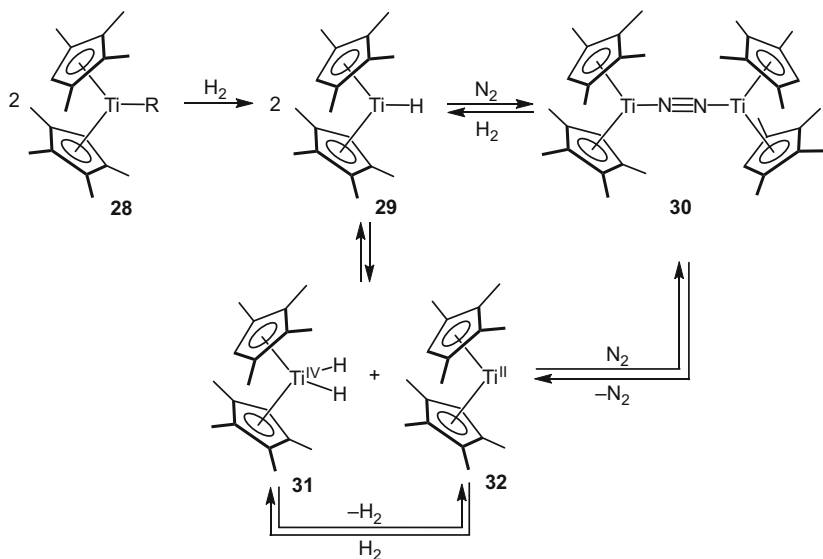
**Scheme 12** Formation of a binuclear molybdenum dinitrogen complex **25**



**Scheme 13** Formation of ammonia from the reaction of the tungsten dinitrogen complex **26** with the ruthenium dihydrogen complex **27**

the presence of  $\text{H}_2$ , the electrons required for the cleavage of  $\text{N}\equiv\text{N}$  bond were provided by the tungsten species.

As to group 5 transition metals, solid surface-supported tantalum hydrides were reported to cleave and hydrogenate  $\text{N}_2$  [56]. However, the activation of dinitrogen by a well-defined mononuclear group 5 transition metal hydride complex remained unknown.

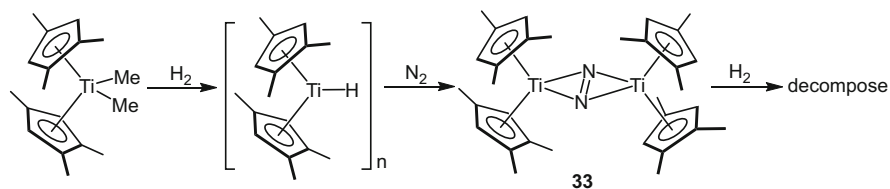


**Scheme 14** Synthesis of the titanocene hydride complex **29** and the formation of an end-on bound dinitrogen complex **30**

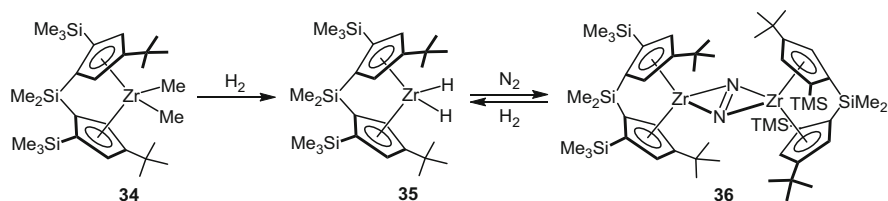
## 2.5 Group 4 Transition Metal Hydrides

The activation of dinitrogen by titanium metallocene hydride complexes bearing different cyclopentadienyl ligands was investigated [57–59]. Acid hydrolysis of a reaction mixture of  $(C_5H_5)_2TiCl_2$  and ethylmagnesium halide in the presence of  $N_2$  was reported to yield  $NH_3$  [59]. It was thought that a titanium hydride species was an active species for the reduction of  $N_2$  in this reaction, though no structural evidence was available. Hydrogenolysis of  $[(C_5Me_5)(C_5Me_4CH_2)TiCH_3]$  with  $H_2$ , followed by introduction of  $N_2$  (1 atm), afforded an end-on coordinated  $N_2$ -bridged complex  $[(C_5Me_5)_2Ti(\mu-N_2)Ti(C_5Me_5)_2]$  [60, 61]. This reaction was proposed to proceed through initial hydrogenolysis of the alkyl complex with  $H_2$  to a dihydride species  $[(C_5Me_5)_2TiH_2]$ , followed by releases of  $H_2$  and incorporation of  $N_2$  to the resulting titanocene species  $[(C_5Me_5)_2Ti]$ . Similarly, hydrogenolysis of the trivalent titanium complexes  $[(C_5Me_4H)_2TiR]$  (**28**) ( $R = Me, Ph$ ) with  $H_2$  followed by the reaction with  $N_2$  afforded the corresponding  $N_2$  complex  $[(C_5Me_4H)_2Ti(\mu-N_2)Ti(C_5Me_4H)_2]$  (**30**) via the hydride complex  $[(C_5Me_4H)_2TiH]$  (**29**) (Scheme 14) [62]. It was found that the Ti(III) metallocene hydride complex **29** could be disproportionated to the Ti(IV) dihydride **31** and the Ti(II) complex **32**. The dihydride **31** could lose  $H_2$  to give **32** in a reversible fashion. The Ti(II) metallocene **32** reacted with  $N_2$  to form the dinuclear titanium  $N_2$  complex **30**. The  $N_2$  ligand in **30** could be released under vacuum to give **32**.

Regarding the bonding mode of dinitrogen, the side-on ( $\eta^2, \eta^2$ ) bridging form is expected to enhance the reactivity of the dinitrogen ligand compared to the end-on



**Scheme 15** Formation of the side-on bound dinitrogen complex **33** from the reaction of a less sterically hindered titanocene hydride complex with  $N_2$



**Scheme 16** Reversible formation of the side-on bound dinitrogen complex **36** from the reaction of the *ansa*-zirconocene hydride complex **35** with  $N_2$

mode [63]. Metallocene complexes bearing less sterically demanding cyclopentadienyl ligands could provide a more sterically accessible and electron-poor metal center that potentially favors side-on  $\eta^2, \eta^2-N_2$  coordination [64]. Indeed, hydrogenolysis of the 1,2,4-trimethylcyclopentadienyl-ligated titanocene dimethyl complex  $[(C_5Me_3H_2)_2TiMe_2]$  with  $H_2$  followed by reaction with  $N_2$  afforded the side-on  $\eta^2, \eta^2-N_2$  complex  $[(C_5Me_3H_2)_2Ti]_2(\mu-\eta^2, \eta^2-N_2)$  (**33**) (Scheme 15) [65]. The reaction of the dinitrogen complex **33** with  $H_2$  (1 atm) did take place, but a characterizable product was not obtained.

The *ansa*-zirconocene dihydride complex **35**, which was formed by hydrogenolysis of the dialkyl precursor **34**, reacted with  $N_2$  reversibly to afford a side-on coordinated dinitrogen complex **36** (Scheme 16) [66]. In contrast, the zirconium metallocene dihydride complex bearing two  $C_5Me_5$  ligands  $[(C_5Me_5)_2ZrH_2]$  did not give an  $N_2$ -incorporated complex under similar conditions [67], suggesting that the *ansa* bridge structure of **35** should play an important role for the formation of the dinitrogen complex **36**.

### 3 Activation and Functionalization of Dinitrogen by Binuclear Transition Metal Hydride Complexes

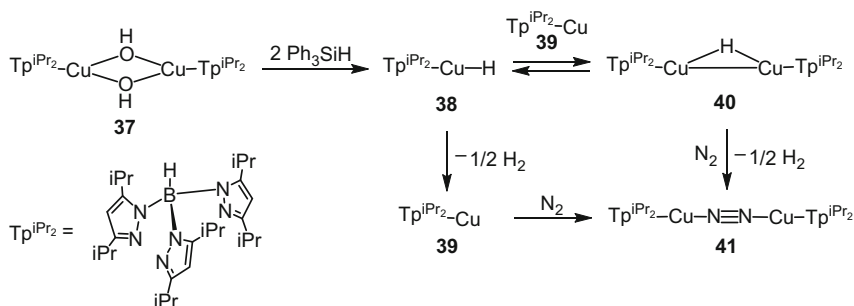
The reaction of a tris(pyrazolyl)borate ( $iPr_2Tp$ )-ligated binuclear copper hydroxide  $[iPr_2TpCu]_2(\mu-OH)_2$  (**37**) with triphenylsilane under an  $N_2$  atmosphere afforded an end-on bridged dinitrogen complex  $[iPr_2TpCu]_2(\mu-N_2)$  (**41**) (Scheme 17) [68]. A mixed valence Cu(I)/Cu(II) binuclear copper monohydride complex  $[iPr_2TpCu]_2(\mu-H)$

(**40**) was isolated as a key intermediate. Complex **40** could be formed via combination of the highly reactive terminal Cu(II) hydride species [ $^{\text{iPr}_2}\text{TpCu-H}$ ] (**38**), which was produced by reaction between  $\text{HSiPh}_3$  and the hydroxide **37**, with the unsaturated Cu(I) species [ $^{\text{iPr}_2}\text{TpCu}$ ] (**39**) generated by release of  $\text{H}_2$  from **38**. Under an  $\text{N}_2$  atmosphere, complex **40** changed to the dinitrogen complex **41** with release of  $\text{H}_2$ . Alternatively, the reaction of **39** with  $\text{N}_2$  could also afford **41**. The  $\text{N}_2$  ligand in **41** is quite labile, which could be replaced by  $^{15}\text{N}_2$ , MeCN, or  $\text{O}_2$ .

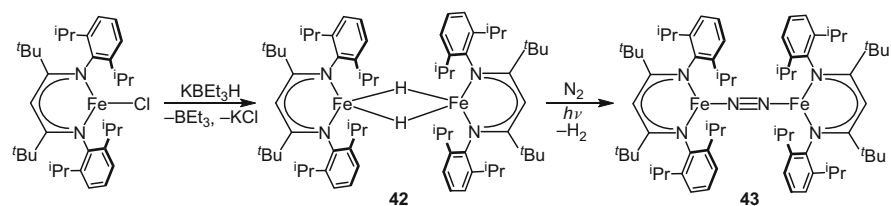
The reaction of the sterically hindered  $\beta$ -diketiminate ligated iron chloride complex with  $\text{KBET}_3\text{H}$  afforded the binuclear Fe(II) dihydride complex **42**, which upon UV irradiation under  $\text{N}_2$  resulted in loss of  $\text{H}_2$  and formation of the end-on dinitrogen complex **43** (Scheme 18) [69, 70].

The  $\beta$ -diketiminate-ligated cobalt and nickel hydride complexes **44** were obtained from the reaction of the chloride precursors with 1.0 equiv. of  $\text{KBET}_3\text{H}$  (Scheme 19) [71, 72]. When 2.0 equiv. of  $\text{KBET}_3\text{H}$  were used to react with the cobalt chloride complex, the potassium-bridged cobalt dihydride complex **45** was formed in high yield [71]. These binuclear dihydride complexes **44** and **45** readily reacted with  $\text{N}_2$  at room temperature to afford the end-on bridged dinitrogen complexes **46** and **47**, respectively (Scheme 19). Attempts to reduce the dinitrogen ligand in the nickel dinitrogen complex with  $\text{H}_2$  led to loss of  $\text{N}_2$  [73].

The reaction of the PNP-ligated zirconium chloride complex [ $\{\text{P}_2\text{N}_2\}\text{ZrCl}_2$ ] with  $\text{KC}_8$  under  $\text{N}_2$  yielded a side-on bound dinitrogen complex of zirconium, [ $\{\text{P}_2\text{N}_2\}\text{Zr}_2(\mu\text{-}\eta^2, \eta^2\text{-N}_2)$ ] (**48**) ( $\text{P}_2\text{N}_2 = \text{PhP}(\text{CH}_2\text{SiMe}_2\text{NSiMe}_2\text{CH}_2)_2\text{PPh}$ ) (Scheme 20) [74].

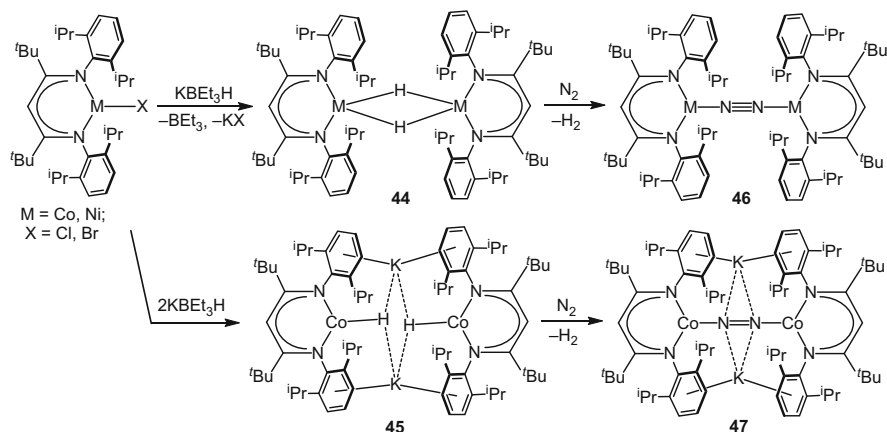


**Scheme 17** Formation of a binuclear copper dinitrogen complex **41**



**Scheme 18** Synthesis of the binuclear iron hydride complex **42** and its reaction with  $\text{N}_2$  to generate the end-on dinitrogen complex **43**



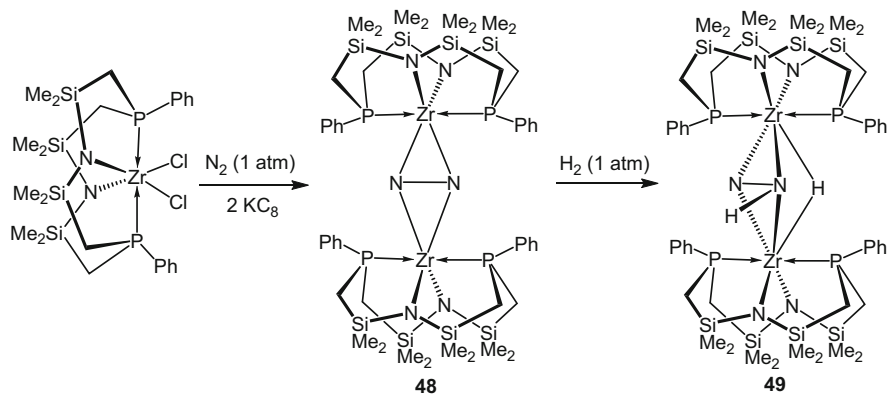


**Scheme 19** Synthesis of binuclear cobalt and nickel hydride complexes **44** and **45** and their reactions with  $\text{N}_2$  to generate the end-on dinitrogen complexes **46** and **47**

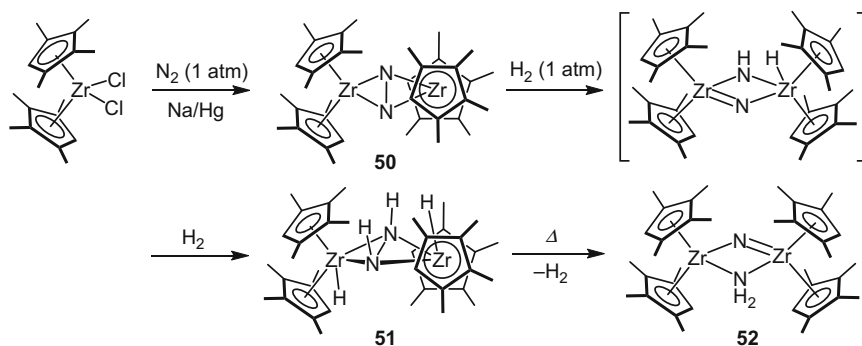
Hydrogenolysis of **48** with  $\text{H}_2$  afforded  $[(\text{P}_2\text{N}_2)\text{Zr}]_2(\mu\text{-}\eta^2, \eta^2\text{-N}_2\text{H})(\mu\text{-H})$  (**49**) containing both a bridging hydride and a bridging hydrazido unit through addition of one molecule of  $\text{H}_2$  across to a  $\text{Zr-N}$  bond. Theoretical studies suggested that addition of a second equivalent of  $\text{H}_2$  is feasible, but this reaction was not observed experimentally [75].

The analogous side-on bound dinitrogen metallocene complex  $[(\text{C}_5\text{M}_4\text{H})_2\text{Zr}]_2(\mu\text{-}\eta^2, \eta^2\text{-N}_2)$  (**50**), which was formed by the reaction of the chloride precursor  $[(\text{C}_5\text{M}_4\text{H})_2\text{ZrCl}_2]$  with  $\text{Na/Hg}$  under  $\text{N}_2$ , underwent the addition of 2 equiv. of  $\text{H}_2$  to furnish a dihydrido/diazenido complex  $[(\text{C}_5\text{M}_4\text{H})_2\text{ZrH}]_2(\mu\text{-}\eta^2, \eta^2\text{-N}_2\text{H}_2)$  (**51**) (Scheme 21) [64, 76, 77]. The reaction proceeded through a concerted, highly ordered transition state, in which the  $\text{H-H}$  bond is simultaneously cleaved with  $\text{Zr-H}$  and  $\text{N-H}$  bond formation. Thermolysis of the dihydrido/diazenido complex **51** caused  $\text{H}_2$  loss and  $\text{N-N}$  bond cleavage to give the nitrido/amido complex  $[(\text{C}_5\text{M}_4\text{H})_2\text{Zr}]_2(\mu\text{-N})(\mu\text{-NH}_2)$  (**52**). In this sequence of the reaction,  $\text{H}_2$  worked as both proton and electron sources. It is also worth noting that thermolysis of the dihydrido/diazenido complex under an  $\text{H}_2$  atmosphere yielded the dihydride complex  $[(\text{C}_5\text{M}_4\text{H})_2\text{ZrH}_2]$  with release of trace amount of ammonia [64].

A binuclear tantalum tetrahydride complex  $([\text{NPN}]\text{Ta})_2(\mu\text{-H})_4$  (**53**) ( $[\text{NPN}] = \text{PhP}(\text{CH}_2\text{SiMe}_2\text{NPh})_2$ ), which was obtained from hydrogenolysis of the trimethyl precursor  $[\text{NPN}]\text{TaMe}_3$ , reacted spontaneously with  $\text{N}_2$  to give a side-on, end-on bound dinitrogen complex  $([\text{NPN}]\text{Ta})_2(\mu\text{-}\eta^1, \eta^2\text{-N}_2)(\mu\text{-H})_2$  (**54**) with elimination of  $\text{H}_2$  (Scheme 22) [78, 79]. In this transformation,  $[\text{N}\equiv\text{N}]$  was formally reduced to  $[\text{N-N}]^{4-}$  by four electrons generated by the reductive elimination of one molecule of  $\text{H}_2$  and the oxidation state change of the two Ta ions from Ta(IV) to Ta(V). The unique side-on end-on coordination fashion of the bridging  $\text{N}_2$  resulted in substantial reactivity of the  $\text{N}_2$  fragment, leading to its cleavage and functionalization. While no apparent reaction of **54** with  $\text{H}_2$  was observed, complete cleavage of the  $\text{N-N}$  bond in **54** was achieved by



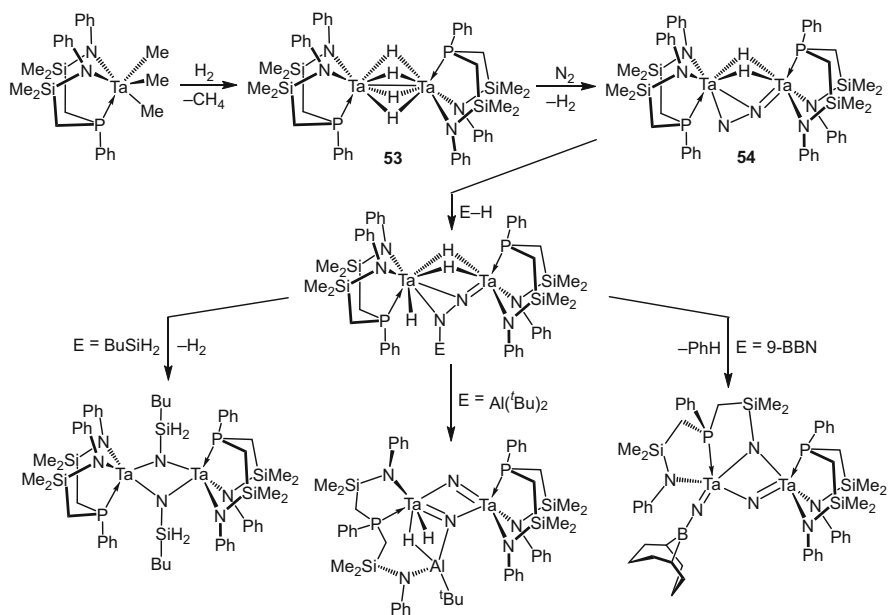
**Scheme 20** Hydrogenation of the binuclear zirconium dinitrogen complex **48** with  $\text{H}_2$



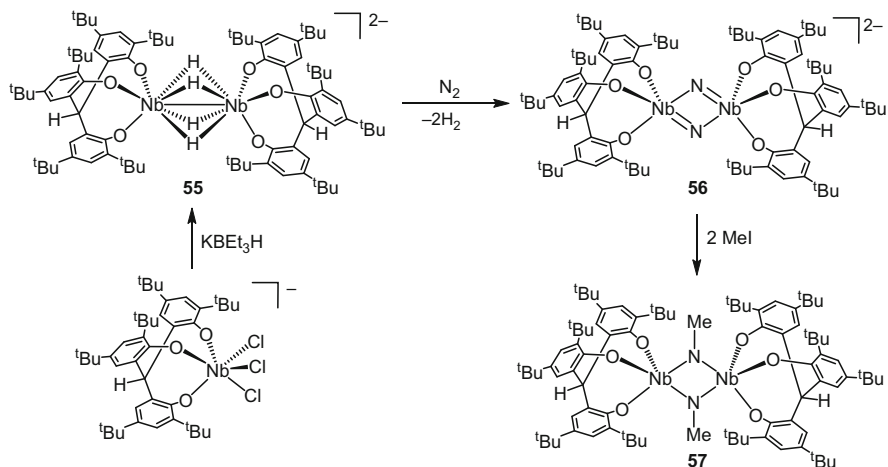
**Scheme 21** Cleavage and hydrogenation of the side-on bound dinitrogen ligand in complex **50** by  $\text{H}_2$

reaction with a variety of hydride reagents ( $\text{E-H} = \text{R}_2\text{BH}$ ,  $\text{R}_2\text{AlH}$ ,  $\text{RSiH}_3$ ) (Scheme 22) [80–82].

The anionic binuclear niobium tetrahydride complex **55** bearing triaryloxy ligands readily reacted with  $\text{N}_2$  (1 atm) to afford the dinitrido complex **56** via N–N bond cleavage without using external reducing agent (Scheme 23) [83, 84]. This process corresponds to an overall six-electron reduction of  $\text{N}_2$ , in which four electrons are provided by formation of two molecules of  $\text{H}_2$  from four hydride ligands and two electrons generated by oxidation of the metal–metal bond. The methylation of the nitride units in **56** by  $\text{MeI}$  proceeded in a stepwise fashion to give the bisimide complex **57** (Scheme 23). A reaction of **56** with  $\text{H}_2$  did not take place.



**Scheme 22** Reaction of a binuclear tantalum tetrahydride complex **53** with  $N_2$  to give a side-on, end-on dinitrogen complex **54** whose N–N bond could be cleaved upon reaction with hydride reagents

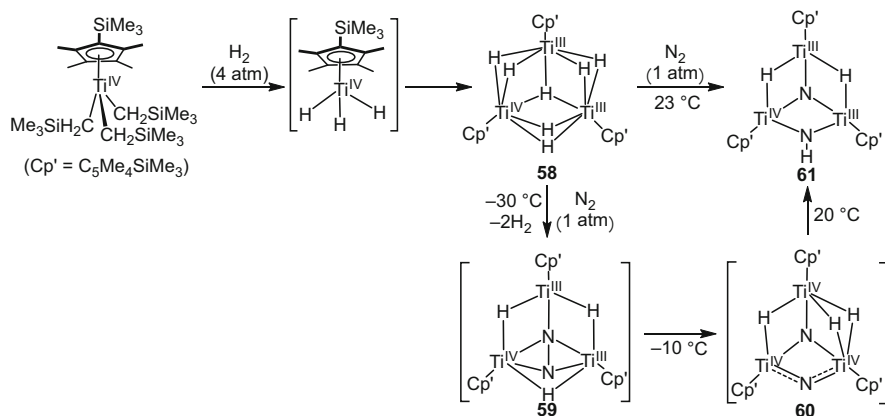


**Scheme 23** Dinitrogen cleavage by a binuclear niobium tetrahydride complex

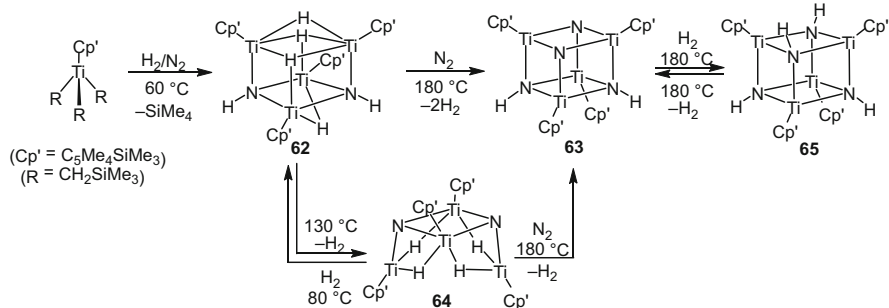
## 4 Activation and Functionalization of Dinitrogen by Tri- and Tetranuclear Transition Metal Hydride Complexes

Hydrogenolysis of the half-sandwich titanium trialkyl complex  $[\text{Cp}'\text{Ti}(\text{CH}_2\text{SiMe}_3)_3]$  ( $\text{Cp}' = \text{C}_5\text{Me}_4\text{SiMe}_3$ ) with  $\text{H}_2$  afforded the mixed valence Ti(III)/Ti(IV) heptahydride complex  $[(\text{Cp}'\text{Ti})_3(\mu_3\text{-H})(\mu\text{-H})_6]$  (**58**) (Scheme 24) [85, 86]. This hydride cluster readily reacted with atmospheric pressure of  $\text{N}_2$  at room temperature, giving an imido/nitrido complex  $[(\text{Cp}'\text{Ti})_3(\mu_3\text{-N})(\mu\text{-NH})(\mu\text{-H})_2]$  (**61**) via N–N bond cleavage and N–H bond formation without the need of extra reducing agent or proton source. Monitoring the reaction by  $^1\text{H}$  and  $^{15}\text{N}$  NMR revealed the initial formation of a dinitrogen complex  $[(\text{Cp}'\text{Ti})_3(\mu_3\text{-}\eta^1, \eta^2, \eta^2\text{-N}_2)(\mu\text{-H})_3]$  (**59**) with release of two molecules of  $\text{H}_2$ , followed by N–N bond cleavage to give a dinitrido ( $\text{N}^{3-}$ ) complex  $[(\text{Cp}'\text{Ti})_3(\mu_3\text{-N})(\mu\text{-N})(\mu\text{-H})_3]$  (**60**), and hydride migration from titanium to the  $\mu_2$ -nitrido unit to give the imido/nitrido complex **61**. The six electrons for the cleavage of the N–N bond were supplied by the reductive elimination of two molecules of  $\text{H}_2$  and the oxidation of two Ti(III) species to two Ti(IV) species. The proton ( $\text{H}^+$ ) for the formation of the N–H bond was generated by oxidation of a bridging hydride ( $\text{H}^-$ ) by two Ti(IV) species which were both reduced to Ti(III). Obviously, the hydride ligands in **58** served as the source of both electron and proton for the dinitrogen cleavage and hydrogenation, resembling in part the industrial Haber–Bosch process at the molecular level.

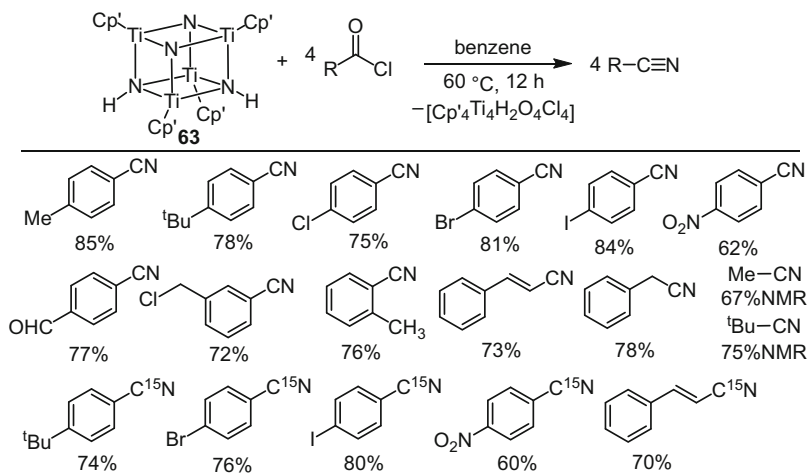
When the hydrogenolysis of the trialkyl titanium complex  $[\text{Cp}'\text{Ti}(\text{CH}_2\text{SiMe}_3)_3]$  with  $\text{H}_2$  was carried out in the presence of  $\text{N}_2$ , a tetranuclear diimido/tetrahydrido complex  $[(\text{Cp}'\text{Ti})_4(\mu_3\text{-NH})_2(\mu\text{-H})_4]$  (**62**), instead of the trinuclear heptahydride complex  $[(\text{Cp}'\text{Ti})_3(\mu_3\text{-H})(\mu\text{-H})_6]$  (**58**), was obtained in high yield (Scheme 25) [85]. The formation of **62** could also be achieved by hydrogenolysis of  $[\text{Cp}'\text{Ti}(\text{CH}_2\text{SiMe}_3)_3]$  in the presence of 1 equiv. of the trinuclear imido/nitrido complex **61**, suggesting that the hydrogenation of **61** with a mononuclear titanium hydride species such as “ $\text{Cp}'\text{TiH}_3$ ”



**Scheme 24** Dinitrogen cleavage and hydrogenation by a trinuclear titanium heptahydride complex **58**



**Scheme 25** Dinitrogen activation and hydrogenation by a tetranuclear titanium diimido/tetrahydrido complex **62**



**Scheme 26** Transformation to nitriles by reaction of **63** with acid chlorides

generated in situ by the hydrogenolysis of [Cp'Ti(CH<sub>2</sub>SiMe<sub>3</sub>)<sub>3</sub>] may take place. No apparent reaction between **61** and H<sub>2</sub> was observed at room or higher temperatures.

Complex **62** reacted with atmospheric pressure of N<sub>2</sub> at 180 °C to afford a mixed diimido/dinitrido complex [(Cp'Ti)<sub>4</sub>(μ<sub>3</sub>-N)<sub>2</sub>(μ<sub>3</sub>-NH)<sub>2</sub>] (**63**) with release of two molecules of H<sub>2</sub> (Scheme 25) [87]. When **62** was heated at 130 °C, one molecule of H<sub>2</sub> was released to give the dinitrido/tetrahydrido complex [(Cp'Ti)<sub>4</sub>(μ<sub>3</sub>-N)<sub>2</sub>(μ-H)<sub>4</sub>] (**64**). Exposure of **64** to H<sub>2</sub> (1 atm) at 80 °C regenerated **62** quantitatively, demonstrating that **62** and **64** are facily interconvertible through dehydrogenation and hydrogenation of the imido/nitrido ligands. When the dinitrido/tetrahydrido complex **64** was heated at 180 °C in the presence of N<sub>2</sub> (1 atm), the diimido/dinitrido complex **63** was formed quantitatively. The hydrogenation of **63** with H<sub>2</sub> to give the tetraimido complex [(Cp'Ti)<sub>4</sub>(μ<sub>3</sub>-NH)<sub>4</sub>] (**65**) took place in a reversible way at 180 °C (Scheme 25).

Remarkably, the imido and nitride species in **63** could be easily converted to nitriles through reaction with acid chlorides at 60 °C (Scheme 26) [87]. This

transformation did not require any extra reagents (either reducing agents or bases) and was compatible with functional groups such as aromatic C–X (X = Cl, Br, I) bonds, nitro group, aldehyde and chloromethyl moieties.  $^{15}\text{N}$ -isotope labeled nitriles could also be efficiently prepared by using the  $^{15}\text{N}$ -enriched analogue  $[(\text{Cp}^*\text{Ti})_4(\mu_3\text{-}^{15}\text{N})_2(\mu_3\text{-}^{15}\text{NH})_2]$  (**63- $^{15}\text{N}$** ) derived from  $^{15}\text{N}_2$  gas.

## 5 Concluding Remarks and Outlook

It is clear from the results described above that molecular transition metal hydride complexes can serve as a platform for dinitrogen activation. Mononuclear transition metal hydride complexes can bind  $\text{N}_2$  to form end-on dinitrogen complexes with loss of  $\text{H}_2$ . This process is generally reversible and N–N bond cleavage is difficult. Binuclear transition metal hydride complexes can show higher reactivity and induce N–N bond cleavage in some cases. A trinuclear titanium polyhydride complex has demonstrated even higher activity for the activation of dinitrogen, which enabled both N–N bond cleavage and N–H bond formation without the need of an external reducing agent or proton source. Obviously, the hydride ligands can serve as the source of both electron and proton for the reduction and hydrogenation of dinitrogen, and the cooperation of multiple metal hydride sites may play an important role in this process. A few functionalization reactions of the nitrogen species generated by the activation of dinitrogen with transition metal hydrides have been reported, among which the recent conversion of a tetranuclear titanium imido/nitrido complex to nitriles is particularly noteworthy. Despite recent progress in this area, the study on the activation and functionalization of dinitrogen by molecular transition metal hydrides, especially multimetallic polyhydride complexes, is still in infancy. The direct use of dinitrogen as a feedstock for organic synthesis remains a challenge.

## References

1. Luo YR (2007) Comprehensive handbook of chemical bond energies. CRC Press, Boca Raton, FL
2. Zhan CG, Nichols JA, Dixon DA (2003) Ionization potential, electron affinity, electronegativity, hardness, and electron excitation energy: molecular properties from density functional theory orbital energies. *J Phys Chem A* 107:4184–4195
3. Hoffman BM et al (2014) Mechanism of nitrogen fixation by nitrogenase: the next stage. *Chem Rev* 114:4041–4062
4. Hoffman BM et al (2013) Nitrogenase: a draft mechanism. *Acc Chem Res* 46:587–595
5. Lukoyanov D et al (2015) Identification of a key catalytic intermediate demonstrates that nitrogenase is activated by the reversible exchange of  $\text{N}_2$  for  $\text{H}_2$ . *J Am Chem Soc* 137:3610–3615
6. Yang ZY et al (2013) On reversible  $\text{H}_2$  loss upon  $\text{N}_2$  binding to FeMo-cofactor of nitrogenase. *Proc Natl Acad Sci U S A* 110:16327–16332

7. Ertl G (2008) Reactions at surfaces: from atoms to complexity (nobel lecture). *Angew Chem Int Ed Engl* 47:3524–3535
8. Honkala K et al (2005) Ammonia synthesis from first-principles calculations. *Science* 307:555–558
9. Ertl G (1980) Surface science and catalysis – studies on the mechanism of ammonia synthesis: the P.H. Emmett award address. *Catal Rev Sci Eng* 21:201–223
10. Rodriguez MM et al (2011) N<sub>2</sub> reduction and hydrogenation to ammonia by a molecular iron-potassium complex. *Science* 334:780–783
11. Logadóttir Á, Nørskov JK (2003) Ammonia synthesis over a Ru(0001) surface studied by density functional calculations. *J Catal* 220:273–779
12. Walter MD (2016) Recent advances in transition metal-catalyzed dinitrogen activation. *Adv Organomet Chem* 65:261–377
13. Yandulov DV, Schrock RR (2003) Catalytic reduction of dinitrogen to ammonia at a single molybdenum center. *Science* 301:76–78
14. Arashiba K, Miyake Y, Nishibayashi Y (2011) A molybdenum complex bearing PNP-type pincer ligands leads to the catalytic reduction of dinitrogen into ammonia. *Nat Chem* 3:120–125
15. Anderson JS, Rittle J, Peters JC (2013) Catalytic conversion of nitrogen to ammonia by an iron model complex. *Nature* 501:84–87
16. Ballmann J, Münhá RF, Fryzuk MD (2010) The hydride route to the preparation of dinitrogen complexes. *Chem Commun* 46:1013–1025
17. Allen AD, Senoff CV (1965) Nitrogenopentammineruthenium(II) complexes. *Chem Commun (London)* 621–622
18. Yamamoto A et al (1967) Study of the fixation of nitrogen. Isolation of tris(triphenylphosphine) cobalt complex co-ordinated with molecular nitrogen. *Chem Commun (London)* 79–80
19. Yamamoto A et al (1967) Reversible combination of molecular nitrogen with a cobalt complex. Exchange reactions of nitrogen–tris(triphenylphosphine)cobalt with hydrogen, ethylene, and ammonia. *J Am Chem Soc* 89:3071
20. Sacco A, Rossi M (1967) Hydride and nitrogen complexes of cobalt. *Chem Commun (London)* 316
21. Yamamoto A et al (1983) Preparation, X-ray molecular structure determination, and chemical properties of dinitrogen-coordinated cobalt complexes containing triphenylphosphine ligands and alkali metal or magnesium. Protonation of the coordinated dinitrogen to ammonia and hydrazine. *Organometallics* 2:1429–1436
22. Yoshida T et al (1979) Preparations and reactions of some hydridodinitrogen-trialkylphosphine complexes of rhodium(I). The structure of a dinitrogen-bridged rhodium(I) dimer, [RhH(P(i-Pr)<sub>3</sub>)<sub>2</sub>]<sub>2</sub>(μ-N<sub>2</sub>). *J Organomet Chem* 181:183–201
23. Yoshida T, Okano T, Otsuka S (1978) Novel three-co-ordinate rhodium(I) hydrido-compounds, [RhH(PBu<sup>t</sup>)<sub>3</sub>]<sub>2</sub> and [RhH{P(cyclohexyl)<sub>3</sub>}]<sub>2</sub>. *J Chem Soc Chem Commun* 855–856
24. Sacco A, Aresta M (1968) Nitrogen fixation: hydrido- and hydrido-nitrogen-complexes of iron(II). *Chem Commun (London)* 1223–1224
25. Aresta M et al (1971) Hydrido-complexes of iron(IV) and iron(II). *Inorg Chim Acta* 5:115–118
26. Aresta M et al (1971) Nitrogen fixation. II. Dinitrogen-complexes of iron. *Inorg Chim Acta* 5:203–206
27. Van Der Sluys LS et al (1990) An attractive “cis-effect” of hydride on neighbor ligands: experimental and theoretical studies on the structure and intramolecular rearrangements of Fe(H)<sub>2</sub>(η<sup>2</sup>-H<sub>2</sub>)(PEtPh<sub>2</sub>)<sub>3</sub>. *J Am Chem Soc* 112:4831–4841
28. Hallman PS, McGarvey BR, Wilkinson G (1968) The preparation and reactions of hydrido-chlorotris(triphenylphosphine)ruthenium(II) including homogeneous catalytic hydrogenation of alk-1-enes. *J Chem Soc A* 3143–3150
29. Knoth WH (1972) Dihydrido(dinitrogen)tris(triphenylphosphine)ruthenium. Dinitrogen bridging ruthenium and boron. *J Am Chem Soc* 94:104–109
30. Yamamoto A, Kitazume S, Ikeda S (1968) Triphenylphosphine complexes of ruthenium and rhodium. Reversible combinations of molecular nitrogen and hydrogen with the ruthenium complex. *J Am Chem Soc* 90:1089–1090

31. Abdur-Rashid K et al (2000) Synthesis and characterization of  $\text{RuH}_2(\text{H}_2)_2(\text{P}^i\text{Pr}_3)_2$  and related chemistry. Evidence for a bis(dihydrogen) structure. *Organometallics* 19:1652–1660
32. Prechtl MHG et al (2007) Synthesis and characterisation of nonclassical ruthenium hydride complexes containing chelating bidentate and tridentate phosphine ligands. *Chem A Eur J* 13:1539–1546
33. Tenorio MJ et al (1997) Hydride, dihydrogen, dinitrogen and related complexes of ruthenium containing the ligand hydrotris(pyrazolyl)borate. X-ray crystal structure of  $[\{\text{HB}(\text{pz})_3\}\text{Ru}(\eta^2\text{-H}_2)(\text{dippe})][\text{BPh}_4]$  (dippe = 1,2-bis(diisopropylphosphino)ethane). *Inorg Chim Acta* 259:77–84
34. Hills A et al (1990) Complexes of tertiary phosphines with iron(II) and dinitrogen, dihydrogen, and other small molecules. *J Organomet Chem* 391:C41–C44
35. Leigh GJ, Jimenez-Tenorio M (1991) Exchange of dinitrogen between iron and molybdenum centers and the reduction of dinitrogen bound to iron: implications for the chemistry of nitrogenases. *J Am Chem Soc* 113:5862–5863
36. Hills A et al (1993) Bis[1,2-bis(dimethylphosphino)ethane]dihydrogenhydridoiron(II) tetraphenylborate as a model for the function of nitrogenases. *J Chem Soc Dalton Trans* 3041–3049
37. Hall DA, Leigh GJ (1996) Reduction of dinitrogen bound at an iron(0) centre. *J Chem Soc Dalton Trans* 3539–3541
38. Gilbertson JD, Szymczak NK, Tyler DR (2004)  $\text{H}_2$  activation in aqueous solution: formation of *trans*- $[\text{Fe}(\text{DMeOPrPE})_2\text{H}(\text{H}_2)]^+$  via the heterolysis of  $\text{H}_2$  in water. *Inorg Chem* 43:3341–3343
39. Gilbertson JD, Szymczak NK, Tyler DR (2005) Reduction of  $\text{N}_2$  to ammonia and hydrazine utilizing  $\text{H}_2$  as the reductant. *J Am Chem Soc* 127:10184–10185
40. Girolami GS et al (1985) Alkyl, hydrido, and tetrahydroaluminato complexes of manganese with 1,2-bis(dimethylphosphino)ethane (dmpe). X-ray crystal structures of  $\text{Mn}_2(\mu\text{-C}_6\text{H}_{11})_2(\text{C}_6\text{H}_{11})_2(\mu\text{-dmpe})$ ,  $(\text{dmpe})_2\text{Mn}(\mu\text{-H})_2\text{AlH}(\mu\text{-H})_2\text{AlH}(\mu\text{-H})_2\text{Mn}(\text{dmpe})_2$ , and  $\text{Li}_4\{\text{MnH}(\text{C}_2\text{H}_4)[\text{CH}_2(\text{Me})\text{PCH}_2\text{CH}_2\text{PMe}_2]_2\}_2 \cdot 2\text{Et}_2\text{O}$ . *J Chem Soc Dalton Trans* 921–929
41. Perthuisot C, Fan M, Jones WD (1992) Catalytic thermal C–H activation with manganese complexes: evidence for  $\eta^2\text{-H}_2$  coordination in a neutral manganese complex and its role in C–H activation. *Organometallics* 11:3622–3629
42. Merwin RK et al (2004) Synthesis and characterization of  $\text{CpMn}(\text{dfepe})(\text{L})$  complexes (dfepe =  $(\text{C}_2\text{F}_5)_2\text{PCH}_2\text{CH}_2\text{P}(\text{C}_2\text{F}_5)_2$ ; L = CO,  $\text{H}_2$ ,  $\text{N}_2$ ): an unusual example of a dihydride to dihydrogen photochemical conversion. *Polyhedron* 23:2873–2878
43. Ginsberg AP (1968) Nine-co-ordinate octahydrido(tertiary phosphine)rhenate complex anions. *Chem Commun (London)* 857–858
44. Tully ME, Ginsberg AP (1973) *trans*-Hydridodinitrogenbis-[1,2-bis(diphenylphosphino)ethane]rhenium(I). *J Am Chem Soc* 95:2042–2044
45. Bradley MG, Roberts DA, Geoffrey GL (1981) Photogeneration of reactive  $[\text{ReH}(\text{diphos})_2]$ . Its reversible coordination of  $\text{CO}_2$  and activation of aromatic C–H bonds. *J Am Chem Soc* 103:379–384
46. Pennella F (1971) Tetrahydrido-complexes of molybdenum. *Chem Commun* 158
47. Bell B et al (1972) Group VI tetrahydrides and stereochemical non-rigidity. *J Chem Soc Chem Commun* 34–35
48. Pierantozzi R, Geoffrey GL (1980) Photoinduced elimination of  $\text{H}_2$  from  $[\text{MoH}_4(\text{diphos})_2]$  and  $[\text{MoH}_4(\text{PPh}_2\text{Me})_4]$ . *Inorg Chem* 19:1821–1822
49. Dzięgielewski JO, Grzybek R (1990) Application of the molybdenum(IV) hydride complexes in cyclohexane solutions to the radiation-catalytic reduction of molecular nitrogen. *Polyhedron* 9:645–651
50. Dzięgielewski JO, Małecki J, Grzybek R (1991) Radiation-catalytic reduction of molecular nitrogen with application of the tungsten(IV) hydride complexes. *Polyhedron* 10:1007–1012
51. Dzięgielewski JO, Małecki J (1991) The cyclic fixation and reduction of molecular nitrogen with  $[\text{WH}_4(\text{Ph}_2\text{PCH}_2\text{CH}_2\text{PPh}_2)_2]$  in  $\gamma$ -irradiated solutions. *Polyhedron* 10:2827–2832
52. Hidai M, Tominari K, Uchida Y (1972) Preparation and properties of dinitrogen–molybdenum complexes. *J Am Chem Soc* 94:110–114



53. Archer LJ, George TA (1979) Reactions of coordinated dinitrogen. 6. Displacement of coordinated dinitrogen by dihydrogen in low-valent molybdenum complexes. *Inorg Chem* 18:2079–2082
54. Green MLH, Silverthorn WE (1971) Arene molybdenum chemistry: some  $\pi$ -allyl, hydrido, and dinitrogen derivatives. *Chem Commun* 557–558
55. Nishibayashi Y, Iwai S, Hidai M (1998) Bimetallic system for nitrogen fixation: ruthenium-assisted protonation of coordinated  $N_2$  on tungsten with  $H_2$ . *Science* 279:540–542
56. Avenier P et al (2007) Dinitrogen dissociation on an isolated surface tantalum atom. *Science* 317:1056–1060
57. Vol'pin ME, Shur VB (1966) Nitrogen fixation by transition metal complexes. *Nature* 209:1236
58. Brintzinger H (1966) Formation of ammonia by insertion of molecular nitrogen into metal-hydride bonds. I. The formation of dimeric dicyclopentadienyltitanium(III) hydride as an intermediate in the Vol'pin-Shur nitrogen-fixing system. *J Am Chem Soc* 88:4305–4307
59. Brintzinger H (1966) Formation of ammonia by insertion of molecular nitrogen into metal-hydride bonds. II. Di- $\mu$ -imido-bis(dicyclopentadienyltitanium(III)) as a product of the reaction between di- $\mu$ -hydrido-bis(dicyclopentadienyltitanium(III)) and molecular nitrogen. *J Am Chem Soc* 88:4307–4308
60. Bercaw JE (1974) Bis(pentamethylcyclopentadienyl)titanium(II) and its complexes with molecular nitrogen. *J Am Chem Soc* 96:5087–5095
61. Sanner RD et al (1976) Structure and magnetism of  $\mu$ -dinitrogen-bis(bis(pentamethylcyclopentadienyl)titanium(II)),  $\{(\eta^5-C_5(CH_3)_5)_2Ti\}_2N_2$ . *J Am Chem Soc* 98:8358–8365
62. de Wolf JM et al (1996) Bis(tetramethylcyclopentadienyl)titanium chemistry. Molecular structures of  $[(C_5HMe_4)(\mu-\eta^1-\eta^5-C_5Me_4)Ti]_2$  and  $[(C_5HMe_4)_2Ti]_2N_2$ . *Organometallics* 15:4977–4983
63. MacLachlan EA, Fryzuk MD (2006) Synthesis and reactivity of side-on-bound dinitrogen metal complexes. *Organometallics* 25:1530–1543
64. Pool JA, Lobkovsky E, Chirik PJ (2004) Hydrogenation and cleavage of dinitrogen to ammonia with a zirconium complex. *Nature* 427:527–530
65. Hanna TE et al (2007) Bis(cyclopentadienyl) titanium dinitrogen chemistry: synthesis and characterization of a side-on bound haptomer. *Organometallics* 26:2431–2438
66. Chirik PJ, Henling LM, Bercaw JE (2001) Synthesis of singly and doubly bridged *ansa*-zirconocene hydrides. Formation of an unusual mixed valence trimeric hydride by reaction of  $H_2$  with  $\{(Me_2Si)_2(\eta^5-C_5H_3)_2\}Zr(CH_3)_2$  and generation of a dinitrogen complex by reaction of  $N_2$  with a zirconocene dihydride. *Organometallics* 20:534–544
67. Manriquez JM et al (1978) Reduction of carbon monoxide promoted by alkyl and hydride derivatives of permethylzirconocene. *J Am Chem Soc* 100:2716–2724
68. Zhang S et al (2016) A dinitrogen dicopper(I) complex via a mixed-valence dicopper hydride. *Angew Chem Int Ed Engl* 55:9927–9931
69. Smith JM et al (2006) Studies of low-coordinate iron dinitrogen complexes. *J Am Chem Soc* 128:756–769
70. Yu Y et al (2008) The reactivity patterns of low-coordinate iron-hydride complexes. *J Am Chem Soc* 130:6624–6638
71. Ding K, Brennessel WW, Holland PL (2009) Three-coordinate and four-coordinate cobalt hydride complexes that react with dinitrogen. *J Am Chem Soc* 131:10804–10805
72. Pfirrmann S et al (2009) A dinuclear nickel(I) dinitrogen complex and its reduction in single-electron steps. *Angew Chem Int Ed Engl* 48:3357–3361
73. Pfirrmann S et al (2009)  $\beta$ -Diketiminato nickel(I) complexes with very weak ligation allowing for  $H_2$  and  $N_2$  activation. *Organometallics* 28:6855–6860
74. Fryzuk MD et al (1997) Transformation of coordinated dinitrogen by reaction with dihydrogen and primary silanes. *Science* 275:1445–1447
75. Basch H, Musaev DG, Morokuma K (2000) Can the binuclear dinitrogen complex  $[P_2N_2]Zr(\mu-\eta^2-N_2)Zr[P_2N_2]$  activate more than one hydrogen molecule? A theoretical study. *Organometallics* 19:3393–3403
76. Pool JA, Bernskoetter WH, Chirik PJ (2004) On the origin of dinitrogen hydrogenation promoted by  $[(\eta^5-C_5Me_4H)_2Zr]_2(\mu_2-\eta^2, \eta^2-N_2)$ . *J Am Chem Soc* 126:14326–14327

77. Bernskoetter WH, Lobkovsky E, Chirik PJ (2005) Kinetics and mechanism of  $N_2$  hydrogenation in bis(cyclopentadienyl) zirconium complexes and dinitrogen functionalization by 1,2-addition of a saturated C–H bond. *J Am Chem Soc* 127:14051–14061
78. Fryzuk MD, Johnson SA, Retting SJ (1998) New mode of coordination for the dinitrogen ligand: a dinuclear tantalum complex with a bridging  $N_2$  unit that is both side-on and end-on. *J Am Chem Soc* 120:11024–11025
79. Fryzuk MD (2009) Side-on end-on bound dinitrogen: an activated bonding mode that facilitates functionalizing molecular nitrogen. *Acc Chem Res* 42:127–133
80. Fryzuk MD, MacKay BA, Patrick BO (2003) Hydrosilylation of a dinuclear tantalum dinitrogen complex: cleavage of  $N_2$  and functionalization of both nitrogen atoms. *J Am Chem Soc* 125:3234–3235
81. MacKay BA, Patrick BO, Fryzuk MD (2005) Hydroalumination of a dinuclear tantalum dinitrogen complex: N–N bond cleavage and ancillary ligand rearrangement. *Organometallics* 24:3836–3841
82. Fryzuk MD et al (2002) Hydroboration of coordinated dinitrogen: a new reaction for the  $N_2$  ligand that results in its functionalization and cleavage. *Angew Chem Int Ed Engl* 41:3709–3712
83. Akagi F, Matsuo T, Kawaguchi H (2007) Dinitrogen cleavage by a diniobium tetrahydride complex: formation of a nitride and its conversion into imide species. *Angew Chem Int Ed Engl* 46:8778–8781
84. Akagi F et al (2013) Reactions of a niobium nitride complex prepared from dinitrogen: synthesis of imide and ureate complexes and ammonia formation. *Eur J Inorg Chem* 3930–3936
85. Shima T et al (2013) Dinitrogen cleavage and hydrogenation by a trinuclear titanium polyhydride complex. *Science* 340:1549–1552
86. Hu S, Shima T, Hou Z (2014) Carbon–carbon bond cleavage and rearrangement of benzene by a trinuclear titanium hydride. *Nature* 512:413–415
87. Guru MM, Shima T, Hou Z (2016) Conversion of dinitrogen to nitriles at a multinuclear titanium framework. *Angew Chem Int Ed Engl* 55:12316–12320

# Reactivity of Group 5 Element Dinitrogen Complexes and N<sub>2</sub>-Derived Nitrides

Yutaka Ishida and Hiroyuki Kawaguchi

**Abstract** Progress in the development of dinitrogen activation by well-defined, molecular complexes of group 5 elements is reviewed. This chapter focuses on the reactivity of dinitrogen coordinated to group 5 metal centers. Functionalization of isolated, molecular group 5 metal nitride species derived from dinitrogen will also be mentioned.

**Keywords** Dinitrogen activation • Dinitrogen complexes • Group 5 elements • Niobium • Nitride • Nitrogen atom transfer • Tantalum • Transition metal complexes • Vanadium

## Contents

1	Introduction .....	46
2	Vanadium .....	46
2.1	Vanadium Dinitrogen Complexes .....	46
2.2	Vanadium Nitride Complexes Prepared from N <sub>2</sub> .....	50
3	Niobium and Tantalum .....	53
3.1	Niobium and Tantalum Dinitrogen Complexes .....	53
3.2	Niobium and Tantalum Dinitrogen Complexes Supported by Mixed Amide-Phosphine Ligands .....	56
3.3	Dinitrogen Cleavage by Niobium Aryloxy Complexes .....	62
3.4	Dinitrogen Cleavage and Nitrogen Atom Transfer Mediated by Niobium Tris(amide) Complexes .....	66
	References .....	67

---

Y. Ishida and H. Kawaguchi (✉)

Department of Chemistry, Tokyo Institute of Technology, Ookayama, Meguro-ku, Tokyo 152-8551, Japan

e-mail: [hkawa@chem.titech.ac.jp](mailto:hkawa@chem.titech.ac.jp)

## 1 Introduction

The research into the coordination chemistry of dinitrogen in group 5 metal compounds has been stimulated by Shilov's findings that the vanadium(II)-magnesium(II) hydroxide system or vanadium(II) compounds with oxygen-donor ligands such as catechol are efficient in conversion of dinitrogen into ammonia and hydrazine in protic solvents at high pH under mild conditions [1, 2]. Niobium(III) and tantalum(III) hydroxides are also found to undergo reduction of dinitrogen but be less efficient in nitrogen fixation than the vanadium-containing system [3]. Coupled with these findings, the role of vanadium in nitrogenase enzymes directed initial research efforts toward the development of vanadium species capable of binding and activating dinitrogen [5]. The scope of these investigations in this field has soon been extended to compounds of heavier group 5 metals, niobium and tantalum, which offers a unique opportunity to elucidate structure-reactivity correlations for nitrogen fixation and provides the possibility to discover new methods for transforming  $N_2$  into valuable materials.

The focus of this chapter is to give an overview of selected current results from the chemistry of well-defined, molecular, group 5 metal complexes relevant to fixation of dinitrogen. Our perspective on these complexes derives primarily from their potential as strong activators in dinitrogen chemistry. Therefore, we will pay particular attention on the reactivity of dinitrogen coordinated to group 5 metal centers, including reductive cleavage of dinitrogen by group 5 metal complexes. Functionalization of isolated, molecular group 5 metal nitride species derived from dinitrogen will also be mentioned. However, we do not intend to cover biomimetic models of nitrogenase, because this area has been reviewed elsewhere [5–7]. Furthermore, dinitrogen reduction by group 5 metal compounds in protic media [1–3, 8] and hydrogenation of  $N_2$  by silica supported tantalum hydrides [9, 10] will be excluded.

## 2 Vanadium

### 2.1 Vanadium Dinitrogen Complexes

The chemistry of vanadium dinitrogen complexes has received considerable attention due to the presence of vanadium as an essential element in synthetic and biological systems that can convert  $N_2$  into  $NH_3$  and/or  $N_2H_4$  [1, 4]. However, the development of well-defined, molecular vanadium complexes relevant to nitrogen fixation has been relatively slow, especially in comparison with neighboring titanium dinitrogen chemistry [11–13]. This might be mainly due to the absence of suitable precursors and the frequently occurring paramagnetism associated with vanadium analogues. Structurally characterized vanadium dinitrogen complexes are listed in Table 1. There is only one report of a fully characterized mononuclear

**Table 1** Structurally characterized vanadium dinitrogen complexes

Compound	N–N (Å)	$\nu(\text{NN})$ ( $\text{cm}^{-1}$ )	Ref.
<i>End-on terminal</i>			
[Na(thf)][(dppe) <sub>2</sub> V(N <sub>2</sub> ) <sub>2</sub> ] ( <b>1</b> )	1.130(16)	1790	[14–16]
<i>End-on bridging</i>			
[(Me <sub>3</sub> CCH <sub>2</sub> ) <sub>3</sub> V] <sub>2</sub> ( $\mu$ -N <sub>2</sub> ) ( <b>2</b> )	1.250(3)	850 ( $\nu(\text{V}=\text{N})$ )	[21]
[(Mes) <sub>3</sub> V] <sub>2</sub> ( $\mu$ -N <sub>2</sub> ) ( <b>3</b> )	1.222(4)		[22]
[K(digly) <sub>3</sub> ][{(Mes) <sub>3</sub> V} <sub>2</sub> ( $\mu$ -N <sub>2</sub> )] ( <b>4</b> )	1.222(4)		[22, 23]
[K(digly)(Mes) <sub>3</sub> V] <sub>2</sub> ( $\mu$ -N <sub>2</sub> ) ( <b>5</b> )	1.233(8)		[22]
[Na(digly) <sub>2</sub> ] <sub>2</sub> [(Mes) <sub>3</sub> V] <sub>2</sub> ( $\mu$ -N <sub>2</sub> ) ( <b>6</b> )	1.225(7)		[22]
[Na(digly) <sub>2</sub> ][Na{(Mes) <sub>3</sub> V} <sub>2</sub> ( $\mu$ -N <sub>2</sub> )] ( <b>7</b> )	1.271(8)		[22, 23]
[(2-Me <sub>2</sub> N-C <sub>6</sub> H <sub>4</sub> )(py)V] <sub>2</sub> ( $\mu$ -N <sub>2</sub> ) ( <b>8</b> )	1.228(4)		[24]
[Cp*{MeC(N <sup>i</sup> Pr) <sub>2</sub> }V] <sub>2</sub> ( $\mu$ -N <sub>2</sub> ) ( <b>10-V, Me</b> )	1.225(2)		[32]
[( <sup>t</sup> Bu <sub>2</sub> MeCO) <sub>3</sub> V] <sub>2</sub> ( $\mu$ -N <sub>2</sub> ) ( <b>11</b> )	1.232(3) 1.225(3)	775 ( $\nu(\text{V}=\text{N})$ )	[33]
[(Ar <sup>t</sup> BuN) <sub>3</sub> Mo]( $\mu$ -N <sub>2</sub> )[V{N <sup>t</sup> Bu(2-NMe <sub>2</sub> -5-Me-C <sub>6</sub> H <sub>3</sub> ) <sub>2</sub> }] <sub>2</sub> ( <b>12</b> ) (Ar = 3,5-Me <sub>2</sub> C <sub>6</sub> H <sub>3</sub> )	1.210(4)	1646	[36]
[[2,5-[(2-C <sub>4</sub> H <sub>3</sub> N)(C <sub>6</sub> H <sub>5</sub> ) <sub>2</sub> C] <sub>2</sub> (MeNC <sub>4</sub> H <sub>2</sub> )]V] <sub>2</sub> ( $\mu$ -N <sub>2</sub> ) ( <b>16</b> )	1.248(5)		[41]
[[{MeC(CH <sub>2</sub> N <sup>i</sup> Pr) <sub>3</sub> }V] <sub>2</sub> ( $\mu$ -N <sub>2</sub> )	1.257(6)		[43]
[[{PhC(NSiMe <sub>3</sub> ) <sub>2</sub> }V] <sub>2</sub> ( $\mu$ -N <sub>2</sub> )	1.235(6)		[44, 45]
[[ <sup>i</sup> Pr <sub>2</sub> N] <sub>3</sub> V] <sub>2</sub> ( $\mu$ -N <sub>2</sub> )	1.27(1)		[46]
[[2,6-(2,6- <sup>i</sup> Pr <sub>2</sub> -C <sub>6</sub> H <sub>3</sub> N=CPh) <sub>2</sub> C <sub>5</sub> H <sub>3</sub> N]V(thf)] <sub>2</sub> ( $\mu$ -N <sub>2</sub> )	1.232(3)		[47, 48]
[[2,6-(2,6- <sup>i</sup> Pr <sub>2</sub> -C <sub>6</sub> H <sub>3</sub> N=CMe) <sub>2</sub> C <sub>5</sub> H <sub>3</sub> N]V(THF)] <sub>2</sub> ( $\mu$ -N <sub>2</sub> )	1.259(6)		[49]
[[2,6-(2,6- <sup>i</sup> Pr <sub>2</sub> -C <sub>6</sub> H <sub>3</sub> NC=CH <sub>2</sub> ) <sub>2</sub> C <sub>5</sub> H <sub>3</sub> N]V(THF)] <sub>2</sub> ( $\mu$ -N <sub>2</sub> )	1.242(5)		[49]
[(C <sub>5</sub> H <sub>4</sub> CH <sub>2</sub> CH <sub>2</sub> NMe <sub>2</sub> )V(PhCCPh)(PMe <sub>3</sub> )] <sub>2</sub> ( $\mu$ -N <sub>2</sub> )	1.212(8)		[50]
[[{N(4-Me-2- <sup>i</sup> Pr <sub>2</sub> P-C <sub>6</sub> H <sub>3</sub> ) <sub>2</sub> }(X)V]( $\mu$ -N <sub>2</sub> ) X = CH <sup>t</sup> Bu	1.246(6)	1370	[51]
X = NC <sup>t</sup> Bu=CH <sup>t</sup> Bu	1.222(4)		[52]
[[N(CH <sub>2</sub> CH <sub>2</sub> NSiMe <sub>3</sub> ) <sub>3</sub> Mo( $\mu$ -N <sub>2</sub> )] <sub>3</sub> V(Cl)(thf)	1.217(7)	1579	[53]

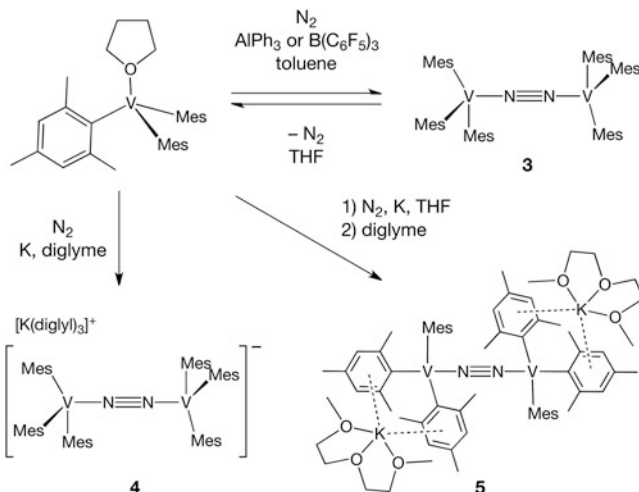
vanadium dinitrogen complex [Na(thf)][(dppe)<sub>2</sub>V(N<sub>2</sub>)<sub>2</sub>] (**1**), [14–16] whereas all other complexes are dinuclear with an end-on bridging N<sub>2</sub> ligand ( $\mu$ - $\eta^1$ : $\eta^1$ -N<sub>2</sub>).

Protonation of the coordinated N<sub>2</sub> has been intensively investigated due to its biological relevance. Products resulting from protonation vary depending on the nature of ligands and oxidation states of metal centers. The mononuclear complex **1** is isoelectronic to neutral molybdenum complexes generally formulated as [(P)<sub>4</sub>Mo(N<sub>2</sub>)<sub>2</sub>] (P is a phosphine ligand) [17–21], and these V and Mo complexes react similarly towards acids. Treatment of **1** with dry HBr results in conversion of 25% of the coordinated N<sub>2</sub> into NH<sub>3</sub> concomitant with a small amount of N<sub>2</sub>H<sub>4</sub>, where protonation may proceed via

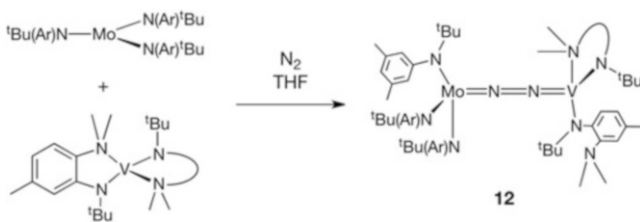
the intermediacy of a hydrazide and/or hydrazinyl complex [14, 15]. In the case of the N<sub>2</sub>-bridged neopentyl (Np) complex [(Np)<sub>3</sub>V]<sub>2</sub>(μ-N<sub>2</sub>) (**2**), protonation of the V–C bond instead of the coordinated N<sub>2</sub> takes place concurrent with quantitative release of N<sub>2</sub> [22]. The mesityl (Mes) analogue [(Mes)<sub>3</sub>V]<sub>2</sub>(μ-N<sub>2</sub>) (**3**) likewise loses N<sub>2</sub> upon protonation, whereas anionic [{(Mes)<sub>3</sub>V}<sub>2</sub>(μ-N<sub>2</sub>)]<sup>n-</sup> (*n* = 1, 2) (**4–7**) prefers to be protonated at the nitrogen atoms of the coordinated N<sub>2</sub> to generate a mixture of NH<sub>3</sub> and N<sub>2</sub>H<sub>4</sub> [23, 24]. This is mainly due to the increased charge density on the coordinated N<sub>2</sub> moiety in going from neutral **3** to anionic **4–7**. When the neutral complex [(2-Me<sub>2</sub>N-C<sub>6</sub>H<sub>4</sub>)(py)-V]<sub>2</sub>(μ-N<sub>2</sub>) (**8**) is protonated, formation of NH<sub>3</sub> and N<sub>2</sub> in a 1:2 ratio is observed [25, 26].

Following the seminal work on the molybdenum system capable of catalyzing conversion of N<sub>2</sub> to NH<sub>3</sub> [27], Schrock and coworkers reported that the sterically encumbering tris(amido)amine ligand scaffold [HIPTN<sub>3</sub>N]<sup>3-</sup> (HIPTN<sub>3</sub>N = (HIPTNCH<sub>2</sub>CH<sub>2</sub>)<sub>3</sub>N, HIPT = 3,5-(2,4,6-<sup>i</sup>Pr<sub>3</sub>C<sub>6</sub>H<sub>2</sub>)<sub>2</sub>C<sub>6</sub>H<sub>3</sub>) was utilized to assess the potential of vanadium species for catalytic reduction of N<sub>2</sub> to NH<sub>3</sub> [28]. A series of vanadium complexes relevant to a hypothetical pathway for dinitrogen reduction has been synthesized by using the THF adduct [(HIPTN<sub>3</sub>N)V(thf)] as a starting material, and these complexes include [{(HIPTN<sub>3</sub>N)V(N<sub>2</sub>)]K (ν(NN) = 1883 cm<sup>-1</sup>), [(HIPTN<sub>3</sub>N)V=NH], and [(HIPTN<sub>3</sub>N)V(NH<sub>3</sub>)]. However, unlike molybdenum complexes, no conversion of N<sub>2</sub> to NH<sub>3</sub> has been observed using these vanadium complexes under conditions described for the [(HIPTN<sub>3</sub>N)Mo] system. In comparison with the molybdenum congener, theoretical considerations suggest that the inability of the vanadium system to mediate reduction of N<sub>2</sub> to NH<sub>3</sub> is attributed to several factors including higher barriers to protonation, lower exergonic character of the N–N bond cleavage step, and the limitation of the NH<sub>3</sub>/N<sub>2</sub> exchange step via a dissociative mechanism [29].

Cummins and coworkers established that the Mo(III) trisamide complex is capable of splitting the triple bond of dinitrogen under mild conditions via an end-on N<sub>2</sub>-bridged dinuclear intermediate [30]. Based on this successful work and some diagonal V/Mo relationship, vanadium derivatives with a d<sup>3</sup> configuration are expected to cleave dinitrogen in a bimolecular fashion. However, there are the numerous examples of stable, end-on N<sub>2</sub>-bridged binuclear complexes with the requisite number of electrons required for N<sub>2</sub> scission. For instance, a d<sup>3</sup> V (II) complex [(nacnac)(ArO)V] (**9**) (nacnac = [ArNC(CH<sub>3</sub>)<sub>2</sub>CH, Ar = 2,6-<sup>i</sup>Pr<sub>2</sub>C<sub>6</sub>H<sub>3</sub>) reversibly binds N<sub>2</sub> to generate [(nacnac)(ArO)V]<sub>2</sub>(μ-N<sub>2</sub>), in which neither thermal nor photochemical N<sub>2</sub> cleavage can be realized [31]. Complex [Cp\*{MeC(N<sup>i</sup>Pr)<sub>2</sub>}V]<sub>2</sub>(μ-N<sub>2</sub>) (**10-V, Me**) is not observed to undergo N<sub>2</sub> cleavage, whereas the heavier group 5 congeners generate the nitride-bridged dinuclear complexes (vide infra) [32]. An alkoxide-supported N<sub>2</sub> complex [(<sup>t</sup>BuMeCO)<sub>3</sub>V]<sub>2</sub>(μ-N<sub>2</sub>) (**11**) does not react with reducing reagents such as Na/Hg, magnesium anthracene, and potassium graphite, resulting in recovery of **11** [33]. The mesityl complex [(Mes)<sub>3</sub>V(thf)] reversibly binds THF in the presence of AlPh<sub>3</sub> or B(C<sub>6</sub>F<sub>5</sub>)<sub>3</sub> under N<sub>2</sub> to produce [{(Mes)<sub>3</sub>V}<sub>2</sub>(μ-N<sub>2</sub>)] (**3**), which can be further reduced with Na or K to generate a series of anionic species [{(Mes)<sub>3</sub>V}<sub>2</sub>(μ-N<sub>2</sub>)]<sup>n-</sup> (*n* = 1, 2) (**4–7**) (Scheme 1) [23]. Regardless of the (V/alkali metal) stoichiometry, the degree of N<sub>2</sub> reduction in



**Scheme 1** Synthesis of vanadium mesityl dinitrogen complexes



**Scheme 2** Synthesis of the molybdenum-vanadium dinuclear complex

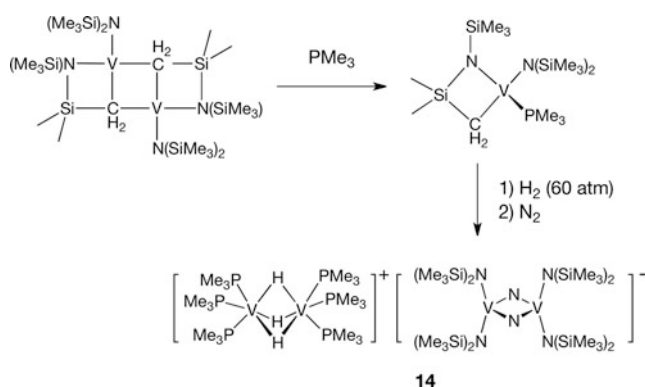
the V<sub>2</sub>(μ-N<sub>2</sub>) unit and the ion-separated/ion-pare structure are found to depend on the nature of the solvent used. The dianionic complexes [ {(Mes)<sub>3</sub>V}<sub>2</sub>(μ-N<sub>2</sub>) ]<sup>2-</sup> with the V(II)–N–N–V(II) skeleton are stable towards N<sub>2</sub> scission. This behavior is in contrast to the d<sup>3</sup> molybdenum(III) analogue, which undergoes N<sub>2</sub> cleavage upon photolysis [34]. Treatment of a mixture of Mo(III) and V(II) precursors in THF under N<sub>2</sub> furnishes a heterodinuclear complex [ {<sup>t</sup>Bu(Ar)N<sub>3</sub>Mo}(μ-N<sub>2</sub>)[V{<sup>t</sup>Bu(2-NMe<sub>2</sub>-5-Me-C<sub>6</sub>H<sub>3</sub>)<sub>2</sub>}]<sub>2</sub> (**12**, Ar = 3,5-Me<sub>2</sub>-C<sub>6</sub>H<sub>3</sub>) (Scheme 2) [35]. Complex **12** liberates N<sub>2</sub> upon thermolysis or photolysis, and further reduction of **12** with KC<sub>8</sub> results in formation of K[(N<sub>2</sub>)Mo(N<sup>t</sup>BuAr)<sub>3</sub>] and the starting V(II) complex. This contrasts with the observation of N–N bond cleavage in the heterodinuclear Mo(μ-N<sub>2</sub>)Nb system (vide infra).

## 2.2 Vanadium Nitride Complexes Prepared from $N_2$

One approach toward achieving conversion of dinitrogen into valuable materials is six-electron reductive  $N_2$  cleavage followed by functionalization of the resulting metal nitride species. One of the simplest systems is reduction of  $VCl_3(thf)_3$  with Mg under  $N_2$ , which produces a black material formulated as  $[VNMg_2Cl_2(thf)]$  (**13**) according to stoichiometry [36]. Compound **13** is diamagnetic, soluble in benzene, and very sensitive to air. The structure of **13** remains unclear, but the nitride group is speculated to bridge between the vanadium and magnesium metal centers. Upon hydrolysis of **13**, formation of 1 mol of  $NH_3$  per vanadium is observed. The reaction of **13** with benzyl chloride gives a mixture of  $[VNMgCl_{1.5}(thf)]$ ,  $MgCl_2(thf)_2$ , and dibenzyl, in which no N–C bond formation is observed. Treatment of **13** with  $CO_2$  results in N–C bond formation and deoxygenation, yielding a cyanate compound  $[VO(NCO)Mg_2Cl_2(thf)_3]$ . The titanium compound analogous to **13** can be prepared in the similar manner, and its reactivity has been intensively studied as a nitrogen source for organic syntheses [37].

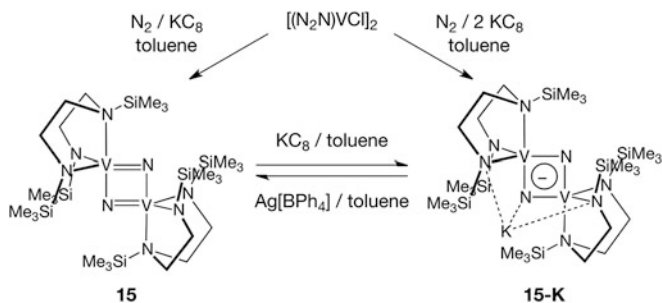
An amide-stabilized mononuclear vanadacyclobutane  $[(Me_3Si)_2N]V\{(CH_2SiMe_2)N(SiMe_3)\}(PMe_3)$  reacts with  $H_2$  (60 atm) to produce  $[(Me_3P)_3V]_2(\mu-H)_3-[(Me_3Si)_2N]_2V_2(\mu-N)_2$  (**14**), which is composed of a hydride-bridged divanadium cation and a nitride-bridged divanadium anion (Scheme 3) [38]. Attempts to prepare **14** following the same procedure under exclusion of  $N_2$  have failed to isolate any tractable material, and the possibility of hydrogenolysis of the N–Si bond is ruled out due to detecting no formation of methane and silanes. These findings suggest that the bridging nitride groups arise from the cleavage of  $N_2$ . During the reaction, the electrons required for the  $N\equiv N$  triple bond scission are partially provided by added  $H_2$  molecules.

The Cloke group demonstrated that reduction of a V(III) precursor  $[(N_2N)VCl]_2$  ( $[N_2N] = (Me_3SiNCH_2CH_2)_2NSiMe_3$ ) with one equivalent of  $KC_8$  (V:K = 1:1) under

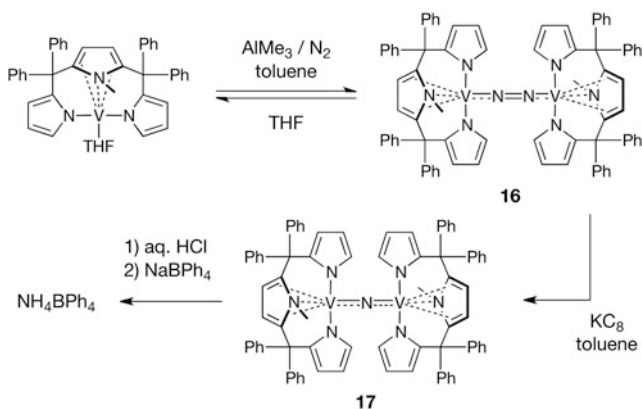


**Scheme 3** Synthesis of the vanadium nitride complex





**Scheme 4** Vanadium nitride complexes derived from N<sub>2</sub> cleavage



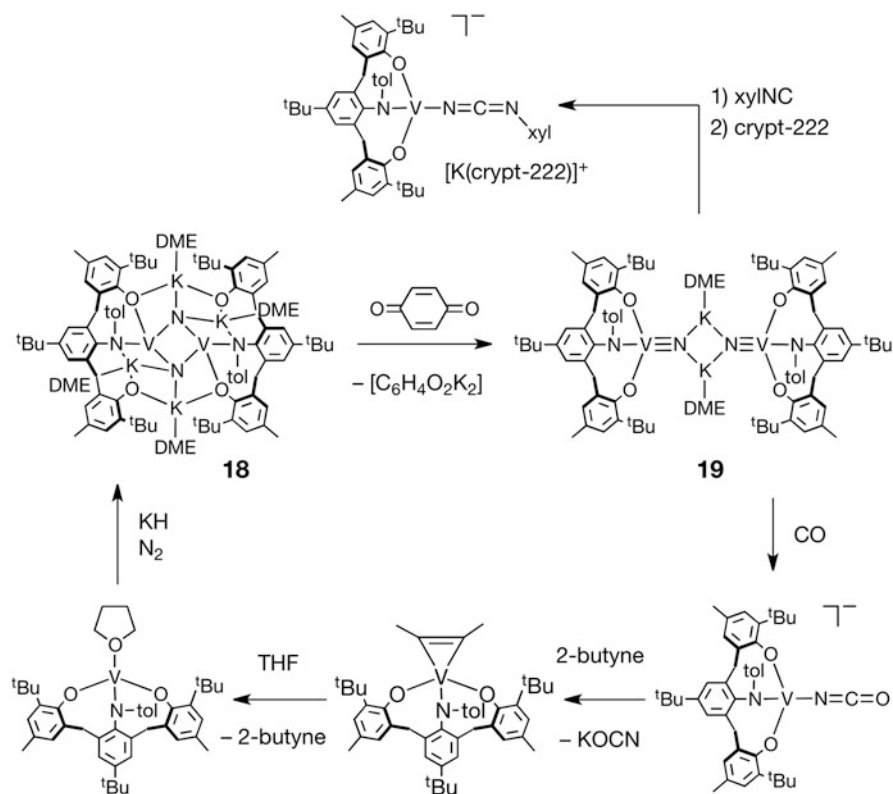
**Scheme 5** N<sub>2</sub> activation by the vanadium complex bearing the tripyrrole ligand

N<sub>2</sub> leads to a mixture of doubly nitride-bridged dimers, [(N<sub>2</sub>N)V]<sub>2</sub>(μ-N)<sub>2</sub> (**15**) and [K{(N<sub>2</sub>N)V}(μ-N)<sub>2</sub>] (**15-K**) (Scheme 4) [39]. Formation of a mixture of **15** and **15-K** is due to the fact that **15** reacts with the available reducing agent faster than does [(N<sub>2</sub>N)VCl]<sub>2</sub>. Increasing the amount of added KC<sub>8</sub> to 2 equivalents (V:K = 1:2) results in isolation of only **15-K**, and oxidation of **15-K** with Ag[BPh<sub>4</sub>] generates **15**. The experiment using a mixture of <sup>14</sup>N<sub>2</sub> and <sup>15</sup>N<sub>2</sub> unambiguously confirmed that both bridging nitride atoms in **15** originate from the same N<sub>2</sub> molecule [40]. With the assumption of a transient V(II) species [(N<sub>2</sub>N)V] as an initial complex upon reduction, computational studies suggest that this V(II) intermediate binds N<sub>2</sub> in a side-on fashion [40]. Further reaction with a second molecule of [(N<sub>2</sub>N)V] would result in the N–N bond cleavage, yielding the final product **15**.

A tripyrrole ligand containing one N-methylated pyrrolyl ring [MeTP]<sup>2-</sup> (H<sub>2</sub>[MeTP] = 2,5-[(2-pyrrolyl)(C<sub>6</sub>H<sub>5</sub>)<sub>2</sub>C]<sub>2</sub>(MeNC<sub>4</sub>H<sub>2</sub>)) can support a V(II) complex [(MeTP)V(thf)], which reversibly loses THF to AlMe<sub>3</sub> under N<sub>2</sub> to form [(MeTP)V]<sub>2</sub>(μ-N<sub>2</sub>) (**16**) (Scheme 5) [41]. Further reduction of **16** with KC<sub>8</sub>

provides a nitride-bridged, mixed-valence V(III)/V(IV) dimer  $[(\text{MeTP})\text{V}_2](\mu\text{-N})$  (**17**) in moderate yield. Treatment of **17** with aqueous HCl followed by addition of  $\text{NaBPh}_4$  results in isolation of  $\text{NH}_4\text{BPh}_4$ , while the  $[(\text{MeTP})\text{V}]$  moiety is completely hydrolyzed and not recovered.

A bis( $\mu$ -nitride) divanadium(IV) complex supported by the  $[\text{ONO}]^{3-}$  ligand ( $[\text{ONO}]^{3-} = 2,6\text{-}(3\text{-}^t\text{Bu}\text{-}5\text{-Me}\text{-}2\text{-OC}_6\text{H}_2\text{CH}_2)_2\text{-}4\text{-}^t\text{Bu}\text{-}(p\text{-tolyl})\text{NC}_6\text{H}_4$ ) can be prepared by reduction of  $[(\text{ONO})\text{V}(\text{thf})]$  with KH under  $\text{N}_2$  (Scheme 6) [42]. This nitride complex  $\{[(\text{ONO})\text{V}]_2(\mu\text{-N})_2\{\text{K}(\text{dme})\}_4\}$  (**18**) is oxidized by *p*-benzoquinone, yielding a V(V) nitride  $\{[(\text{ONO})\text{VN}]_2\{\text{K}(\text{dme})\}_2\}$  (**19**). The reactions of **19** with CO and xyllyl isocyanide (xylINC) afford isocyanate and carbodiimide complexes, in which the metal center is reduced from V(V) to V(III). The isocyanate complex liberates KOCN upon addition of 2-butyne to give an alkyne complex, which can be recycled back to the starting complex  $[(\text{ONO})\text{V}(\text{thf})]$ . These results establish a synthetic cycle for production of cyanate from  $\text{N}_2$  and CO, which proceeds under relatively mild conditions.



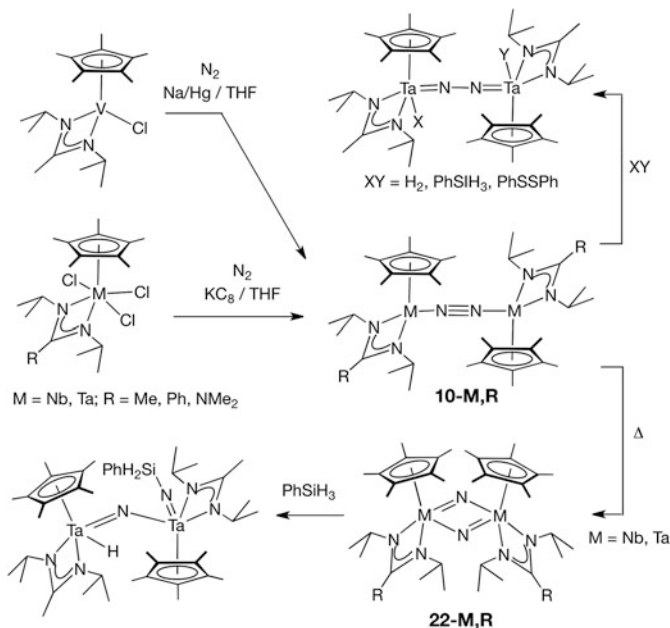
**Scheme 6** Assembly of  $\text{N}_2$  and CO into  $\text{OCN}^-$  by vanadium  $[\text{ONO}]$ -supported complexes

### 3 Niobium and Tantalum

#### 3.1 Niobium and Tantalum Dinitrogen Complexes

Structurally characterized dinitrogen complexes of niobium and tantalum are listed in Tables 2 and 3, respectively. Compared to vanadium, the congeners of the heavier group 5 elements, niobium and tantalum, are known to contain more strongly activated N<sub>2</sub> ligands and generate more robust M–N–N–M linkages. For example, ligand replacement reactions using [(MCl<sub>3</sub>)(thf)<sub>2</sub>]<sub>2</sub>(μ-N<sub>2</sub>) (M = Nb, Ta) as starting complexes generate a series of binuclear Nb and Ta complexes with retention of the M–N–N–M framework [54, 55]. Studies on protonation of [M(S<sub>2</sub>CNEt<sub>2</sub>)<sub>3</sub>]<sub>2</sub>(μ-N<sub>2</sub>) (**20-M**, M = Nb, Ta) with an excess of anhydrous HX (X = Cl, Br) have revealed that the reaction proceeds in a stepwise manner to produce an NHNH<sub>2</sub>-bridged dinuclear intermediate, which subsequently undergoes fragmentation via M–N bond cleavage and further protonation, resulting in a stoichiometric amount of [M(S<sub>2</sub>CNEt<sub>2</sub>)<sub>3</sub>X<sub>2</sub>] and hydrazine [21, 54, 56, 57].

The Sita group reported that a series of paramagnetic, μ-η<sup>1</sup>:η<sup>1</sup>-N<sub>2</sub> complexes of group 5 elements [Cp\*{RC(N<sup>i</sup>Pr)<sub>2</sub>}M]<sub>2</sub>(μ-N<sub>2</sub>) (**10-M,R**; M = V, R = Me; M = Nb, R = Me, Ph; M = Ta, R = Me, Ph, NMe<sub>2</sub>) are prepared by treating Cp\*{RC(N<sup>i</sup>Pr)<sub>2</sub>}MCl<sub>2</sub> (M = Nb, Ta) or Cp\*{MeC(N<sup>i</sup>Pr)<sub>2</sub>}VCl with KC<sub>8</sub> or 0.5% Na/Hg under N<sub>2</sub> (Scheme 7) [32]. The tantalum and niobium complexes contain more strongly



**Scheme 7** Synthesis of group 5 element N<sub>2</sub> complexes supported by the Cp-amidinate ligand systems

**Table 2** Structurally characterized niobium dinitrogen complexes

Compound	N–N (Å)	$\nu(\text{NN})$ ( $\text{cm}^{-1}$ )	Ref.
<i>End-on bridging</i>			
$[(\text{Et}_2\text{NCS}_2)_3\text{Nb}]_2(\mu\text{-N}_2)$	1.252(16)		[53]
$[\text{Cp}^*\{\text{PhC}(\text{N}^i\text{Pr})_2\}\text{Nb}]_2(\mu\text{-N}_2)$ ( <b>10-Nb,Ph</b> )	1.300(3)		[61]
$[(\text{P}_2\text{N}_2)\text{Nb}]_2(\mu\text{-N}_2)$ ( <b>23</b> )	1.272(5)		[64]
$[(\text{NPN})(\text{Cl})\text{Nb}]_2(\mu\text{-N}_2)$ ( <b>26</b> )	1.237(4)		[65]
$[(\text{PNP})(\text{Cl})_2\text{Nb}]_2(\mu\text{-N}_2)$ ( <b>27</b> )	1.277(6)		[79, 80]
$[\text{Na}(\text{digly})_2]_2[\{(\text{calix})\text{Nb}\}_2(\mu\text{-N}_2)]$ ( <b>38</b> )	1.390(17)	1372	[87]
$[\{(\text{Ar}^t\text{BuN})_3\text{Mo}\}(\mu\text{-N}_2)[\text{Nb}\{\text{N}^i\text{Pr}(\text{Ar})\}_3]$	1.235(10)	1583	[89]
$[(\text{Cy}_2\text{N})_3\text{Nb}]_2(\mu\text{-N}_2)$	1.34(1)		[90]
$[(^t\text{Bu}_3\text{SiO})_3\text{Nb}]_2(\mu\text{-N}_2)$	1.310(4)		[91]
$[(\text{PhMe}_2\text{P})_4(\text{Cl})\text{W}]_2(\mu\text{-N}_2)[\text{Nb}(\text{Cl})_3\text{Cp}]$	1.254(9)	1395	[92]
$[(\text{P}_2\text{N}_2)\text{MeNb}]_2(\mu\text{-N}_2)$	1.280(7)		
<i>Side-on bridging</i>			
$[\{(\text{calix})\text{Nb}\}_2(\mu\text{-}\eta^2\text{:}\eta^2\text{-N}_2)\text{Na}_4(\text{dme})_5]$ ( <b>40</b> )	1.402(8)		[80]
$[\{(\text{calix})\text{Nb}\}_2(\text{O})(\mu\text{-}\eta^2\text{:}\eta^2\text{-N}_2)\text{Na}_4(\text{dme})_4]$	1.424(5)		[53]

activated  $\text{N}_2$  ligands than the vanadium analogue as evidenced by N–N bond distances. Each metal center in these  $\text{N}_2$  dinuclear complexes is formally  $d^2$  for V and  $d^1$  for niobium and tantalum. The tantalum complex **10-Ta,Me** undergoes 1,4-addition of  $\text{H}_2$ ,  $\text{PhSiH}_3$ , and  $\text{PhSSPh}$  across the Ta– $\text{N}_2$ –Ta linkage to form the dihydride, silyl-hydride, and dithiolate complexes  $[\text{Cp}^*\{\text{RC}(\text{N}^i\text{Pr})_2\}_2\text{Ta}_2(\text{X})(\text{Y})](\mu\text{-N}_2)$  (X, X = H, H; H,  $\text{SiH}_2\text{Ph}$ ; SPh, SPh), respectively, along with oxidation of Ta(IV) to Ta(V). During all these reactions, the dinuclear structure is retained without affecting the end-on-bridging  $\text{N}_2$  moiety [58, 59]. In contrast, when **10-Ta,R** is oxidized with  $\text{N}_2\text{O}$ , the  $\text{N}_2$  coordination mode changes from  $\mu\text{-}\eta^1\text{:}\eta^1$  (end-on) to  $\mu\text{-}\eta^2\text{:}\eta^2$  (side-on) to form  $[\text{Cp}^*\{\text{RC}(\text{N}^i\text{Pr})_2\}\text{Ta}]_2(\mu\text{-}\eta^2\text{:}\eta^2\text{-N}_2)(\mu\text{-O})$  (**21**) [32]. This finding indicates that the  $\mu\text{-O}$  moiety can act as an efficient ligand to enforce the side-on binding  $\text{N}_2$  coordination mode.

In a series of these  $\text{Cp}^*$ -amidinate group 5 metal complexes **10-M,R**, two metal centers could supply totally six electrons to reduce the coordinated  $\text{N}_2$  to two nitride  $\text{N}^{3-}$  moieties. Indeed, the niobium and tantalum complexes are thermolyzed to quantitatively produce the corresponding bis( $\mu$ -nitride) dimers  $[\text{Cp}^*\{\text{RC}(\text{N}^i\text{Pr})_2\}\text{M}]_2(\mu\text{-N})_2$  (**22-M,R**; M = Nb, R = Me; M = Ta, R = Me, Ph,  $\text{NMe}_2$ ) [32, 58]. This contrasts the thermal stability of the vanadium congener, in which formation of nitride complexes through cleavage of the coordinated  $\text{N}_2$  ligand is unfavorable. The  $\text{Ta}_2(\mu\text{-N})_2$  core is found to undergo hydrosilylation. Treatment of the bis( $\mu$ -nitride) complex **22-Ta,Me** with  $\text{PhSiH}_3$  results in formation of an imide-nitride complex  $[\text{Cp}^*\{\text{RC}(\text{N}^i\text{Pr})_2\}\text{Ta}]_2(\text{H})(\text{NSiH}_2\text{Ph})(\mu\text{-N})$  through  $\sigma$ -bond metathesis of a Ta–N single bond [58].

Kinetic and mechanistic investigations of thermal conversion of **10-M,R** to **22-M,R** suggest that the process of the nitride formation is first-order in the  $\text{N}_2$  complex with appreciable negative entropies of activation and that no significant

**Table 3** Structurally characterized tantalum dinitrogen complexes

Compound	N–N (Å)	$\nu(\text{NN})$ (cm <sup>-1</sup> )	Ref.
<i>End-on bridging</i>			
[(2,6- <sup>i</sup> Pr <sub>2</sub> -C <sub>6</sub> H <sub>3</sub> O) <sub>3</sub> (thf)Ta] <sub>2</sub> ( $\mu$ -N <sub>2</sub> )	1.32(1)		[54]
[(2,6- <sup>i</sup> Pr <sub>2</sub> -C <sub>6</sub> H <sub>3</sub> S) <sub>3</sub> (thf)Ta] <sub>2</sub> ( $\mu$ -N <sub>2</sub> )	1.29(6)		[54]
[Cp*{RC(N <sup><i>i</i></sup> Pr) <sub>2</sub> }Ta] <sub>2</sub> ( $\mu$ -N <sub>2</sub> ) R = Ph ( <b>10-Ta,Ph</b> ) R = Me ( <b>10-Ta,Me</b> ) R = NMe <sub>2</sub> ( <b>10-Ta,NMe<sub>2</sub></b> )	1.308(2) 1.313(4) 1.306(5)		[32] [32, 58] [32]
[Cp*{MeC(N <sup><i>i</i></sup> Pr) <sub>2</sub> }(X)Ta] <sub>2</sub> ( $\mu$ -N <sub>2</sub> ) X = H, SiH <sub>2</sub> Ph X = H, H X = SPh, SPh	1.284(4) 1.307(6) 1.297(3)		[58] [58] [59]
[(Bz <sub>3</sub> P)(thf)(Cl) <sub>3</sub> Ta] <sub>2</sub> ( $\mu$ -N <sub>2</sub> )	1.282(6)		[93]
[( <sup>t</sup> BuCH)( <sup>t</sup> BuCH <sub>2</sub> )(Me <sub>3</sub> P) <sub>2</sub> Ta] <sub>2</sub> ( $\mu$ -N <sub>2</sub> )	1.298(12)		[94, 95]
[( <sup>t</sup> Bu <sub>3</sub> SiO) <sub>2</sub> (Cl)Ta] <sub>2</sub> ( $\mu$ -N <sub>2</sub> )	1.355(11)		[96]
[{C <sub>4</sub> H <sub>4</sub> BN(CHMe <sub>2</sub> ) <sub>2</sub> }(Cl)(PMe <sub>3</sub> ) <sub>2</sub> Ta] <sub>2</sub> ( $\mu$ -N <sub>2</sub> )	1.309(9)	1720	[97]
[Cp* <sub>2</sub> (Cl)Ta] <sub>2</sub> ( $\mu$ -N <sub>2</sub> )	1.235(13)		[98]
[(C <sub>5</sub> Me <sub>4</sub> Et)(Cl) <sub>2</sub> Ta] <sub>2</sub> ( $\mu$ -N <sub>2</sub> )	1.280(6)		[99]
[Cp*(4-MeC <sub>6</sub> H <sub>4</sub> S) <sub>2</sub> Ta] <sub>2</sub> ( $\mu$ -N <sub>2</sub> )	1.280(6)		[100]
[Cp*{(2,6-Me <sub>2</sub> C <sub>6</sub> H <sub>3</sub> )N <sup><i>i</i></sup> BuC(O)}(Cl)Ta] <sub>2</sub> ( $\mu$ -N <sub>2</sub> )	1.292(4) 1.290(4)		[101]
[(PhMe <sub>2</sub> P) <sub>4</sub> (Cl)W]( $\mu$ -N <sub>2</sub> )[Ta(Cl) <sub>3</sub> Cp]	1.275(9)	1435	[91]
<i>Side-on bridging</i>			
[Cp*{RC(N <sup><i>i</i></sup> Pr) <sub>2</sub> }Ta] <sub>2</sub> ( $\mu$ - $\eta^2$ : $\eta^2$ -N <sub>2</sub> )( $\mu$ -O) ( <b>21</b> ) R = Ph  R = Me  R = NMe <sub>2</sub>	1.504(4) 1.489(4) 1.493(14) 1.507(13) 1.499(4)		[32]
<i>Side-on end-on bridging</i>			
[(NPN)Ta] <sub>2</sub> ( $\mu$ -H) <sub>2</sub> ( $\mu$ - $\eta^2$ : $\eta^1$ -N <sub>2</sub> ) R = Ph ( <b>28</b> ) R = Cy	1.319(6) 1.328(7)	1165	[64, 69] [67]

N–N bond cleavage occurs in the transition state [32]. The N–N bond cleavage step is postulated to proceed via a  $\mu$ - $\eta^2$ : $\eta^2$ -N<sub>2</sub> dinuclear intermediate. The activation barrier is higher for the tantalum reaction than the niobium reaction. The thermal stability of these  $\mu$ - $\eta^1$ : $\eta^1$ -N<sub>2</sub> complexes can be modulated by the choice of the distal R-substituent groups of the amidinate ligands, and the sterically demanding phenyl substituent is crucial for kinetically stabilizing the  $\mu$ - $\eta^1$ : $\eta^1$ -N<sub>2</sub> diniobium complex **10-Nb,Me**. This process is reminiscent of the N–N bond cleavage mechanism proposed in the [(calix[4]arene)Nb] system (vide infra).

### 3.2 Niobium and Tantalum Dinitrogen Complexes Supported by Mixed Amide-Phosphine Ligands

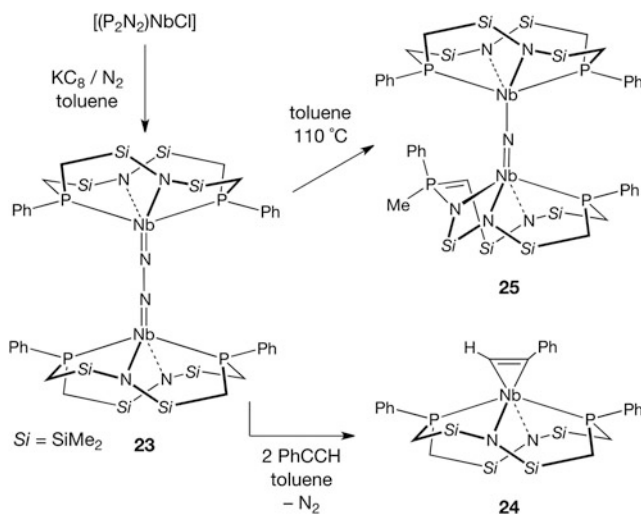
Fryzuk and coworkers have developed the mixed amide-phosphine hybrid multidentate ligands and have very successfully employed  $[\text{P}_2\text{N}_2]^{2-}$  and  $[\text{NPN}]^{2-}$  ligands to expand the coordination chemistry of dinitrogen in niobium and tantalum ( $[\text{P}_2\text{N}_2]^{2-} = [(\text{PhP})_2(\text{CH}_2\text{SiMe}_2\text{NSiMe}_2\text{CH}_2)_2]^{2-}$ ;  $[\text{NPN}]^{2-} = [\text{PhP}(\text{CH}_2\text{SiMe}_2\text{NPh})_2]^{2-}$ ) [60–62]. These ligand systems incorporate hard amide and soft phosphine donors into their ligand frameworks, allowing them to stabilize a variety of oxidation states and facilitate intriguing molecular transformations including  $\text{N}_2$  activation.

Reduction of  $[(\text{P}_2\text{N}_2)\text{NbCl}]$  with  $\text{KC}_8$  under  $\text{N}_2$  leads to formation of a paramagnetic  $\mu\text{-}\eta^1\text{:}\eta^1\text{-N}_2$  dinioibium complex  $[(\text{P}_2\text{N}_2)\text{Nb}]_2(\mu\text{-N}_2)$  (**23**), in which two Nb (IV) centers are bridged by a formal  $[\text{N}_2]^{4-}$  unit as evidenced by EPR and variable-temperature magnetic susceptibility measurements [63]. Complex **23** is found to be inert toward  $\text{H}_2$  and primary silanes, while the coordinated  $\text{N}_2$  is replaced with phenylacetylene to afford an alkyne complex  $[(\text{P}_2\text{N}_2)\text{Nb}(\eta^2\text{-PhCCH})]$  (**24**) (Scheme 8). Protonation of **23** by  $\text{Me}_3\text{N}\cdot\text{HCl}$  produces hydrazine in 62% yield. Upon thermolysis, the dinitrogen complex **23** undergoes conversion to  $\{[(\text{P}_2\text{N}_2)\text{Nb}](\mu\text{-N})\{[\text{PN}_3]\text{Nb}\}\}$  (**25**) ( $[\text{PN}_3] = \text{PhPMe}(\text{CHSiMe}_2\text{NSiMe}_2\text{CH}_2\text{P}(\text{Ph})\text{CH}_2\text{SiMe}_2\text{NSiMe}_2\text{N})$ ). It has been proposed that the arrangements leading to **25** include N–N bond scission of the  $\mu\text{-}\eta^2\text{:}\eta^2\text{-N}_2$  dinuclear intermediate and nucleophilic attack of a phosphine to the bridging nitride. The metal centers change their oxidation states from Nb(IV)–Nb(IV) to Nb(III)–Nb(V), which is consistent with magnetic data.

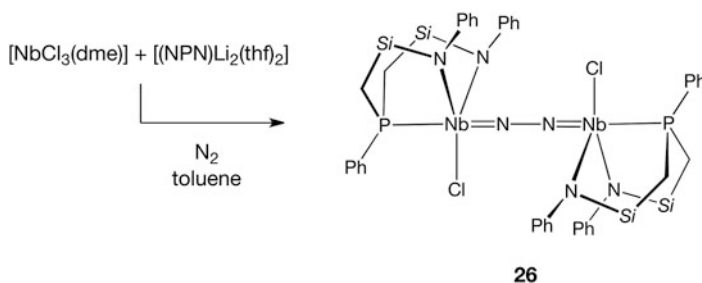
In parallel studies, coordination of the  $[\text{NPN}]$  ligand to niobium has been investigated. Treatment of  $[\text{NbCl}_3(\text{dme})]$  with  $[(\text{NPN})\text{Li}_2(\text{thf})_2]$  under  $\text{N}_2$  results in formation of a diamagnetic  $\mu\text{-}\eta^1\text{:}\eta^1\text{-N}_2$  complex  $[(\text{NPN})\text{NbCl}]_2(\mu\text{-N}_2)$  (**26**) (Scheme 9) [64].

Mindiola and coworkers reported the related  $[\text{PNP}]$ -supported complex  $[(\text{PNP})\text{-NbCl}_2]_2(\mu\text{-N}_2)$  (**27**,  $[\text{PNP}]^- = \text{N}(2\text{-P}^i\text{Pr}_2\text{-4-methylphenyl})_2$ ), which is prepared in good yields by reacting  $[(\text{NbCl}_3)(\text{thf})_2]_2(\mu\text{-N}_2)$  with  $[(\text{PNP})\text{Li}]$  or reducing  $[(\text{PNP})\text{-NbCl}_3]$  with  $\text{Bu}_3\text{SnH}$  under  $\text{N}_2$  [65]. According to the structural parameters of **26** and **27**, the  $\text{Nb}=\text{N}=\text{Nb}$  resonance formula is thought best to represent the bonding situation. Computational studies suggest that two-electron reduction of **27** does not induce N–N bond rupture. Indeed, further reduction using reagents such as  $\text{KC}_8$ ,  $[\text{Mg}(\text{thf})_3(\text{anthracene})]$ ,  $[\text{Na}(\text{C}_{10}\text{H}_8)]$ ,  $\text{Na/Hg}$ , and  $\text{Bu}_3\text{SnH}$  leads to decomposition mixtures or no reaction.

The utility of the  $[\text{NPN}]$  ligand has been extended to tantalum, resulting in the synthesis of a ditantalum dinitrogen complex  $[(\text{NPN})\text{Ta}]_2(\mu\text{-H})_2(\mu\text{-N}_2)$  (**28**) [64, 66, 67]. Complex **28** contains a  $\mu\text{-}\eta^1\text{:}\eta^2$  (side-on end-on) bound  $\text{N}_2$ , which is strongly activated as evidenced by a long N–N bond distance (1.319(6) Å). The hydrides bridging two metals in close proximity is responsible for the observation of side-on end-on  $\text{N}_2$  coordination in **28**. Besides the unique binding mode of  $\text{N}_2$ , this complex



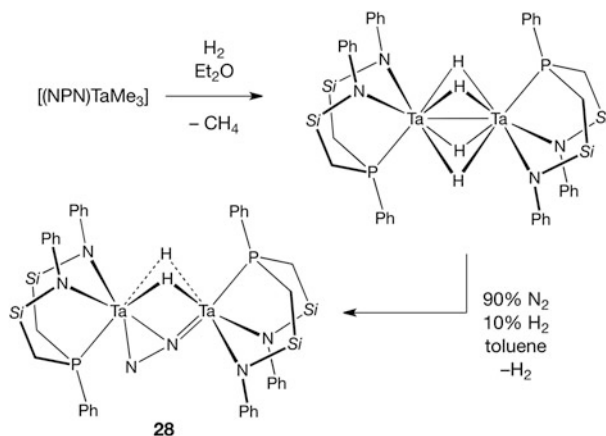
**Scheme 8** Synthesis and reactions of the niobium N<sub>2</sub> complex supported by the [P<sub>2</sub>N<sub>2</sub>] ligand



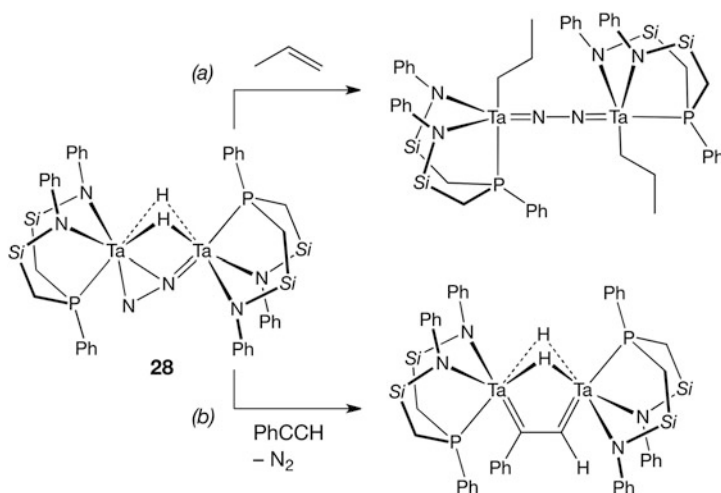
**Scheme 9** Synthesis of the [NPN]-supported niobium N<sub>2</sub> complex

is notable for its synthetic procedure. A tetrahydride ditantalum complex [(NPN)-Ta]<sub>2</sub>(μ-H)<sub>4</sub>, prepared by hydrogenolysis of [NPN]TaMe<sub>3</sub>, spontaneously reacts with N<sub>2</sub> along with H<sub>2</sub> reductive elimination to form the dinitrogen complex **28** (Scheme 10). In the two-step synthesis of **28** starting from [NPN]TaMe<sub>3</sub>, H<sub>2</sub> is utilized as a reducing reagent, and the use of strong reducing reagents such as Na/Hg or KC<sub>8</sub> can be avoided. Thus, this strategy offers attractive avenues for the synthesis of strongly activated N<sub>2</sub> complexes and for the use of N<sub>2</sub> as a nitrogen source.

Complex **28** exhibits a wide range of reactivity patterns due to the ability of the side-on end-on bound N<sub>2</sub> moiety and/or the bridging hydrides to engage in interactions with a substrate [62]. This complex is found to (a) insert propene into Ta–H bonds, a reaction characteristic of metal hydride complexes (Scheme 11a) [64], (b) serve as a precursor for low-valent species via N<sub>2</sub> displacement upon reacting with terminal alkynes (Scheme 11b) [68], and (c) display dinitrogen-based reactivity, often concurrent with N–N bond cleavage (Schemes 12–16).



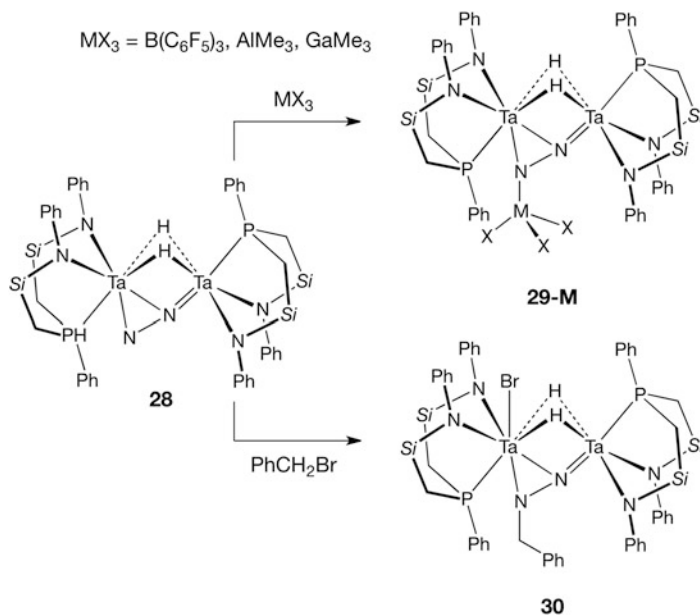
**Scheme 10** Synthesis of the side-on end-on  $N_2$  tantalum complex



**Scheme 11** Reactions of the side-on end-on  $N_2$  tantalum complex with propene and phenylacetylene

The terminal nitrogen of the side-on end-on bound  $N_2$  in **28** is nucleophilic, and a series of adducts  $\{[(NPN)Ta]_2(\mu-\eta^1;\eta^2-N_2MX_3)(\mu-H)_2\}$  (**29-M**;  $M = B, Al, Ga$ ) are readily derived by treating with Group 13 Lewis acids  $MX_3$  such as  $B(C_6F_5)_3$ ,  $AlMe_3$ , and  $GaMe_3$  (Scheme 12) [69]. Adduct formation with Lewis acids increases the extent of dinitrogen activation, which is reflected in elongation of the N–N bond distances (**28**, 1.319(6) Å; **29-B**, 1.393(7) Å; **29-Al**, 1.363(7) Å; **29-Ga**, 1.356(18) Å). When benzyl bromide is used as an electrophile, alkylation at the terminal nitrogen is observed to give  $\{[(NPN)Ta](\mu-\eta^1;\eta^2-N_2CH_2Ph)(\mu-H)_2\{TaBr(NPN)\}$

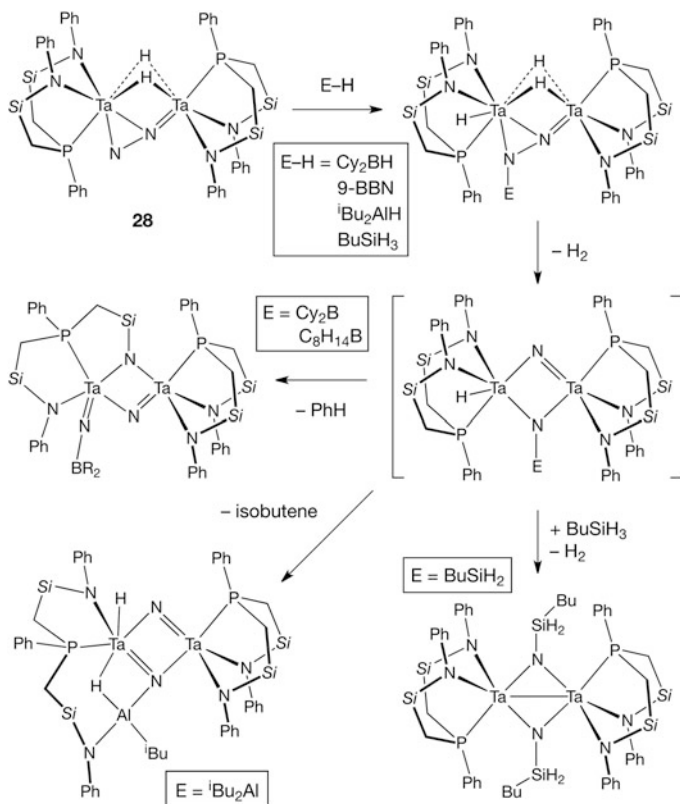




**Scheme 12** Reactions of the side-on end-on N<sub>2</sub> tantalum complex with group 3 Lewis acids and benzyl bromide

**(30)** [64]. In all these products, the bridging hydrides remain intact, which accounts for the retention of the  $\mu\text{-}\eta^1;\eta^2$  binding N<sub>2</sub> moiety.

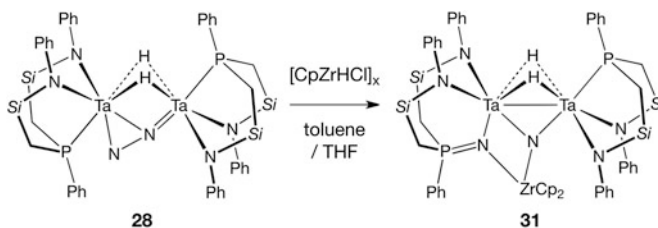
Further functionalization of the side-on end-on bound N<sub>2</sub> moiety concomitant with N–N bond cleavage is achieved by treating **28** with main-group element hydrides (E–H) such as R<sub>2</sub>BH, R<sub>2</sub>AlH, and RH<sub>2</sub>SiH (Scheme 13) [70–74]. In all these transformations, the first step is E–H addition across the Ta–N bond at the terminal nitrogen of the side-on end-on bound N<sub>2</sub>. The next step includes elimination of H<sub>2</sub> along with N–N bond cleavage, generating a nitride-imide species as a key intermediate. The last step is observed to depend on the nature of the E–H hydride reagents. For example, the reactions of **28** with 9-BBN and Cy<sub>2</sub>BH lead to auxiliary ligand rearrangement involving the silyl group migration and benzene elimination [70, 71]. With <sup>1</sup>Bu<sub>2</sub>AlH, loss of isobutene takes place with a phosphine arm of one [NPN] ligand migrating from tantalum to aluminum [72]. When slightly more than 2 equivalents of BuSiH<sub>3</sub> are used, the coordinated N<sub>2</sub> moiety is converted into two bridging bis(silylimide) groups concomitant with H<sub>2</sub> evolution [73–75]. In contrast to hydroboration and hydroalumination, hydrosilylation of the coordinated N<sub>2</sub> moiety takes place with the [NPN] ligands remaining intact. However, in the presence of excess BuSiH<sub>3</sub>, one phenyl substitute of the [NPN] ligand is ortho-cyclometalated. Therefore, auxiliary ligand degradations have hampered attempts to extrude N-containing products such as N(SiH<sub>2</sub>Bu)<sub>3</sub> and regenerate the starting hydride complex [(NPN)Ta]<sub>2</sub>( $\mu\text{-H}$ )<sub>4</sub> in the **28**/E–H reaction systems.



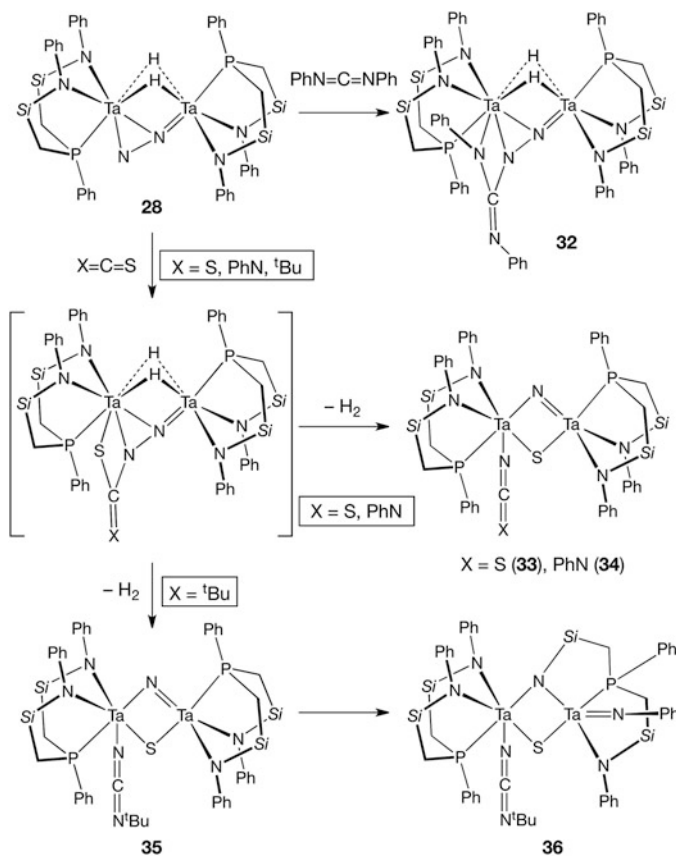
**Scheme 13** Reactions of the side-on end-on N<sub>2</sub> tantalum complex with main-group element hydrides

As an extension of Fryzuk's work on addition of hydride reagents to the side-on end-on bound N<sub>2</sub>, the reaction of **28** with [Cp<sub>2</sub>ZrHCl]<sub>x</sub> was investigated (Scheme 14) [76]. The reaction proceeds differently, where the zirconocene hydride behaves as a Zr(II) precursor. The reaction would be initiated by coordination of the Zr (II) fragment to the N<sub>2</sub> unit and subsequent inner-sphere two-electron reduction concomitant with N–N bond cleavage, yielding a transient nitride-bridged species. Finally, nucleophilic attack of a phosphine to one of the bridging nitrides results in formation of [ {(NP(N)N)Ta} (μ-N)(μ-H)<sub>2</sub> { [NPN]Ta } (ZrCp<sub>2</sub>) } ] (**31**). The analogous reactions of **28** with [Cp<sub>2</sub>ZrH<sub>2</sub>]<sub>2</sub> and [Cp<sub>2</sub>Zr(py)(Me<sub>3</sub>SiC≡CSiMe<sub>3</sub>)] afford the same product **31** in better yields.

Another intriguing transformation of the side-on end-on bound N<sub>2</sub> is C–N bond formation by the reaction of **28** with 1,2-cumulenes X=C=Y (X, Y = N, S) (Scheme 15) [77]. This transformation is proposed to include initial formation of a [2+2] cycloaddition species. Upon reacting with PhN=C=NPh, the cycloaddition product can be isolated as [ {(NPN)Ta }<sub>2</sub> (μ-H)<sub>2</sub> { μ-PhNC(NPh)N<sub>2</sub> } ] (**32**) and undergo no further reaction. With S=C=S and PhN=C=S, H<sub>2</sub> elimination

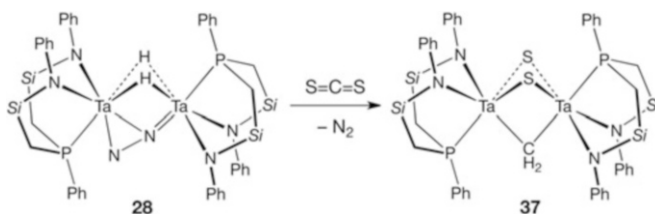


**Scheme 14** Reaction of the side-on end-on N<sub>2</sub> tantalum complex with zirconocene hydride



**Scheme 15** Reactions of the side-on end-on N<sub>2</sub> tantalum complex with 1,2-cumulenes

subsequently occurs to generate  $\mu$ -nitride,  $\mu$ -sulfide complexes  $[\{(\text{NPN})\text{Ta}\}_2(\mu\text{-N})(\mu\text{-S})(\text{NCS})]$  (**33**) and  $[\{(\text{NPN})\text{Ta}\}_2(\mu\text{-N})(\mu\text{-S})(\text{NCNPh})]$  (**34**) concomitant with successive cleavage of N–N and C–S bonds. The reaction of **28** with  $^t\text{BuN}=\text{C}=\text{S}$



**Scheme 16** Reaction of the side-on end-on  $N_2$  tantalum complex with  $CS_2$

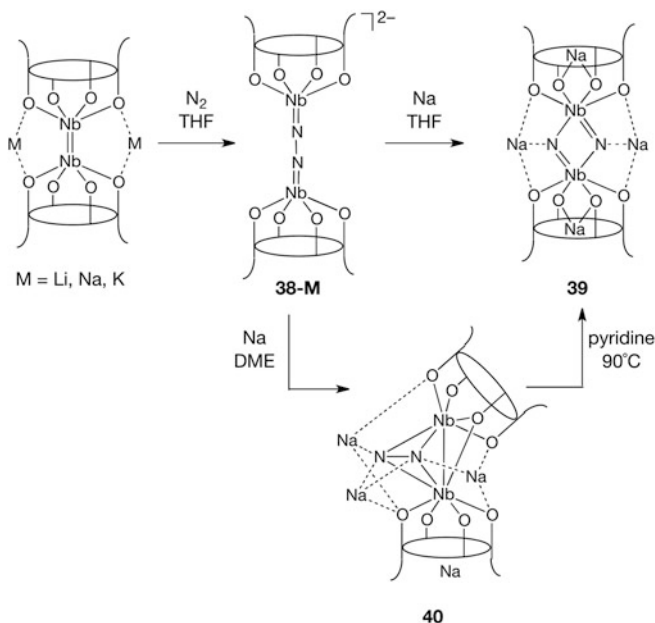
proceeds in a similar manner, but the corresponding nitride-sulfide species  $[(NPN)Ta]_2(\mu-H)_2(\mu-S)(NCN^tBu)$  (**35**) is thermally unstable and undergoes auxiliary ligand rearrangement, resulting in amide-to-nitride silyl migration and formation of **36**.

The outcome of the reaction of **28** with carbon disulfide  $S=C=S$  may be altered dramatically by changing the reaction conditions to higher temperatures (Scheme 16) [78]. In so doing, conversion of carbon disulfide into two bridging sulfides and one bridging methylene is observed to produce  $[(NPN)Ta]_2(\mu-CH_2)(\mu-S)_2$  (**37**). This process includes  $N_2$  displacement, C–S bond cleavage, and CS insertion into the bridging hydrides.

### 3.3 Dinitrogen Cleavage by Niobium Aryloxy Complexes

Aryloxy ligands are effective at stabilizing novel early transition metal chemistry and employed to prepare reactive metal complexes that imitate or surpass the role of the metal anchored to heterogeneous, oxygen-rich surfaces. In this context, calixarenes have the potential to provide a preorganized set of oxygen donors that mimics oxide surfaces. Floriani and coworkers presented stepwise cleavage of  $N_2$  by a niobium calix[4]arene complex, where electrons stored in the metal–metal bond are used to reduce  $N_2$  (Scheme 17) [79, 80]. A diniohium complex  $[(\{p^tBu\text{-calix[4]-(O)}_4\}Nb)_2(\mu-M)_2]$  ( $M = Li, Na, K$ ) containing a Nb(III)=Nb(III) double bond reacts with  $N_2$  to afford an end-on  $N_2$  bridged dimer  $[(\{p^tBu\text{-calix[4]-(O)}_4\}Nb)_2(\mu-\eta^1:\eta^1-N_2)(M)_2]$  (**38-M**;  $M = Li, Na, K$ ), in which the long N–N bond distance (1.390(17) Å) corresponds to a four-electron reduced form  $[N_2]^{4-}$ . The  $\mu-\eta^1:\eta^1-N_2$  complex **38** can accept two extra electrons by treating with sodium, which facilitates complete N–N bond cleavage and formation of a dinuclear species with two bridging nitrides  $[(\{p^tBu\text{-calix[4]-(O)}_4\}Nb)_2(\mu-N)_2(\mu-Na)_2(Na)_2]$  (**39**).

Two reaction pathways for conversion of **38** into **39** are proposed. In both pathways, reduction of niobium by sodium initially generates a biradical system containing two  $d^1$  Nb(IV) centers. In one pathway, N–N bond cleavage proceeds via a transition state with a zigzag Nb=N–N=Nb structure. This process closely resembles N–N bond cleavage in the molybdenum trisamide  $N_2$  complex  $[(R(Ar)-N)_3Mo]_2(\mu-N_2)$  [81]. The resulting monomeric nitride complex dimerizes to

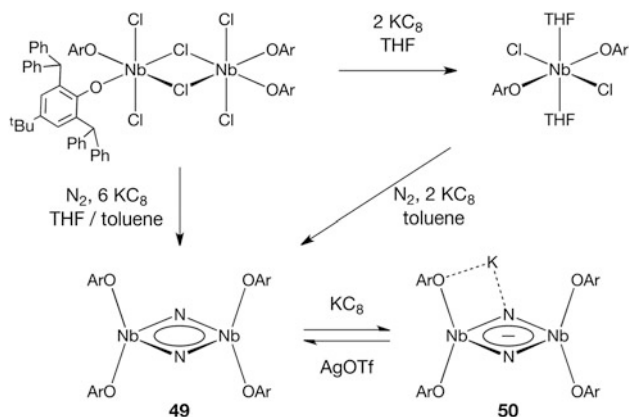


**Scheme 17** N<sub>2</sub> cleavage by the calix[4]arene-supported niobium complex

produce **39**. The other pathway includes formation of a metal–metal bond, which stores two electrons supplied by sodium and stabilizes a side-on bound N<sub>2</sub> intermediate [ $\{(\text{p-}^t\text{Bu-calix[4]-(O)}_4)\text{Nb}\}_2(\mu\text{-}\eta^2\text{:}\eta^2\text{-N}_2)(\mu\text{-Na})_3\text{Na}$ ] (**40**). This intermediate undergoes intramolecular two-electron transfer from the metal–metal bond to the N–N bond, with accompanying cleavage of the N–N and the Nb–Nb bonds and yielding the bis( $\mu$ -nitride) dimer **39**. The reaction of **38** with sodium is dependent on the nature of the solvent used. In THF, the reaction leads to isolation of **39** as a major product. When the reaction is carried out in DME, the side-on N<sub>2</sub>-bridged complex **40** is obtained along with a small amount of **39**. Complex **40** is thermally unstable, and heating a pyridine solution of **40** at 90 °C provides **39** as a unique product.

A related ligand system to calix[4]arene is a triaryloxy ligand [OOO]<sup>3-</sup>, known as the Koebner trimer. This [OOO] ligand system lacks the fourth aryloxy unit found in calix[4]arene and has an acyclic structure. A niobium chloride [(OOO)NbCl<sub>2</sub>]<sub>2</sub> was treated with LiBHET<sub>3</sub> under N<sub>2</sub> to produce a bis( $\mu$ -nitride) dimer [ $\{(\text{OOO})\text{Nb}\}_2(\mu\text{-N})_2\{\text{Li}(\text{thf})_2\}$ ] (**41**) (Scheme 18) [82]. Computational studies suggest that N<sub>2</sub> is  $\mu\text{-}\eta^1\text{:}\eta^2$ -coordinated to the Nb(III) dinuclear core bridged by two hydrides and reduced to the [N<sub>2</sub>]<sup>4-</sup> form [83]. The additional two electrons required for N–N cleavage are provided by migration of one hydride to an N atom. In the final step, the N-bound H atom is coupled with the remaining hydride to produce the bis( $\mu$ -nitride) dimer **41** along with H<sub>2</sub> elimination.

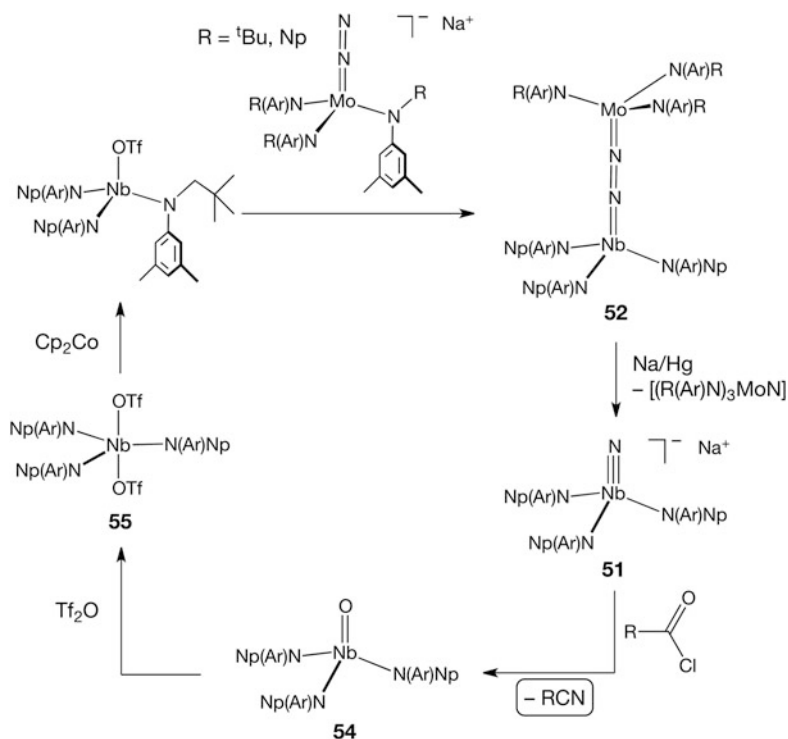




**Scheme 20** N<sub>2</sub> cleavage by the niobium aryloxide complex

triple bond cleavage requires no external reducing reagents. The reaction spontaneously proceeds, where two electrons are provided by the metal–metal cleavage and four additional electrons are supplied by H<sub>2</sub> elimination. The bridging nitrides in **43** are nucleophilic enough to undergo protonation and methylation [84, 85]. Addition of 2,6-lutidinium chloride to **43** affords NH<sub>3</sub> and the anionic complex [(O<sub>3</sub>)NbCl<sub>3</sub>]<sup>−</sup>. The reaction of this anionic complex with KBHET<sub>3</sub> regenerates the hydride complex **42**, thereby completing a synthetic cycle for conversion of N<sub>2</sub> to NH<sub>3</sub> [85]. Methylation of **43** with methyl iodide proceeds in a stepwise manner to yield a μ-nitride-imide and a bis(μ-imide) dimer, [(O<sub>3</sub>)Nb]<sub>2</sub>(μ-N)(μ-NMe){K(thf)} (**44**) and [(O<sub>3</sub>)Nb]<sub>2</sub>(μ-NMe)<sub>2</sub> (**45**) [84]. The μ-imide dimer **45** is inert toward CO<sub>2</sub>. However, treatment of **45** with pyridine affords a monomeric imide species [(O<sub>3</sub>)Nb(NMe)(py)<sub>2</sub>] (**46**). This imide monomer **46** is observed to undergo [2+2] cycloaddition with CO<sub>2</sub> to give an ureate complex [(O<sub>3</sub>)Nb(MeNCONMe)(py)] (**47**) and a bis(μ-oxo) dimer [(O<sub>3</sub>)Nb](μ-O)<sub>2</sub> (**48**) in a 2:1 ratio [85].

Mindiola and coworkers accomplished dinitrogen cleavage by niobium complexes bearing a sterically encumbering aryloxide ligand, 2,6-bis(diphenylmethyl)-4-tert-butylphenoxide (OAr) (Scheme 20) [86]. The reaction of [(ArO)<sub>2</sub>Nb<sub>2</sub>Cl<sub>3</sub>]<sub>2</sub> or [(ArO)<sub>2</sub>NbCl<sub>2</sub>(thf)<sub>2</sub>] with KC<sub>8</sub> under N<sub>2</sub> provides a bis(μ-nitride) dimer [(ArO)<sub>2</sub>Nb]<sub>2</sub>(μ-N)<sub>2</sub> (**49**), which can be further reduced by 1 equivalent of KC<sub>8</sub> to provide a paramagnetic nitride species [(ArO)<sub>2</sub>Nb]<sub>2</sub>(μ-N)<sub>2</sub>K (**50**). Conversion of **49** to **50** is reversible, and **49** is regenerated by oxidation of **50** with AgOTf. This behavior is similar to that found in the V<sub>2</sub>(μ-N)<sub>2</sub> structure reported by the Cloke group (vide supra). Upon protonation by anhydrous HCl, both nitride complexes give NH<sub>4</sub>Cl and free ArOH in a 1:2 ratio.



**Scheme 21** Conversion of acid chloride into organic nitrile by the  $\text{N}_2$ -derived niobium nitride complex

### 3.4 Dinitrogen Cleavage and Nitrogen Atom Transfer Mediated by Niobium Tris(amide) Complexes

The Cummins group established the connection between  $\text{N}_2$  cleavage reaction and N-atom transfer reactivity by utilizing the reactivity of an anionic niobium nitride complex  $[(\text{Np}(\text{Ar})\text{N})_3\text{NbNNa}]$  (**51**) derived from  $\text{N}_2$  activation (Scheme 21). An end-on  $\text{N}_2$ -bridged Mo/Nb complex  $[\{(\text{R}(\text{Ar})\text{N})_3\text{Mo}\}(\mu\text{-}\eta^1:\eta^1\text{-N}_2)\{\text{NbN}(\text{Ar})\text{Np}\}]$  (**52**), which is prepared by salt metathesis of  $[(\text{Np}(\text{Ar})\text{N})_3\text{NbCl}]$  or  $[(\text{Np}(\text{Ar})\text{N})_3\text{NbOTf}]$  with  $[\text{Na}(\text{thf})_x][(\text{R}(\text{Ar})\text{N})_3\text{Mo}(\text{N}_2)]$ , has served as an entry to dinitrogen chemistry of the niobium tris(amide) system [87, 88]. Reduction of the Mo/Nb dinitrogen complex **52** with Na/Hg results in a 1:1 mixture of the anionic niobium nitride **51** and the neutral molybdenum nitride  $[(\text{R}(\text{Ar})\text{N})_3\text{MoN}]$  (**53**). These complexes **51** and **53** could be easily separated by differential solubility.

The anionic nitride **51** readily reacts with acid chlorides  $\text{RC}(\text{O})\text{Cl}$  ( $\text{R} = \text{Me}, {}^t\text{Bu}, \text{Ph}, 1\text{-adamantyl}, \text{CH}=\text{CH}_2$ ), yielding the corresponding organic nitriles  $\text{RCN}$  along with a niobium oxo complex  $[(\text{R}(\text{Ar})\text{N})_3\text{NbO}]$  (**54**) [88]. According to experimental and computational studies, formation of organic nitriles could be ascribed to retro



[2+2] fragmentation by a transient niobacyclobutene Nb–N=C(R)–O species. To achieve a synthetic cycle for conversion of N<sub>2</sub> to organic nitriles, treatment of the oxo complex **54** with triflic anhydride affords a bistriflate complex [(R(Ar)N)<sub>3</sub>Nb(OTf)<sub>2</sub>] (**55**). The bis(triflate) complex **55** is subsequently one-electron reduced using cobaltocene or magnesium anthracene to regenerate the starting monotriflic complex [(R(Ar)N)<sub>3</sub>Nb(OTf)].

## References

1. Shilov A, Denisov N, Efimov O, Shuvalov N, Shuvalova N, Shilova A (1971) *Nature* 231:460
2. Nikonova LA, Isaeva SA, Pershikova NI, Shilov AE (1975) *J Mol Catal* 1:367
3. Shilov AE (1987) *J Mol Catal* 41:221
4. Robson RL, Eady RR, Richardson TH, Miller RW, Hawkins M, Postgate JR (1986) *Nature* 322:388
5. Slebondnick C, Hamstra BJ, Pecoraro VL (1997) *Struct Bond* 89:51
6. Rehder D (1999) *Coord Chem Rev* 182:297
7. Janas Z, Sobota P (2005) *Coord Chem Rev* 249:2144
8. Bazhenova TA, Shilov AE (1995) *Coord Chem Rev* 144:69
9. Avenier P, Taoufik M, Lesage A, Solans-Monfort X, Baudouin A, de Mallmann A, Veyre L, Basset JM, Eisenstein O, Emsley L, Quadrelli EA (2007) *Sience* 317:1056
10. Solans-Monfort X, Chow C, Gouré E, Kaya Y, Basset JM, Taoufik M, Quadrelli EA, Eisenstein O (2012) *Inorg Chem* 51:7237
11. Chatt J, Dilworth JR, Richards RL (1978) *Chem Rev* 78:589
12. Hidai M, Mizobe Y (1995) *Chem Rev* 98:1115
13. MacKay BA, Fryzuk MD (2004) *Chem Rev* 104:385
14. Rehder D, Woitha C, Priebsch W, Gailus H (1992) *J Chem Soc Chem Commun* 364
15. Gailus H, Woitha C, Rehder D (1994) *J Chem Soc Dalton Trans* 3471
16. Woitha C, Rehder D (1990) *Angew Chem Int Ed Engl* 29:1438
17. Chatt J, Pearman AJ, Richards RL (1975) *Nature* 253:39
18. Hidai M, Mizobe Y (2002) *Met Ions Biol Syst* 39:121
19. Rosenblat MC, Henderson RA (2002) *Inorg Chim Acta* 331:270
20. Tanabe Y, Nishibayashi Y (2016) *Chem Rec* 16:1549
21. Henderson RA (1990) *Transition Met Chem* 15:330
22. Buijink JKF, Meetsma A, Teuben JH (1993) *Organometallics* 12:2004
23. Ferguson R, Solari E, Floriani C, Osella D, Ravera M, Re N, Chiesi-Villa A, Rizzoli C (1997) *J Am Chem Soc* 119:10104
24. Ferguson R, Solari E, Floriani C, Chiesi-Villa A, Rizzoli C (1993) *Angew Chem Int Ed Engl* 32:396
25. Edema JJH, Meetsma A, Gambarotta S (1989) *J Am Chem Soc* 111:6878
26. Leigh GJ, Prieto-Alcón R, Sanders JR (1991) *J Chem Soc Chem Commun* 921
27. Yandulov DV, Schrock RR (2003) *Science* 301:76
28. Smythe NC, Schrock RR, Müller P, and Weare WW (2006) *Inorg Chem* 45:9197
29. Guha AK, Phukan AK (2011) *Inorg Chem* 50:8826
30. Laplaza CE, Cummins CC (1995) *Science* 268:861
31. Tran BL, Pinter B, Nichols AJ, Konopka FT, Thompson R, Chen CH, Krzystek J, Ozarowski A, Telsler J, Baik MH, Meyer K, Minjiola DJ (2012) *J Am Chem Soc* 134:13035
32. Keane AJ, Yonke BL, Hirotsu M, Zavalij PY, Sita LR (2014) *J Am Chem Soc* 136:9906
33. Groyzman S, Villagrán D, Freedman DE, Nocera DG (2011) *Chem Commun* 47:10242

34. Solari E, Da Silva C, Iacono B, Hesschenbrouck J, Rizzoli C, Scopelliti R, Floriani C (2001) *Angew Chem Int Ed* 40:3907
35. Cozzolino AF, Silvia JS, Lopez N, Cummins CC (2014) *Dalton Trans* 43:4639
36. Yamamoto A, Go S, Ookawa M, Takahashi M, Ikeda S, Keii T (1972) *Bull Chem Soc Jpn* 45:3110
37. Mori M, Akashi M, Hori M, Hori K, Nishida M, Sato Y (2004) *Bull Chem Soc Jpn* 77:1655
38. Berno P, Gambarotta S (1995) *Angew Chem Int Ed Engl* 34:822
39. Clentsmith GKB, Bates VME, Hitchcock PB, Cloke FGN (1999) *J Am Chem Soc* 121:10444
40. Bates VME, Clentsmith GKB, Cloke FGN, Green JC, Jenkin HDL (2000) *Chem Commun* 927
41. Vidyaratne I, Crewdson P, Lefebvre E, Gambarotta S (2007) *Inorg Chem* 46:8836
42. Ishida Y, Kawaguchi H (2014) *J Am Chem Soc* 136:16990
43. Desmangles N, Jenkins H, Ruppia KB, Gambarotta S (1996) *Inorg Chim Acta* 250:1
44. Berno P, Hao S, Minhas R, Gambarotta S (1994) *J Am Chem Soc* 116:7417
45. Hao S, Berno P, Minhas RK, Gambarotta S (1996) *Inorg Chim Acta* 244:37
46. Song JI, Berno P, Gambarotta S (1994) *J Am Chem Soc* 116:6927
47. Milsmann C, Turner ZR, Semproni SP, Chirik PJ (2012) *Angew Chem Int Ed* 51:5386
48. Milsmann C, Semproni SP, Chirik PJ (2014) *J Am Chem Soc* 136:12099
49. Vidyaratne I, Gambarotta S, Korobkov I, Budzelaar PHM (2005) *Inorg Chem* 44:1187
50. Liu G, Liang X, Meetsma A, Hessen B (2010) *Dalton Trans* 39:7891
51. Kilgore UJ, Sengelaub CA, Pink M, Fout AR, Mindiola DJ (2008) *Angew Chem Int Ed* 47:3769
52. Kilgore UJ, Sengelaub CA, Fan H, Tomaszewski J, Karty JA, Baik MH, Mindiola DJ (2009) *Organometallics* 28:843
53. O'Donoghue MB, Davis WM, Schrock RR, Reiff WM (1999) *Inorg Chem* 38:243
54. Dilworth JR, Henderson RA, Hills A, Hughes DL, Macdonald C, Stephens AN, Walton DRM (1990) *J Chem Soc Dalton Trans* 1077
55. Schrock RR, Wesolek M, Liu AH, Wallace KC, Dewan JC (1988) *Inorg Chem* 27:2050
56. Henderson RA, Morgan SH, Stephens AN (1990) *J Chem Soc Dalton Trans* 1101
57. Henderson RA, Morgan SH (1990) *J Chem Soc Dalton Trans* 1107
58. Hirotsu M, Fontaine PP, Epshteyn A, Zavalij PY, Sita LR (2007) *J Am Chem Soc* 129:9284
59. Yonke BL, Keane AJ, Zavalij PY, Sita LR (2012) *Organometallics* 31:345
60. Burford RJ, Yeo A, Fryzuk MD *Coord Chem Rev* DOI: <http://dx.doi.org/10.1016/j.ccr.2016.06.015>
61. MacLachlan EA, Fryzuk MD (2006) *Organometallics* 25:1530
62. Fryzuk MD (2009) *Acc Chem Res* 42:127
63. Fryzuk MD, Kozak CM, Bowdridge MR, Patrick BO, Rettig SJ (2002) *J Am Chem Soc* 124:8389
64. Fryzuk MD, Johnson SA, Patrick BO, Albinati A, Mason SA, Koetzle TF (2001) *J Am Chem Soc* 123:3960
65. Kilgore UJ, Yang X, Tomaszewski J, Huffman JC, Mindiola DJ (2006) *Inorg Chem* 45:10712
66. Fryzuk MD, Johnson SA, Rettig SJ (1998) *J Am Chem Soc* 120:11024
67. Yeo A, Shaver MP, Fryzuk MD (2015) *Z Anorg Allg Chem* 641:123
68. Shaver MP, Johnson SA, Fryzuk MD (2005) *Can J Chem* 83:652
69. Studt F, MacKay BA, Johnson SA, Patrick BO, Fryzuk MD, Tuczek F (2005) *Chem A Eur J* 11:604
70. Fryzuk MD, MacKay BA, Johnson SA, Patrick BO (2002) *Angew Chem Int Ed* 41:3709
71. MacKay B, Johnson SA, Patrick BO, Fryzuk MD (2005) *Can J Chem* 83:315
72. MacKay BA, Patrick BO, Fryzuk MD (2005) *Organometallics* 24:3836
73. Fryzuk MD, MacKay BA, Patrick BO (2003) *J Am Chem Soc* 125:3234
74. MacKay BA, Munha RF, Fryzuk MD (2006) *J Am Chem Soc* 128:9472
75. Studt F, MacKay BA, Fryzuk MD, Tuczek F (2006) *Dalton Trans* 1137

76. Spencer LP, MacKay BA, Patrick BO (2006) Fryzuk MD Proc. Natl Acad Sci U S A 103:17094
77. Ballmann J, Yeo A, Patrick BO, Fryzuk MD (2011) Angew Chem Int Ed 50:507
78. Ballmann J, Yeo A, MacKay BA, Rijt SV, Patrick BO, Fryzuk MD (2010) Chem Commun 46:8794
79. Zanotti-Gerosa A, Solari E, Giannini L, Floriani C, Chiesi-Villa A, Rizzoli C (1998) J Am Chem Soc 120:437
80. Caselli A, Solari E, Scopelliti R, Floriani C, Re N, Rizzoli C, Chiesi-Villa A (2000) J Am Chem Soc 122:3652
81. Laplaza CE, Johnson MJA, Peters JC, Odom AL, Kim E, Cummins CC, George GN, Pickering IJ (1996) J Am Chem Soc 118:8623
82. Kawaguchi H, Matsuo T (2002) Angew Chem Int Ed 41:2792
83. Tanaka H, Shiota Y, Matsuo T, Kawaguchi H, Yoshizawa K (2009) Inorg Chem 48:3875
84. Akagi F, Matsuo T, Kawaguchi H (2007) Angew Chem Int Ed 46:8778
85. Akagi F, Suzuki S, Ishida Y, Hatanaka T, Matsuo T, Kawaguchi H (2013) Eur J Inorg Chem 3930
86. Searles K, Carroll PJ, Chen CH, Pink M, Mindiola DJ (2015) Chem Commun 51:3526
87. Mindiola DJ, Meyer K, Cherry JPF, Baker TA, Cummins CC (2000) Organometallics 19:1622
88. Figueroa JS, Piro NA, Clough CR, Cummins CC (2006) J Am Chem Soc 128:940
89. Berno P, Gambarotta S (1995) Organometallics 14:2159
90. Hulley EB, Williams VA, Hirsekorn KF, Wolczanski PT, Lancaster KM, Lobkovsky EB (2016) Polyhedron 103:105
91. Ishino H, Nagano T, Kuwata S, Yokobayashi Y, Ishii Y, Hidai M (2001) Organometallics 20:188
92. Fryzuk MD, Kozak CM, Patrick BO (2003) Inorg Chim Acta 345:53
93. Churchill MR, Wasserman HJ (1982) Inorg Chem 21:218
94. Churchill MR, Wasserman HJ (1981) Inorg Chem 20:2899
95. Turner HW, Fellmann JD, Rocklage SM, Schrock RR, Churchill MR, Wasserman HJ (1980) J Am Chem Soc 102:7809
96. Hulley EB, Bonanno JB, Wolczanski PT, Cundari TR, Lobkovsky EB (2010) Inorg Chem 49:8524
97. Sperry CK, Cotter WD, Lee RA, Lachicotte RJ, Bazan GC (1998) J Am Chem Soc 120:7791
98. Bregel DC, Oldham SM, Lachicotte RJ, Eisenberg R (2002) Inorg Chem 41:4371
99. Lee TY, Wooten AJ, Luci JJ, Swenson DC, Messerle L (2005) Chem Commun 5444
100. Takada R, Hirotsu M, Nishioka T, Hashimoto H, Kinoshita I (2011) Organometallics 30:4232
101. Horrillo-Martinez P, Patrick BO, Schafer LL, Fryzuk MD (2012) Dalton Trans 41:1609

# Functionalization of N<sub>2</sub> by Mid to Late Transition Metals via N–N Bond Cleavage

Isabel Klopsch, Ekaterina Yu Yuzik-Klimova, and Sven Schneider

**Abstract** This review focuses on the recent efforts to functionalize dinitrogen via complete cleavage of the N≡N bond with particular emphasis on mid to late transition metal complexes. The relationships of electronic and structural parameters for the most common N<sub>2</sub>-bonding modes (end-on and side-on bridging) with N<sub>2</sub>-splitting reactivity are discussed. This analysis points towards electronic configurations with  $\pi^{10}$  (end-on) and  $\pi^8\delta^2$  (side-on) electrons within the M<sub>2</sub>N<sub>2</sub>-cores for full N–N bond cleavage into terminal and bridging nitride complexes, respectively. The full body of work on N<sub>2</sub>-splitting with group 6–8 metals is comprehensively presented. Ligand electronic and steric effects are discussed in detail for privileged platforms, such as low coordinate, electron rich complexes with  $\pi$ -donating ligands. Finally, several strategies for functionalization of the nitrides resulting from N<sub>2</sub>-splitting are presented that lead to N–C bond formation. The developed pseudo-catalytic cycles reported so far that combine N<sub>2</sub>-cleavage, nitride functionalization, and N-transfer provide guidelines for rational catalyst design.

**Keywords** Bonding • Dinitrogen splitting • Nitrogen fixation • Transition metal nitrides

## Contents

1 Nitrogenase, Haber-Bosch, and Catalytic N <sub>2</sub> Fixation .....	72
2 Bonding in N <sub>2</sub> -Bridged Complexes .....	73
2.1 General Considerations .....	73
2.2 End-On Bridging N <sub>2</sub> .....	74
2.3 Side-On Bridging N <sub>2</sub> .....	77

---

I. Klopsch, E.Y. Yuzik-Klimova, and S. Schneider (✉)  
Institute for Inorganic Chemistry, University of Goettingen, Tammannstrasse 4, 37077  
Goettingen, Germany  
e-mail: [sven.schneider@chemie.uni-goettingen.de](mailto:sven.schneider@chemie.uni-goettingen.de)

3	Splitting of N <sub>2</sub> into Nitride Complexes of Group 6 Elements and Beyond .....	81
3.1	N <sub>2</sub> -Splitting by Homoleptic Group 6 Amide Complexes .....	81
3.2	N <sub>2</sub> -Splitting by Group 6 and 7 Pincer Complexes .....	85
3.3	N <sub>2</sub> -Splitting by Group 6 Cyclopentadienide Complexes .....	89
3.4	N <sub>2</sub> -Splitting Beyond Group 7 Elements .....	91
4	Nitride Functionalization Following N <sub>2</sub> -Splitting .....	94
4.1	Formation of Heterocummulenes .....	95
4.2	Formation of Nitriles .....	98
5	Conclusions .....	103
	References .....	104

## 1 Nitrogenase, Haber-Bosch, and Catalytic N<sub>2</sub> Fixation

Nitrogen is, next to oxygen, hydrogen, and carbon, one of the main elements found in organic compounds, but atmospheric N<sub>2</sub>, which constitutes about 78 vol% of air and more than 99% of global nitrogen, is chemically highly inert. Hence, its conversion into the more reactive nitrogen source ammonia by biological [1, 2] “nitrogen fixation” was crucial for the development of life. Furthermore, our modern societies strongly rely on the industrial Haber-Bosch process [3, 4] for the production of fertilizers and as feedstock for the chemical synthesis of organic nitrogen compounds, the latter consuming approx. 20% of industrially produced NH<sub>3</sub> [5]. Fundamentally different mechanisms were proposed for the conversion of N<sub>2</sub> via these two processes. Nitrogen fixation by the enzyme [Fe,Mo]-nitrogenase proceeds through a series of alternating nitrogen reduction and protonation steps with gradual N–N bond order reduction. In contrast, heterogeneously catalyzed ammonia synthesis proceeds via initial, turn-over limiting dissociative chemisorption of N<sub>2</sub> on the catalyst surface and subsequent stepwise N–H bond formation. These pathways provide the basis for the development of synthetic catalysts that enable the transformation of N<sub>2</sub> at ambient conditions, which is a longstanding goal. To date, a small number of well-defined, biomimetic homogeneous catalysts were reported [6–8]. Alternative electrochemical and photochemical approaches are currently intensively studied, but still suffer from comparatively low selectivities (H<sub>2</sub> evolution) and energy efficiency [9, 10]. Full N<sub>2</sub>-splitting into well-defined molecular nitrides was also reported on several instances, but homogeneous catalysts that operate via initial N<sub>2</sub>-cleavage remain elusive. However, this approach might offer alternatives to nitrogen fixation beyond NH<sub>3</sub>. Molecular nitride chemistry is well developed and several methods for C–N bond formation starting from nitrides are known [11]. Hence, catalysts that directly transform dinitrogen into nitrogen compounds, such as amines, nitriles, or isocyanates, via N<sub>2</sub>-splitting and nitride transfer cycles are attractive goals and recent examples that demonstrated stoichiometric routes fuel this idea [5, 12]. In this context, the current review focuses on well-defined molecular systems that enable the functionalization of N<sub>2</sub> via initial full cleavage of the N–N bond with the aim at developing some guidelines that ultimately lead to the design of catalysts for the synthesis of value added nitrogen compounds directly from N<sub>2</sub>.

## 2 Bonding in N<sub>2</sub>-Bridged Complexes

### 2.1 General Considerations

The high bond dissociation (941 kJ mol<sup>-1</sup>) and ionization energies (15.6 eV), low proton (5.1 eV) and electron affinities (−1.9 eV), and the lack of a dipole moment all account for the high thermodynamic and kinetic stability of dinitrogen [13–15]. Cleavage of the first N–N bond defines a major challenge and requires about half of the total triple bond energy (410 kJ mol<sup>-1</sup>). In comparison, acetylene features an even stronger triple bond (962 kJ mol<sup>-1</sup>) but the  $\pi$ -bonds are much weaker (222 kJ mol<sup>-1</sup>), which provides a rationale for the higher reactivity compared with N<sub>2</sub> [16]. A wide range of charge transfer to coordinated N<sub>2</sub>-ligands is well documented, reaching from barely activated, neutral N<sub>2</sub> to highly reduced hydrazide [N<sub>2</sub>]<sup>4-</sup> (Table 1). This degree of activation is expressed within spectroscopic (N–N stretching vibration) and structural parameters (N–N bond distance) [17, 18], which are inversely proportional according to Badger's rule [19]. While reduction to diazenide (N<sub>2</sub><sup>2-</sup>) and hydrazide (N<sub>2</sub><sup>4-</sup>) ligands are more commonly observed only a few examples for complexes with [N<sub>2</sub>]<sup>3-</sup> radical anion ligands were reported [20]. The monoanionic N<sub>2</sub><sup>-</sup> radical was only detected in solid matrix upon photodecomposition of metal azide single crystals and adsorbed on MO (M = Mg, Ca) surfaces at low temperatures [21–24]. According to computations, the unknown free radical species HN<sub>2</sub> is endothermic with respect to decay into N<sub>2</sub> and H by  $\Delta E = 9$  kcal/mol and has a lifetime of only around 10<sup>-10</sup> s at room temperature [25]. Hence, the unfavorable one-electron reduction of N<sub>2</sub> emphasizes the use of multi-electron redox catalysts for nitrogen fixation. The current model for nitrogenase also implies initial two-electron N<sub>2</sub>-reduction. These electrons are stored within two Fe–H bonds and charge transfer is triggered by H<sub>2</sub> reductive elimination from the active site [2]. Besides vibrational and structural data, the spin state can also provide information on the redox state of coordinated N<sub>2</sub>-ligands due to magnetic coupling of the metal ion with radical ligands, such as N<sub>2</sub><sup>2-</sup> (S = 1). Alternatively, a covalent picture can be very useful to rationalize bonding with metal ions that have efficient orbital overlap with N<sub>2</sub>-ligands (see below).

Four coordination modes of N<sub>2</sub> to metal ions are most frequently found (Fig. 1), i.e., mononuclear end-on (1), dinuclear end-on (2), dinuclear side-on (3), and

**Table 1** Bond distances and stretching frequencies for free and coordinated nitrogen species

Free N <sub>2</sub> [26]		1.10 Å	2,331 cm <sup>-1</sup>
N≡N	S = 0	≈1.10–1.20 Å	≈1,700–2,331 cm <sup>-1</sup>
[N≡N] <sup>-</sup>	S = ½	n.a.	n.a.
Free H <sub>2</sub> N <sub>2</sub> [27, 28]		1.25 Å	1,583/1,529 cm <sup>-1</sup>
[N=N] <sup>2-</sup>	S = 1	≈1.20–1.35 Å	≈1,200–1,700 cm <sup>-1</sup>
[N=N] <sup>3-</sup> [20]	S = ½	1.40 Å	989–1,040 cm <sup>-1</sup>
Free H <sub>4</sub> N <sub>2</sub> [29]		1.45 Å	885 cm <sup>-1</sup>
[N–N] <sup>4-</sup>	S = 0	≈1.40–1.60 Å	≈700–1,100 cm <sup>-1</sup>

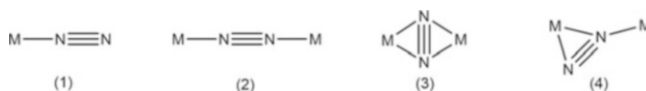
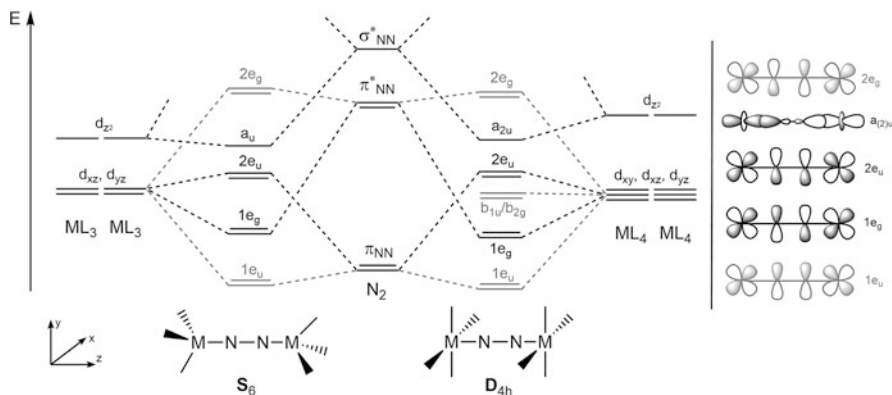


**Fig. 1** Most common bonding motifs in  $N_2$  complexes

dinuclear side-on-end-on (4), with (1) being predominant. More than one metal ion will be required for full 6-electron reduction to nitrides. Therefore, only multinuclear activation is discussed in this review. These coordination modes generally show different degrees of  $N_2$ -activation, which can be attributed to metal- $N_2$  bonding and will therefore be discussed in the next two sections for the more common coordination modes (2) and (3). As an important difference, the terminal binding mode (1) and particularly the side-on modes (3) and (4) generally exhibit enhanced reactivity, e.g., with respect to N–H, N–C, or N–Si bond formation. In contrast, such  $N_2$  functionalization reactions were not observed directly for the end-on bridging mode (2). However, (2) proved to be important en route to full  $N_2$ -splitting into nitrides, which will be discussed below and in Sect. 3.

## 2.2 End-On Bridging $N_2$

The end-on bridging mode,  $M-(\mu-\eta^1-\eta^1-N_2)-M$ , is most frequently observed for dinuclear complexes.  $N_2$  activation upon  $\eta^1$ -coordination to the first metal ion increases the electron density on the ligand thus increasing its basicity for binding of the second metal. Charge delocalization over the whole  $M-N-N-M$  unit in the dinuclear complex further stabilizes the dinuclear binding motif [30]. End-on bridging  $N_2$ -complexes, which are best described by diazenide  $N_2^{2-}$  ( $M-N=N-M$ ) and hydrazide  $N_2^{4-}$  ( $M=N-N=M$ ) resonance structures, are well documented, while radical  $N_2$ -ligands ( $N_2^-$  or  $N_2^{3-}$ ) were not reported in this bonding mode [31]. The charge transfer to the  $N_2$ -ligand can be rationalized based on orbital interactions as first considered by *Gray* and *Chatt* [32, 33].  $N_2$  activation is a consequence of back donation from the metal to the  $N-N$   $\pi^*$ -antibonding orbitals. In threefold symmetry, two metal d-orbitals ( $d_{xz}$ ,  $d_{yz}$ ) are available from each metal ion for  $\pi$ -bonding [46]. Linear combination with the nitrogen  $\pi$  and  $\pi^*$  orbitals gives rise to four sets of degenerate  $\pi$ -orbitals ( $1e_u$ ,  $1e_g$ ,  $2e_u$ ,  $2e_g$ ; Scheme 1). It was pointed out in early theoretical work from *Fenske-Hall* computations that mixing of the  $N-N$   $\pi$ -bonding orbitals with metal d-orbitals is weak, i.e., that occupation of the  $e_u$ -levels contributes to  $M-N$  bonding and  $N_2$  activation to a minor extend [34]. However, the effect of occupation of the  $2e_u$  level on  $N_2$  activation was demonstrated by *Cummins* and coworkers within the redox series  $[(ArfBuN)_3Mo]_2(\mu-\eta^1:\eta^1-N_2)^{n+}$  ( $n = 0-2$ ; Fig. 2; see below for discussion). Besides the  $M-N-N-M$   $\pi$ -manifold, the frontier orbitals are complemented by  $M-N$  bonding MOs ( $a_u/a_{2u}$ ) that result from mixing of metal  $d_{22}$ -orbitals with the  $N-N$   $\sigma$ -antibonding orbital [37, 101]. This MO is strongly  $N-N$  antibonding in



**Scheme 1** Qualitative orbital interaction diagram for end-on N<sub>2</sub> bridged dinuclear complexes in threefold and fourfold geometry (*left*) and symmetry of the M–N–N–M  $\sigma$ - and  $\pi$ -type MOs (*right*) as an extension of Fryzuk's scheme [46]. MOs less relevant for N<sub>2</sub>-activation and splitting drawn in grey

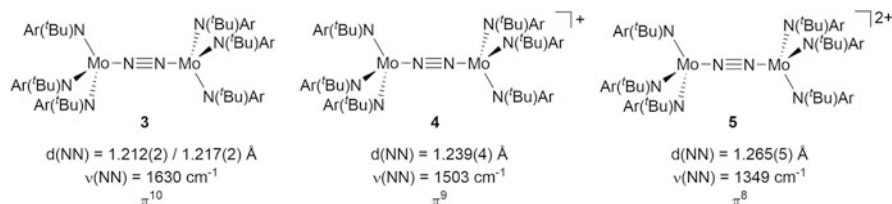


**Fig. 2** Bond distances, stretching frequencies, and number of electrons in the MNNM  $\pi$ -system for  $\{\text{Mo}[\text{N}(\text{tBu})(\text{Ar})]_3\}_2(\mu\text{-}\eta^1\text{-}\eta^1\text{-N}_2)^{n+}$  ( $n = 0\text{--}2$ ) [36, 37]

nature. Hence, its occupation strongly weakens the N<sub>2</sub> bond. Furthermore, it drops in energy upon splitting the N<sub>2</sub>-complex into terminal nitrides (see Scheme 7). In addition to these  $\sigma$ - and  $\pi$ -M<sub>2</sub>N<sub>2</sub> interactions, in fourfold symmetry (octahedral or square pyramidal geometry) two metal-based non-bonding MOs with  $\delta/\delta^*$ -character are derived from  $d_{xy}$ . In threefold symmetry these MOs should be much higher in energy due to interaction with the auxiliary ligands.

Based on this simple qualitative MO scheme, the degree of N<sub>2</sub>-activation can be correlated to  $\pi$ -orbital occupancy within closely related systems upon filling the MOs with the four electrons from N<sub>2</sub>  $\pi$ -bonding and the valence electrons contributed from the two ML<sub>*n*</sub> fragments. Occupation of the  $e_g$  levels weakens the N–N bond in contrast to the MOs with  $e_u$  symmetry. Hence, it is evident that a  $\pi^8$  valence electron configuration should result in maximal N<sub>2</sub> bond weakening. For example, the N<sub>2</sub>-bridged diruthenium complex  $[(\text{NH}_3)_5\text{RuN}_2\text{Ru}(\text{NH}_3)_5]^{4+}$  (**1**) exhibits a  $\pi^{12}$  configuration ( $(1e_u)^4(1e_g)^4(b_{1u})^2(b_{2u})^2(2e_u)^4(2e_g)^0$ ) with a very small degree of N<sub>2</sub> bond weakening ( $d_{\text{NN}} = 1.12$  Å,  $\nu_{\text{NN}} = 2,100$   $\text{cm}^{-1}$ ) [32]. In contrast, the bimetallic complex  $[(\text{PMe}_2\text{Ph})_4\text{ClReN}_2\text{MoCl}_4(\text{OMe})]$  (**2**) with  $\pi^8$  configuration ( $(1e_u)^4(1e_g)^4$ )



$(b_{1u})^2(b_{2u})^1(2e_u)^0(2e_g)^0$ ) displays much stronger  $N_2$ -activation ( $d_{NN} = 1.21 \text{ \AA}$ ,  $\nu_{NN} = 1,660 \text{ cm}^{-1}$ ) [35].

This dependence of the degree of activation on valence electron configuration is nicely reflected within the redox series  $[(Ar\text{tBuN})_3Mo]_2(\mu-\eta^1:\eta^1-N_2)]^{n+}$  ( $n = 0$  (**3**), 1 (**4**), 2 (**5**); Ar = 3,5- $C_6H_3Me_2$ ; Fig. 2) reported by Cummins and coworkers [36, 37]. According to this model, these compounds adopt  $(1e_u)^4(1e_g)^4(2e_u)^{(2-n)}(2e_g)^0$  configurations, i.e., 10 ( $n = 0$ , **3**), 9 ( $n = 1$ , **4**), and 8 ( $n = 2$ , **5**) electrons in Mo–N–N–Mo  $\pi$ -type orbitals, respectively. The electronic triplet (**3**), doublet (**4**), and singlet (**5**) ground states and the increasing activation upon oxidation of the parent  $\pi^{10}$  system **3** (Fig. 2) are in agreement with the bonding model. Interestingly, while **4** and **5** are thermally stable, only the supposedly least activated  $N_2$ -complex **3** splits into the terminal nitrides  $[NMo(N\text{tBuAr})_3]$  [38]. Splitting of the  $\pi^{10}$ -dimer **3** produces two closed shell, pseudo-tetrahedral molybdenum(VI) nitrides. As the N–N  $\sigma$ -antibonding  $a_u$ -orbital drops in energy upon splitting, two electrons are transferred from the  $\pi$ - to the  $\sigma$ -manifold (Scheme 7). In comparison, the oxidized dimers **4** and **5** are short by one and two electrons, respectively, to form nitrides where all M–N  $\sigma$ - and  $\pi$ -bonding orbitals are fully occupied. These simple considerations emphasize the preference for a  $\pi^{10}$ -configuration in splitting of linearly  $N_2$ -bridged dinuclear complexes into terminal nitrides. The same arguments were applied to analogous systems, which are discussed in more detail in Sect. 3.

The subtle influence of different metals within strongly related coordination spheres on  $N_2$ -activation was systematically examined by Sita and coworkers. They reported a series of group 4–6  $\eta^5$ -cyclopentadienyl/ $\eta^2$ -amidinate complexes ( $am = N(iPr)C(Me)N(iPr)$ ; M = Ti (**6**), Zr (**7**), Hf (**8**), V (**9**), Nb (**10**), Ta (**11**), Mo (**12**), W (**13**); Fig. 3 and Table 2) [39–41]. Except for Zr and Hf, isostructural end-on bridging  $N_2$ -coordination was found. The diamagnetic Ti-complex **6** was described as two  $Ti^{III}$   $d^1$ -ions spin-coupled with an  $N_2^{2-}$  bridge. The high fourth ionization potential of Ti prevents further reduction of  $N_2$  [42]. Slightly less activation was observed for the analogous vanadium complex **9**, leading to the description as two antiferromagnetically coupled  $V^{II}$ -ions bridged by  $N_2$ , which qualitatively reflects the decreased reduction potential compared with titanium. The higher degree of activation for the niobium and tantalum dimers **10** and **11** also reflects the trends in reduction potential upon moving down group 5. These compounds were described as containing  $Ta^{IV}$  and  $Nb^{IV}$ , respectively, which are bridged by  $[N_2]^{4-}$  ligands. For **11**, preliminary magnetic data supported a singlet ground state and thermally populated triplet state with antiferromagnetic exchange above 2K. **11** also splits the strongly reduced  $N_2$ -ligand to form the tantalum(V)

**Fig. 3** Sita's isostructural  $(Cp^*amM)_2(\mu-N_2)$  complexes

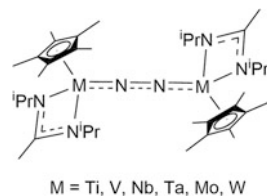


**Table 2** N–N bond distances in (Cp<sup>\*</sup>amM)<sub>2</sub>(μ-N<sub>2</sub>) complexes

Metal	Coordination mode	d(NN) [Å]	Reference
Ti ( <b>6</b> )	(μ-η <sup>1</sup> -η <sup>1</sup> -N <sub>2</sub> )	1.270(2)	[40]
Zr <sup>a</sup> ( <b>7</b> )	(μ-η <sup>2</sup> -η <sup>2</sup> -N <sub>2</sub> )	1.518(2)	[43]
Hf ( <b>8</b> )	(μ-η <sup>2</sup> -η <sup>2</sup> -N <sub>2</sub> )	1.611(4)	[43]
V ( <b>9</b> )	(μ-η <sup>1</sup> -η <sup>1</sup> -N <sub>2</sub> )	1.225(2)	[41]
Nb <sup>b</sup> ( <b>10</b> )	(μ-η <sup>1</sup> -η <sup>1</sup> -N <sub>2</sub> )	1.300(3)	[41]
Ta ( <b>11</b> )	(μ-η <sup>1</sup> -η <sup>1</sup> -N <sub>2</sub> )	1.313(4)	[39]
Mo ( <b>12</b> )	(μ-η <sup>1</sup> -η <sup>1</sup> -N <sub>2</sub> )	1.267(2)	[40]
W ( <b>13</b> )	(μ-η <sup>1</sup> -η <sup>1</sup> -N <sub>2</sub> )	1.277(8)	[40]

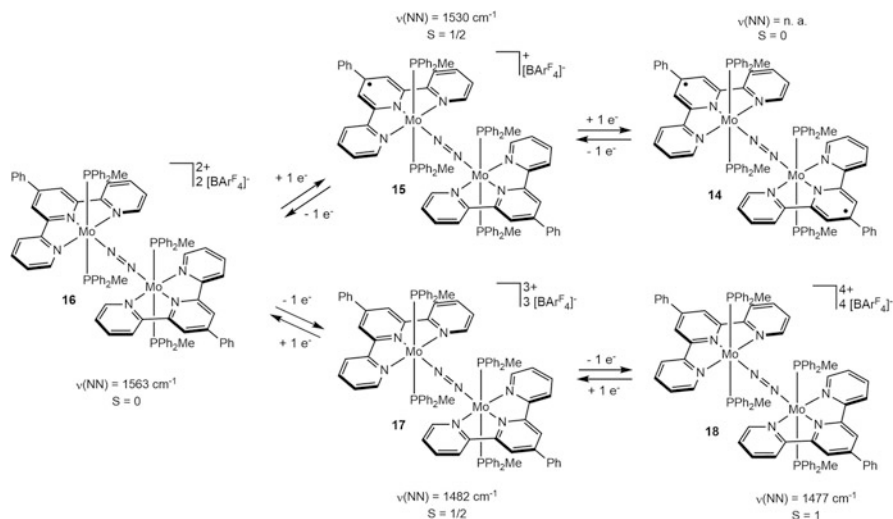
<sup>a</sup>Exchange of methyl group in amidinate against NMe<sub>2</sub><sup>b</sup>Exchange of methyl group in amidinate against phenyl

nitride bridged complex [(Cp<sup>\*</sup>(am)Ta)<sub>2</sub>(μ-N)<sub>2</sub>] above 0°C. In turn, the diamagnetic group 6 analogues **12** and **13** are again in agreement with decreasing reduction potential and show weaker activation of the N<sub>2</sub> bridge compared to Nb and Ta. While **12** and **13** are thermally stable, N<sub>2</sub>-splitting was realized photochemically (c.f. Sect. 3).

Strong ligand influences on N<sub>2</sub>-activation are also well documented. An instructive example was provided by the group of *Chirik*, who reported the isolation of the extensive terpyridine dimolybdenum dinitrogen series [(<sup>Ph</sup>Tpy)(PPh<sub>2</sub>Me)<sub>2</sub>Mo]<sub>2</sub>(μ-η<sup>1</sup>:η<sup>1</sup>-N<sub>2</sub>)[BAR<sup>F</sup><sub>4</sub>]<sub>n</sub> (*n* = 0 (**14**), 1 (**15**), 2 (**16**), 3 (**17**), 4 (**18**); Scheme 2) [44]. Spectroscopic data of the dicationic complex **16** indicates an N<sub>2</sub><sup>2-</sup> bridge. DFT computations support a π<sup>10</sup>(δ<sup>4</sup>) configuration, yet with a singlet ground state as the degeneracy of the frontier π\*-MOs is strongly lifted due to electronic coupling with the Tpy ligand. Single and double oxidation leads to stronger N<sub>2</sub>-activation as the electrons are removed from the N–N bonding π\*-orbital. Intriguingly, reduction also results in N–N bond weakening since the SOMO of **15** is Tpy-ligand centered, which was also found for the second reduction. The use of redox active ligands for electron storage provides an attractive approach for multi-electron redox reactions like nitrogen fixation.

### 2.3 Side-On Bridging N<sub>2</sub>

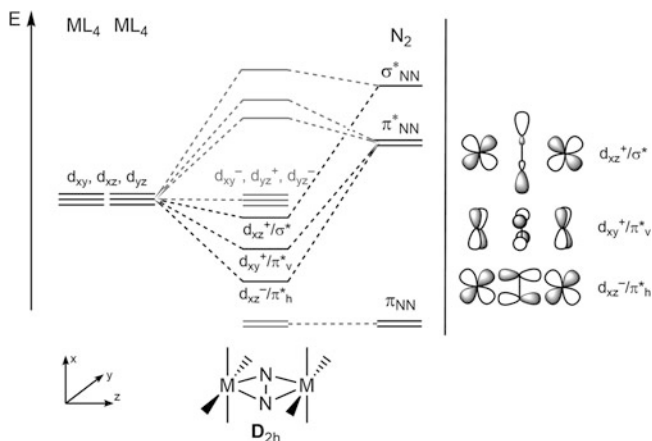
The side-on N<sub>2</sub>-bridging coordination mode is less common in dinuclear complexes than end-on coordination [17, 45, 46]. First evidence was provided by the linkage isomerization of the isotopomers of [(NH<sub>3</sub>)<sub>5</sub>Ru(<sup>14/15</sup>N<sub>2</sub>)]<sup>2+</sup> which is too fast to proceed via N<sub>2</sub> dissociation, suggesting intermediate side-on coordination [47]. The first structurally characterized side-on N<sub>2</sub> complex, a polynuclear nickel-lithium compound, was reported in 1973 [48, 49]. By now, several other examples were reported, mostly with early transition metals and f-block elements, exhibiting varying degrees of activation, as exemplified by *Evans*' [(Cp<sup>\*</sup><sub>2</sub>Sm)<sub>2</sub>(μ-η<sup>2</sup>:η<sup>2</sup>-N<sub>2</sub>)] (**19**, d<sub>NN</sub> = 1.088(12) Å) vs. *Fryzuk*'s [(PNP)ZrCl]<sub>2</sub>(μ-η<sup>2</sup>:η<sup>2</sup>-N<sub>2</sub>)] (**20**,



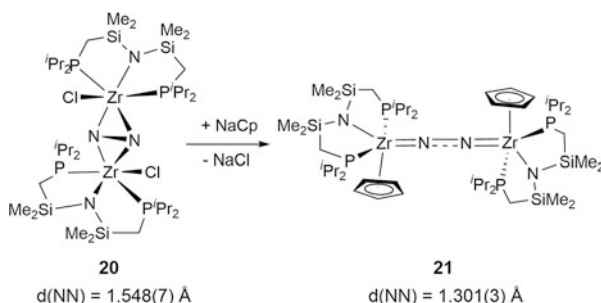
**Scheme 2**  $\{[(^{\text{Ph}}\text{Tpy})(\text{PPh}_2\text{Me})_2\text{Mo}]_2(\mu\text{-}\eta^1\text{-}\eta^1\text{-N}_2)\}[\text{BAr}^{\text{F}}_4]_n$  ( $n = 0\text{--}4$ ) redox series reported by Chirik and coworkers [44]

[PNP] = (*i*Pr<sub>2</sub>PCH<sub>2</sub>SiMe<sub>2</sub>)<sub>2</sub>N (d<sub>NN</sub> = 1.548(7) Å) [50, 51]. Bonding of the two metal centers with side-on bound N<sub>2</sub> is more complex compared with the end-on isomer, as considerable distortion from planarity of the M<sub>2</sub>N<sub>2</sub> core is often observed. A simplified model for two side-on N<sub>2</sub>-bridged square-pyramidal ML<sub>4</sub> fragments is shown in Scheme 3, based on considerations first described by Fryzuk and coworkers [46]. Metal N<sub>2</sub> bonding should be dominated by back donation from suitable d-orbitals into the N<sub>2</sub> π\*-orbitals. In contrast to end-on coordination, only one π-interaction results from out of phase combination of the two d<sub>xz</sub> orbitals and the horizontal N<sub>2</sub> π\*-level. In addition, an interaction with δ-symmetry is constructed by the in-phase d<sub>xy</sub> combination with the vertical N<sub>2</sub> π\*-orbital. Both MOs are N–N antibonding in character. However, weaker orbital overlap for the δ-with respect to π-interactions suggests an energetic preference for end-on N<sub>2</sub>-coordination. In fact, isolable mononuclear complexes with side-on terminal η<sup>1</sup>-η<sup>1</sup>-N<sub>2</sub>-coordination remain unknown [52].

One reason for the occurrence of side-on bridging N<sub>2</sub>-ligands can be the absence of an accessible d-orbital that is suitable to form the second π-bond. Semi-empirical computations for the model complex  $\{[\text{Zr}(\text{Cl})\text{N}(\text{SiH}_2\text{CH}_2\text{PH}_2)_2]_2(\mu\text{-}\eta^2\text{:}\eta^2\text{-N}_2)\}$  confirmed this picture revealing that one of the d-orbitals required for π-bonding is raised in energy due to π-donation by the amide and chloride ligands [46]. In fact, ligand exchange of chloride vs. cyclopentadienide (Cp) results in N<sub>2</sub> linkage isomerization and isolation of the end-on bridged complex  $\{[(\text{PNP})\text{ZrCp}]_2(\mu\text{-}\eta^1\text{:}\eta^1\text{-N}_2)\}$  (**21**, Scheme 4) [46]. Hence, exchange of chloride by Cp stabilizes the end-on coordination by reducing the Cl<sup>−</sup>/N<sub>2</sub> π-MO competition and destabilizes the side-on coordination as the Cp ligand overlaps with a d-orbital that would be required for



**Scheme 3** Qualitative orbital interaction diagram for side-on N<sub>2</sub> bridged dinuclear complexes (*left*) and symmetry of the relevant MOs (*right*) as an extension of Fryzuk's scheme [46]. MOs less relevant for N<sub>2</sub>-activation and splitting drawn in grey



**Scheme 4** Transformation of side-on to end-on N<sub>2</sub> configuration by ligand exchange [46]

$\delta$ -bonding with a side-on N<sub>2</sub> complex. The remaining N<sub>amide</sub>-Zr-N<sub>2</sub>  $\pi$ -interaction is expressed in an unusually long Zr-N<sub>amide</sub> bond of **21** (2.306(3)/2.303(3) Å) [53, 54]. Bonding analysis of the zirconium system on a higher computational level (DFT) by Tuzcek and coworkers qualitatively confirmed the earlier picture and showed that distortion of the M<sub>2</sub>N<sub>2</sub> core from planarity to a butterfly structure aids at charge delocalization of the N<sub>2</sub>-ligand [55]. Furthermore, the LUMO was described as a non-bonding, metal-based MO from out of phase combination of two d<sub>xy</sub> orbitals (d<sub>xy</sub><sup>-</sup>). Slightly higher, an MO was found from combination of metal d-orbitals with the N<sub>2</sub>  $\sigma^*$ -orbital (drawn below d<sub>xy</sub><sup>-</sup> in simplified Scheme 3). Occupation of this MO should strongly weaken the N–N bond. However, the Zr<sub>2</sub>N<sub>2</sub> core does not contain enough electrons for full N<sub>2</sub> cleavage. In contrast, model computations for [SiMe<sub>3</sub>N(CH<sub>2</sub>CH<sub>2</sub>NSiMe<sub>3</sub>)<sub>2</sub>V]<sub>2</sub>( $\mu$ - $\eta^2$ : $\eta^2$ -N<sub>2</sub>), which in fact splits the N<sub>2</sub>-ligand into the dinitride bridged divanadium(V) isomer [56], indicate the population of such an MO with N<sub>2</sub>  $\sigma^*$ -character [57, 58]. Together

with the filled  $N_2$   $\pi$ -orbitals, this picture emphasizes an overall  $\pi^8\delta^2$  valence electron configuration to be favorable for  $N_2$ -splitting for the side-on coordination. Importantly, comparison of the two simplified MO-schemes for end-on ( $D_{4h}$ ) and side-on ( $D_{2h}$ ) coordination suggests that a lower valence electron count of the  $ML_4$  fragments is required for splitting from the side-on linkage isomer. This is in fact corroborated by computational DFT analysis of the conversion of  $[\{Cp^*(am)Ta\}_2(\mu-N_2)]$  into  $[\{Cp^*(am)Ta\}_2(\mu-N)_2]$  [41, 59]. The proposed mechanism proceeds via initial isomerization of the triplet end-on ( $\pi^8$ ) to the singlet side-on ( $\pi^8\delta^2$ ) form prior to  $N_2$ -splitting, in full agreement with this very simple model.

The electronic structures of  $[\{R_2M\}_2(\mu-\eta^2:\eta^2-N_2)]$  ( $M = \text{group 4-9}$ ,  $R = \text{amide, cyclopentadienide}$ ) complexes with planar  $M_2N_2$ -cores were examined computationally by *Stranger* and coworkers [60]. An increase in activation was found upon descending a group, presumably due to more diffuse d-orbitals resulting in better overlap. Furthermore, the conformation of  $M(NH_2)_2$  fragments with respect to the  $M_2N_2$ -core was predicted to have a strong impact on  $N_2$  activation and cleavage. In general, perpendicular arrangement leads to stronger activation due to better electron delocalization into the MNNM moiety. Moving along the transition series eventually results in  $N_2$ -splitting as predicted by the simple model in Scheme 3. Additional metal–metal interactions stabilize the nitride bridged products.

Besides these electronic considerations, sterics also play an important role, as the two metal moieties are closer in the side-on bonding mode. This was demonstrated for a series of zirconocenes [61, 62]. In contrast to *Bercaw's* classic decamethylzirconocene dimer  $[\{Cp^*_2Zr(\eta^1-N_2)\}_2(\mu-\eta^1-\eta^1-N_2)]$  (**22**;  $Cp^* = C_5Me_5$ ) and analogous  $[\{Cp^*Cp'Zr(\eta^1-N_2)\}_2(\mu-\eta^1:\eta^1-N_2)]$  (**23**;  $Cp' = C_5Me_4H$ ), removal of a second methyl group results in the side-on bridged octamethylzirconocene dimer  $[(Cp'_2Zr)_2(\mu-\eta^2:\eta^2-N_2)]$  (**24**) with side-on bridging  $N_2$  (Fig. 4) [63–65]. DFT calculations predict the relative stability of side-on  $N_2$  bridged isomers to increase down group 4 in the periodic table [42]. This trend is confirmed experimentally for the series  $[(Cp^*amM)_2(\mu-N_2)]$  ( $M = Ti, Zr, Hf$ ), which exhibits end-on for Ti (**6**) and side-on configuration for the Zr (**7**) and Hf (**8**) complexes (Table 2) [40]. It is assumed that only the larger Zr and Hf (ionic radii: 1.75 Å) are able to accommodate the more crowded side-on coordination, while the smaller homologue Ti (1.60 Å) and other metals like V (1.53 Å), Nb (1.64 Å), or Mo (1.54 Å) adopt the end-on bonding motif with this ligand set.

An important difference between end-on and side-on bridging coordination is the reactivity. In fact, the only  $N_2$ -functionalization reaction that is known for the end-on bridging mode is splitting into nitrides. In contrast, reactions like C–N coupling with CO, which can lead to full scission of the N–N bond, are well

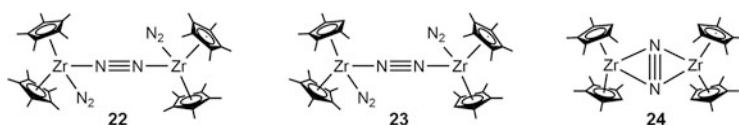
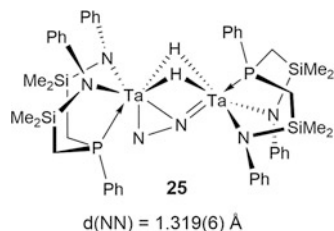


Fig. 4 Steric effect on end-on vs. side-on  $N_2$  binding

**Fig. 5** Side-on end-on N<sub>2</sub> bridged tantalum complex [68]



documented for side-on bonding [63, 66] and computations indicate that side-on binding is a prerequisite for N<sub>2</sub>-hydrogenation [67]. Related reactivity was also observed for the rare, side-on/end-on coordination mode, e.g., for [ $\{(\text{NPN})\text{Ta}\}_2(\mu\text{-H})_2(\mu\text{-}\eta^1\text{:}\eta^2\text{-N}_2)$ ] (**25**, NPN = (Ph)P(CH<sub>2</sub>SiMe<sub>2</sub>NPh)<sub>2</sub>) (Fig. 5) [68, 69]. This compound is formed upon reaction of dinuclear Ta(IV) hydride complex [ $\{(\text{NPN})\text{Ta}\}_2(\mu\text{-H})_4$ ] (NPN = PhP(CH<sub>2</sub>SiMe<sub>2</sub>NPh)<sub>2</sub>) with N<sub>2</sub> under partial release of H<sub>2</sub>. Hence, the reducing equivalents for N<sub>2</sub> reduction are stored in two Ta–H bonds providing an early model for nitrogenase reactivity. The energetic advantage of maintaining the remaining bridging hydrides, which force the two metal centers in **25** in close proximity, is believed to prevail over the energy difference to dinuclear end-on coordination. Subsequent treatment with boranes [70], silanes [71–73], alanes [74], zirconocenes [75], or with 1,2-cumulenes [76] led to full cleavage of the dinitrogen bond.

### 3 Splitting of N<sub>2</sub> into Nitride Complexes of Group 6 Elements and Beyond

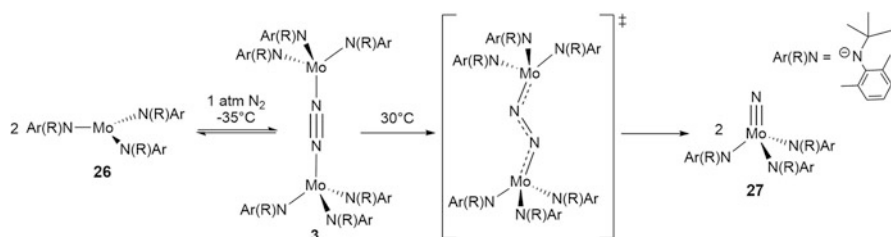
As discussed in Sect. 2, the type of metal, oxidation state, coordination geometry, ligand type, and electronic configuration are essential features that govern the ability of N<sub>2</sub>-bridged multinuclear complexes to split into nitrides. In this section, we want to illustrate these principles with a comprehensive overview over N<sub>2</sub>-splitting reactions mediated by mid to late transition metal complexes (group 6–8). Other examples from group 4–5 and f-block chemistry are not part of this section, but will be covered by other reviews in this book.

#### 3.1 N<sub>2</sub>-Splitting by Homoleptic Group 6 Amide Complexes

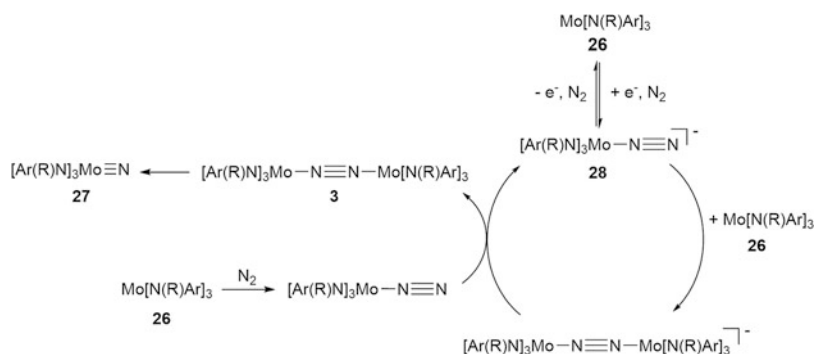
Arguably the best examined system regarding both N<sub>2</sub>-splitting and transfer of the resulting nitride ligands is *Cummins'* molybdenum triamides, which also marks the first example for N<sub>2</sub>-cleavage into well-defined nitrides [36, 38]. [ $(\text{Ar}t\text{BuN})_3\text{Mo}(\mu\text{-}\eta^1\text{-}\eta^1\text{-N}_2)\text{Mo}(\text{N}t\text{BuAr})_3$ ] (**3**, Ar = 3,5-C<sub>6</sub>H<sub>3</sub>Me<sub>2</sub>) forms upon reaction of the isolable molybdenum(III) complex [ $\text{Mo}(\text{N}t\text{BuAr})_3$ ] (**26**) at –35°C under N<sub>2</sub>

(1 atm) and splits into the molybdenum(VI) nitrides  $[\text{NMo}(\text{N}t\text{BuAr})_3]$  (**27**) when warmed to room temperature (Scheme 5) in near quantitative yield.  $\text{N}_2$ -splitting was computed to be exothermic by about 20 kcal/mol [77], but  $\text{N}_2$ -uptake on this route requires several days. It can be significantly accelerated by addition of reductants, and isolation of terminal dinitrogen complex  $\text{Na}[(\text{N}_2)\text{Mo}(\text{N}t\text{BuAr})_3]$  (**28**) allowed for the proposal of a redox-catalytic mechanism (Scheme 6) [78].

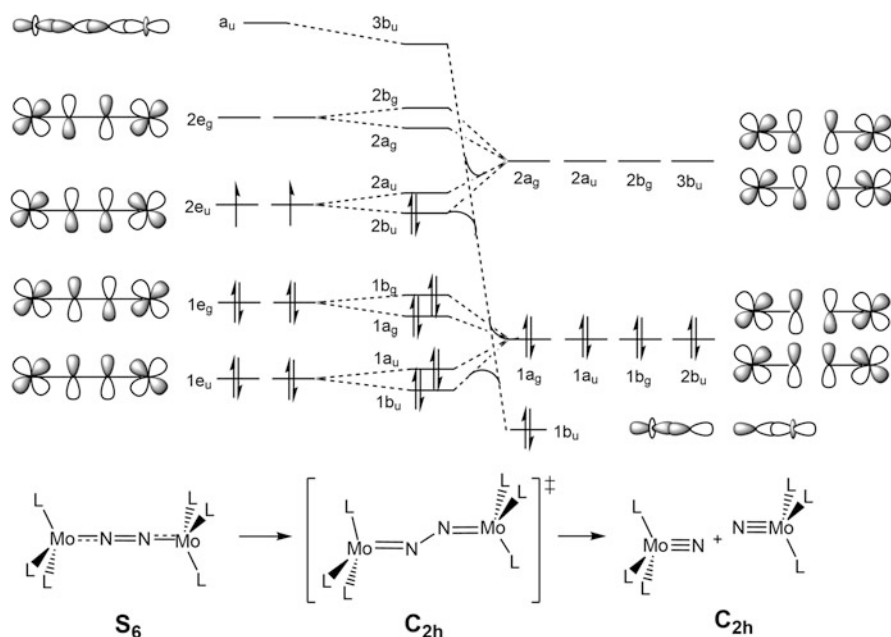
The spectroscopic, magnetic, and structural features of intermediate **3** indicate moderate to strong  $\text{N}_2$ -activation, in agreement with  $\text{Mo}^{\text{IV}}\{\text{N}_2^{2-}\}\text{Mo}^{\text{IV}}$  and the covalent  $\pi^{10}$  bonding model described above [36, 37]. The reaction can also be rationalized by extension of the  $\pi$ -MO scheme in the dimer. Full splitting into nitride complexes requires additional charge transfer to the  $\text{N}_2$ -ligand, more exactly form the  $2e_u$   $\pi$ -orbitals to the  $a_u$   $\sigma^*$ -MO of triplet **3** (Scheme 7), which drops in energy upon N–N bond cleavage and formation of the closed-shell molybdenum (VI) nitride products. Hence, dissociation of the dimer along the N–N bond vector is symmetry forbidden but requires breaking of the high symmetry of **3** ( $S_6$ ) for  $\sigma/\pi$ -MO-mixing. Accordingly, *Morokuma* and coworkers computed a zigzag transition state (TS) with approximate N–N single bond character for model complex  $[(\text{NH}_2)_3\text{MoN}_2\text{Mo}(\text{NH}_2)_3]_2$  [77]. In the TS the antibonding character of the  $3b_u$  is reduced upon M–N–N–M bending and mixing with the  $2b_u$  orbital enabling charge



**Scheme 5** Cleavage of  $\text{N}_2$  in terminal nitrides mediated by a triamido molybdenum(III) complex [38]



**Scheme 6** Redox-catalytic mechanism for  $\text{N}_2$ -splitting from **26** into **27** [78]



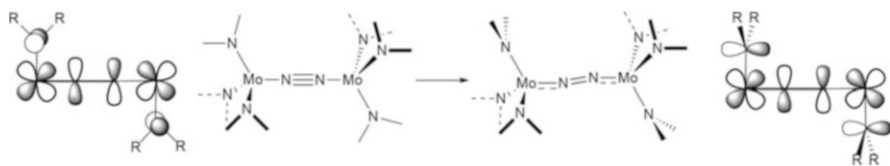
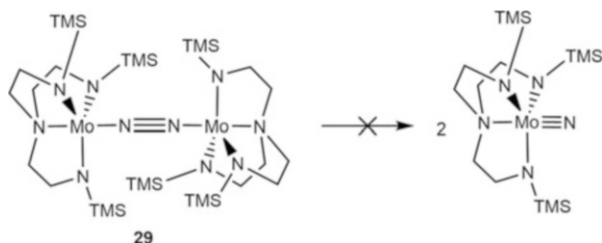
**Scheme 7** MO scheme for N<sub>2</sub> cleavage in terminal nitrides out of a Mo(III) dinuclear dimer in S<sub>6</sub> symmetry [36]

transfer to the nitride. This picture also resolves the apparent dichotomy observed for the oxidized compounds [(Ar*t*BuN)<sub>3</sub>Mo(μ-η<sup>1</sup>-η<sup>1</sup>-N<sub>2</sub>)Mo(N*t*BuAr)<sub>3</sub>]<sup>+</sup> (**4**) and [(Ar*t*BuN)<sub>3</sub>Mo(μ-η<sup>1</sup>-η<sup>1</sup>-N<sub>2</sub>)Mo(N*t*BuAr)<sub>3</sub>]<sup>2+</sup> (**5**). While the π<sup>9</sup> (**4**) and π<sup>8</sup> (**5**) configurations exhibit stronger N<sub>2</sub> activation (see Sect. 2) in the ground state, they are short by one and two electrons, respectively, to split into stable closed-shell nitrido complexes.

An interesting comparison is given with *Schrock's* related triamidoamine dimer [(R'*N*CH<sub>2</sub>CH<sub>2</sub>)<sub>3</sub>NMo]<sub>2</sub>(μ-η<sup>1</sup>:η<sup>1</sup>-N<sub>2</sub>) (**29**, R' = *t*BuMe<sub>2</sub>Si) [36, 79, 80]. Both **3** and **29** exhibit the same formal oxidation and spin states and display similar structural parameters within the central Mo–N–N–Mo moiety. However, *Schrock's* dimer does not split into the respective nitrides (Scheme 8), which could be prepared on another route. This observation can be attributed to the *trans*-influence of the additional amine donor, which destabilizes σ-bonding with the nitride ligand and the a<sub>u</sub> orbital in the dimer. Hence, splitting is both thermodynamically and kinetically more unfavorable and splitting of a simplified model of **29** was calculated to be endothermic [77]. Computational work on truncated models by *Stranger* and coworkers suggests that the conformational rigidity of the triamidoamine vs. the monodentate amido ligands might also contribute to the difference in reactivity [81, 82]. Rotation of an amido ligand by 90° increases charge transfer from the metal to N<sub>2</sub> (Scheme 9). This conformation also stabilizes an electronic singlet with respect to the triplet state, en route to the singlet zigzag transition state. However, in



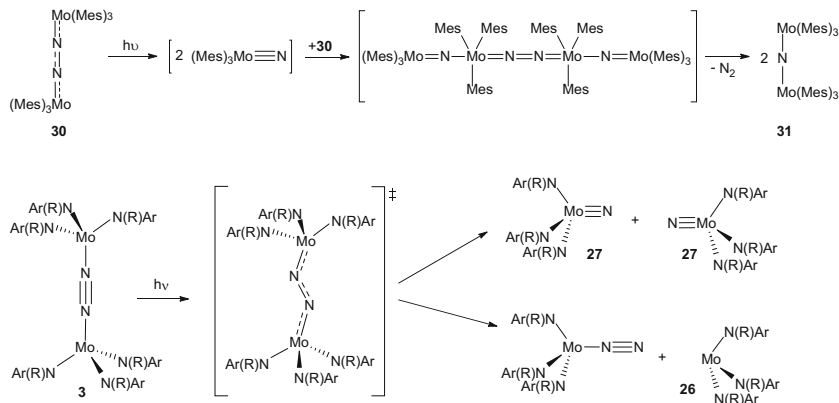
**Scheme 8** Comparison of *Schrock's* triamidoamine Mo(III) and *Cummins'* triamido Mo(III) N<sub>2</sub> dimers towards N<sub>2</sub> cleavage



**Scheme 9** Rotation of one NR<sub>2</sub> group at each Mo center in [Mo(NR<sub>2</sub>)<sub>3</sub>]<sub>2</sub>(μ-N<sub>2</sub>)

agreement with the experimentally confirmed triplet ground state of **3** [37], computations on full **3** revealed that the bulky *tert*-butylamide ligands strongly destabilize the singlet and N<sub>2</sub>-splitting might in fact not pass through this intermediate [83].

$\pi$ -Donor ancillary ligands generally lead to stronger N<sub>2</sub> activation and more exothermic splitting [77, 81]. In fact, the triaryl analogue [(Mes<sub>3</sub>Mo)<sub>2</sub>( $\mu$ - $\eta^1$ : $\eta^1$ -N<sub>2</sub>)] (**30**, Mes = 2,4,6-Me<sub>3</sub>C<sub>6</sub>H<sub>2</sub>) reported by *Floriani* and coworkers is stable in refluxing benzene [84]. However, irradiation in the UV range ( $\lambda = 365.0$  nm) produces the nitride bridged dimer [(Mes<sub>3</sub>Mo)<sub>2</sub>( $\mu$ -N)] (**31**), which marked the first example of photochemical N<sub>2</sub>-splitting. The authors proposed a mechanism (Scheme 10, top) via initial photolysis into monomeric nitrides, which form a transient tetranuclear intermediate with parent **30** and finally the nitride bridged dinuclear product **31** after N<sub>2</sub>-loss. *Cummins* proposed an alternative mechanism based on detailed examination of the triamido platform. Bulk irradiation of **3** with visible light ( $\lambda \geq 480$  nm) at  $-78^\circ\text{C}$  produces a 1:1 mixture of nitride **27** and parent [Mo(*Nt*BuAr)<sub>3</sub>] **26** (Scheme 10, bottom) [37]. Frequency resolved pump-probe spectroscopy revealed that excitation at 2.3 eV creates an excited triplet state, which relaxes through internal conversion (IC) within 300 fs. to a vibrationally excited ground state [85]. Rapid cooling of the hot ground state (sub-ps) explains the modest quantum yield ( $\Phi = 0.05$ ) for the two Mo–N and N–N dissociative reaction channels. Importantly, coupling of IC with structural distortions of the Mo–N–N–Mo core facilitates the entry into the higher barrier N–N cleavage channel through the singlet zigzag transition state and thereby compensates the thermal bias for Mo–N cleavage, which results in the photochemical 1:1 product mixture. Such distortions were predicted computationally for the photochemical states of linearly bridged diiron and -ruthenium  $\mu$ -N<sub>2</sub> complexes (M = Fe, Ru) by *Reiher* et al. [86].

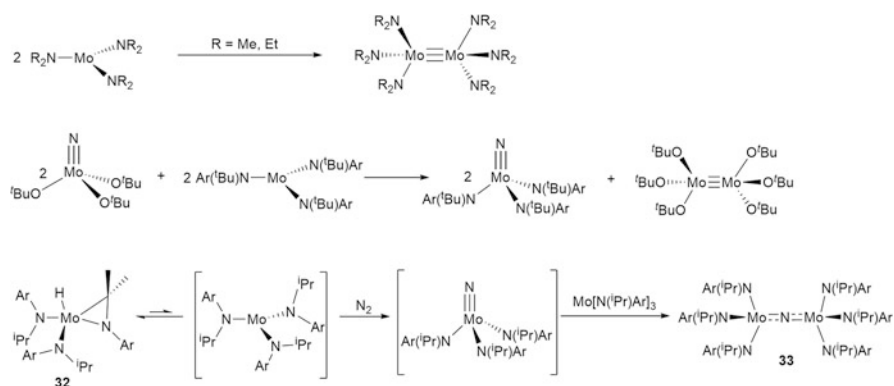


**Scheme 10** Proposed photolysis mechanisms for *Floriani's* dimer **30** (top) and *Cummins'* dimer **3** (bottom) [37, 84]

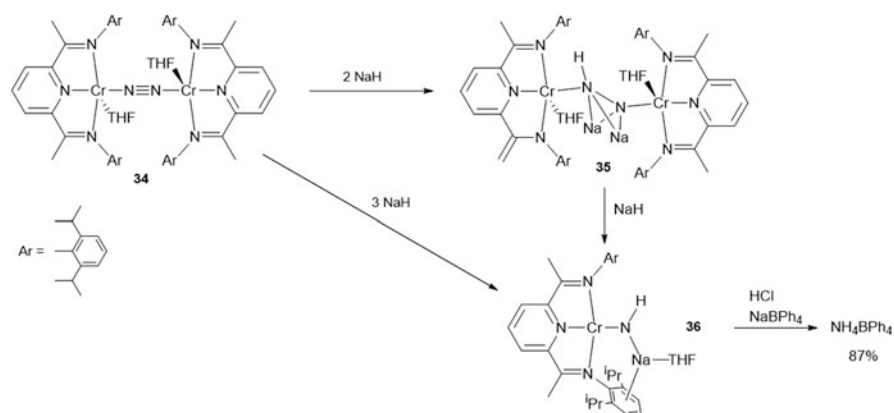
The necessity for **3** to distort from linearity for N–N bond cleavage indicates that ligand sterics are crucial not only for the formation of N<sub>2</sub>-bridged complexes but also for splitting into nitrides. For example, [Mo(NAdAr)<sub>3</sub>] (Ad = 1-adamantyl) does not form nitrides under N<sub>2</sub>, presumably due to the excessive steric bulk of the amide ligands [78]. However, steric shielding is required to prevent metal–metal bonding and formation, as found for Mo<sub>2</sub>(NR<sub>2</sub>)<sub>6</sub> (NR<sub>2</sub> = NMe<sub>2</sub>, NMeEt, NEt<sub>2</sub>), which do not react with N<sub>2</sub> (Scheme 11, top) [87]. These considerations were confirmed by DFT computations [88]. For the same reason, use of alkoxide ligands was unsuccessful, although rapid nitride transfer between the alkoxide and amide platforms was demonstrated (Scheme 11, mid) [89–91]. N<sub>2</sub>-splitting with a smaller isopropylamide ligand was also reported (Scheme 11, bottom). However, in case of the *iso*-propylamide metal–metal bond formation is suppressed by reversible methyne C–H cyclometalation [92]. Reaction of [MoH(η<sup>2</sup>-Me<sub>2</sub>C=NAr)(NiPrAr)<sub>2</sub>] (**32**) with N<sub>2</sub> gives the nitride bridged complex [{(Ar'PrN)<sub>3</sub>Mo}<sub>2</sub>(μ-N)] (**33**). The proposed mechanism implies a CH reductive elimination preequilibrium, N<sub>2</sub>-splitting, and dimerization with the parent triamide. Mixing **32** and [NMo(NiPrAr)<sub>3</sub>] gives the same product.

### 3.2 N<sub>2</sub>-Splitting by Group 6 and 7 Pincer Complexes

Tridentate, monoanionic, meridionally coordinating (“pincer”) ligands are extensively used in small molecule activation and homogeneous catalysis [93, 94]. Bulky substituents aid in enforcing rigid square-planar, square-pyramidal, or octahedral coordination geometries and direct the reactivity to predefined sites. Four accounts on N<sub>2</sub> cleavage into nitrides with group 6 and 7 complexes were reported that carry pincer-type or related ligands. *Schrock* pointed out that N<sub>2</sub> activation with



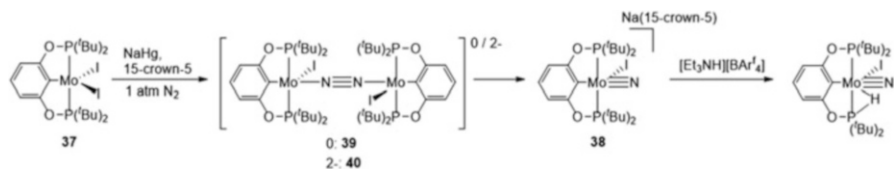
**Scheme 11** Dimerization of molybdenum triamides/trialkoxides



**Scheme 12**  $N_2$  cleavage by reduction of a chromium  $N_2$  bridged dimer with NaH [96]

chromium is more difficult compared with molybdenum due to low lying high-spin states and the weak reduction potential of  $Cr^{III}$ -compounds [95]. In addition, DFT calculations by *Stranger* predict unfavorable thermochemistry of  $N_2$ -splitting for chromium triamides [81]. Regardless, *Budzelaar*, *Gambarotta*, and coworkers reported  $N_2$ -cleavage mediated by a well-defined chromium complex [96]. Reduction of  $N_2$  bridged  $[(NNN)Cr(THF)]_2(\mu-\eta^1-\eta^1-N_2)$  (**34**,  $NNN=C_5H_3N-2,6-(2,6-iPr_2C_6H_3)N=C(CH_3)_2$ ) with 2 eq. of NaH led to the protonated hydrazide species **35** (Scheme 12). The hydrogen atom of the  $N_2H$  ligand was transferred from a methyl group of the diimine ligand. Treatment with an additional equivalent NaH results in full N–N bond scission and formation of imide **36**. Ammonia could be collected in 87% yield after addition of aqueous HCl.

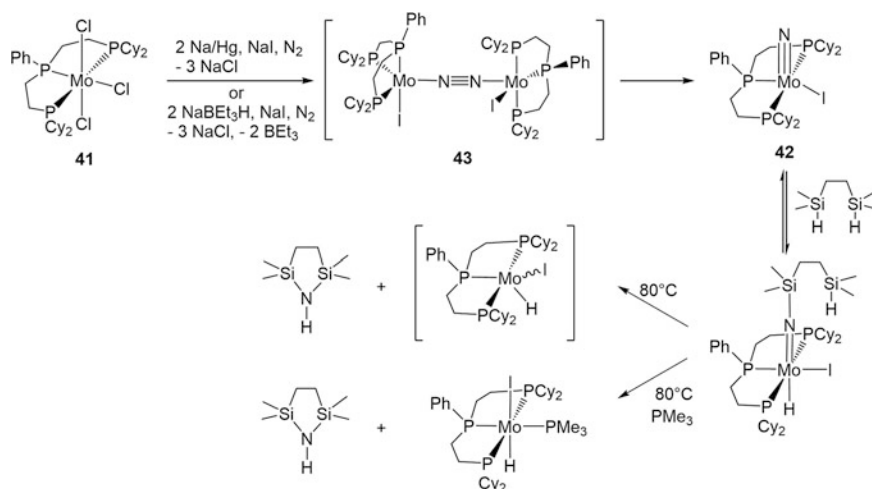
*Schrock* and coworkers reported full  $N_2$ -cleavage into terminal nitrides for the reduction of molybdenum(III) pincer complex  $[MoI_2(POCOP)]$  (**37**,  $POCOP=C_6H_3-$



**Scheme 13** N<sub>2</sub> cleavage and subsequent protonation of the terminal nitride in *Schrock's* {POCOP}Mo system [97]

2,6-(OP<sup>t</sup>Bu<sub>2</sub>)<sub>2</sub> with Na/Hg under N<sub>2</sub> in the presence of crown ether 15-crown-5 (Scheme 13) [97]. The square-pyramidal, diamagnetic nitrido molybdate(IV) [Na(15-crown-5)][Mo(N)(POCOP)] (**38**) was isolated. The authors proposed a mechanism via an end-on N<sub>2</sub>-bridged dinuclear intermediate, which splits into nitrides, in analogy with *Cummins'* molybdenum trianilide system. Two reducing equivalents are overall required per {Mo(POCOP)} moiety which raises the question about the electronic configuration of the state that undergoes N–N bond scission. The authors favored cleavage on the neutral [(POCOP)IMo(N<sub>2</sub>)MoI(POCOP)] (**39**) stage into intermediate molybdenum(V) nitrides over splitting of [(POCOP)IMo(N<sub>2</sub>)MoI(POCOP)]<sup>2-</sup> (**40**) into the final molybdenum(IV) product. Within a simplified covalent binding model in idealized fourfold symmetry (Scheme 1), the Mo–N–N–Mo core of neutral dimer **39** exhibits a π<sup>8</sup> electronic configuration (in case of low spin) vs. π<sup>10</sup> expected for dianionic **40**. Within this simple isolobal analogy the putative dianionic π<sup>10</sup> dimer **40** with Mo in square-pyramidal geometry resembles *Cummins'* π<sup>10</sup> trianilide dimer **3** in threefold symmetry more closely. Alternatively, splitting of **39** implies additional charge transfer from the metal to the N<sub>2</sub>-ligand when starting from a singlet π<sup>8</sup> ground state, e.g., by crossing to a π<sup>10</sup> quintet en route to a molybdenum(V) nitride splitting product, which is then further reduced to final **38**. Experimental or computational information about the reaction pathway or the structures and spin-states of intermediates are not yet available. Protonation of the molybdenum(IV) nitrido complex **38** with [Et<sub>3</sub>NH][BAR<sup>F</sup><sub>4</sub>] leads to formation of a hydride species in which the proton bridges the metal ion and a phosphorous ligand. Nitride protonation was not observed and with a mixture of organometallic reductants and acid only around 0.3 equivalents of ammonia were detected.

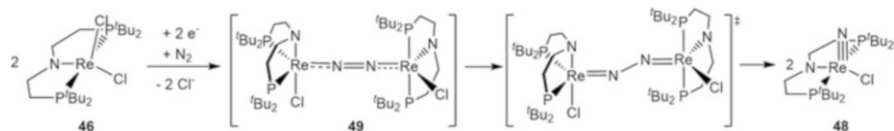
In analogy to *Schrock's* pincer system, the group of *Mézailles* reported N<sub>2</sub>-splitting upon reduction of molybdenum trichloride [MoCl<sub>3</sub>(PPP<sup>Cy</sup>)] (**41**, PPP<sup>Cy</sup> = PhP(CH<sub>2</sub>CH<sub>2</sub>PCy<sub>2</sub>)<sub>2</sub>) with Na/Hg in the presence of NaI under N<sub>2</sub> atmosphere [98]. The terminal nitride [Mo(N)I(PPP<sup>Cy</sup>)] (**42**) was observed in 80% spectroscopic and 60% isolated yield (Scheme 14). The authors also proposed N<sub>2</sub>-cleavage of dinuclear intermediate [(PPP<sup>Cy</sup>)IMo]<sub>2</sub>(μ:η<sup>1</sup>-η<sup>1</sup>-N<sub>2</sub>) (**43**) into the nitride **42**. Notably, such an intermediate should have a π<sup>10</sup> electronic configuration resembling the *Cummins* dimer **3**. Interestingly, the molybdenum(0) complexes [(PPP<sup>Cy</sup>)(N<sub>2</sub>)<sub>2</sub>Mo]<sub>2</sub>(μ:η<sup>1</sup>-η<sup>1</sup>-N<sub>2</sub>) (**44**) and [(PPP<sup>tBu</sup>)(N<sub>2</sub>)<sub>2</sub>Mo]<sub>2</sub>(μ:η<sup>1</sup>-η<sup>1</sup>-N<sub>2</sub>) (**45**) with weakly activated bridging N<sub>2</sub> were independently reported by *Nishibayashi* and *Mezailles* [99, 100]. They are excellent precatalysts for ammonia generation and N<sub>2</sub> silylation but do not split into nitrides. Starting from nitride **42**, *Mezailles* and



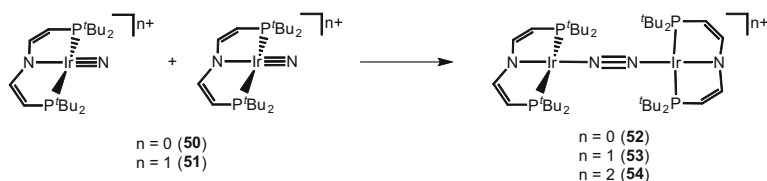
**Scheme 14** 2 Electron reduction of (PPP)MoCl<sub>3</sub> yielding the terminal nitride (PPP)Mo(N)I [98]

coworkers were also able to transfer the nitrogen upon metal re-reduction with silanes [98]. Heating with 1,2-bisdimethylsilyethane results in release of the free bis(silyl)amine and presumably reduction of the metal to a molybdenum(II) hydride which was trapped in the presence of PMe<sub>3</sub> as [ $\{\text{Mo}^{\text{II}}(\text{H})\text{I}(\text{PMe}_3)(\text{PPP}^{\text{tBu}})\}$ ]. Full regeneration of the metal in terms of a synthetic or even catalytic cycle could not be accomplished so far.

*Schneider* and coworkers extended this approach beyond group 6. Reduction of the rhenium(III) PNP pincer complexes [ $\text{ReCl}_2(\text{PNP})$ ] (**46**, PNP = N(CH<sub>2</sub>CH<sub>2</sub>P<sup>*f*</sup>Bu<sub>2</sub>)<sub>2</sub>) or [ $\text{ReCl}_3(\text{PNP})$ ] (**47**) with Na/Hg under N<sub>2</sub> atmosphere gives the rhenium(V) nitride [ $\text{Re}(\text{N})\text{Cl}(\text{PNP})$ ] (**48**) in spectroscopic yields up to 90% (Scheme 15) [101, 102]. Alternatively, milder organometallic reductants such as CoCp\*<sub>2</sub> can also be used, albeit with slightly lower yield. Intermediates were not detected, but DFT computations supported a mechanism via formation of dinuclear complex [ $\{(\text{PNP})\text{ClRe}\}_2(\mu:\eta^1-\eta^1-\text{N}_2)$ ] (**49**). For this putative intermediate, triplet, open shell singlet (BS[1,1]), and singlet wavefunctions were found close in energy. However, they all resemble the  $\pi^{10}$  configuration expected for such a dimer from the simple symmetry considerations in Scheme 1, again in analogy with *Cummins*' molybdenum triamide and possibly with *Schrock's* and *Mézailles'* pincer systems (see above). Splitting of **49** into **48** was computed to be exergonic by  $\Delta G^0 = 98 \text{ kJ mol}^{-1}$  via a zigzag hydrazido transition state with a moderate kinetic barrier ( $\Delta G^\ddagger = 84 \text{ kJ mol}^{-1}$ ). The PNP pincer ligand also features a strongly  $\pi$ -donating dialkylamide group in the ligand backbone. It can overlap with the Re–N–N–Re  $\pi$ -manifold to promote charge transfer to N<sub>2</sub>, which requires ligand rotation for the triamide platform where the amide ligands are orthogonal (see above). Starting from nitride **48** the group of *Schneider* also reported nitrogen transfer by formation of acetonitrile within a synthetic cycle, which will be discussed in Sect. 4.



**Scheme 15** Proposed N<sub>2</sub>-splitting mechanism mediated by a rhenium PNP pincer complex [101]

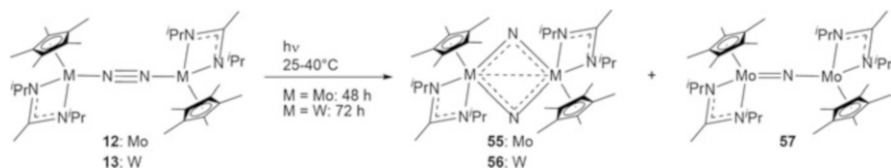


**Scheme 16** Coupling of neutral and cationic (PNP)Ir nitrides to (μ-N<sub>2</sub>)-complexes [103, 105]

The microscopic reverse, i.e., nitride coupling to N<sub>2</sub>, was also examined with pincer complexes, to elucidate the boundaries for the covalent N<sub>2</sub>-bonding model [103–105]. *Schneider* and coworkers examined the coupling of the iridium nitrides [IrN(PNP)]<sup>n+</sup> (*n* = 0 (**50**), 1 (**51**); PNP = N(CHCHP*t*Bu<sub>2</sub>)<sub>2</sub>) to the three possible N<sub>2</sub>-bridged dimers of the Ir<sup>I</sup>/Ir<sup>II</sup> redox series [(PNP)IrN<sub>2</sub>Ir(PNP)]<sup>n+</sup> (*n* = 0 (**52**), 1 (**53**), 2 (**54**)), and structurally characterized them [105] (Scheme 16). From a simple isolobal relationship with octahedral L<sub>5</sub>M–N–ML<sub>5</sub> complexes (Scheme 1), the square-planar geometry gives rise to π<sup>12</sup> configuration for Ir<sup>I</sup>/Ir<sup>I</sup> dimer **52**, π<sup>11</sup> for mixed-valent Ir<sup>I</sup>/Ir<sup>II</sup> species **53** and π<sup>10</sup> for dicationic Ir<sup>II</sup>/Ir<sup>II</sup> compound **54**, which was qualitatively confirmed by DFT computations. All three coupling reactions were found to be thermodynamically downhill and all proceed via zigzag transition states in analogy to the reverse N<sub>2</sub>-splitting. Hence, N<sub>2</sub>-splitting of the π<sup>10</sup> dimer **54** is thermodynamically unfavorable due to weak M–N multiple bonding for late transition metals such as iridium. This observation emphasizes the limitations of the covalent N<sub>2</sub>-bonding scheme with respect to N<sub>2</sub>-splitting reactivity. However, a decreasing driving force for coupling to dimers **52** (Δ*G* = –102 kcal/mol), **53** (Δ*G* = –97 kcal/mol), and **54** (Δ*G* = –74 kcal/mol) was computed, respectively. This trend in fact reflects the MO picture, as for the π<sup>11</sup> (**53**) and π<sup>12</sup> (**52**) dimers the respective iridium(IV) nitride **50** is destabilized by population of antibonding Ir–N π\*-MO [103].

### 3.3 N<sub>2</sub>-Splitting by Group 6 Cyclopentadienide Complexes

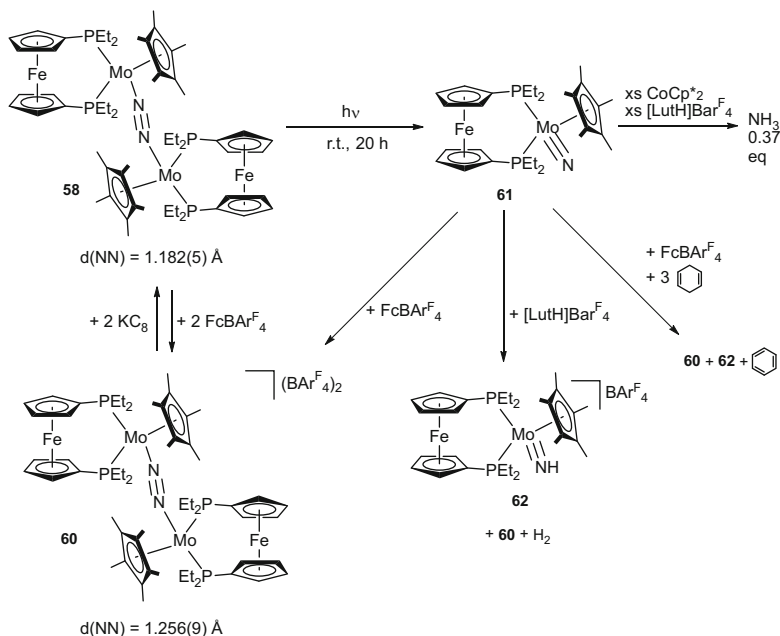
The end-on bridged dinuclear group 6 dinitrogen complexes [{Cp\**M*(am)}<sub>2</sub>(μ-N<sub>2</sub>)] (*M* = Mo (**12**), W (**13**); am = *i*PrNC(Me)NiPr) were prepared by *Sita* and coworkers upon reduction of the respective M<sup>IV</sup> dichlorides [40]. These diamagnetic



**Scheme 17** N<sub>2</sub> cleavage in  $\mu$ -nitrido and bis( $\mu$ -nitrido) complexes by Sita's group [106]

complexes exhibit a  $\pi^8$  M–N–N–M core with moderate activation and are thermally stable with respect to splitting into nitrides. However, irradiation with a mercury lamp results in splitting of the N–N bond to the dimeric, diamagnetic M<sup>V</sup> nitrides [ $\{\text{Cp}^*\text{M}(\text{am})\}_2(\mu\text{-N})_2$ ] (M = Mo (**55**), W (**56**)) and, in case of M = Mo, together with mixed valent Mo<sup>IV</sup>/Mo<sup>III</sup> mononitride bridged [ $\{\text{Cp}^*\text{Mo}(\text{am})\}_2(\mu\text{-N})$ ] (**57**) (Scheme 17) [106]. The mechanism of this reaction is not known. However, the product distribution is reminiscent of the photolysis of *Cummins'* trianilide [ $\{(\text{Ar}t\text{BuN})_3\text{Mo}\}_2(\mu\text{-}\eta^1\text{-}\eta^1\text{-N}_2)$ ] **3** (see Sect. 3.1). There, relaxation of a hot ground state that arises from photoexcitation and internal conversion provides entry to competing N–N and Mo–N cleavage pathways upon coupling with vibrational distortions of the Mo–N–N–Mo core. In the present case, such a mechanism could result in the formation of [ $\text{Cp}^*\text{Mo}(\text{am})\text{N}$ ] and [ $\text{Cp}^*\text{Mo}(\text{am})$ ] which subsequently dimerize to a statistical mixture of the dinitride and nitride dimers. Importantly, such a mechanism implies the formation of the molybdenum(V) (d<sup>1</sup>) nitride from the  $\pi^8$ -dimer. Hence, charge transfer from metal-based d-orbitals to the N<sub>2</sub>-ligand required for N–N bond splitting might be possible at least photochemically. This photochemical N<sub>2</sub>-splitting reaction was complemented with nitride transfer within a synthetic cycle producing isocyanate with CO<sub>2</sub> and chlorosilane. This reaction is discussed in Sect. 4.

This work is related to the reactivity of a redox series of N<sub>2</sub>-bridged dimolybdenum piano-stool complexes supported by a ferrocenyldiphosphine ligand. The three complexes [ $\{\text{Cp}^*\text{Mo}(\text{depf})\}_2(\mu\text{-}\eta^1\text{-}\eta^1\text{-N}_2)$ ][ $\text{BAr}^F_4$ ]<sub>n</sub> (n = 0 (**58**), 1 (**59**), 2 (**60**); depf = 1,1'-bisdiethylphosphinoferrocene; Scheme 18) were reported by *Nishibayashi* and *Yoshizawa* [107, 108]. The solution magnetic properties of **60** (diamagnetic), **59** ( $\mu_{\text{eff}} = 2.1 \mu_{\text{B}}$ ), and **58** ( $\mu_{\text{eff}} = 3.2 \mu_{\text{B}}$ ) at room temperature in combination with the moderate (**58**:  $d_{\text{NN}} = 1.182(5) \text{ \AA}$ ) to strong (**60**:  $d_{\text{NN}} = 1.256(9) \text{ \AA}$ ) degrees of N<sub>2</sub> activation support low-spin  $\pi^8$  (**60**),  $\pi^9$  (**59**),  $\pi^{10}$  (**58**), configurations, respectively. This is reminiscent of the series **3-5** [ $\{(\text{Ar}t\text{BuN})_3\text{Mo}\}_2(\mu\text{-}\eta^1\text{-}\eta^1\text{-N}_2)$ ]<sup>n+</sup> (n = 0–2; see Sect. 3.1) reported by *Cummins*. In analogy, the allegedly least activated N<sub>2</sub> complex **58** splits into nitride [ $\{\text{Cp}^*\text{Mo}^{\text{IV}}\text{N}(\text{depf})_2\}$ ] (**61**) upon irradiation at  $400 < \lambda < 580 \text{ nm}$ . TD-DFT computations point towards a transition at  $\lambda_{\text{calc}} = 495 \text{ nm}$  with strong metal to N<sub>2</sub>-ligand charge transfer character that might be relevant for the splitting reactivity. Importantly, oxidation of **61** with ferrocenium results in the reverse, i.e., thermal coupling to dinitrogen complex **60**. This inversion of the N<sub>2</sub>-splitting/coupling thermochemistry is in line with the electronic configurations of **58** ( $\pi^{10}$ : splitting) and **60** ( $\pi^8$ : coupling), respectively. Interestingly,



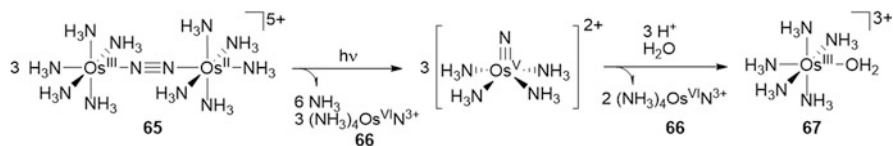
**Scheme 18** N<sub>2</sub> cleavage and functionalization mediated by a {Mo(depf)(Cp\*)} complex [107]

oxidation of **61** in the presence of the hydrogen atom donor 1,4-cyclohexadiene results in the hydrogen atom transfer product [ $\{\text{Cp}^*\text{Mo}^{\text{IV}}(\text{NH})(\text{depf})_2\}^+$  (**62**) besides nitride coupling, which might give entry into nitride transfer reactivity. Moreover, protonation of **61** gives the same products, but the mechanism for this disproportionation remains unclear.

### 3.4 N<sub>2</sub>-Splitting Beyond Group 7 Elements

Group 8 elements, in particular iron, are the metals used as catalysts for the *Haber-Bosch* process, which in fact proceeds via initial, turnover limiting dissociative N<sub>2</sub> chemisorption. However, despite intense efforts [109–113], for a long time only the reverse reaction of N<sub>2</sub>-splitting, i.e., nitride coupling, were known for molecular iron [114–116], ruthenium [117], and osmium [118–122] complexes. Most of these dimerize as octahedral or square-planar M<sup>V</sup> nitrides. They are destabilized due to the population of an antibonding M–N  $\pi^*$ -MO, which drives dimerization to the N<sub>2</sub>-bridged complexes with  $\pi^{12}$  M–N–N–M cores. The same situation was shown for isolobal, square-planar group 9 M<sup>IV</sup> (M = Rh, Ir) nitrides, which were examined by *Schneider* and coworkers (see Sect. 3.2). In contrast, the iron(IV) nitride [FeN(BP<sub>3</sub>)] (BP<sub>3</sub><sup>−</sup> = PhB(CH<sub>2</sub>P*i*Pr<sub>2</sub>)<sub>3</sub><sup>−</sup>) (**63**) also undergoes coupling at room temperature, yet exhibiting an electronic closed-shell ground state. Coupling produces



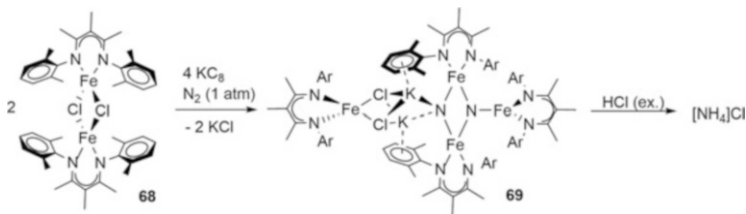


**Scheme 19** Photoinduced N<sub>2</sub> cleavage mediated by an osmium complex [123]

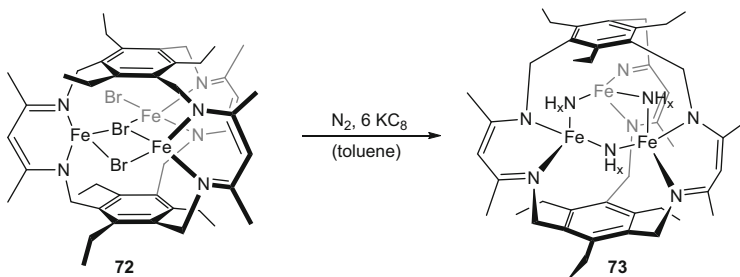
[{(BP<sub>3</sub>)Fe]<sub>2</sub>(μ-η<sup>1</sup>-η<sup>1</sup>-N<sub>2</sub>)] (**64**) with two exchange-coupled high-spin Fe(I) ions in threefold symmetry bridged by neutral N<sub>2</sub>. Analysis of the magnetic data favored this valence state assignment over a three-spin model constituted by two high-spin Fe(II) ions bridged by N<sub>2</sub><sup>2-</sup> (S = 1). Hence, the metal high-spin state reduces charge transfer to the N<sub>2</sub> ligand resulting in only moderate activation ( $d_{\text{NN}} = 1.138$  (6) Å) thereby contributing to the instability of the iron(IV) nitride.

The first report of N<sub>2</sub>-cleavage beyond group 6 was reported by *Kunkely* and *Vogler* in 2010. Irradiation of mixed-valent Os<sup>II</sup>/Os<sup>III</sup> N<sub>2</sub>-complex [(NH<sub>3</sub>)<sub>5</sub>Os](μ-η<sup>1</sup>-η<sup>1</sup>-N<sub>2</sub>)]<sup>5+</sup> (**65**) in acidic aqueous solution was reported to yield osmium(VI) nitride [OsN(NH<sub>3</sub>)<sub>4</sub>]<sup>3+</sup> (**66**) and [Os<sup>III</sup>(NH<sub>3</sub>)<sub>5</sub>(H<sub>2</sub>O)]<sup>3+</sup> (**67**) (Scheme 19) [123]. The authors proposed a mechanism via photochemical N<sub>2</sub>-splitting into Os<sup>VI</sup> and transient Os<sup>V</sup> nitrides. The latter disproportionates with subsequent hydrolysis forming ammonia with an overall yield of 16%.

Shortly after, *Holland* and coworkers presented the first example of N<sub>2</sub>-splitting to a well-defined molecular iron nitride complex. Reduction of the dimeric iron(II) β-diketimate complex [FeCl(L)]<sub>2</sub> (L = MeC[C(Me)N(2,6-Me<sub>2</sub>C<sub>6</sub>H<sub>3</sub>)<sub>2</sub>]) (**68**) with KC<sub>8</sub> under N<sub>2</sub> affords the isolation of the remarkable dinitride complex K<sub>2</sub>[(L)<sub>4</sub>(μ-N)<sub>2</sub>(μ-Cl)<sub>2</sub>] (**69**) (Scheme 20) upon full scission of the N–N bond ( $d_{\text{NN}} = 2.799(2)$  Å) [124]. NMR studies indicate that the complex, multinuclear structure is maintained in solution. Mössbauer spectra suggest the valence assignments as two high-spin Fe<sup>II</sup> and two high-spin Fe<sup>III</sup> ions, in agreement with the overall charge balance for 6-electron N<sub>2</sub> reduction. The cooperativity of four iron centers avoids the unfavorable formation of high-valent iron. Previous work from that group emphasizes the strong influence of subtle ligand variations. Reduction of the mononuclear β-diketimate complex [(L')FeCl] (L' = HC[C<sup>t</sup>Bu)N(2,6-<sup>i</sup>Pr<sub>2</sub>C<sub>6</sub>H<sub>3</sub>)<sub>2</sub>) (**70**) yields N<sub>2</sub>-bridged K<sub>2</sub>[(L')Fe]<sub>2</sub>(μ-η<sup>1</sup>-η<sup>1</sup>-N<sub>2</sub>)] (**71**), which exhibits strong N<sub>2</sub>-activation ( $d_{\text{NN}} = 1.23$  Å,  $\nu_{\text{NN}} = 1,589$  cm<sup>-1</sup>) but does not split into nitrides [125]. This difference was attributed to ligand sterics, which prevent nitride stabilization by cluster formation in the latter case. Computational analysis for **68** suggested initial formation of a Fe–N–N–Fe core followed by side-on coordination of a third Fe(I) fragment for the smaller ligand [126]. After structural rearrangement to a side-on/side-on/end-on conformation, coordination of the fourth iron fragment leads to N–N cleavage. This study and subsequent experimental work emphasized an important influence of the alkaline cation in stabilizing the nitride cluster and enabling N<sub>2</sub>-splitting [127, 128]. Splitting is reversible as demonstrated by addition of the strong π-acceptor CO, which results in N<sub>2</sub> reductive elimination



**Scheme 20** N<sub>2</sub> cleavage and ammonia formation mediated by a dinuclear iron compound [124]



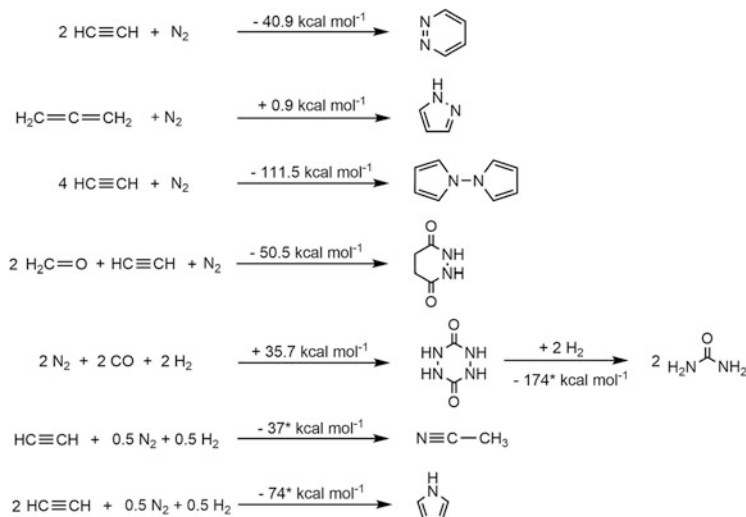
**Scheme 21** N<sub>2</sub> cleavage by a designed trinuclear Fe complex [132]

[129]. Addition of several acids to **68** yields ammonia in up to 96% yield [130]. An impressive number of intermediates could be isolated for the protonolysis, giving insights into a potential mechanism for ammonia formation. They also illustrate the strong basicity of the system and the strong reductants that are required for stepwise reduction/protonation can be offset by proton-coupled electron transfer reactions. Removal of the supporting potassium ion in **68** by addition of 18-crown-6 reveals a very basic nitrogen moiety, which ends up in intramolecular C–H activation of a benzylic CH<sub>3</sub> group of the ancillary ligand to form N–H bonds [131]. Strong nucleophilicity of the unmasked nitride is also displayed by C–N bond formation with methyl tosylate resulting in a bridging imide/nitride.

*Murray* and coworkers used a multimetallic, cooperative approach to split N<sub>2</sub> upon reduction of a triiron(II) complex **72** with KC<sub>8</sub> (Scheme 21) [132]. The three Fe ions in the main product **73** were found to bridge through three NH<sub>x</sub> functions. Mössbauer spectra show the presence of localized triiron(II/II/III) at low temperatures. The presence of three nitrogen atoms per cluster suggests intra- and intermolecular cooperativity. The origin of the hydrogen atoms in the bridging NH<sub>x</sub> moieties could not be determined so far. Reaction in silylated glassware, deuterium labeling experiments, and addition of compounds with weak C–H bonds (9,10-dihydroanthracene) did not give a satisfactory explanation. Addition of HCl to this compound yields about 30% ammonia, indicating that only one of three nitrogen units can be liberated in this way.

## 4 Nitride Functionalization Following N<sub>2</sub>-Splitting

The reactivity of transition metal nitrides, as depending on the metal type and oxidation state, was extensively examined and summarized in several comprehensive review articles [11, 133, 134]. Nitride ligands mostly exhibit nucleophilic reactivity except for some examples of high-valent late transition metal nitride complexes (Ru, Os, Ir). Accordingly, the reactivity of nitrides that originated from N<sub>2</sub>-splitting with electrophiles was examined. Several groups reported the generation of ammonia upon protonolysis of well-defined N<sub>2</sub>-derived nitride complexes. Concerning group 6-8 metals the reports by the groups of *Budzelaar* (Cr) [96], *Nishibayashi* (Mo) [107], *Vogler* (Os) [123], *Holland* (Fe) [113, 124], and *Murray* (Fe) [132] were already presented in the preceding section. Besides these, further examples from *Chirik* (Ti) [63], *Hou* (Ti) [135], *Gambarotta* (Ti and V) [136, 137], *Kawaguchi* (Nb) [138], and *Mindiola* (Nb) [139] using early transition metals are also known. However, the generation of ammonia is not in the main focus of this review. Instead, in this section the transfer of nitrogen from N<sub>2</sub> by N–C bond formation via initial N<sub>2</sub>-splitting will be discussed. When considering possible target molecules for the synthesis of organics with N<sub>2</sub> as nitrogen source it is instructive to assess the thermochemistry of hypothetical reactions. *Caulton* and coworkers discussed several reactions where N<sub>2</sub> is incorporated into organic molecules with retention of one or two N–N bonds (selected reactions in Scheme 22) [140]. With high energy starting materials like acetylenes and N-heterocycles as synthetic targets, particularly when stabilized by aromaticity, several



**Scheme 22** Computed reaction enthalpies  $\Delta H_r$  for N<sub>2</sub> functionalization from *Caulton* and coworkers [140] (numbers marked with \* are experimental values for gas phase reactions retrieved from Ref. [142])

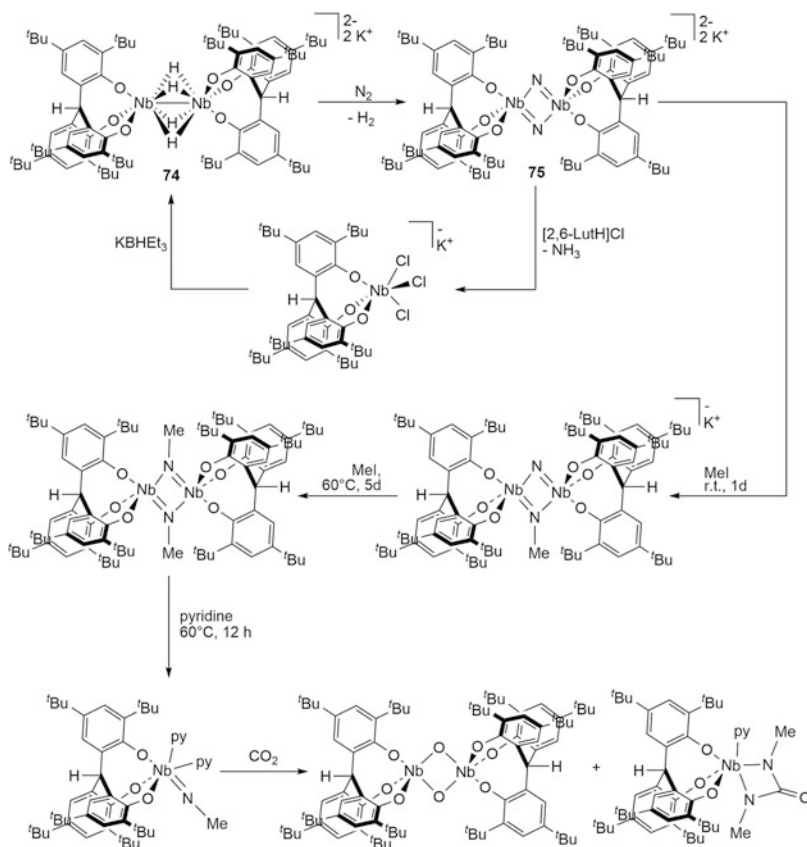
thermodynamically accessible reactions were pointed out. In addition, formation of strong C=N (e.g., heterocummulenes) or C≡N (nitriles) bonds can offset the high energy demand for complete N<sub>2</sub> cleavage [141]. For example the C≡N bond dissociation energy ( $D^0(\text{HC}\equiv\text{N}) = 937 \text{ kJ mol}^{-1}$ ) is close to that of N<sub>2</sub> providing a driving force for catalytic transformations of N<sub>2</sub> to nitriles. Unfavorable reactions can be turned exothermic by simultaneous hydrogenation. Besides, H<sub>2</sub> can serve as attractive mild reductant for nitrogen.

#### 4.1 Formation of Heterocummulenes

The group of *Kawaguchi* demonstrated N<sub>2</sub> cleavage upon reaction of a Nb(V) dichloride with a chelating triphenoxide ligand with LiHBEt<sub>3</sub> (6 eq.) [143]. Subsequent work with a related triphenoxy ligand gave further insights into the mechanism (Scheme 23). The (μ-H)<sub>4</sub>-bridged dimer K<sub>2</sub>[(L<sup>OPh3</sup>Nb<sup>IV</sup>)<sub>2</sub>(μ-H)<sub>4</sub>] (**74**) directly reacts with N<sub>2</sub> upon H<sub>2</sub> elimination and N–N bond cleavage to the bis(μ-nitrido) complex K<sub>2</sub>[(L<sup>OPh3</sup>Nb)<sub>2</sub>(μ-N)<sub>2</sub>] (**75**; L<sup>OPh3</sup> = HC-*o*-(C<sub>6</sub>H<sub>2</sub>O-4,6-tBu<sub>2</sub>)<sub>3</sub>) [138]. Within a series of stoichiometric reactions, this compound could be transformed to a mononuclear ureate complex via nitride alkylation, dimer cleavage with pyridine and oxo/imido-metathesis with CO<sub>2</sub> [144]. Importantly, the immediate product from N<sub>2</sub>-splitting does not react with CO<sub>2</sub>, presumably because of low nucleophilicity of the bridging nitride and steric bulk. Ureate formation from the imide intermediate is proposed to proceed via initial [2 + 2] addition of CO<sub>2</sub> and subsequent extrusion of methyl isocyanate. Besides the dimeric oxo complex, the ureate would then result from MeNCO addition to another parent imido complex. However, reaction intermediates or free MeNCO could not be detected. Liberation of free heterocummulenes like isocyanate or carbodiimide or of dimethylurea was not reported.

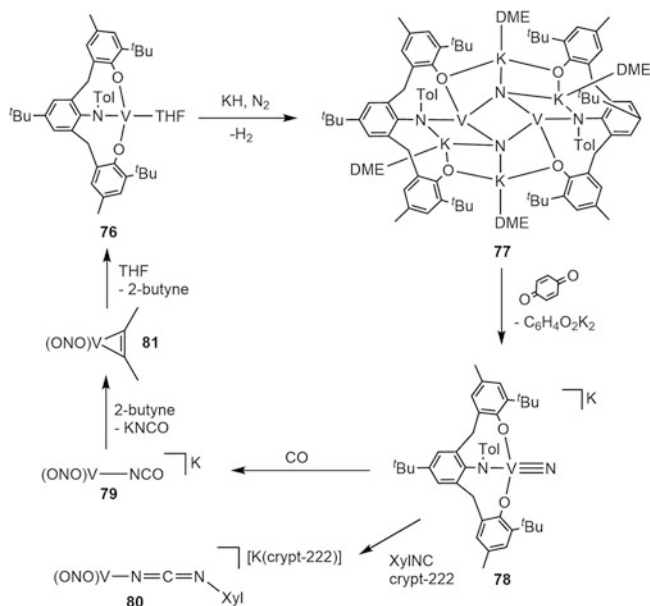
The same group later established a full synthetic cycle for isocyanate from N<sub>2</sub> formation with a related system. Reduction of vanadium complex [(ONO)V<sup>III</sup>(THF)] (ONO = 2,6-(3-*t*Bu-5-Me-2-OC<sub>6</sub>H<sub>2</sub>CH<sub>2</sub>)-4-*t*Bu-(*p*-tolyl)NC<sub>6</sub>H<sub>4</sub>) (**76**) with KH (2 equiv) under N<sub>2</sub> atmosphere gives the nitride bridged [(K(DME))<sub>2</sub>{(ONO)V<sup>IV</sup>(μ-N)}<sub>2</sub>] (**77**) in 61% yield (Scheme 24) [145]. Oxidation with benzoquinone affords the terminal vanadium(V) nitride K[(ONO)V<sup>V</sup>N] (**78**). Regeneration of the V<sup>IV</sup> nitride dimer with KH was not successful, suggesting that the V<sup>V</sup> nitride is not an intermediate in N<sub>2</sub>-splitting. Nitrogen atom transfer to CO or isonitriles was accomplished, generating the respective vanadium(III) isocyanate (**79**) and carbodiimide (**80**) complexes. After C–N bond formation free potassium isocyanate precipitates in toluene upon trapping the alkyne complex [(ONO)V(η<sup>2</sup>-MeCCMe)] (**81**) with dimethylacetylene. From there, parent **76** could be regenerated by dissolving **81** in THF.

A full synthetic cycle to isocyanates from N<sub>2</sub> could also be established by *Sita* and coworkers [106]. Earlier work of this group demonstrated thermal N<sub>2</sub>-splitting for the N<sub>2</sub>-bridged group 5 complexes [(Cp<sup>\*</sup>(am)M)<sub>2</sub>(μ:η<sup>1</sup>-η<sup>1</sup>-N<sub>2</sub>)] (M = Nb (**10**),

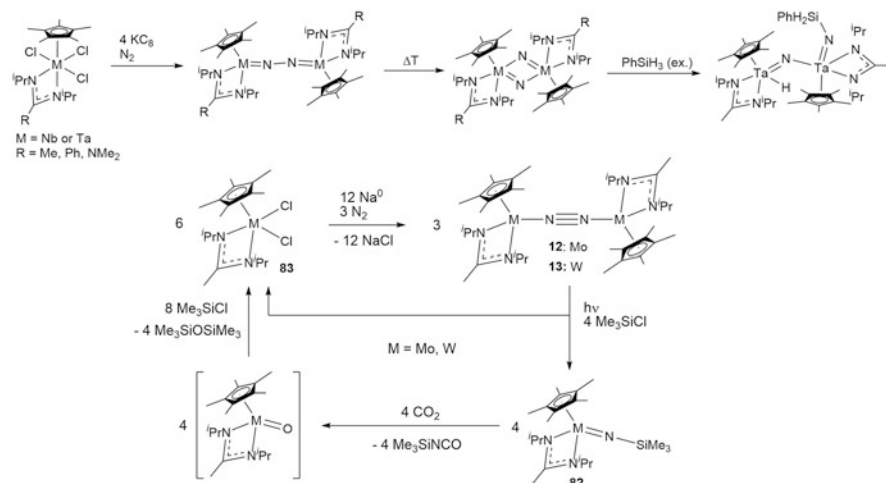


**Scheme 23** N<sub>2</sub>-splitting by a Nb hydrido complex and functionalization of the resulting bis (μ-nitrido) [138, 144]

Ta (**11**); Scheme 25, top), which exhibit strong N<sub>2</sub> activation in the ground state (see Sect. 2.2) [39, 41]. Functionalization of the tantalum nitride was achieved by N–Si bond formation with silanes [39], reminiscent of work by the group of *Mézailles* (c.f. Sect. 3.2). This approach could be transferred to the analogous group 6 system. Photolysis of [ $\text{Cp}^*(\text{am})\text{M}$ ]<sub>2</sub>(μ:η<sup>1</sup>-η<sup>1</sup>-N<sub>2</sub>) (M = Mo (**12**), W (**13**)) yields nitride-bridged dinuclear complexes **55** and **56** (c.f. Sect. 3.3) [40]. Addition of R<sub>3</sub>ECl (R<sub>3</sub>E = Me<sub>3</sub>Si, Ph<sub>3</sub>Si, Me<sub>3</sub>Ge, Me<sub>3</sub>C) to the bis(μ-nitrido) complexes **55** and **56** produces a 1:1 mixture of the mononuclear nitride [Cp\**M*(am)M(N)Cl] and the imide [Cp\**M*(am)(N-ER<sub>3</sub>)] (**82**). A radical mechanism was proposed. In contrast, irradiation of **12** or **13** in the presence of Me<sub>3</sub>SiCl gives the imide complex **82** and dichloride [Cp\**M*(am)Cl<sub>2</sub>] (**83**) in 2:1 ratio (Scheme 25, bottom). Reaction of the imide with CO affords free silylisocyanate in up to 64% yield and the bis(carbonyl) complex [Cp\**M*(am)(CO)<sub>2</sub>] [106, 146]. To close the synthetic cycle, the latter complexes could be converted to the respective dichlorides **83** either by reaction



**Scheme 24** Synthetic cycle for N<sub>2</sub> to isocyanate conversion promoted by vanadium complexes [145]



**Scheme 25** N<sub>2</sub>-splitting and functionalization mediated by group 5 complexes (*top*, [39]) and a synthetic cycle for N<sub>2</sub> to isocyanate conversion by group 6 metal complexes (*bottom*, [146])

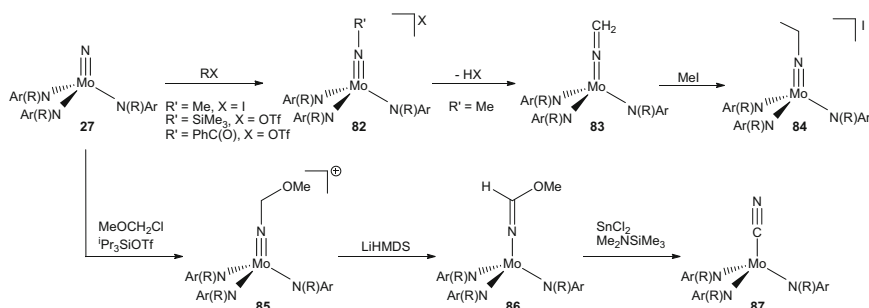
with CO<sub>2</sub> and subsequent treatment of the resulting oxo complex with Me<sub>3</sub>SiCl or directly by reaction of the silylimide under CO<sub>2</sub> (1.4–4.8 bar) in the presence of Me<sub>3</sub>SiCl (Scheme 25). On this route, free isocyanate could be generated from N<sub>2</sub> in

a pseudo-catalytic, four step one-pot synthesis with up to 82% recovered catalyst per cycle.

Attempts to get isocyanates from the reaction of CO with *Cummins'* molybdenum(VI) nitride  $[\text{MoN}(\text{N}t\text{BuAr})_3]$ , which results from  $\text{N}_2$ -splitting failed [147]. While DFT computations predicted that this reaction should be thermodynamically possible, a large kinetic barrier presumably arises from the lack of a carbonyl complex intermediate that can rearrange to an isocyanate. In comparison, this pathway was computationally proposed for a related vanadium(V) nitride, which forms isocyanates with CO, but which is not derived from  $\text{N}_2$  [147–149].

## 4.2 Formation of Nitriles

Nitriles represent another synthetic target that was addressed by several groups using molybdenum (*Cummins*), rhenium (*Schneider*), and titanium (*Hou*) platforms. Seminal work in this area was reported by *Cummins* and coworkers starting from the trisanilide molybdenum(VI) nitrides that arise from  $\text{N}_2$ -splitting (c.f. Sect. 3.1).  $[\text{Mo}(\text{N})(\text{N}t\text{BuAr})_3]$  (**27**) exhibits only weak nucleophilicity but can be activated with strong Lewis acids, including alkylation, silylation, and acylation with  $\text{MeOTf}$ ,  $\text{Me}_3\text{SiOTf}$ , or in situ prepared  $\text{PhC}(\text{O})\text{OTf}$ , respectively [150]. The methylimido complex **84** can be deprotonated (Scheme 26). The resulting ketimide **85**, with approximately linear  $\text{Mo}=\text{N}=\text{CH}_2$  unit, is a C-nucleophile giving the ethylimide  $[\text{Mo}(\text{NEt})(\text{N}t\text{BuAr})_3]^+$  **86** with  $\text{MeI}$ . Interestingly, the ethylimide could not be obtained by direct ethylation of the nitride with  $\text{EtOTf}$ ,  $\text{EtI}$ , or  $[\text{Et}_3\text{O}]\text{BF}_4$ , respectively [150]. As an extension of this work, *Cummins* later reported the formation of a cyanide complex from nitride **27** (Scheme 26). With a mixture of  $\text{MeOCH}_2\text{Cl}$  and  $^i\text{Pr}_3\text{SiOTf}$  a methoxymethylimide complex **85** was obtained and deprotonation leads to the respective alkoxyketimide  $[\text{Mo}(\text{NCHOMe})(\text{N}t\text{BuAr})_3]$  (**88**) [151]. Release of free prussic acid with Lewis acid was not successful, but a mixture of Lewis acid/Brønsted base ( $\text{SnCl}_2/\text{Me}_3\text{SiNMe}_2$ ) gave the molybdenum (IV) cyanide complex  $[\text{Mo}(\text{CN})(\text{N}t\text{BuAr})_3]$  (**89**). While this approach of



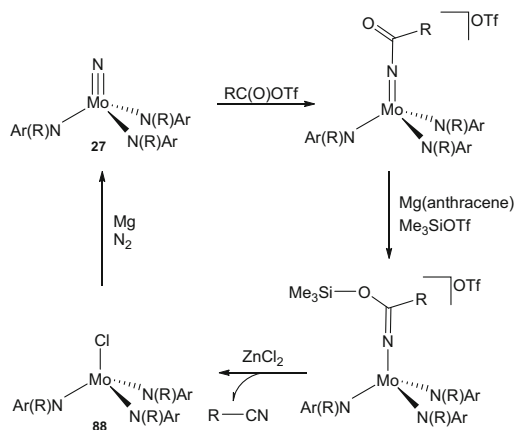
**Scheme 26** Functionalization of  $\text{N}_2$ -derived terminal nitrido complex **27** with electrophiles

N<sub>2</sub>-functionalization via splitting, alkylation, and ligand oxidation processes did not lead to pseudo-catalytic synthetic cycles or even catalysis with this system yet, it is conceptually relevant concerning the redox-balance. It demonstrates that metal-re-reduction, in this case Mo<sup>VI</sup> to Mo<sup>IV</sup>, can at least in part be accomplished without external reducing equivalents, but through a charge transfer from the ligand to metal that is coupled with imide deprotonation. In fact, deprotonation of alkylimides to ketimides and even double deprotonation to nitriles – a formal transfer of four electrons to the metal – were well known but previously not applied to N<sub>2</sub> functionalization [152, 153]. This approach was later also picked up by *Schneider* and coworkers to establish a full synthetic cycle for nitrile generation from N<sub>2</sub> (see below).

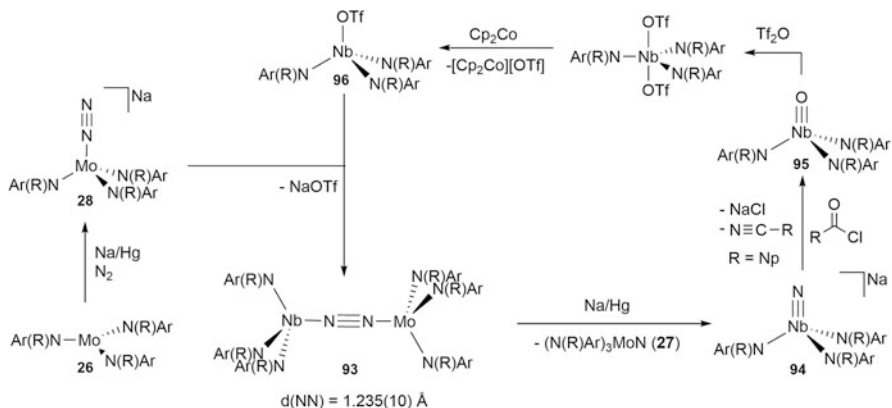
*De Vries* and coworkers were the first ones to transfer the N<sub>2</sub>-derived nitride from *Cummins*' system to an organic compound. Reaction of **27** with trifluoroacetic anhydride in DMF results in release of free amide CF<sub>3</sub>C(O)NH<sub>2</sub> in high yield with respect to nitrogen [154]. However, the molybdenum trisanilide platform is degraded and, in fact, the *tert*-butylamide groups serve as proton source, preventing catalytic turnover. An elegant route for full nitrogen transfer starting from **27** was provided by *Cummins* in 2006 [155]. Acylation with RC(O)Cl/SiMe<sub>3</sub>OTf (R = Ph, <sup>t</sup>Bu, Me) gives the respective acylimide complexes **90** (Scheme 27). These can be reduced with Mg/anthracene in the presence of Me<sub>3</sub>SiCl to a trimethylsiloxy-ketimide **91**. Salt metathesis with Lewis acids like SnCl<sub>2</sub> or ZnCl<sub>2</sub> results in fragmentation to the free organonitrile and molybdenum(IV) chloride [MoCl(N<sup>t</sup>BuAr)<sub>3</sub>] (**92**). Further reduction restores the parent Mo<sup>III</sup> triamide. In this synthetic cycle, nitriles were produced in up to 38% yield over all steps. Each molybdenum center is oxidized by 3 electrons upon N<sub>2</sub> cleavage and re-reduction is a purely metal centered process.

This system was later extended to heterobimetallic (Mo/Nb) N<sub>2</sub>-cleavage and -functionalization. N<sub>2</sub>-bridged (π<sup>9</sup>-electron) complex [(Ar<sup>t</sup>BuN)<sub>3</sub>Mo(μ-η<sup>1</sup>-η<sup>1</sup>-N<sub>2</sub>)Nb(N<sup>t</sup>PrAr)<sub>3</sub>] (**93**) splits into Mo<sup>VI</sup> nitride **27** and Nb<sup>V</sup> nitride [NbN(N<sup>t</sup>PrAr)<sub>3</sub>]<sup>-</sup>

**Scheme 27** Synthetic cycle for N<sub>2</sub> cleavage and conversion to nitriles [155]



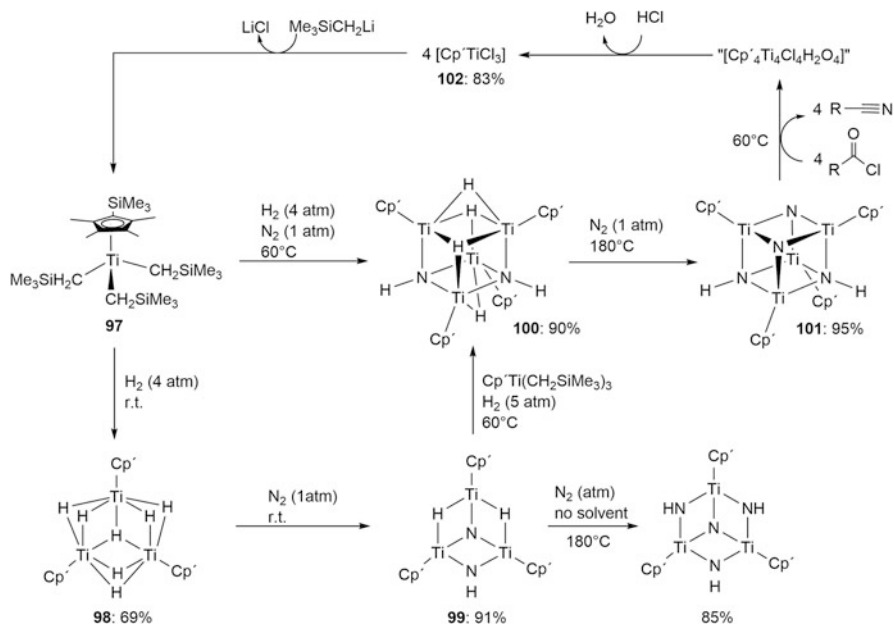




**Scheme 28** Synthetic cycle for  $\text{N}_2$  to organonitrile conversion mediated by a heterobimetallic Nb/Mo system [156, 157]

(**94**) upon reduction (Scheme 28) [156]. This nitrido niobate is more reactive than the isoelectronic Mo complex. With acyl chlorides, unusual oxo/nitride metathesis is observed directly producing the free nitrile and the  $\text{Nb}^{\text{V}}$  oxo complex (**95**) [157]. Closing of the cycle with respect to niobium was accomplished by addition of trifluoromethanesulfonic anhydride, reduction with  $\text{CoCp}_2$  and metathesis of the  $\text{Nb}^{\text{IV}}$  triflate **96** with  $[(\text{N}_2)\text{Mo}(\text{N}^t\text{BuAr})_3]^-$  **28**. Ligand modification allowed for trapping of an  $\text{Nb}^{\text{V}}$  acylimido complex, which converts into the oxo-complex upon heating. A variety of nitriles can be synthesized in high yield, providing the opportunity of selective, atom-efficient  $^{15}\text{N}$ -labelling employing  $^{15}\text{N}_2$ . However, while this synthetic cycle is pseudo-catalytic in Nb it is still stoichiometric in Mo.

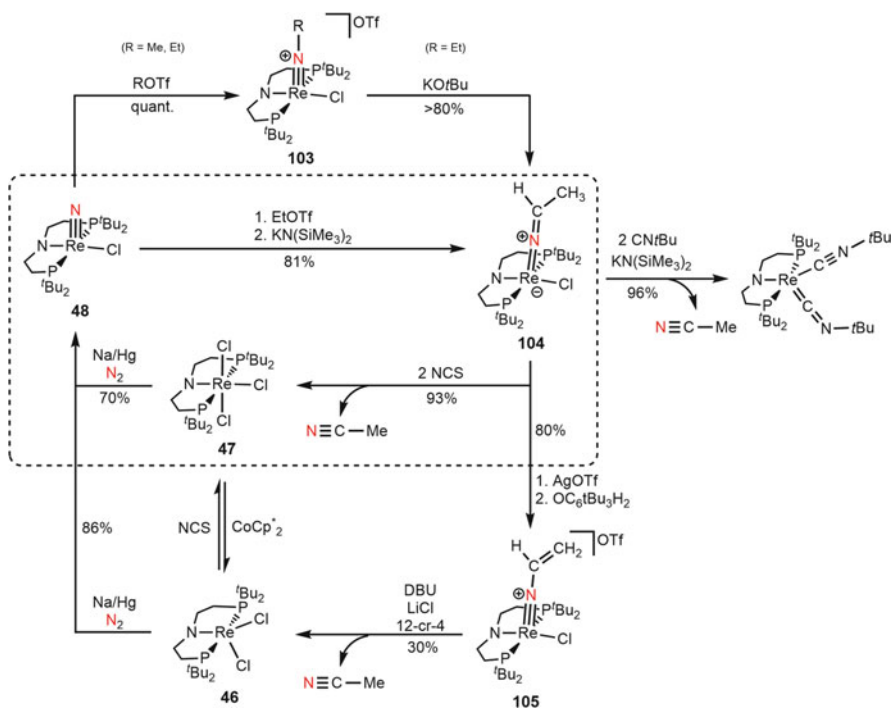
Related work was reported by *Hou* and coworkers with a titanium cyclopentadienide platform, which even enabled the use of  $\text{H}_2$  as reductant for  $\text{N}_2$ -cleavage. (Scheme 29) [135, 158]. Hydrogenolysis of the titanium(IV) alkyl complex  $[\text{Cp}^*\text{Ti}(\text{CH}_2\text{SiMe}_3)_3]$  ( $\text{Cp}^* = \text{C}_5\text{Me}_4\text{SiMe}_3$ ) (**97**) with dihydrogen (4 atm) affords a mixture of the partially reduced, mixed-valent, trinuclear polyhydride  $[(\text{Cp}^*\text{Ti})_3(\mu_3\text{-H})(\mu_2\text{-H})_6]$  (**98**: 69%) and  $[(\text{Cp}^*\text{Ti})_4(\mu\text{-H})_8]$  (10%, not shown in Scheme 29).  $[(\text{Cp}^*\text{M})_4(\mu\text{-H})_8]$  is the main product in case of homologous Zr and Hf [159]. However, only **98** reacts with  $\text{N}_2$  (1 atm) upon partial  $\text{H}_2$  elimination and formation of  $[(\text{Cp}^*\text{Ti})_3(\mu_2\text{-NH})(\mu_3\text{-N})(\mu_2\text{-H})_2]$  (**99**) with full  $\text{N}_2$ -cleavage and retention of the formal metal oxidation states  $\{\text{Ti}^{\text{III}}_2/\text{Ti}^{\text{IV}}\}$ . The side-on end-on  $\text{N}_2$ -bridged complex  $[(\text{Cp}^*\text{Ti})_3(\mu\text{-}\eta^1:\eta^2:\eta^2\text{-N}_2)(\mu\text{-H})_3]$  was spectroscopically identified as an intermediate at  $-30^\circ\text{C}$ . Above  $-10^\circ\text{C}$ ,  $\text{N}_2$ -splitting is observed to the bis- $\mu$ -nitride  $[(\text{Cp}^*\text{Ti})_3(\mu_3\text{-N})(\mu_2\text{-N})(\mu_2\text{-H})_3]$ , which isomerizes to the final product at  $20^\circ\text{C}$ . Further  $\text{N}_2$ -incorporation was observed upon prolonged heating as solid at  $180^\circ\text{C}$ . Importantly, direct reaction of  $[\text{Cp}^*\text{Ti}(\text{CH}_2\text{SiMe}_3)_3]$  under  $\text{H}_2$  (4 atm) and  $\text{N}_2$  (1 atm) at  $60^\circ\text{C}$  gives the bisimide complex  $[(\text{Cp}^*\text{Ti})_3(\mu_3\text{-NH})_2(\mu_2\text{-H})_4]$  (**100**) in 90% yield. Heating of the latter under  $\text{N}_2$  ( $180^\circ\text{C}$ , neat) also results in more  $\text{N}_2$ -incorporation to the diimide dinitride complex  $[(\text{Cp}^*\text{Ti})_4(\mu^3\text{-NH})_2(\mu^3\text{-N})_2]$  (**101**) in about 95%



**Scheme 29** N<sub>2</sub> functionalization via polynuclear titanium hydrides [135, 160]

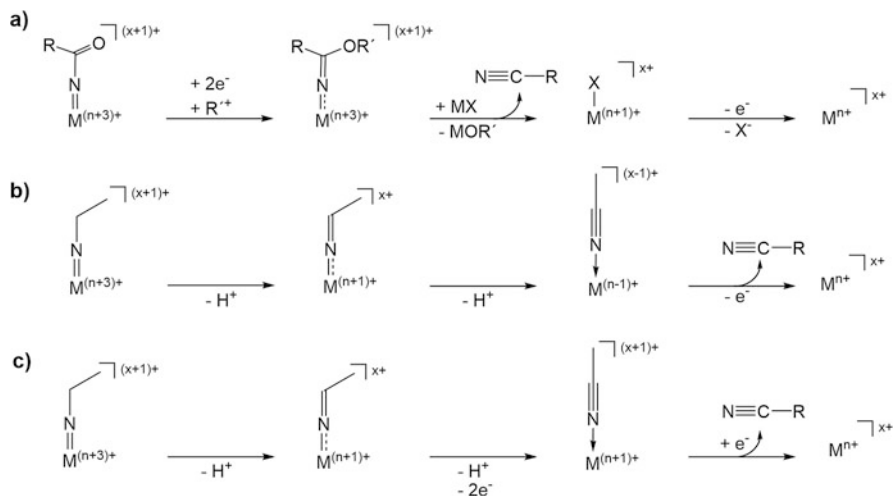
yield (Scheme 29) [160]. This complex directly forms a variety of organic nitriles in good yields (60–85%) with acyl chlorides (60°C, 12 h) allowing for nitrogen transfer from N<sub>2</sub> into organic substrates in two simple reaction steps. The μ-oxo complex [(Cp'TiCl<sub>2</sub>)<sub>2</sub>(μ-O)] and several unidentified paramagnetic titanium species also result, which can be recovered as [Cp'TiCl<sub>3</sub>] (**102**) in 83% yield upon addition of ethereal HCl to the crude mixture. This enabled a full synthetic cycle by salt metathesis with lithium neosyl. Most importantly, this system does not require strong reductants like alkali metals.

*Schneider* and coworkers also reported the formation of acetonitrile with N<sub>2</sub> as nitrogen source within a synthetic cycle based on their rhenium pincer platform (Scheme 30). The nitride [Re(N)Cl(PNP)] (**48**, PNP = N(CH<sub>2</sub>CH<sub>2</sub>PtBu<sub>2</sub>)<sub>2</sub>), which results from N<sub>2</sub>-splitting (c.f. Sect. 3.2), does not react with H<sub>2</sub> (3 bar) in contrast with the related square-planar group 8 compounds [M(N)(PNP)] (M = Ru, Os) that form ammonia in high yield [161, 162]. This lack of reactivity was attributed to the strong *trans*-effect of the nitride ligand, which prevents H<sub>2</sub> heterolysis in *trans*-position. However, **48** can be N-alkylated by strong electrophiles, such as alkyltriflates ROTf (R = Me, Et) to the respective imido complexes [Re(NR)Cl(PNP)]<sup>+</sup> [102]. In contrast, with Brønsted acids protonation at the amide instead of the nitride nitrogen is observed. The different selectivity follows the computed thermochemical preference for reaction with protons and C-nucleophiles, respectively. *Caution* and coworkers reported similar findings for a ruthenium(IV) nitride that was obtained with azide as nitrogen source [163]. Deprotonation of ethylimide [Re(NEt)Cl(PNP)]<sup>+</sup> (**103**) gives the respective ketimide [Re(N=CHMe)Cl(PNP)]



**Scheme 30** Synthetic cycle for  $N_2$  to acetonitrile conversion mediated by rhenium PNP pincer complex (DBU = 1,8-Diazabicyclo[5.4.0]undec-7-en, NCS = *N*-chlorosuccinimide). The *dashed box* describes the most efficient cycle [102]

**(104)** in near quantitative yield. The Re–N (1.822(4) Å) and C=N (1.273(7) Å) bond distances and near linearity indicate strong 1-azavinylidene  $Re=N=C$  heterocummulene character, also explaining the observation of two stereoisomers of **104**. The formation of **104** directly from the nitride can also be carried out in a two-step, one-pot synthesis. Previous work on other group 6 and group 7 alkylimides that were not derived from  $N_2$  suggests the formation of nitriles ( $M \leftarrow N\equiv CR$ ) upon double deprotonation of primary alkylimides ( $M=N-CH_2R$ ) via ketimido ( $M-N=CHR$ ) intermediates [152, 153]. Both deprotonation steps also represent formal 2-electron reductions of the metal. Hence, this route implies intramolecular proton coupled metal reduction, instead of the use of external reductants used in the protocols of *Cummins* (Mg/anthracene) and *Hou* ( $H_2$ ), respectively. Deprotonation of **104** was possible upon trapping of the resulting rhenium(I) species with strong  $\pi$ -acceptor ligands, like isonitriles, with concomitant free acetonitrile release in near quantitative yield. Alternatively, external oxidants can be used to avoid the need for additional  $\pi$ -accepting ligands. Net  $2e^-/H^+$  removal by stepwise, one-pot oxidation with  $Ag^+$  and subsequent hydrogen atom abstraction with tri-*tert*-butylphenoxy radical gave the vinylimide  $[Re(NCHCH_2)Cl(PNP)]^+$  (**105**) in high yield. The preference of the  $Re^V$  vinylimido vs. the  $Re^{III}$



**Scheme 31** Schematic pathways of nitrile synthesis after functionalization of N<sub>2</sub>-derived nitrides: Nitride acylation (a) and alkylation (b, c) [102]

nitrile complex tautomer emphasizes the electron rich nature of the {Re(PNP)}-platform. However, release of free acetonitrile from **105** is possible by adding a chloride source with catalytic amounts of base (DBU) for tautomerization, albeit in moderate yields. The most efficient route for acetonitrile release from ketimide **104** was obtained using N-chlorosuccinimide (NCS) as combined oxidant, chloride source and base, giving free MeCN and rhenium(IV) chloride [ReCl<sub>3</sub>(PNP)] **47** in over 90% yield. Versatile reduction of **47** closes a full synthetic cycle.

In comparing the synthetic strategies of the three nitrile protocols discussed above it is instructive to assess the overall redox economy. Both *Cummins* (Mo, Mo/Nb) and *Hou* (Ti) used organic acyl electrophiles for C–N bond formation. Hence, a full cycle comprising N<sub>2</sub>-splitting and N-transfer further requires three electrons per N-atom for re-reduction of the metal (Scheme 31a). This can be accomplished with external chemical reductants, like electropositive metals (*Cummins*) or H<sub>2</sub> (*Hou*). In contrast, the strategy evaluated by *Schneider* and coworkers relies on intramolecular proton-coupled ligand-to-metal charge transfer. Each deprotonation step is associated with formal 2-electron reduction of the metal. Odd electron N<sub>2</sub> reduction (3e<sup>-</sup> per N-atom) requires additional reductive or oxidative redox steps for (pseudo)catalytic turnover (Scheme 31b and c).

## 5 Conclusions

In this tutorial review, the electronic structures of the most common end-on and side-on bridging N<sub>2</sub>-complexes and the parameters that determine splitting into nitrides were discussed. Some general trends such as increasing N<sub>2</sub>-activation of the

heavier metal homologues due to better orbital overlap are apparent. Importantly, dinuclear  $N_2$ -complexes with  $\pi^{10}$  (end-on) and  $\pi^8\delta^2$  (side-on) electrons within the  $M_2N_2$  core, respectively, were pointed out as preferred electronic configurations for splitting into nitrides. Several other parameters, such as  $\pi$ -donating auxiliary ligands, steric influences, high/low-spin transitions, and decreasing  $M\equiv N$  bond strengths along the transition series complicate this simplified picture. However, it provides a good starting point in future efforts to design catalyst platforms that functionalize  $N_2$  via splitting into nitrides. For nitride functionalization that follows  $N_2$ -splitting, several synthetic targets were pointed out that could offset cleavage of the strong  $N_2$  bond, such as nitriles, heterocycles, or heterocumulenes. Catalytic protocols that proceed through  $N_2$ -splitting are yet to be developed. However, several stoichiometric and pseudo-catalytic variants offer possible solutions to combine C–N bond formation and 6-electron redox reactivity and open up a path towards catalytic  $N_2$  functionalization beyond ammonia in the future.

## References

1. Hoffman BM, Dean DR, Seefeldt LC (2009) Climbing nitrogenase: toward a mechanism of enzymatic nitrogen fixation. *Acc Chem Res* 42:609–619. doi:10.1021/ar8002128
2. Hoffman BM, Lukoyanov D, Yang ZY, Dean DR, Seefeldt LC (2014) Mechanism of nitrogen fixation by nitrogenase: the next stage. *Chem Rev* 114:4041–4062. doi:10.1021/cr400641x
3. Haber F (1910) Über die Darstellung des Ammoniaks aus Stickstoff und Wasserstoff. *Z Elektrochem Angew Phys Chem* 16:244–246. doi:10.1002/bbpc.19100160709
4. Ertl G (2008) Reactions at surfaces: from atoms to complexity (nobel lecture). *Angew Chem Int Ed* 47:3524–3535. doi:10.1002/anie.200800480
5. Bezdek MJ, Chirik PJ (2016) Expanding boundaries:  $N_2$  cleavage and functionalization beyond early transition metals. *Angew Chem Int Ed* 55:7892–7896. doi:10.1002/anie.201603142
6. Yandulov DV, Schrock RR (2003) Catalytic reduction of dinitrogen to ammonia at a single molybdenum center. *Science* 301:76–78. doi:10.1126/science.1085326
7. Arashiba K, Miyake Y, Nishibayashi Y (2011) A molybdenum complex bearing PNP-type pincer ligands leads to the catalytic reduction of dinitrogen into ammonia. *Nat Chem* 3:120–125. doi:10.1038/nchem.906
8. Anderson JS, Rittle J, Peters JC (2013) Catalytic conversion of nitrogen to ammonia by an iron model complex. *Nature* 501:84–87. doi:10.1038/nature12435
9. van der Ham CJM, Koper MTM, Hettterscheid DGH (2014) Challenges in reduction of dinitrogen by proton and electron transfer. *Chem Soc Rev* 43:5183–5191. doi:10.1039/c4cs00085d
10. Ali M, Zhou F, Chen K, Kotzur C, Xiao C, Bourgeois L, Zhang X, MacFarlane DR (2016) Nanostructured photoelectrochemical solar cell for nitrogen reduction using plasmon-enhanced black silicon. *Nat Commun* 7:11335. doi:10.1038/ncomms11335
11. Smith JM (2014) Reactive transition metal nitride complexes. In: Karlin KD (ed) *Progress in inorganic chemistry*, vol 58. Wiley, Hoboken, pp 417–470. doi: 10.1002/9781118792797.ch06
12. Hidai M (1999) Chemical nitrogen fixation by molybdenum and tungsten complexes. *Coord Chem Rev* 185–186:99–108. doi:10.1016/s0010-8545(98)00250-1
13. Sellmann D (1974) Dinitrogen-transition metal complexes: synthesis, properties, and significance. *Angew Chem Int Ed Engl* 13:639–649. doi:10.1002/anie.197406391

14. Bazhenova TA, Shilov AE (1995) Nitrogen fixation in solution. *Coord Chem Rev* 144:69–145. doi:[10.1016/0010-8545\(95\)01139-g](https://doi.org/10.1016/0010-8545(95)01139-g)
15. Jia HP, Quadrelli EA (2014) Mechanistic aspects of dinitrogen cleavage and hydrogenation to produce ammonia in catalysis and organometallic chemistry: relevance of metal hydride bonds and dihydrogen. *Chem Soc Rev* 43:547–564. doi:[10.1039/c3cs60206k](https://doi.org/10.1039/c3cs60206k)
16. Shilov AE (2003) Catalytic reduction of molecular nitrogen in solutions. *Russ Chem Bull* 52:2555–2562. doi:[10.1023/b:rucb.0000019873.81002.60](https://doi.org/10.1023/b:rucb.0000019873.81002.60)
17. Fryzuk MD, Johnson SA (2000) The continuing story of dinitrogen activation. *Coord Chem Rev* 200–202:379–409. doi:[10.1016/s0010-8545\(00\)00264-2](https://doi.org/10.1016/s0010-8545(00)00264-2)
18. MacKay BA, Fryzuk MD (2004) Dinitrogen coordination chemistry: on the biomimetic borderlands. *Chem Rev* 104:385–401. doi:[10.1021/cr020610c](https://doi.org/10.1021/cr020610c)
19. Badger RM (1934) A relation between internuclear distances and bond force constants. *J Chem Phys* 2:128–131. doi:[10.1063/1.1749433](https://doi.org/10.1063/1.1749433)
20. Evans WJ, Fang M, Zucchi GL, Furche F, Ziller JW, Hoekstra RM, Zink JI (2009) Isolation of dysprosium and yttrium complexes of a three-electron reduction product in the activation of dinitrogen, the (N<sub>2</sub>)<sup>3-</sup> radical. *J Am Chem Soc* 131:11195–11202. doi:[10.1021/ja9036753](https://doi.org/10.1021/ja9036753)
21. Gelerinter E, Silsbee RH (1966) Electron spin resonance identification of an N<sub>2</sub><sup>-</sup> defect in X-irradiated sodium azide. *J Chem Phys* 45:1703–1709. doi:[10.1063/1.1727818](https://doi.org/10.1063/1.1727818)
22. Marinkas PL, Bartram RH (1968) ESR of N<sub>2</sub><sup>-</sup> in UV-irradiated single crystals of anhydrous barium azide. *J Chem Phys* 48:927–930. doi:[10.1063/1.1668738](https://doi.org/10.1063/1.1668738)
23. Brailsford JR, Morton JR, Vannotti LE (1969) Electron spin resonance spectrum of N<sub>2</sub><sup>-</sup> trapped in KCl, KBr, and KI. *J Chem Phys* 50:1051–1055. doi:[10.1063/1.1671155](https://doi.org/10.1063/1.1671155)
24. Chiesa M, Giamello E, Murphy DM, Pacchioni G, Paganini MC, Soave R, Sojka Z (2001) Reductive activation of the nitrogen molecule at the surface of “electron-rich” MgO and CaO. The N<sub>2</sub><sup>-</sup> surface adsorbed radical ion. *J Phys Chem B* 105:497–505. doi:[10.1021/jp002794+](https://doi.org/10.1021/jp002794+)
25. Bozkaya U, Turney JM, Yamaguchi Y, Schaefer III HF (2010) The barrier height, unimolecular rate constant, and lifetime for the dissociation of HN<sub>2</sub>. *J Chem Phys* 132:064308. doi:[10.1063/1.3310285](https://doi.org/10.1063/1.3310285)
26. Stoicheff BP (1954) High resolution raman spectroscopy of gases: III. Raman spectrum of nitrogen. *Can J Phys* 32:630–634. doi:[10.1139/p54-066](https://doi.org/10.1139/p54-066)
27. Carlotti M, Johns JWC, Trombetti A (1974) The ν<sub>5</sub> fundamental bands of N<sub>2</sub>H<sub>2</sub> and N<sub>2</sub>D<sub>2</sub>. *Can J Phys* 52:340–344. doi:[10.1139/p74-048](https://doi.org/10.1139/p74-048)
28. Craig NC, Levin IW (1979) Vibrational assignment and potential function for *trans*-diazene (diimide): predictions for *cis*-diazene. *J Chem Phys* 71:400. doi:[10.1063/1.438084](https://doi.org/10.1063/1.438084)
29. Goubeau J, Kull U (1962) Die Schwingungsspektren von Natrium- und Zinkhydrazid. *Z Anorg Allg Chem* 316:182–189. doi:[10.1002/zaac.19623160310](https://doi.org/10.1002/zaac.19623160310)
30. Shaver MP, Fryzuk MD (2003) Activation of molecular nitrogen: coordination, cleavage and functionalization of N<sub>2</sub> mediated by metal complexes. *Adv Synth Catal* 345:1061–1076. doi:[10.1002/adsc.200303081](https://doi.org/10.1002/adsc.200303081)
31. Studt F, Tuzek F (2006) Theoretical, spectroscopic, and mechanistic studies on transition-metal dinitrogen complexes: implications to reactivity and relevance to the nitrogenase problem. *J Comput Chem* 27:1278–1291. doi:[10.1002/jcc.20413](https://doi.org/10.1002/jcc.20413)
32. Treitel IM, Flood MT, Marsh RE, Gray HB (1969) Molecular and electronic structure of μ-nitrogen-decaamminediruthenium(II). *J Am Chem Soc* 91:6512–6513. doi:[10.1021/ja01051a070](https://doi.org/10.1021/ja01051a070)
33. Chatt J, Fay RC, Richards RL (1971) Preparation and characterisation of the dinuclear dinitrogen complex, trichloro-μ-dinitrogen-bis(tetrahydrofuran){chlorotetrakis[dimethyl-(phenyl)phosphine]rhenium(I)chromium(III)} [(PMe<sub>2</sub>Ph)<sub>4</sub>ClReN<sub>2</sub>CrCl<sub>3</sub>(thf)<sub>2</sub>]. *J Chem Soc A* 702–704. doi:[10.1039/J19710000702](https://doi.org/10.1039/J19710000702)
34. Powell CB, Hall MB (1984) Molecular orbital calculations on dinitrogen-bridged transition-metal dimers. *Inorg Chem* 23:4619–4627. doi:[10.1021/ic00194a042](https://doi.org/10.1021/ic00194a042)
35. Mercer M, Crabtree RH, Richards RL (1973) A μ-dinitrogen complex with a long N–N bond. X-ray crystal structure of [(PMe<sub>2</sub>Ph)<sub>4</sub>ClReN<sub>2</sub>MoCl<sub>4</sub>(OMe)]. *J Chem Soc Chem Commun* 808–809. doi:[10.1039/C39730000808](https://doi.org/10.1039/C39730000808)

36. Laplaza CE, Johnson MJA, Peters JC, Odom AL, Kim E, Cummins CC, George GN, Pickering IJ (1996) Dinitrogen cleavage by three-coordinate molybdenum(III) complexes: mechanistic and structural data. *J Am Chem Soc* 118:8623–8638. doi:[10.1021/ja960574x](https://doi.org/10.1021/ja960574x)
37. Curley JJ, Cook TR, Reece SY, Müller P, Cummins CC (2008) Shining light on dinitrogen cleavage: structural features, redox chemistry, and photochemistry of the key intermediate bridging dinitrogen complex. *J Am Chem Soc* 130:9394–9405. doi:[10.1021/ja8002638](https://doi.org/10.1021/ja8002638)
38. Laplaza CE, Cummins CC (1995) Dinitrogen cleavage by a three-coordinate molybdenum (III) complex. *Science* 268:861–863. doi:[10.1126/science.268.5212.861](https://doi.org/10.1126/science.268.5212.861)
39. Hirotsu M, Fontaine PP, Epshteyn A, Zavalij PY, Sita LR (2007) Dinitrogen activation at ambient temperatures: new modes of H<sub>2</sub> and PhSiH<sub>3</sub> additions for an “end-on-bridged” [Ta(IV)]<sub>2</sub>(μ-η<sup>1</sup>:η<sup>1</sup>-N<sub>2</sub>) complex and for the bis(μ-nitrido) [Ta(V)(μ-N)]<sub>2</sub> product derived from facile N≡N bond cleavage. *J Am Chem Soc* 129:9284–9285. doi:[10.1021/ja072248v](https://doi.org/10.1021/ja072248v)
40. Fontaine PP, Yonke BL, Zavalij PY, Sita LR (2010) Dinitrogen complexation and extent of N≡N activation within the group 6 “end-on-bridged” dinuclear complexes, {(η<sup>5</sup>-C<sub>5</sub>Me<sub>5</sub>)M[N(i-Pr)C(Me)N(i-Pr)]}<sub>2</sub>(μ-η<sup>1</sup>:η<sup>1</sup>-N<sub>2</sub>) (M=Mo and W). *J Am Chem Soc* 132:12273–12285. doi:[10.1021/ja100469f](https://doi.org/10.1021/ja100469f)
41. Keane AJ, Yonke BL, Hirotsu M, Zavalij PY, Sita LR (2014) Fine-tuning the energy barrier for metal-mediated dinitrogen N≡N bond cleavage. *J Am Chem Soc* 136:9906–9909. doi:[10.1021/ja505309j](https://doi.org/10.1021/ja505309j)
42. Peigné B, Cano J, Aullón G (2012) On the coordination of dinitrogen to group 4 metallocenes. *Eur J Inorg Chem* 797–806. doi: [10.1002/ejic.201100788](https://doi.org/10.1002/ejic.201100788)
43. Hirotsu M, Fontaine PP, Zavalij PY, Sita LR (2007) Extreme N≡N bond elongation and facile N-atom functionalization reactions within two structurally versatile new families of group 4 bimetallic “side-on-bridged” dinitrogen complexes for zirconium and hafnium. *J Am Chem Soc* 129:12690–12692. doi:[10.1021/ja0752989](https://doi.org/10.1021/ja0752989)
44. Bezdek MJ, Guo S, Chirik PJ (2016) Terpyridine molybdenum dinitrogen chemistry: synthesis of dinitrogen complexes that vary by five oxidation states. *Inorg Chem* 55:3117–3127. doi:[10.1021/acs.inorgchem.6b00053](https://doi.org/10.1021/acs.inorgchem.6b00053)
45. MacLachlan EA, Fryzuk MD (2006) Synthesis and reactivity of side-on-bound dinitrogen metal complexes. *Organometallics* 25:1530–1543. doi:[10.1021/om051055i](https://doi.org/10.1021/om051055i)
46. Fryzuk MD, Haddad TS, Mylvaganam M, McConville DH, Rettig SJ (1993) End-on versus side-on bonding of dinitrogen to dinuclear early transition-metal complexes. *J Am Chem Soc* 115:2782–2792. doi:[10.1021/ja00060a028](https://doi.org/10.1021/ja00060a028)
47. Armor JN, Taube H (1970) Linkage isomerization in nitrogen-labeled [Ru(NH<sub>3</sub>)<sub>5</sub>N<sub>2</sub>]Br<sub>2</sub>. *J Am Chem Soc* 92:2560–2562. doi:[10.1021/ja00711a066](https://doi.org/10.1021/ja00711a066)
48. Jonas K (1973) π-Bonded nitrogen in a crystalline nickel-lithium complex. *Angew Chem Int Ed Engl* 12:997–998. doi:[10.1002/anie.197309971](https://doi.org/10.1002/anie.197309971)
49. Krüger C, Tsay YH (1973) Molecular structure of a π-dinitrogen-nickel-lithium complex. *Angew Chem Int Ed Engl* 12:998–999. doi:[10.1002/anie.197309981](https://doi.org/10.1002/anie.197309981)
50. Evans WJ, Ulibarri TA, Ziller JW (1988) Isolation and X-ray crystal structure of the first dinitrogen complex of an f-element metal, [(C<sub>5</sub>Me<sub>5</sub>)<sub>2</sub>Sm]<sub>2</sub>N<sub>2</sub>. *J Am Chem Soc* 110:6877–6879. doi:[10.1021/ja00228a043](https://doi.org/10.1021/ja00228a043)
51. Fryzuk MD, Haddad TS, Rettig SJ (1990) Reduction of dinitrogen by a zirconium phosphine complex to form a side-on-bridging N<sub>2</sub> ligand. Crystal structure of {[Pr<sup>3</sup>₂PCH<sub>2</sub>SiMe<sub>2</sub>)<sub>2</sub>N]ZrCl}<sub>2</sub>(μ-η<sup>2</sup>:η<sup>2</sup>-N<sub>2</sub>). *J Am Chem Soc* 112:8185–8186. doi: [10.1021/ja00178a063](https://doi.org/10.1021/ja00178a063)
52. Thorn DL, Tulip TH, Ibers JA (1979) The structure of *trans*-chloro(dinitrogen)bis(triisopropylphosphine)-rhodium(I): an X-ray study of the structure in the solid state and a nuclear magnetic resonance study of the structure in solution. *J Chem Soc Dalton Trans* 2022–2025. doi: [10.1039/dt9790002022](https://doi.org/10.1039/dt9790002022)
53. Peterson EJ, Von Dreele RB, Brown TM (1976) Crystal and molecular structure of tetraiso-thiocyanatobis(2,2'-bipyridine)niobium(IV) and -zirconium(IV). *Inorg Chem* 15:309–315. doi:[10.1021/ic50156a014](https://doi.org/10.1021/ic50156a014)

54. Archer RD, Day RO, Illingsworth ML (1979) Transition-metal eight-coordination. 13. Synthesis, characterization, and crystal and molecular structure of the Schiff-base chelate bis(*N,N'*-disalicylidene-1,2-phenylenediamino)zirconium(IV) benzene solvate. *Inorg Chem* 18:2908–2916. doi:10.1021/ic50200a056
55. Studt F, Morello L, Lehnert N, Fryzuk MD, Tuzcek F (2003) Side-on bridging coordination of N<sub>2</sub>: spectroscopic characterization of the planar Zr<sub>2</sub>N<sub>2</sub> core and theoretical investigation of its butterfly distortion. *Chem A Eur J* 9:520–530. doi:10.1002/chem.200390055
56. Clentsmith GKB, Bates VME, Hitchcock PB, Cloke FGN (1999) Reductive cleavage of dinitrogen by a vanadium diamidoamine complex: the molecular structures of [V(Me<sub>3</sub>SiN{CH<sub>2</sub>CH<sub>2</sub>NSiMe<sub>3</sub>})<sub>2</sub>(μ-N)]<sub>2</sub> and K[V(Me<sub>3</sub>SiN{CH<sub>2</sub>CH<sub>2</sub>NSiMe<sub>3</sub>})<sub>2</sub>(μ-N)]<sub>2</sub>. *J Am Chem Soc* 121:10444–10445. doi:10.1021/ja9921219
57. Bates VME, Clentsmith GKB, Cloke GN, Green JC, Jenkin HDL (2000) Theoretical investigation of the pathway for reductive cleavage of dinitrogen by a vanadium diamidoamine complex. *Chem Commun* 927–928. doi: 10.1039/b002534h
58. Studt F, Lamarche VME, Clentsmith GKB, Cloke FGN, Tuzcek F (2005) Vibrational and electronic structure of the dinuclear bis(μ-nitrido) vanadium(V) complex [V(N{N<sup>⋄</sup>})<sub>2</sub>(μ-N)]<sub>2</sub>: spectroscopic properties of the M<sub>2</sub>(μ-N)<sub>2</sub> diamond core. *Dalton Trans* 1052–1057. doi: 10.1039/b418856j
59. Zhang W, Tang Y, Lei M, Morokuma K, Musaev DG (2011) Ditantalum dinitrogen complex: reaction of H<sub>2</sub> molecule with “end-on-bridged” [Ta<sup>IV</sup>]<sub>2</sub>(μ-η<sup>1</sup>:η<sup>1</sup>-N<sub>2</sub>) and bis(μ-nitrido) [Ta<sup>V</sup>]<sub>2</sub>(μ-N)<sub>2</sub> complexes. *Inorg Chem* 50:9481–9490. doi:10.1021/ic201159z
60. Cavigliasso G, Wilson L, McAlpine S, Attar M, Stranger R, Yates BF (2010) Activation and cleavage of the N–N bond in side-on bound [L<sub>2</sub>M–NN–ML<sub>2</sub>] (L=NH<sub>2</sub>, NMe<sub>2</sub>, N<sup>i</sup>Pr<sub>2</sub>, C<sub>5</sub>H<sub>5</sub>, C<sub>5</sub>Me<sub>4</sub>H) dinitrogen complexes of transition metals from groups 4 through 9. *Dalton Trans* 39:4529–4540. doi:10.1039/b924999k
61. Bobadova-Parvanova P, Wang Q, Morokuma K, Musaev DG (2005) How many methyl groups in [(η<sup>5</sup>-C<sub>5</sub>Me<sub>n</sub>H<sub>5-n</sub>)<sub>2</sub>Zr]<sub>2</sub>(μ<sub>2</sub>,η<sup>2</sup>,η<sup>2</sup>-N<sub>2</sub>) are needed for dinitrogen hydrogenation? A theoretical study. *Angew Chem Int Ed* 44:7101–7103. doi:10.1002/anie.200501371
62. Chirik PJ (2010) Group 4 transition metal sandwich complexes: still fresh after almost 60 years. *Organometallics* 29:1500–1517. doi:10.1021/om100016p
63. Pool JA, Lobkovsky E, Chirik PJ (2004) Hydrogenation and cleavage of dinitrogen to ammonia with a zirconium complex. *Nature* 427:527–530. doi:10.1038/nature02274
64. Manriquez JM, Bercau JE (1974) Preparation of a dinitrogen complex of bis(pentamethylcyclopentadienyl)zirconium(II). Isolation and protonation leading to stoichiometric reduction of dinitrogen to hydrazine. *J Am Chem Soc* 96:6229–6230. doi:10.1021/ja00826a071
65. Pool JA, Bernskoetter WH, Chirik PJ (2004) On the origin of dinitrogen hydrogenation promoted by [(η<sup>5</sup>-C<sub>5</sub>Me<sub>4</sub>H)<sub>2</sub>Zr]<sub>2</sub>(μ<sub>2</sub>,η<sup>2</sup>,η<sup>2</sup>-N<sub>2</sub>). *J Am Chem Soc* 126:14326–14327. doi:10.1021/ja045566s
66. Knobloch DJ, Lobkovsky E, Chirik PJ (2010) Dinitrogen cleavage and functionalization by carbon monoxide promoted by a hafnium complex. *Nat Chem* 2:30–35. doi:10.1038/nchem.477
67. Bobadova-Parvanova P, Wang Q, Quinonero-Santiago D, Morokuma K, Musaev DG (2006) Does dinitrogen hydrogenation follow different mechanisms for [(η<sup>5</sup>-C<sub>5</sub>Me<sub>4</sub>H)<sub>2</sub>Zr]<sub>2</sub>(μ<sub>2</sub>,η<sup>2</sup>,η<sup>2</sup>-N<sub>2</sub>) and [(PhP(CH<sub>2</sub>SiMe<sub>2</sub>NSiMe<sub>2</sub>CH<sub>2</sub>)PPh)Zr]<sub>2</sub>(μ<sub>2</sub>,η<sup>2</sup>,η<sup>2</sup>-N<sub>2</sub>) complexes? A computational study. *J Am Chem Soc* 128:11391–11403. doi:10.1021/ja057937q
68. Fryzuk MD, Johnson SA, Rettig SJ (1998) New mode of coordination for the dinitrogen ligand: a dinuclear tantalum complex with a bridging N<sub>2</sub> unit that is both side-on and end-on. *J Am Chem Soc* 120:11024–11025. doi:10.1021/ja982377z
69. Fryzuk MD, Johnson SA, Patrick BO, Albinati A, Mason SA, Koetzle TF (2001) New mode of coordination for the dinitrogen ligand: formation, bonding, and reactivity of a tantalum complex with a bridging N<sub>2</sub> unit that is both side-on and end-on. *J Am Chem Soc* 123:3960–3973. doi:10.1021/ja0041371



70. Fryzuk MD, MacKay BA, Johnson SA, Patrick BO (2002) Hydroboration of coordinated dinitrogen: a new reaction for the  $N_2$  ligand that results in its functionalization and cleavage. *Angew Chem Int Ed* 41:3709–3712. doi:[10.1002/1521-3773\(20021004\)41:19<3709::aid-anie3709>3.0.co;2-u](https://doi.org/10.1002/1521-3773(20021004)41:19<3709::aid-anie3709>3.0.co;2-u)
71. Fryzuk MD, MacKay BA, Patrick BO (2003) Hydrosilylation of a dinuclear tantalum dinitrogen complex: cleavage of  $N_2$  and functionalization of both nitrogen atoms. *J Am Chem Soc* 125:3234–3235. doi:[10.1021/ja034303f](https://doi.org/10.1021/ja034303f)
72. MacKay BA, Munha RF, Fryzuk MD (2006) Substituent effects in the hydrosilylation of coordinated dinitrogen in a ditantalum complex: cleavage and functionalization of  $N_2$ . *J Am Chem Soc* 128:9472–9483. doi:[10.1021/ja061508q](https://doi.org/10.1021/ja061508q)
73. Yeo A, Shaver MP, Fryzuk MD (2015) A new side-on end-on ditantalum dinitrogen complex and its reaction with  $BuSiH_3$ . *Z Anorg Allg Chem* 641:123–127. doi:[10.1002/zaac.201400167](https://doi.org/10.1002/zaac.201400167)
74. MacKay BA, Patrick BO, Fryzuk MD (2005) Hydroalumination of a dinuclear tantalum dinitrogen complex: N–N bond cleavage and ancillary ligand rearrangement. *Organometallics* 24:3836–3841. doi:[10.1021/om050208z](https://doi.org/10.1021/om050208z)
75. Spencer LP, MacKay BA, Patrick BO, Fryzuk MD (2006) Inner-sphere two-electron reduction leads to cleavage and functionalization of coordinated dinitrogen. *Proc Natl Acad Sci U S A* 103:17094–17098. doi:[10.1073/pnas.0602132103](https://doi.org/10.1073/pnas.0602132103)
76. Ballmann J, Yeo A, Patrick BO, Fryzuk MD (2011) Carbon-nitrogen bond formation by the reaction of 1,2-cumulenes with a ditantalum complex containing side-on- and end-on-bound dinitrogen. *Angew Chem Int Ed* 50:507–510. doi:[10.1002/anie.201005704](https://doi.org/10.1002/anie.201005704)
77. Cui Q, Musaeov DG, Svensson M, Sieber S, Morokuma K (1995)  $N_2$  cleavage by three-coordinate group 6 complexes. W(III) Complexes would be better than Mo(III) complexes. *J Am Chem Soc* 117:12366–12367. doi:[10.1021/ja00154a052](https://doi.org/10.1021/ja00154a052)
78. Peters JC, Cherry JPF, Thomas JC, Baraldo L, Mindiola DJ, Davis WM, Cummins CC (1999) Redox-catalyzed binding of dinitrogen by molybdenum *N-tert*-hydrocarbylanilide complexes: implications for dinitrogen functionalization and reductive cleavage. *J Am Chem Soc* 121:10053–10067. doi:[10.1021/ja991435t](https://doi.org/10.1021/ja991435t)
79. Kol M, Schrock RR, Kempe R, Davis WM (1994) Synthesis of molybdenum and tungsten complexes that contain triamidoamine ligands of the type  $(C_6F_5NCH_2CH_2)_3N$  and activation of dinitrogen by molybdenum. *J Am Chem Soc* 116:4382–4390. doi:[10.1021/ja00089a028](https://doi.org/10.1021/ja00089a028)
80. Shih KY, Schrock RR, Kempe R (1994) Synthesis of molybdenum complexes that contain silylated triamidoamine ligands. A  $\mu$ -dinitrogen complex, methyl and acetylide complexes, and coupling of acetylides. *J Am Chem Soc* 116:8804–8805. doi:[10.1021/ja00098a048](https://doi.org/10.1021/ja00098a048)
81. Christian G, Driver J, Stranger R (2003) Dinitrogen activation in sterically-hindered three-coordinate transition metal complexes. *Faraday Discuss* 124:331–341. doi:[10.1039/b211335j](https://doi.org/10.1039/b211335j)
82. Christian G, Stranger R, Yates BF, Graham DC (2005) Ligand rotation in  $[Ar(R)N]_3M-N_2-M [N(R)Ar]_3$  ( $M, M' = Mo^{III}, Nb^{III}$ ,  $R = ^iPr$  and  $^tBu$ ) dimers. *Dalton Trans* 962–968. doi:[10.1039/b413766c](https://doi.org/10.1039/b413766c)
83. Brookes NJ, Graham DC, Christian G, Stranger R, Yates BF (2009) The influence of peripheral ligand bulk on nitrogen activation by three-coordinate molybdenum complexes – a theoretical study using the ONIOM method. *J Comput Chem* 30:2146–2156. doi:[10.1002/jcc.21199](https://doi.org/10.1002/jcc.21199)
84. Solari E, Da Silva C, Iacono B, Hesselbrouck J, Rizzoli C, Scopelliti R, Floriani C (2001) Photochemical activation of the  $N\equiv N$  bond in a dimolybdenum–dinitrogen complex: formation of a molybdenum nitride. *Angew Chem Int Ed* 40:3907–3909. doi:[10.1002/1521-3773\(20011015\)40:20<3907::aid-anie3907>3.0.co;2-#](https://doi.org/10.1002/1521-3773(20011015)40:20<3907::aid-anie3907>3.0.co;2-#)
85. Huss AS, Curley JJ, Cummins CC, Blank DA (2013) Relaxation and dissociation following photoexcitation of the  $(\mu-N_2)[Mo(N[t-Bu]Ar)_3]_2$  dinitrogen cleavage intermediate. *J Phys Chem B* 117:1429–1436. doi:[10.1021/jp310122x](https://doi.org/10.1021/jp310122x)
86. Reiher M, Kirchner B, Hutter J, Sellmann D, Hess BA (2004) A photochemical activation scheme of inert dinitrogen by dinuclear  $Ru^{II}$  and  $Fe^{II}$  complexes. *Chem A Eur J* 10:4443–4453. doi:[10.1002/chem.200400081](https://doi.org/10.1002/chem.200400081)

87. Chisholm MH, Cotton FA, Frenz BA, Reichert WW, Shive LW, Stults BR (1976) The molybdenum–molybdenum triple bond. 1. Hexakis(dimethylamido)dimolybdenum and some homologues: preparation, structure, and properties. *J Am Chem Soc* 98:4469–4476. doi:[10.1021/ja00431a024](https://doi.org/10.1021/ja00431a024)
88. Hahn J, Landis CR, Nasluzov VA, Neyman KM, Rösch N (1997) Steric effects on dinitrogen cleavage by three-coordinate molybdenum(III) complexes: a molecular mechanics study. *Inorg Chem* 36:3947–3951. doi:[10.1021/ic961466e](https://doi.org/10.1021/ic961466e)
89. Johnson MJA, Lee PM, Odom AL, Davis WM, Cummins CC (1997) Atom-bridged intermediates in N- and P-atom transfer reactions. *Angew Chem Int Ed Engl* 36:87–91. doi:[10.1002/anie.199700871](https://doi.org/10.1002/anie.199700871)
90. Cummins CC (1998) Reductive cleavage and related reactions leading to molybdenum–element multiple bonds: new pathways offered by three-coordinate molybdenum(III). *Chem Commun* 1777–1786. doi: [10.1039/a802402b](https://doi.org/10.1039/a802402b)
91. Laplaza CE, Johnson AR, Cummins CC, October RV (1996) Nitrogen atom transfer coupled with dinitrogen cleavage and Mo–Mo triple bond formation. *J Am Chem Soc* 118:709–710. doi:[10.1021/ja953573y](https://doi.org/10.1021/ja953573y)
92. Tsai YC, Johnson MJA, Mindiola DJ, Cummins CC, Klooster WT, Koetzle TF (1999) A cyclometalated resting state for a reactive molybdenum amide: favorable consequences of  $\beta$ -hydrogen elimination including reductive cleavage, coupling, and complexation. *J Am Chem Soc* 121:10426–10427. doi:[10.1021/ja9917464](https://doi.org/10.1021/ja9917464)
93. van Koten G, Milstein D (eds) (2013) Organometallic pincer chemistry. Topics in organometallic chemistry, vol 40. Springer, Heidelberg
94. Szabo KJ, Wendt OF (eds) (2014) Pincer and pincer-type complexes: applications in organic synthesis and catalysis. Wiley-VCH, Weinheim
95. Smythe NC, Schrock RR, Müller P, Weare WW (2006) Synthesis of [(HIPTNCH<sub>2</sub>CH<sub>2</sub>)<sub>3</sub>N]Cr compounds (HIPT=3,5-(2,4,6-*i*-Pr<sub>3</sub>C<sub>6</sub>H<sub>2</sub>)<sub>2</sub>C<sub>6</sub>H<sub>3</sub>) and an evaluation of chromium for the reduction of dinitrogen to ammonia. *Inorg Chem* 45:7111–7118. doi:[10.1021/ic060549k](https://doi.org/10.1021/ic060549k)
96. Vidyaratne I, Scott J, Gambarotta S, Budzelaar PHM (2007) Dinitrogen activation, partial reduction, and formation of coordinated imide promoted by a chromium diiminepyridine complex. *Inorg Chem* 46:7040–7049. doi:[10.1021/ic700810f](https://doi.org/10.1021/ic700810f)
97. Hebden TJ, Schrock RR, Takase MK, Müller P (2012) Cleavage of dinitrogen to yield a (*t*-BuPOCOP)molybdenum(IV) nitride. *Chem Commun* 48:1851–1853. doi:[10.1039/c2cc17634c](https://doi.org/10.1039/c2cc17634c)
98. Liao Q, Cavallé A, Saffon-Merceron N, Mézailles N (2016) Direct synthesis of silylamine from N<sub>2</sub> and a silane: mediated by a tridentate phosphine molybdenum fragment. *Angew Chem Int Ed* 55:11212–11216. doi:[10.1002/anie.201604812](https://doi.org/10.1002/anie.201604812)
99. Liao Q, Saffon-Merceron N, Mézailles N (2015) N<sub>2</sub> reduction into silylamine at tridentate phosphine/Mo center: catalysis and mechanistic study. *ACS Catal* 5:6902–6906. doi:[10.1021/acscatal.5b01626](https://doi.org/10.1021/acscatal.5b01626)
100. Arashiba K, Kinoshita E, Kuriyama S, Eizawa A, Nakajima K, Tanaka H, Yoshizawa K, Nishibayashi Y (2015) Catalytic reduction of dinitrogen to ammonia by use of molybdenum–nitride complexes bearing a tridentate triphosphine as catalysts. *J Am Chem Soc* 137:5666–5669. doi:[10.1021/jacs.5b02579](https://doi.org/10.1021/jacs.5b02579)
101. Klopsch I, Finger M, Würtele C, Milde B, Werz DB, Schneider S (2014) Dinitrogen splitting and functionalization in the coordination sphere of rhenium. *J Am Chem Soc* 136:6881–6883. doi:[10.1021/ja502759d](https://doi.org/10.1021/ja502759d)
102. Klopsch I, Kinauer M, Finger M, Würtele C, Schneider S (2016) Conversion of dinitrogen into acetonitrile under ambient conditions. *Angew Chem Int Ed* 55:4786–4789. doi:[10.1002/anie.201600790](https://doi.org/10.1002/anie.201600790)
103. Scheibel MG, Askevold B, Heinemann FW, Reijerse EJ, de Bruin B, Schneider S (2012) Closed-shell and open-shell square-planar iridium nitrido complexes. *Nat Chem* 4:552–558. doi:[10.1038/nchem.1368](https://doi.org/10.1038/nchem.1368)

104. Scheibel MG, Wu Y, Stückl AC, Krause L, Carl E, Stalke D, de Bruin B, Schneider S (2013) Synthesis and reactivity of a transient, terminal nitrido complex of rhodium. *J Am Chem Soc* 135:17719–17722. doi:[10.1021/ja409764j](https://doi.org/10.1021/ja409764j)
105. Abbenseth J, Finger M, Würtele C, Kasanmascheff M, Schneider S (2016) Coupling of terminal iridium nitrido complexes. *Inorg Chem Front* 3:469–477. doi:[10.1039/c5qi00267b](https://doi.org/10.1039/c5qi00267b)
106. Keane AJ, Farrell WS, Yonke BL, Zavalij PY, Sita LR (2015) Metal-mediated production of isocyanates,  $R_3EN=C=O$  from dinitrogen, carbon dioxide, and  $R_3ECl$ . *Angew Chem Int Ed* 54:10220–10224. doi:[10.1002/anie.201502293](https://doi.org/10.1002/anie.201502293)
107. Miyazaki T, Tanaka H, Tanabe Y, Yuki M, Nakajima K, Yoshizawa K, Nishibayashi Y (2014) Cleavage and formation of molecular dinitrogen in a single system assisted by molybdenum complexes bearing ferrocenyldiphosphine. *Angew Chem Int Ed* 53:11488–11492. doi:[10.1002/anie.201405673](https://doi.org/10.1002/anie.201405673)
108. Rebreyend C, de Bruin B (2015) Photolytic  $N_2$  splitting: a road to sustainable  $NH_3$  production? *Angew Chem Int Ed* 54:42–44. doi:[10.1002/anie.201409727](https://doi.org/10.1002/anie.201409727)
109. Crossland JL, Tyler DR (2010) Iron–dinitrogen coordination chemistry: dinitrogen activation and reactivity. *Coord Chem Rev* 254:1883–1894. doi:[10.1016/j.ccr.2010.01.005](https://doi.org/10.1016/j.ccr.2010.01.005)
110. Khoenkhoen N, de Bruin B, Reek JNH, Dzik WI (2015) Reactivity of dinitrogen bound to mid- and late-transition-metal centers. *Eur J Inorg Chem* 567–598. doi: [10.1002/ejic.201403041](https://doi.org/10.1002/ejic.201403041)
111. McWilliams SF, Holland PL (2015) Dinitrogen binding and cleavage by multinuclear iron complexes. *Acc Chem Res* 48:2059–2065. doi:[10.1021/acs.accounts.5b00213](https://doi.org/10.1021/acs.accounts.5b00213)
112. Hazari N (2010) Homogeneous iron complexes for the conversion of dinitrogen into ammonia and hydrazine. *Chem Soc Rev* 39:4044–4056. doi:[10.1039/b919680n](https://doi.org/10.1039/b919680n)
113. MacLeod KC, Holland PL (2013) Recent developments in the homogeneous reduction of dinitrogen by molybdenum and iron. *Nat Chem* 5:559–565. doi:[10.1038/nchem.1620](https://doi.org/10.1038/nchem.1620)
114. Betley TA, Peters JC (2004) A tetrahedrally coordinated  $L_3Fe-N_x$  platform that accommodates terminal nitride ( $Fe^{IV}\equiv N$ ) and dinitrogen ( $Fe^I-N_2-Fe^I$ ) ligands. *J Am Chem Soc* 126:6252–6254. doi:[10.1021/ja048713v](https://doi.org/10.1021/ja048713v)
115. Hendrich MP, Gunderson W, Behan RK, Green MT, Mehn MP, Betley TA, Lu CC, Peters JC (2006) On the feasibility of  $N_2$  fixation via a single-site  $Fe^I/Fe^{IV}$  cycle: spectroscopic studies of  $Fe^I(N_2)Fe^I$ ,  $Fe^{IV}\equiv N$ , and related species. *Proc Natl Acad Sci U S A* 103:17107–17112. doi:[10.1073/pnas.0604402103](https://doi.org/10.1073/pnas.0604402103)
116. Krahe O, Bill E, Neese F (2014) Decay of iron(V) nitride complexes by a N–N bond-coupling reaction in solution: a combined spectroscopic and theoretical analysis. *Angew Chem Int Ed* 53:8727–8731. doi:[10.1002/anie.201403402](https://doi.org/10.1002/anie.201403402)
117. Kane-Maguire LAP, Sheridan PS, Basolo F, Pearson RG (1970) Azidoruthenium(III) complexes as precursors for molecular nitrogen and nitrene complexes. *J Am Chem Soc* 92:5865–5872. doi:[10.1021/ja00723a009](https://doi.org/10.1021/ja00723a009)
118. Buhr JD, Taube H (1979) Oxidation of  $[Os(NH_3)_5CO]^{2+}$  to  $[(Os(NH_3)_4CO)_2N_2]^{4+}$ . *Inorg Chem* 18:2208–2212. doi:[10.1021/ic50198a032](https://doi.org/10.1021/ic50198a032)
119. Che CM, Lam HW, Tong WF, Lai TF, Lau TC (1989) Model reactions for nitrogen fixation. Photo-induced formation and X-ray crystal structure of  $[Os_2(NH_3)_8(MeCN)_2(N_2)]^{5+}$  from  $[Os^VI(NH_3)_4N]^{3+}$ . *J Chem Soc Chem Commun* 1883–1884. doi: [10.1039/c39890001883](https://doi.org/10.1039/c39890001883)
120. Ware DC, Taube H (1991) Substitution-induced N–N coupling for nitride coordinated to osmium(VI). *Inorg Chem* 30:4605–4610. doi:[10.1021/ic00024a029](https://doi.org/10.1021/ic00024a029)
121. Demadis KD, Meyer TJ, White PS (1997) Localization in *trans,trans*- $[(tpy)(Cl)_2Os^{III}(N_2)Os^{II}(Cl)_2(tpy)]^+$  ( $tpy=2,2':6',2''$ -Terpyridine). *Inorg Chem* 36:5678–5679. doi:[10.1021/ic970885o](https://doi.org/10.1021/ic970885o)
122. Seymore SB, Brown SN (2002) Polar effects in nitride coupling reactions. *Inorg Chem* 41:462–469. doi:[10.1021/ic010844z](https://doi.org/10.1021/ic010844z)
123. Kunkely H, Vogler A (2010) Photolysis of aqueous  $[(NH_3)_5Os(\mu-N_2)Os(NH_3)_5]^{5+}$ : cleavage of dinitrogen by an intramolecular photoredox reaction. *Angew Chem Int Ed* 49:1591–1593. doi:[10.1002/anie.200905026](https://doi.org/10.1002/anie.200905026)
124. Rodriguez MM, Bill E, Brennessel WW, Holland PL (2011)  $N_2$  reduction and hydrogenation to ammonia by a molecular iron-potassium complex. *Science* 334:780–783. doi:[10.1126/science.1211906](https://doi.org/10.1126/science.1211906)

125. Smith JM, Lachicotte RJ, Pittard KA, Cundari TR, Lukat-Rodgers G, Rodgers KR, Holland PL (2001) Stepwise reduction of dinitrogen bond order by a low-coordinate iron complex. *J Am Chem Soc* 123:9222–9223. doi:[10.1021/ja016094+](https://doi.org/10.1021/ja016094+)
126. Figg TM, Holland PL, Cundari TR (2012) Cooperativity between low-valent iron and potassium promoters in dinitrogen fixation. *Inorg Chem* 51:7546–7550. doi:[10.1021/ic300150u](https://doi.org/10.1021/ic300150u)
127. Grubel K, Brennessel WW, Mercado BQ, Holland PL (2014) Alkali metal control over N–N cleavage in iron complexes. *J Am Chem Soc* 136:16807–16816. doi:[10.1021/ja507442b](https://doi.org/10.1021/ja507442b)
128. McWilliams SF, Rodgers KR, Lukat-Rodgers G, Mercado BQ, Grubel K, Holland PL (2016) Alkali metal variation and twisting of the FeNNFe core in bridging diiron dinitrogen complexes. *Inorg Chem* 55:2960–2968. doi:[10.1021/acs.inorgchem.5b02841](https://doi.org/10.1021/acs.inorgchem.5b02841)
129. MacLeod KC, Vinyard DJ, Holland PL (2014) A multi-iron system capable of rapid N<sub>2</sub> formation and N<sub>2</sub> cleavage. *J Am Chem Soc* 136:10226–10229. doi:[10.1021/ja505193z](https://doi.org/10.1021/ja505193z)
130. MacLeod KC, McWilliams SF, Mercado BQ, Holland PL (2016) Stepwise N–H bond formation from N<sub>2</sub>-derived iron nitride, imide and amide intermediates to ammonia. *Chem Sci* 7:5736–5746. doi:[10.1039/c6sc00423g](https://doi.org/10.1039/c6sc00423g)
131. MacLeod KC, Menges FS, McWilliams SF, Craig SM, Mercado BQ, Johnson MA, Holland PL (2016) Alkali-controlled C–H cleavage or N–C bond formation by N<sub>2</sub>-derived iron nitrides and imides. *J Am Chem Soc* 138:11185–11191. doi:[10.1021/jacs.6b04984](https://doi.org/10.1021/jacs.6b04984)
132. Lee Y, Sloane FT, Blondin G, Abboud KA, García-Serres R, Murray LJ (2015) Dinitrogen activation upon reduction of a triiron(II) complex. *Angew Chem Int Ed* 54:1499–1503. doi:[10.1002/anie.201409676](https://doi.org/10.1002/anie.201409676)
133. Eikey RA, Abu-Omar MM (2003) Nitrido and imido transition metal complexes of groups 6–8. *Coord Chem Rev* 243:83–124. doi:[10.1016/S0010-8545\(03\)00048-1](https://doi.org/10.1016/S0010-8545(03)00048-1)
134. Berry JF (2009) Terminal nitrido and imido complexes of the late transition metals. *Comm Inorg Chem* 30:28–66. doi:[10.1080/02603590902768875](https://doi.org/10.1080/02603590902768875)
135. Shima T, Hu S, Luo G, Kang X, Luo Y, Hou Z (2013) Dinitrogen cleavage and hydrogenation by a trinuclear titanium polyhydride complex. *Science* 340:1549–1552. doi:[10.1126/science.1238663](https://doi.org/10.1126/science.1238663)
136. Nikiforov GB, Vidyaratne I, Gambarotta S, Korobkov I (2009) Titanium-promoted dinitrogen cleavage, partial hydrogenation, and silylation. *Angew Chem Int Ed* 48:7415–7419. doi:[10.1002/anie.200903648](https://doi.org/10.1002/anie.200903648)
137. Vidyaratne I, Crewdson P, Lefebvre E, Gambarotta S (2007) Dinitrogen coordination and cleavage promoted by a vanadium complex of a  $\sigma,\pi,\sigma$ -donor ligand. *Inorg Chem* 46:8836–8842
138. Akagi F, Matsuo T, Kawaguchi H (2007) Dinitrogen cleavage by a diniobium tetrahydride complex: formation of a nitride and its conversion into imide species. *Angew Chem Int Ed* 46:8778–8781. doi:[10.1002/anie.200703336](https://doi.org/10.1002/anie.200703336)
139. Searles K, Carroll PJ, Chen CH, Pink M, Mindiola DJ (2015) Niobium-nitrides derived from nitrogen splitting. *Chem Commun* 51:3526–3528. doi:[10.1039/c4cc09563d](https://doi.org/10.1039/c4cc09563d)
140. Andino JG, Mazumder S, Pal K, Caulton KG (2013) New approaches to functionalizing metal-coordinated N<sub>2</sub>. *Angew Chem Int Ed* 52:4726–4732. doi:[10.1002/anie.201209168](https://doi.org/10.1002/anie.201209168)
141. Benson SW (1965) Bond energies. *J Chem Educ* 42:502–518. doi:[10.1021/ed042p502](https://doi.org/10.1021/ed042p502)
142. Burgess DR. Thermochemical data. In: Linstrom PJ, Mallard WG (eds) NIST chemistry WebBook, NIST standard reference database number 69. National Institute of Standards and Technology, Gaithersburg MD. <http://webbook.nist.gov>
143. Kawaguchi H, Matsuo T (2002) Dinitrogen-bond cleavage in a niobium complex supported by a tridentate aryloxy ligand. *Angew Chem Int Ed* 41:2792–2794. doi:[10.1002/1521-3773\(20020802\)41:15<2792::aid-anie2792>3.0.co;2-k](https://doi.org/10.1002/1521-3773(20020802)41:15<2792::aid-anie2792>3.0.co;2-k)
144. Akagi F, Suzuki S, Ishida Y, Hatanaka T, Matsuo T, Kawaguchi H (2013) Reactions of a niobium nitride complex prepared from dinitrogen: synthesis of imide and ureate complexes and ammonia formation. *Eur J Inorg Chem* 3930–3936. doi: [10.1002/ejic.201300172](https://doi.org/10.1002/ejic.201300172)
145. Ishida Y, Kawaguchi H (2014) Nitrogen atom transfer from a dinitrogen-derived vanadium nitride complex to carbon monoxide and isocyanide. *J Am Chem Soc* 136:16990–16993. doi:[10.1021/ja510317h](https://doi.org/10.1021/ja510317h)

146. Yonke BL, Reeds JP, Fontaine PP, Zavalij PY, Sita LR (2014) Catalytic production of isocyanates via orthogonal atom and group transfers employing a shared formal group 6 M (II)/M(IV) redox cycle. *Organometallics* 33:3239–3242. doi:[10.1021/om500532s](https://doi.org/10.1021/om500532s)
147. Cozzolino AF, Silvia JS, Lopez N, Cummins CC (2014) Experimental and computational studies on the formation of cyanate from early metal terminal nitrido ligands and carbon monoxide. *Dalton Trans* 43:4639–4652. doi:[10.1039/c3dt52738g](https://doi.org/10.1039/c3dt52738g)
148. Silvia JS, Cummins CC (2009) Two-electron reduction of a vanadium(V) nitride by CO to release cyanate and open a coordination site. *J Am Chem Soc* 131:446–447. doi:[10.1021/ja807767w](https://doi.org/10.1021/ja807767w)
149. Tran BL, Pink M, Gao X, Park H, Mendiola DJ (2010) Low-coordinate and neutral nitrido complexes of vanadium. *J Am Chem Soc* 132:1458–1459. doi:[10.1021/ja908303k](https://doi.org/10.1021/ja908303k)
150. Sceats EL, Figueroa JS, Cummins CC, Loening NM, Van der Wel P, Griffin RG (2004) Complexes obtained by electrophilic attack on a dinitrogen-derived terminal molybdenum nitride: electronic structure analysis by solid state CP/MAS <sup>15</sup>N NMR in combination with DFT calculations. *Polyhedron* 23:2751–2768. doi:[10.1016/j.poly.2004.08.010](https://doi.org/10.1016/j.poly.2004.08.010)
151. Curley JJ, Cozzolino AF, Cummins CC (2011) Nitrogen fixation to cyanide at a molybdenum center. *Dalton Trans* 40:2429–2432. doi:[10.1039/c0dt01326a](https://doi.org/10.1039/c0dt01326a)
152. Sivasankar C, Tuzcek F (2006) Double deprotonation of coordinated ethylimide to CH<sub>3</sub>CN: molecular mechanism and relevance to the chemistry of Mo and W organoimides. *Dalton Trans* 3396–3398. doi: [10.1039/b602038k](https://doi.org/10.1039/b602038k)
153. Kukushkin VY, Pombeiro AJL (2002) Additions to metal-activated organonitriles. *Chem Rev* 102:1771–1802. doi:[10.1021/cr0103266](https://doi.org/10.1021/cr0103266)
154. Henderickx H, Kwakkenbos G, Peters A, van der Spoel J, de Vries K (2003) Direct formation of an organonitrogen compound from a molybdenum nitrido species. *Chem Commun* 897:2050–2051. doi:[10.1039/b305774g](https://doi.org/10.1039/b305774g)
155. Curley JJ, Sceats EL, Cummins CC (2006) A cycle for organic nitrile synthesis via dinitrogen cleavage. *J Am Chem Soc* 128:14036–14037. doi:[10.1021/ja066090a](https://doi.org/10.1021/ja066090a)
156. Mendiola DJ, Meyer K, Cherry JPF, Baker TA, Cummins CC (2000) Dinitrogen cleavage stemming from a heterodinuclear niobium/molybdenum N<sub>2</sub> complex: new nitridoniobium systems including a niobazene cyclic trimer. *Organometallics* 19:1622–1624. doi:[10.1021/om000159k](https://doi.org/10.1021/om000159k)
157. Figueroa JS, Piro NA, Clough CR, Cummins CC (2006) A nitridoniobium(V) reagent that effects acid chloride to organic nitrile conversion: synthesis via heterodinuclear (Nb/Mo) dinitrogen cleavage, mechanistic insights, and recycling. *J Am Chem Soc* 128:940–950. doi:[10.1021/ja056408j](https://doi.org/10.1021/ja056408j)
158. Hou Z, Shima T, Hu S, Endo Y (2014) Novel complex and use of same. WO Patent 2014080939 A1, US Patent 20150291635
159. Hu S, Shima T, Luo Y, Hou Z (2013) Tetranuclear zirconium and hafnium polyhydride complexes composed of the “CpMH<sub>2</sub>” units. *Organometallics* 32:2145–2151. doi:[10.1021/om400012a](https://doi.org/10.1021/om400012a)
160. Guru MM, Shima T, Hou Z (2016) Conversion of dinitrogen to nitriles at a multinuclear titanium framework. *Angew Chem Int Ed*. doi: [10.1002/anie.201607426](https://doi.org/10.1002/anie.201607426)
161. Askevold B, Nieto JT, Tussupbayev S, Diefenbach M, Herdweck E, Holthausen MC, Schneider S (2011) Ammonia formation by metal-ligand cooperative hydrogenolysis of a nitrido ligand. *Nat Chem* 3:532–537. doi:[10.1038/nchem.1051](https://doi.org/10.1038/nchem.1051)
162. Schendzielorz FS, Finger M, Volkmann C, Würtele C, Schneider S (2016) A terminal osmium(IV) nitride: ammonia formation and ambiphilic reactivity. *Angew Chem Int Ed* 55:11417–11420. doi:[10.1002/anie.201604917](https://doi.org/10.1002/anie.201604917)
163. Walstrom A, Fan H, Pink M, Caulton KG (2010) Unexpected selectivity in electrophilic attack on (PNP)RuN. *Inorg Chim Acta* 363:633–636. doi:[10.1016/j.ica.2008.11.010](https://doi.org/10.1016/j.ica.2008.11.010)

# Synthetic Nitrogen Fixation with Mononuclear Molybdenum(0) Phosphine Complexes: Occupying the *trans*-Position of Coordinated N<sub>2</sub>

Nadja Stucke, Thomas Weyrich, Mareike Pfeil, Katharina Grund, Andrei Kindjajev, and Felix Tuczek

**Abstract** Synthetic nitrogen fixation with molybdenum phosphine complexes has witnessed a renaissance recently due to the discovery that such systems are competent to catalytically convert N<sub>2</sub> to ammonia. In the framework of this research area, we have prepared complexes of the type [Mo(N<sub>2</sub>)(PEP)(P<sub>2</sub>)] (E = N, P; P<sub>2</sub> = dp<sub>3</sub>pm, dmp<sub>3</sub>m) in which the linear PEP ligand coordinates in a facial geometry. Similar complexes have been prepared using mixed carbene–phosphine (PCP) ligands. Furthermore, molybdenum bis(dinitrogen) complexes have been synthesized which are facially coordinated by a tripod ligand and contain the bidentate coligands dp<sub>3</sub>pm and dmp<sub>3</sub>m. Recently, both of these approaches have been united in the synthesis of a Mo(0)–N<sub>2</sub> complex supported by a pentadentate tetrapodal (pentaPod) ligand. The structural, electronic, and vibrational properties of all of these dinitrogen complexes have been investigated by NMR, IR, and Raman spectroscopy, and their reactivities in a nitrogen fixing cycle have been evaluated. To this end, protonated derivatives have been investigated as well. On the basis of these results and DFT calculations, these systems are promising candidates for the catalytic conversion of N<sub>2</sub> to ammonia.

**Keywords** Mixed phosphine/carbene ligands • Molybdenum complexes • Multidentate phosphine ligands • Nitrogen fixation

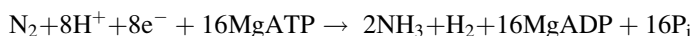
## Contents

1 Introduction .....	114
2 Mo(0)–Dinitrogen Complexes Supported by Tridentate PEP Ligands (E = P, N) .....	115

3	Mo(0)–Dinitrogen Complexes Supported by Mixed Imidazol–Ylidene/Phosphanyl Hybrid Ligands .....	119
4	Mo(0)–Dinitrogen Complexes Supported by Tripodal Ligands with Aryl Substituents .....	130
5	Mo(0)–Dinitrogen Complexes Supported by Hybrid Tripodal Ligands with Mixed Dialkylphosphine/Diarylphosphine Donor Groups .....	135
6	Mo(0)–Dinitrogen Complexes Supported by Tetradentate NP <sub>3</sub> Ligands .....	139
7	Mo(0)–Dinitrogen Complex Supported by a Pentadentate Tetrapodal Phosphine (pentaPod <sup>P</sup> ) Ligand .....	144
8	Summary and Conclusion .....	149
	References .....	150

## 1 Introduction

One of the grand challenges of biological, inorganic, and organometallic chemistry is the conversion of molecular dinitrogen to ammonia under ambient conditions [1]. In nature, this process is catalyzed by the enzyme nitrogenase according to the equation [2]:



This process is highly energy consuming [3], and during the reduction not only ammonia but also H<sub>2</sub> is developed. Nitrogenase consists of two proteins. The larger one, called molybdenum–iron (MoFe) protein, is an α<sub>2</sub>β<sub>2</sub>-tetramer which contains two iron–sulfur clusters, the P-clusters, and two iron–molybdenum cofactors (FeMoco) which are the active site of the enzyme where the reduction of dinitrogen occurs [4–7]. The electrons needed are provided by the iron (Fe) protein by forming a complex with the MoFe protein. One electron is transferred from the Fe protein; then the Fe protein dissociates and is recharged, so it is able to reduce the MoFe protein again. After accomplishing this process eight times, one catalytic cycle is completed [8].

Dinitrogen can also be converted to ammonia under ambient conditions by transition metal complexes [9, 10]. In the last years, synthetic model systems have been established that even allow a catalytic ammonia synthesis in a nitrogenase-like fashion with turnover numbers of up to 60 per mononuclear catalytic metal site [11, 12]. The earliest of these systems was discovered by Schrock and coworkers in 2003 and is based on a molybdenum complex with a sterically shielding HIPTN<sub>3</sub>N ligand (HIPTN<sub>3</sub>N = [{3,5-(2,4,6-*i*Pr<sub>3</sub>C<sub>6</sub>H<sub>2</sub>)<sub>2</sub>C<sub>6</sub>H<sub>3</sub>NCH<sub>2</sub>CH<sub>2</sub>}]<sub>3</sub>N]<sup>3-</sup>) [13, 14]. Using decamethylchromocene as reductant and lutidinium BAR<sup>F</sup> (BAR<sup>F</sup> = tetrakis[3,5-bis(trifluoromethyl)phenyl]borate) as proton source, ammonia was generated from N<sub>2</sub> with this system in four cycles with an overall yield of 65% [14]. A few years later, Nishibayashi et al. established a dinuclear molybdenum–dinitrogen complex supported by a PNP-pincer ligand [15–17]. With a combination of decamethylcobaltocene and lutidinium triflate, this system generated 12 equiv. NH<sub>3</sub> per molybdenum center. Most recently, the original catalyst was modified by applying tridentate triphosphine ligands instead of the PNP-pincer ligand which led to a further increase in catalytic activity

(63 NH<sub>3</sub>/Mo, respectively) [18]. In 2013, Peters et al. demonstrated that a catalytic synthesis of ammonia from N<sub>2</sub> is also possible based on iron complexes [19]. Using KC<sub>8</sub> and HBAR<sup>F</sup> at low temperature, up to 64 eq. NH<sub>3</sub> are generated per Fe center [12].

The earliest complete mechanistic scenario for synthetic nitrogen fixation is the Chatt cycle. This reactive scheme is based on mononuclear bis(dinitrogen) phosphine-Mo/W dinitrogen complexes supported by diphosphine ligands like dppe (dppe = Ph<sub>2</sub>PCH<sub>2</sub>CH<sub>2</sub>PPh<sub>2</sub>) or depe (depe = Et<sub>2</sub>PCH<sub>2</sub>CH<sub>2</sub>PEt<sub>2</sub>), which first have been synthesized by the groups of Chatt and Hidai [20–24]. Our group has been involved in synthetic, spectroscopic, and theoretical investigations of these complexes and their protonated/reduced derivatives over the last years [25–37]. The classic Chatt cycle, however, suffers from a couple of drawbacks that have limited its performance in a catalytic reaction mode. In particular, the conjugate base of the acid applied for protonation displaces one of the dinitrogen ligands in the parent bis(dinitrogen) complex, leading to a loss of 50% of bound substrate. Moreover, the presence of anionic coligands causes disproportionation at the Mo(I) stage which corresponds to 50% loss of reactive complex [38].

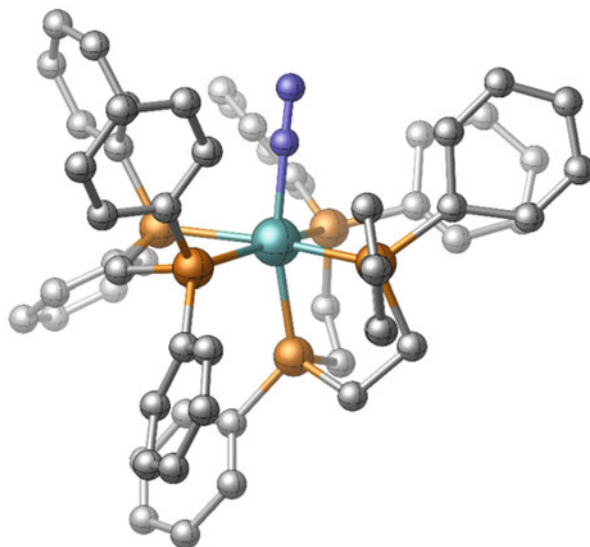
Herein we describe our attempts to modify the design of the original mononuclear Mo(0) phosphine complexes in order to eventually achieve a catalytic action of these systems. This in particular involves shielding the *trans*-position of coordinated N<sub>2</sub> in order to prevent ligand-exchange reactions at this site. The last stage of these developments is a molybdenum(0)–N<sub>2</sub> complex supported by a pentadentate tetrapodal (pentaPod) ligand. The N<sub>x</sub>H<sub>y</sub> (*x* = 1, 2; *y* = 0–3) intermediates in these types of systems should be related to those of the Schrock cycle and the Fe-based systems of Peters, but differ from those of Nishibayashi's system which does involve ligand-exchange reactions at the *trans*-position of coordinated N<sub>2</sub>.

## 2 Mo(0)–Dinitrogen Complexes Supported by Tridentate PEP Ligands (E = P, N)

A first approach to occupy the *trans*-position of the coordinated dinitrogen ligand involved the use of tridentate PEP ligands. With the diphosphine coligand dmpm (dmpm = Me<sub>2</sub>PCH<sub>2</sub>PMe<sub>2</sub>), we synthesized dinitrogen pentaphosphine complexes of the type [Mo(N<sub>2</sub>)(PEP)(dmpm)] in which the *trans*-position of N<sub>2</sub> is occupied by the central donor atom E (E = P or N) of the tridentate ligand PEP. In 1988, George et al. had already prepared the mono(dinitrogen) complex [Mo(N<sub>2</sub>)(dpepp)(dmpm)] supported by the tridentate ligand dpepp (dpepp = PhP(CH<sub>2</sub>CH<sub>2</sub>PPh<sub>2</sub>)<sub>2</sub>) [39]. The authors were also able to generate the corresponding NNH<sub>2</sub> complex by protonation with trifluoromethane sulfonic acid [40]. It should be mentioned that a range of molybdenum bis(dinitrogen) complexes with PEP ligands have been described in the literature [41–45], but – apart from [Mo(N<sub>2</sub>)(dpepp)(dmpm)] and the related complex [Mo(N<sub>2</sub>)(dpepp)(dppm)] (**1**) – no other molybdenum mono(dinitrogen) complexes with facially coordinating PEP ligands (E = P, N) were described. It was possible to obtain single crystals of **1** suitable for single crystal X-ray structure



**Fig. 1** Single crystal X-ray structure of  $[\text{Mo}(\text{N}_2)(\text{dpepp})(\text{dppm})]$  (**1**). Hydrogen atoms are omitted for clarity [41]



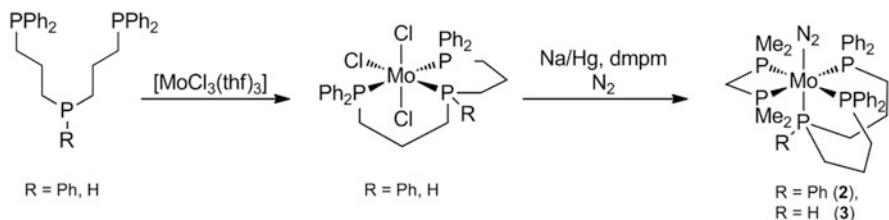
analysis (Fig. 1; [41]) demonstrating that the dpepp ligand coordinates facially to the molybdenum center.

In order to further explore such systems, we decided to investigate molybdenum–dinitrogen complexes with tridentate PEP ligands, varying the central donor atom E (E = N, P) and the chain length of the aliphatic linkages. Our goal was thereby to examine the stability of the respective  $\text{N}_2$  complexes and the activation of the  $\text{N}_2$  ligand [46]. A similar problem will be addressed when comparing the literature-known  $\text{NP}_3$  ligand [47] ( $\text{NP}_3 = \text{N}(\text{CH}_2\text{CH}_2\text{PPh}_2)_3$ ) with the new  $\text{prNP}_3$  ( $\text{prNP}_3 = \text{N}(\text{CH}_2\text{CH}_2\text{CH}_2\text{PPh}_2)_3$ ) ligand which has  $\text{C}_3$  bridges (cf. Sect. 6) [48].

Elongation of the  $\text{C}_2$  linkage of the tridentate ligand dpepp by an additional methylene group leads to the literature-known ligand  $\text{prPP}(\text{Ph})\text{P}$  ( $\text{prPP}(\text{Ph})\text{P} = \text{PhP}(\text{CH}_2\text{CH}_2\text{CH}_2\text{PPh}_2)_2$ ) [49, 50]. In 1986, Dahlenburg et al. synthesized the corresponding molybdenum(III) complex  $[\text{MoCl}_3(\text{prPP}(\text{Ph})\text{P})] \cdot \text{CH}_2\text{Cl}_2$  which was converted to the bis(dinitrogen) complex  $[\text{Mo}(\text{N}_2)_2(\text{prPP}(\text{Ph})\text{P})(\text{PR}_3)]$  by sodium amalgam reduction using different monotertiary phosphines ( $\text{PR}_3$ ) [50]. To the best of our knowledge, however, a corresponding molybdenum mono(dinitrogen) complex has not been synthesized yet. By sodium amalgam reduction of  $[\text{MoCl}_3(\text{prPP}(\text{Ph})\text{P})] \cdot \text{CH}_2\text{Cl}_2$  under a dinitrogen atmosphere in tetrahydrofuran in the presence of dmpm, we obtained the complex  $[\text{Mo}(\text{N}_2)(\text{prPP}(\text{Ph})\text{P})(\text{dmpm})]$  (**2**) (Scheme 1) [46].

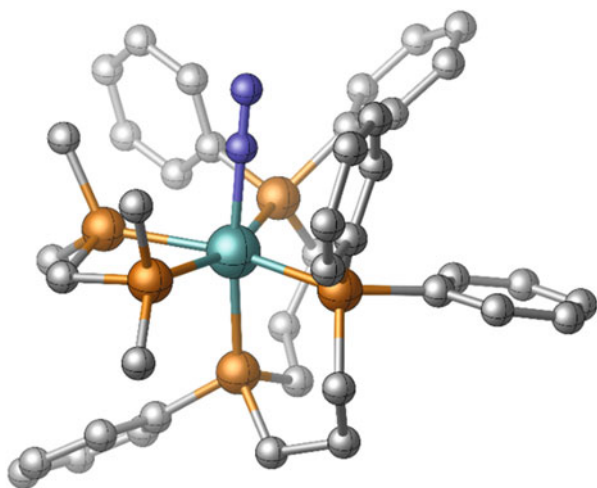
An X-ray single crystal structure determination of **2** has been performed (Fig. 2) [46]. Comparison with  $[\text{Mo}(\text{N}_2)(\text{dpepp})(\text{dppm})]$  **1** (Fig. 1) reveals similar bond lengths and angles (note that no crystal structure of  $[\text{Mo}(\text{N}_2)(\text{dpepp})(\text{dmpm})]$  is available).

Nevertheless, the  $\text{Mo}-\text{P}_{\text{ax}}$  bond of  $[\text{Mo}(\text{N}_2)(\text{dpepp})(\text{dppm})]$  **1** is about  $0.0246(18)$  Å shorter than in **2** ( $2.4460(6)$  Å) [41, 46]. This significant difference is certainly due to higher steric demand of the  $\text{C}_3$  bridges compared to the  $\text{C}_2$  counterparts [46].



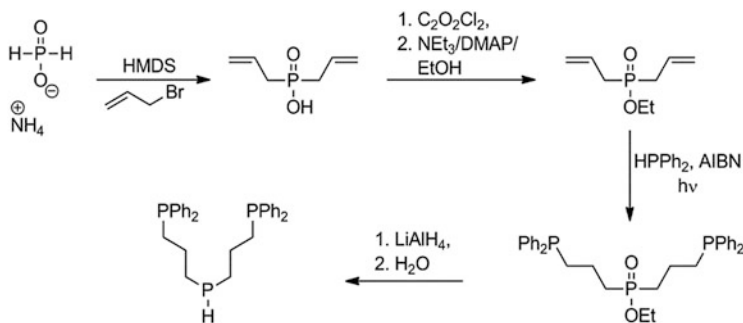
**Scheme 1** Synthesis of the complexes  $[\text{Mo}(\text{N}_2)(\text{prPP}(\text{Ph})\text{P})(\text{dmpm})]$  (**2**) and  $[\text{Mo}(\text{N}_2)(\text{prPPHP})(\text{dmpm})]$  (**3**)

**Fig. 2** Single crystal X-ray structure of  $[\text{Mo}(\text{N}_2)(\text{prPP}(\text{Ph})\text{P})(\text{dmpm})]$  (**2**). Hydrogen atoms are omitted for clarity [46]



The degree of activation of the  $\text{N}_2$  ligand can be investigated with the help of vibrational spectroscopy. Interestingly, replacement of the  $\text{C}_2$  by a  $\text{C}_3$  linkage hardly influences the  $\text{N-N}$  stretching frequency. For  $[\text{Mo}(\text{N}_2)(\text{dpepp})(\text{dmpm})]$   $\tilde{\nu}_{\text{NN}}$  is located at  $1,966 \text{ cm}^{-1}$  [39], and for  $[\text{Mo}(\text{N}_2)(\text{prPP}(\text{Ph})\text{P})(\text{dmpm})]$  (**2**) a strong  $\text{NN}$  stretching vibration is observed at  $\tilde{\nu}_{\text{NN}} = 1,970 \text{ cm}^{-1}$ . Because of broadened signals and a quintet associated with the *trans*-phosphine in the  $^{31}\text{P}$ -NMR spectrum of  $[\text{Mo}(\text{N}_2)(\text{prPP}(\text{Ph})\text{P})(\text{dmpm})]$  (**2**), we assume that several conformers exist in solution. The corresponding complex  $[\text{Mo}(\text{N}_2)(\text{dpepp})(\text{dppm})]$  (**1**) shows a triplet for the *trans*-phosphine instead of a quintet. The presence of several conformers of **2** can be explained by the higher flexibility of the  $\text{C}_3$  linkages as compared to the  $\text{C}_2$  bridges of *dpepp* in  $[\text{Mo}(\text{N}_2)(\text{dpepp})(\text{dmpm})]$  [39].

In view of the fact that the flexibility of the ligand backbone is restricted by phenyl groups [51], we wanted to know what happens if the tertiary phosphine *trans* to the  $\text{N}_2$  ligand is replaced by a secondary phosphine. Therefore we synthesized the complex  $[\text{Mo}(\text{N}_2)(\text{prPPHP})(\text{dmpm})]$  (**3**) with the ligand *prPPHP* (*prPPHP* =  $\text{HP}(\text{CH}_2\text{CH}_2\text{CH}_2\text{PPh}_2)_2$ ) (Scheme 2). The synthesis of the diallylphosphonic acid ethyl ester was adapted from Bujard et al. [52]. After addition of diphenylphosphine,



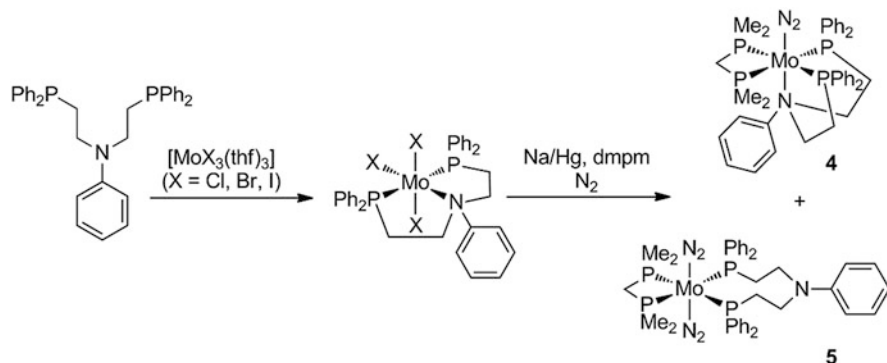
**Scheme 2** Synthesis of the ligand prPPHP

promoted by AIBN, we obtained ethyl-bis(3-(diphenylphosphino)propyl)phosphinate, which was subjected to a lithium aluminium hydride reduction, leading to the ligand prPPHP [46].

By amalgam reduction of the Mo(III) precursor, the Mo(0)–N<sub>2</sub> complex [Mo(N<sub>2</sub>)(prPPHP)(dmpm)] (**3**) was obtained. Again the <sup>31</sup>P-NMR spectrum indicates the presence of several conformers. Moreover a strongly high-field shifted signal for the *trans* secondary phosphine is observed [46]. A single crystal structure of **3** shows similar bond lengths and angles as compared to **2**. However, with 2.4015(6) Å the Mo–P<sub>ax</sub> bond is significantly shorter than those present in [Mo(N<sub>2</sub>)(prPP(Ph)P)(dmpm)] (**2**) (2.4460(6) Å) [46] and [Mo(N<sub>2</sub>)(dpepp)(dppm)] (2.4214(18) Å) [41]. This is readily explained by the smaller steric demand of the PH group as compared to the PPh moiety [46]. Interestingly the NN stretching band of **3** ( $\tilde{\nu}_{\text{NN}} = 1,974 \text{ cm}^{-1}$ ) is nearly the same as in **2** ( $\tilde{\nu}_{\text{NN}} = 1,970 \text{ cm}^{-1}$ ) so that the activation of N<sub>2</sub> is not influenced by replacing the PPh moiety by PH [46].

The effect of changing the central donor atom of the PEP ligand was investigated by replacing the central phosphorus donors of dpepp and prPP(Ph)P by nitrogen, leading to the ligands PN(Ph)P (PN(Ph)P = PhN(CH<sub>2</sub>CH<sub>2</sub>PPh<sub>2</sub>)<sub>2</sub>) and prPN(Ph)P (prPN(Ph)P = PhN(CH<sub>2</sub>CH<sub>2</sub>CH<sub>2</sub>PPh<sub>2</sub>)<sub>2</sub>). The former ligand has been prepared earlier by Kostas [53]. The ligand PN(Ph)P was converted to Mo(III) complexes [MoX<sub>3</sub>(PN(Ph)P)] using the Mo(III) precursors [MoCl<sub>3</sub>(thf)<sub>3</sub>], [MoBr<sub>3</sub>(thf)<sub>3</sub>], and [MoI<sub>3</sub>(thf)<sub>3</sub>] (Scheme 3) [54–56]. The highest yield was achieved with the precursor [MoI<sub>3</sub>(thf)<sub>3</sub>] [46]. Interestingly ligand prPN(Ph)P could only be converted to the Mo(III) complex with [MoI<sub>3</sub>(thf)<sub>3</sub>] [46].

Reduction of the Mo(III) complexes with sodium amalgam under a dinitrogen atmosphere predominantly leads to the mono(dinitrogen) complex [Mo(N<sub>2</sub>)(PN(Ph)P)(dmpm)] (**4**) and the bis(dinitrogen) complex [Mo(N<sub>2</sub>)<sub>2</sub>(κ<sup>2</sup>-PN(Ph)P)(dmpm)] (**5**; Scheme 3) [46]. A similar pathway has been employed to synthesize the corresponding prPN(Ph)P complexes [Mo(N<sub>2</sub>)(prPN(Ph)P)(dmpm)] (**6**) and the [Mo(N<sub>2</sub>)<sub>2</sub>(κ<sup>2</sup>-prPN(Ph)P)(dmpm)] (**7**). The occurrence of the bis(dinitrogen) complexes in both systems indicates a partial dissociation of the N-donor in *trans*-position of the N<sub>2</sub> ligand. Thereby a κ<sup>2</sup>-coordination of the prPN(Ph)P ligand results and another N<sub>2</sub>



**Scheme 3** Synthesis of the complexes  $[\text{MoX}_3(\text{PN}(\text{Ph})\text{P})]$  ( $\text{X} = \text{Cl}, \text{Br}, \text{I}$ ),  $[\text{Mo}(\text{N}_2)(\text{PN}(\text{Ph})\text{P})(\text{dmpm})]$  (**4**), and  $[\text{Mo}(\text{N}_2)_2(\text{PN}(\text{Ph})\text{P})(\text{dmpm})]$  (**5**)

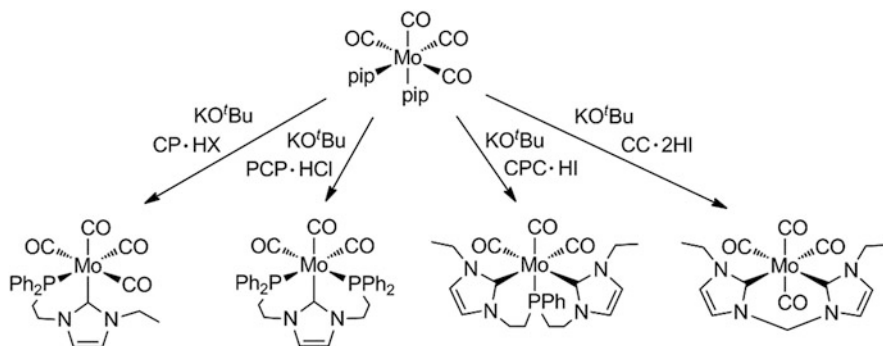
ligand coordinates at the free position (Scheme 3). Note that the smallest fraction of the respective bis(dinitrogen) complex was observed if  $[\text{MoI}_3(\text{PN}(\text{Ph})\text{P})]$  was used as a precursor [46].

The NN stretching vibration of  $[\text{Mo}(\text{N}_2)(\text{PN}(\text{Ph})\text{P})(\text{dmpm})]$  (**4**) is observed at  $1,940 \text{ cm}^{-1}$  and that of  $[\text{Mo}(\text{N}_2)(\text{prPN}(\text{Ph})\text{P})(\text{dmpm})]$  (**6**) at  $1,939 \text{ cm}^{-1}$ . This demonstrates again that an elongation of the  $\text{C}_2$  to a  $\text{C}_3$  linkage does not influence the  $\text{N}_2$  activation (vide infra). Comparing the NN stretch of  $[\text{Mo}(\text{N}_2)(\text{PN}(\text{Ph})\text{P})(\text{dmpm})]$  (**4**) with that of the phosphorus analogue  $[\text{Mo}(\text{N}_2)(\text{dpepp})(\text{dmpm})]$  ( $\tilde{\nu}_{\text{NN}} = 1,966 \text{ cm}^{-1}$ ), a low-frequency shift of  $26 \text{ cm}^{-1}$  is observed. Exchange of a phosphine by an amine in *trans*-position to the  $\text{N}_2$  ligand thus drastically increases the activation of  $\text{N}_2$ . Supported by DFT calculations, we assume that the absence of a  $\pi$ -backbonding interaction in the PNP system ensures a better activation. By contrast, a P-donor *trans* to the  $\text{N}_2$  ligand shows significant  $\pi$ -backbonding, leading to a stronger bond between the metal and the *trans* P-donor which reduces the activation of  $\text{N}_2$  [46].

Summing up, the elongation of a  $\text{C}_2$  to a  $\text{C}_3$  linkage and the exchange of tertiary phosphine by a secondary phosphine hardly influence the activation of  $\text{N}_2$  but an N-donor *trans* to  $\text{N}_2$  leads to a better activation of  $\text{N}_2$ . On the other hand, mono (dinitrogen) complexes with PNP ligands are less stable than their PPP counterpart ligands so that bis(dinitrogen) complexes are formed [46].

### 3 Mo(0)–Dinitrogen Complexes Supported by Mixed Imidazol-Ylidene/Phosphanyl Hybrid Ligands

Since the isolation of the first stable N-heterocyclic carbene by Arduengo and coworkers in 1991 [57, 58], these molecules have become increasingly important, particularly in organometallic catalysis [59–63]. For that reason, it appeared of significant interest to explore the application of mixed phosphine/carbene ligands in the field of small



**Scheme 4** Different molybdenum complexes have been prepared starting from the precursor  $[\text{Mo}(\text{CO})_4(\text{pip})_2]$

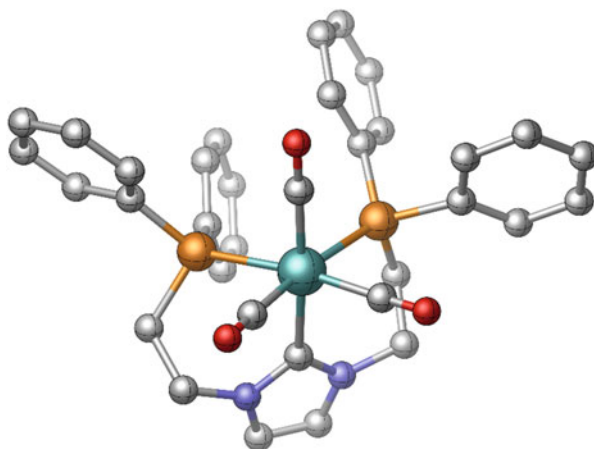
molecule activation, especially molybdenum-based dinitrogen fixation [64–66]. In our studies of molybdenum–dinitrogen complexes supported by multidentate phosphine ligands, we investigated the electronic influences of aryl and alkyl substituents in detail [46, 67–71]. Far more drastic changes are to be expected if a phosphine group is replaced by a carbene residue [64]. To determine the impact of N-heterocyclic carbenes coordinating to a molybdenum center on the activation of small molecules, Gradert et al. synthesized a range of molybdenum tricarbonyl complexes supported by different carbene and mixed carbene/phosphine ligands. Starting from the precursor  $[\text{Mo}(\text{CO})_4(\text{pip})_2]$  and replacing the piperidine ligands (and one carbonyl ligand), four new complexes have been obtained (Scheme 4). Using vibrational spectroscopy and single crystal X-ray structure analysis, these complexes have been characterized. Furthermore DFT calculations have been performed to determine the electronic properties of the carbene unit [64].

As evident from Scheme 4, the bidentate CP ligand and the CC ligand coordinate to the molybdenum center via the phosphine and carbene unit or the pure carbene groups, respectively. The PCP ligand and the CPC ligand substitute the two piperidine ligands and one CO ligand of the precursor  $[\text{Mo}(\text{CO})_4(\text{pip})_2]$ .

In almost all cases, potassium *tert*-butoxide was used as deprotonating agent. The free carbene reacts with the metal precursor in tetrahydrofuran to yield the molybdenum complexes  $[\text{Mo}(\text{CO})_4(\text{CP})]$ ,  $[\text{Mo}(\text{CO})_3(\text{PCP})]$ ,  $[\text{Mo}(\text{CO})_3(\text{CPC})]$ , and  $[\text{Mo}(\text{CO})_4(\text{CC})]$  supported by mixed NHC/phosphine ligands. It could be shown that the  $[\text{Mo}(\text{CO})_4(\text{pip})_2]$  precursor with its internal base piperidine is able to act as the deprotonating agent. Consequently the use of an external base was not required. The molybdenum tricarbonyl complexes containing the PCP or CPC ligand have been investigated using vibrational spectroscopy, nuclear magnetic resonance spectroscopy, and single crystal X-ray structure analysis. Importantly, the tridentate ligand PCP coordinates facially to the molybdenum center (Fig. 3); the same is observed for the CPC ligand [64].

Relevant information regarding the properties of the metal–carbene bond could be obtained from single crystal X-ray structure determination. Comparing the

**Fig. 3** Crystal structure of *fac*-[Mo(CO)<sub>3</sub>(PCP)]. Hydrogen atoms are omitted for clarity [64]



impact of the carbene unit on the carbonyl ligand in *trans*-position with the influence of a phosphine group in *trans*-position to a carbonyl ligand, it became clear that the C–O bond distance of the carbonyl ligand *trans* to the carbene (1.158 Å) is longer than the C–O distances of the CO ligands *trans* to the phosphines (1.149 Å/1.150 Å). This was interpreted as evidence that carbene is a weaker  $\pi$ -acceptor than phosphine. To assess the  $\sigma$ -donor capabilities of the different donor atoms of the PCP ligand, the metal–C<sub>Carbonyl</sub> bond distances of the three CO ligands were compared. The metal–C<sub>Carbonyl</sub> distance of the CO *trans* to the carbene (1.969 Å) is marginally shorter than the distances of the CO ligands *trans* to the phosphine moieties (1.978 Å/1.972 Å). Because of the missing elongation of the metal–C<sub>CO</sub> bond *trans* to the carbene unit, the  $\sigma$ -donor capability of the carbene has to be comparable to that of the phosphine [64].

To check these conclusions, DFT calculations have been performed. Between the lone pair of the carbene and the metal  $d\sigma$  orbital, a distinct, strong  $\sigma$ -interaction exists. Furthermore a  $\pi$ -interaction between the C<sub>carbene</sub> atom and the metal center is conceivable. Depending on the nature of the metal center (number of d electrons), the  $\pi$ -contribution varies between 10 and 30% [72]. In a molybdenum(0) center, the  $d_{xy}$ ,  $d_{yz}$ , and  $d_{xz}$  orbitals are doubly occupied so that the lone pair of the carbene donates into the  $d_{x^2-y^2}$  ([Mo(CO)<sub>4</sub>(CP)] and [Mo(CO)<sub>4</sub>(CC)]) and  $d_{z^2}$  ([Mo(CO)<sub>3</sub>(PCP)], [Mo(CO)<sub>3</sub>(CPC)]) orbitals, respectively. Comparing the different contributions of the carbene and phosphine lone pairs, it is obvious that the  $\sigma$ -donor capability of these groups is of about equal strength. This is illustrated by the isodensity plots of the frontier orbitals shown in Fig. 4.

Regarding the carbene moiety in Fig. 4, it becomes clear that there is no  $\pi$ -interaction (neither  $\pi$ -bonding nor  $\pi$ -backbonding) between the  $d\pi$  orbitals of the metal center and the carbene C atom. DFT thus indicates that the carbene unit of the PCP ligand coordinating to a Mo(0) center is only a strong  $\sigma$ -donor, but not a  $\pi$ -acceptor [64].

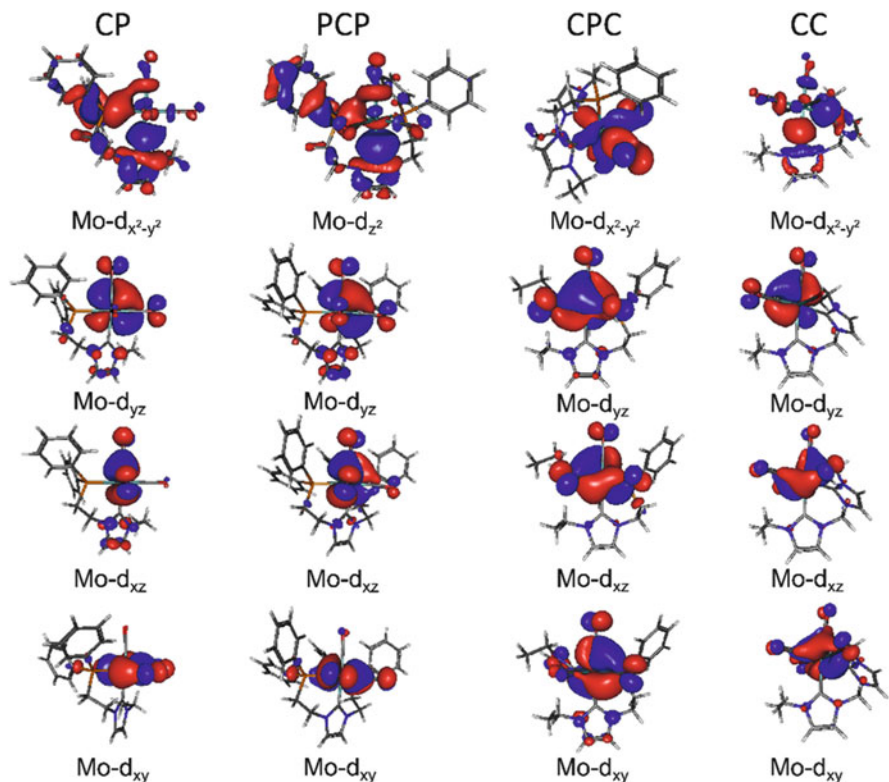
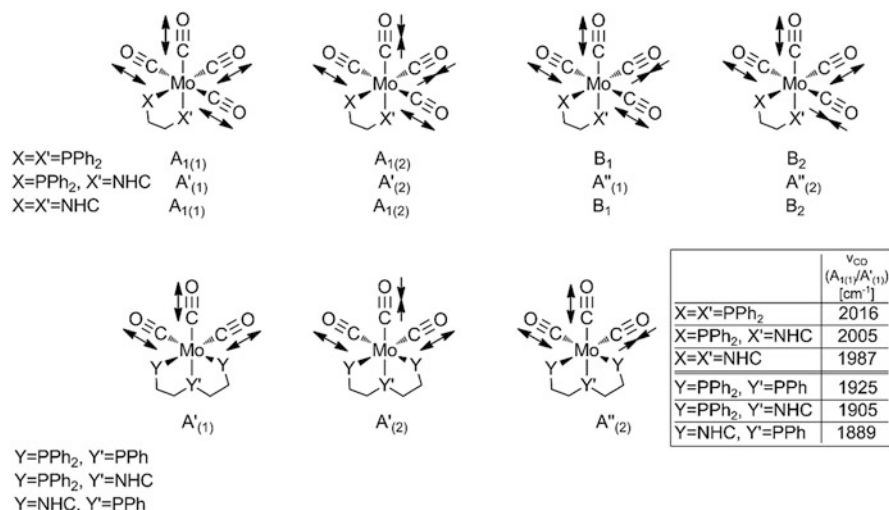


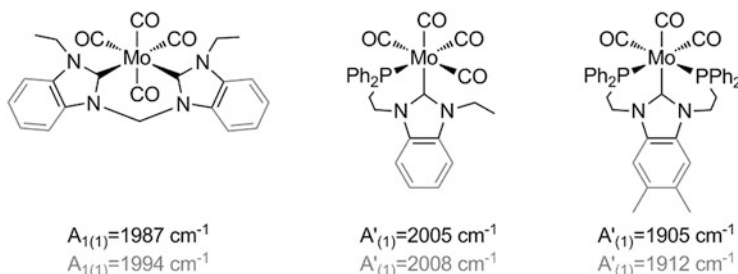
**Fig. 4** Isodensity plots of the frontier molecular orbitals of  $[\text{Mo}(\text{CO})_4(\text{CP})]$ ,  $[\text{Mo}(\text{CO})_3(\text{PCP})]$ ,  $[\text{Mo}(\text{CO})_3(\text{CPC})]$ , and  $[\text{Mo}(\text{CO})_4(\text{CC})]$ . The  $\sigma$ -donor capability of the phosphine and carbene unit is of comparable strength [64]

The results of vibrational spectroscopy support these findings. The bond length between two atoms correlates with the vibrational frequency; that is, the longer the bond, the lower the frequency. In order to obtain information regarding this issue, seven complexes with phosphine, carbene, and mixed phosphine/carbene donor sets have been synthesized and investigated with IR and Raman spectroscopy (Scheme 5). Four complexes are tetracarbonyl complexes containing bidentate coligands, whereas three complexes are tricarbonyl complexes supported by tridentate coligands. Complexes  $[\text{Mo}(\text{CO})_4(\text{CC})]$  and  $[\text{Mo}(\text{CO})_4(\text{dppp})]$  ( $\text{dppp} = \text{Ph}_2\text{PCH}_2\text{CH}_2\text{CH}_2\text{PPh}_2$ ) exhibit  $\text{C}_{2v}$  symmetry; hence four bands ( $2^*A_1$ ,  $B_1$ , and  $B_2$ ) appear in the vibrational spectrum. Due to the mixed ligand sphere, the point group of  $[\text{Mo}(\text{CO})_4(\text{CP})]$  is lowered to  $\text{C}_s$ , and as a result the four observable bands transform according to  $2^*A'$  and  $2^*A''$  [64].

The frequency of the totally symmetric mode  $A_1/A'$  in the complexes with PP, CP, and CC ligands decreases from  $2,016 \text{ cm}^{-1}$  (PP) over  $2,005 \text{ cm}^{-1}$  (CP) to  $1,987 \text{ cm}^{-1}$  (CC). This indicates that carbonyl ligands are more activated in carbene complexes than in complexes with pure phosphine ligands. The same behavior can be observed



**Scheme 5** Analysis of the vibrational modes depending on the symmetry of the complexes



**Scheme 6** New synthesized molybdenum complexes bearing benzimidazole-based mixed NHC/phosphine ligands

in the complexes with tridentate ligands. Three bands are observed in the IR and Raman spectra of  $[Mo(CO)_3(CPC)]$ ,  $[Mo(CO)_3(PCP)]$ , and  $[Mo(CO)_3(dpepp)]$  which in  $C_s$  symmetry transform according to  $2^*A'$  and  $A''$  [73]. The stretching vibration of  $[Mo(CO)_3(CPC)]$  is located at  $1,889\text{ cm}^{-1}$ , the vibration of  $[Mo(CO)_3(PCP)]$  at  $1,905\text{ cm}^{-1}$ , and the totally symmetric mode of  $[Mo(CO)_3(dpepp)]$  is located at  $1,925\text{ cm}^{-1}$  [64]; that is, the more carbene units are coordinated to the metal center, the lower are the CO frequencies.

In a later study, Gradert et al. synthesized similar molybdenum carbonyl complexes with mixed N-heterocyclic/phosphine ligands. The effect of a carbene unit with a benzimidazole backbone towards small molecules like CO was also investigated and compared to the imidazole-based carbene moiety. In Scheme 6, the new complexes  $[Mo(CO)_4(\text{Benz-CC})]$ ,  $[Mo(CO)_4(\text{Benz-CP})]$ , and  $[Mo(CO)_4(\text{DMBenz-PCP})]$  are shown [65, 74].



Vibrational studies showed that the benzimidazole-based ligands have comparable properties to the imidazole-based counterparts. However, the CO stretching vibrations of the molybdenum complexes coordinated by the carbene ligand with benzimidazole backbones are slightly shifted to higher wavenumbers (Scheme 6). In comparison to the  $[\text{Mo}(\text{CO})_4(\text{CC})]$  complex, e.g., the stretching frequency of the benzimidazole analogue  $[\text{Mo}(\text{CO})_4(\text{Benz-CC})]$  is shifted by  $7\text{ cm}^{-1}$  to  $1994\text{ cm}^{-1}$ . The same effect can be observed in the complexes with tridentate ligands, where the totally symmetric stretching mode in the benzimidazole-based NHC/phosphine CO complex is shifted by  $7\text{ cm}^{-1}$  to higher frequency compared to the imidazole-based analogue [64, 65]. Two explanations can be invoked to explain these findings: (1) The carbene unit of the benzimidazole-based ligand is a weaker  $\sigma$ -donor than the carbene of the imidazole-based ligand. (2) The  $\sigma$ -donor capabilities of both ligand systems are comparable and the benzimidazole-based carbene ligand also functions as a  $\pi$ -acceptor. To evaluate these possibilities, DFT calculations were performed. As evident from Fig. 5, the isodensity plots of the uncoordinated benzimidazole ligand exhibit an unoccupied  $\pi^*$  orbital which is located at the carbene atom (LUMO,  $-0.59\text{ eV}$ ) [65]. Backbonding to this orbital could in principle be possible. Although the DFT-optimized and the X-ray structure exhibit a slightly shortened  $\text{Mo}-\text{C}_{\text{NHC}}$  bond for  $[\text{Mo}(\text{CO})_3(\text{DMBenz-PCP})]$ , no significant contribution of  $\pi^*$  orbitals is found in the  $d\pi$  orbitals of the molybdenum atom of the complex. Consequently the lower activation of the carbonyl ligand in the

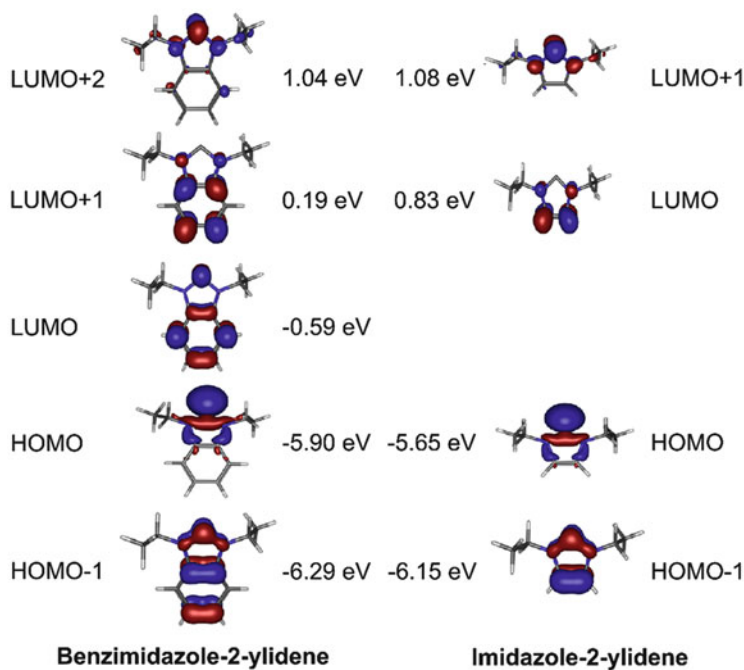


**Fig. 5** Isodensity plots of the frontier molecular orbitals of the imidazole and benzimidazole-based PCP ligands and the energies [65]

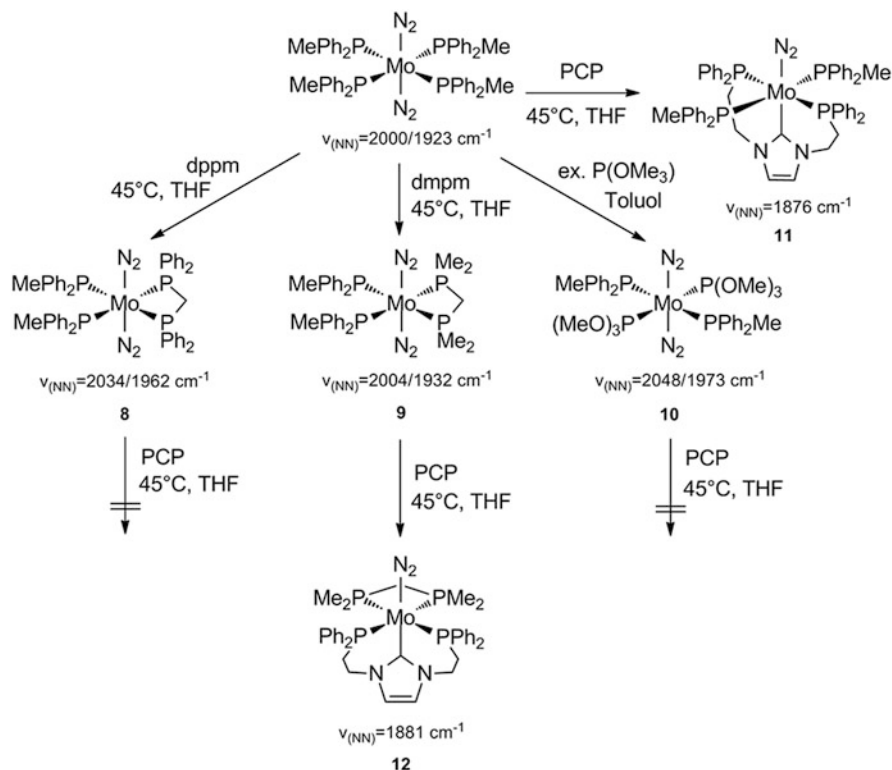
benzimidazole–PCP moiety is caused by a lower  $\sigma$ -donor capability of the carbene moiety as compared to the imidazole-based system [65].

In conclusion, the first molybdenum carbonyl complexes supported by mixed phosphine/NHC ligands have been prepared and characterized by different methods. In agreement with single crystal X-ray structure determination and vibrational spectroscopy, DFT calculations indicate that the carbene unit within the ligand systems is a pure  $\sigma$ -donor, in contrast to a phosphine moiety which is a  $\sigma$ -donor/ $\pi$ -acceptor. Due to the missing  $\pi$ -acceptor properties, the carbonyl ligands in the carbene complexes are significantly more activated than those in complexes with pure phosphine coligands [64]. Additionally three carbonyl complexes containing mixed benzimidazole-based NHC/phosphine ligands have been prepared, characterized, and compared to their imidazole analogues. The benzimidazole-based ligand is a weaker  $\sigma$ -donor than the imidazole-based ligand and, therefore, the CO ligands are slightly less activated in molybdenum carbonyl complexes supported by benzimidazole- as compared to imidazole-based ligands [65].

Having analyzed the bonding properties of NHC ligands based on molybdenum carbonyl complexes, the next step involved the application of the mixed NHC/phosphine ligands in molybdenum-based nitrogen fixation [66]. The tridentate mixed NHC/phosphine ligand 1,3-bis(2-diphenylphosphanylethyl)imidazol-2-ylidene (PCP) was chosen for the synthesis of molybdenum–dinitrogen complexes. Starting from the precursor  $[\text{Mo}(\text{N}_2)_2(\text{PPh}_2\text{Me})_4]$ , ligand-exchange reactions were explored to synthesize mono(dinitrogen) complexes containing the PCP ligand or to *synthesize* other suitable precursors (Scheme 7) [66, 75–77]. The four monophosphine ligands in the complex  $[\text{Mo}(\text{N}_2)(\text{PPh}_2\text{Me})_4]$  can easily be substituted by two diphosphine ligands or two phosphite ligands. The resulting molybdenum–dinitrogen complexes have been investigated using NMR and vibrational spectroscopy. Depending on the dpmm, dmpm, or two trimethyl phosphite ligands, the dinitrogen moieties are more or less activated. The symmetric stretching mode is located at  $2,034\text{ cm}^{-1}$  ( $[\text{Mo}(\text{N}_2)_2(\text{dpmm})(\text{PPh}_2\text{Me})_2]$  (**8**)), at  $2,004\text{ cm}^{-1}$  ( $[\text{Mo}(\text{N}_2)_2(\text{dmpm})(\text{PPh}_2\text{Me})_2]$  (**9**)), and at  $2,048\text{ cm}^{-1}$  ( $[\text{Mo}(\text{N}_2)_2(\text{PPh}_2\text{Me})_2(\text{P}(\text{OMe})_3)_2]$  (**10**)). The typical AA'XX' coupling pattern can be observed for the two complexes with pure phosphine ligands  $[\text{Mo}(\text{N}_2)_2(\text{dpmm})(\text{PPh}_2\text{Me})_2]$  (**8**) and  $[\text{Mo}(\text{N}_2)_2(\text{dmpm})(\text{PPh}_2\text{Me})_2]$  (**9**) [66].

Starting from  $[\text{Mo}(\text{N}_2)_2(\text{PPh}_2\text{Me})_4]$ , the ligand-exchange reaction with the PCP ligand has been monitored using IR spectroscopy. Within 2 h, the symmetric and antisymmetric stretching modes of the bis(dinitrogen) precursors disappear and a new band emerges at  $1,876\text{ cm}^{-1}$  (Fig. 6) [66].

Due to the very strong activation of the  $\text{N}_2$  ligand and the results of the investigations of the molybdenum carbonyl complexes supported by the PCP ligand, it can be assumed that the dinitrogen ligand coordinates in *trans*-position to the carbene atom. Because of the flexibility of the PCP ligand and steric hindrance of the phenyl groups, the constitution corresponds to the meridionally coordinated complex *mer*- $[\text{Mo}(\text{N}_2)(\text{PCP})(\text{PPh}_2\text{Me})_2]$  (**11**). However, the strong activation of the  $\text{N}_2$  ligand is accompanied by a high thermal instability of the dinitrogen complex, and therefore further investigations using NMR spectroscopy could not be performed. Reaction of the precursor  $[\text{Mo}(\text{N}_2)_2(\text{dpmm})(\text{PPh}_2\text{Me})_2]$  (**8**) with the carbene ligand did not lead



**Scheme 7** Dinitrogen complexes with different phosphine and phosphite ligands

to the expected  $\text{N}_2$  complex. A possible reason is the high steric demand of the phenyl groups of the dppm ligand. The PCP ligand has to coordinate facially to the molybdenum center, so that the four phenyl groups in the horizontal plane interfere excessively. The analogous complex with the dmpm coligand could be obtained, exhibiting an NN stretching vibration at  $1,881 \text{ cm}^{-1}$ . Time-dependent NMR spectroscopy revealed the formation of the *fac*- $[\text{Mo}(\text{N}_2)(\text{dmpm})(\text{PCP})]$  (**12**) complex during the reaction. Nevertheless, due to the strong activation of the dinitrogen ligand, the product also was thermally unstable. The strong activation of the  $\text{N}_2$  ligand and the thermal instability of the complex are caused by the pure  $\sigma$ -donor and the missing  $\pi$ -acceptor character of the PCP ligand. In order to obtain dinitrogen complexes which exhibit a higher thermal stability, the PCP ligand was substituted by the DMBenzPCP ligand [74]. However, the desired complexes could not be isolated [66].

In view of these results, we decided to replace the phosphine coligands by less activating trimethyl phosphite ligands. This way the electron density at the molybdenum center should be reduced so that the coordinating  $\text{N}_2$  ligand is less activated and the corresponding complex is stable at room temperature. First of all a ligand-exchange reaction starting from  $[\text{Mo}(\text{N}_2)_2(\text{PPh}_2\text{Me})_2(\text{P}(\text{OMe})_3)_2]$  (**10**) with the PCP

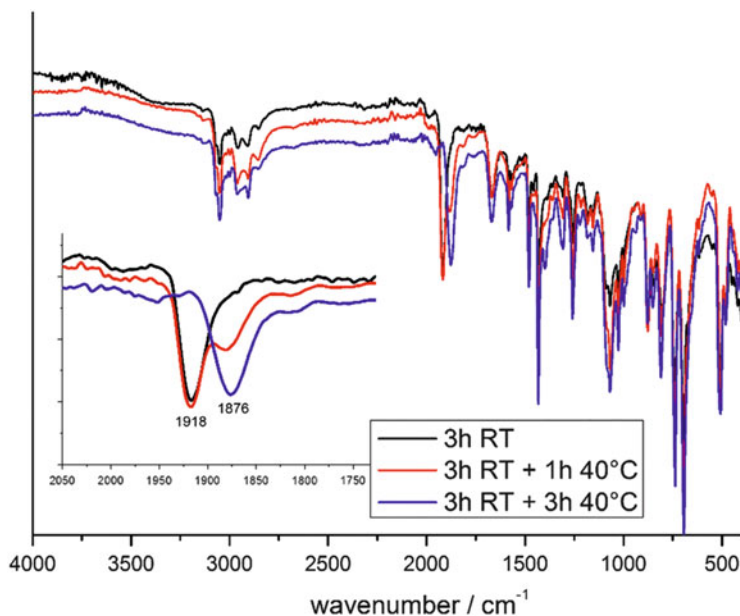
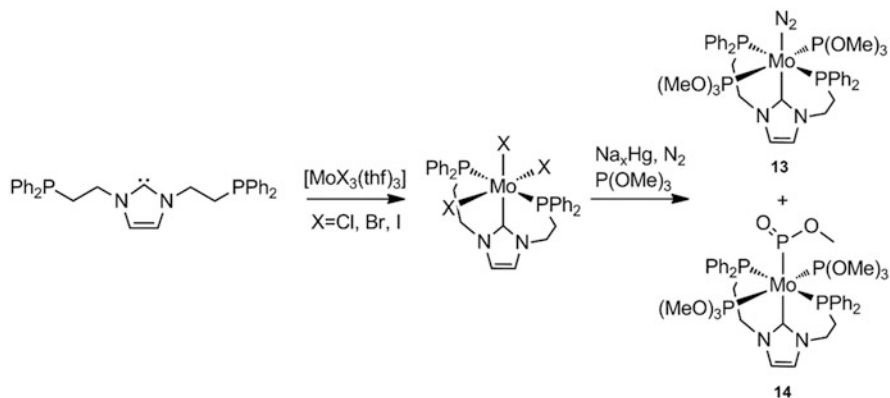


Fig. 6 IR spectra of the reaction of  $[\text{Mo}(\text{N}_2)_2(\text{PPh}_2\text{Me})_4]$  and the PCP ligand [66]

ligand has been performed. The structure of the precursor  $[\text{Mo}(\text{N}_2)_2(\text{PPh}_2\text{Me})_2(\text{P}(\text{OMe})_3)_2]$  (**10**) was proven by single X-ray structure analysis in the solid state and by NMR spectroscopy in solution. In the solid state, the pure *trans-trans* isomer exists, where the two phosphines as well as the two phosphites are in *trans*-position to each other. In solution, this complex converts into several isomers. Hence the ligand-exchange reaction of this precursor with the PCP ligand does not yield the dinitrogen complex.

A further possibility to obtain molybdenum(0)-dinitrogen complexes is the reduction of a molybdenum(III) complex by use of, e.g., sodium amalgam. The single crystal X-ray structure determination of the precursor  $[\text{MoCl}_3(\text{PCP})]$  proves a meridional coordination of the PCP ligand. Comparing this coordination geometry to that of the molybdenum tricarbonyl complexes (*vide supra*), it becomes clear that the coordination mode of the PCP ligand depends on the electronic properties of the coligand (chloride vs. carbonyl) [66]. Sodium amalgam reduction of the molybdenum(III) precursor  $[\text{MoCl}_3(\text{PCP})]$  under  $\text{N}_2$  atmosphere in the presence of two equivalents of trimethyl phosphite finally led to two molybdenum(0) complexes **13** and **14** (Scheme 8).

The target complex *mer*- $[\text{Mo}(\text{N}_2)(\text{PCP})(\text{P}(\text{OMe})_3)_2]$  (**13**) could be obtained this way and was found to be thermally stable. In accordance to our expectations, the NN stretching vibration of this dinitrogen complex is located at higher wavenumbers at  $1,932\text{ cm}^{-1}$ . The decrease in the activation of the dinitrogen ligand leads to a stable product which could be characterized completely. DFT calculations of the complex *mer*- $[\text{Mo}(\text{N}_2)(\text{PCP})(\text{P}(\text{OMe})_3)_2]$  (**13**) exhibit no  $\pi$ -backbonding into  $\pi^*$  orbitals of



**Scheme 8** Reaction of the free carbene with the molybdenum precursor  $[\text{MoCl}_3(\text{thf})_3]$  and the sodium amalgam reduction under  $\text{N}_2$  atmosphere and two equivalents of trimethyl phosphite

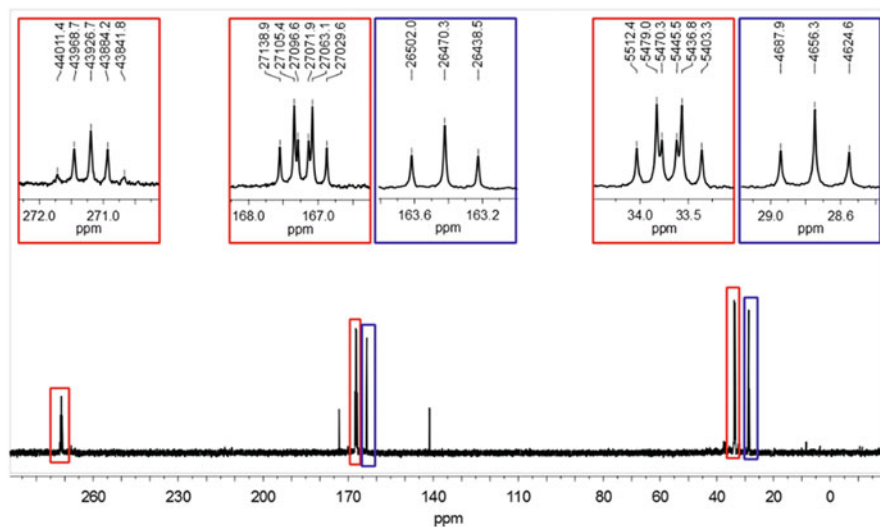


**Fig. 7**  $^{31}\text{P}$ -NMR spectrum of *mer*- $[\text{Mo}(\text{N}_2)(\text{PCP})(\text{P}(\text{OMe})_3)_2]$  (**13**) (blue) and  $[\text{Mo}(\text{PCP})(\text{P}(\text{OMe})_3)_2(\text{P}(\text{O})(\text{OMe}))]$  (**14**) (red) [66]

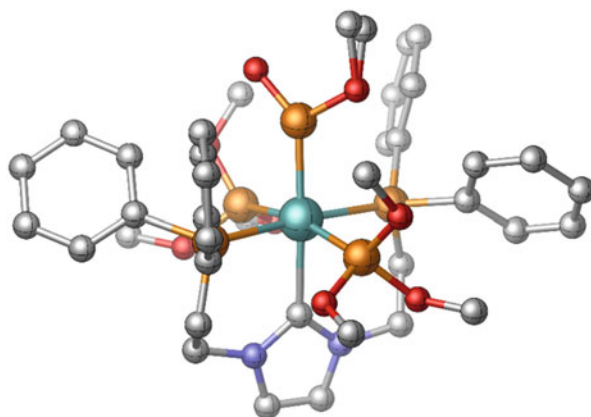
the PCP ligand. Again, the carbene atom of the PCP ligand is a pure  $\sigma$ -donor. Regarding the  $^{31}\text{P}$ -NMR spectrum of the product of the sodium amalgam reduction, it is apparent that an additional product has been formed. Because of the signal in the  $^{13}\text{C}$  HMBC NMR spectrum at 193.8 ppm, the coordination of the carbene atom to the molybdenum center in this additional product is proven. In the  $^{31}\text{P}$ -NMR spectrum, the expected two triplets of the dinitrogen complex can be observed (Fig. 7) [66].

Furthermore three additional signals of the other product are visible. A multiplet at 271.0 ppm points towards a new phosphorus species coordinated to the molybdenum center. This strong shift is not compatible with the trimethyl phosphite or phosphine groups. Ultimately, the structure of the by-product **14** could be solved by single X-ray structure determination. It is shown in Fig. 8 [66].

In *trans*-position to the carbene unit, the species P(O)(OMe) coordinates to the molybdenum center. The Mo–P<sub>P(O)(OMe)</sub> bond is significantly shortened (2.254(1) Å) compared to the other Mo–P bonds (2.397(8) Å and 2.453(8) Å). As a result of this, it can be inferred that the Mo–P<sub>P(O)(OMe)</sub> bond has a double-bond character. Vibrational spectroscopic analysis reveals a P–O<sub>P(O)(OMe)</sub> stretching vibration at 1,146 cm<sup>-1</sup> which is indicative of a double bond. The ligand P(O)(OMe) can be described as an ester of meta phosphorous acid, so it can be denoted as a meta phosphite ligand [78–82]. By varying the amount of trimethyl phosphite, it is possible to change the ratio of the dinitrogen complex and the meta phosphite complex up to 3:2 (1.4 equiv. of trimethyl phosphite). However, it is not possible to suppress the formation of the meta phosphite complex completely. By further lowering the amount of trimethyl phosphite, the yield of the dinitrogen complex decreases but the ratio of the products is unchanged. Using an excess of trimethyl phosphite leads to the exclusive formation of the meta phosphite complex. These experiments show that the formation of the meta phosphite complex [Mo(PCP)(P(OMe)<sub>3</sub>)<sub>2</sub>(P(O)(OMe))] (**14**) is preferred; that is, this is the thermodynamically stable product [66].

The formation of this complex has been investigated in more detail. Using the ligand dpepp instead of PCP during the sodium amalgam reduction and applying an excess of trimethyl phosphite lead to the molybdenum complex *fac*-[Mo(P(OMe)<sub>3</sub>)<sub>3</sub>(dpepp)]. No formation of a meta phosphite complex is observed. Accordingly the reaction of trimethyl phosphite to a meta phosphite ligand is exclusively mediated by the Mo–NHC unit. During time-dependent NMR studies of the product mixture ([Mo(PCP)(P(OMe)<sub>3</sub>)<sub>2</sub>(P(O)(OMe))] (**14**) and *mer*-[Mo(N<sub>2</sub>)(PCP)(P(OMe)<sub>3</sub>)<sub>2</sub>] (**13**)) in presence of an excess of trimethyl phosphite, the ratio of the starting products

**Fig. 8** Crystal structure of [Mo(PCP)(P(OMe)<sub>3</sub>)<sub>2</sub>(P(O)(OMe))] (**14**). Hydrogen atoms are omitted for clarity [66]



does not change. Thus the sodium amalgam reduction of a molybdenum(III) complex to a molybdenum(0) complex is needed to generate the meta phosphite [66].

The reactivity of the dinitrogen complex *mer*-[Mo(N<sub>2</sub>)(PCP)(P(OMe)<sub>3</sub>)<sub>2</sub>] (**13**) towards Brønsted and Lewis acids has been investigated in order to evaluate the influence of the NHC unit. Intermediates like NNH<sub>2</sub><sup>-</sup> or AlMe<sub>3</sub> complexes could not be observed during the reaction using <sup>31</sup>P-NMR spectroscopy. Instead the meta phosphite complex reacts with the Lewis acid AlMe<sub>3</sub> under formation of two different products, in which the AlMe<sub>3</sub> coordinates to the two different oxygen atoms of the meta phosphite ligand [66].

To summarize, new molybdenum complexes containing the imidazole- and benzimidazole-based pincer ligand PCP (1,3-bis(2-diphenylphosphanylethyl)imidazol-2-ylidene, resp., 1,3-bis(2-diphenylphosphanylethyl)benzimidazol-2-ylidene) have been synthesized, characterized, and investigated in connection with small molecule, especially dinitrogen fixation [64–66]. It became apparent that the carbene atom of the PCP ligand is a pure σ-donor because of the exact cancellation of the π-donor and π-acceptor properties. Hence small molecules like carbonyl or dinitrogen coordinating to the metal center exhibit a very strong activation of the triple bond [64–66]. Unfortunately, this high activation of the dinitrogen ligand is accompanied by a thermal instability of the resulting complexes [66]. Therefore the electron density at the metal center has been reduced using phosphite ligands. A stable dinitrogen molybdenum complex with a mixed phosphine/carbene ligand could be obtained and characterized. During this reaction, the by-product [Mo(PCP)(P(OMe)<sub>3</sub>)<sub>2</sub>(P(O)(OMe))] (**14**) with a meta phosphite ligand has emerged as the thermodynamically stable product. The derivatization of the dinitrogen complex *mer*-[Mo(N<sub>2</sub>)(PCP)(P(OMe)<sub>3</sub>)<sub>2</sub>] (**13**) only leads to a decomposition [66]. The study of the mixed ligands with phosphine and carbene units revealed the remarkable properties of the PCP ligand although the application in mononuclear molybdenum–dinitrogen complexes is delicate [64–66].

## 4 Mo(0)–Dinitrogen Complexes Supported by Tripodal Ligands with Aryl Substituents

In this section, we return to molybdenum–dinitrogen complexes supported by polydentate phosphine ligands. In Sect. 2, the use of linear tridentate PEP ligands was explored, varying the donor atom E (N, P) and the chain length of the phosphine arms (C<sub>2</sub> vs. C<sub>3</sub>). A potential disadvantage especially of the dpepp system is the possibility of the existence of different facial isomers, leading to different degrees of N<sub>2</sub> activation [41, 83].

In order to establish a design that both remedies the drawbacks of the Chatt system and avoids the problem of isomerization, our working group explored the use of tripodal triphosphine ligands for molybdenum-based nitrogen fixation. In contrast to their linear PPP counterparts, especially the dpepp ligand, these ligands

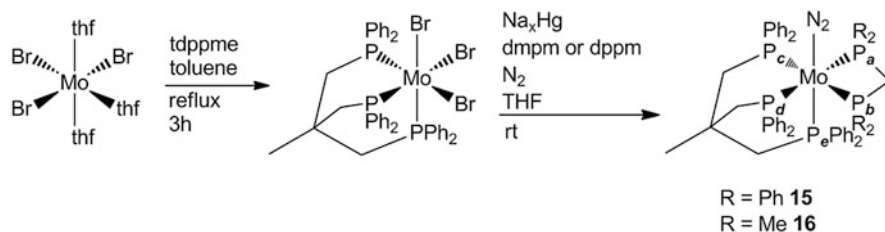
enforce facial coordination [84]. In this way, the pivotal *trans*-position to the dinitrogen ligand is also saturated. Moreover, due to the chelating effect of the ligand, an increased stability at higher oxidation states of the metal center is expected. In this respect, tripodal triphosphine ligands represent an alternative to tridentate macrocyclic P3 ligands [85]. In 2011, we reported the first successful coordination of the tripod ligand *tdppme* (*tdppme* = 1,1,1-tris(diphenylphosphanylmethyl)ethane) to a low-valent Mo–dinitrogen complex along with the bidentate coligands *dmpm* and *dppm*, respectively [67]. The applied synthetic approach involved the reaction of strong reducing agents like sodium amalgam with Mo(III) halide complexes to generate – along with the respective coligands under a dinitrogen atmosphere – the corresponding molybdenum–dinitrogen complexes (vide supra). In the case of the *tdppme* ligand, the best results were achieved by starting from  $[\text{MoBr}_3(\text{thf})_3]$  (Scheme 9). Reaction with the tripod led to  $[\text{MoBr}_3(\text{tdppme})]$ ; notably that the *mer*-isomer of  $[\text{MoBr}_3(\text{thf})_3]$  changes to the *fac*-isomer of  $[\text{MoBr}_3(\text{tdppme})]$  in the course of the reaction. The sodium amalgam reduction under an  $\text{N}_2$  atmosphere in the presence of the appropriate diphos coligand ultimately produced the complexes  $[\text{Mo}(\text{N}_2)(\text{tdppme})(\text{diphos})]$  (**15**, **16**).

The constitution of these complexes in the solid state was elucidated by the single crystal X-ray structure analysis of the complex  $[\text{Mo}(\text{N}_2)(\text{tdppme})(\text{dmpm})]$  (**16**) (Fig. 9). The data show a rather small bite angle of  $66.86^\circ$  of the *dmpm* coligand which seems to fit to the higher steric demand of the tripod ligand exhibiting a larger bite angle of the equatorial phosphines ( $82.30^\circ$ ).

This solid state structure also exists in solution. The  $^{31}\text{P}$ -NMR spectra of both **15** and **16** show an AA'XX'M signal structure, which can be attributed to the pentaphosphine environment surrounding the molybdenum center.

For the complex  $[\text{Mo}(\text{N}_2)(\text{tdppme})(\text{dppm})]$  (**15**), three signals at 43.92, 33.32, and 10.58 ppm are observed (Fig. 10, top).

The multiplet at 43.92 ppm corresponds to the equatorially bound P-donor atoms of the tripod ligand while the signal for the *trans*-phosphine donor can be found at 33.32 ppm. The multiplet at 10.58 ppm is attributed to the P-donor atoms of the *dppm* ligand. After extraction of the coupling constants, a corresponding  $^{31}\text{P}$ -NMR spectrum has been simulated (Fig. 10, bottom). The same signal structure is observed for the complex  $[\text{Mo}(\text{N}_2)(\text{tdppme})(\text{dmpm})]$  (**16**), however, with slightly different chemical shifts.



**Scheme 9** Synthesis of  $[\text{Mo}(\text{N}_2)(\text{tdppme})(\text{diphos})]$  (**15**, **16**) via reduction of the reactive precursor  $[\text{MoBr}_3(\text{tdppme})]$  (diphos = *dmpm*, *dppm*)



**Fig. 9** Single crystal structure of  $[\text{Mo}(\text{N}_2)(\text{tdppme})(\text{dmpm})]$  (**16**). Hydrogen atoms are omitted for clarity [67]

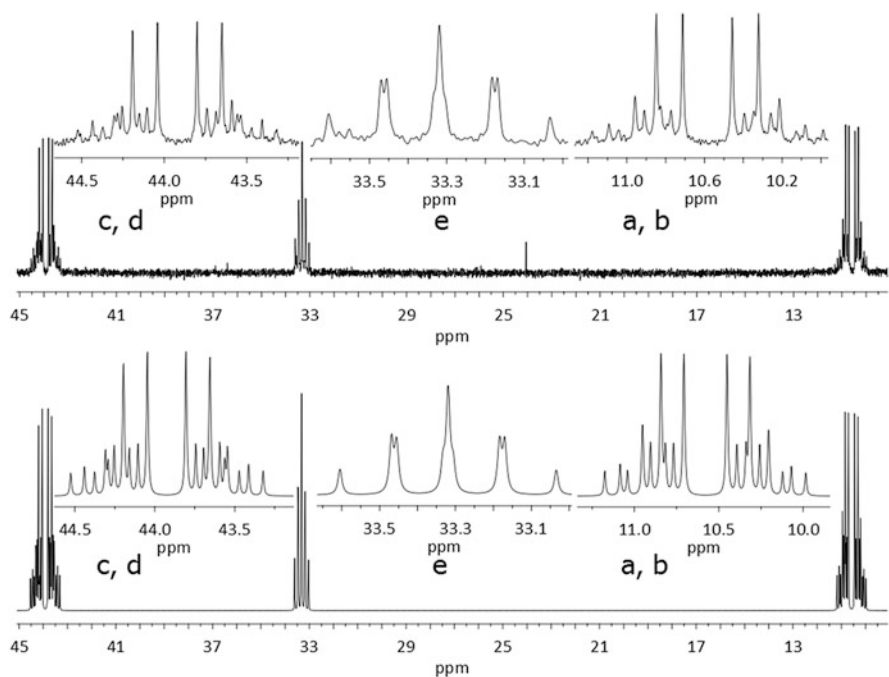
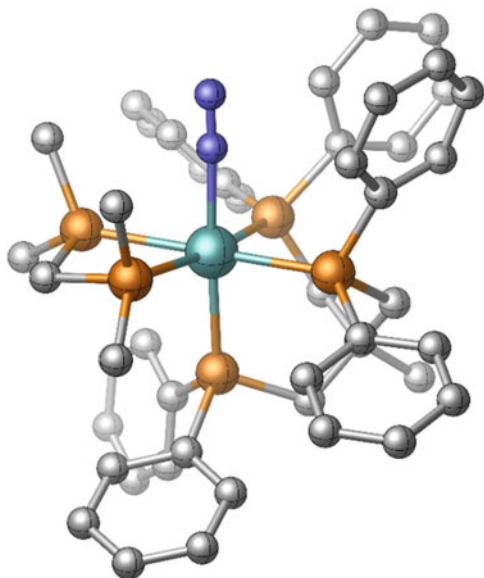


**Fig. 10** Comparison of the measured (*top*) and the simulated (*bottom*)  $^{31}\text{P}$ -NMR spectrum of  $[\text{Mo}(\text{N}_2)(\text{tdppme})(\text{dppm})]$  (**15**). Simulation of a  $^{31}\text{P}$ -NMR spectrum has been carried out after extraction of the coupling constants [67]

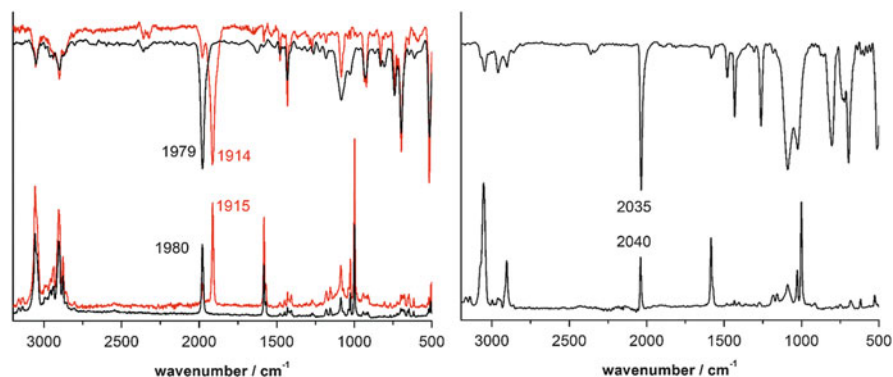


**Fig. 11** IR (*top*) and Raman (*bottom*) spectra of  $[\text{Mo}(\text{N}_2)(\text{tdppme})(\text{dmpm})]$  (**16**, *left*, *black*) and  $[\text{Mo}(\text{N}_2)(\text{tdppme})(\text{dppm})]$  (**15**, *right*). *Left*:  $[\text{Mo}^{15}\text{N}_2](\text{tdppme})(\text{dmpm})]$  ( $^{15}\text{N}$ -**16**) (*red*) [67]

After confirming the constitution of the Mo–N<sub>2</sub> complexes **15** and **16**, the next step was to obtain information regarding the degree of activation of the N<sub>2</sub> ligand. Compared to the free dinitrogen molecule ( $\tilde{\nu}_{\text{NN}} = 2,331 \text{ cm}^{-1}$ ), moderately activated N<sub>2</sub> complexes exhibit stretching frequencies lower than  $2,000 \text{ cm}^{-1}$  [86]. While the complex  $[\text{Mo}(\text{N}_2)(\text{tdppme})(\text{dmpm})]$  (**16**) shows an NN stretching frequency at  $1,979 \text{ cm}^{-1}$  and thus is considered to be activated moderately, the complex  $[\text{Mo}(\text{N}_2)(\text{tdppme})(\text{dppm})]$  (**15**) exhibits a stretching frequency of the coordinated N<sub>2</sub> ligand at  $2,035 \text{ cm}^{-1}$  and thus is out of the range of moderately activated N<sub>2</sub> complexes (Fig. 11).

Clearly, the coligand has a significant influence on the degree of activation. In order to activate the N<sub>2</sub> ligand, electron density has to be transferred from d orbitals of the metal center to the antibonding orbitals of the dinitrogen ligand which ultimately leads to a weakening of the NN bond. By employing an alkyl phosphine coligand like dmpm, more electron density is donated to the metal center than in case of the dppm coligand. Due to the electron withdrawing character of phenyl groups present in the latter ligand, less electron density is located at the metal center, leading to a shift of  $\tilde{\nu}_{\text{NN}}$  to higher frequency by  $55 \text{ cm}^{-1}$ .

The next step was the investigation of the reactivity of the N<sub>2</sub> complexes **15** and **16** towards strong acids. As mentioned above,  $[\text{Mo}(\text{N}_2)(\text{tdppme})(\text{dppm})]$  (**15**), which is less activated than  $[\text{Mo}(\text{N}_2)(\text{tdppme})(\text{dmpm})]$  (**16**), does not exhibit any reactivity towards acids. However, the N<sub>2</sub> ligand of  $[\text{Mo}(\text{N}_2)(\text{tdppme})(\text{dmpm})]$  (**16**) could be protonated using 2 equiv. of trifluoromethanesulfonic acid, leading to the

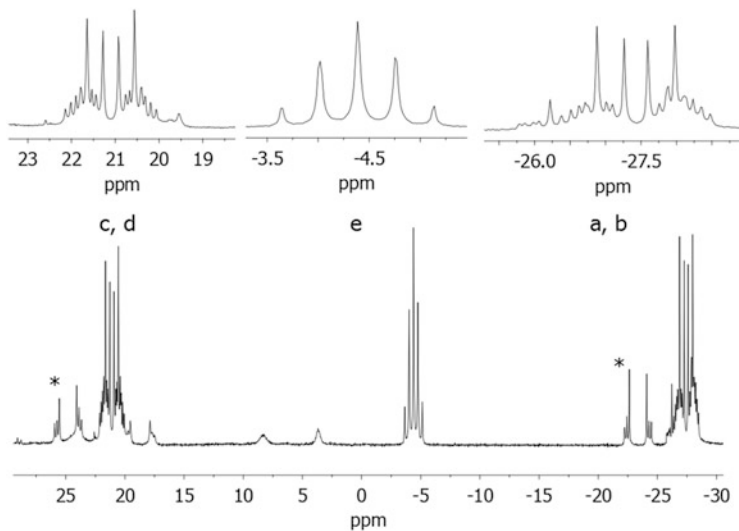


**Fig. 12**  $^{31}\text{P}$ -NMR spectrum of  $[\text{Mo}(\text{NNH}_2)(\text{tdppme})(\text{dmpm})](\text{OTf})_2$  ( $\text{NNH}_2$ -**16**). Signals marked by asterisks at 24.82 and  $-23.35$  ppm (AA'XX') are probably a consequence of a decomposition product during the NMR measurement [67]

diamagnetic complex  $[\text{Mo}(\text{NNH}_2)(\text{tdppme})(\text{dmpm})](\text{OTf})_2$  ( $\text{NNH}_2$ -**16**). The conversion occurred under full retention of the pentaphosphine environment as evidenced by the  $^{31}\text{P}$ -NMR spectrum which still exhibits an AA'XX'M signal structure (Fig. 12). In comparison to the parent complex  $[\text{Mo}(\text{N}_2)(\text{tdppme})(\text{dmpm})]$  (**16**), all resonances shift to higher field by 10–44 ppm.

Derivatization of  $\text{N}_2$  in the isotopomer  $[\text{Mo}(^{15}\text{N}_2)(\text{tdppme})(\text{dmpm})]$  ( $^{15}\text{N}$ -**16**) has been carried out as well using 2 equiv. of HOTf. Coupling of the protons of the  $^{15}\text{N}^{15}\text{NH}_2$  species to the terminal  $\text{N}_\beta$  atom was detected via  $^1\text{H}$ - $^{15}\text{N}$  HMQC-NMR. With the help of vibrational spectroscopy, more information was obtained regarding the  $\text{NNH}_2$  species (Fig. 13). Signals at 3,301 and  $3,238\text{ cm}^{-1}$  of the complex  $[\text{Mo}(\text{NNH}_2)(\text{tdppme})(\text{dmpm})](\text{OTf})_2$  ( $\text{NNH}_2$ -**16**) can be assigned to the antisymmetric and symmetric  $\text{NH}_2$  stretches. A shift to lower wavenumbers of the  $\text{NH}_2$  stretch has been detected as well for the  $^{15}\text{N}_2$  marked isotopomer  $[\text{Mo}(^{15}\text{N}^{15}\text{NH}_2)(\text{tdppme})(\text{dmpm})](\text{OTf})_2$  ( $^{15}\text{N}^{15}\text{NH}_2$ -**16**;  $3,289\text{ cm}^{-1}$  and  $3,230\text{ cm}^{-1}$  respectively; Fig. 13). Moreover, the NN stretch of the  $\text{NNH}_2$  complex can be identified at  $1,410\text{ cm}^{-1}$  (Fig. 13).

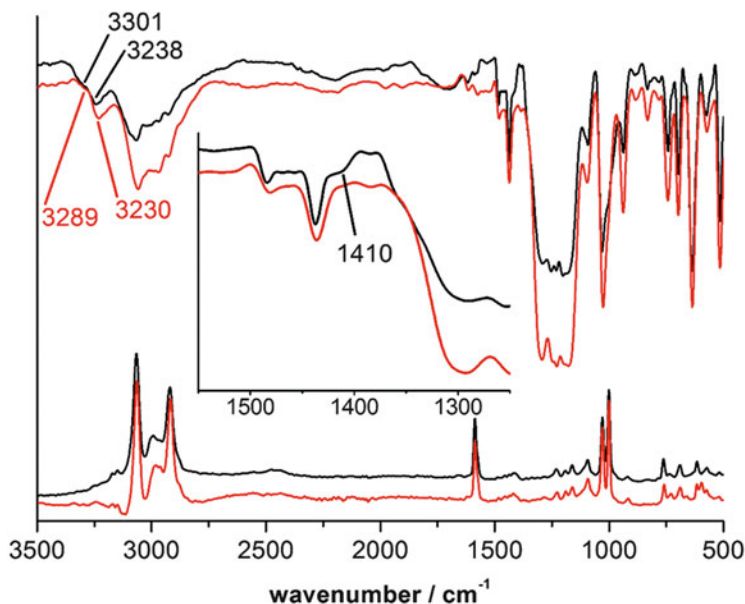


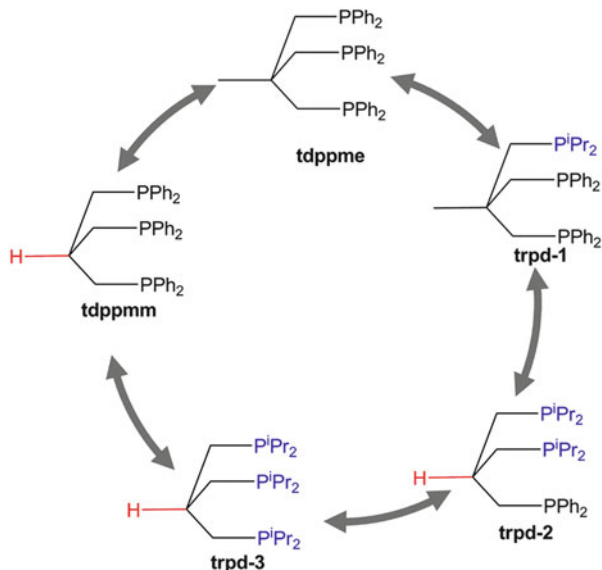
**Fig. 13** IR (top) and Raman (bottom) spectra of  $[\text{Mo}(\text{NNH}_2)(\text{tdppme})(\text{dmpm})]$  ( $\text{NNH}_2$ -**16**) (black) and  $[\text{Mo}(^{15}\text{N}^{15}\text{NH}_2)(\text{tdppme})(\text{dmpm})]$  ( $^{15}\text{N}^{15}\text{NH}_2$ -**16**) (red). Inset: enlargement of the range of the NN stretching vibration of ( $\text{NNH}_2$ -**16**) [67]

## 5 Mo(0)–Dinitrogen Complexes Supported by Hybrid Tripodal Ligands with Mixed Dialkylphosphine/ Diarylphosphine Donor Groups

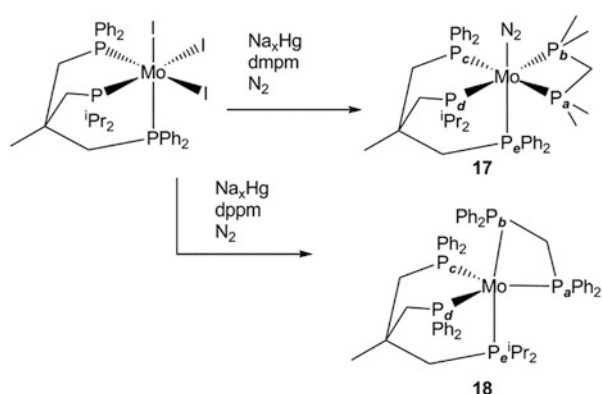
As shown in the previous section, changing the coligand in tripod-supported molybdenum–dinitrogen complexes from dppm to dmpm leads to a higher activation of  $\text{N}_2$  [67]. As a next stage in our investigations of these systems, we also wanted to implement this increase of activation by replacing aryl- by alkylphosphine groups in the tripod ligand. In the framework of this project, we prepared a set of different tripod ligands in which the diphenylphosphine donor groups of tdpme are substituted in a stepwise fashion by diisopropylphosphine groups [68].

By exchanging one diphenylphosphine group of the tdpme ligand by a diisopropylphosphine moiety, the ligand trpd-1 was obtained. The corresponding ligands trpd-2 and trpd-3 possess two and three diisopropylphosphine groups, respectively. Due to preparative reasons, trpd-2 and trpd-3 contain an isobutyl backbone [87]. To investigate the effect of the backbone on the coordination behavior of these ligands, a fourth ligand has been synthesized which contains three diphenylphosphine groups on an isobutyl backbone (Scheme 10) [88]. All four ligands were utilized in combination with the coligands dppm and dmpm to synthesize molybdenum–dinitrogen complexes [69].

**Scheme 10** Schematic representation of the substitution pattern of the tripod ligand. Note that the ligands trpd-2, trpd-3, and tdppmm are based on an isobutyl backbone



**Scheme 11** Representation of the sodium amalgam reduction of the reactive precursor  $[\text{MoI}_3(\text{trpd-1})]$  in the presence of dmpm or dppm, respectively



In order to obtain the desired  $\text{N}_2$  complexes, the typical procedure has been applied (vide supra). First, the tripod ligands are coordinated to a reactive  $\text{Mo(III)}$  precursor, secondly a reduction of the molybdenum(III) complexes through sodium amalgam in an  $\text{N}_2$  atmosphere with addition of a coligand affords the corresponding  $\text{Mo-N}_2$  complexes (Scheme 11). For our set of tripod ligands, we used  $[\text{MoI}_3(\text{thf})_3]$  [55, 89] as a precursor, because it enabled preparation of the  $\text{Mo(III)}$  tripod complexes in good yields and purities.

Subsequent reduction of the aforementioned complexes by sodium amalgam and addition of the coligand (dppm or dmpm) yielded in cases of trpd-2, trpd-3 and tdppmm complexes with a  $\kappa^2$ -coordination. One explanation for this observation is the high steric demand of the diisopropylphosphine groups incorporated in the

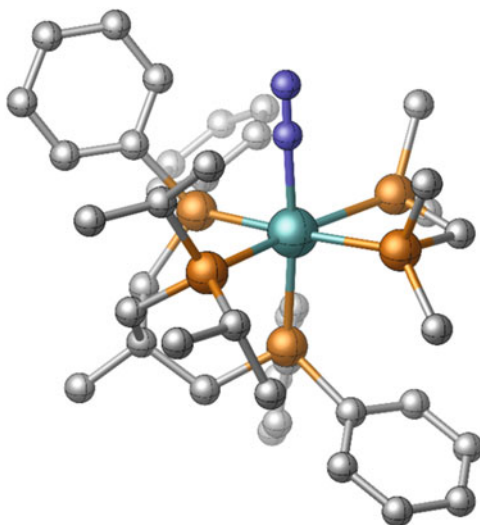
ligands trpd-2 and trpd-3. Another problem is the isobutyl backbone. While the apical methyl group in the neopentyl backbone supports the facial coordination of the tripod ligand, the isobutyl backbone does not possess this methyl group. Because the pivotal *trans*-position to  $N_2$  is not saturated by the ligand, the  $\kappa^2$ -complexes are not suitable for further investigations.

Interestingly, sodium amalgam reduction of  $[MoI_3(trpd-1)]$  precursor and dppm as coligand resulted in a molybdenum complex without coordinated dinitrogen. Although the  $^{31}P$ -NMR spectrum showed five sets of signals, which are indicative of five different phosphorus species coordinated to the metal center, no signals or traces of dinitrogen could be found by elemental analysis or vibrational spectroscopy. Thus the complex  $[Mo(trpd-1)(dppm)]$  (**18**) has been obtained which possesses a rare fivefold coordination, certainly due to the high steric demand of the  $P^iPr_2$  [90] group and the bigger coligand dppm.

On the other hand, a six-coordinate  $Mo(0)-N_2$  complex has been successfully synthesized with trpd-1 and dmpm as coligand. Single crystal X-ray structure analysis of this complex (**17**) shows that the diisopropylphosphine group is located in the equatorial plane, i.e., *cis* to the axial  $N_2$  ligand. As expected, the structure determination proved the existence of five coordinated phosphine donor groups besides the  $N_2$  ligand. Compared to the symmetric tdppme complex **16**, the trpd-1 complex **17** possesses a distorted octahedral structure (Fig. 14).

$^{31}P$ -NMR spectroscopy has been applied to gain further information concerning the structure of the complex (Fig. 15). This spectrum shows different sets of ddd-signals which can be found at 47.3, 41.1, 40.3, and  $-24.5$  ppm. The signals at  $-24.5$  ppm can be ascribed to the P atoms of the dmpm coligand and are in the range of our previous result for  $[Mo(N_2)(tdppme)(dmpm)]$  (**16**) [67]. The signal at 40.3 ppm corresponds to the diphenylphosphine group *trans* to the  $N_2$  ligand of the

**Fig. 14** Single crystal structure of  $[Mo(N_2)(trpd-1)(dmpm)]$  (**17**). Hydrogen atoms are omitted for clarity [69]



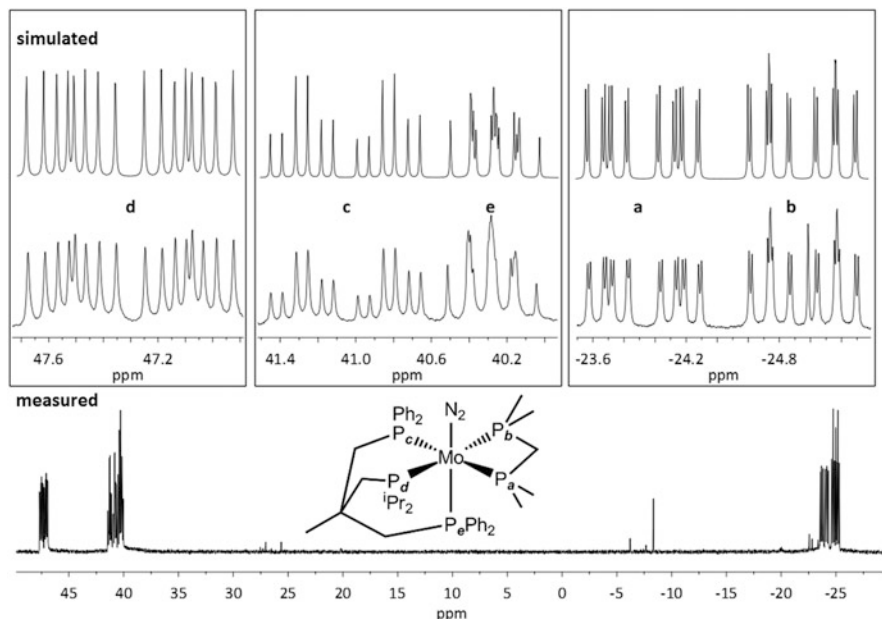


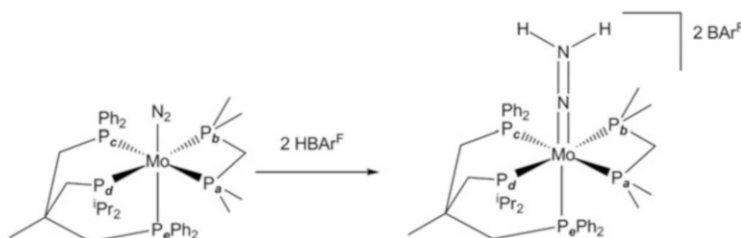
**Fig. 15**  $^{31}\text{P}$ -NMR of  $[\text{Mo}(\text{N}_2)(\text{trpd-1})(\text{dmpm})]$  (**17**) with the detailed zoom for the simulation (*top*) and the measurement (*bottom*) [69]

complex. The second diphenylphosphine group can be found at 41.1 ppm, while the signal of the diisopropylphosphine group is located at 47.3 ppm (Fig. 15).

IR and Raman spectra of the dinitrogen complex **17** show an NN stretch at  $1,965\text{ cm}^{-1}$  which is in the range of moderately activated dinitrogen complexes. Moreover, the additional alkylphosphine group of the aforementioned complex increased the activation of the  $\text{N}_2$  ligand compared to the parent system  $[\text{Mo}(\text{N}_2)(\text{tdppme})(\text{dmpm})]$  (**16**) ( $\tilde{\nu}_{\text{NN}} = 1,979\text{ cm}^{-1}$ ) [67].

The reactivity of this complex towards acids has been investigated as well. Although several experiments with  $\text{HOTf}$ ,  $\text{H}_2\text{SO}_4$ , or  $\text{HCl}$  have been performed, the desired  $\text{NNH}_2$  complex could not be obtained. However, application of  $\text{HBAr}^{\text{F}}$  [91] led to generation and detection of the  $\text{NNH}_2$  species under retention of the pentaphosphine coordination, as evidenced by subsequent  $^{31}\text{P}$ -NMR measurement.

Obviously,  $\text{HBAr}^{\text{F}}$  is a suitable acid for this experiment because of the non-coordinating anion (Scheme 12). The signals of the complex  $[\text{Mo}(\text{NNH}_2)(\text{trpd-1})(\text{dmpm})](\text{BAr}^{\text{F}})_2$  ( $\text{NNH}_2$ -**17**) are shifted to high field as evidenced before for the complex  $[\text{Mo}(\text{NNH}_2)(\text{tdppme})(\text{dmpm})](\text{OTf})_2$  ( $\text{NNH}_2$ -**16**) (Fig. 16).



**Scheme 12** Derivatization of the ligand  $N_2$  by using 2 equiv. of the acid  $HBARF$

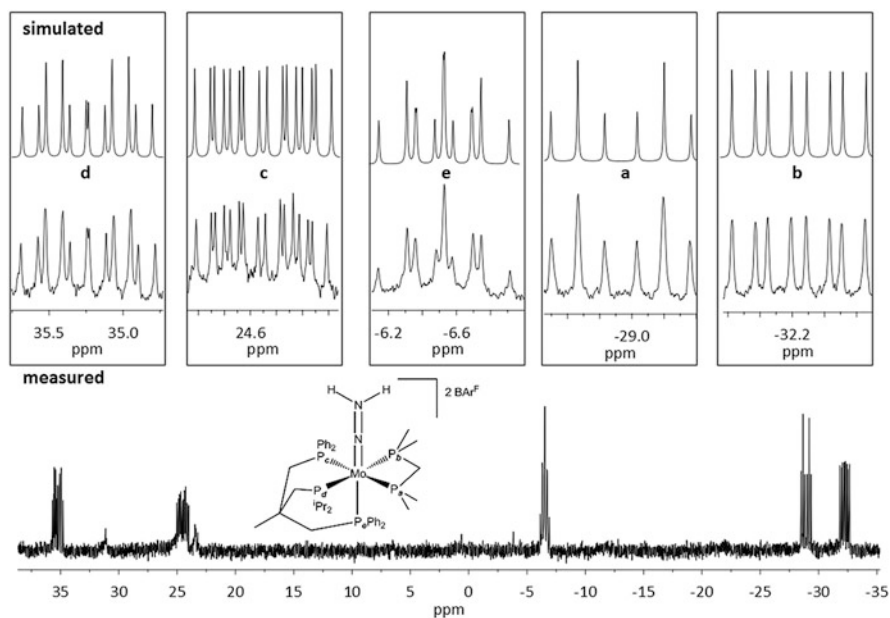


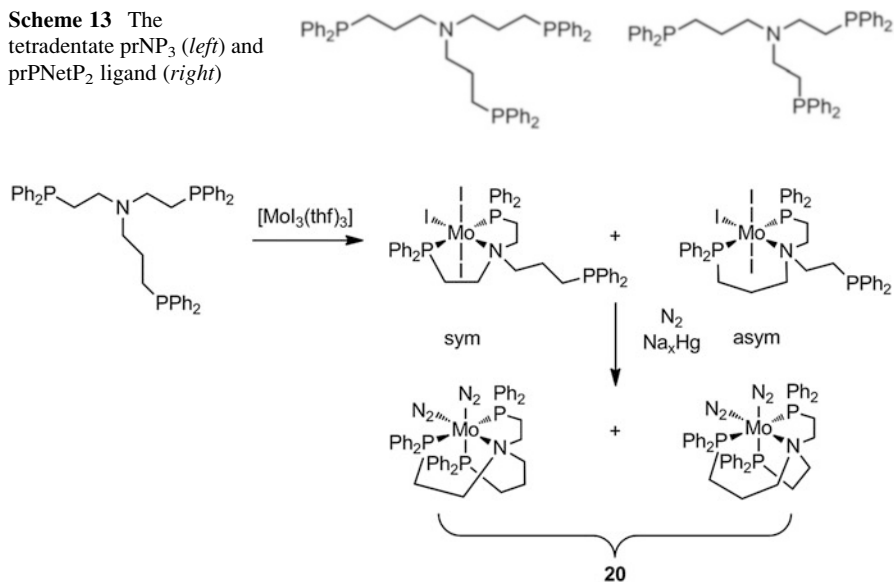
**Fig. 16**  $^{31}P$ -NMR of  $[Mo(NNH_2)(trpd-1)(dmpm)]$  ( $NNH_2$ -17) with detailed zoom of the simulated (*top*) and measured (*bottom*) spectra [69]

## 6 Mo(0)–Dinitrogen Complexes Supported by Tetradentate $NP_3$ Ligands

A further approach towards occupying the *trans*-position of a dinitrogen ligand in molybdenum–dinitrogen complexes is based on tetradentate  $NP_3$  ligands. Towards this goal, our group synthesized the new tetradentate ligands  $prNP_3$  ( $NP_3 = N(CH_2CH_2CH_2PPh_2)_3$ ) and  $prPNetP_2$  ( $prPNetP_2 = (Ph_2PCH_2CH_2CH_2)N(CH_2CH_2PPh_2)_2$ ) (Scheme 13). The ligand  $prPNetP_2$  is an asymmetric ligand which contains mixed ethylene/propylene bridges. The coordination of these ligands to molybdenum(0) centers and their impact to the activation of the  $N_2$  ligand have been studied [48].



**Scheme 13** The tetradentate prNP<sub>3</sub> (left) and prPNetP<sub>2</sub> ligand (right)



**Scheme 14** Synthesis of the complexes [MoI<sub>3</sub>(prPNetP<sub>2</sub>)] and [Mo(N<sub>2</sub>)<sub>2</sub>(prPNetP<sub>2</sub>)] (**20**)

To obtain Mo(0)–dinitrogen complexes, we first synthesized the Mo(III) complexes [MoCl<sub>3</sub>(prNP<sub>3</sub>)] and [MoI<sub>3</sub>(prPNetP<sub>2</sub>)] by reaction of prNP<sub>3</sub> and prPNetP<sub>2</sub> with [MoCl<sub>3</sub>(thf)<sub>3</sub>] and [MoI<sub>3</sub>(thf)<sub>3</sub>]. Reduction of the respective Mo(III) complexes with sodium amalgam in a dinitrogen atmosphere led to the *cis*-bis(dinitrogen) Mo(0) complexes [Mo(N<sub>2</sub>)<sub>2</sub>(prNP<sub>3</sub>)] (**19**) and [Mo(N<sub>2</sub>)<sub>2</sub>(prPNetP<sub>2</sub>)] (**20**). The synthesis of the latter is shown in Scheme 14 [48].

Reaction of the asymmetric prPNetP<sub>2</sub> ligand with the Mo(III) precursor [MoI<sub>3</sub>(thf)<sub>3</sub>] leads to formation of two isomers: (1) *sym* (coordination of prPNetP<sub>2</sub> by two ethylene bridged phosphines) and (2) *asym* (coordination of prPNetP<sub>2</sub> by one ethylene and one propylene bridged phosphines; Scheme 14). With the help of DFT calculations, we found out that the *sym*-isomer is energetically disfavored by 7.4 kcal mol<sup>-1</sup> [48]. Reduction with Na<sub>x</sub>Hg generates the corresponding dinitrogen complexes, which also exist in different isomeric forms (vide infra). Importantly, we observed a κ<sup>4</sup>-coordination of the new ligands prPNetP<sub>2</sub> and prNP<sub>3</sub> for all bis(dinitrogen) Mo(0) complexes in solution. However, the thermal stability of the new complexes is limited [48].

The new Mo(0)–dinitrogen complexes [Mo(N<sub>2</sub>)<sub>2</sub>(prNP<sub>3</sub>)] (**19**) and [Mo(N<sub>2</sub>)<sub>2</sub>(prPNetP<sub>2</sub>)] (**20**) were characterized by vibrational and NMR spectroscopy [48]. The IR spectrum of [Mo(N<sub>2</sub>)<sub>2</sub>(prNP<sub>3</sub>)] (**19**) shows a symmetric (1,950 cm<sup>-1</sup>) and an antisymmetric (1,904 cm<sup>-1</sup>) combination of NN vibrations, reflecting a moderate activation of N<sub>2</sub>. The relative intensities of the two vibrations indicate that the *cis*-bis(dinitrogen) complex **19** was obtained [48]. It was expected that in the <sup>31</sup>P-NMR spectrum of [Mo(N<sub>2</sub>)<sub>2</sub>(prNP<sub>3</sub>)] (**19**) an A<sub>2</sub>M spin system appears, similar to the literature-known complex *cis*-[Mo(N<sub>2</sub>)<sub>2</sub>(NP<sub>3</sub>)] (**21**) of Fernández-Trujillo et al.

( $\text{NP}_3 = \text{N}(\text{CH}_2\text{CH}_2\text{PPh}_2)_3$ ) [48]. However, in place of an  $\text{A}_2\text{M}$  spin system an AMX system was observed (Fig. 17) [48].

The observation of the AMX spectrum can be explained by DFT. In Fig. 18, the geometry optimized structures of *cis*- $[\text{Mo}(\text{N}_2)_2(\text{NP}_3)]$  (**21**) and  $[\text{Mo}(\text{N}_2)_2(\text{prNP}_3)]$  (**19**) are shown. In the structure of *cis*- $[\text{Mo}(\text{N}_2)_2(\text{NP}_3)]$  (**21**) (Fig. 18, left), the phosphines *trans* to each other are symmetric with respect to a plane containing both dinitrogen ligands and thus are magnetically equivalent. In contrast, the optimized structure of  $[\text{Mo}(\text{N}_2)_2(\text{prNP}_3)]$  (**19**) (Fig. 18, right) shows a rotation of the *prNP*<sub>3</sub> ligand around the N–Mo–N<sub>2</sub> axis. Therefore the phosphines *trans* to each other are not equivalent anymore. Breaking the mirror symmetry of the parent complex **21** is the reason for the splitting of the signals in the <sup>31</sup>P-NMR spectrum (Fig. 19) [48].

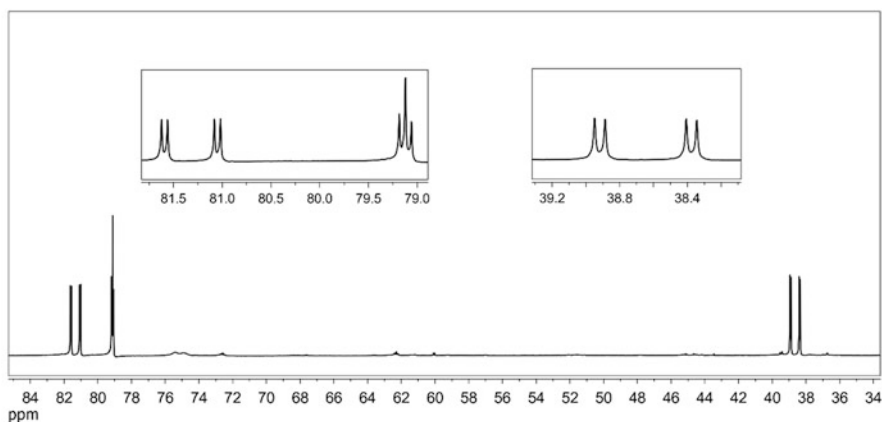


Fig. 17 <sup>31</sup>P-NMR spectrum of  $[\text{Mo}(\text{N}_2)_2(\text{prNP}_3)]$  (**19**) [46]

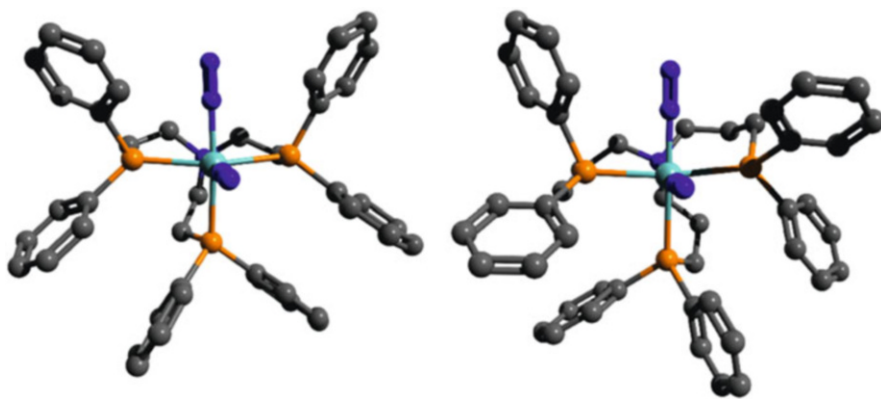
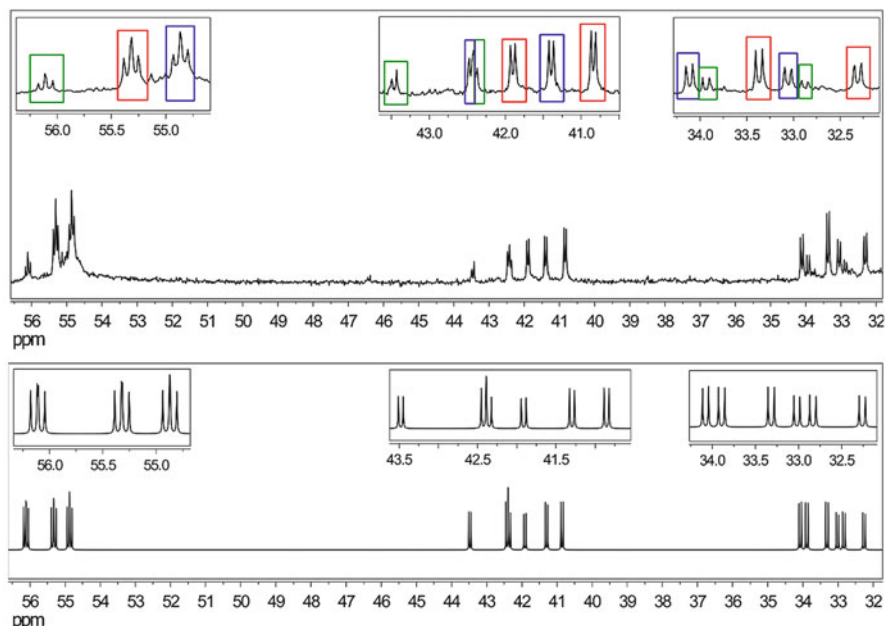


Fig. 18 Geometry optimized structures of  $[\text{Mo}(\text{N}_2)_2(\text{NP}_3)]$  (**21**, left) and  $[\text{Mo}(\text{N}_2)_2(\text{prNP}_3)]$  (**19**, right) [46]



**Fig. 19**  $^{31}\text{P}$ -NMR spectrum of  $[\text{Mo}(\text{N}_2)_2(\text{prPNetP}_2)]$  (**20**) (*top*: measured; *bottom*: simulated). Three types of frames (*green*, *red*, and *blue*) indicate the AMX subspectra of three species [48]

The IR spectrum of  $[\text{Mo}(\text{N}_2)_2(\text{prPNetP}_2)]$  (**20**) exhibits a symmetric ( $1,991\text{ cm}^{-1}$ ) and an antisymmetric ( $1,925\text{ cm}^{-1}$ ) stretching vibration of the  $\text{N}_2$  ligands. Again, the relative intensities indicate that the *cis*-bis(dinitrogen) complex is formed [48]. In the  $^{31}\text{P}$ -NMR spectrum of **20** (Fig. 19), three AMX patterns are observed. Due to the appearance of AMX systems, it can be inferred that the two phosphines *trans* to each other are magnetically inequivalent (*vide supra*) [48]. The observation of three AMX patterns leads to the conclusion that three different isomers of the complex **20** have been formed during the reaction.

With the help of DFT calculations, more information about the structure of possible isomers was obtained. The geometry optimized structures are shown in Figs. 20 and 21. All these isomers differ with respect to the configuration of the  $\text{C}_3$  bridge relative to the *cis*- $\text{C}_2$  bridge. The calculated relative energies (in  $\text{kcal mol}^{-1}$ ) for the *asym*-isomers are 0 for **20e**, +0.28 for **20b**, +2.22 for **20c**, +3.94 for **20d**, and for the *sym*-isomer (**20a**) +2.53 [48].

Probably, all of the signals in the  $^{31}\text{P}$ -NMR spectrum belong to the *asym* form of the  $[\text{Mo}(\text{N}_2)_2(\text{prPNetP}_2)]$  complex (**20**). In the *asym* form, the ethylene and propylene bridges are located within the PNP plane and a mirror plane is lacking. Comparing the *trans* coupling constant of the phosphorus nuclei in  $[\text{Mo}(\text{N}_2)_2(\text{prPNetP}_2)]$  (**20**) with the equivalent phosphorus species in  $[\text{Mo}(\text{N}_2)_2(\text{prNP}_3)]$  (**19**), it can be noted that the coupling constants are significantly different. On the other hand, the respective coupling constants of the three isomers are nearly equal. If one of the isomers was

**Fig. 20** Optimized structure of the isomer of *sym*-[Mo(N<sub>2</sub>)<sub>2</sub>(prPNetP<sub>2</sub>)] (**20a**) [48]

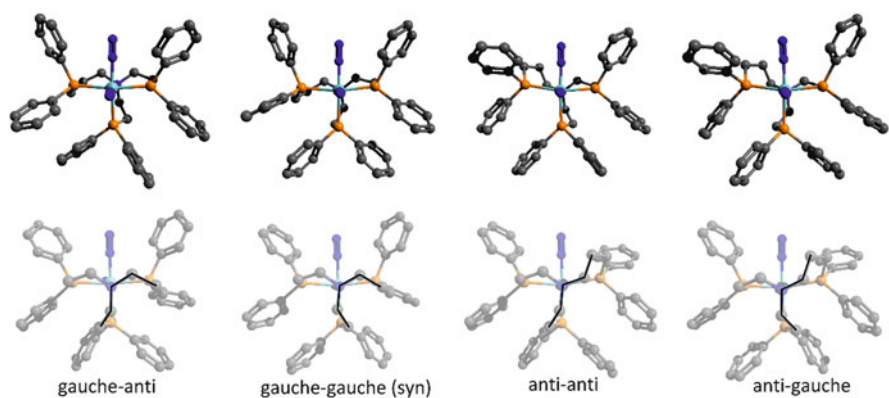
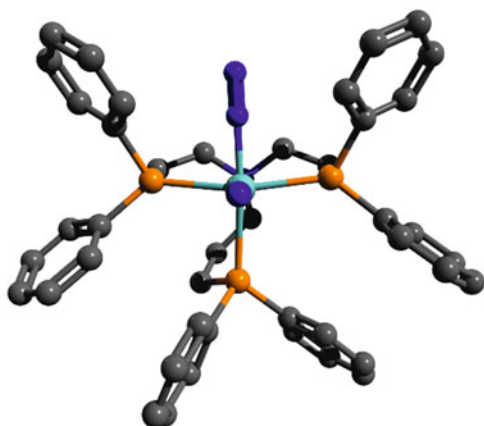


**Fig. 21** Optimized structures of the four possible isomers of *asym*-[Mo(N<sub>2</sub>)<sub>2</sub>(prPNetP<sub>2</sub>)] (*asym*-**20**) (left to right: **20b**, **20c**, **20d**, and **20e**). *Top*: front view; *bottom*: rear view with indication of the conformation [48]

the *sym*-isomer, we would observe one different *trans* coupling constant. Therefore we assume that the three species observed in the <sup>31</sup>P-NMR spectrum are *asym*-isomers. Maybe the product distribution of the Mo(0) complexes is also influenced by the Mo(III) precursor, where the *sym*-isomer is disfavored (*vide supra*) [48].

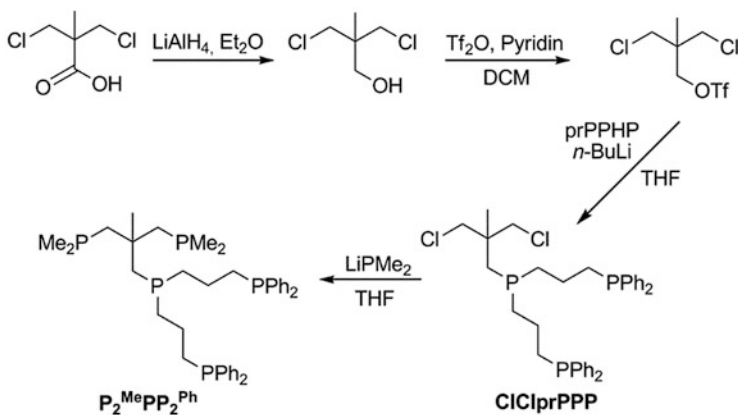
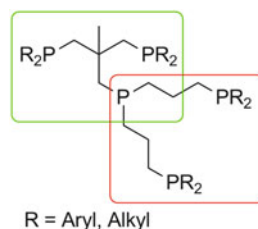
According to the DFT calculations, the formation of four *asym*-isomers is in principle possible (**20b–e**, Fig. 21), but only three sets of AMX signals are apparent in the <sup>31</sup>P-NMR spectrum (Fig. 19). Compound **20d** is the energetically least favorable product; consequently, we assume that this complex is not formed during the reaction [48].

## 7 Mo(0)–Dinitrogen Complex Supported by a Pentadentate Tetrapodal Phosphine (pentaPod<sup>P</sup>) Ligand

In the preceding sections, several possibilities to occupy the *trans*-position of coordinated N<sub>2</sub> in Chatt type systems have been explored. Our first attempt towards this goal was based on complexes with a combination of a trident and a diphos ligand as present in, e.g., [Mo(N<sub>2</sub>)(dpepp)(dppm)] [41]. Then, in order to ensure a higher stability of the phosphine environment, the use of tripod ligands was explored. The neopentyl backbone enforces a facial coordination of these ligands [67, 69, 70]. However, also in these systems the phosphine group in the axial position to the N<sub>2</sub> ligand was found to be prone to dissociation, leading to coordination of external ligands such as the conjugated base of the acid employed for protonation or a solvent molecule. The ultimate solution to this problem is the synthesis of a pentadentate tetrapodal phosphine (pentaPod<sup>P</sup>) ligand [92]. This type of ligand derives from the fusion of a tripod and a trident ligand (Fig. 22).

The synthesis of the pentaPod<sup>P</sup> ligand is shown in Scheme 15. The trident part of the ligand is composed of bis(3-(diphenylphosphino)propyl)phosphine (prPPHP) which has already been presented in Sect. 2. The synthesis of the tripod part starts

**Fig. 22** The pentaPod<sup>P</sup> ligand consists of a tripod part (*green*) and a tridentate part (*red*)



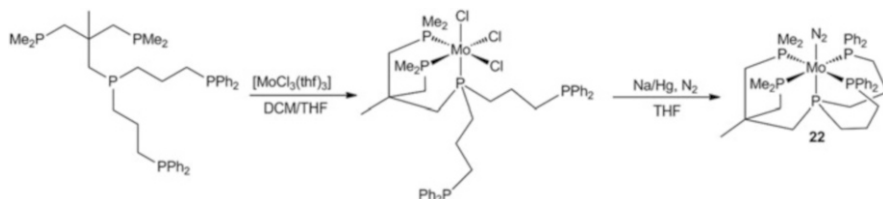
**Scheme 15** Synthesis of the pentapod<sup>P</sup> ligand P<sub>2</sub>MePP<sub>2</sub>Ph

from 3,3-dichloropivalic acid. After reduction of the acid function and the conversion of the resulting alcohol residue to the triflate [93], prPPLiP was reacted with the triflate function of the tripod part to yield the proligand ClClPrPPP. The last step of the reaction required 2 eq. of LiPMe<sub>2</sub> which reacted with ClClPrPPP to ultimately produce the pentaPod<sup>P</sup> ligand P<sub>2</sub><sup>Me</sup>PP<sub>2</sub><sup>Ph</sup> [92].

Coordination of the pentadentate phosphine ligand (P<sub>2</sub><sup>Me</sup>PP<sub>2</sub><sup>Ph</sup>) was achieved by addition of an equimolar amount of [MoCl<sub>3</sub>(thf)<sub>3</sub>] [50, 92, 94]. Due to the incorporation of different phosphine donor groups in the trident and the tripod part of the ligand (alkyl vs. aryl phosphines), the pentaPod<sup>P</sup> ligand possesses a unique coordination behavior. While the tripod part inevitably leads to a facially coordinated product, coordination of the trident part is more likely to result in a complex with a meridional isomer [67, 95]. It is expected that the tripod part of P<sub>2</sub><sup>Me</sup>PP<sub>2</sub><sup>Ph</sup> coordinates selectively to [MoCl<sub>3</sub>(thf)<sub>3</sub>], yielding *fac*(trpd)-[MoCl<sub>3</sub>(P<sub>2</sub><sup>Me</sup>PP<sub>2</sub><sup>Ph</sup>)] (trpd = tripod) (Scheme 16). This is a consequence of the stronger σ-donor character and the smaller steric demand of the dimethylphosphines in comparison to the diphenylphosphine donor groups. Subsequent sodium amalgam reduction of *fac*(trpd)-[MoCl<sub>3</sub>(P<sub>2</sub><sup>Me</sup>PP<sub>2</sub><sup>Ph</sup>)] leads to a mononuclear dinitrogen complex with coordination of the remaining diphenylphosphine donor groups of the trident part of the ligand [92].

This way, the desired pentaphosphine environment, which is necessary to minimize the shortcomings of Chatt type systems, has been achieved by the employment of just one ligand. The structure of **22** was proven by <sup>31</sup>P-NMR spectroscopy and single crystal structure determination. As explained earlier, an AA'XX'M signal structure in the <sup>31</sup>P-NMR spectrum is expected for a complex with five coordinated phosphine donors (Fig. 23). After extraction of the necessary coupling constants, a simulation has been performed [96].

A further proof for the structure of **22** was obtained by single crystal X-ray structure determination (Fig. 24). The data clearly show the pentaPod<sup>P</sup> ligand occupying five coordination sites of the molybdenum center and the dinitrogen ligand binding to the remaining coordination site. The activation of N<sub>2</sub> in the complex [Mo(N<sub>2</sub>)(P<sub>2</sub><sup>Me</sup>PP<sub>2</sub><sup>Ph</sup>)] (**22**) leads to an elongation of the N<sub>α</sub>N<sub>β</sub> distance (1.099(5) Å) compared to elemental N<sub>2</sub> (1.0975 Å).



**Scheme 16** Coordination of the pentaPod<sup>P</sup> ligand P<sub>2</sub><sup>Me</sup>PP<sub>2</sub><sup>Ph</sup> on [MoCl<sub>3</sub>(thf)<sub>3</sub>] and subsequent sodium amalgam reduction under the atmosphere of N<sub>2</sub> to generate the molybdenum–dinitrogen complex [Mo(N<sub>2</sub>)(P<sub>2</sub><sup>Me</sup>PP<sub>2</sub><sup>Ph</sup>)] (**22**)

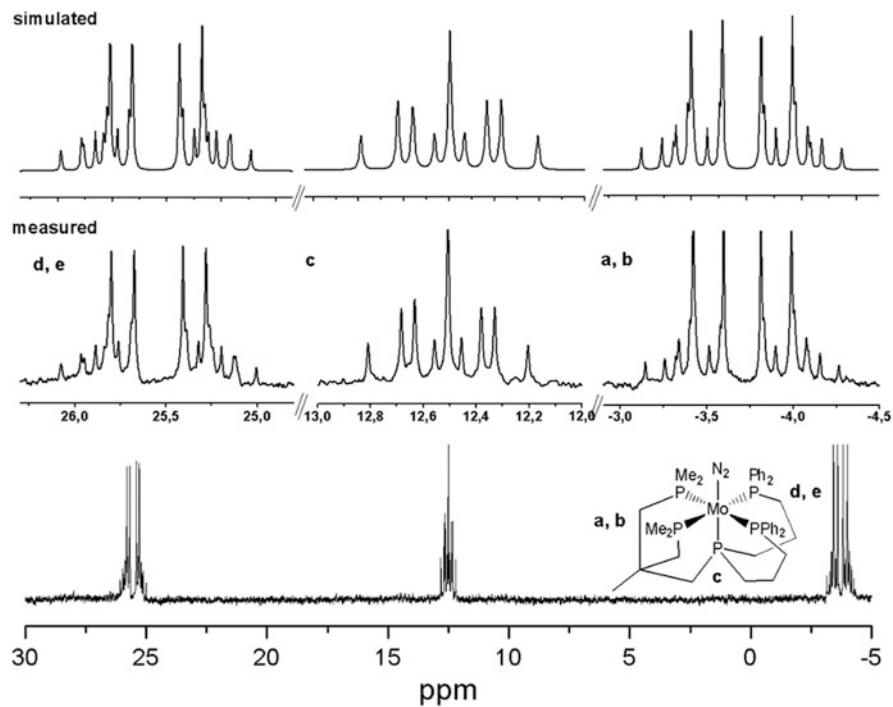
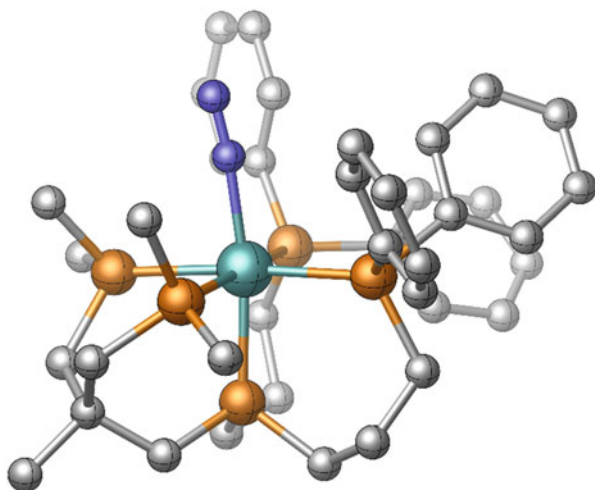


**Fig. 23**  $^{31}\text{P}$ -NMR spectrum of  $[\text{Mo}(\text{N}_2)(\text{P}_2^{\text{Me}}\text{PP}_2^{\text{Ph}})]$  (22) (bottom) with magnifications of the simulation (top) and the measurement (middle) [92]

**Fig. 24** Crystal structure of  $[\text{Mo}(\text{N}_2)(\text{P}_2^{\text{Me}}\text{PP}_2^{\text{Ph}})]$  (22). Hydrogen atoms are omitted for clarity [92]



While the bond lengths between the equatorially bound phosphine donor atoms and the molybdenum atom ( $\text{Mo-P}_{\text{eq}}$ ) exhibit an average value of 2.4481 Å, the phosphine donor atom located *trans* to the dinitrogen ligand shows quite a short bond length (2.3868(5) Å) to the metal center. This proves the successful strapping of the central phosphine donor in the pentaPod<sup>P</sup> design. The strong  $\text{Mo-P}_{\text{ax}}$  bond hinders dissociation at this position, solving one of the problems of the original Chatt systems [92].

IR and Raman spectra were measured to examine the degree of activation of the coordinated dinitrogen ligand (Fig. 25). The spectra show an NN stretching vibration at 1,929  $\text{cm}^{-1}$ . To the best of our knowledge, this is the lowest value of an NN stretch for a mononuclear molybdenum–dinitrogen complex with phosphine ligands. For comparison and further characterization, the  $^{15}\text{N}_2$ -complex of  $[\text{Mo}(\text{N}_2)(\text{P}_2^{\text{Me}}\text{PP}_2^{\text{Ph}})]$  (**22**) has been synthesized as well. The NN stretching frequency of  $[\text{Mo}(^{15}\text{N}_2)(\text{P}_2^{\text{Me}}\text{PP}_2^{\text{Ph}})]$  ( $^{15}\text{N}$ -**22**) is observed at 1,868  $\text{cm}^{-1}$ . Theoretically ( $\Delta_{\text{theo}} = 65 \text{ cm}^{-1}$ ) and experimentally determined ( $\Delta_{\text{exp}} = 61 \text{ cm}^{-1}$ ) isotope shifts are in good agreement [92].

The reactivity of the complex  $[\text{Mo}(\text{N}_2)(\text{P}_2^{\text{Me}}\text{PP}_2^{\text{Ph}})]$  (**22**) towards acids was investigated as well. For the protonation reactions, two different acids have been employed, HOTf and  $\text{HBAr}^{\text{F}}$  [92]. Protonation with trifluoromethanesulfonic acid in THF was unsuccessful because ligand-exchange reactions with solvent molecules took place. Analysis of the protonation products was performed using NMR and IR

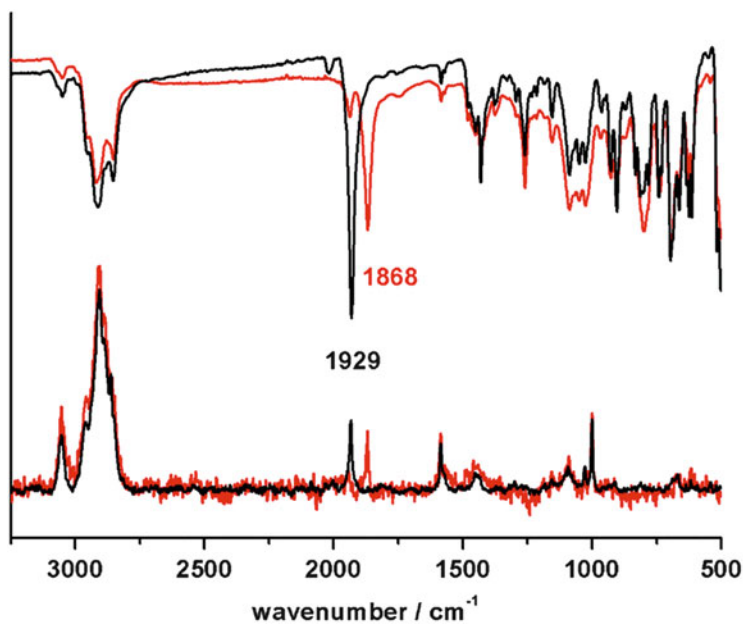


**Fig. 25** Comparison of IR and Raman spectra of  $[\text{Mo}(\text{N}_2)(\text{P}_2^{\text{Me}}\text{PP}_2^{\text{Ph}})]$  (**22**) (black) and  $[\text{Mo}(^{15}\text{N}_2)(\text{P}_2^{\text{Me}}\text{PP}_2^{\text{Ph}})]$  ( $^{15}\text{N}$ -**22**) (red) [92]



spectroscopy [12, 69]. It was possible to characterize the  $[\text{Mo}(\text{NNH}_2)(\text{P}_2^{\text{Me}}\text{PP}_2^{\text{Ph}})]$  ( $\text{NNH}_2\text{-22}$ ) species at a temperature of 250 K, whereas it became unstable at 270 K. The  $^{31}\text{P}$ -NMR spectrum of  $\text{NNH}_2\text{-22}$  shows a shift of the signals to high field compared to **22**; in particular, a shift for *trans*-phosphine by 45.9 ppm has been observed (Fig. 26). Moreover, a signal at  $-234$  ppm could be obtained from  $^{15}\text{N}$ -INEPT-NMR spectroscopy, reflecting a doubly protonated  $\text{N}_\beta$  atom, which indicates a successful protonation experiment [97, 98].

In situ IR investigations revealed that upon protonation the NN stretch at  $1,929\text{ cm}^{-1}$  disappears and two new NH stretching vibrations emerge at  $3,198\text{ cm}^{-1}$  and  $3,179\text{ cm}^{-1}$ , respectively (Fig. 27) [67]. Again, these findings indicate formation of the  $\text{NNH}_2$  complex.

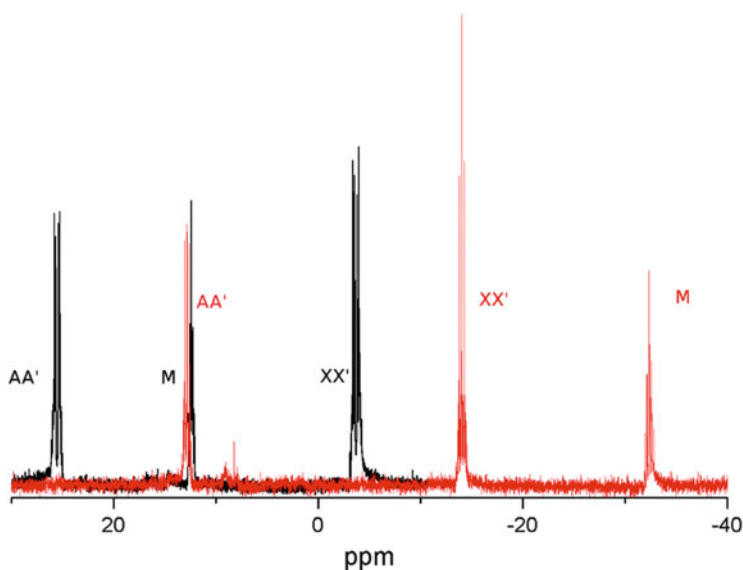


**Fig. 26** Comparison of  $^{31}\text{P}$ -NMR spectra of  $[\text{Mo}(\text{N}_2)(\text{P}_2^{\text{Me}}\text{PP}_2^{\text{Ph}})]$  (**22**) (black) and  $[\text{Mo}(\text{NNH}_2)(\text{P}_2^{\text{Me}}\text{PP}_2^{\text{Ph}})](\text{NNH}_2\text{-22})$  (red). All signals undergo a downfield shift which is most significant for the M signal [92]

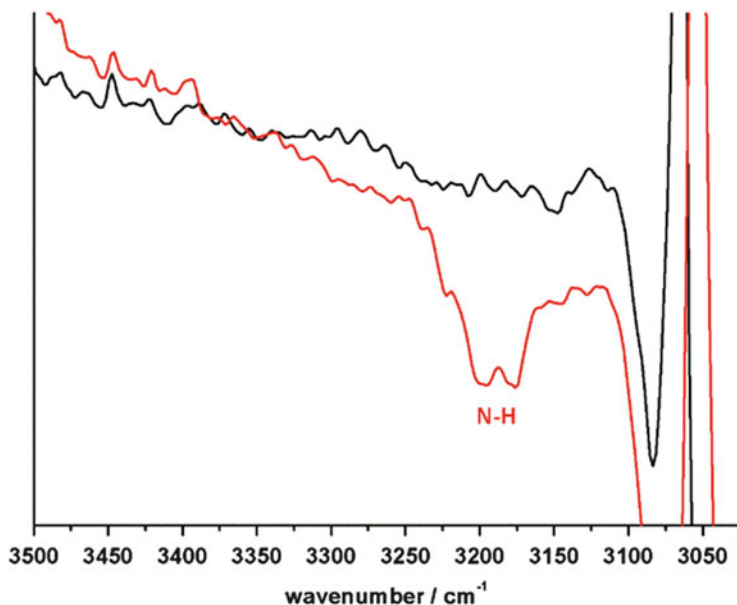


**Fig. 27** Comparison of the NH-vibration regions of Mo-N<sub>2</sub>- (**22**, black) and Mo-NNH<sub>2</sub>- (NNH<sub>2</sub>-**22**, red) complexes. The protonation was carried out with HBAr<sup>F</sup> [92]

## 8 Summary and Conclusion

In the present review, our synthetic efforts towards the development of an efficient catalyst for N<sub>2</sub> reduction on the basis of mononuclear Mo(0) phosphine complexes are described. One of the major problems of the Chatt system is the disproportionation reaction at the level of the Mo(I) complex which is caused by the coordination of an anionic ligand in *trans*-position of the N<sub>2</sub> ligand. To prevent this problematic reaction, the *trans*-position must be blocked by the ligand system. Several concepts to achieve this goal have been pursued. Our first approach involved the use of PEP ligands with the donor atom E (N, P) in *trans*-position to N<sub>2</sub>. Interestingly, dinitrogen complexes with PNP ligands exhibited a much higher activation of N<sub>2</sub> than their analogues supported by PPP ligands. Then, complexes with PCP ligands were examined, the central carbon donor being contained in an N-heterocyclic carbene. Importantly, the presence of a carbene donor in *trans*-position of N<sub>2</sub> caused a dramatic increase in the activation of this ligand. On the other hand, the corresponding dinitrogen complexes became thermally unstable, which could be remedied by employing phosphite instead of phosphine coligands.

A major focus in our investigations has also been directed towards the synthesis of molybdenum–dinitrogen complexes supported by tripod ligands. We started these investigations with the commercially available ligand tris(diphosphinomethyl)ethane (tdppme), complemented by dppm and dmpm coligands. Later on, we also replaced the diphenylphosphine endgroups of the tdppme ligand by aliphatic phosphine groups

PR<sub>2</sub>, starting with R = isopropyl substituents. The resulting Mo(0)–dinitrogen complexes exhibited a greater activation of N<sub>2</sub> than their tdpmpme-supported counterparts, but the accommodation of more than one diisopropylphosphine group in the tripod ligand proved to be difficult.

The ultimate stage of our studies involved the development of pentaPod<sup>P</sup> ligands which derive from the fusion of a PEP and a tripod ligand. Importantly, this ligand contains PMe<sub>2</sub> groups on the tripod and PPh<sub>2</sub> groups on the trident part of the pentaPod backbone. This allows a stepwise coordination of this ligand to Mo centers, leading to the first molybdenum–dinitrogen complex supported by a pentadentate tetrapodal phosphine ligand.

An important aspect in the design of these multidentate phosphine ligands is the proper choice of the chain length in tridentate PEP ligands and the tridentate parts of pentaPod<sup>P</sup> ligands, respectively. This problem has both been investigated on the basis of the above-mentioned, tridentate PNP/PPP ligands and on the basis of tetradentate NP<sub>3</sub> ligands. While the replacement of C<sub>2</sub> by C<sub>3</sub> groups has little influence on the activation of N<sub>2</sub> in Mo(0) complexes supported by these types of ligands, the presence of C<sub>3</sub> bridges leads to a higher flexibility of the ligand framework which is reflected by the appearance of conformers and/or line broadening in the <sup>31</sup>P-NMR spectra. With regard to the pentaPod<sup>P</sup> design, the use of C<sub>3</sub> bridges in the trident part appears to provide a stable, yet flexible coordination environment. The reactivity of the [Mo(N<sub>2</sub>)(pentaPod<sup>P</sup>)] complex **22** towards acids and reductants now is being studied in detail, as well as the conversion of N<sub>2</sub> to ammonia on the basis of this system.

## References

1. MacKay BA, Fryzuk MD (2004) *Chem Rev* 104:385–401
2. Burgess BK, Lowe DJ (1996) *Chem Rev* 96:2983–3011
3. Alberty RA, Goldberg RN (2004) *Biochemistry* 31:10610–10615
4. Burgess BK (1990) *Chem Rev* 90:1377–1406
5. Kim JS, Rees DC (1992) *Nature* 360:553–560
6. Lancaster KM, Roemelt M, Ettenhuber P, Hu Y, Ribbe MW, Neese F, Bergmann U, DeBeer S (2011) *Science* 334:974–977
7. Spatzal T, Aksoyoglu M, Zhang L, Andrade SLA, Schleicher E, Weber S, Rees DC, Einsle O (2011) *Science* 334:940–940
8. Thorneley RNF, Lowe DJ (1985) In: Spiro TG (ed) *Molybdenum enzymes*. Wiley, New York
9. Hinrichsen S, Broda H, Gradert C, Söncksen L, Tuzcek F (2012) *Annu Rep Prog Chem Sect A Inorg Chem* 108:17–47
10. Henderson RA, Leigh GJ, Pickett CJ (1983) *Adv Inorg Chem* 27:197–292
11. Arashiba K, Kinoshita E, Kuriyama S, Eizawa A, Nakajima K, Tanaka H, Yoshizawa K, Nishibayashi Y (2015) *J Am Chem Soc* 137:5666–5669
12. Del Castillo TJ, Thompson NB, Peters JC (2016) *J Am Chem Soc* 138:5341–5350
13. Schrock RR (2005) *Acc Chem Res* 38:955–962
14. Yandulov CV, Schrock RR (2003) *Science* 301:76–78
15. Arashiba K, Miyake Y, Nishibayashi Y (2011) *Nat Chem* 3:120–125
16. Kinoshita E, Arashiba K, Kuriyama S, Miyake Y, Shimazaki R, Nakanishi H, Nishibayashi Y (2012) *Organometallics* 31:8437–8443

17. Kuriyama S, Arashiba K, Nakajima K, Tanaka H, Kamaru N, Yoshizawa K, Nishibayashi Y (2014) *J Am Chem Soc* 136:9719–9731
18. Nishibayashi Y (2015) *C R Chim* 18:776–784
19. Anderson JS, Rittle J, Peters JC (2013) *Nature* 501:84–87
20. Chatt J, Dilworth JR, Richards RL (1978) *Chem Rev* 78:589–625
21. Chatt J, Pearman AJ, Richards RL (1975) *Nature* 253:39–40
22. Hidai M, Tominari K, Uchida Y, Misono A (1969) *J Chem Soc D Chem Commun*:1392
23. Hidai M, Tominari K, Uchida Y (1972) *J Am Chem Soc* 94:110–114
24. Hidai M, Mizobe Y (1995) *Chem Rev* 95:1115–1133
25. Broda H, Hinrichsen S, Tuczek F (2013) *Coord Chem Rev* 257:587–598
26. Dreher A, Stephan G, Tuczek F (2009) *Adv Inorg Chem* 61:367–405
27. Römer R, Stephan G, Habeck C, Hoberg C, Peters G, Näther C, Tuczek F (2008) *Eur J Inorg Chem* 21:3258–3263
28. Römer R, Gradert C, Bannwarth A, Peters G, Näther C, Tuczek F (2011) *Dalton Trans* 40:3229–3236
29. Sönksen L, Römer R, Näther C, Peters G, Tuczek F (2011) *Inorg Chim Acta* 374:472–479
30. Lehnert N, Tuczek F (1999) *Inorg Chem* 38:1659–1670
31. Lehnert N, Tuczek F (1999) *Inorg Chem* 38:1671–1682
32. Horn KH, Lehnert N, Tuczek F (2003) *Inorg Chem* 42:1076–1086
33. Horn KH, Böres N, Lehnert N, Mersmann K, Näther C, Peters G, Tuczek F (2005) *Inorg Chem* 44:3016–3030
34. Mersmann K, Horn KH, Böres N, Lehnert N, Studt F, Paulat F, Peters G, Ivanovic-Burmazovic I, van Eldik R, Tuczek F (2005) *Inorg Chem* 44:3031–3045
35. Mersmann K, Hauser A, Lehnert N, Tuczek F (2006) *Inorg Chem* 45:5044–5056
36. Dreher A, Mersmann K, Näther C, Ivanovic-Burmazovic I, van Eldik R, Tuczek F (2009) *Inorg Chem* 48:2078–2093
37. Dreher A, Meyer S, Näther C, Westphal A, Broda H, Sarkar B, Kaim W, Kurz P, Tuczek F (2013) *Inorg Chem* 52:2335–2352
38. Stephan G, Sivasankar C, Studt F, Tuczek F (2008) *Chem A Eur J* 14:644–652
39. George TA, Tisdale RC (1988) *Inorg Chem* 27:2909–2912
40. George TA, Ma L, Shailh SN, Tisdale RC, Zubieta J (1990) *Inorg Chem* 29:4789–4796
41. Stephan G, Peters G, Lehnert N, Habeck CM, Näther C, Tuczek F (2005) *Can J Chem* 83:385–402
42. George TA, Jackson MA (1988) *Inorg Chem* 27:924–926
43. Weiss CJ, Groves AN, Mock MT, Dougherty WG, Kassel WS, Helm ML, DuBois DL, Bullock RM (2012) *Dalton Trans* 41:4517–4529
44. Ogawa T, Kajita Y, Wasada-Tsutsui Y, Wasada H, Masuda H (2013) *Inorg Chem* 52:182–195
45. Stephan G, Näther C, Sivasankar C, Tuczek F (2008) *Inorg Chim Acta* 361:1008–1019
46. Hinrichsen S, Schnoor AC, Grund K, Flöser B, Schlimm A, Näther C, Krahmer J, Tuczek F (2016) *Dalton Trans* 45:14801–14813
47. Fernández-Trujillo MJ, Basallote MG, Valerga P, Puerta MC (1993) *J Chem Soc Dalton Trans*:923–926
48. Schnoor AC, Gradert C, Schlepner M, Krahmer J, Tuczek F (2015) *Z Anorg All Chem* 641:83–90
49. Green LM, Meek DW (1990) *Polyhedron* 9:35–45
50. Dahlenburg L, Pietsch B (1986) *Z Naturforsch B Anorg Chem Org Chem* 41:70–75
51. Batke S, Kothe T, Haas M, Wadepohl H, Ballmann J (2016) *Dalton Trans* 45:3528–3540
52. Bujard M, Gouverneur V, Mioskowski C (1999) *J Org Chem* 64:2119–2123
53. Kostas ID (2001) *J Organomet Chem* 626:221–226
54. Stoffelbach F, Saurenz D, Poli R (2001) *Eur J Inorg Chem*:2699–2703
55. Owens BE, Poli R, Rheingold AL (1989) *Inorg Chem* 28:1456–1462
56. Poli R, Krueger ST, Mattamana SP, Dunbar KR, Hanhua Z (1998) *Inorg Synth* 32:198–203
57. Arduengo III AJ, Harlow RL, Kline M (1991) *J Am Chem Soc* 113:361–363

58. Enders D, Niemeier O, Henseler A (2007) *Chem Rev* 107:5606–5655
59. Scholl M, Trnka TM, Morgan JP, Grubbs RH (1999) *Tetrahedron Lett* 40:2247–2250
60. Herrmann WA, Köcher C (1997) *Angew Chem* 109:2256–2282; *Angew Chem Int Ed* (1997) 36:2162–2187
61. Fürstner A, Alcarazo M, Radkowski K, Lehmann CW (2008) *Angew Chem* 120:8426–8430; *Angew Chem Int Ed* (2008) 47:8302–8306
62. Dorta R, Stevens ED, Hoff CD, Nolan SP (2003) *J Am Chem Soc* 125:10490–10491
63. Hillier AC, Sommer WJ, Yong BS, Petersen JL, Cavallo L, Nolan SP (2003) *Organometallics* 22:4322–4326
64. Gradert C, Krahmer J, Sönnichsen FD, Näther C, Tuczek F (2013) *Eur J Inorg Chem*:3943–3955
65. Gradert C, Krahmer J, Sönnichsen FD, Näther C, Tuczek F (2014) *J Organomet Chem* 770:61–68
66. Gradert C, Stucke N, Krahmer J, Näther C, Tuczek F (2015) *Chem A Eur J* 21:1130–1137
67. Krahmer J, Broda H, Peters G, Näther C, Thimm W, Tuczek F (2011) *Eur J Inorg Chem*:4377–4386
68. Krahmer J, Peters G, Tuczek F (2014) *Z Anorg Allg Chem* 640:2834–2838
69. Söncksen L, Gradert C, Krahmer J, Näther C, Tuczek F (2013) *Inorg Chem* 52:6576–6589
70. Broda H, Hinrichsen S, Krahmer J, Näther C, Tuczek F (2014) *Dalton Trans* 43:2007–2012
71. Broda H, Krahmer J, Tuczek F (2014) *Eur J Inorg Chem*:3564–3571
72. Jacobsen H, Correa A, Costabile C, Cavallo L (2006) *J Organomet Chem* 691:4350–4358
73. Cotton FA, Kraihanzel CS (1962) *J Am Chem Soc* 84:4432–4438
74. Hahn FE, Jahnke MC, Pape T (2006) *Organometallics* 25:5927–5936
75. Lazarowych NJ, Morris RH, Ressler JM (1986) *Inorg Chem* 25:3926–3932
76. Yuki M, Miyake Y, Nishibayashi Y (2009) *Organometallics* 28:5821–5827
77. Yuki M, Midorikawa T, Miyake Y, Nishibayashi Y (2009) *Organometallics* 28:4741–4746
78. Schnöckel H, Schunck S (1987) *Z Anorg Allg Chem* 548:161–164
79. Brupbacher-Gatehouse B, Brupbacher T (1999) *J Chem Phys* 111:6300–6310
80. Niecke E, Engelmann M, Zorn H, Krebs B, Henkel G (1980) *Angew Chem* 92:738–739; *Angew Chem Int Ed Engl* (1980) 19:710–712
81. Niecke E, Zorn H, Krebs B, Henkel G (1980) *Angew Chem* 92:737–738; *Angew Chem Int Ed Engl* (1980) 19:709–710
82. Keck H, Kuchen W, Renneberg H, Terlouw JK, Visser HC (1991) *Angew Chem* 103:331–333; *Angew Chem Int Ed* (1991) 30:318–320
83. Klatt K, Stephan G, Peters G, Tuczek F (2008) *Inorg Chem* 47:6541–6550
84. Seitz T, Muth A, Huttner G (1994) *Chem Ber* 127:1837–1842
85. Fox MA, Campbell KA, Kyba EP (1981) *Inorg Chem* 20:4163–4165
86. Studt F, Tuczek F (2006) *J Comput Chem* 27:1278–1291
87. Muth A, Walter O, Huttner G, Asam A, Zsolnai L, Emmerich C (1994) *J Organomet Chem* 468:149–163
88. Janssen BC, Asam A, Huttner G, Sernau V, Zsolnai L (1994) *Chem Ber* 127:501–506
89. Poli R, Krueger ST, Mattamana SP, Dunbar KR, Hanhua Z (1998) *Inorg Synth* 32:198–203
90. Tolman CA (1977) *Chem Rev* 77:313–348
91. Brookhart M, Grant B, Volpe AF (1992) *Organometallics* 11:3920–3922
92. Hinrichsen S, Kindjajev A, Adomeit S, Krahmer J, Näther C, Tuczek F (2016) *Inorg Chem* 55:8712–8722
93. Card PJ, Hitz WD (1984) *J Am Chem Soc* 106:5348–5350
94. Walter O, Huttner G, Zsolnai L (1993) *Z Naturforsch B Chem Sci* 48:636–640
95. Hofacker P, Friebe C, Dehnicke K, Bäuml P, Hiller W, Strahle J (1989) *Z Naturforsch B Chem Sci* 44:1161–1166
96. Günther H (1972) *Angew Chem* 84:907–920; *Angew Chem Int Ed Engl* (1972) 11:861–874
97. Haymore BL, Hughes M, Mason J, Richards RL (1988) *J Chem Soc Dalton Trans*:2935–2940
98. Donovan-Mtsunzi S, Richards RL, Mason J (1984) *J Chem Soc Dalton Trans*:1329–1332

# Catalytic Nitrogen Fixation Using Molybdenum–Dinitrogen Complexes as Catalysts

Aya Eizawa and Yoshiaki Nishibayashi

**Abstract** This chapter describes recent advances of molybdenum-catalyzed catalytic nitrogen fixation such as catalytic formation of silylamine and ammonia from dinitrogen under ambient reaction conditions. Hidai, Nishibayashi, Masuda, Mézailles, and their coworkers have achieved the molybdenum-catalyzed silylation and Schrock, Nishibayashi, and their coworkers have achieved the molybdenum-catalyzed formation of ammonia from nitrogen gas under ambient reaction conditions.

**Keywords** Ammonia • Catalyst • Dinitrogen • Molybdenum • Reduction • Silylamine

## Contents

1	Introduction: Brief History of Preparation of Transition Metal–Dinitrogen Complexes and Their Use for Stoichiometric Nitrogen Fixation .....	154
2	Catalytic Transformation of Dinitrogen to Silylamine with Molybdenum Complexes . .	155
3	Catalytic Transformation of Dinitrogen to Ammonia with Molybdenum Complexes . . .	158
3.1	Molybdenum Complexes Bearing Tetradentate Ligands as Catalysts .....	158
3.2	Molybdenum Complexes Bearing Pincer Ligands as Catalysts .....	161
4	Perspective .....	166
	References .....	166

---

A. Eizawa and Y. Nishibayashi (✉)

Department of Systems Innovation, School of Engineering, The University of Tokyo, Hongo, Bunkyo-ku, Tokyo 113-8656, Japan  
e-mail: [ynishiba@sys.t.u-tokyo.ac.jp](mailto:ynishiba@sys.t.u-tokyo.ac.jp)

# 1 Introduction: Brief History of Preparation of Transition Metal–Dinitrogen Complexes and Their Use for Stoichiometric Nitrogen Fixation

In 1965, the first transition metal–dinitrogen complex  $[\text{Ru}(\text{N}_2)(\text{NH}_3)_5]^{2+}$  (**1**) was reported by Allen and Senoff (Fig. 1) [1]. The first transition metal–dinitrogen complex  $[\text{Co}(\text{N}_2)\text{H}(\text{PPh}_3)_3]$  (**2**), whose dinitrogen ligand was directly derived from nitrogen gas, was reported by Yamamoto and coworkers in 1967 [2]. With regard to molybdenum–dinitrogen complex, the first example is *trans*- $[\text{Mo}(\text{N}_2)_2(\text{dppe})_2]$  (**3**, dppe = 1,2-bis(diphenylphosphino)ethane) reported by Hidai and coworkers in 1969 [3].

The first conversion of coordinated dinitrogen ligand to ammonia was achieved by Chatt and coworkers in 1975 (Fig. 2) [4, 5]. The reaction of *cis*- $[\text{M}(\text{N}_2)_2(\text{PMe}_2\text{Ph})_4]$  ( $\text{M} = \text{Mo}$ , **4**;  $\text{M} = \text{W}$ , **5**) with strong acids such as sulfuric acid and hydrobromic acid afforded up to 0.88 equivalents of ammonia for **4** and up to 1.98 equivalents of ammonia for **5**. Stoichiometric reactions of **4** and **5** with strong acids afforded the corresponding hydrazido(2-) complexes, which were considered to be reactive intermediates in the

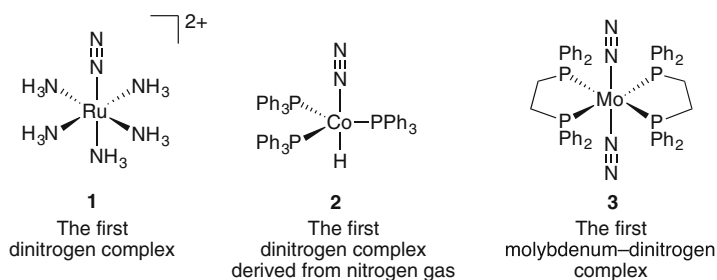


Fig. 1 Historic transition metal–dinitrogen complexes

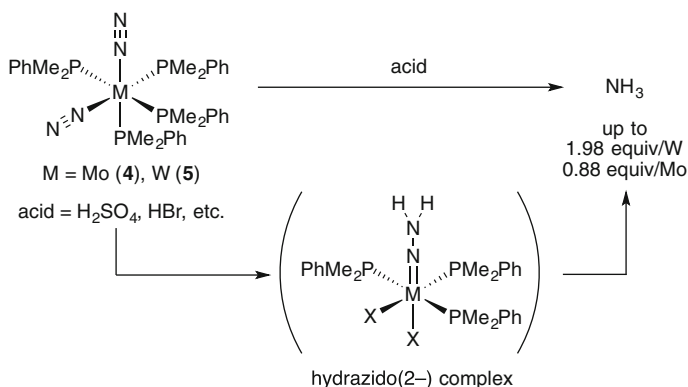


Fig. 2 Protonation of molybdenum– and tungsten–dinitrogen complexes with strong acids

formation of ammonia from dinitrogen complexes [6–8]. Since this discovery, synthesis and reactivity of a number of molybdenum–dinitrogen complexes have been reported [9–29]. In this chapter, we describe a recent advance on catalytic conversion of nitrogen gas using molybdenum–dinitrogen and related complexes as catalysts under ambient reaction conditions.

## 2 Catalytic Transformation of Dinitrogen to Silylamine with Molybdenum Complexes

Catalytic transformation of dinitrogen to silylamine was first accomplished by Shiina using chromium trichloride  $\text{CrCl}_3$  as a catalyst in 1972 [30]. However, the possibility of lithium–nitride as nitrogen source was not completely excluded because Li was used as a reductant. With regard to molybdenum catalysis, the first example was achieved by Hidai, Mizobe, and coworkers in 1989 [31]. This report is the first example of catalytic transformation of the coordinated dinitrogen into silylamine. In the presence of a molybdenum–dinitrogen complex *cis*-[Mo(N<sub>2</sub>)<sub>2</sub>(PMe<sub>2</sub>Ph)<sub>4</sub>] (**4**) as a catalyst, the reaction of an atmospheric pressure of nitrogen gas with sodium and Me<sub>3</sub>SiCl in THF at room temperature afforded 24.3 equivalents of tris(trimethylsilyl)amine (N(SiMe<sub>3</sub>)<sub>3</sub>) (Fig. 3). After this report, several molybdenum-catalyzed reactions of nitrogen gas into silylamine were reported by some research groups. In 2011, the use of a molybdenum–dinitrogen complex bearing ferrocenyldiphosphine ligands (**6**) as a catalyst was found to produce 226 equivalents of silylamine per catalyst by Nishibayashi, Yoshizawa, and coworkers [32]. Masuda and coworkers reported that a molybdenum–dinitrogen complex bearing diphosphine ligands (**7**) worked as a catalyst in transforming dinitrogen into silylamine [33]. Recently, molybdenum–bis(silyl)hydrazido(2–) complexes bearing a tetradentate tetraphosphine ligand (**8**) [34] and a tridentate triphosphine ligand (**9**) [35] have also been revealed to work as effective catalysts for the catalytic silylation by Mézailles and coworkers. Quite recently, Nishibayashi and coworkers found that the use of molybdenum–dinitrogen complexes bearing azaferrocene-based PNP pincer ligands **10** and **11** promoted the same catalytic reaction [36]. Typical results are shown in Fig. 3.

Novel plausible reaction pathways for the catalytic silylation using **6**, **8**, and **9** as catalysts have been examined (Fig. 4). As to the catalytic cycle for using **6**, a reaction pathway was studied with DFT calculations (Fig. 4a) [32]. Chlorotrimethylsilane is reduced to generate trimethylsilyl radical, which is a real silylating agent for this catalytic reaction. At first, one of the dinitrogen ligands of **I** is silylated to form [Mo(NNSiMe<sub>3</sub>)] (**II**) and then [Mo(NN(SiMe<sub>3</sub>)<sub>2</sub>)] (**III**) species. Then further silylation proceeds at the nitrogen atom adjacent to the molybdenum atom to generate a silylhydrazido(1–) (**IV**) species. Successive one-electron reduction liberates (Me<sub>3</sub>Si)<sub>2</sub>NN(SiMe<sub>3</sub>)<sup>–</sup> and the coordination of another dinitrogen molecule to the vacant site of the molybdenum atom of **V** regenerates the molybdenum–dinitrogen complex **I**. The generated (Me<sub>3</sub>Si)<sub>2</sub>NN(SiMe<sub>3</sub>) anion would be converted to two



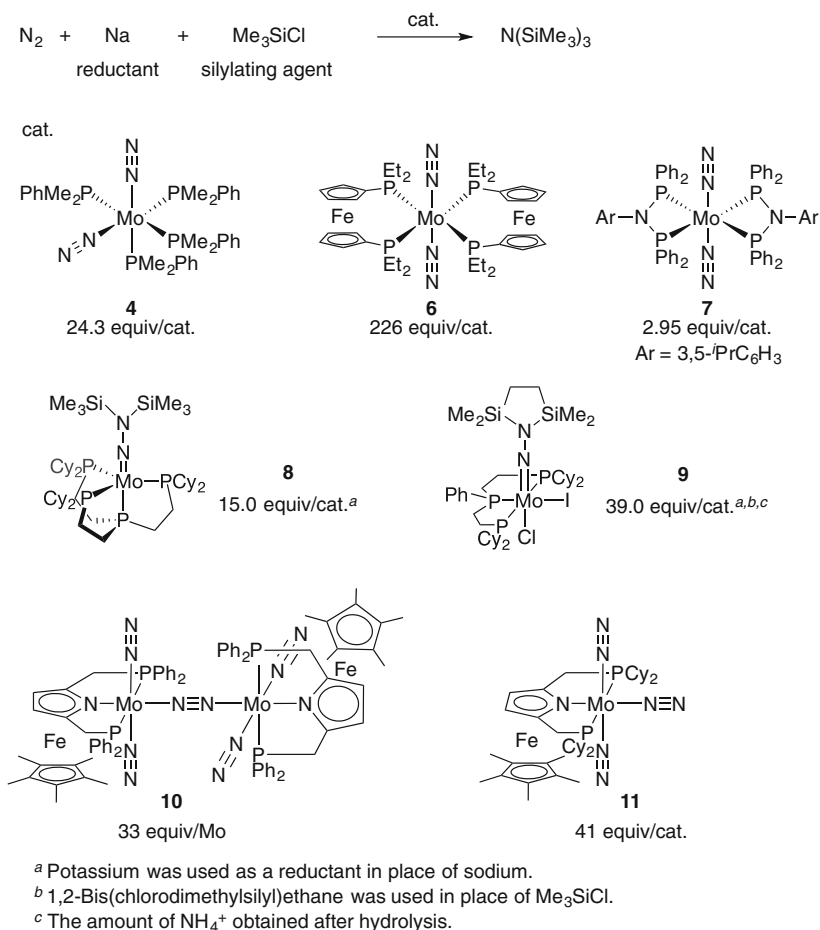
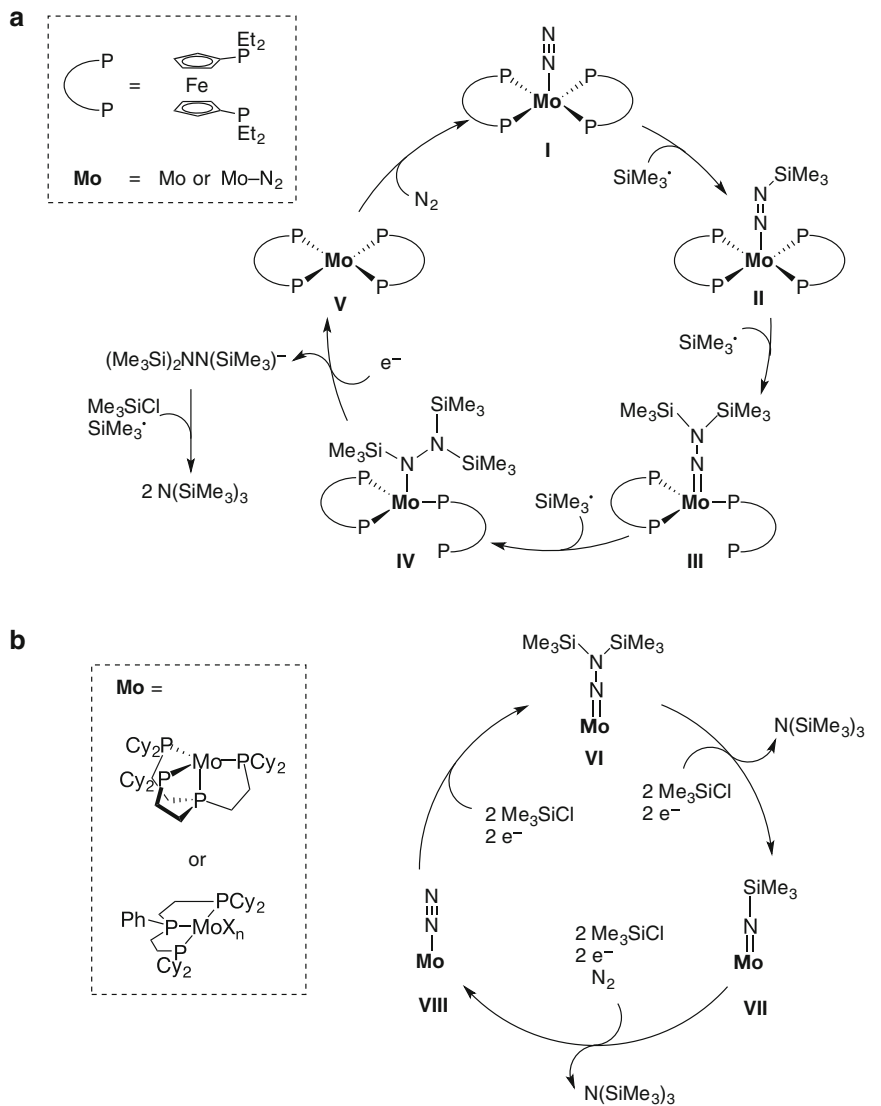


**Fig. 3** Molybdenum-catalyzed catalytic conversion of nitrogen gas to silylamine

molecules of N(SiMe<sub>3</sub>)<sub>3</sub>. On the other hand, Mézailles and coworkers carried out stoichiometric reactions of the molybdenum complexes **8** and **9** with reductants and/or silylating agents to obtain information on the catalytic cycle. Based on the stoichiometric reactions, a reaction pathway has been proposed (Fig. 4b) [34, 35]. First, a molybdenum–bis(silyl)hydrazido(2–) species **VI** is silylated to afford one molecule of silylamine and a molybdenum–imido complex **VII**. Further silylation of **VII** affords another silylamine and the coordination of another dinitrogen molecule generates a molybdenum–dinitrogen species **VIII**. Silylation to the dinitrogen ligand regenerates **VI**.



### 3 Catalytic Transformation of Dinitrogen to Ammonia with Molybdenum Complexes

#### 3.1 Molybdenum Complexes Bearing Tetradentate Ligands as Catalysts

The first successful example of the catalytic transformation of dinitrogen to ammonia under ambient reaction conditions was reported by Yandulov and Schrock in 2003 [37]. Employing a molybdenum–dinitrogen complex bearing a triamidoamine ligand [HIPTN<sub>3</sub>N]MoN<sub>2</sub> (**12**, HIPTN<sub>3</sub>N = (3,5-(2,4,6-*i*-Pr<sub>3</sub>C<sub>6</sub>H<sub>2</sub>)<sub>2</sub>C<sub>6</sub>H<sub>3</sub>NCH<sub>2</sub>CH<sub>2</sub>)<sub>3</sub>N) as a catalyst, the reaction of an atmospheric pressure of nitrogen gas with decamethylchromocene (CrCp\*<sub>2</sub>, Cp\* = η<sup>5</sup>-C<sub>5</sub>Me<sub>5</sub>; a reductant) and 2,6-lutidinium tetraarylborate ([LutH]BAR<sup>F</sup><sub>4</sub>, Lut = 2,6-lutidine, Ar<sup>F</sup> = 3,5-(CF<sub>3</sub>)<sub>2</sub>C<sub>6</sub>H<sub>3</sub>; a proton source) in heptane at room temperature afforded 7.56 equivalents of ammonia per catalyst (Fig. 5). A plausible reaction pathway is shown in Fig. 6, based on intensive stoichiometric reactions of **12** with a proton source and/or a reductant [16, 17, 38–41]. At first, the formation of a diazenido species **XI** from **12** proceeds via either one of the following two reaction pathways. One is the stepwise reduction and protonation of the coordinating dinitrogen ligand in **12**. The other pathway is the protonation of one of the amido nitrogens in the supporting ligand in **12** to give **X** and then successive protonation and reduction of **X** to afford **XI**. Next, stepwise protonation and reduction liberates one ammonia molecule and gives a nitrido species **XV**. Further protonation and reduction of **XV** affords an ammonia complex **XXI**. Finally, the ligand exchange liberates the second ammonia molecule and regenerates **12**. Electrochemical mechanistic study strongly suggested a proton-coupled electron transfer in the catalytic cycle

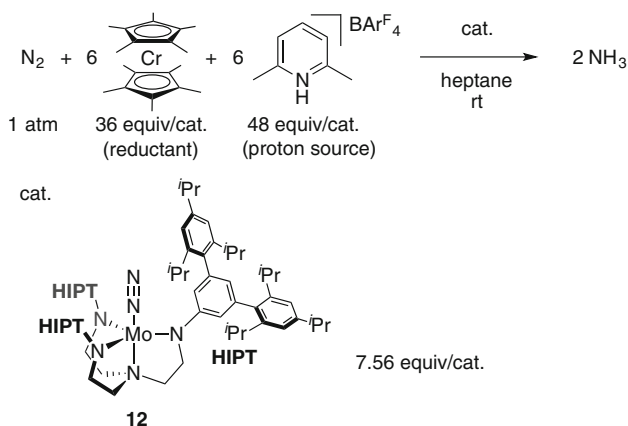


**Fig. 5** The first catalytic transformation of nitrogen gas to ammonia using Schrock molybdenum–dinitrogen complex as a catalyst

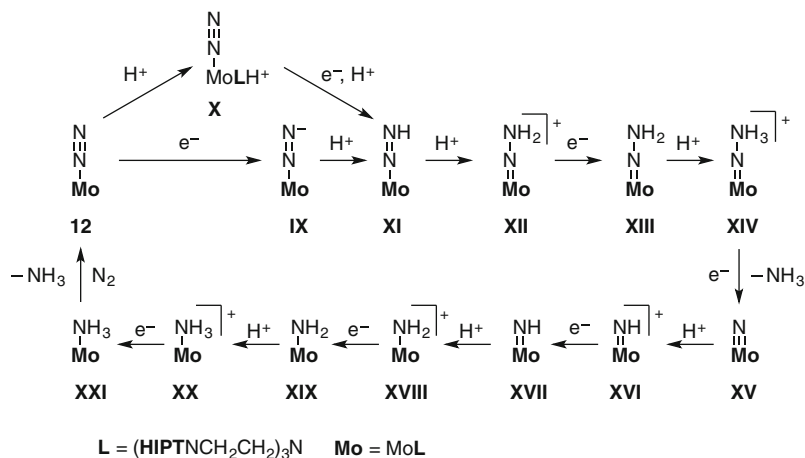


**Fig. 6** A plausible reaction pathway of the catalytic transformation of dinitrogen to ammonia employing **12** as a catalyst

[42]. Some key intermediates **IX**, **XI**, **XII**, **XV**, **XVI**, **XX**, and **XXI** were isolated and characterized spectroscopically. Complexes **XI**, **XV**, and **XX** have almost the same catalytic activity as **12**.

Dozens of molybdenum complexes bearing slightly modified tetradentate ligands were synthesized and their catalytic activity was examined in detail (Fig. 7). Typical examples are as follows: molybdenum complexes with triamidoamine ligands containing hexa-*tert*-butylterphenyl groups (**13**), hexamethylterphenyl groups (**14**), *p*-bromohexaisopropylterphenyl groups (**15**) [43], DPP groups (**16**, DPP = 3,5-bis(2,5-diisopropylpyrrolyl)<sub>2</sub>C<sub>6</sub>H<sub>3</sub>) [44], and with asymmetrical tetradentate ligands such as [(HIPTNCH<sub>2</sub>CH<sub>2</sub>)<sub>2</sub>NCH<sub>2</sub>CH<sub>2</sub>N-aryl] ligands (**17–20**) [45] and diamidopyrrolyl ligand (**21**) [46]. Unfortunately, most of them, except for **15**, failed to catalytically convert dinitrogen to ammonia under the same reaction conditions.

Some other transition metal complexes bearing a HIPTN<sub>3</sub>N ligand such as vanadium (**22**) [47], chromium (**23**) [48], and tungsten (**24**) [49] complexes were synthesized and their catalytic activity was examined in detail (Fig. 8). However, no catalytic reaction occurred at all when these complexes were used as catalysts.

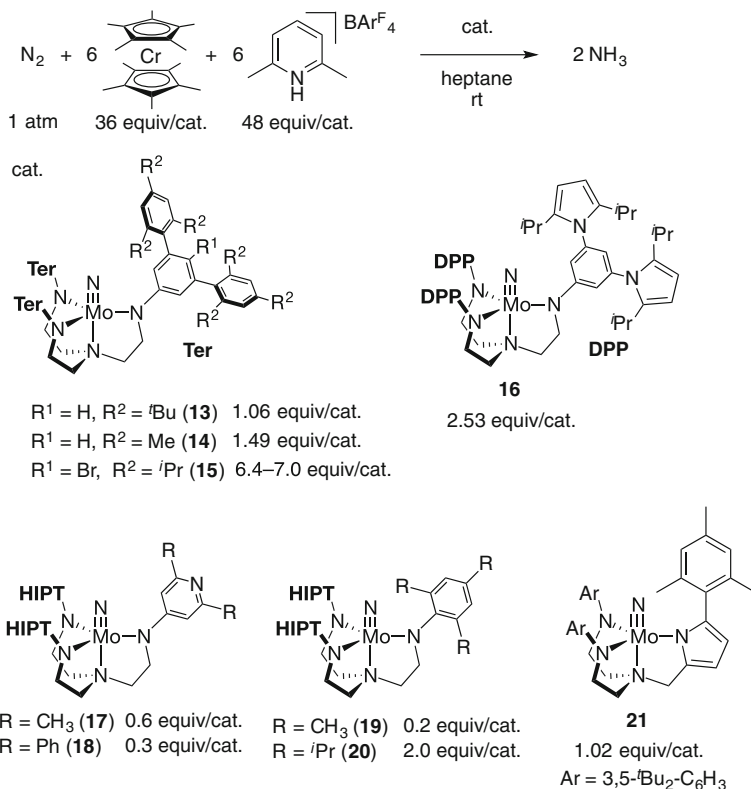


**Fig. 7** Catalytic activity of molybdenum complexes bearing slightly modified tetradentate ligands

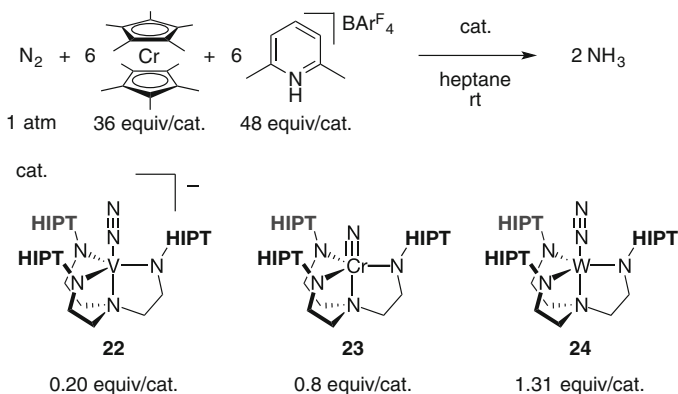


**Fig. 8** Catalytic activity of vanadium-, chromium-, and tungsten-HIPTN<sub>3</sub>N complexes

### 3.2 Molybdenum Complexes Bearing Pincer Ligands as Catalysts

The second example of the catalytic transformation of dinitrogen into ammonia under ambient reaction conditions was reported by Nishibayashi and coworkers in 2011 [50]. The catalyst for this reaction system is a dinitrogen-bridged dimolybdenum–dinitrogen complex bearing PNP-type pincer ligands (**25**, PNP = 2,6-bis(di-*tert*-butylphosphinomethyl)pyridine; Fig. 9). The molecular structure of the molybdenum catalyst was determined to maintain its dinuclear structure also in a solution by measuring  $^{15}\text{N}$  NMR of the  $^{15}\text{N}_2$ -labeled complex. In the presence of **25** as a catalyst, the reaction of an atmospheric pressure of nitrogen gas with lutidinium trifluoromethanesulfonate ([LutH]OTf; OTf =  $\text{OSO}_2\text{CF}_3$ ; a proton source) and cobaltocene ( $\text{CoCp}_2$ ; Cp =  $\eta^5\text{-C}_5\text{H}_5$ ; a reductant) at room temperature afforded up to 23.2 equivalents of ammonia together with 43.5 equivalents of dihydrogen (Fig. 9). Since then, the preparation of a series of molybdenum complexes and the investigation of their catalytic activity have been reported by Nishibayashi and coworkers [51–55].

Detailed experimental studies on a plausible reaction pathway have been conducted by Nishibayashi, Yoshizawa, and coworkers [51]. Some molybdenum–nitrido complexes bearing the same PNP ligand were synthesized and their catalytic activity was investigated in detail (Fig. 10). The use of molybdenum–nitrido complexes **26** and **27** as catalysts produced a similar amount of ammonia with that using **25**. The result of DFT calculations indicated that a nitrido complex such as **27** is one of key reactive intermediates in the catalytic transformation of ammonia catalyzed by **25**.

A plausible reaction pathway is shown in Fig. 11. At first, one of the terminal dinitrogen ligands in **25** is protonated to give **XXII**. Successive protonation and reduction liberate one ammonia molecule and nitrido complex **XXIII**. Further stepwise protonation and reduction of **XXIII** afford an ammonia complex **XXIV** and ligand exchange liberates another ammonia molecule to regenerate **25**. A theoretical study also revealed that the dinuclear structure of the dinitrogen-bridged dimolybdenum complex is essential to the first protonation of one of the terminal

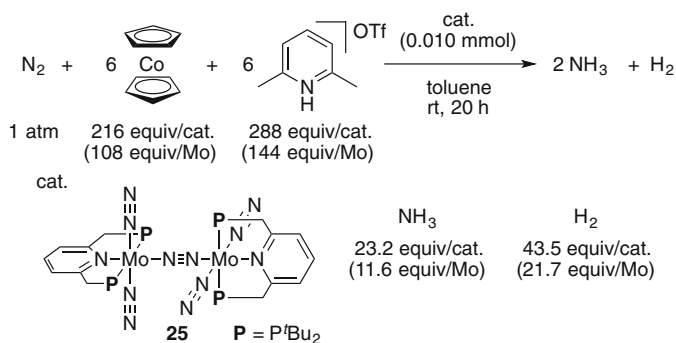


**Fig. 9** Catalytic conversion of nitrogen gas to ammonia under ambient conditions employing **25** as a catalyst

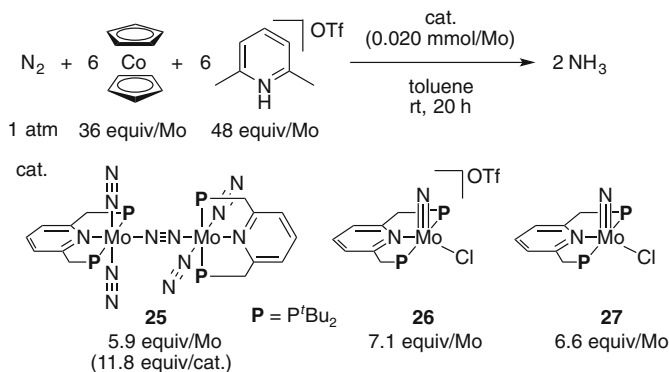


**Fig. 10** Catalytic conversion of nitrogen gas to ammonia using molybdenum–dinitrogen complex and molybdenum–nitrido complexes as catalysts

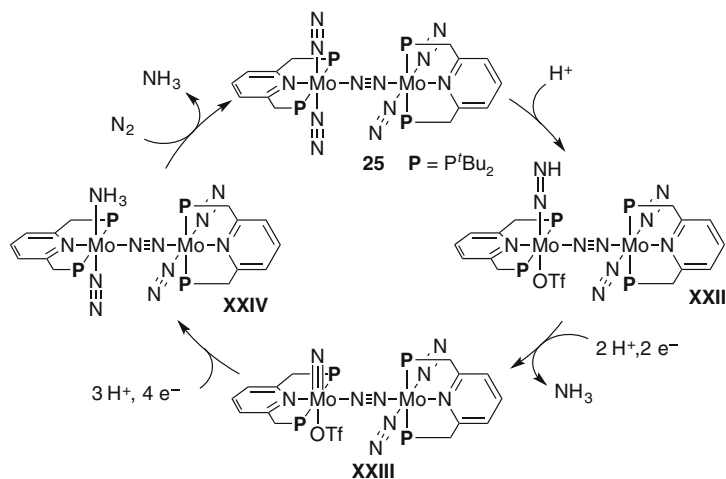


**Fig. 11** Proposed catalytic cycle of converting dinitrogen to ammonia using **25** as a catalyst

dinitrogen ligands in **25** for the catalytic cycle (Fig. 12). Yoshizawa and Tanaka describe more detailed results in this book (Sect. 3.1 in ref. [56]).

Substituent effects on the phosphorus atoms of the PNP ligand were examined by Nishibayashi, Yoshizawa, and coworkers [50–52]. From the PNP ligand bearing either isopropyl (<sup>i</sup>Pr) groups or 1-adamantyl (Ad) groups in place of *tert*-butyl (<sup>t</sup>Bu) groups on both phosphorus atoms, the corresponding dimolybdenum–dinitrogen complexes cannot be prepared by the same procedure as that for **25**. On the other hand, dinitrogen-bridged dimolybdenum complexes bearing asymmetrical PNP ligands, where one phosphorus atom in the PNP ligand has two *tert*-butyl (<sup>t</sup>Bu) groups and the other has two other substituents such as 1-adamantyl (Ad), phenyl (Ph), isopropyl, and cyclohexyl (Cy) groups, can be prepared (**28**, **29**, **30**, and **31**,

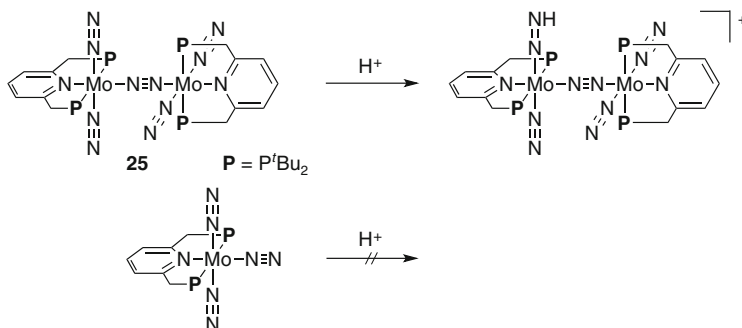


**Fig. 12** The first protonation step of molybdenum–dinitrogen complex **25**

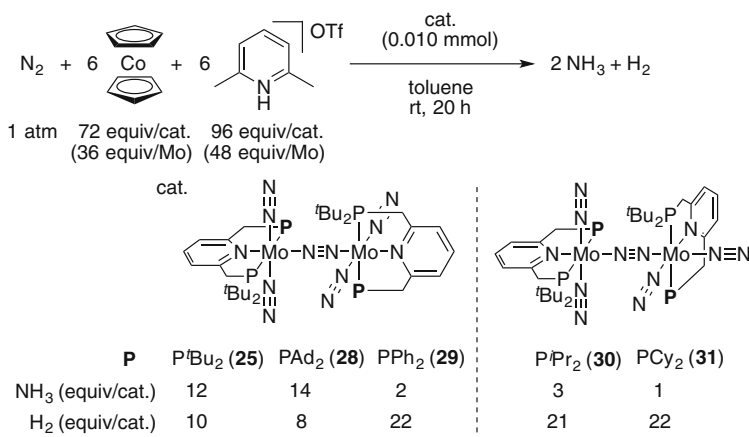


**Fig. 13** Catalytic activity of molybdenum–dinitrogen complexes bearing asymmetrical PNP ligands

respectively; Fig. 13). Molecular structures of **28** and **29** were almost the same as **25**, where two *trans*-[Mo(N<sub>2</sub>)<sub>2</sub>(PNP)] units are bridged by one dinitrogen ligand in an end-on fashion. On the other hand, from the PNP ligands bearing isopropyl or cyclohexyl groups on one phosphorus atom, the complexes bearing a *trans*-[Mo(N<sub>2</sub>)<sub>2</sub>(PNP)] unit and a *cis*-[Mo(N<sub>2</sub>)<sub>2</sub>(PNP)] unit bridged by one dinitrogen ligand in an end-on fashion were obtained. The catalytic activity of **28–31** was also investigated in detail. In the presence of **28**, the reaction of an atmospheric pressure of nitrogen gas with 72 equivalents of CoCp<sub>2</sub> and 96 equivalents of [LutH]OTf in toluene at room temperature produced 14 equivalents of ammonia, which are comparable to the result using **25**. Meanwhile, the use of **29–31** as catalysts produced only a stoichiometric amount of ammonia under the same conditions (Fig. 13). These results show that the presence of bulky substituents on the phosphorus atoms in PNP ligands is necessary for catalytic conversion of nitrogen gas into ammonia.



Substituent effects at the 4-position in the pyridine ring of the PNP ligands were also explored (Fig. 14) [53]. The introduction of electron-withdrawing groups such as phenyl group (**32**) and trimethylsilyl group (**33**) at the 4-position in the pyridine ring weakened the activation of terminal dinitrogen ligands of the complexes. On the other hand, that of electron-donating groups such as *tert*-butyl group (**34**), methyl group (**35**), and methoxy group (**36**) strengthened the activation of the terminal dinitrogen ligands. In the presence of **32–36** as catalysts, reactions of an atmospheric pressure of nitrogen gas with 216 equivalents of  $\text{CoCp}_2$  and 288 equivalents of  $[\text{LutH}]\text{OTf}$  in toluene at room temperature produced 21, 23, 28, 31, and 34 equivalents of ammonia and 46, 44, 45, 36, and 36 equivalents of dihydrogen, respectively. The activation of terminal dinitrogen ligands of the complexes succeeded in improving the catalytic activity to convert dinitrogen into ammonia. This is due to the acceleration of the first protonation step of the terminal dinitrogen ligand. The activation of terminal dinitrogen ligands of the complexes also succeeded in suppressing the formation of dihydrogen, which competes with ammonia formation. In addition, turnover frequency (TOF, defined as equivalents of ammonia produced in the initial 1 h) of catalytic reactions using **25**, **35**, and **36** as catalysts was monitored. For **25** and **35**, the TOFs were 17 and  $28 \text{ h}^{-1}$ , respectively. On the other hand, the TOF was  $7 \text{ h}^{-1}$  when **36** was used as a catalyst. These results indicated that the use of **36** as a catalyst reduces the reaction rate because of the difficulty of reducing steps.

Redox active substituents such as ferrocene were also introduced at the 4-position of the PNP ligand (**37**, Fig. 15) [54]. The introduction of a ferrocene moiety to the PNP ligand did not affect the activation of terminal dinitrogen ligands, but an electronic interaction appeared between the molybdenum atom and the iron atom of ferrocene on the cyclic voltammetry of the molybdenum complexes bearing a ferrocene-substituted PNP ligand. In the presence of **37** as a catalyst, the reaction of an atmospheric pressure of nitrogen gas with 216 equivalents of  $\text{CoCp}_2$  and

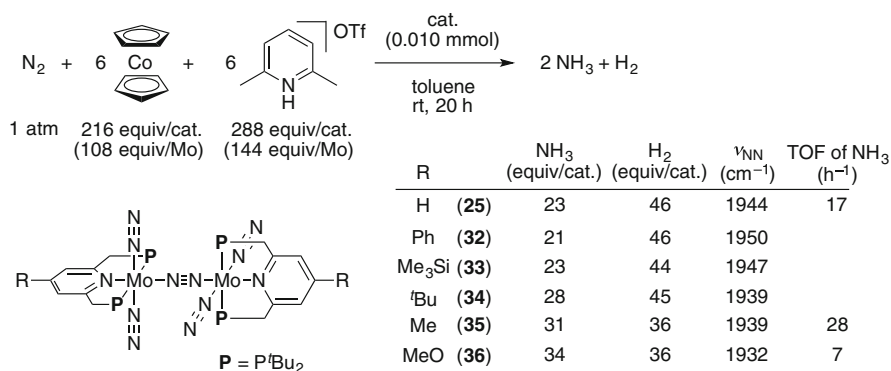


**Fig. 14** Catalytic conversion of nitrogen gas to ammonia using molybdenum–dinitrogen complexes bearing 4-substituted PNP ligands

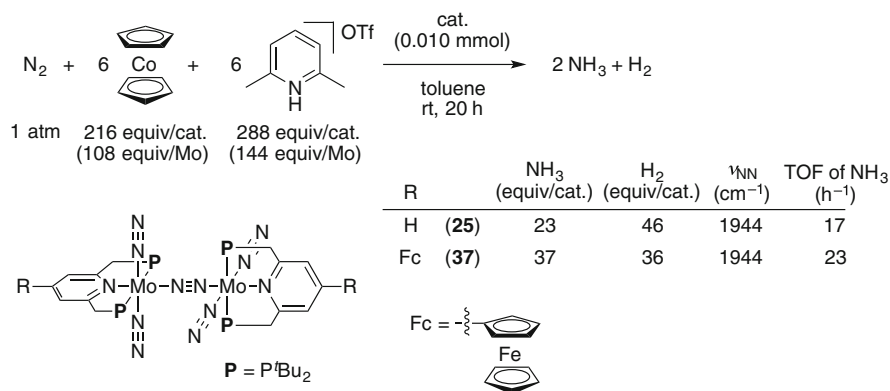


**Fig. 15** Catalytic conversion of nitrogen gas to ammonia using a molybdenum–dinitrogen complex bearing 4-Fc-PNP ligands **37** as a catalyst

288 equivalents of [LutH]OTf in toluene at room temperature produced 37 equivalents of ammonia and 36 equivalents of dihydrogen, respectively. Mechanistic study indicates that an intramolecular electron transfer from the iron atom of ferrocene to the molybdenum center may accelerate the reduction step in the catalytic cycle.

The employment of PPP-type (PPP = bis(di-*tert*-butylphosphinoethyl)phenylphosphine) pincer ligand to the molybdenum complexes was investigated in detail [55]. The phosphines in the PPP ligand had advantages of lower Brønsted basicity and higher stability for the protonation in the catalytic reaction. Furthermore, the  $\pi$ -accepting property of the PPP ligand can stabilize a variety of molybdenum complexes bearing a broad range of oxidation states of the molybdenum center in the catalytic cycle. The corresponding dinitrogen-bridged dimolybdenum complex bearing the PPP ligands could not be prepared probably due to the low bond energy of the terminal dinitrogen ligand; however, molybdenum–nitrido complexes **38** and **39** were prepared according to the previous procedure (Fig. 16). In the presence of **38** and **39** as catalysts, reactions of an atmospheric pressure of nitrogen gas with 36 equivalents of decamethylcobaltocene (CoCp\*<sub>2</sub>; a reductant) and 48 equivalents of 2,4,6-trimethylpyridinium trifluoromethanesulfonate ([CoH]OTf, CoL = 2,4,6-trimethylpyridine; a proton source) per molybdenum atom in toluene at room temperature produced 9.6 and 11.0 equivalents of ammonia and 1.1 and 0.3 equivalents of dihydrogen per molybdenum atom, respectively. The presence of PPP ligand greatly suppressed the formation of dihydrogen. It is noteworthy that a molybdenum–trichloride complex bearing the PPP ligand **40** also worked as an effective catalyst, where 6.4 equivalents of ammonia were produced under the same reaction conditions. Finally, the use of a larger amount of a reductant and a proton source using **39** as a catalyst resulted in the formation of up to 63 equivalents of ammonia per molybdenum atom (Fig. 17). The molybdenum–nitrido complex **39** showed much higher performance for the catalytic conversion of dinitrogen into ammonia than other molybdenum complexes.

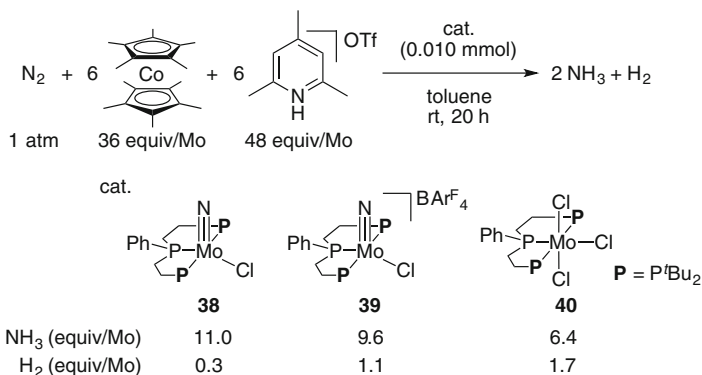


**Fig. 16** Catalytic conversion of nitrogen gas to ammonia using molybdenum–nitrido complexes and a molybdenum–trichloride complex bearing PPP ligand

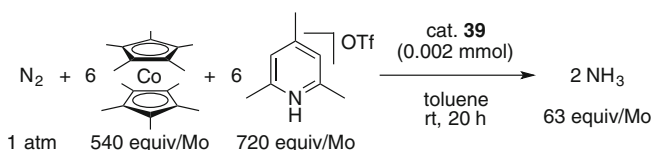


**Fig. 17** Catalytic conversion of dinitrogen to ammonia using **39** as a catalyst with larger amounts of reductant and proton source

## 4 Perspective

As described in this chapter, a number of molybdenum–dinitrogen complexes have been prepared and their catalytic activity has been examined for the last decade. Subtle tuning of supporting ligands greatly improved the catalytic activity. Surely the catalytic activity is improved year by year, but multiple breakthroughs for improving catalytic activity are yet necessary for the industrial application [56].

## References

- Allen AD, Senoff CV (1965) Nitrogenopentammineruthenium(II) complexes. *Chem Commun*:621–622. doi:10.1039/c19650000621
- Yamamoto A, Kitazume S, Pu LS, Ikeda S (1967) Study of the fixation of nitrogen. Isolation of tris(triphenylphosphine) cobalt complex coordinated with molecular nitrogen. *Chem Commun*:79–80. doi:10.1039/c19670000079
- Hidai M, Tominari K, Uchida Y, Misono A (1969) A *trans*-dinitrogen complex of molybdenum. *Chem Commun*:1392–1392. doi:10.1039/c29690001392
- Chatt J, Pearman AJ, Richards RL (1975) The reduction of mono-coordinated molecular nitrogen to ammonia in a protic environment. *Nature* 253:39–40. doi:10.1038/253039b0

- Chatt J, Pearman AJ, Richards RL (1977) Conversion of dinitrogen in its molybdenum and tungsten complexes into ammonia and possible relevance to the nitrogenase reaction. *J Chem Soc Dalton Trans*:1852–1860. doi:[10.1039/dt9770001852](https://doi.org/10.1039/dt9770001852)
- Chatt J, Pearman AJ, Richards RL (1975) Diazenido (iminonitrosyl) ( $N_2H$ ), hydrazido(2–) ( $N_2H_2$ ), and hydrazido(1–) ( $N_2H_3$ ) ligands as intermediates in the reduction of ligating dinitrogen to ammonia. *J Organomet Chem* 101:C45–C47. doi:[10.1016/s0022-328x\(00\)92481-1](https://doi.org/10.1016/s0022-328x(00)92481-1)
- Chatt J, Pearman AJ, Richards RL (1978) Hydrazido(2–)-complexes of molybdenum and tungsten formed from dinitrogen complexes by protonation and ligand exchange. *J Chem Soc Dalton Trans*:1766–1776. doi:[10.1039/dt9780001766](https://doi.org/10.1039/dt9780001766)
- Anderson SN, Fakley ME, Richards RL, Chatt J (1981) Hydrazido(2–)-complexes as intermediates in the conversion of ligating dinitrogen into ammonia and hydrazine. *J Chem Soc Dalton Trans*:1973–1980. doi:[10.1039/dt9810001973](https://doi.org/10.1039/dt9810001973)
- Chatt J (1975) The reactions of dinitrogen in its mononuclear complexes. *J Organomet Chem* 100:17–28. doi:[10.1016/s0022-328x\(00\)88931-7](https://doi.org/10.1016/s0022-328x(00)88931-7)
- Chatt J, Richards RL (1982) The reactions of dinitrogen in its metal complexes. *J Organomet Chem* 239:65–77. doi:[10.1016/s0022-328x\(00\)94103-2](https://doi.org/10.1016/s0022-328x(00)94103-2)
- Hidai M, Mizobe Y (1995) Recent advances in the chemistry of dinitrogen complexes. *Chem Rev* 95:1115–1133. doi:[10.1021/cr00036a008](https://doi.org/10.1021/cr00036a008)
- Hidai M, Ishii Y (1996) Toward direct synthesis of organonitrogen compounds from dinitrogen: the chemistry of diazoalkane complexes derived from dinitrogen complexes. *Bull Chem Soc Jpn* 69:819–831. doi:[10.1246/bcsj.69.819](https://doi.org/10.1246/bcsj.69.819)
- Fryzuk MD, Johnson SA (2000) The continuing story of dinitrogen activation. *Coord Chem Rev* 200–202:379–409. doi:[10.1016/s0010-8545\(00\)00264-2](https://doi.org/10.1016/s0010-8545(00)00264-2)
- Shaver MP, Fryzuk MD (2003) Activation of molecular nitrogen: coordination, cleavage and functionalization of  $N_2$  mediated by metal complexes. *Adv Synth Catal* 345:1061–1076. doi:[10.1002/adsc.200303081](https://doi.org/10.1002/adsc.200303081)
- MacKay BA, Fryzuk MD (2004) Dinitrogen coordination chemistry: on the biomimetic borderlands. *Chem Rev* 104:385–401. doi:[10.1021/cr020610c](https://doi.org/10.1021/cr020610c)
- Schrock RR (2005) Catalytic reduction of dinitrogen to ammonia at a single molybdenum center. *Acc Chem Res* 38:955–962. doi:[10.1021/ar0501121](https://doi.org/10.1021/ar0501121)
- Schrock RR (2008) Catalytic reduction of dinitrogen to ammonia by molybdenum: theory versus experiment. *Angew Chem Int Ed* 47:5512–5522. doi:[10.1002/anie.200705246](https://doi.org/10.1002/anie.200705246)
- Hinrichsen S, Broda H, Gradert C, Söncksen L, Tucek F (2012) Recent developments in synthetic nitrogen fixation. *Annu Rep Prog Chem Sect A Inorg Chem* 108:17–47. doi:[10.1039/c2ic90033e](https://doi.org/10.1039/c2ic90033e)
- Nishibayashi Y (2012) Molybdenum-catalyzed reduction of molecular dinitrogen under mild reaction conditions. *Dalton Trans* 41:7447–7453. doi:[10.1039/c2dt30105a](https://doi.org/10.1039/c2dt30105a)
- Broda H, Hinrichsen S, Tucek F (2013) Molybdenum(0) dinitrogen complexes with polydentate phosphine ligands for synthetic nitrogen fixation: geometric and electronic structure contributions to reactivity. *Coord Chem Rev* 257:587–598. doi:[10.1016/j.ccr.2012.05.010](https://doi.org/10.1016/j.ccr.2012.05.010)
- Tanabe Y, Nishibayashi Y (2013) Developing more sustainable processes for ammonia synthesis. *Coord Chem Rev* 257:2551–2564. doi:[10.1016/j.ccr.2013.02.010](https://doi.org/10.1016/j.ccr.2013.02.010)
- Sivasankar C, Baskaran S, Tamizmani M, Ramakrishna K (2014) Lessons learned and lessons to be learned for developing homogeneous transition metal complexes catalyzed reduction of  $N_2$  to ammonia. *J Organomet Chem* 752:44–58. doi:[10.1016/j.jorganchem.2013.11.024](https://doi.org/10.1016/j.jorganchem.2013.11.024)
- Khoenkhoen N, de Bruin B, Reek JNH, Dzik WI (2015) Reactivity of dinitrogen bound to mid- and late-transition-metal centers. *Eur J Inorg Chem*:567–598. doi:[10.1002/ejic.201403041](https://doi.org/10.1002/ejic.201403041)
- Nishibayashi Y (2015) Molybdenum-catalyzed reduction of molecular dinitrogen into ammonia under ambient reaction conditions. *C R Chim* 18:776–784. doi:[10.1016/j.crci.2015.01.014](https://doi.org/10.1016/j.crci.2015.01.014)
- Nishibayashi Y (2015) Recent progress in transition-metal-catalyzed reduction of molecular dinitrogen under ambient reaction conditions. *Inorg Chem* 54:9234–9247. doi:[10.1021/acs.inorgchem.5b00881](https://doi.org/10.1021/acs.inorgchem.5b00881)

26. Tanaka H, Nishibayashi Y, Yoshizawa K (2016) Interplay between theory and experiment for ammonia synthesis catalyzed by transition metal complexes. *Acc Chem Res* 49:987–995. doi:[10.1021/acs.accounts.6b00033](https://doi.org/10.1021/acs.accounts.6b00033)
27. Ohki Y, Seino H (2016) N-heterocyclic carbenes as supporting ligands in transition metal complexes of N<sub>2</sub>. *Dalton Trans* 45:874–880. doi:[10.1039/c5dt04298d](https://doi.org/10.1039/c5dt04298d)
28. Tanabe Y, Nishibayashi Y (2016) Catalytic dinitrogen fixation to form ammonia at ambient reaction conditions using transition metal–dinitrogen complexes. *Chem Rec* 16:1549–1577. doi:[10.1002/tcr.201600025](https://doi.org/10.1002/tcr.201600025)
29. Flöser BM, Tuczek F (2016) Synthetic nitrogen fixation with mononuclear molybdenum complexes: electronic-structural and mechanistic insights from DFT. *Coord Chem Rev.* doi:[10.1016/j.ccr.2016.11.003](https://doi.org/10.1016/j.ccr.2016.11.003)
30. Shiina K (1972) Reductive silylation of molecular nitrogen *via* fixation to tris(trialkylsilyl) amine. *J Am Chem Soc* 94:9266–9267. doi:[10.1021/ja00781a068](https://doi.org/10.1021/ja00781a068)
31. Komori K, Oshita H, Mizobe Y, Hidai M (1989) Catalytic conversion of molecular nitrogen into silylamines using molybdenum and tungsten dinitrogen complexes. *J Am Chem Soc* 111:1939–1940. doi:[10.1021/ja00187a092](https://doi.org/10.1021/ja00187a092)
32. Tanaka H, Sasada A, Kouno T, Yuki M, Miyake Y, Nakanishi H, Nishibayashi Y, Yoshizawa K (2011) Molybdenum-catalyzed transformation of molecular dinitrogen into silylamine: experimental and DFT study on the remarkable role of ferrocenyldiphosphine ligands. *J Am Chem Soc* 133:3498–3506. doi:[10.1021/ja109181n](https://doi.org/10.1021/ja109181n)
33. Ogawa T, Kajita Y, Wasada-Tsutsui Y, Wasada H, Masuda H (2013) Preparation, characterization, and reactivity of dinitrogen molybdenum complexes with bis(diphenylphosphino) amine derivative ligands that form a unique 4-membered P–N–P chelate ring. *Inorg Chem* 52:182–195. doi:[10.1021/ic301577a](https://doi.org/10.1021/ic301577a)
34. Liao Q, Saffon-Merceron N, Mézailles N (2014) Catalytic dinitrogen reduction at the molybdenum center promoted by a bulky tetradentate phosphine ligand. *Angew Chem Int Ed* 53:14206–14210. doi:[10.1002/anie.201408664](https://doi.org/10.1002/anie.201408664)
35. Liao Q, Saffon-Merceron N, Mézailles N (2015) N<sub>2</sub> reduction into silylamine at tridentate phosphine/Mo center: catalysis and mechanistic study. *ACS Catal* 5:6902–6906. doi:[10.1021/acscatal.5b01626](https://doi.org/10.1021/acscatal.5b01626)
36. Kuriyama S, Arashiba K, Nakajima K, Tanaka H, Yoshizawa K, Nishibayashi Y (2016) Azaferrocene-based PNP-type pincer ligand: synthesis of molybdenum, chromium, and iron complexes and reactivity toward nitrogen fixation. *Eur J Inorg Chem*:4856–4861. doi:[10.1002/ejic.201601051](https://doi.org/10.1002/ejic.201601051)
37. Yandulov DV, Schrock RR (2003) Catalytic reduction of dinitrogen to ammonia at a single molybdenum center. *Science* 301:76–78. doi:[10.1126/science.1085326](https://doi.org/10.1126/science.1085326)
38. Yandulov DV, Schrock RR (2002) Reduction of dinitrogen to ammonia at a well-protected reaction site in a molybdenum triamidoamine complex. *J Am Chem Soc* 124:6252–6253. doi:[10.1021/ja020186x](https://doi.org/10.1021/ja020186x)
39. Yandulov DV, Schrock RR, Rheingold AL, Ceccarelli C, Davis WM (2003) Synthesis and reactions of molybdenum triamidoamine complexes containing hexaisopropylterphenyl substituents. *Inorg Chem* 42:796–813. doi:[10.1021/ic0205051](https://doi.org/10.1021/ic0205051)
40. Yandulov DV, Schrock RR (2005) Studies relevant to catalytic reduction of dinitrogen to ammonia by molybdenum triamidoamine complexes. *Inorg Chem* 44:1103–1117. doi:[10.1021/ic040095w](https://doi.org/10.1021/ic040095w)
41. Weare WW, Dai X, Byrnes MJ, Chin JM, Schrock RR, Müller P (2006) Catalytic reduction of dinitrogen to ammonia at a single molybdenum center. *Proc Natl Acad Sci U S A* 103:17099–17106. doi:[10.1073/pnas.0602778103](https://doi.org/10.1073/pnas.0602778103)
42. Munisamy T, Schrock RR (2012) An electrochemical investigation of intermediates and processes involved in the catalytic reduction of dinitrogen by [HIPTN<sub>3</sub>N]Mo (HIPTN<sub>3</sub>N = (3,5-(2,4,6-*i*-Pr<sub>3</sub>C<sub>6</sub>H<sub>2</sub>)<sub>2</sub>C<sub>6</sub>H<sub>3</sub>NCH<sub>2</sub>CH<sub>2</sub>)<sub>3</sub>N). *Dalton Trans* 41:130–137. doi:[10.1039/c1dt11287b](https://doi.org/10.1039/c1dt11287b)

43. Ritleng V, Yandulov DV, Weare WW, Schrock RR, Hock AS, Davis WM (2004) Molybdenum triamidoamine complexes that contain hexa-*tert*-butylterphenyl, hexamethylterphenyl, or *p*-bromohexaisopropylterphenyl substituents. An examination of some catalyst variations for the catalytic reduction of dinitrogen. *J Am Chem Soc* 126:6150–6163. doi:[10.1021/ja0306415](https://doi.org/10.1021/ja0306415)
44. Reithofer MR, Schrock RR, Müller P (2010) Synthesis of [(DPPNCH<sub>2</sub>CH<sub>2</sub>)<sub>3</sub>N]<sup>3-</sup> molybdenum complexes (DPP = 3,5-(2,5-diisopropylpyrrolyl)<sub>2</sub>C<sub>6</sub>H<sub>3</sub>) and studies relevant to catalytic reduction of dinitrogen. *J Am Chem Soc* 132:8349–8358. doi:[10.1021/ja1008213](https://doi.org/10.1021/ja1008213)
45. Weare WW, Schrock RR, Hock AS, Müller P (2006) Synthesis of molybdenum complexes that contain “hybrid” triamidoamine ligands, [(hexaisopropylterphenyl-NCH<sub>2</sub>CH<sub>2</sub>)<sub>2</sub>NCH<sub>2</sub>CH<sub>2</sub>N-aryl]<sup>3-</sup>, and studies relevant to catalytic reduction of dinitrogen. *Inorg Chem* 45:9185–9196. doi:[10.1021/ic0613457](https://doi.org/10.1021/ic0613457)
46. Chin JM, Schrock RR, Müller P (2010) Synthesis of diamidopyrrolyl molybdenum complexes relevant to reduction of dinitrogen to ammonia. *Inorg Chem* 49:7904–7916. doi:[10.1021/ic100856n](https://doi.org/10.1021/ic100856n)
47. Smythe NC, Schrock RR, Müller P, Weare WW (2006) Synthesis of [(HIPTNCH<sub>2</sub>CH<sub>2</sub>)<sub>3</sub>N]V compounds (HIPT = 3,5-(2,4,6-*i*-Pr<sub>3</sub>C<sub>6</sub>H<sub>2</sub>)<sub>2</sub>C<sub>6</sub>H<sub>3</sub>) and an evaluation of vanadium for the reduction of dinitrogen to ammonia. *Inorg Chem* 45:9197–9205. doi:[10.1021/ic061554r](https://doi.org/10.1021/ic061554r)
48. Smythe NC, Schrock RR, Müller P, Weare WW (2006) Synthesis of [(HIPTCH<sub>2</sub>CH<sub>2</sub>)<sub>3</sub>N]Cr compounds (HIPT = 3,5-(2,4,6-*i*-Pr<sub>3</sub>C<sub>6</sub>H<sub>2</sub>)<sub>2</sub>C<sub>6</sub>H<sub>3</sub>) and an evaluation of chromium for the reduction of dinitrogen to ammonia. *Inorg Chem* 45:7111–7118. doi:[10.1021/ic060549k](https://doi.org/10.1021/ic060549k)
49. Yandulov DV, Schrock RR (2005) Synthesis of tungsten complexes that contain hexaisopropylterphenyl-substituted triamidoamine ligands, and reactions relevant to the reduction of dinitrogen to ammonia. *Can J Chem* 83:341–357. doi:[10.1139/v05-013](https://doi.org/10.1139/v05-013)
50. Arashiba K, Miyake Y, Nishibayashi Y (2011) A molybdenum complex bearing PNP-type pincer ligands leads to the catalytic reduction of dinitrogen into ammonia. *Nat Chem* 3:120–125. doi:[10.1038/nchem.906](https://doi.org/10.1038/nchem.906)
51. Tanaka H, Arashiba K, Kuriyama S, Sasada A, Nakajima K, Yoshizawa K, Nishibayashi Y (2014) Unique behaviour of dinitrogen-bridged dimolybdenum complexes bearing pincer ligand towards catalytic formation of ammonia. *Nat Commun* 5:3737. doi:[10.1038/ncomms4737](https://doi.org/10.1038/ncomms4737)
52. Kinoshita E, Arashiba K, Kuriyama S, Miyake Y, Shimazaki R, Nakanishi H, Nishibayashi Y (2012) Synthesis and catalytic activity of molybdenum–dinitrogen complexes bearing unsymmetric PNP-type pincer ligands. *Organometallics* 31:8437–8443. doi:[10.1021/om301046t](https://doi.org/10.1021/om301046t)
53. Kuriyama S, Arashiba K, Nakajima K, Tanaka H, Kamaru N, Yoshizawa K, Nishibayashi Y (2014) Catalytic formation of ammonia from molecular dinitrogen by use of dinitrogen-bridged dimolybdenum–dinitrogen complexes bearing PNP-pincer ligands: remarkable effect of substituent at PNP-pincer ligand. *J Am Chem Soc* 136:9719–9731. doi:[10.1021/ja5044243](https://doi.org/10.1021/ja5044243)
54. Kuriyama S, Arashiba K, Nakajima K, Tanaka H, Yoshizawa K, Nishibayashi Y (2015) Nitrogen fixation catalyzed by ferrocene-substituted dinitrogen-bridged dimolybdenum–dinitrogen complexes: unique behavior of ferrocene moiety as redox active site. *Chem Sci* 6:3940–3951. doi:[10.1039/c5sc00545k](https://doi.org/10.1039/c5sc00545k)
55. Arashiba K, Kinoshita E, Kuriyama S, Eizawa A, Nakajima K, Tanaka H, Yoshizawa K, Nishibayashi Y (2015) Catalytic reduction of dinitrogen to ammonia by use of molybdenum–nitride complexes bearing a tridentate triphosphine as catalysts. *J Am Chem Soc* 137:5666–5669. doi:[10.1021/jacs.5b02579](https://doi.org/10.1021/jacs.5b02579)
56. Tanaka H, Yoshizawa K (2017) Computational approach to nitrogen fixation on molybdenum–dinitrogen complexes. *Top Organomet Chem* 60:171–196. doi:[10.1007/3418\\_2016\\_7](https://doi.org/10.1007/3418_2016_7)

# Computational Approach to Nitrogen Fixation on Molybdenum–Dinitrogen Complexes

Hiromasa Tanaka and Kazunari Yoshizawa

**Abstract** The transformation of  $N_2$  into  $NH_3$  (nitrogen fixation) on transition metal complexes generally involves complicated elementary reaction steps and a number of possible reaction intermediates because at least six pairs of proton and electron (or six hydrogen atoms) must take part in this process. Mechanistic details of nitrogen fixation will be disclosed by close liaison between theory and experiment. In this chapter, recent advances in the mechanistic understanding of the catalytic transformation of  $N_2$  to  $NH_3$  on mono- and dinuclear Mo– $N_2$  complexes are overviewed from a theoretical perspective. In particular, catalytic mechanisms of nitrogen fixation by dinitrogen-bridged dimolybdenum complexes bearing pincer ligands are discussed in detail based on density-functional-theory calculations corroborated by experimental findings.

**Keywords** Catalytic mechanism • Molybdenum • Nitrogen fixation • Pincer ligand • Theoretical calculation

## Contents

1	Introduction .....	172
2	Nitrogen Fixation Catalyzed by an Mo–Triamidoamine Complex: The Yandulov–Schrock Cycle .....	174
3	Nitrogen Fixation Catalyzed by Dinitrogen-Bridged Dimolybdenum Complexes .....	175
3.1	Dimolybdenum Complexes Bearing PNP-Type Pincer Ligands .....	175
3.2	Dimolybdenum Complexes Bearing Substituted PNP-Type Pincer Ligands .....	183
3.3	Dimolybdenum Complexes Bearing PCP-Type Pincer Ligands .....	185
4	Conclusions .....	193
	References .....	195

---

H. Tanaka (✉) and K. Yoshizawa (✉)  
Institute for Materials Chemistry and Engineering and IRCCS, Kyushu University, Nishi-ku,  
Fukuoka 819-0395, Japan  
e-mail: [h-tanaka@ms.ifoc.kyushu-u.ac.jp](mailto:h-tanaka@ms.ifoc.kyushu-u.ac.jp); [kazunari@ms.ifoc.kyushu-u.ac.jp](mailto:kazunari@ms.ifoc.kyushu-u.ac.jp)

## 1 Introduction

As a part of the global nitrogen cycle on the earth, biological nitrogen fixation is efficiently accomplished by nitrogenases in certain bacteria. The Mo-containing nitrogenase has a double cubane-type iron–molybdenum–sulfur complex  $\text{MoFe}_7\text{S}_9\text{C}$  called FeMo-cofactor at the active site, and the multinuclear transition-metal complex binds dinitrogen ( $\text{N}_2$ ) and reduces it to ammonia ( $\text{NH}_3$ ) at ambient temperature under atmospheric pressure (Fig. 1a) [1–4]. According to the optimal reaction, eight pairs of proton and electron are utilized for the formation of two molecules of  $\text{NH}_3$  and the obligatory evolution of one molecule of  $\text{H}_2$ . Although the exact reaction mechanism of the biological nitrogen fixation has not been fully understood, a compelling mechanism is proposed on the basis of a series of excellent spectroscopic studies [5]. In the proposed mechanism, the binding of  $\text{N}_2$  occurs at the  $\text{E}_4$  intermediate, where four pairs of proton and electron are accumulated in the FeMo cofactor and two of the hydrogens bridge between iron atoms to form  $[\text{Fe}–\text{H}–\text{Fe}]$  moieties (Fig. 1b).

The biological nitrogen fixation system is an attractive model for designing an alternative to the industrial Haber–Bosch process, in which  $\text{NH}_3$  is produced from  $\text{N}_2$  and  $\text{H}_2$  under harsh conditions. It should be noted that more than 90% of the total energy for the industrial  $\text{NH}_3$  production is consumed for the production of  $\text{H}_2$  (and  $\text{CO}_2$ ) from fossil fuels [6]. From an environmental point of view, much attention has been paid to novel nitrogen fixation systems that operate without the use of  $\text{H}_2$  under ambient conditions in the homogeneous phase. Since the discovery of the first transition-metal– $\text{N}_2$  complex in 1965 [7], a large number of metal– $\text{N}_2$  complexes have been synthesized and the stoichiometric reactivity of coordinated  $\text{N}_2$  has been thoroughly examined [8–12]. At present, however, very limited transition metal complexes are known to work as catalysts for the direct formation of  $\text{NH}_3$  from  $\text{N}_2$  in the presence of proton and electron sources (Fig. 2) [13–22]. Interestingly, all the catalysts ever reported contain Mo and Fe at their metal centers, similar to the FeMo cofactor. Quite recently, two research groups have independently demonstrated a cobalt-catalyzed transformation of  $\text{N}_2$  into  $\text{NH}_3$  [23, 24]. Unfortunately, the turnover numbers of all the catalysts mentioned above are still low compared with

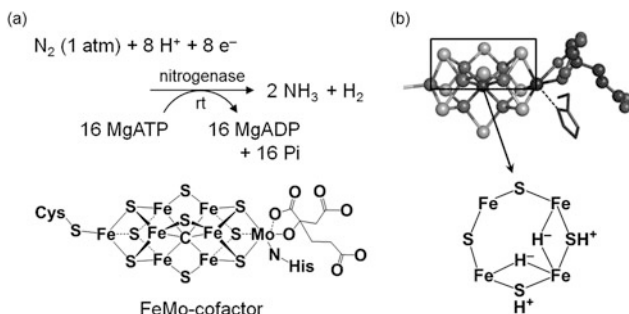


**Fig. 1** (a) Biological nitrogen fixation by the Mo-containing nitrogenase. (b) A possible structure of the  $\text{E}_4$  intermediate



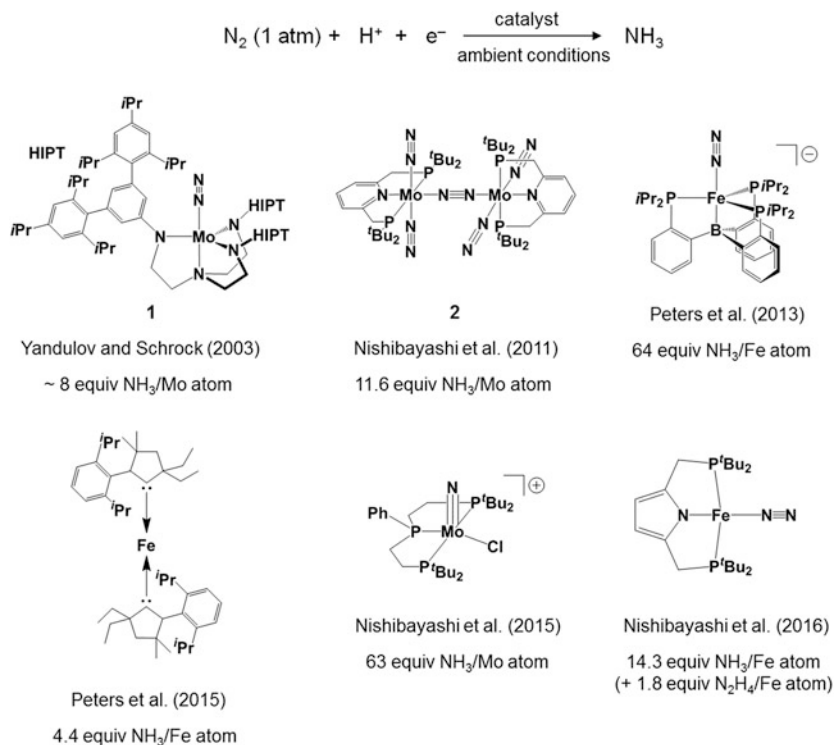


**Fig. 2** Mo and Fe-based synthetic catalysts for nitrogen fixation with their turnover numbers of  $\text{NH}_3$  production per metal atom

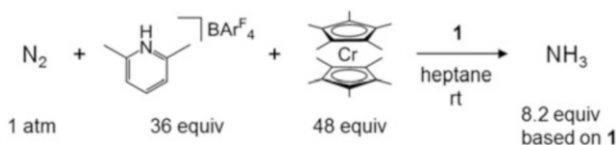
heterogeneous Fe catalysts utilized for the Haber-Bosch process. Relevant to the biological nitrogen fixation by the Mo-containing nitrogenase, it should be noted that Fe and Co complexes bearing an anionic PNP pincer ligand catalyzes the formation of  $\text{NH}_3$  and hydrazine  $\text{N}_2\text{H}_4$  [22, 24], where  $\text{N}_2\text{H}_4$  is known as an intermediate during the biological  $\text{N}_2$  reduction [1]. Very recently, Ashley and coworkers reported a selective catalytic reduction of  $\text{N}_2$  to  $\text{N}_2\text{H}_4$  using an Fe (0) complex  $\text{Fe}(\text{depe})_2(\text{N}_2)$  ( $\text{depe}=\text{Et}_2\text{PCH}_2\text{CH}_2\text{PEt}_2$ ) [25].

To develop more effective nitrogen fixation catalysts under ambient conditions in the homogenous phase, we must extract as much information as possible from the limited successful examples. Computational chemistry will be able to provide useful mechanistic insights into the complicated catalytic cycles involving short-lived intermediates that are often difficult to detect or characterize experimentally. In particular for the Mo-catalyzed nitrogen fixation systems in Fig. 2, quantum chemical calculations by density-functional-theory (DFT) methods have been applied for elucidating detailed mechanisms of the transformation of  $\text{N}_2$  based on experimental findings, and also been exploited for designing more effective catalysts [15, 26]. In this chapter, we overview recent advances in the mechanistic understanding of catalytic transformation of  $\text{N}_2$  to  $\text{NH}_3$  by mono- and dimolybdenum complexes from a theoretical perspective.

## 2 Nitrogen Fixation Catalyzed by an Mo–Triamidoamine Complex: The Yandulov–Schrock Cycle

In 2003, Yandulov and Schrock showed a pioneering example of the direct formation of  $\text{NH}_3$  from  $\text{N}_2$  under ambient conditions using an Mo–triamidoamine complex,  $[\text{HIPTN}_3\text{N}]\text{Mo}(\text{N}_2)$  **1** (HIPT = hexaisopropylterphenyl). In the presence of 2,6-lutidinium tetrakis[3,5-bis(trifluoromethyl)phenyl]borate ( $[\text{LuH}]\text{BAr}^{\text{F}}_4$ ) as a proton source and decamethylchromocene ( $\text{CrCp}^*_2$ ) as a reducing reagent, **1** served as the catalyst for nitrogen fixation at room temperature, where up to 8.2 equiv of  $\text{NH}_3$  was produced based on **1** (Scheme 1) [16]. Unfortunately, the turnover number of the catalyst has not been updated despite various modifications of the original complex **1**. The preparation and characterization of intermediates relevant to the catalytic reaction led them to propose a catalytic mechanism involving a stepwise addition of protons and electrons, the so-called Yandulov–Schrock cycle [16, 26–29]. Their proposal based on concrete experimental evidence received much interest from theoretical researchers, and the validity of the proposed catalytic mechanism has been advocated by intensive computational studies on the energetics of possible reaction pathways conducted by Cao et al. [30], Studt and Tuzek [31], Magistrato et al. [32], and Reiher and coworkers [33–38].

Figure 3 describes the Yandulov–Schrock cycle for nitrogen fixation catalyzed by **1**, where  $[\text{Mo}]$  represents  $[\text{HIPTN}_3\text{N}]\text{Mo}$ . The catalytic formation of  $\text{NH}_3$  in the Yandulov–Schrock cycle involves a successive protonation of the distal N atom of coordinated  $\text{N}_2$ , which is the one far from Mo. Each protonation step is followed by one-electron reduction step. Addition of three pairs of proton/electron to **1** affords a nitride intermediate  $[\text{Mo}(\equiv\text{N})]$  and the first molecule of  $\text{NH}_3$  via the formation of diazenide  $[\text{Mo}(\text{N}=\text{NH})]$ , hydrazide(2-)  $[\text{Mo}(\text{NNH}_2)]$ , and hydrazidium  $[\text{Mo}$



**Scheme 1** Transformation of  $\text{N}_2$  into  $\text{NH}_3$  catalyzed by a Mo–triamidoamine complex **1**

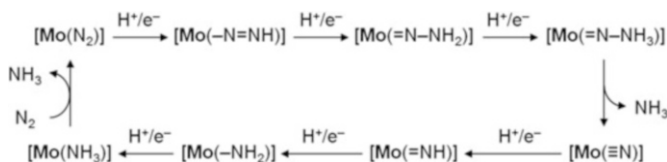


**Fig. 3** The Yandulov–Schrock cycle for the transformation of dinitrogen into ammonia catalyzed by **1**.  $[\text{Mo}]$  represents  $[\text{HIPTN}_3\text{N}]\text{Mo}$

( $\text{NNH}_3$ ) intermediates. Protonation of the proximal N atom of the  $\text{N}_2$  ligand, which is the one directly connected with Mo, is not considered in this catalytic cycle because diazene ( $\text{HN}=\text{NH}$ ) and hydrazine ( $\text{H}_2\text{N}-\text{NH}_2$ ) were not observed experimentally. The remaining nitride N atom in  $[\text{Mo}(\equiv\text{N})]$  is then protonated and reduced to give an ammine intermediate  $[\text{Mo}(\text{NH}_3)]$  via imide  $[\text{Mo}(\text{NH})]$  and amide  $[\text{Mo}(\text{NH}_2)]$  intermediates. Finally the  $\text{NH}_3$  ligand is replaced by an incoming  $\text{N}_2$  molecule to complete the catalytic cycle. For the first protonation of **1**, Reiher and coworkers theoretically suggested an alternative pathway in which protonation of an amide N atom of the  $\text{HIPTN}_3\text{N}$  ligand precedes protonation of the  $\text{N}_2$  ligand [33, 35]. Later, Schrock and coworkers confirmed this computational suggestion by ENDOR spectroscopy [28].

### 3 Nitrogen Fixation Catalyzed by Dinitrogen-Bridged Dimolybdenum Complexes

#### 3.1 Dimolybdenum Complexes Bearing PNP-Type Pincer Ligands

In 2011, Nishibayashi and coworkers reported a new nitrogen fixation system operating under mild conditions using a dinitrogen-bridged dimolybdenum complex bearing a pyridine-based PNP-type pincer ligand,  $[\{\text{Mo}(\text{N}_2)_2(\text{PNP})\}_2(\mu\text{-N}_2)]$  (**2**; PNP=2,6-bis(di-*tert*-butylphosphinomethyl)pyridine), as a catalyst (Scheme 2) [17]. In the presence of  $[\text{LutH}]\text{OTf}$  ( $\text{OTf}=\text{CF}_3\text{SO}_3$ ) as a proton source and cobaltocene ( $\text{CoCp}_2$ ) as a reducing reagent, up to 23 equiv of  $\text{NH}_3$  based on the catalyst was produced from  $\text{N}_2$  gas. In this first report, they postulated a catalytic mechanism of the transformation of  $\text{N}_2$  into  $\text{NH}_3$  by reference to the Yandulov–Schrock mechanism, i.e., mononuclear Mo– $\text{N}_2$  complexes separated from **2**, such as  $[\text{Mo}(\text{N}_2)_3(\text{PNP})]$ , work as key reactive intermediates in the catalytic cycle (Fig. 4a). Batista and coworkers pointed out a remarkable role of dinuclear Mo complexes in the catalytic activity of **2** based on theoretical calculations from a thermodynamic aspect [39]. To get a mechanistic insight into nitrogen fixation in the dimolybdenum system, Yoshizawa, Nishibayashi, and coworkers demonstrated a synergetic relationship between theory and experiment [40].

A theoretically plausible catalytic cycle described in Fig. 4b is corroborated by the following experimental findings: [17, 40] (1) Dimolybdenum complex **2** contains five  $\text{N}_2$  ligands, four terminal and one bridging. The terminal  $\text{N}_2$  ligands can be replaced by CO molecules to afford  $[\{\text{Mo}(\text{CO})_2(\text{PNP})\}_2(\mu\text{-N}_2)]$ . The CO-substituted dimolybdenum complex produced less than a stoichiometric amount of  $\text{NH}_3$ . (2) A six-coordinate mononuclear Mo– $\text{N}_2$  complex, *trans*- $[\text{Mo}(\text{N}_2)_2(\text{PMe}_2\text{Ph})(\text{PNP})]$ , showed no catalytic activity. (3) The catalytic activity of **2** strongly depends on the nature of the counter anion of the proton source ( $\text{LutH}^+$ ). The amount of produced  $\text{NH}_3$  was drastically decreased when  $[\text{LutH}]\text{Cl}$  and  $[\text{LutH}]\text{BAr}_4^{\text{F}}$  were adopted as proton

**Scheme 2** Transformation of  $N_2$  into  $NH_3$  catalyzed by a dimolybdenum complex bearing PNP-type pincer ligands **2**

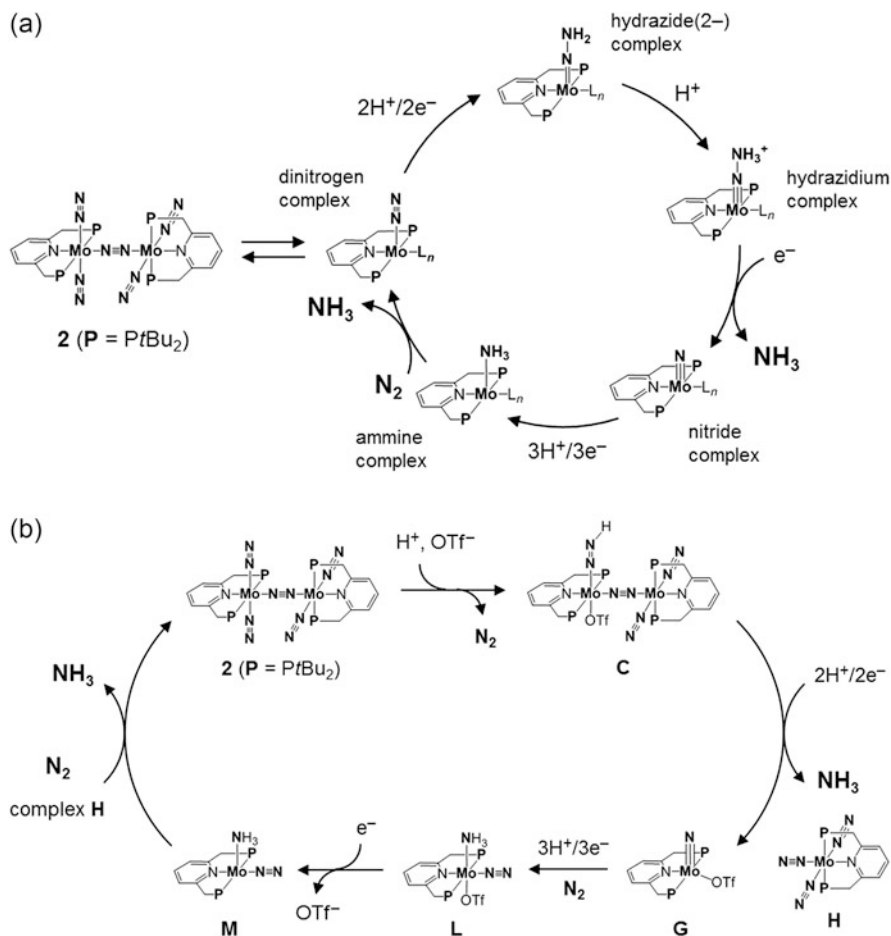
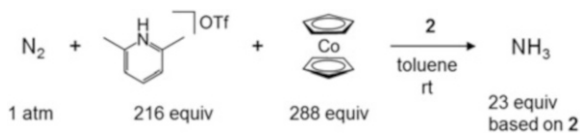


**Fig. 4** Proposed catalytic cycles of the transformation of  $N_2$  into  $NH_3$  by **2**. (a) First proposed mechanism [17]. (b) Theory-based mechanism corroborated by experimental findings [39]. The numbering of intermediates is presented in Fig. 5

sources. (4) Two Mo–nitride complexes,  $[Mo(\equiv N)(PNP)Cl]$  and  $[Mo(\equiv N)(PNP)Cl]OTf$  exhibited almost the same catalytic activity as **2**. (5) Fragments assignable to  $[Mo(\equiv N)(OTf)(PNP)-N\equiv N-Mo(N_2)(PNP)]$  and  $[Mo(\equiv N)(OTf)(PNP)]$  were observed by mass spectrometry from the stoichiometric reaction of **2** with 2 equiv of  $[LutH]OTf$  in toluene at room temperature. (6) A mononuclear Mo–imide complex  $[Mo(=NH)$

(C<sub>5</sub>H<sub>5</sub>N)(PNP)Cl]OTf, in which a pyridine molecule occupies the equatorial coordination site, was isolated. (7) A fragment assignable to [Mo(NH<sub>3</sub>)(PNP)–N≡N–Mo(N<sub>2</sub>)<sub>2</sub>(PNP)] or [Mo(NH<sub>3</sub>)(N<sub>2</sub>)(PNP)–N≡N–Mo(N<sub>2</sub>)(PNP)] was observed by mass spectrometry from a reaction mixture of the catalytic reaction of **2** with excess amounts of [LutH]OTf and CoCp<sub>2</sub>. These experimental findings were exploited for developing a hypothesis in the theory-based proposal: (a) Terminal N<sub>2</sub> ligands are essential for the catalytic formation of NH<sub>3</sub>. (b) Dimolybdenum complexes with the bridging N<sub>2</sub> ligand must be involved in the catalytic cycle. (c) Triflate (OTf<sup>−</sup>) as the counter anion of LutH<sup>+</sup> would play a role in the catalytic cycle. (d) A dinuclear Mo complex is separated into mononuclear ones to afford [Mo(≡N)(OTf)(PNP)] as a key intermediate at a certain stage in the catalytic cycle. (e) Six-coordinate mononuclear Mo-imide complexes such as [Mo(=NH)(OTf)(N<sub>2</sub>)(PNP)] and its cation, in which N<sub>2</sub> occupies the equatorial site, are formed in the course of protonation and reduction of [Mo(≡N)(OTf)(PNP)]. This process is prepared for regeneration of **2** to complete the catalytic cycle.

The proposed catalytic cycle shown in Fig. 4b involves hydrogenations of an N<sub>2</sub> ligand in **2** leading to generation of the first NH<sub>3</sub> molecule without separation of the dinuclear Mo–N≡N–Mo structure. The numbering of intermediates is given in Fig. 5. The first protonation should occur at one of the terminal N<sub>2</sub> ligands in **2** and is followed by exchange of the N<sub>2</sub> ligand *trans* to the protonated N<sub>2</sub> ligand for the counter anion of the proton source, OTf<sup>−</sup> (**2** → **C**). Addition of two proton/electron pairs to **C** leads to the formation of the first NH<sub>3</sub> molecule. The protonation and reduction of the NNH group in **C** prompts a facile dissociation of a dative Mo–N<sub>2</sub> bond between an Mo atom and the bridging N<sub>2</sub> ligand to give two mononuclear Mo complexes, a nitride complex **G** and a dinitrogen complex **H**. Addition of three proton/electron pairs to **G** accompanied by the coordination of N<sub>2</sub> at the equatorial position results in the formation of a six-coordinate ammine complex **L**. Addition of the sixth electron to **L** liberates the OTf<sup>−</sup> ligand to form a five-coordinate ammine complex **M**, which couples with **H** to regenerate a dimolybdenum complex. The regeneration of the Mo–N≡N–Mo structure is linked with the replacement of the NH<sub>3</sub> ligand by an incoming N<sub>2</sub> molecule to complete the catalytic cycle.

Figure 5 presents the energetics of detailed reaction pathways for the transformation of N<sub>2</sub> into NH<sub>3</sub> catalyzed by **2**. Alternating protonation/reduction steps were assumed in the calculated pathways. Activation energies of the proton transfer from LutH<sup>+</sup> were evaluated for all protonation steps. Energy profiles of the reduction steps were obtained as the energy difference between protonated and neutral intermediates. The values in *italics* correspond to the reaction energies calculated based on the equation [XH]<sup>+</sup> + [CoCp<sub>2</sub>] → [XH] + [CoCp<sub>2</sub>]<sup>+</sup>, where [XH]<sup>+</sup> is a protonated intermediate. The latter values should be carefully treated because each species in the equation is separately calculated at infinite distance [35]. Energy changes (Δ*E*) and activation energies (*E*<sub>a</sub> in parenthesis) were calculated at the B3LYP\* level of theory [41, 42]. For optimization, the LANL2DZ and 6-31G(d) basis sets were chosen for the Mo atom and the other atoms, respectively (BS1). To determine the energy profiles of individual reaction steps, single-point energy calculations were performed at the optimized geometries by BS1 using the Stuttgart-Dresden pseudopotentials (SDD)

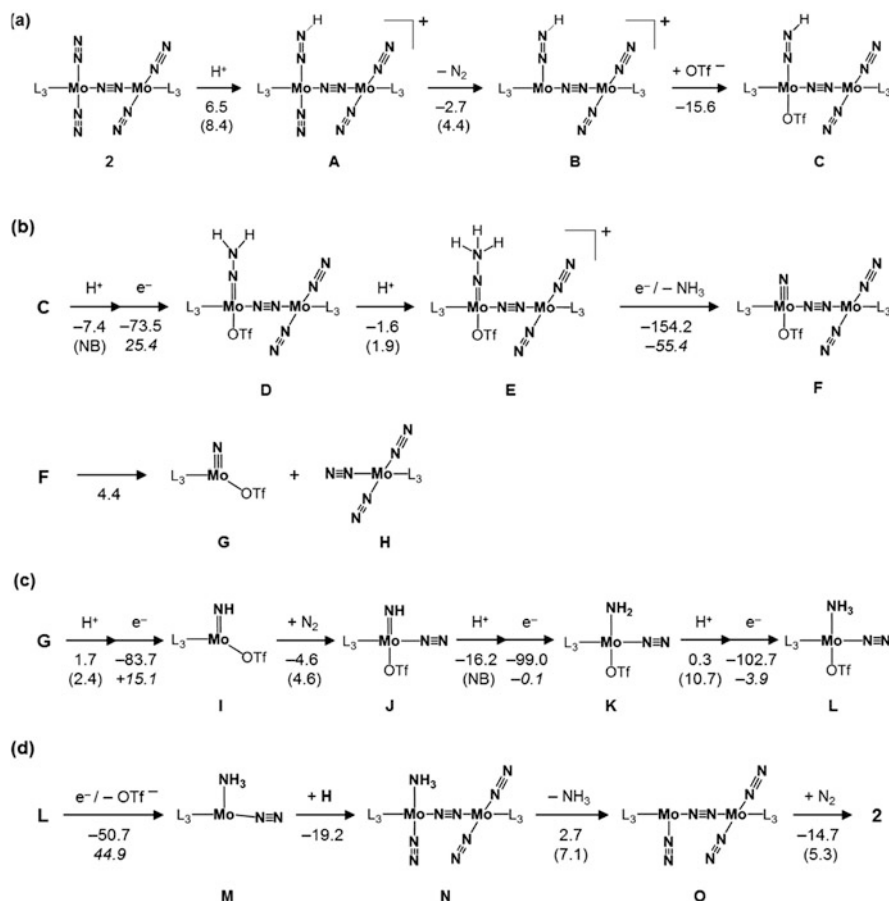


**Fig. 5** (a) Protonation of a terminal  $N_2$  ligand. (b) First  $NH_3$  formation and separation into mononuclear Mo complexes. (c) Second  $NH_3$  formation. (d) Regeneration of dinuclear structure and ligand exchange. A possible reaction pathway for the transformation of  $N_2$  into  $NH_3$  starting from **2**.  $L_3$  represents the PNP pincer ligand. Energy changes and activation energies (in parenthesis) for individual reaction steps were calculated at the B3LYP\*/BS2 level of theory (units in  $\text{kcal mol}^{-1}$ ). NB means that the corresponding reaction has no activation barrier. Protons are supplied by lutidinium. For reduction steps, energy difference between protonated and neutral species is presented. Values in *italics* correspond to the reaction energies obtained with cobaltocene

and 6-311+G(d,p) basis sets (BS2) in place of the LANL2DZ and 6-31G(d) basis sets, respectively. In this review, we concentrate on the three important steps in the catalytic cycle, (1) the protonation of a terminal  $N_2$  ligand in **2** leading to **C**, (2) the formation of mononuclear Mo–nitride complex **G**, and (3) the ligand exchange of  $NH_3$  for  $N_2$  at the final step of the catalytic cycle.

To start the catalytic cycle for the transformation of  $\text{N}_2$ , one of the  $\text{N}_2$  ligands in **2** must be protonated. Dinitrogen complex **2** has at least two possible sites for protonation, four equivalent terminal  $\text{N}_2$  ligands and one bridging  $\text{N}_2$  ligand. The  $\text{N}\equiv\text{N}$  stretching frequencies of **2** in THF were experimentally observed at  $1944\text{ cm}^{-1}$  (terminal  $\text{N}_2$ ) and  $1890\text{ cm}^{-1}$  (bridging  $\text{N}_2$ ), indicating that the bridging  $\text{N}_2$  ligand is more strongly activated [17]. However, as shown in Fig. 6a, the protonation of the bridging  $\text{N}_2$  ligand is not likely to occur at room temperature due to its extremely high activation energy ( $40.7\text{ kcal mol}^{-1}$ ). In contrast, the activation energy for the protonation of a terminal  $\text{N}_2$  ligand is relatively low ( $8.4\text{ kcal mol}^{-1}$ ) although the reaction is endothermic by  $6.5\text{ kcal mol}^{-1}$ . A space-filling model of **2** will give a clue for the difference in reactivity of coordinated  $\text{N}_2$  with  $\text{LutH}^+$  (Fig. 6b). Eight *tert*-butyl groups in **2** makes  $\text{LutH}^+$  inaccessible to the bridging  $\text{N}_2$  ligand without a large distortion in the  $\text{Mo-N}\equiv\text{N-Mo}$  moiety. On the other hand, the distal N atom of terminal  $\text{N}_2$  ligands that sticks out from the molecular surface is likely to accept a proton from  $\text{LutH}^+$ . It should be noted that the separation of **2** into two mononuclear  $\text{Mo-N}_2$  complexes [ $\text{Mo}(\text{N}_2)_3(\text{PNP})$ ] **H** and *trans*- $[\text{Mo}(\text{N}_2)_2(\text{PNP})]$  is endothermic by  $24.9\text{ kcal mol}^{-1}$ . The calculated results strongly suggest that the formation of mononuclear  $\text{Mo-N}_2$  complexes from **2** is an unacceptable reaction pathway for the transformation of  $\text{N}_2$  into  $\text{NH}_3$ .

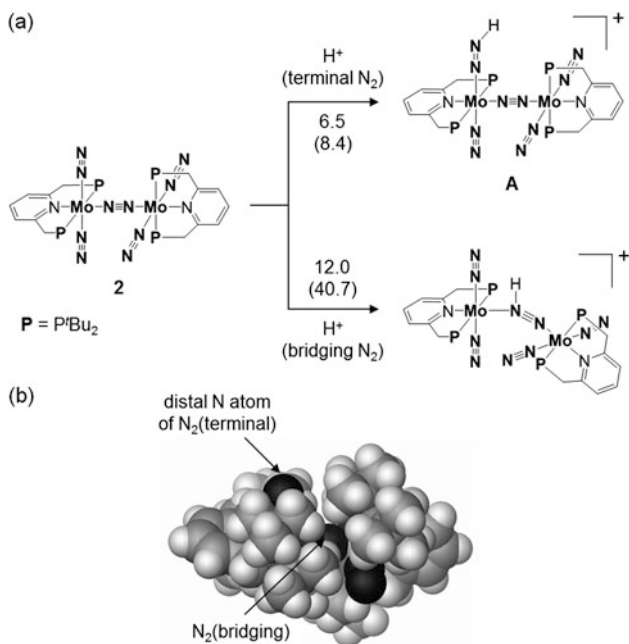


**Fig. 6** (a) Energy profiles of protonation of terminal and bridging  $\text{N}_2$  ligands by  $\text{LutH}^+$ . Energy changes and activation energies (in parenthesis) are given in  $\text{kcal mol}^{-1}$ . (b) A space-filling model of **2**. The bridging  $\text{N}_2$  ligand is sterically protected by *t*Bu groups in the pincer ligands

As shown in Fig. 5a, the proton detachment from **A**, which is the backward reaction of the protonation of **2**, can easily proceed due to a very small activation energy of  $1.9 \text{ kcal mol}^{-1}$ . On the other hand, the protonation of **2** dramatically activates the Mo–N<sub>2</sub> bond between the Mo atom and the N<sub>2</sub> ligand *trans* to the NNH group. The elimination of the N<sub>2</sub> ligand is endothermic by  $14.7 \text{ kcal mol}^{-1}$  ( $E_a = 20.0 \text{ kcal mol}^{-1}$ ) for **2** and *exothermic* by  $2.7 \text{ kcal mol}^{-1}$  ( $E_a = 4.4 \text{ kcal mol}^{-1}$ ) for **A**. After the N<sub>2</sub> elimination, the counter anion of LutH<sup>+</sup> (OTf<sup>−</sup>) will attack the vacant coordinate site in **B** to compensate electric charges. This speculation is reasonable because OTf<sup>−</sup> can exist in the vicinity of **B** after the protonation of a terminal N<sub>2</sub> ligand in **2**. The coordination of OTf<sup>−</sup> to **B** is exothermic by  $15.6 \text{ kcal mol}^{-1}$ , and thereby the NNH moiety is thermodynamically stabilized for the following protonation/reduction steps. Totally, the first protonation process (**2** → **C**) is exothermic by  $11.8 \text{ kcal mol}^{-1}$ .

In the proposed catalytic cycle, mononuclear Mo–nitride complex [Mo(≡N)(OTf)(PNP)] **G** is regarded as a key reaction intermediate (Fig. 4b). It is reasonable to consider the formation of dinuclear Mo–nitride complex **F**, [Mo(≡N)(OTf)(PNP)–NN–Mo(N<sub>2</sub>)<sub>2</sub>(PNP)], based on the experimental observation of a fragment assignable to [Mo(≡N)(OTf)(PNP)–NN–Mo(N<sub>2</sub>)<sub>2</sub>(PNP)] by mass spectrometry. Actually, the dissociation energy of the Mo–N<sub>2</sub> bond between the Mo(≡N) atom and the bridging N<sub>2</sub> ligand in **F** is calculated to be only  $4.4 \text{ kcal mol}^{-1}$  (Fig. 5b). The small bond dissociation energy indicates that **F** should be separated into the corresponding mononuclear complexes **G** and **H**. It should be emphasized here that [Mo(N<sub>2</sub>)<sub>3</sub>(PNP)] **H** does not accept a proton from LutH<sup>+</sup>. All efforts to obtain a product complex consisting of the protonated **H** and Lut resulted in failure, and instead, only a reactant complex consisting of **H** and LutH<sup>+</sup> was optimized. The computational result suggests that a dimolybdenum complex with the Mo–N≡N–Mo structure must be regenerated to start the next catalytic cycle.

As described in Fig. 5d, the regeneration of dimolybdenum complex **2** as the final step of the catalytic cycle involves the exchange of the coordinated NH<sub>3</sub> for a newly incoming N<sub>2</sub> molecule (**N** → **O** → **2**). For Schrock's Mo–triamidoamine system, interconversion of Mo–NH<sub>3</sub> and Mo–N<sub>2</sub> complexes has been investigated both experimentally [26, 27, 43] and theoretically [34–36] in great detail. In this system, the Mo–NH<sub>3</sub> complex readily reacted with N<sub>2</sub> to yield the Mo–N<sub>2</sub> complex, and 1–2 h was required to establish the thermal equilibrium between Mo–NH<sub>3</sub>, Mo–N<sub>2</sub>, N<sub>2</sub>, and NH<sub>3</sub> [43]. Reiher and coworkers reported that energy change ( $\Delta E$ ) in the exchange of NH<sub>3</sub> for N<sub>2</sub> is calculated to be  $-9.8 \text{ kcal mol}^{-1}$  by using full [HIPTN<sub>3</sub>N]Mo complexes [35]. Very recently, Tucek and coworkers reported  $\Delta E = -7.6 \text{ kcal mol}^{-1}$  [44]. Reiher and coworkers investigated the ligand exchange step with Car-Parrinello molecular dynamics simulations followed by stationary DFT calculations [36]. They found that N<sub>2</sub> can access the Mo center through an entrance channel in the plane of three amide N atoms of [HIPTN<sub>3</sub>N]Mo(NH<sub>3</sub>) to form a six-coordinate intermediate [HIPTN<sub>3</sub>N]Mo(N<sub>2</sub>)(NH<sub>3</sub>).

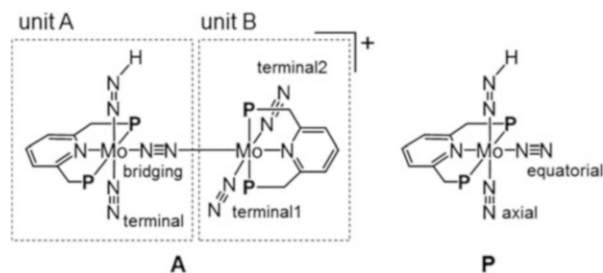
For the exchange of NH<sub>3</sub> for N<sub>2</sub> in the dimolybdenum system, DFT calculations predicted a dissociation–addition mechanism via the formation of a five-coordinate intermediate [Mo(N<sub>2</sub>)(PNP)–NN–Mo(N<sub>2</sub>)<sub>2</sub>(PNP)] **O** (Fig. 5d). Elimination of the NH<sub>3</sub> ligand in [Mo(NH<sub>3</sub>)(N<sub>2</sub>)(PNP)–NN–Mo(N<sub>2</sub>)<sub>2</sub>(PNP)] **N** is endothermic by only



2.7 kcal mol<sup>-1</sup> with an activation energy of 7.1 kcal mol<sup>-1</sup>. Addition of N<sub>2</sub> to **O**, the final step toward the regeneration of **2**, is exothermic by 14.7 kcal mol<sup>-1</sup> with a low activation barrier of 5.3 kcal mol<sup>-1</sup>. Totally, the ligand exchange is exothermic by 12.0 kcal mol<sup>-1</sup> and it will be smoothly attained at room temperature via the dissociation–addition mechanism.

Mononuclear Mo–N<sub>2</sub> complexes such as [Mo(N<sub>2</sub>)<sub>3</sub>(PNP)] and [Mo(N<sub>2</sub>)<sub>2</sub>(PNP)] do not serve as active catalytic species since their N<sub>2</sub> ligands cannot be protonated by LutH<sup>+</sup>. This is the reason why the regeneration of dinuclear complex **2** is considered as the final step of the catalytic cycle in Fig. 4b. Cooperation between the two Mo units in **2** apparently plays an essential role in exhibiting the catalytic activity. The origin of the catalytic activity can be explained in terms of atomic charge of N<sub>2</sub> in the dinuclear and mononuclear Mo–N<sub>2</sub> complexes and their protonated ones at the first protonation step. Table 1 summarizes calculated differences ( $\Delta q$ ) in the NPA atomic charge ( $q$ ) [45] between the Mo–N<sub>2</sub> and Mo–NNH<sup>+</sup> complexes for the dinuclear (**2** and **A**) and mononuclear (**H** and **P**) Mo complexes. The values of  $\Delta q$  obtained for the Mo atoms, N<sub>2</sub>, NNH and PNP indicate how the positive charge of the added proton is redistributed in the Mo–NNH<sup>+</sup> complexes. In the mononuclear system, the protonation of an axial N<sub>2</sub> ligand varies the NPA charges of the Mo atom, the NNH ligand, the remaining axial N<sub>2</sub> ligand, the equatorial N<sub>2</sub> ligand, and the pincer ligand by +0.38, +0.07, +0.17, +0.09, and +0.29, respectively ( $\Delta q = +1.00$  in total). The  $\Delta q$  values of

**Table 1** Differences in the NPA atomic charge ( $\Delta q$ ) between Mo–N<sub>2</sub> and protonated complexes obtained for dinuclear (**2** and **A**) and mononuclear (**H** and **P**) molybdenum complexes



		$q(\mathbf{A})$	$q(\mathbf{B})$	$\Delta q(\mathbf{A}-2)$		$q(\mathbf{P})$	$q(\mathbf{H})$	$\Delta q(\mathbf{P}-\mathbf{H})$
Unit A	Mo	-0.02	-0.35	+0.33	Mo	0.00	-0.38	+0.38
	NN(H)	-0.15	-0.12	-0.03	NN(H)	-0.04	-0.11	+0.07
	NN <sub>terminal</sub>	+0.04	-0.13	+0.17	NN <sub>axial</sub>	+0.06	-0.11	+0.17
	NN <sub>bridging</sub>	-0.13	-0.08	-0.05	NN <sub>equatorial</sub>	-0.01	-0.10	+0.09
	Pincer	+0.89	+0.64	+0.24	Pincer	+0.99	+0.70	+0.29
	Total			+0.66	Total			+1.00
Unit B	Mo	-0.24	-0.35	+0.11				
	NN <sub>terminal1</sub>	-0.10	-0.13	+0.03				
	NN <sub>terminal2</sub>	-0.10	-0.13	+0.03				
	Pincer	+0.81	+0.64	+0.17				
	Total			+0.34				

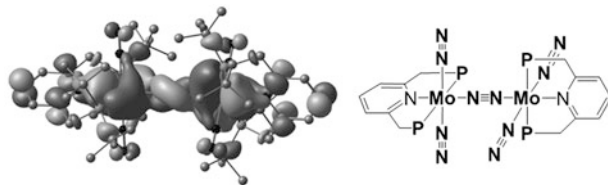


Fig. 7 Spatial distribution of the HOMO of **2**

the dinuclear system were obtained for units A and B separately, where unit A is identical to **H**. Comparison between  $\Delta q$  (**A-2**) of unit A and  $\Delta q$  (**P-H**) provides insight into the function of unit B in the protonation of **2**. The total  $\Delta q$  values of units A (+0.66) and B (+0.34) indicate that a large amount of electron ( $0.34e^-$ ) is donated from unit B to unit A upon protonation. The donated electron mainly distributes on the NNH ligand and bridging  $N_2$  ligand. Large differences in  $\Delta q$  between unit A of **A-2** and **P-H** are observed for the NNH ligand ( $-0.10$ ) and the bridging  $N_2$  ( $-0.14$ ). The electron transfer between the two Mo units enhances the Brønsted basicity of the terminal  $N_2$  ligand attacked by  $LutH^+$ , and an unprotonated Mo unit (unit B in this case) works as a mobile ligand in the first protonation step.

In general the degree of  $N_2$  activation in a metal- $N_2$  complex is experimentally judged from elongation of the  $N\equiv N$  bond and red-shift of the  $N\equiv N$  stretching frequency relative to free  $N_2$ . Deeth and Field [46], and Studt and Tuczec [47] reported that atomic charges on coordinated  $N_2$  is also a useful criterion for judging the degree of  $N_2$  activation. In a biomimetic nitrogen fixation system, a catalytic cycle starts with protonation of  $N_2$  on a metal center (reduction may occur first). Therefore, the reactivity of a metal- $N_2$  complex with a proton donor should closely correlate with the amount of negative charge on the coordinated  $N_2$ . Yoshizawa and coworkers reported that the gross NPA charge on an  $N_2$  ligand in  $M-N_2$  ( $M = Mo, Ru, \text{ and } W$ ) complexes showed a good correlation with activation energies of protonation by  $LutH^+$  [48]. As shown in Table 1, the gross NPA charges on a terminal/axial  $N_2$  ligand are almost identical in the di- and mononuclear  $Mo-N_2$  complexes ( $-0.12$  for **2** and  $-0.11$  for **H**). From the criteria of atomic charge, the degree of  $N_2$  activation in **2** is not sufficient for the protonation by  $LutH^+$ . The small negative charge on  $N_2$  in **2** implies that the terminal  $N_2$  ligand to be protonated is not “preactivated” but activated through an on-demand electron transfer between the two Mo units induced by the approach of  $LutH^+$ . Synergy of the two Mo centers in **2** can be understood by looking at the HOMO (Fig. 7). The HOMO of **2** is highly delocalized between  $d$  orbitals of the two Mo atoms and a  $\pi$  orbital of the bridging  $N_2$  ligand. Their overlap is distorted due to the twisted connection between the two

Mo units, where the dihedral angle of  $\text{N}_2\text{--Mo--Mo--N}_2$  is  $-54.4^\circ$ . The intermetallic electron transfer allows **2** to receive a proton from  $\text{LutH}^+$  at the first step toward the catalytic transformation of  $\text{N}_2$  into  $\text{NH}_3$ .

### 3.2 Dimolybdenum Complexes Bearing Substituted PNP-Type Pincer Ligands

The theory-based reaction pathways supported by the experimental findings (Fig. 4b) give useful information on the development of more effective catalysts for nitrogen fixation using dinitrogen-bridged dimolybdenum complexes. The computational results indicate that the protonation of a terminal  $\text{N}_2$  ligand in **2** is one of the most energetically unfavorable steps. As a strategy for the improvement of catalytic activity of **2**, introduction of an electron-donating group to the pyridine ring in PNP is expected to reinforce the backdonating ability of the Mo atoms. Enhancing the electron-donating ability of PNP will lead to the increase of electron density on the  $\text{N}_2$  ligands to strongly attract a proton at the first protonation step.

Yoshizawa and coworkers theoretically assessed the impact of introduction of electron-donating groups to the 4-position of the pyridine ring in PNP [49]. Substituent effects of the electron-donating groups were evaluated based on the energetics of the first protonation process in Fig. 5a. In the presence of  $[\text{LutH}]\text{OTf}$  as a proton source, this process involves three elementary reaction steps: protonation of a terminal  $\text{N}_2$  ligand, elimination of the  $\text{N}_2$  ligand *trans* to the generated NNH ligand, and coordination of  $\text{OTf}^-$  to prevent the Mo–NNH complex from proton detachment. Figure 8 shows energy profiles of the first protonation process for **2a** (equivalent to **2**), methyl-substituted **2b**, and methoxy-substituted **2c**. While the use of methyl- and methoxy-substituted PNP ligands does not significantly affect the trend of the energy profiles, the introduction of an electron-donating group lowers the activation barrier for the protonation and stabilizes the generated diazenide complex **A**. The activation energy for the protonation step is decreased from  $8.4 \text{ kcal mol}^{-1}$  (**2a**) to  $7.4 \text{ kcal mol}^{-1}$  (**2b**) and  $7.0 \text{ kcal mol}^{-1}$  (**2c**). In addition, the backward reaction from **A** to **2** will be suppressed by using **2b** and **2c** as catalysts. The corresponding activation energies are calculated to be  $2.4 \text{ kcal mol}^{-1}$  for **2b** and  $3.7 \text{ kcal mol}^{-1}$  for **2c**, both of which are higher than that of **2a** ( $1.9 \text{ kcal mol}^{-1}$ ). On the other hand, the introduction of the methyl and methoxy groups does not change the energetics of the  $\text{N}_2$  elimination step. The elimination of the *trans*  $\text{N}_2$  ligand is exothermic by  $2.6\text{--}2.8 \text{ kcal mol}^{-1}$  and requires activation energies of  $4.4\text{--}4.5 \text{ kcal mol}^{-1}$  for all complexes. The  $\text{N}\equiv\text{N}$  stretching frequency calculated for **2a** ( $1960 \text{ cm}^{-1}$  in THF) is slightly red-shifted by introducing the methyl group (**2b**,  $1958 \text{ cm}^{-1}$ ) and the methoxy group (**2c**,  $1954 \text{ cm}^{-1}$ ). The gross NPA charge on a terminal  $\text{N}_2$  ligand is slightly increased from  $-0.125$  (**2a**) to  $-0.127$  (**2b**) and  $-0.133$  (**2c**). The characteristics of the  $\text{N}_2$  ligands indicate a higher degree of  $\text{N}_2$  activation in the Mo complexes bearing the substituted PNP-pincer ligands. DFT calculations have predicted that the introduction of an electron-donating group to

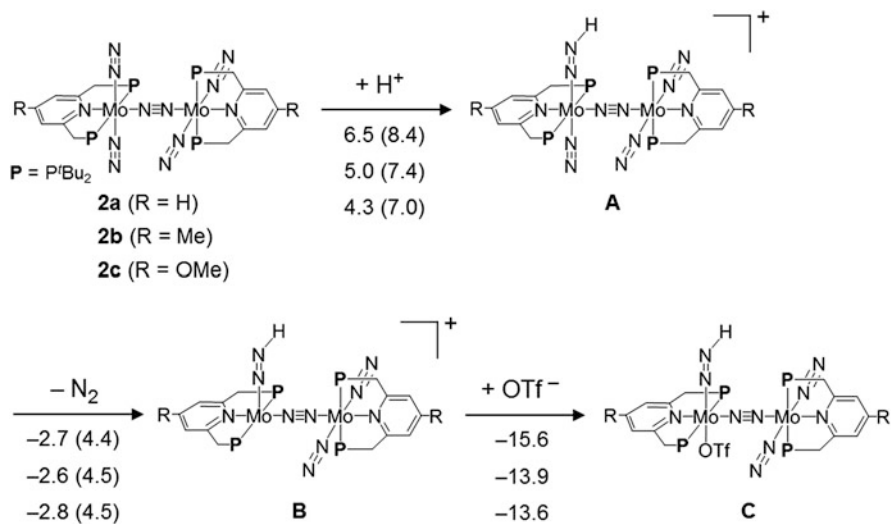
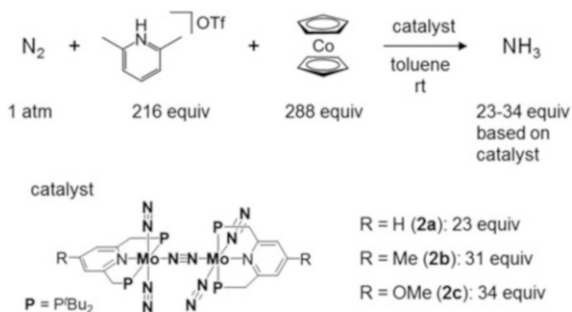


**Fig. 8** Energy profiles of the first protonation process of **2a-2c** calculated at the B3LYP\*/BS2//B3LYP\*/BS1 level of theory. Energy changes and activation energies (in parenthesis) are presented in kcal mol<sup>-1</sup>. Proton is transferred from LutH<sup>+</sup>

**Scheme 3** Transformation of N<sub>2</sub> into NH<sub>3</sub> catalyzed by dimolybdenum complexes bearing substituted PNP-type pincer ligands



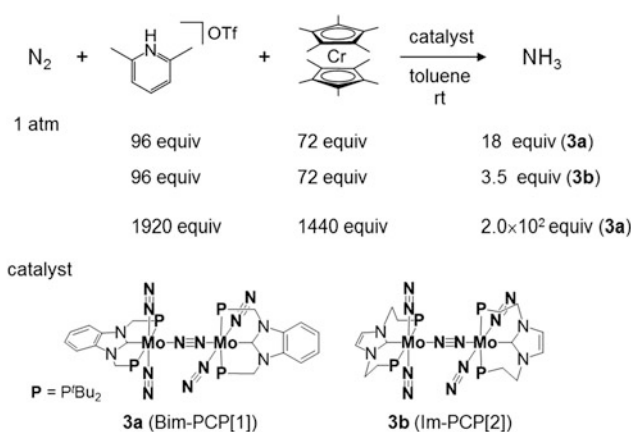
PNP facilitated the protonation of **2** and the methoxy-substituted **2c** would serve as an effective catalyst.

Nishibayashi and coworkers synthesized a series of substituted dinitrogen-bridged dimolybdenum complexes including **2b** and **2c**, and examined the catalytic transformation of N<sub>2</sub> into NH<sub>3</sub> using them as catalysts (Scheme 3) [49]. The N≡N stretching frequencies were observed at 1944 cm<sup>-1</sup> (**2a**), 1939 cm<sup>-1</sup> (**2b**), and 1932 cm<sup>-1</sup> (**2c**) in THF, which reasonably agreed with the computational trend. In accordance with the theory-based design, the methoxy-substituted **2c** produced the largest amount of NH<sub>3</sub> (34 equiv) based on the catalyst. They eventually succeeded in producing 52 equiv of NH<sub>3</sub> by using **2c** in the presence of larger amounts of [LutH]OTf (480 equiv) and CoCp<sub>2</sub> (360 equiv).

### 3.3 Dimolybdenum Complexes Bearing PCP-Type Pincer Ligands

Experimental and theoretical investigations on a series of dimolybdenum complexes bearing PNP-type pincer ligands have provided three important clues to designing a new pincer ligand for the development of more effective catalysts for nitrogen fixation. (1) As mentioned in the former section, enhancement of the backdonating ability of the Mo centers will accelerate the protonation of a terminal N<sub>2</sub> ligand, which is energetically less favorable. (2) The dinitrogen-bridged dimolybdenum (Mo–N≡N–Mo) structure must be retained because the intermetallic electron transfer via the bridging N<sub>2</sub> ligand is essential for the protonation of a terminal N<sub>2</sub> ligand. (3) The pincer ligand must be strongly coordinated to the Mo center in order to extend the lifetime of the catalyst. Dissociation of PNP from the Mo center was generally observed after the catalytic reaction, and it should lead to deactivation of the catalyst.

As a candidate pincer ligand that could meet the above requirements, Nishibayashi and coworkers adopted an *N*-heterocyclic carbene-based PCP-type pincer ligand [50]. *N*-heterocyclic carbene (NHC) is known to serve as a  $\sigma$  donor stronger than pyridine as well as a  $\pi$  acceptor [51–55], which is expected to coordinate to a metal center tightly. They newly synthesized two dinitrogen-bridged dimolybdenum complexes bearing two types of PCP pincer ligands containing 1,3-bis((di-*tert*-butylphosphino)methyl)benzimidazol-2-ylidene (Bim-PCP[1], **3a**) and 1,3-bis(2-(di-*tert*-butylphosphino)ethyl)imidazol-2-ylidene (Im-PCP[2], **3b**) (Scheme 4). These PCP ligands were prepared for investigating how the length of methylene linkers between the NHC framework and P<sup>*t*</sup>Bu<sub>2</sub> groups influences the catalytic activity for nitrogen fixation. The catalytic activities of **3a** and **3b** for nitrogen fixation were quite different. In the presence of 96 equiv of [LutH]OTf as a proton source and 72 equiv of decamethylchromocene (CrCp\*<sub>2</sub>) as a reducing agent, **3a** worked as a

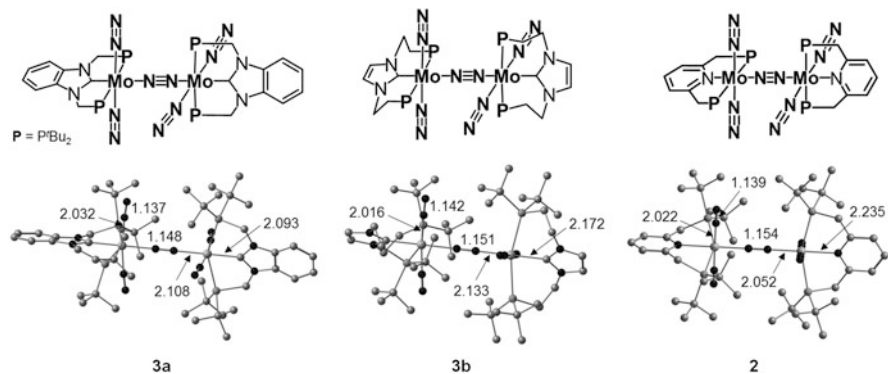


**Scheme 4** Transformation of N<sub>2</sub> into NH<sub>3</sub> catalyzed by dimolybdenum complexes bearing PCP-type pincer ligands

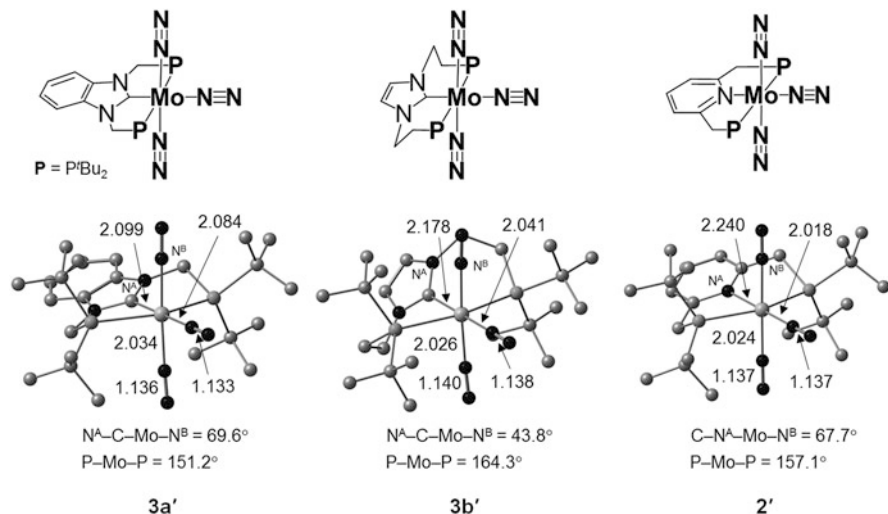
catalyst for nitrogen fixation to produce 18 equiv of  $\text{NH}_3$  based on the catalyst in toluene at room temperature. On the other hand, **3b** produced only 3.5 equiv of  $\text{NH}_3$  under the same reaction conditions. Surprisingly, the amount of generated  $\text{NH}_3$  reached  $2.0 \times 10^2$  equiv by using **3a** as a catalyst in the presence of larger amounts of  $[\text{LutH}]\text{OTf}$  (1920 equiv) and  $\text{CrCp}^*_2$  (1440 equiv), which is about an order of magnitude greater than the Mo–PNP complex **2a**. A sharp contrast between **3a** and **3b** was observed in the stability of the dimolybdenum structure. IR and  $^{15}\text{N}\{^1\text{H}\}$  NMR measurements in THF as a solvent revealed that **3b** was separated into two mononuclear Mo– $\text{N}_2$  complexes, such as  $[\text{Mo}(\text{N}_2)_3(\text{Im-PCP}[2])]$  **3b'** at room temperature.

Figure 9 depicts structures of **3a** and **3b** optimized at the B3LYP\* level of theory. The SDD and 6-31G\* basis sets (BS3) were employed for the Mo atoms and the others, respectively. The Mo–N bond distance for the bridging  $\text{N}_2$  ligand is 2.108 Å (**3a**) and 2.133 Å (**3b**), indicating a weaker binding of the bridging  $\text{N}_2$  ligand to the Mo atom in **3b**. In terms of the separation of a dimolybdenum complex into two mononuclear complexes, the bond dissociation energy (BDE) of the Mo– $\text{N}_2$ (bridging) bond of **3b** is calculated to be  $9.0 \text{ kcal mol}^{-1}$ , which is much lower than that of **3a** ( $18.8 \text{ kcal mol}^{-1}$ ). The low BDE of the Mo– $\text{N}_2$ (bridging) bond of **3b** can be associated with the IR and  $^{15}\text{N}\{^1\text{H}\}$  NMR spectra of **3b** measured in solution. Moreover, the low reactivity of **3b** for nitrogen fixation experimentally proves the importance of the dinuclear Mo– $\text{N}\equiv\text{N}$ –Mo structure for exhibiting the catalytic activity. In fact, DFT calculations demonstrated that mononuclear Mo– $\text{N}_2$  complexes such as  $[\text{Mo}(\text{N}_2)_3(\text{Bim-PCP}[1])]$  **3a'** and  $[\text{Mo}(\text{N}_2)_3(\text{Im-PCP}[2])]$  **3b'** cannot be protonated by  $\text{LutH}^+$  in a similar manner as  $[\text{Mo}(\text{N}_2)_3(\text{PNP})]$  **G** presented in the former section.

Optimized structures of **3a'** and **3b'** in Fig. 10 and their space-filling models in Fig. 11 explain how the length of  $\text{CH}_2$  linkers in the PCP ligands influences thermodynamic stability of the dimolybdenum structure. The Mo–N distances for the equatorial  $\text{N}_2$  ligand are 2.084 Å for **3a'** and 2.041 Å for **3b'**, and they are increased by 0.024 Å (**3a'**  $\rightarrow$  **3a**) and 0.092 Å (**3b'**  $\rightarrow$  **3b**) upon formation of the



**Fig. 9** Optimized structures of dimolybdenum complexes **3a**, **3b**, and **2** calculated at the B3LYP\*/BS3 level of theory. Bond distances are given in Å



**Fig. 10** Optimized structures of mononuclear Mo–N<sub>2</sub> complexes **3a'**, **3b'**, and **2'** calculated at the B3LYP\*/BS3 level of theory. Bond distances are given in Å

corresponding dimolybdenum complexes. Contrary to the large difference in the BDE of the Mo–N<sub>2</sub>(bridging) bond between **3a** and **3b**, the BDEs of the Mo–N<sub>2</sub>(equatorial) bond are almost identical for **3a'** and **3b'**, 21.2 and 21.5 kcal mol<sup>−1</sup>, respectively. These results would imply that steric hindrance between *tert*-butyl groups on the phosphorus atoms in the PCP ligands governs the thermodynamic stability of the Mo–N≡N–Mo structure. The bond angle of P–Mo–P in **3b'** (164.3°) is larger than that in **3a'** (151.2°) due to the longer CH<sub>2</sub> linkers in Im-PCP[2]. As shown in space-filling models in Fig. 11, the *tert*-butyl groups in Im-PCP[2] stick out along the equatorial N<sub>2</sub> ligand compared to those in Bim-PCP[1] so as to effectively protect the N<sub>2</sub> ligand utilized for the connection with another Mo unit. As a result, the Mo–N≡N–Mo structure of **3b** is destabilized by steric repulsions between the *tert*-butyl groups in two mononuclear Mo units facing each other.

Reaction pathways for the transformation of N<sub>2</sub> into NH<sub>3</sub> using **3a** as a catalyst are expected to be basically similar to those using **2** as a catalyst shown in Fig. 5. As the first step toward the mechanistic understanding of the nitrogen fixation catalyzed by **3a**, theoretical investigations [50] have been particularly focused on the first protonation process because this process involves one of the most energetically unfavorable reaction steps in the catalytic cycle proposed for **2**.

Figure 12 compares energy profiles of two possible reaction pathways of the first protonation process leading to intermediate **C** from **3a** and **2**. The pathway shown above (**Path I**) is the same one as shown in Fig. 5a, i.e. the transformation of N<sub>2</sub> starts with the protonation of a terminal N<sub>2</sub> ligand. The protonation of **3a** by LutH<sup>+</sup> (**3a** → **A**-PCP) is endothermic by 8.1 kcal mol<sup>−1</sup> with an activation energy of 8.3 kcal mol<sup>−1</sup>. This energy profile indicates that the backward reaction to release H<sup>+</sup> from N<sub>2</sub> would occur very rapidly due to a very low activation energy of 0.2 kcal mol<sup>−1</sup>, which is

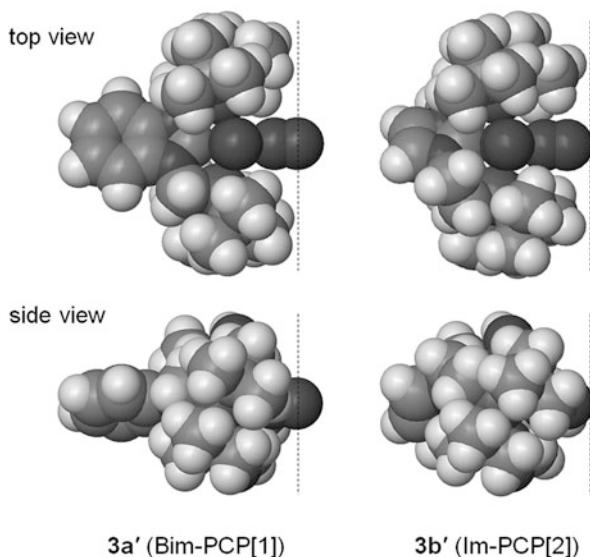


**Fig. 11** Space-filling models of **3a'** and **3b'**. *tert*-Butyl groups in Im-PCP[2] stick out to destabilize a dimolybdenum structure connected through the equatorial N<sub>2</sub> ligand

much lower than that in the Mo–PNP system (1.9 kcal mol<sup>-1</sup>). On the other hand, the following N<sub>2</sub> elimination step (A-PCP → B-PCP) is exothermic by 5.2 kcal mol<sup>-1</sup> with a low activation energy of 4.0 kcal mol<sup>-1</sup>. The low reactivity of terminal N<sub>2</sub> ligands in **3a** with LutH<sup>+</sup> appears to be strange because the NHC-based PCP ligands were expected to work as a strong electron donor compared with the pyridine-based PNP ones.

Another possible pathway to **C** (**Path II** in Fig. 12) involves the elimination of a terminal N<sub>2</sub> ligand in the initial complex **3a** (**2**) followed by the protonation of the remaining terminal N<sub>2</sub> ligand (**3a** (**2**) → **Q** → **B** → **C**). In the Mo–PCP system, the elimination reaction (**3a** → **Q**-PCP) proceeds in an endothermic way by 11.9 kcal mol<sup>-1</sup> and requires an activation energy of 19.7 kcal mol<sup>-1</sup>, which is acceptable for a reaction occurring at room temperature. In the Mo–PNP system, this reaction is endothermic by 14.4 kcal mol<sup>-1</sup> with an activation energy of 20.0 kcal mol<sup>-1</sup>. Since the energy changes calculated here correspond to the BDEs of the Mo–N<sub>2</sub>(terminal) bond in **3a** and **2**, the Mo–N<sub>2</sub>(terminal) bond in **3a** is 2.5 kcal mol<sup>-1</sup> weaker than that in **2**. The weaker Mo–N<sub>2</sub>(terminal) bond as well as the lower reactivity of **3a** with LutH<sup>+</sup> in **Path I** can be associated with less activation of the terminal N<sub>2</sub> ligands. The N≡N stretching frequencies of terminal N<sub>2</sub> ligands in **3a** and **2** were experimentally observed at 1978 and 1936 cm<sup>-1</sup> in the solid state, respectively, indicating that the terminal N<sub>2</sub> ligands in **3a** are less activated than those in **2**. The N≡N stretching frequencies calculated for **3a** (2012 cm<sup>-1</sup> in vacuo) and **2** (1993 cm<sup>-1</sup> in vacuo) reproduced the experimental trend; 1978 cm<sup>-1</sup> (KBr) for **3a** [50] and 1936 cm<sup>-1</sup> (KBr) for **2** [17]. The dissociation of the terminal N<sub>2</sub> ligand in **3a** markedly activates the remaining N<sub>2</sub> ligand at the *trans*





**Table 2** Changes in the NPA atomic charge ( $\Delta q$ ) in the coordination of the pincer ligands to the  $\text{Mo}(\text{N}_2)_3$  moiety

	$q(\mathbf{3a}')$	$q(\text{free})$	$\Delta q$	$q(\mathbf{2}')$	$q(\text{free})$	$\Delta q$	$q(\mathbf{3b}')$	$q(\text{free})$	$\Delta q$
Mo	-0.55	0	-0.55	-0.39	0	-0.39	-0.54	0	-0.54
$\text{N}_2$ ligands	-0.26	0	-0.26	-0.31	0	-0.31	-0.36	0	-0.36
$\text{P}'\text{Bu}_2$ (1)	+0.59	+0.30	+0.29	+0.60	+0.31	+0.29	+0.59	+0.29	+0.30
$\text{P}'\text{Bu}_2$ (2)	+0.59	+0.30	+0.29	+0.60	+0.31	+0.29	+0.59	+0.29	+0.30
NHC (Py)	-0.37	-0.60	+0.23	-0.50	-0.62	+0.12	-0.28	-0.58	+0.30

The values of  $\Delta q$  are obtained as differences of the NPA charges ( $q$ ) between mononuclear  $\text{Mo}-\text{N}_2$  complexes ( $\mathbf{3a}'$ ,  $\mathbf{2}'$ , and  $\mathbf{3b}'$ ) and free pincer ligands (Bim-PCP[1] for  $\mathbf{3a}'$ , PNP for  $\mathbf{2}'$ , and Im-PCP[2] for  $\mathbf{3b}'$ )

**Table 3** Selected bond distances ( $\text{\AA}$ ) in  $\mathbf{3a}'$  and  $\mathbf{2}'$  and bond dissociation energies of the  $\text{Mo}-\text{N}_2$ (equatorial) and  $\text{Mo}-\text{N}_2$ (axial) bonds ( $\text{kcal mol}^{-1}$ )

		$\mathbf{3a}'$	$\mathbf{2}'$
Distance	Mo-C(carbene)	2.099 (0.91)	
	Mo-N(pyridine)		2.240 (0.39)
	Mo- $\text{N}_2$ (equatorial)	2.084 (0.50)	2.018 (0.62)
	Mo- $\text{N}_2$ (axial)	2.034 (0.53)	2.024 (0.54)
BDE	Mo- $\text{N}_2$ (equatorial)	21.2	30.1
	Mo- $\text{N}_2$ (axial)	12.5	14.0

The values in parenthesis present the Mayer bond order

properties of mononuclear  $\text{Mo}-\text{N}_2$  complexes [ $\text{Mo}(\text{N}_2)_3(\text{Bim-PCP}[1])$ ]  $\mathbf{3a}'$  and [ $\text{Mo}(\text{N}_2)_3(\text{PNP})$ ]  $\mathbf{2}'$  have been investigated in detail.

Table 2 compares the electron-donating ability of Bim-PCP[1] and PNP in terms of the NPA charge. Changes in the NPA charge ( $\Delta q$ ) between the  $\text{Mo}-\text{N}_2$  complexes and the free pincer ligands were calculated for estimating the amount of electron donated from the pincer ligands to the Mo center and three  $\text{N}_2$  ligands during complexation. The  $\Delta q$  values were independently calculated for four moieties in  $\mathbf{3a}'$  ( $\mathbf{2}'$ ); the NHC (pyridine) moiety with the  $\text{CH}_2$  linkers, the  $\text{P}'\text{Bu}_2$  groups, the Mo atom, and the  $\text{N}_2$  ligands. The NPA charges of the Mo and  $\text{N}_2$  ligands were set to be zero for the free ligands, and hence  $\Delta q$  of the  $\text{Mo}(\text{N}_2)_3$  moiety is identical to the sum of the NPA charges assigned to this moiety. As shown in Table 2, Bim-PCP[1] and PNP donate  $0.81e^-$  and  $0.70e^-$  to the  $\text{Mo}(\text{N}_2)_3$  moiety during complexation, respectively. From a viewpoint of atomic charge, the NHC-based pincer ligand surely works as a strong electron-donor compared with the pyridine-based one. The electron-donating ability of the pincer ligands is governed by the

NHC and pyridine moieties because  $\Delta q$  of the  $P^tBu_2$  groups are identical (+0.29) in both Bim-PCP[1] and PNP. The difference in the amount of the donated electron comes from the  $\Delta q$  values of the NHC moiety (+0.23) and the pyridine moiety (+0.12).

Optimized structures in Fig. 10 and BDEs of the Mo–N<sub>2</sub>(equatorial) and Mo–N<sub>2</sub>(axial) bonds also provide useful information on the evaluation of the electron-donating ability of the pincer ligands. Table 3 summarizes geometric parameters around the Mo center in **3a'** and **2'**, together with the BDEs of the Mo–N<sub>2</sub> bonds. The Mo–C(carbene) bond distance of 2.099 Å in **3a'** is much shorter than the Mo–N(pyridine) bond distance of 2.240 Å in **2'**, indicating a stronger binding of Bim-PCP[1] to the Mo center. The Mayer bond orders (b.o.) [56] of the Mo–C(carbene) bond (0.91) and Mo–N(pyridine) bond (0.39) also suggest a strong bonding interaction between the Mo center and Bim-PCP[1]. The solid connection between Mo and Bim-PCP[1] well explains the experimental result that **3a** has a long lifetime as a catalyst for nitrogen fixation with a high turnover number of NH<sub>3</sub> production compared with **2**. On the other hand, the Mo–N<sub>2</sub>(equatorial) bond is weakened by a strong *trans* influence of the NHC moiety. The Mo–N<sub>2</sub>(equatorial) bond distance

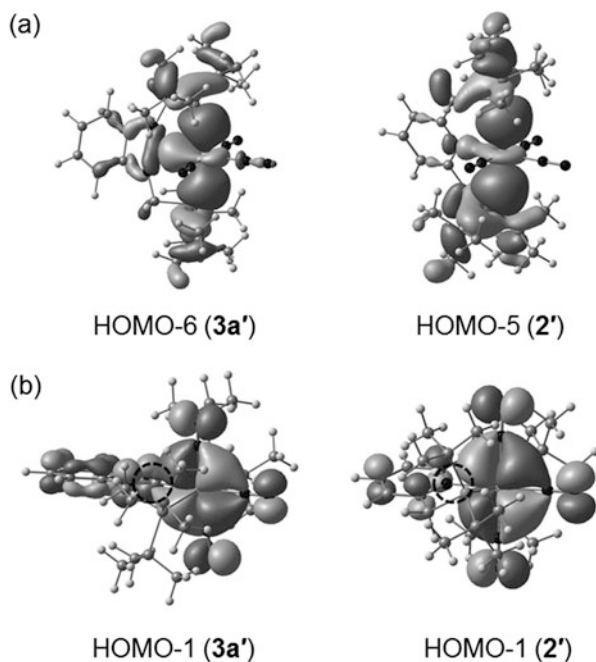


**Fig. 13** Spatial distribution of frontier orbitals of **3a'** and **2'**: (a) HOMO-6 (**3a'**) and HOMO-5 (**2'**) contributing to  $\sigma$  donation from the pincer ligand to Mo, and (b) HOMO-1 contributing to  $\pi$  backdonation from Mo to both equatorial and axial N<sub>2</sub> ligands. An “extra” backdonation from Mo to the pincer ligand is observed only in **3a'** (dashed circle). The molecular structures in (b) are rotated by 90° along the axis containing the Mo atom and the equatorial N<sub>2</sub> ligand from those in (a)

of 2.084 Å (b.o. = 0.50) in **3a'** is much longer than that of 2.018 Å (b.o. = 0.62) in **2'**. The elongated Mo–N<sub>2</sub>(equatorial) bond in **3a'** results in a low BDE of 21.2 kcal mol<sup>-1</sup> compared with that of **2'** (30.1 kcal mol<sup>-1</sup>). It is notable that the coordination of Bim-PCP[1] influences not only the equatorial N<sub>2</sub> ligand but also the axial N<sub>2</sub> ligands so as to weaken all Mo–N<sub>2</sub> bonds. The Mo–N<sub>2</sub>(axial) bond distances (b.o.) are 2.034 Å (0.53) for **3a'** and 2.024 Å (0.54) for **2'**, while the BDEs are 12.5 kcal mol<sup>-1</sup> for **3a'** and 14.0 kcal mol<sup>-1</sup> for **2'**. Dimolybdenum complexes **3a** and **2** show a similar trend in the BDEs of the Mo–N<sub>2</sub>(bridging) and Mo–N<sub>2</sub>(terminal) bonds. The BDEs of the Mo–N<sub>2</sub>(bridging) and Mo–N<sub>2</sub>(terminal) bonds are 18.8 and 11.9 kcal mol<sup>-1</sup> for **3a**, respectively, both of which are lower than those for **2** (24.9 and 14.4 kcal mol<sup>-1</sup>).

The influence of coordination of the NHC-based PCP ligand to the Mo center can be rationalized by spatial distribution of frontier orbitals responsible for the Mo–C (carbene) and Mo–N<sub>2</sub> bonds. The HOMO-6 (**3a'**) and HOMO-5 (**2'**) in Fig. 13a contribute to a  $\sigma$  bond between the Mo center and the carbene C atom (or the pyridine N atom). The large amplitude of the lobe observed between Mo and C implies a strong  $\sigma$ -donating ability of Bim-PCP[1] compared to PNP. The HOMO-1 in Fig. 13b shows

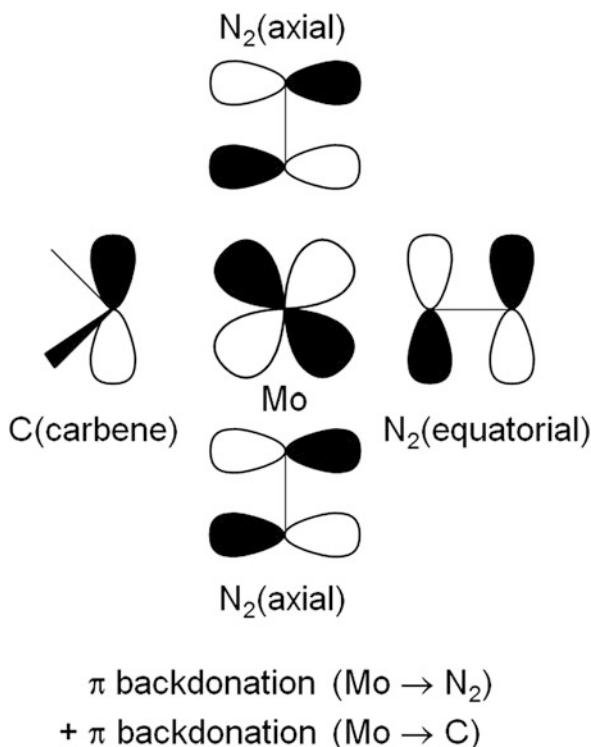


**Fig. 14** Schematic drawing of the  $\pi$ -bonding interaction between the Mo atom and ligands in the HOMO-1 of **3a'**

$\pi$  backdonation from an out-of-plane  $d$  orbital of Mo to a  $\pi^*$  orbital of  $N_2$  ligands. In general the  $\pi$  backdonation from metal to  $N_2$  plays an essential role in the binding and activation of  $N_2$  upon formation of a metal– $N_2$  complex. It should be emphasized here that *both* equatorial and axial  $N_2$  ligands are affected by occupation of the HOMO-1. A large difference between the HOMO-1 of **3a'** and **2'** is the presence of  $\pi$  backdonation from Mo to the vacant  $p$  orbital of the carbene C atom in **3a'**. The weak Mo– $N_2$  bonds in **3a'** can be ascribed to the  $\pi$ -accepting ability of the NHC that decreases the propensity of Mo for  $\pi$  backdonation to both equatorial and axial  $N_2$  ligands (Fig. 14). Actually, as presented in Table 2,  $\Delta q$  of the three  $N_2$  ligands in **3a'** ( $-0.26$ ) is smaller than that in **3b'** ( $-0.31$ ) despite the higher electron-donating ability of Bim-PCP[1]. Whereas the  $\pi$  backdonation to the NHC weakens the Mo– $N_2$  bonding in **3a'**, it also contributes to the solid connection between Mo and Bim-PCP[1].

On the other hand, the contribution of the  $\pi$  backdonation seems to be less significant for the bonding between Mo and Im-PCP[2] in [Mo( $N_2$ )<sub>3</sub>(Im-PCP[2])] **3b'**. As shown in Fig. 10, the coordination of the NHC moiety of Im-PCP[2] to Mo is highly twisted due to the ethylene linkers; the dihedral angle of  $N^A-C-Mo-N^B$  in **3b'** ( $43.8^\circ$ ) is much smaller than that in **3a'** ( $69.6^\circ$ ) and the dihedral angle of  $C-N^A-Mo-N^B$  in **2'** ( $67.7^\circ$ ). Because the overlap between the vacant  $p$  orbital of the carbene C atom and the out-of-plane  $d$  orbital of the Mo atom is maximized at the  $N^A-C-Mo-N^B$  dihedral angle of  $90^\circ$ , the twisted coordination of the NHC moiety decreases the propensity of Mo for  $\pi$  backdonation to the NHC. As a result, Im-PCP[2] only exhibits a very strong  $\sigma$ -donating ability and donates  $0.90e^-$  to the Mo atom during complexation. The gross NPA charge on the three  $N_2$  ligands ( $-0.36$ ) as well as a high BDE of the Mo– $N_2$ (axial) bond of **3b'** ( $14.3 \text{ kcal mol}^{-1}$ ) indicates that the coordination of Im-PCP[2] effectively activates the  $N_2$  ligands compared with Bim-PCP[1]. However, the  $N_2$  ligands in the mononuclear Mo complex **3b'** are not sufficiently activated for the reaction with  $LutH^+$ , as mentioned in Sect. 3.1. Again, the low catalytic activity of **3b** for nitrogen fixation would stem from the thermodynamic instability of the Mo– $N\equiv N$ –Mo structure caused by the ethylene linkers of Im-PCP[2].

## 4 Conclusions

In this chapter, we have overviewed recent topics in the mechanistic understanding of artificial nitrogen fixation catalyzed by mono- and dimolybdenum complexes from a theoretical point of view. The Yandulov–Schrock cycle proposed for the mononuclear Mo–triamidoamine system involves alternating protonation/reduction steps via the formation of a Mo–nitride ( $Mo\equiv N$ ) intermediate. The validity of the Yandulov–Schrock cycle has been thoroughly investigated both experimentally and theoretically, and this cycle is now accepted as an established catalytic mechanism of nitrogen fixation at a single metal site.

In the dimolybdenum Mo–PNP system, a dinuclear Mo–NN–Mo structure plays a decisive role in the transformation of  $N_2$  into  $NH_3$ , particularly in the protonation of

coordinated  $N_2$ . While the catalytic cycle deduced from experimental and theoretical findings is analogous to the Yandulov–Schrock cycle in that one of the terminal  $N_2$  ligands at an Mo unit of **2** is converted to two molecules of  $NH_3$  via the formation of a Mo–nitride intermediate, a main difference from the Mo–triamidoamine system is that the other Mo unit works as a mobile ligand to donate electron in the first protonation process. Intermetallic electron transfer between the two Mo units through the bridging  $N_2$  ligand efficiently activates the terminal  $N_2$  ligand to be protonated, and opens the path to further protonation and reduction steps leading to the generation of  $NH_3$ . Based on the catalytic mechanism proposed for the Mo–PNP system, dimolybdenum complexes bearing substituted PNP–pincer ligands were designed to achieve higher catalytic activity than the original complex. As predicted by theoretical calculations, the introduction of electron-donating groups to the pyridine moiety of the pincer ligand improved the turnover number of  $NH_3$  production from 23 (**2a**) to 52 (**2c**) equiv/catalyst.

As an alternative strategy for enhancing the electron-donating ability of pincer ligands, dimolybdenum complexes bearing *N*-heterocyclic carbene-based PCP-type pincer ligands (Bim-PCP[1] and Im-PCP[2]) have been newly designed and synthesized. Dimolybdenum complex **3a** bearing Bim-PCP[1] exhibited high catalytic activity for nitrogen fixation, where up to 200 equiv of  $NH_3$  was produced on the catalyst. On the other hand, **3b** bearing Im-PCP[2] exhibited very low catalytic activity. Separation of **3b** into mononuclear Mo– $N_2$  complexes observed in solution was rationalized by a low bond dissociation energy calculated for the Mo– $N_2$ (bridging) bond of **3b**. The large differences in catalytic activity and behavior in solution testify the theory-based proposal that the dinuclear Mo–NN–Mo structure must be preserved at a certain stage of the nitrogen fixation in the Mo–PCP system (probably also the Mo–PNP system). Calculated reaction pathways of the first protonation process toward the transformation of  $N_2$  into  $NH_3$  by **3a** demonstrated that a weak Mo– $N_2$ (terminal) bond of **3a** may be associated with the high catalytic activity. The strong  $\sigma$  donation as well as  $\pi$  backdonation between Mo and Bim-PCP[1] provides a solid connection between the metal center and pincer ligand in **3a**, and would contribute to the long lifetime of **3a** as a catalyst. The catalytic activity of dimolybdenum complexes bearing pincer ligands is exquisitely controlled by both geometric and electronic factors. The former mainly influences the thermodynamic stability of the dimolybdenum structure through steric hindrance stemmed from the length of the phosphorus arms. The latter affects the binding of a pincer ligand to Mo through the  $\sigma$  donation and  $\pi$  backdonation. A pincer ligand with a strong  $\sigma$ -donating ability binds to Mo tightly, but its pronounced *trans* influence can decrease the thermodynamic stability of the dimolybdenum structure. The  $\pi$ -accepting ability of a pincer ligand should also be considered in tuning the catalytic activity of a dimolybdenum complex because the backdonation from Mo to the pincer ligand can weaken all the Mo– $N_2$  bonds.

The mechanism of nitrogen fixation is quite complicated because at least six pairs of proton and electron must take part in the transformation of  $N_2$  into  $NH_3$ . Therefore, the catalytic reaction pathway should compete with unexpected side reactions that limit the turnover number of  $NH_3$  production, but they are often

difficult to observe and characterize experimentally. Automated screening techniques can be applied for locating such undesired pathways leading to deactivation of catalysts. For example, a heuristics-guided protocol for the automatic exploration of chemical reaction spaces developed by Reiher and coworkers [38] has recently been exploited for finding possible elementary reactions in the Mo–triamidoamine system. In their study, about 10,000 intermediates and more than 2000 transition states were optimized using a simplified model complex of **1**. Computational and experimental researches in close coordination become increasingly important for accelerating the development of more effective nitrogen fixation catalysts working under ambient reaction conditions.

## References

1. Burgess BK, Lowe DJ (1996) *Chem Rev* 96:2983–3011
2. Einsle O, Tezcan FA, Andrade SLA, Schmid B, Yoshida M, Howard JB, Rees DC (2002) *Science* 297:1696–1700
3. Spatzal T, Aksoyoglu M, Zhang L, Andrade SLA, Schleicher E, Weber S, Rees DC, Einsle O (2011) *Science* 334:940
4. Lancaster KM, Roemelt M, Ettenhuber P, Hu Y, Ribbe MW, Neese F, Bergmann U, DeBeer S (2011) *Science* 334:974–977
5. Hoffman BM, Lukoyanov D, Yang Z-Y, Dean DR, Seefeldt LC (2014) *Chem Rev* 114:4041–4062
6. Liu H (2013) *Ammonia synthesis catalysts: innovation and practice*. Chemical Industry Press & World Scientific, Singapore
7. Allen AD, Senoff CV (1965) *Chem Commun* 24:621–622
8. Chatt J, Dilworth JR, Richards RL (1978) *Chem Rev* 78:589–625
9. Hidayi M, Mizobe Y (1995) *Chem Rev* 95:1115–1133
10. MacKay BA, Fryzuk MD (2004) *Chem Rev* 104:385–401
11. Nishibayashi Y (2012) *Dalton Trans* 41:7447–7453
12. Tanabe Y, Nishibayashi Y (2013) *Coord Chem Rev* 257:2551–2564
13. Nishibayashi Y (2015) *Inorg Chem* 54:9234–9247
14. Khoenkhoen N, de Bruin B, Reek JNH, Dzik WI (2015) *Eur J Inorg Chem* 567–598
15. Tanaka H, Nishibayashi Y, Yoshizawa K (2016) *Acc Chem Res* 49:987–995
16. Yandulov DV, Schrock RR (2003) *Science* 301:76–78
17. Arashiba K, Miyake Y, Nishibayashi Y (2011) *Nat Chem* 3:120–125
18. Anderson JS, Rittle J, Peters JC (2013) *Nature* 501:84–87
19. Del Castillo TJ, Thompson NB, Peters JC (2016) *J Am Chem Soc* 138:5341–5350
20. Ung G, Peters JC (2015) *Angew Chem Int Ed* 54:532–535
21. Arashiba K, Kinoshita E, Kuriyama S, Eizawa A, Nakajima K, Tanaka H, Yoshizawa K, Nishibayashi Y (2015) *J Am Chem Soc* 137:5666–5669
22. Kuriyama S, Arashiba K, Nakajima K, Matsuo Y, Tanaka H, Ishii K, Yoshizawa K, Nishibayashi Y (2016) *Nat Commun* 7:12181
23. Del Castillo TJ, Thompson NB, Suess DLM, Ung G, Peters JC (2015) *Inorg Chem* 54:9256–9262
24. Kuriyama S, Arashiba K, Tanaka H, Matsuo Y, Nakajima K, Yoshizawa K, Nishibayashi Y (2016) *Angew Chem Int Ed* 55:14291–14295
25. Hill PJ, Doyle LR, Crawford AD, Myers WK, Ashley AE (2016) *J Am Chem Soc* 138:13521–13524
26. Schrock RR (2008) *Angew Chem Int Ed* 47:5512–5522
27. Yandulov DV, Schrock RR (2005) *Inorg Chem* 44:1103–1117
28. Kinney RA, McNaughton RL, Chin JM, Schrock RR, Hoffman BM (2011) *Inorg Chem* 50:418–420
29. Munisamy T, Schrock RR (2012) *Dalton Trans* 41:130–137

30. Cao Z, Zhou Z, Wan H, Zhang Q (2005) *Int J Quantum Chem* 103:344–353
31. Studt F, Tuzcek F (2005) *Angew. Chem Int Ed* 44:5639–5642
32. Magistrato A, Robertazzi A, Carloni P (2007) *J Chem Theory Comput* 3:1708–1720
33. Reiher M, Le Guennic B, Kirchner B (2005) *Inorg Chem* 44:9640–9642
34. Le Guennic B, Kirchner B, Reiher M (2005) *Chem Eur J* 11:7448–7460
35. Schenk S, Le Guennic B, Kirchner B, Reiher M (2008) *Inorg Chem* 47:3634–3650
36. Schenk S, Kirchner B, Reiher M (2009) *Chem Eur J* 15:5073–5082
37. Schenk S, Reiher M (2009) *Inorg Chem* 48:1638–1648
38. Bergeler M, Simm GN, Proppe J, Reiher M (2015) *J Chem Theory Comput* 11:5712–5722
39. Tian Y-H, Pierpont AW, Batista ER (2014) *Inorg Chem* 53:4177–4183
40. Tanaka H, Arashiba K, Kuriyama S, Sasada A, Nakajima K, Yoshizawa K, Nishibayashi Y (2014) *Nat Commun* 5:3737
41. Reiher M, Salomon O, Hess BA (2001) *Theor Chem Acc* 107:48–55
42. Reiher M (2002) *Inorg Chem* 41:6928–6935
43. Schrock RR (2005) *Acc Chem Res* 38:955–962
44. Thimm W, Gradert C, Broda H, Wennmohs F, Neese F, Tuzcek F (2015) *Inorg Chem* 54:9248–9255
45. Reed AE, Curtiss LA, Weinhold F (1988) *Chem Rev* 88:899–926
46. Deeth RJ, Field CN (1994) *J Chem Soc Dalton Trans* 1943–1948
47. Studt F, Tuzcek F (2006) *J Comput Chem* 27:1278–1291
48. Tanaka H, Ohsako F, Seino H, Mizobe Y, Yoshizawa K (2010) *Inorg Chem* 49:2464–2470
49. Kuriyama S, Arashiba K, Nakajima K, Tanaka H, Kamaru N, Yoshizawa K, Nishibayashi Y (2014) *J Am Chem Soc* 136:9719–9731
50. Eizawa A, Arashiba K, Tanaka H, Kuriyama S, Matsuo Y, Nakajima K, Yoshizawa K, Nishibayashi Y (2017) *Nat Commun* 8:14874
51. Hopkinson MN, Richter C, Schedler M, Glorius F (2014) *Nature* 510:485–496
52. Trnka TM, Grubbs RH (2001) *Acc Chem Res* 34:18–29
53. Ohki Y, Seino H (2016) *Dalton Trans* 45:874–880
54. Comas-Vives A, Harvey JN (2011) *Eur J Inorg Chem* 5025–5035
55. Nelson DJ, Nolan SP (2013) *Chem Soc Rev* 42:6723–6753
56. Mayer I (1983) *Chem Phys Lett* 97:270–274



# Sulfur-Supported Iron Complexes for Understanding N<sub>2</sub> Reduction

Amy L. Speelman and Patrick L. Holland

**Abstract** This chapter focuses on the use of synthetic complexes for modeling iron sites in the iron-molybdenum nitrogenase enzyme, particularly on those with sulfur donors in the coordination sphere. This is an under-explored area that has promise to elucidate the way that Fe–S bonds contribute to N<sub>2</sub> binding and activation. We review iron complexes with sulfide, thiolate, and thioether-containing supporting ligands and discuss the binding of N<sub>2</sub> as well as reduced species such as hydrazine and diazene. The structures, spectroscopy, reactions, and other properties of key complexes are described, including recent results.

**Keywords** Dinitrogen • Iron • Nitrogenase • Sulfur

## Contents

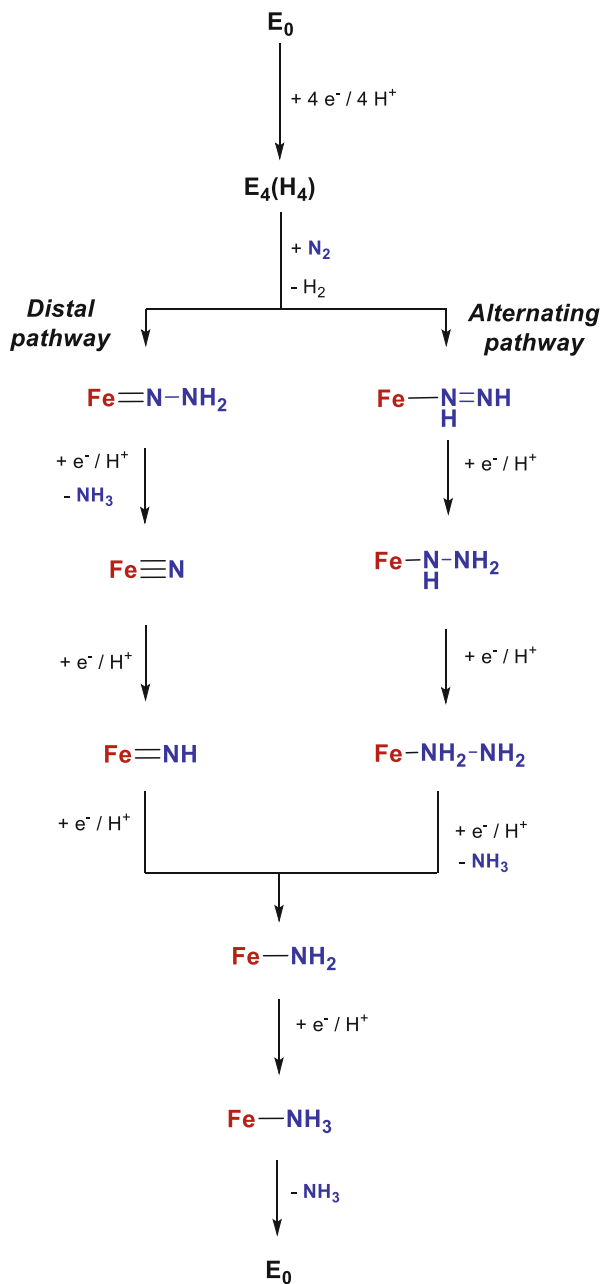
1	N <sub>2</sub> Reduction in Biological Systems .....	198
2	Fe–N <sub>2</sub> Complexes with S Ligands .....	201
2.1	N <sub>2</sub> Complexes with Thioether-Containing Ligands .....	202
2.2	N <sub>2</sub> Complexes with Thiolate Ligands .....	203
2.3	Interaction of N <sub>2</sub> with Iron–Sulfide Clusters .....	204
3	Fe Complexes with N <sub>x</sub> H <sub>y</sub> Ligands .....	205
3.1	N <sub>x</sub> H <sub>y</sub> Complexes with Iron–Sulfide Clusters .....	205
3.2	N <sub>x</sub> H <sub>y</sub> Complexes with Thioether/Thiolate Ligands .....	206
3.3	N <sub>x</sub> H <sub>y</sub> Complexes with Thiolate Ligands .....	208
3.4	N <sub>x</sub> H <sub>y</sub> Complexes with Thiolate and Cp Ligands .....	209
4	Conclusions .....	210
	References .....	211



that are based on the Lowe–Thorneley kinetic scheme [2, 15], which specifies that from the resting state ( $E_0$ ), four electrons and four protons are added to give the intermediate  $E_4$ , which is the state that binds N<sub>2</sub>. Electron-nuclear double resonance (ENDOR) studies indicate that  $E_4$  has two hydrides bridging between iron centers, implying that the other two H atoms are probably protonated sulfides [16–18]. According to the Lowe–Thorneley model, the reversible reductive elimination of H<sub>2</sub> is accompanied by N<sub>2</sub> binding to iron [15]. Seefeldt and Hoffman propose that the bound N<sub>2</sub> is immediately converted to a species at the diazene redox level, although the steps in this transformation and the structure of the resulting “N<sub>2</sub>H<sub>2</sub>” species are not clear. The sites of subsequent protonation are also unclear, but the possibilities are typically categorized as distal and alternating (see Fig. 2). In the distal pathway, proposed by analogy to small molecule molybdenum complexes [19, 20], the first molecule of ammonia is released following three protonations at the distal nitrogen. This results in the formation of a nitride that can accept three more protons and electrons to release a second equivalent of ammonia. In the alternating pathway, each N atom is protonated in turn to eventually yield a hydrazine species that undergoes N–N bond cleavage. The alternating mechanism has generally been favored for the FeMoco on the basis that diazene and hydrazine (which are intermediates unique to the alternating pathway) are also nitrogenase substrates, and that hydrazine is released from the enzyme during turnover under some conditions [5]. Although species following N–N cleavage (which are common to both the alternating and distal pathways) have been trapped and characterized by pulsed EPR [5], no intermediate that is unique to the distal or alternating pathway has been observed in the FeMoco. Furthermore, a recent study of a model complex suggests that crossover between intermediates in the distal and alternating pathways should also be considered [21]. Within each limiting mechanism, there are additional ambiguities to be resolved because the intermediates may be terminally bound or bridging between metal centers, and their coordination modes could change throughout the catalytic cycle. Thus, many questions remain about the mechanism of NH<sub>3</sub> formation, even in the best-understood nitrogenase.

Only the resting state of the FeMoco has been structurally characterized. Rearrangement of synthetic iron–sulfur clusters upon ligand binding or redox changes is known [22–24], and therefore it is reasonable to predict that internal bond cleavage might occur upon reduction and N<sub>2</sub> binding in the FeMoco. Additional evidence for this hypothesis comes from experimental studies of nitrogenase. For example, in the crystal structure of the CO-inhibited form of nitrogenase, one of the central bridging sulfides (S2B; see Fig. 1) is replaced by CO [25]. When CO is removed and the enzyme is exposed to catalytic conditions, the bridging sulfide is reincorporated and the enzyme regains full activity. In another example, Rees and coworkers replaced S2B with a selenide. Crystallographic studies demonstrated that the selenide migrates to the other central “belt” sites and is eventually extruded from the active site (with reincorporation of a sulfide) during acetylene reduction [26]. The fate of the released S<sup>2-</sup> or Se<sup>2-</sup> and the mechanism of the exchange processes in these experiments are not yet clear. Nevertheless, these studies demonstrate that sulfide dissociation and cluster rearrangement certainly can occur during turnover. However, <sup>13</sup>C and <sup>14</sup>C labeling

**Fig. 2** Distal and alternating pathways for  $N_2$  reduction. Although all intermediates are drawn as terminally coordinated, bridging coordination modes are also plausible



studies confirm that the central carbide does not exchange during reduction of  $C_2H_2$ , CO, or  $N_2$  [27].

Given the uncertainty surrounding the mechanism of nitrogenase and its structure during turnover, many different intermediates could be postulated. A wide variety of mechanistic steps have been proposed based on DFT calculations [28–39]. Synthetic model compounds have been used to test the feasibility of some of these proposed chemical transformations. Iron complexes that cleave N<sub>2</sub> [40–43] as well as iron complexes that catalytically reduce N<sub>2</sub> to ammonia and/or silylamine [44–49] have been reported. However, these compounds and others that bind N<sub>2</sub> and/or partially reduced N<sub>2</sub> species (N<sub>x</sub>H<sub>y</sub>;  $x = 1-2$ ,  $y = 1-4$ ) typically contain phosphorus, nitrogen, and/or carbon donors and it is unclear what effects these abiological ligands have on catalysis. Nitrogenase-relevant compounds with these types of ligand frameworks have been reviewed elsewhere [20, 50–56].

Iron complexes with sulfur supporting ligands that bind N<sub>x</sub>H<sub>y</sub> fragments can give distinctive insight into the reactivity patterns that can be expected in the FeMoco [57]. As shown in the examples below, the sulfur donors may serve as functional models for sulfides, for example, by facilitating proton delivery or by stabilizing N<sub>x</sub>H<sub>y</sub> species through hydrogen bonding interactions. Furthermore, these complexes can replicate the weak ligand field, the low coordination number, and the high-spin electronic configuration of the iron sites in the FeMoco. Complexes containing sulfides are the most relevant to nitrogenase, but more often thiolates are used as anionic donors. A number of iron complexes with thioether ligands, which model protonated sulfides in nitrogenases, are also known. Here, we discuss these iron complexes with sulfur-containing ligands that bind N<sub>2</sub> and N<sub>x</sub>H<sub>y</sub> fragments in the context of nitrogenase modeling.

## 2 Fe–N<sub>2</sub> Complexes with S Ligands

A variety of coordination modes have been proposed for N<sub>2</sub> in the FeMoco [30, 33, 58]. These include bridging, terminal, and side-on coordination, in some cases involving rearrangement of the cofactor. Model complexes can illustrate the plausibility of N<sub>2</sub> binding in these coordination modes in a sulfur-rich coordination environment.

The interaction of N<sub>2</sub> with transition metals consists primarily of  $\pi$ -backbonding from filled iron d-orbitals into the empty  $\pi^*$  orbitals of N<sub>2</sub>, which results in a weakening of the N–N triple bond [50, 59]. The deviation of the N–N bond length and/or N–N stretching frequency from the values for free N<sub>2</sub> can be used as measures of the degree of activation of the N–N bond. The parameters for structurally characterized N<sub>2</sub> complexes with sulfur supporting ligands are given in Table 1. These complexes, along with other species that can be shown by reactivity or spectroscopic studies to bind N<sub>2</sub>, are discussed below.

**Table 1** Key bond lengths and N≡N stretching frequencies of N<sub>2</sub> complexes with sulfur donors

Complex	Fe–N (Å)	N–N (Å)	$\nu_{\text{NN}}$ (cm <sup>-1</sup> )	Ref.
Free N <sub>2</sub>	–	1.098	2,359	[60]
<i>Thioether complexes</i>				
[Fe( <sup>i</sup> PrPDI)(N <sub>2</sub> )] ( <b>1</b> )	1.797(2) 1.799(2)	1.118(3) 1.111(3)	2,045	[61]
[Fe(SiP <sup>i</sup> Pr <sub>3</sub> )(N <sub>2</sub> ) <sup>+</sup> ( <b>2</b> )	1.913(2)	1.091(3)	2,143	[62]
[Fe(SiP <sup>i</sup> Pr <sub>2</sub> S <sup>Ad</sup> )(N <sub>2</sub> ) <sup>+</sup> ( <b>3</b> )	1.954(3)	1.037(5)	2,156	[63]
[Fe(SiP <sup>i</sup> PrS <sup>Ad</sup> <sub>2</sub> )(H)(N <sub>2</sub> )] ( <b>5</b> )	1.828(2)	1.116(3)	2,060	[63]
<i>Thiolate complexes</i>				
[Fe <sup>I</sup> (N <sub>2</sub> )(μ-SAr)Fe <sup>I</sup> (N <sub>2</sub> ) <sup>-</sup> ( <b>7</b> )	1.808(1) 1.822(1)	1.128(1) 1.122(2)	2,017, 1,979	[64]
[Fe <sup>I</sup> (N <sub>2</sub> )(μ-SAr)Fe <sup>II</sup> (N <sub>2</sub> )] ( <b>8</b> )	1.854(7)	1.05(1)	2,070, 1,983	[64]
[Fe <sup>II</sup> (N <sub>2</sub> )(μ-SAr)Fe <sup>II</sup> (N <sub>2</sub> ) <sup>+</sup> ( <b>9</b> )	1.889(3) 1.917(3)	1.048(5) 1.034(5)	2,129	[64]
[Fe <sup>I</sup> (N <sub>2</sub> )(H)(μ-SAr)Fe <sup>II</sup> (N <sub>2</sub> ) <sup>-</sup> ( <b>10</b> )	1.804(3) 1.819(3)	1.124(4) 1.120(6)	1,981, 2,044	[64]
[Fe <sup>II</sup> (N <sub>2</sub> )(H)(μ-SAr)Fe <sup>II</sup> (N <sub>2</sub> )] ( <b>11</b> )	1.8392(9)	1.110(1)	2,036, 2,096	[64]
[Fe(L)(N <sub>2</sub> ) <sup>2-</sup> ( <b>13</b> )	1.790(5)	1.132(8)	1,880	[65]

Values in parentheses are estimated standard deviations (esd)

## 2.1 N<sub>2</sub> Complexes with Thioether-Containing Ligands

The first structurally characterized iron–N<sub>2</sub> complex with any type of sulfur donor was the tetrahydrothiophene (THT) adduct of the complex [Fe(<sup>i</sup>PrPDI)(N<sub>2</sub>)] (**1**) [61] (Fig. 3). Peters and coworkers later reported a set of thioether derivatives of the complex [Fe(SiP<sup>i</sup>Pr<sub>3</sub>)(N<sub>2</sub>)<sup>+</sup> (**2**) [62, 63]. When a thioether was incorporated in place of one of the phosphine ligands in **2**, the complex was still able to bind N<sub>2</sub>, although the replacement of the phosphine with thioether made the N<sub>2</sub> more labile and slightly less activated, as demonstrated by the increase in  $\nu_{\text{NN}}$  from 2,143 cm<sup>-1</sup> in the parent complex **2** to 2,156 cm<sup>-1</sup> in **3**. When a second phosphine was replaced with a thioether, N<sub>2</sub> binding was no longer observed. Addition of a hydride led to N<sub>2</sub> binding to both the mono and bis(thioether) complexes and a more activated N<sub>2</sub> ligand as compared to analogous complexes without a hydride ligand, as shown by the 101 cm<sup>-1</sup> decrease in  $\nu_{\text{NN}}$  in **4** ( $\nu_{\text{NN}} = 2,055$  cm<sup>-1</sup>) as compared to **3**. The formation of hydrides could play a similar role in promoting N<sub>2</sub> binding and activation in the FeMoco. Although it could not be crystallographically characterized, the mixed-valence iron(I)/iron(II) bridging N<sub>2</sub> complex **6** was also accessible via treatment of the solvent adduct [Fe(SiP<sup>i</sup>PrS<sup>Ad</sup><sub>2</sub>)(Et<sub>2</sub>O)]<sup>+</sup> with 0.5 equivalents of CrCp<sub>2</sub> or CoCp<sub>2</sub>. Complex **6** exhibits an N–N stretching vibration at 1,881 cm<sup>-1</sup>, significantly lower than any of the monometallic complexes with this ligand, which illustrates how N<sub>2</sub> binding and activation could be facilitated by multimetallic cooperativity [66].



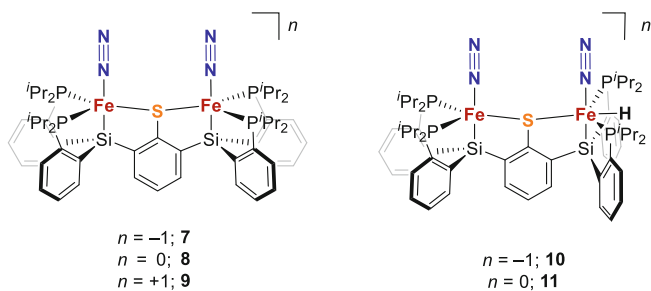


**Fig. 4**  $N_2$  complexes incorporating a bridging thiolate

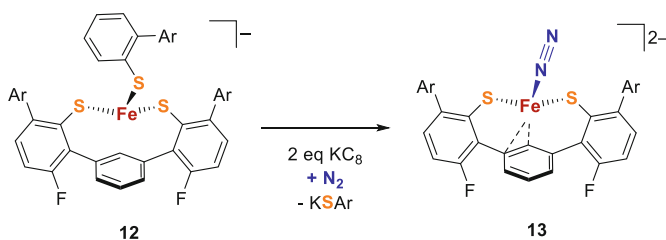


**Fig. 5**  $N_2$  binding to an iron site containing exclusively sulfur and carbon donors.  $Ar = 2,4,6$ -triisopropylphenyl

### 2.3 Interaction of $N_2$ with Iron–Sulfide Clusters

The study of synthetic iron–sulfur clusters in the context of nitrogenase has also been the topic of a significant body of work [22–24, 67, 68]. Although there are no structurally characterized iron–sulfur clusters with bound  $N_2$  ligands, catalytic and spectroscopic studies have demonstrated that  $N_2$  can bind to synthetic iron–sulfur clusters. Electrochemical reduction of  $N_2$  to  $NH_3$  is catalyzed by  $[Fe_4S_4(SPh)_4]^{2-}$  and  $[Mo_2Fe_6S_8(SPh)_9]^{3-}$  clusters, albeit with very low Faradaic efficiency [69]. More recently, the photochemical conversion of  $N_2$  to  $NH_3$  by chalcogenide aerogels (chalcogels) containing  $Mo_2Fe_6S_8(SPh)_3$  and  $Fe_4S_4$  clusters has been reported [70, 71]. Using infrared spectroscopy, N–N stretching bands were observed at 1,746 and 1,753  $cm^{-1}$  upon irradiation of these chalcogels with visible light under  $N_2$  atmosphere. The N–N stretching frequencies are even lower than the  $S_2C$  supported complex above and are indicative of some form of reduced  $N_2$  species, but the redox and protonation state of this species are not known. Nevertheless, these data provide evidence for the formation of a cluster-bound  $N_xH_y$  species during turnover.  $N_2$  binding to  $Fe_2S_2^+$ ,  $Fe_3S_3^+$ , and  $Fe_4S_4^+$  clusters in the gas phase has also been observed by mass spectrometry in ion-trapping experiments [72]. The structures of the  $N_2$  adducts are not known experimentally but were suggested from DFT calculations.

Finally, in a recent study, a diferrous iron sulfide hydride complex with a  $\beta$ -diketiminate coligand was reduced under  $N_2$  to give a diiron(0)  $N_2$  complex in 24% spectroscopic yield [73]. Gas chromatography indicates that  $H_2$  is produced during



this process. The reactivity of this complex thus models the E<sub>4</sub> state of the FeMoco, in which H<sub>2</sub> loss from an iron hydride sulfide core results in N<sub>2</sub> binding [14, 74–76]. However, in the model complex the H<sub>2</sub> production results from a bimolecular reaction, the N<sub>2</sub>-containing product did not also contain a sulfide, and mechanistic studies of the reaction leading to sulfide extrusion and N<sub>2</sub> binding were precluded by the presence of a significant number of unidentified byproducts in the reaction mixture.

### 3 Fe Complexes with N<sub>x</sub>H<sub>y</sub> Ligands

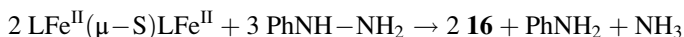
There are no examples of N<sub>2</sub> functionalization giving a well-defined N<sub>x</sub>H<sub>y</sub> complex for iron complexes with sulfur supporting ligands. However, a number of diazene (HN=NH) and hydrazine (NH<sub>2</sub>–NH<sub>2</sub>) complexes are known with sulfur-based supporting ligands, as are alkyl- or aryl-substituted diazene and hydrazine derivatives. Generation of the hydrazine species typically proceeds in a straightforward manner by addition of hydrazine to precursor complexes. In some cases, hydrazine addition instead results in isolable diazene complexes accompanied by formation of amines, implying that the diazene was generated via hydrazine disproportionation. The generation of diazene complexes via direct addition of diazene to a precursor is more problematic because diazene is unstable in solution [77–79], but there are examples where diazene is generated and trapped in situ by iron complexes. Isolated diazene complexes are most commonly synthesized by hydrazine disproportionation or by oxidation of corresponding hydrazine species. In this section, we discuss the generation, structural characterization, and reactivity of these N<sub>x</sub>H<sub>y</sub> compounds.

#### 3.1 N<sub>x</sub>H<sub>y</sub> Complexes with Iron–Sulfide Clusters

An early report demonstrated that the electrochemical reduction of hydrazine is catalyzed with high Faradaic efficiency by [Fe<sub>4</sub>S<sub>4</sub>(SPh)<sub>4</sub>]<sup>2-</sup> and [Mo<sub>2</sub>Fe<sub>6</sub>S<sub>8</sub>(SPh)<sub>9</sub>]<sup>3-</sup> clusters, but the mechanism of NH<sub>3</sub> formation was not examined [80]. Chemical reduction of vanadium- and molybdenum-containing iron–sulfur cubanes also generates ammonia from hydrazine, but in all of these cases the V or Mo centers were implicated as the sites of hydrazine binding and reduction [81–89].

The only examples of structurally characterized iron N<sub>x</sub>H<sub>y</sub> complexes incorporating sulfides are the β-diketiminato supported complexes **14–16** [90, 91] (Fig. 6). Reaction of the diferrous monosulfide-bridged precursor with ammonia, methylhydrazine, or 1,1-dimethylhydrazine yielded 2:1 complexes in which one of the N-donors is bound to each iron center (**14**). In contrast, reaction with the parent hydrazine yielded complex **15** in which an N<sub>2</sub>H<sub>4</sub> ligand bridges between the iron centers. Treatment of the diferrous precursor with 1.5 equivalents of phenylhydrazine

resulted in the formation of the mixed-valence iron(II)/iron(III) phenylhydrazido-bridged complex **16** via the overall reaction:



This reactivity demonstrates that sulfide-bridged iron centers are capable of N–N bond cleavage. The phenylhydrazido species **16** was also the subject of a detailed ENDOR study, which enabled the first determination of the hyperfine coupling parameters of a well-defined bridging hydrazido species that could be compared to the ENDOR parameters of nitrogenase intermediates [92].

### 3.2 $\text{N}_x\text{H}_y$ Complexes with Thioether/Thiolate Ligands

Sellmann and coworkers reported a series of complexes with supporting ligands containing two thiolate donors with additional thioether, amine, and/or pyridine groups [93–95]. Of particular note are several *trans* diazene complexes (two representative examples are shown in Fig. 7), which were generated either by air oxidation of a corresponding hydrazine species [96, 97] or by trapping of diazene generated in situ from potassium azodicarboxylate or benzenesulfonic acid hydrazide [98, 99]. In these complexes, the diazene ligand bridges between two iron centers, with the protons of the diazene forming one long ( $\sim 2.8 \text{ \AA}$ ) and one short ( $\sim 2.2 \text{ \AA}$ ) hydrogen bond to the

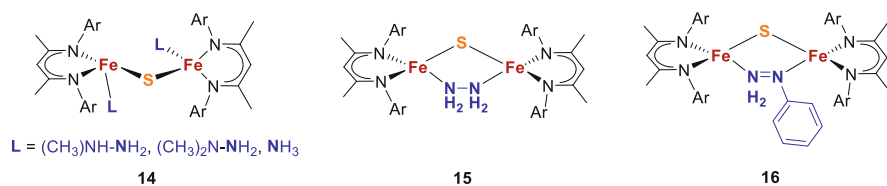


**Fig. 6** Sulfide-bridged  $\beta$ -diketiminato complexes with nitrogenase-relevant  $\text{N}_x\text{H}_y$  fragments. *Ar* = 2,6-diisopropylphenyl

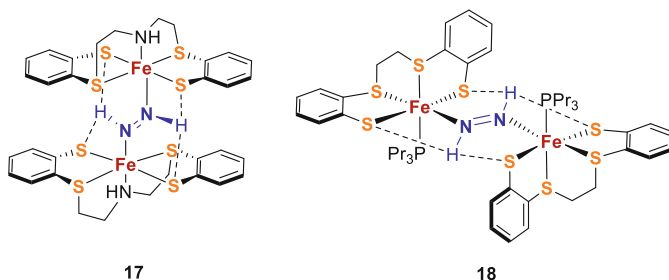


**Fig. 7** Structure of diazene-bridged complexes **17** and **18**

thiolate moieties of the supporting ligand [96, 97, 99]. DFT calculations suggest that the strong hydrogen-bonding interaction contributes significantly to the overall stability of the complex [100, 101]. The sulfides in the FeMoco, as well as adjacent amino acids, may play a similar role in stabilizing intermediates during N<sub>2</sub> reduction. A further contribution to the stability of these complexes arises from the strong  $\pi$ -backbonding interaction between the iron center and the diazene ligand, as demonstrated by their intense blue color that arises from an iron to diazene charge transfer transition [102, 103]. This interaction leads to slight weakening of the N–N bond as compared to free diazene: for example, in complex **17**, the N–N bond length [96] is 1.301(5) Å compared to 1.252 Å in free diazene [104]. The N–N stretching frequency is 1,382 cm<sup>-1</sup> [103], which falls between the values for free diazene ( $\nu_{\text{NN}} = 1,529$  cm<sup>-1</sup> [105]) and free hydrazine ( $\nu_{\text{NN}} = 876$  cm<sup>-1</sup> [106]). Using normal coordinate analysis, Lehnert and coworkers determined an N–N bond order of 1.6 for this complex indicating partial reduction to a hydrazido(2-) species [103]. SCF-X $\alpha$ -SW calculations indicated that the LUMO of this complex consists primarily of a diazene  $\pi^*$  orbital, which implies that reduction of the complex should further weaken the N–N bond of the diazene moiety [102]. However, in practice the reduction occurred at an extremely negative potential and led instead to decomposition of the complex.

Although structurally characterized monometallic iron complexes that bind hydrazine [107–109] and ammonia [107] are also known in these systems, a corresponding N<sub>2</sub> species could not be generated. Interestingly, however, oxidation of the diazene complex **18** with two equivalents of ferrocenium at -78 °C caused a color change from blue to purple [110, 111]. Since the HOMO of complex **18** is primarily an iron orbital [102], this oxidation was expected to result in the formation of a diferric diazene species. Warming the purple oxidized species above -40 °C resulted in N<sub>2</sub> evolution and formation of a green ferrous product. This implies that the purple species may be a ferrous N<sub>2</sub> complex, which is a valence tautomer of the expected diferric diazene complex (Fig. 8). This process would model the reverse of N<sub>2</sub> binding in the FeMoco and illustrate how sulfides could facilitate proton transfer. Unfortunately, the instability of the purple oxidized species prevented further characterization and its identity remains unclear.

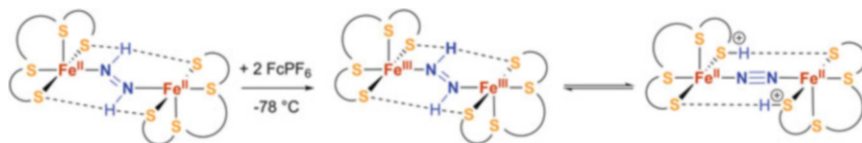


**Fig. 8** Two-electron oxidation of diazene complex **18**, with the presumed product shown in two tautomeric forms: a diferric diazene complex and a diferrous dinitrogen adduct. The supporting ligands have been omitted for clarity

### 3.3 $N_xH_y$ Complexes with Thiolate Ligands

Other complexes containing thiolate donors are also known to bind  $N_2H_4$  and  $NH_3$ . In these systems, like those described above, the hydrazine ligands often form extensive hydrogen-bonding networks with the thiolates and/or solvents of crystallization. For example, Sellmann and coworkers crystallized iron bis(benzenedithiolate) complexes with hydrazine bound in bridging [112] and terminal [113] coordination modes. The terminal complex in particular contains an extensive hydrogen-bonding network between the metal-bound hydrazine and  $N_2H_4$  and  $N_2H_5$  molecules in the crystal lattice.

Upon reaction of the sterically hindered thiolate-bridged dimer  $Fe_2(\mu\text{-STriph})_2(\text{STriph})_2$  ( $\text{STriph} = 2,4,6\text{-triphenylbenzenethiolate}$ ) with hydrazine, rearrangement to the hydrazine-bridged dimer  $Fe_2(\mu\text{-}N_2H_2)_2(N_2H_2)_2(\text{STriph})_4$  (**19**) was observed [114] (Fig. 9). The precursor complex  $Fe_2(\mu\text{-}N_2H_2)_2(\text{STriph})_2$  also reacted with amines to yield mono- and bimetallic coordination compounds and was observed to catalyze the disproportionation of 1,2-diphenylhydrazine to aniline and azobenzene ( $\text{PhN}=\text{NPh}$ ). Complex **20** also coordinates ammonia and hydrazine [115]. The  $NH_3$  and  $N_2H_4$  ligands in **20** are labile in solution but are stabilized in the solid state by hydrogen-bonding interactions to solvent molecules. This complex catalyzes hydrazine reduction, but the number of turnovers is low and no intermediates could be observed during the reaction.

Hydrazine cleavage at iron sites has also been observed in other systems. A series of ferric iron-imide heterocubanes (**21**) were generated by the reaction of ferrous complexes containing sterically hindered thiolate ligands with 1,2-diarylhydrazines [116, 117]. The mechanism of the N–N bond cleavage step leading to imide formation is not clear but was proposed to occur through formation of a diferrous complex containing an arylhydrazine bound in a  $\mu\text{-}\eta^2\text{:}\eta^2$  fashion, followed by electron transfer from the ferrous centers to the hydrazine resulting in N–N bond cleavage. A similar reaction leading to N–N bond cleavage and formation of a bridging imide could be envisioned in the FeMoco. Note that these cubane structures were obtained only with sterically hindered thiolates and 1,2-diarylhydrazines; all other substrates gave mixtures of products. In a different set of studies, iron-imide-sulfide heterocubanes were also structurally and spectroscopically characterized [118, 119].

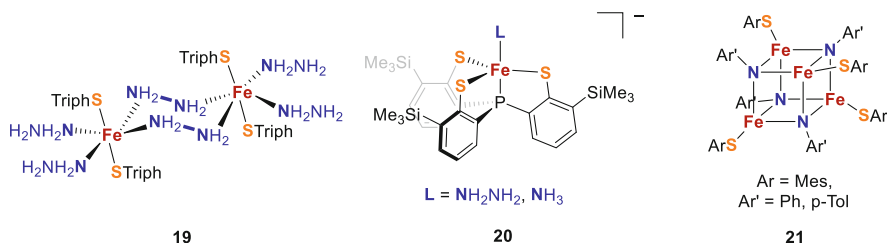
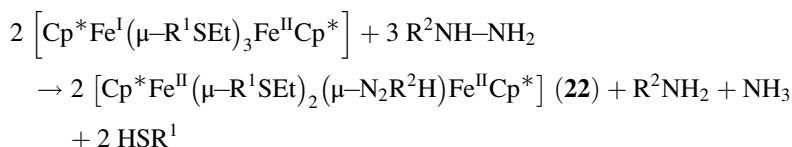


**Fig. 9** Complexes generated by the addition of hydrazines to iron precursors with sterically bulky thiolate ligands

### 3.4 N<sub>x</sub>H<sub>y</sub> Complexes with Thiolate and Cp Ligands

Several complexes incorporating thiolate and Cp donors are also known to catalyze the N–N bond cleavage of hydrazines. Qu and coworkers reported that alkylthiolate-bridged iron complexes react with hydrazines to form *cis* diazene complexes (**22**) [120, 121]:



In the presence of reductant and acid, these compounds catalytically cleave the N–N bond of various alkyl- and aryl-substituted hydrazines. No intermediates could be detected in this reaction, but DFT calculations suggested that protonation and reduction of diazene involves isomerization to a (μ-NH)-NH<sub>2</sub> species [122]. The strong donation of the thiolates and their ability to shift coordination mode are thought to be important in allowing this isomerization to occur. Nishibayashi and coworkers reported a similar system containing an *ortho*-substituted aryl thiolate in which a methyl-diazene (CH<sub>3</sub>–N=NH) or methyl-diazenido (N=NCH<sub>3</sub><sup>–</sup>) moiety is bound side-on between two iron centers (**23–24**) [123] (Fig. 10). In this case, the bridging structure was important for promoting selective hydrazine cleavage; a corresponding monomeric complex promoted H<sub>2</sub> formation rather than NH<sub>3</sub> production. Again, however, the mechanism of N–N bond cleavage was not clear and the key hydrazido (R<sub>2</sub>N–NR<sup>–</sup>) intermediate could not be detected.

In another system, Qu and coworkers studied the generation of ammonia from treatment of a benzenedithiolate-bridged diiron complex with hydrazine [124]. Several intermediates along the pathway to NH<sub>3</sub> release were accessible via stepwise protonation and/or reduction. Starting from a diferrous complex with *cis*-diazene bound μ-η<sup>1</sup>:η<sup>1</sup> between the iron centers (**25**), protonation led to electron transfer from the iron centers to the diazene ligand and rearrangement to afford a diferric complex in which a hydrazido (N<sub>2</sub>H<sub>3</sub><sup>–</sup>) ligand is bound asymmetrically in a μ-η<sup>1</sup>:η<sup>2</sup> fashion (**26**). The bridging benzenedithiolate ligand also rearranged to a μ-η<sup>1</sup>:η<sup>2</sup> coordination mode, which resembles the hypothesized rearrangement of sulfides in the FeMoco during turnover. Subsequent two-electron reduction and protonation of **26** resulted in ammonia release and formation of an amido-bridged diferrous complex (**27**). DFT calculations suggest that the ammonia comes from the non-bridging NH<sub>2</sub> of the hydrazido species via the mechanism shown in Fig. 11. Note that this process involves an NH–NH<sub>3</sub> intermediate that is not part of the traditional distal or alternating pathways but has been proposed for the FeMoco based on computational results [34]. The amido complex **27** also produces NH<sub>3</sub> upon further reduction and protonation, although the yield is low due to competitive proton reduction.

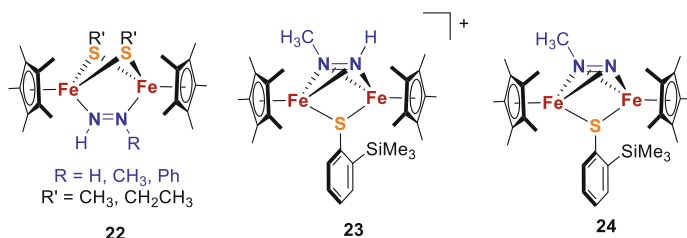


**Fig. 10** Structures of Cp-supported thiolate-bridged diazene complexes reported by Qu and Nishibayashi

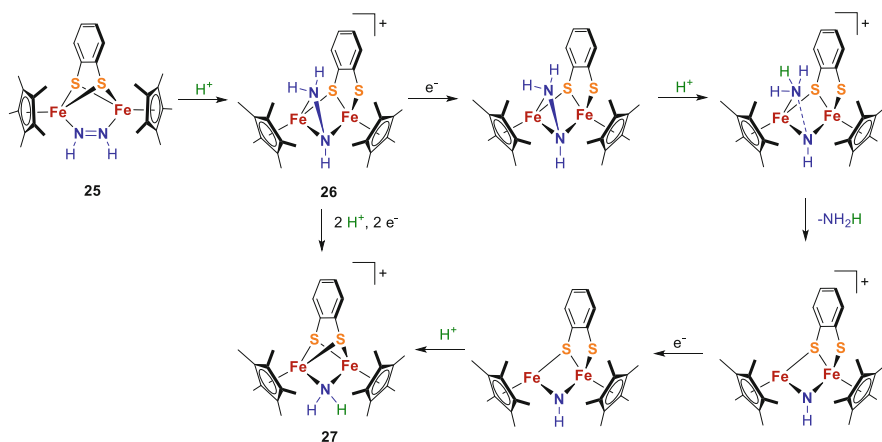


**Fig. 11** Proposed mechanism of NH<sub>3</sub> release leading to the formation of **27** upon protonation and reduction of **25** via **26**. Of the complexes shown in this figure, only **26** and **27** are structurally characterized, although the structure of **25** (which is an isolable species) can be inferred based on the structure of the analogous one-electron oxidized species. The sequence of protonation and electron transfer steps is proposed based on DFT calculations

## 4 Conclusions

The results presented above show the variety of synthetic strategies that have yielded N<sub>2</sub> and N<sub>x</sub>H<sub>y</sub> complexes of iron with sulfur-containing supporting ligands. It is becoming clear that the coordinative flexibility, electron-rich character, and hydrogen-bonding capability of sulfur atoms can influence the behavior of bound N<sub>2</sub> and N<sub>x</sub>H<sub>y</sub> coligands. Understanding the electronic structure and reactivity of these compounds has begun to provide insight into the possible role(s) of the sulfides in the FeMoco of nitrogenase.

**Acknowledgement** The authors thank the National Institutes of Health (GM065313) for funding.

## References

1. Ribbe M (ed) (2011) Nitrogen fixation. Humana, New York, NY
2. Burgess BK, Lowe DJ (1996) Chem Rev 96:2983
3. Holland PL (2004) Nitrogen fixation. In: McCleverty J, Meyer TJ (eds) Comprehensive Coordination Chemistry II. Elsevier, Oxford, Vol. 8, pp 569–599
4. Hu Y, Ribbe MW (2015) J Biol Inorg Chem 20:435
5. Hoffman BM, Lukoyanov D, Yang Z-Y, Dean DR, Seefeldt LC (2014) Chem Rev 114:4041
6. Eady RR (1996) Chem Rev 96:3013
7. Krahn E, Weiss BJR, Kröckel M, Groppe J, Henkel G, Cramer SP, Trautwein AX, Schneider K, Müller A (2002) J Biol Inorg Chem 7:37
8. Seefeldt LC, Dance IG, Dean DR (2004) Biochemistry 43:1401
9. Spatzal T, Schlesier J, Burger E-M, Sippel D, Zhang L, Andrade SLA, Rees DC, Einsle O (2016) Nat Commun 7:10902
10. Björnsson R, Lima FA, Spatzal T, Weyhermüller T, Glatzel P, Bill E, Einsle O, Neese F, DeBeer S (2014) Chem Sci 5:3096
11. Hoffman BM, Dean DR, Seefeldt LC (2009) Acc Chem Res 42:609
12. Seefeldt LC, Hoffman BM, Dean DR (2009) Annu Rev Biochem 78:701
13. Hoffman BM, Lukoyanov D, Dean DR, Seefeldt LC (2013) Acc Chem Res 46:587
14. Lukoyanov D, Yang Z-Y, Khadka N, Dean DR, Seefeldt LC, Hoffman BM (2015) J Am Chem Soc 137:3610
15. Thorneley RNF, Lowe DJ (1985) Met Ions Biol 7:221
16. Igarashi RY, Laryukhin M, Dos Santos PC, Lee H-I, Dean DR, Seefeldt LC, Hoffman BM (2005) J Am Chem Soc 127:6231
17. Lukoyanov D, Yang Z-Y, Dean DR, Seefeldt LC, Hoffman BM (2010) J Am Chem Soc 132:2526
18. Doan PE, Telser J, Barney BM, Igarashi RY, Dean DR, Seefeldt LC, Hoffman BM (2011) J Am Chem Soc 133:17329
19. Schrock RR (2005) Acc Chem Res 38:955
20. Nishibayashi Y (2015) Inorg Chem 54:9234
21. Rittle J, Peters JC (2016) J Am Chem Soc 138:4243
22. Lee SC, Holm RH (2003) Proc Natl Acad Sci U S A 100:3595
23. Lee SC, Holm RH (2004) Chem Rev 104:1135
24. Lee SC, Lo W, Holm RH (2014) Chem Rev 114:3579
25. Spatzal T, Perez KA, Einsle O, Howard JB, Rees DC (2014) Science 345:1620
26. Spatzal T, Perez KA, Howard JB, Rees DC (2015) Elife 4:e11620
27. Wiig JA, Lee CC, Hu Y, Ribbe MW (2013) J Am Chem Soc 135:4982
28. Dance I (2008) Dalton Trans 5977
29. Dance I (2008) Dalton Trans 5992
30. Dance I (2012) Dalton Trans 41:4859
31. Dance I (2014) A unified chemical mechanism for hydrogenation reactions catalyzed by nitrogenase. In: Weigand W, Schollhammer P (eds) Bioinspired catalysis. Wiley, Weinheim, pp 249–288
32. Huniar U, Ahlrichs R, Coucouvanis D (2004) J Am Chem Soc 126:2588
33. Schimpl J, Petrilli HM, Blöchl PE (2003) J Am Chem Soc 125:15772
34. Kästner J, Blöchl PE (2007) J Am Chem Soc 129:2998
35. Hinnemann B, Nørskov JK (2004) J Am Chem Soc 126:3920
36. Varley JB, Wang Y, Chan K, Studt F, Nørskov JK (2015) Phys Chem Chem Phys 17:29541
37. Rao L, Xu X, Adamo C (2016) ACS Catalysis 6:1567
38. McKee ML (2016) J Phys Chem A 120:754
39. Siegbahn PEM (2016) J Am Chem Soc 138:10485
40. Rodriguez MM, Bill E, Brennessel WW, Holland PL (2011) Science 334:780
41. Grubel K, Brennessel WW, Mercado BQ, Holland PL (2014) J Am Chem Soc 136:16807

42. MacLeod KC, McWilliams SF, Mercado BQ, Holland PL (2016) *Chem Sci* 7:5736
43. Lee Y, Sloane FT, Blondin G, Abboud KA, Garcia-Serres R, Murray LJ (2015) *Angew Chem Int Ed Engl* 54:1499
44. Anderson JS, Rittle J, Peters JC (2013) *Nature* 501:84
45. Creutz SE, Peters JC (2014) *J Am Chem Soc* 136:1105
46. Ung G, Peters JC (2015) *Angew Chem Int Ed Engl* 54:532
47. Del Castillo TJ, Thompson NB, Peters JC (2016) *J Am Chem Soc* 138:5341
48. Yuki M, Tanaka H, Sasaki K, Miyake Y, Yoshizawa K, Nishibayashi Y (2012) *Nat Commun* 3:1254
49. Kuriyama S, Arashiba K, Nakajima K, Matsuo Y, Tanaka H, Ishii K, Yoshizawa K, Nishibayashi Y (2016) *Nat Commun* 7:12181
50. MacKay BA, Fryzuk MD (2004) *Chem Rev* 104:385
51. Crossland JL, Tyler DR (2010) *Coord Chem Rev* 254:1883
52. Hazari N (2010) *Chem Soc Rev* 39:4044
53. MacLeod KC, Holland PL (2013) *Nat Chem* 5:559
54. Köthe C, Limberg C (2015) *Z Anorg Allg Chem* 641:18
55. Tanabe Y, Nishibayashi Y (2016) *Chem Rec* 16:1549
56. Ohki Y, Seino H (2016) *Dalton Trans* 45:874
57. Čorić I, Holland PL (2016) *J Am Chem Soc* 138:7200
58. Hallmen PP, Kästner J (2015) *Z Anorg Allg Chem* 641:118
59. Bazhenova TA, Shilov AE (1995) *Coord Chem Rev* 144:69
60. NIST Computational Chemistry Comparison and Benchmark Database (2015) National Institute of Standards and Technology. <http://cccbdb.nist.gov/>. Accessed 21 Sept 2015
61. Bart SC, Lobkovsky E, Bill E, Wieghardt K, Chirik PJ (2007) *Inorg Chem* 46:7055
62. Lee Y, Mankad NP, Peters JC (2010) *Nat Chem* 2:558
63. Takaoka A, Mankad NP, Peters JC (2011) *J Am Chem Soc* 133:8440
64. Creutz SE, Peters JC (2015) *J Am Chem Soc* 137:7310
65. Čorić I, Mercado BQ, Bill E, Vinyard DJ, Holland PL (2015) *Nature* 526:96
66. McWilliams SF, Holland PL (2015) *Acc Chem Res* 48:2059
67. Venkateswara Rao P, Holm RH (2004) *Chem Rev* 104:527
68. Henderson RA (2014) Binding substrates to synthetic Fe–S-based clusters and the possible relevance to nitrogenases. In: Weigand W, Schollhammer P (eds) *Bioinspired catalysis*. Wiley, Weinheim, pp 289–324
69. Tanaka K, Hozumi Y, Tanaka T (1982) *Chem Lett* 11:1203
70. Banerjee A, Yuhua BD, Margulies EA, Zhang Y, Shim Y, Wasielewski MR, Kanatzidis MG (2015) *J Am Chem Soc* 137:2030
71. Liu J, Kelley MS, Wu W, Banerjee A, Douvalis AP, Wu J, Zhang Y, Schatz GC, Kanatzidis MG (2016) *Proc Natl Acad Sci U S A* 113:5530
72. Heim HC, Bernhardt TM, Lang SM, Barnett RN, Landman U (2016) *J Phys Chem C* 120:12549
73. Arnet NA, Dugan TR, Menges FS, Mercado BQ, Brennessel WW, Bill E, Johnson MA, Holland PL (2015) *J Am Chem Soc* 137:13220
74. Yang Z-Y, Khadka N, Lukoyanov D, Hoffman BM, Dean DR, Seefeldt LC (2013) *Proc Natl Acad Sci U S A* 110:16327
75. Lukoyanov D, Khadka N, Yang Z-Y, Dean DR, Seefeldt LC, Hoffman BM (2016) *J Am Chem Soc* 138:10674
76. Lukoyanov D, Khadka N, Yang Z-Y, Dean DR, Seefeldt LC, Hoffman BM (2016) *J Am Chem Soc* 138:1320
77. Stanbury DM (1991) *Inorg Chem* 30:1293
78. Liao G-L, Palmer G (1998) *Biochemistry* 37:15583
79. Barney BM, McCleod J, Lukoyanov D, Laryukhin M, Yang T-C, Dean DR, Hoffman BM, Seefeldt LC (2007) *Biochemistry* 46:6784
80. Hozumi Y, Imasaka Y, Tanaka K, Tanaka T (1983) *Chem Lett* 12:897



81. Coucouvanis D, Mosier PE, Demadis KD, Patton S, Malinak SM, Kim CG, Tyson MA (1993) *J Am Chem Soc* 115:12193
82. Malinak SM, Demadis KD, Coucouvanis D (1995) *J Am Chem Soc* 117:3126
83. Demadis KD, Malinak SM, Coucouvanis D (1996) *Inorg Chem* 35:4038
84. Malinak SM, Simeonov AM, Mosier PE, McKenna CE, Coucouvanis D (1997) *J Am Chem Soc* 119:1662
85. Palermo RE, Singh R, Bashkin JK, Holm RH (1984) *J Am Chem Soc* 106:2600
86. Coucouvanis D (1996) *J Biol Inorg Chem* 1:594
87. Demadis KD, Coucouvanis D (1994) *Inorg Chem* 33:4195
88. Demadis KD, Coucouvanis D (1995) *Inorg Chem* 34:3658
89. Coucouvanis D, Demadis KD, Malinak SM, Mosier PE, Tyson MA, Laughlin LJ (1996) *J Mol Catal A Chem* 107:123
90. Vela J, Stoian S, Flaschenriem CJ, Münck E, Holland PL (2004) *J Am Chem Soc* 126:4522
91. Stubbert BD, Vela J, Brennessel WW, Holland PL (2013) *Z Anorg Allg Chem* 639:1351
92. Lees NS, McNaughton RL, Vargas Gregory W, Holland PL, Hoffman BM (2008) *J Am Chem Soc* 130:546
93. Sellmann D, Sutter J (1997) *Acc Chem Res* 30:460
94. Sellmann D, Utz J, Blum N, Heinemann FW (1999) *Coord Chem Rev* 190–192:607
95. Sellmann D, Sutter J (1996) *J Biol Inorg Chem* 1:587
96. Sellmann D, Soglowek W, Knoch F, Moll M (1989) *Angew Chem Int Ed Engl* 28:1271
97. Sellmann D, Friedrich H, Knoch F, Moll M (1994) *Z Naturforsch B* 49:76
98. Sellmann D, Hennige A (1997) *Angew Chem Int Ed Engl* 36:276
99. Sellmann D, Blum DCF, Heinemann FW (2002) *Inorg Chim Acta* 337:1
100. Reiher M, Sellmann D, Hess AB (2001) *Theor Chem Acc* 106:379
101. Reiher M, Salomon O, Sellmann D, Hess BA (2001) *Chem Eur J* 7:5195
102. Lehnert N, Wiesler BE, Tuzcek F, Hennige A, Sellmann D (1997) *J Am Chem Soc* 119:8869
103. Lehnert N, Wiesler BE, Tuzcek F, Hennige A, Sellmann D (1997) *J Am Chem Soc* 119:8879
104. Carlotti M, Johns JWC, Trombetti A (1974) *Can J Phys* 52:340
105. Bondybey VE, Nibler JW (1973) *J Chem Phys* 58:2125
106. Giguère PA, Liu ID (1952) *J Chem Phys* 20:136
107. Sellmann D, Soglowek W, Knoch F, Ritter G, Dengler J (1992) *Inorg Chem* 31:3711
108. Sellmann D, Shaban S, Heinemann F (2004) *Eur J Inorg Chem* 2004:4591
109. Sellmann D, Blum N, Heinemann F (2001) *Z Naturforsch B* 56:581
110. Sellmann D, Hennige A, Heinemann FW (1998) *Inorg Chim Acta* 280:39
111. Sellmann D, Hofmann T, Knoch F (1994) *Inorg Chim Acta* 224:61
112. Sellmann D, Kreutzer P, Huttner G, Frank A (1978) *Z Naturforsch B* 33:1341
113. Sellmann D, Friedrich H, Knoch F (1994) *Z Naturforsch B* 49:660
114. Zdilla MJ, Verma AK, Lee SC (2008) *Inorg Chem* 47:11382
115. Chang Y-H, Chan P-M, Tsai Y-F, Lee G-H, Hsu H-F (2014) *Inorg Chem* 53:664
116. Verma AK, Lee SC (1999) *J Am Chem Soc* 121:10838
117. Zdilla MJ, Verma AK, Lee SC (2011) *Inorg Chem* 50:1551
118. Chen X-D, Duncan JS, Verma AK, Lee SC (2010) *J Am Chem Soc* 132:15884
119. Chen X-D, Zhang W, Duncan JS, Lee SC (2012) *Inorg Chem* 51:12891
120. Chen Y, Zhou Y, Chen P, Tao Y, Li Y, Qu J (2008) *J Am Chem Soc* 130:15250
121. Chen Y, Liu L, Peng Y, Chen P, Luo Y, Qu J (2011) *J Am Chem Soc* 133:1147
122. Luo Y, Li Y, Yu H, Zhao J, Chen Y, Hou Z, Qu J (2012) *Organometallics* 31:335
123. Yuki M, Miyake Y, Nishibayashi Y (2012) *Organometallics* 31:2953
124. Li Y, Li Y, Wang B, Luo Y, Yang D, Tong P, Zhao J, Luo L, Zhou Y, Chen S, Cheng F, Qu J (2013) *Nat Chem* 5:320

# Catalytic Transformations of Molecular Dinitrogen by Iron and Cobalt–Dinitrogen Complexes as Catalysts

Shogo Kuriyama and Yoshiaki Nishibayashi

**Abstract** This chapter describes the recent advances of the iron and cobalt-catalyzed transformations of molecular dinitrogen into not only silylamine but also ammonia and hydrazine under mild reaction conditions. In both reaction systems, reaction pathways are proposed based on the experimental and theoretical studies on iron and cobalt–dinitrogen complexes.

**Keywords** Ammonia • Catalyst • Cobalt • Dinitrogen • Iron • Reduction • Silylamine

## Contents

1	Introduction .....	216
2	Iron–Dinitrogen Complexes .....	217
2.1	Background of Iron–Dinitrogen Complexes .....	217
2.2	Catalytic Silylation of Dinitrogen Using Iron Catalysts .....	217
2.3	Catalytic Formation of Ammonia Using Iron Catalysts .....	219
2.4	Catalytic Formation of Ammonia and Hydrazine Using Iron–Dinitrogen Complex as Catalyst .....	226
3	Cobalt–Dinitrogen Complexes .....	229
3.1	Background of Cobalt–Dinitrogen Complexes .....	229
3.2	Catalytic Silylation of Dinitrogen Using Cobalt Catalysts .....	230
3.3	Catalytic Formation of Ammonia Using Cobalt Catalysts .....	230
4	Summary .....	232
	References .....	233

---

S. Kuriyama and Y. Nishibayashi (✉)

Department of Systems Innovation, School of Engineering, The University of Tokyo, Hongo, Bunkyo-ku, Tokyo 113-8656, Japan

e-mail: [ynishiba@sys.t.u-tokyo.ac.jp](mailto:ynishiba@sys.t.u-tokyo.ac.jp)

## 1 Introduction

Nitrogen is an essential element for living things. Because nitrogen gas, which is abundant in atmosphere, cannot be directly utilized by most of the living things, the development of nitrogen fixation, ammonia formation from nitrogen gas, is one of the most important reactions in chemistry. Industrially, the Haber–Bosch process produces ammonia from nitrogen and hydrogen gases (Fig. 1) [1]. This process produces ca. 1.6 million tons of ammonia annually and the produced ammonia is used for fertilizer and other materials. Because the Haber–Bosch process requires harsh reaction conditions such as high temperature and high pressure and consumes at least 1–2% of the annual primary energy supply in the world, the development of nitrogen fixation under mild reaction conditions has been strongly desired for human beings.

In biological nitrogen fixation, nitrogenase enzymes convert nitrogen gas into ammonia under ambient reaction conditions (Fig. 2) [2]. The recent spectroscopic and X-ray studies revealed the structure of the active site of nitrogenase in FeMo cofactor (Fig. 2) [3–6]. The active site consists of a thiolate-bridged polynuclear complex containing carbon, iron, and molybdenum atoms. The FeV- and Fe-only nitrogenases, which contain vanadium and iron atoms in place of the molybdenum atom in the FeMo cofactor, are also known, although the catalytic activity of these nitrogenases is lower than that of FeMo-nitrogenase. Despite extensive mechanistic studies, the detailed mechanism of dinitrogen reduction by nitrogenases remains unclear. However, nitrogenase provides a fundamental clue to a design for nitrogen fixation system under mild reaction conditions, where transition metal–dinitrogen complexes play a key role in converting nitrogen gas into ammonia [7–10].

Iron–dinitrogen complexes have been extensively studied because the iron atom plays an essential role in both industrial and biological nitrogen fixations [11–14]. Especially, the existence of iron atoms in all types of nitrogenases has prompted chemists to synthesize a variety of iron–dinitrogen complexes as model complexes and to use them as catalysts for nitrogen fixation. On the other hand, the development of nitrogen fixation by use of cobalt–dinitrogen complexes as catalysts has also attracted attention recently after 50 years when Yamamoto and co-workers prepared a cobalt dinitrogen complex as the first example of the transition metal–dinitrogen complex bearing a dinitrogen ligand directly derived from nitrogen gas [15]. This chapter describes a quite recent advance of the catalytic transformation of nitrogen gas by using iron and cobalt–dinitrogen complexes as catalysts.

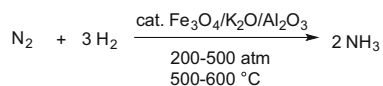


**Fig. 1** Industrial nitrogen fixation by Haber–Bosch process

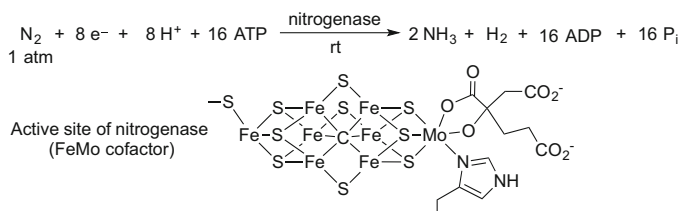


**Fig. 2** Biological nitrogen fixation by nitrogenase

## 2 Iron–Dinitrogen Complexes

### 2.1 Background of Iron–Dinitrogen Complexes

Since the discovery of the first iron–dinitrogen complex in 1968 [16], synthesis and reactivity of a variety of iron–dinitrogen complexes bearing various phosphine ligands have been extensively studied by Leigh, Tyler, Field, and other groups [11–14]. Protonation of iron–dinitrogen complexes  $[\text{Fe}(\text{N}_2)(\text{diphosphine})_2]$  with HCl or HOTf afforded a mixture of ammonia and hydrazine. Based on the reactivities of isolated and generated intermediates, Tyler and co-workers have proposed a reaction pathway for the formation of ammonia from an iron–dinitrogen complex **1**, where symmetrical protonation of the coordinated dinitrogen ligand occurs to afford the corresponding diazene (NHNH) and hydrazine ( $\text{NH}_2\text{NH}_2$ ) complexes as reactive intermediates (Fig. 3) [17]. However, no catalytic reduction of dinitrogen was achieved in this reaction system.

### 2.2 Catalytic Silylation of Dinitrogen Using Iron Catalysts

Tris(trimethylsilyl)amine ( $\text{N}(\text{SiMe}_3)_3$ ) is considered as an equivalent to ammonia because  $\text{N}(\text{SiMe}_3)_3$  can be quantitatively converted into ammonia upon hydrolysis. Generally,  $\text{N}(\text{SiMe}_3)_3$  is produced from the reaction of nitrogen gas with alkali metals (Na and K) as reductants and chlorotrimethylsilane ( $\text{Me}_3\text{SiCl}$ ) as a silylating agent in the presence of transition metal complexes as catalysts [18–24], where the catalytic formation using transition metal–dinitrogen complexes has so far been achieved only in the case of molybdenum complexes. Although chromium- and titanium-catalyzed reactions were reported by using Li as a reductant, the possibility of lithium–nitride as nitrogen source was not completely excluded [18–24].

In 2012, Nishibayashi and co-workers found the iron-catalyzed silylation of nitrogen gas under ambient reaction conditions (Fig. 4) [25]. Even simple iron complexes such as iron carbonyls and ferrocene derivatives worked as effective catalysts for the formation of  $\text{N}(\text{SiMe}_3)_3$  from an atmospheric pressure of nitrogen gas with sodium as a reductant and  $\text{Me}_3\text{SiCl}$  as a silylating agent. Especially, trimethylsilyl-substituted ferrocene **2** produced the largest amount of  $\text{N}(\text{SiMe}_3)_3$

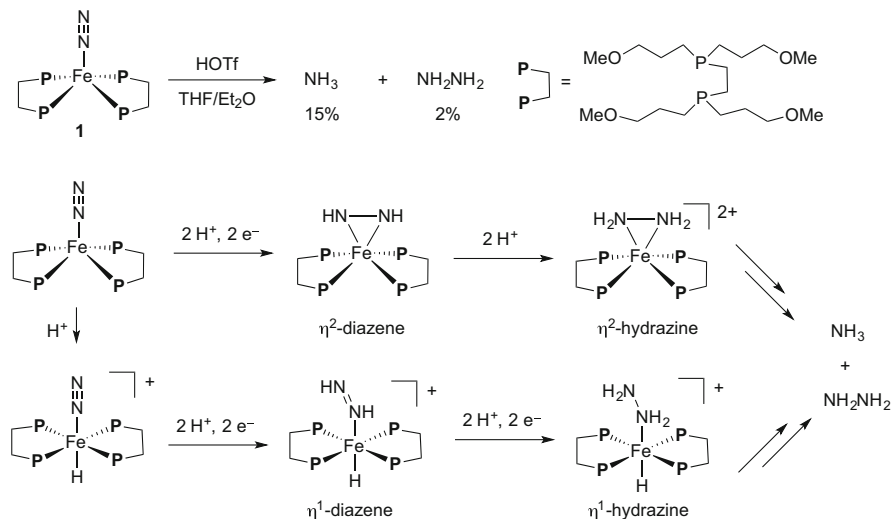


**Fig. 3** The plausible reaction pathways for the formation of ammonia and hydrazine starting from an iron–dinitrogen complex bearing diphosphine ligands

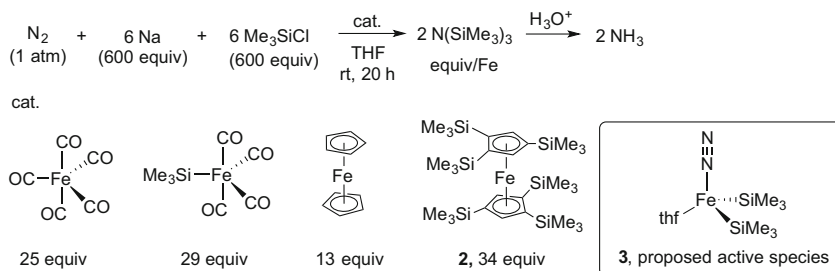


**Fig. 4** Catalytic formation of  $\text{N}(\text{SiMe}_3)_3$  from molecular dinitrogen using iron complexes as catalysts

(34 equiv. based on the iron atom in the catalyst). On the other hand, ferrous chloride and  $[\text{Fe}\{\text{N}(\text{SiMe}_3)_2\}_2]$  did not exhibit any catalytic activity under the same reaction conditions.

No catalytically relevant intermediate or dinitrogen complexes were detected in the reaction system. However, the possibility that iron nanoparticles generated in situ worked as an active species was excluded because the addition of a large excess amount of Hg did not affect the catalytic activity. As proposed in the previous molybdenum systems [18–24], a trimethylsilyl radical is considered to play an important role to promote the reduction of nitrogen gas. Based on the results of DFT calculations, an iron–dinitrogen complex bearing trimethylsilyl groups **3**, which was generated in situ from Na,  $\text{Me}_3\text{SiCl}$ , and iron precatalysts, was proposed to work as a real active species.

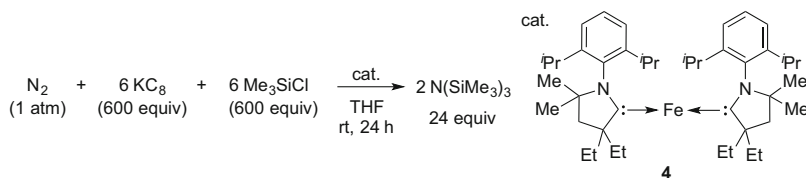


**Fig. 5** Catalytic silylation of molecular dinitrogen using an iron complex bearing cyclic (alkyl)(amino)carbenes as a catalyst

In 2015, Peters and a co-worker reported that an iron complex bearing two cyclic (alkyl)(amino)carbene (CAAC) ligands **4** worked as a catalyst for the formation of  $N(\text{SiMe}_3)_3$ , where 24 equiv. of  $N(\text{SiMe}_3)_3$  were formed based on the iron atom of the catalyst (Fig. 5) [26]. In this system, the presence of  $\text{KC}_8$  was necessary to produce  $N(\text{SiMe}_3)_3$ . Only a trace amount of  $N(\text{SiMe}_3)_3$  was obtained when Na was used as a reductant.

## 2.3 Catalytic Formation of Ammonia Using Iron Catalysts

### 2.3.1 Iron–Dinitrogen Complexes Bearing Triphosphineborane Ligand

Peters and a co-worker studied iron–dinitrogen and related complexes bearing a triphosphineborane (TPB) ligand. The electronic nature of the TPB ligand changes Fe–B interaction to stabilize both  $\pi$ -acidic and  $\pi$ -basic ligands. In 2011, Peters and a co-worker reported the synthesis of formally iron(0)- and iron(-I)-dinitrogen complexes bearing the TPB ligand **5–7** as well as the corresponding *N*-aryl imide complex **8** (Fig. 6) [27]. The strong iron–boron interaction was observed in the iron(-I) complexes (**6** and **7**), whereas the interaction between Fe and B atoms was weak in the imide complex. This flexibility of the Fe–B bond is considered to realize the catalytic transformation of nitrogen gas under mild reaction conditions.

### 2.3.2 Catalytic Conversion of Nitrogen Gas into Ammonia

In 2013, Peters and co-workers reported the first example of the iron-catalyzed reduction of nitrogen gas into ammonia [28]. The reaction of an atmospheric pressure of nitrogen gas with  $[\text{H}(\text{OEt}_2)_2]\text{BAr}^{\text{F}}_4$  (46 equiv.) as a proton source and  $\text{KC}_8$  (50 equiv.) as reductant in  $\text{Et}_2\text{O}$  at  $-78^\circ\text{C}$  for 1 h in the presence of the iron–dinitrogen complex **7** afforded 7.0 equiv. of ammonia based on the iron atom in the catalyst (Fig. 7). Hydrogen gas was obtained as a by-product in 35% yield based on the proton source (5.1 equiv.) in this reaction. No hydrazine was detected as a by-product under this reaction conditions. Separately, it was confirmed that hydrazine was completely converted into ammonia under the catalytic reaction conditions, suggesting that hydrazine cannot be detected even if hydrazine is formed as a

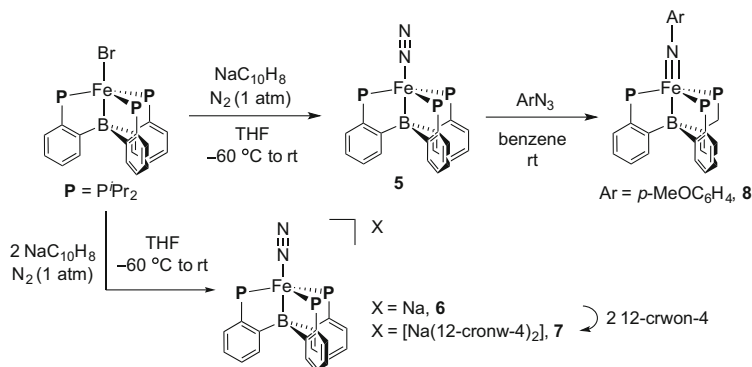


**Fig. 6** Synthesis of iron–dinitrogen and –imide complexes bearing a triphosphineborane ligand

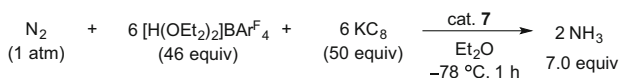


**Fig. 7** Catalytic formation of ammonia from molecular dinitrogen using an iron–dinitrogen complex **7** as a catalyst

primary product. When simple iron complexes such as  $\text{FeCl}_2$ ,  $\text{FeCl}_3$ , ferrocene, and  $\text{Fe}(\text{CO})_5$  were used as catalysts, only a trace amount of ammonia was formed under the same reaction conditions. The reaction using a well-known iron–dinitrogen complex  $[\text{Fe}(\text{depe})_2(\text{N}_2)]$  as a catalyst gave only less than 1 equiv. of ammonia based on the iron atom. In the absence of any iron complex, the reaction of  $\text{KC}_8$  and  $[\text{H}(\text{OEt}_2)_2]\text{BAR}^{\text{F}_4}$  in  $\text{Et}_2\text{O}$  at  $-78^\circ\text{C}$  under  $\text{N}_2$  afforded only hydrogen gas in  $>75\%$  yield.

The catalytic reaction should be carried out at a low temperature such as  $-78^\circ\text{C}$  to inhibit the direct reaction between the reductant and the proton source forming hydrogen gas. Strong acidity and non-coordinating nature of  $[\text{H}(\text{OEt}_2)_2]\text{BAR}^{\text{F}_4}$  are of importance in the present catalytic reaction. In fact, trifluoromethanesulfonic acid, hydrogen chloride, and  $[2,6\text{-lutidinium}]\text{BAR}^{\text{F}_4}$  did not work as an efficient proton source at all. Strong reducing power of  $\text{KC}_8$  was necessary to promote the catalytic reaction. Metallocenes such as  $\text{CoCp}^*_2$  and  $\text{CrCp}^*_2$  did not work as an efficient reductant because of their weaker reducing ability. When the electrolysis of a cationic complex  $[(\text{TPB})\text{Fe}]\text{BAR}^{\text{F}_4}$  (**9**) was held at  $-2.3 \text{ V}$  vs.  $\text{FeCp}_2^{0/+}$  in the presence of  $[\text{H}(\text{OEt}_2)_2]\text{BAR}^{\text{F}_4}$  (50 equiv.) in  $\text{Et}_2\text{O}$  at  $-78^\circ\text{C}$  under  $\text{N}_2$  for 17 h, 2.2 equiv. of ammonia based on the Fe atom was obtained in 25% faradaic efficiency (Fig. 8) [29].

The time profile of ammonia formation using **7** as a catalyst indicated that the reaction was completed within 1 h at  $-78^\circ\text{C}$  [29]. The initial turnover frequency (TOF), which was determined as moles of ammonia produced per minute per an iron atom, was estimated to be  $1.2 \text{ min}^{-1}$ . The kinetic measurement also revealed that the reaction is the first order in an iron complex and zero order in a proton

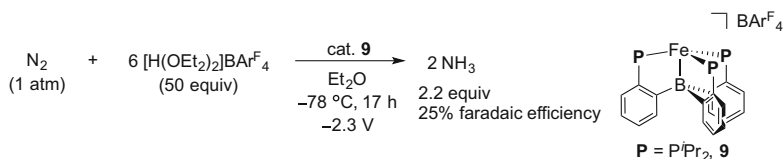


**Fig. 8** Control potential electrolysis of an iron–dinitrogen complex **9** under 1 atm of  $\text{N}_2$

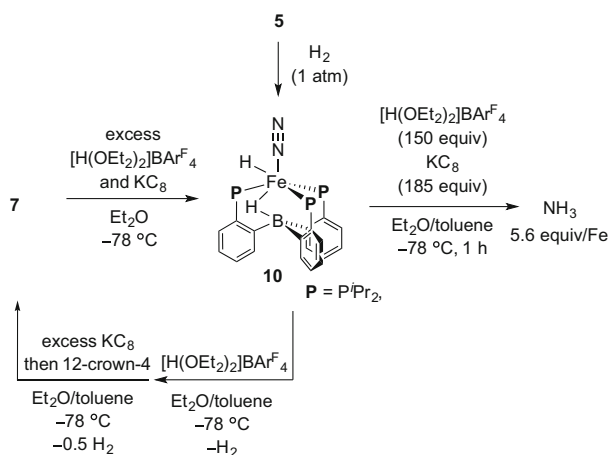


**Fig. 9** Reactivity of a borohydride-hydride complex **10**

source, indicating that a monomeric iron species is involved in the rate-determining step for the formation of ammonia. The time profile of dihydrogen formation in the presence or absence of the catalyst showed that both iron-catalyzed and background hydrogen formation competed with ammonia formation in the catalytic reaction. Mössbauer spectra of the catalytic reaction mixture indicated the formation of a Fe(-1)-dinitrogen complex **6**, a Fe(0)-dinitrogen complex **5**, and a Fe-hydride complex **10** as the iron species during the reaction (Fig. 9) [29]. Based on the results of stoichiometric and catalytic reactions of **10** shown in Figs. 9 and 10, complex **10** is considered as a resting state of the catalytic system.

### 2.3.3 Nature of Ligands in Catalytic Reaction

Peters and co-workers investigated the catalytic activity of isostructural Fe–dinitrogen complexes bearing (triphosphine)alkyl (TPC) [30] and (triphosphine)silyl (TPSi) [28, 31] ligands (**11** and **12**) to check the effect of the atom at the *trans* position to the dinitrogen ligand. The reaction using these complexes as catalysts afforded 59, 36, and 3.8 equiv. of ammonia, respectively, when larger amounts of  $\text{KC}_8$  (1600–1800 equiv.) and  $[\text{H}(\text{OEt}_2)_2]\text{BARF}_4$  (1500 equiv.) were loaded (Fig. 10) [29]. The Fe–B bond was revealed to be the most flexible, while the Fe–Si bond was



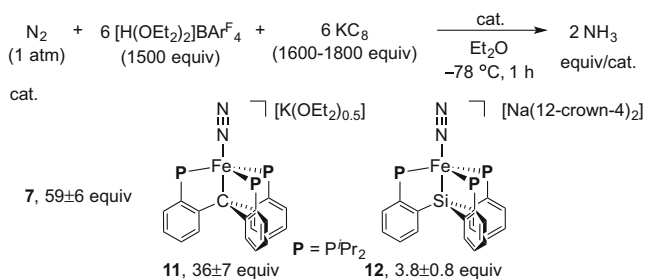


**Fig. 10** Catalytic activities of iron–dinitrogen complexes bearing TPB, TPC, and TPSi ligands for the formation of ammonia from molecular dinitrogen

the least. The flexibility of the Fe–B bond of the complex realized appropriate geometric and redox environment on the Fe center to exhibit the catalytic activity.

Peters and a co-worker also reported the catalytic formation of ammonia by using **4** as a catalyst (Fig. 11) [26]. When the catalytic reaction was carried out at a very low reaction temperature such as  $-95^\circ\text{C}$ , 3.3 equiv. of ammonia were produced based on the iron atom. At  $-95^\circ\text{C}$ , an anionic dinitrogen complex **14** was formed from the reduction of the corresponding dinitrogen complex **13**, which was formed below  $-80^\circ\text{C}$  (Fig. 11). Furthermore, Peters and co-workers investigated the catalytic activity of two kinds of diiron–dinitrogen complexes (Fig. 12) [32, 33]. One is a diiron–dinitrogen complex bearing bridging hydride ligands **15**, and the other is a diiron–dinitrogen complex bearing a bridging thiolate ligand **16**. However, both complexes did not show any catalytic activity toward the formation of ammonia.

### 2.3.4 Stoichiometric Reactivity of Iron–Dinitrogen Complexes

Peters and co-workers succeeded in isolation and characterization of several key intermediates relating to nitrogen fixation using their iron–dinitrogen complexes [34–36]. An amido complex  $[(\text{TPB})\text{FeNH}_2]$  (**17**) was prepared from the reaction of the cationic complex **9** with  $\text{NaNH}_2$  in  $\text{Et}_2\text{O}$  (Fig. 13). Protonation of **17** with  $[\text{H}(\text{OEt}_2)_2]\text{BAr}^{\text{F}}_4$  in  $\text{Et}_2\text{O}$  afforded the corresponding ammonia complex **18**. Reduction of **18** with  $\text{KC}_8$  under atmospheric pressure of nitrogen gas gave the dinitrogen complex **5** together with ammonia (Fig. 13). Treatment of **9** with hydrazine afforded the corresponding hydrazine complex **19**, which decomposed into **18** upon standing in solution at room temperature (Fig. 13) [34]. The same research group also reported the reaction of the dinitrogen complex **7** with an excess amount (10 equiv.) of  $[\text{H}(\text{OEt}_2)_2]\text{BAr}^{\text{F}}_4$  in 2-MeTHF at  $-136^\circ\text{C}$  or  $\text{Et}_2\text{O}$  at  $-78^\circ\text{C}$  to give the corresponding hydrazide(2-) complex **20** (Fig. 14) [35]. The complex **20** was thermally unstable and decomposed at higher temperature such as  $-40^\circ\text{C}$ .

Peters and a co-worker succeeded in elucidating the crystal structure and reactivity of the corresponding hydrazide complex in the TPSi system [36]. Treatment of a complex  $[(\text{TPSi})\text{Fe}(\text{N}_2)](\text{K}(\text{THF})_x)$  (**21**) with a slight excess amount of either

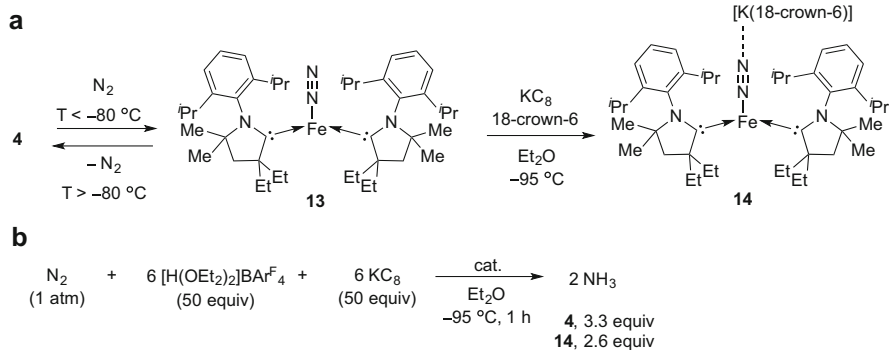


**Fig. 11** Reactivity and catalytic activities of iron complexes bearing CAAC ligands

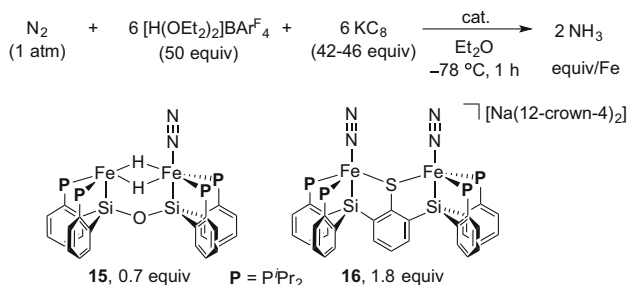


**Fig. 12** Catalytic activities of diiron–dinitrogen complexes supported by bridging-hydride and -thiolate ligands

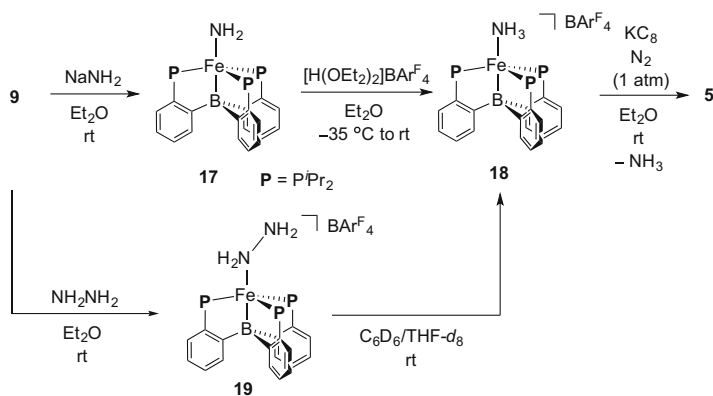


**Fig. 13** Synthesis and reactivities of iron–amide, –ammonia, and –hydrazine complexes bearing the TPB ligand

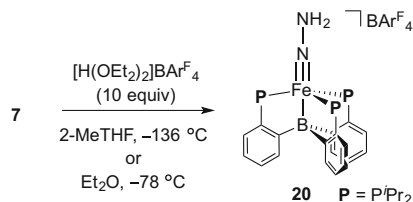


**Fig. 14** Protonation of **7** at low temperature to afford a hydrazide(2-) complex **20**

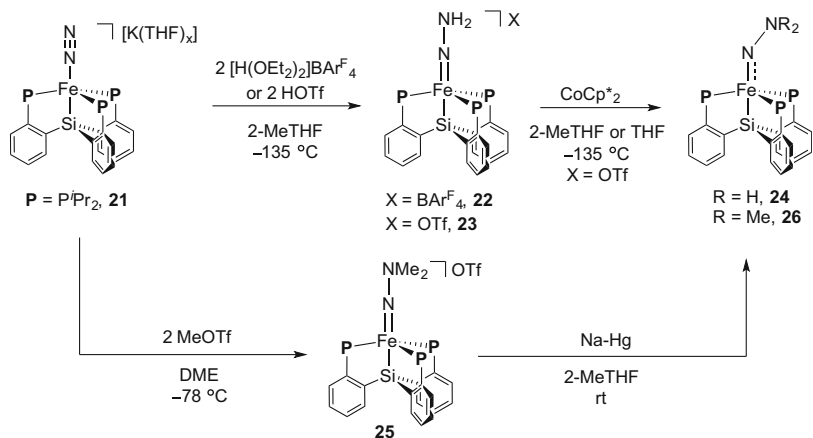


**Fig. 15** Synthesis of cationic and neutral hydrazide(2-) complexes bearing a TPSi ligand

$[\text{H}(\text{OEt}_2)_2]\text{BARF}_4$  or HOTf in 2-MeTHF at  $-135^\circ\text{C}$  afforded the corresponding hydrazide complexes **22** and **23**, respectively (Fig. 15). Crystal structures of these complexes showed that they have an  $\text{NNH}_2$  ligand making hydrogen bonding interactions with  $\text{Et}_2\text{O}$  (**22**) or OTf (**23**). The structure of **23** featured a short Fe–N distance and a long N–N distance. Reduction of **23** with 1 equiv. of  $\text{CoCp}^*_2$  in 2-MeTHF at  $-135^\circ\text{C}$  afforded the corresponding neutral hydrazide complex **24**, which was rapidly decomposed upon warming to  $-78^\circ\text{C}$  (Fig. 15). Methylated analogues of the cationic and the neutral hydrazide complexes **25** and **26** were isolated and fully characterized (Fig. 15). When the complex **24**, generated in situ from **23** at  $-135^\circ\text{C}$ , was warmed to room temperature, the reaction of **24** with **23** afforded nearly equal amounts of hydrazine and dinitrogen complexes **27** and **28** as major products. In this reaction, further disproportionation of **27** gave a mixture of a triflate complex **29** and a cationic ammonia complex **30** as minor products (Fig. 16).

Separately, the complex **30** was obtained from the one-pot reaction of **21** with HOTf and  $\text{CoCp}^*_2$  in 2-MeTHF at  $-135^\circ\text{C}$  (Fig. 17). Quenching this reaction with HCl 10 min after warming afforded a mixture of hydrazine (0.53 equiv.) and ammonia (0.16 equiv.) (Fig. 17). When the reaction was quenched after stirring at

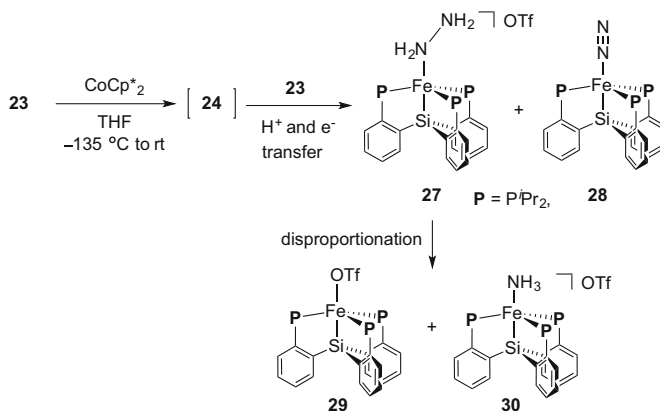


**Fig. 16** Reactivity of the hydrazide(2-) complexes bearing a TPSi ligand

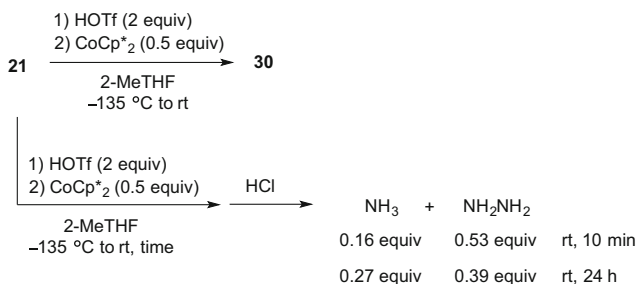


**Fig. 17** Reactions of the dinitrogen complex bearing a TPSi ligand with an acid and a reductant

room temperature for 24 h, further conversion of hydrazine into ammonia was observed (Fig. 17).

### 2.3.5 Overview of Catalytic Cycle

By careful investigation of the TPB and TPSi systems [29, 34–36], Peters and co-workers revealed the following: (1)  $[(\text{TPB})\text{Fe}(\text{N}_2)]^-$  and  $[(\text{TPSi})\text{Fe}(\text{N}_2)]^-$  were doubly protonated at low temperature to produce the corresponding hydrazide(2-) complexes  $[\text{Fe}(\text{NNH}_2)]^+$ , (2) reduction of  $[(\text{TPSi})\text{Fe}(\text{NNH}_2)]^+$  at low temperature afforded  $[(\text{TPSi})\text{Fe}(\text{NNH}_2)]$ , which was converted into  $[(\text{TPSi})\text{Fe}(\text{NH}_2\text{NH}_2)]^+$  and  $[(\text{TPSi})\text{Fe}(\text{N}_2)]$ , (3) disproportionation of the hydrazine ligand on  $[(\text{TPSi})\text{Fe}]$  or  $[(\text{TPB})\text{Fe}]$  proceeded smoothly to give the corresponding ammonia complexes, and (4) protonation of  $[(\text{TPB})\text{Fe}(\text{NH}_2)]$  afforded  $[(\text{TPB})\text{Fe}(\text{NH}_3)]^+$ , which was reduced to  $[(\text{TPB})\text{Fe}(\text{N}_2)]$  or  $[(\text{TPB})\text{Fe}(\text{N}_2)]^-$  together with ammonia. Based on these findings, they proposed a reaction pathway as shown in Fig. 18. As the former part, protonation of dinitrogen complex proceeded via a distal pathway or the Chatt

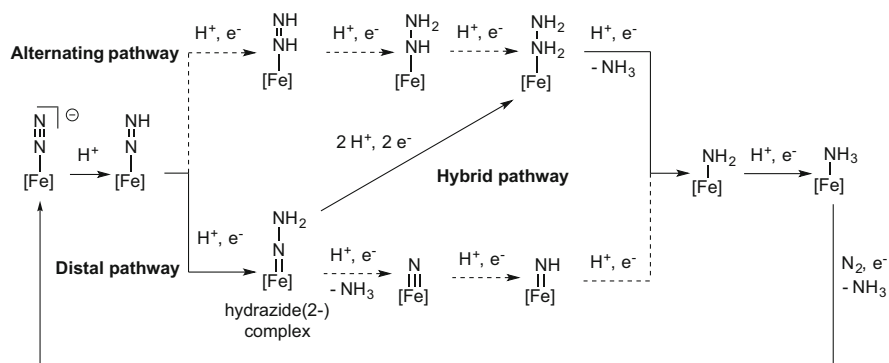


**Fig. 18** Possible reaction pathways for the catalytic formation of ammonia from molecular dinitrogen

cycle to give hydrazide(2-) complex. A hybrid of the distal and alternating pathways was proposed as the latter part. Hydrazide(2-) complex was converted into an ammonia complex via a hydrazine complex as a reactive intermediate. However, unfortunately, no formation of hydrazine was observed in the Peters system.

## 2.4 Catalytic Formation of Ammonia and Hydrazine Using Iron–Dinitrogen Complex as Catalyst

### 2.4.1 Synthesis and Catalytic Activity

Nishibayashi and co-workers found that an iron–dinitrogen complex bearing a pyrrole-based PNP pincer ligand **31** worked as a catalyst for the formation of ammonia and hydrazine from nitrogen gas (Fig. 19) [37]. The pyrrole-based PNP-pincer ligand was used because this ligand contains both hard and soft donors to stabilize metal centers of various oxidation states. Reduction of an iron (II) chloride complex **32** with  $\text{KC}_8$  under an atmospheric pressure of nitrogen gas in THF at room temperature afforded a paramagnetic iron(I)–dinitrogen complex **31**, which has a square planar geometry around the iron atom (Fig. 19). The corresponding hydride and methyl complexes **33** and **34** were also prepared from reactions of iron chloride complex with  $\text{KHBET}_3$  and  $\text{MeMgCl}$ , respectively (Fig. 19).

The catalytic activity of these iron complexes toward nitrogen fixation was investigated under the Peters' reaction conditions. The reaction of an atmospheric pressure of nitrogen gas with  $\text{KC}_8$  (50 equiv.) as a reductant and  $[\text{H}(\text{OEt}_2)_2]\text{BAR}^{\text{F}_4}$  (46 equiv.) as a proton source in  $\text{Et}_2\text{O}$  at  $-78^\circ\text{C}$  in the presence of **31** afforded 4.4 equiv. of ammonia and 0.2 equiv. of hydrazine based on the iron atom of the catalyst (Fig. 20a). The use of larger amounts of both reductant and proton source

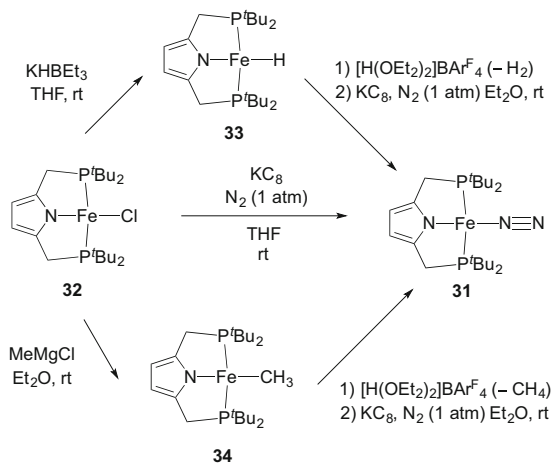


**Fig. 19** Synthesis of iron complexes bearing a pyrrole-based PNP-pincer ligand

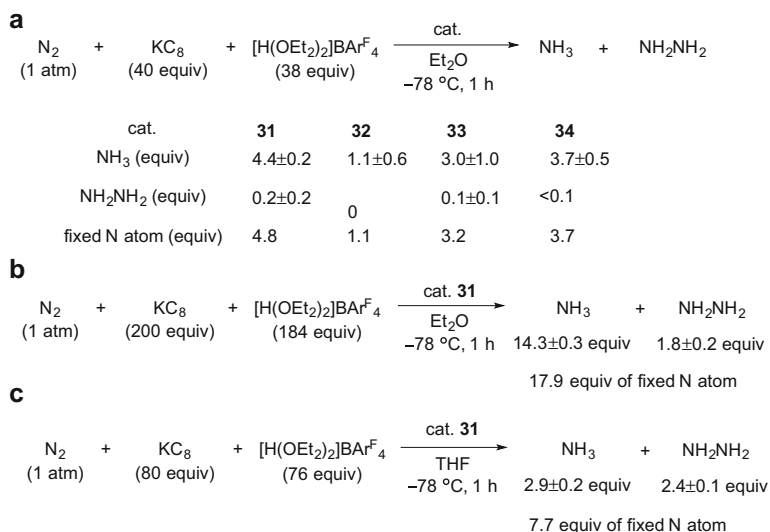


**Fig. 20** Catalytic formation of ammonia and hydrazine from molecular dinitrogen using iron complexes as catalysts

increased the catalytic activity. The largest amounts of ammonia and hydrazine (14.3 equiv. of ammonia and 1.8 equiv. of hydrazine) were obtained when 200 equiv. of  $\text{KC}_8$  and 184 equiv. of  $[\text{H}(\text{OEt}_2)_2]\text{BAR}^{\text{F}}_4$  were employed under the same reaction conditions (Fig. 20b). Interestingly, the ratio of ammonia to hydrazine depended on the nature of solvent employed. Thus, when THF was used in place of  $\text{Et}_2\text{O}$ , hydrazine became the major product, where up to 2.4 equiv. of

hydrazine (4.8 equiv. based on fixed N atom) and 2.9 equiv. of ammonia were produced based on the iron atom of the catalyst (Fig. 20c).

Complexes **33** and **34** also had a similar catalytic activity and produced 3.0 equiv. and 3.7 equiv. of ammonia based on the iron atom of the catalyst, respectively (Fig. 20a). Separately, it was confirmed that both **33** and **34** were converted into **31** together with hydrogen gas and methane by treatment with  $[\text{H}(\text{OEt}_2)_2]\text{BAr}^{\text{F}}_4$  and  $\text{KC}_8$  under an atmospheric pressure of nitrogen gas in  $\text{Et}_2\text{O}$  at room temperature, respectively. These results indicated that **33** and **34** are easily converted into **31** under the catalytic reaction conditions. When **32** was subjected to the catalytic conditions, only a stoichiometric amount of ammonia was formed (Fig. 20a).

#### 2.4.2 Mechanistic Consideration

In contrast to the Peters' system described in the previous section, both ammonia and hydrazine were formed when Fe-PNP complexes were used as catalysts. In this reaction system, the conversion of hydrazine into ammonia proceeded under the catalytic reaction conditions. Interestingly, the use of THF as a solvent inhibited the full conversion of hydrazine into ammonia. The detailed reaction pathway has not yet been clarified, but the catalytic reaction was proposed to proceed via a hydrazine complex as a key reactive intermediate.

After the catalytic reaction using Fe-PNP complexes as catalysts, only a free PNP ligand was detected without any iron species. The reaction of the dinitrogen complex **31** with  $[\text{H}(\text{OEt}_2)_2]\text{BAr}^{\text{F}}_4$  in  $\text{Et}_2\text{O}$  at room temperature afforded the corresponding dinitrogen complex bearing the protonated pyrrole ring of PNP ligand (**35**) (Fig. 21). Reduction of the protonated dinitrogen complex **35** with  $\text{KC}_8$  at room temperature gave a mixture of the starting dinitrogen complex **31** and free PNP ligand (Fig. 21). Unfortunately, the protonated dinitrogen complex **35** showed only a low catalytic activity for nitrogen fixation. These results indicate that the protonated dinitrogen complex should be one of the deactivated species in the catalytic reaction.

Reduction of **32** with an excess amount of sodium in the presence of 15-crown-5 gave the corresponding dinitrogen complex **31** together with an anionic dinitrogen complex **36** (Fig. 22). This result indicated that a similar dinitrogen complex may be formed under the catalytic reaction conditions.

Nishibayashi and co-workers also carried out DFT calculations on the first protonation step of the dinitrogen complexes (Fig. 23). The result of the protonation of **31** indicated that protonation on the  $\beta$ -carbon atom on the pyrrole ring proceeds in an exergonic way with a low activation barrier, while that on the  $\text{N}_2$  ligand requires a similar activation barrier and is endergonic (Fig. 23a). On the other hand, protonation of an anionic dinitrogen complex **37** occurred on both dinitrogen ligand and a pyrrole moiety in an exergonic way (Fig. 23b). However, the former requires a lower activation barrier than the latter. As a result, the complex **37** was considered to work as a key intermediate in the catalytic cycle.

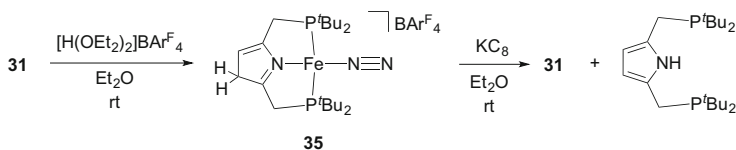
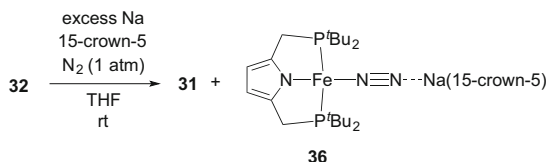
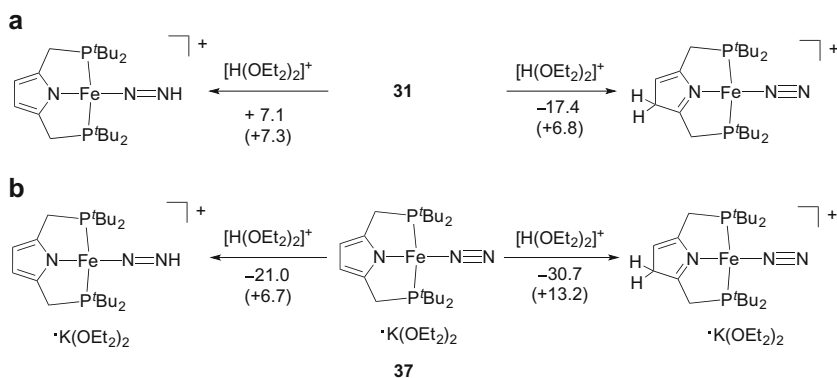
Fig. 21 Protonation of the iron–dinitrogen complex **31**

Fig. 22 Synthesis of an anionic iron(0)–dinitrogen complex



Gibbs free energy changes at 195 K are presented in kcal/mol

Fig. 23 DFT calculations on protonation on iron(I)- and iron(0)-dinitrogen complexes with  $[\text{H}(\text{OEt}_2)_2]^+$ 

### 3 Cobalt–Dinitrogen Complexes

#### 3.1 Background of Cobalt–Dinitrogen Complexes

In 1967, Yamamoto and co-workers reported the first cobalt–dinitrogen complex  $[\text{Co}(\text{N}_2)\text{H}(\text{PPh}_3)_3]$  (**38**) [15]. After this discovery, some stoichiometric reactions of **38** were investigated in detail, but any formation of ammonia was not observed. In contrast, the protonation of an anionic dinitrogen complex **39**, which was prepared by deprotonation of **38** with strong bases such as  $t\text{BuLi}$ , afforded a mixture of ammonia and hydrazine (Fig. 24) [38].



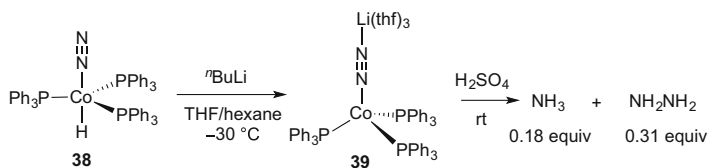


Fig. 24 Reactivity of the complex **38**

### 3.2 Catalytic Silylation of Dinitrogen Using Cobalt Catalysts

In 2015, Lu and co-workers reported the first example of cobalt-catalyzed reduction of nitrogen gas into  $\text{N}(\text{SiMe}_3)_3$  under ambient reaction conditions. In this reaction system, a dicobalt complex bearing a trisphosphino(triamido)amine ligand **40** worked as the most effective catalyst for the formation of  $\text{N}(\text{SiMe}_3)_3$  (Fig. 25) [39]. The reaction of an atmospheric pressure of nitrogen gas with  $\text{KC}_8$  (2000 equiv. to the catalyst) as a reductant and  $\text{Me}_3\text{SiCl}$  (2000 equiv. to the catalyst) as a silylating agent in the presence of **40** as a catalyst afforded 98 equiv. of  $\text{N}(\text{SiMe}_3)_3$  based on the cobalt atom in the catalyst (195 equiv. based on the catalyst). In two consecutive catalytic reactions using **40**, the overall amount of silylamine was 160 equiv. based on the cobalt atom in the catalyst. An anionic dicobalt dinitrogen complex **41** had a similar catalytic activity, while an isostructural cobalt–aluminum dinuclear complex **42** worked as a less efficient catalyst. Simple cobalt phosphine complexes such as  $\text{CoCl}(\text{PPh}_3)_3$  also worked as catalysts.

Independently, at the same time, Nishibayashi and co-workers reported the cobalt-catalyzed transformation of nitrogen gas into  $\text{N}(\text{SiMe}_3)_3$  under similar reaction conditions [40]. Some simple cobalt complexes such as  $[\text{Co}_2(\text{CO})_8]$  and  $[\text{Co}(\text{SiMe}_3)(\text{CO})_4]$  worked as effective catalysts using Na as a reductant and  $\text{Me}_3\text{SiCl}$  as a silylating agent (Fig. 26). Addition of 2,2'-bipyridine as a ligand to the cobalt complex was found to substantially increase the catalytic activity, where up to 49 equiv. of  $\text{N}(\text{SiMe}_3)_3$  based on the catalyst were produced. Interestingly, Yamamoto's dinitrogen complex also worked as an effective catalyst under the same reaction conditions. The negative results of Hg- and quantitative-poisoning tests suggested that some cobalt complexes truly worked as the active species in the catalytic reaction. Based on the results of DFT calculations, a cobalt–dinitrogen complex bearing trimethylsilyl groups and 2,2'-bipyridine **43**, which may be generated in situ, worked as a real active species.

### 3.3 Catalytic Formation of Ammonia Using Cobalt Catalysts

Peters and co-workers investigated the reactivity of a series of cobalt–dinitrogen complexes toward the catalytic formation of ammonia from nitrogen gas (Fig. 27) [41]. The reaction using an anionic cobalt–dinitrogen complex bearing the TPB

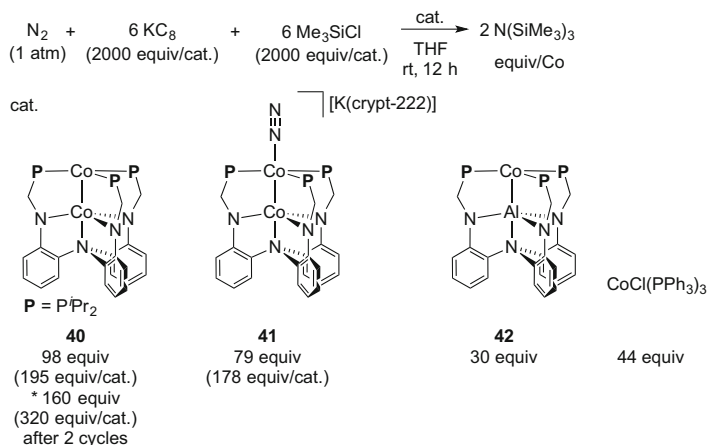


**Fig. 25** Cobalt-catalyzed silylation of molecular dinitrogen reported by Lu and co-workers

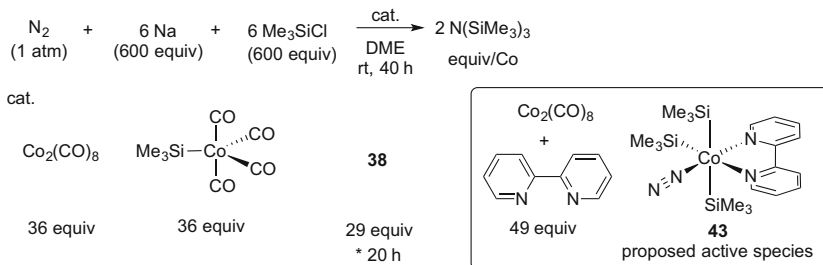


**Fig. 26** Cobalt-catalyzed silylation of molecular dinitrogen reported by Nishibayashi and co-workers

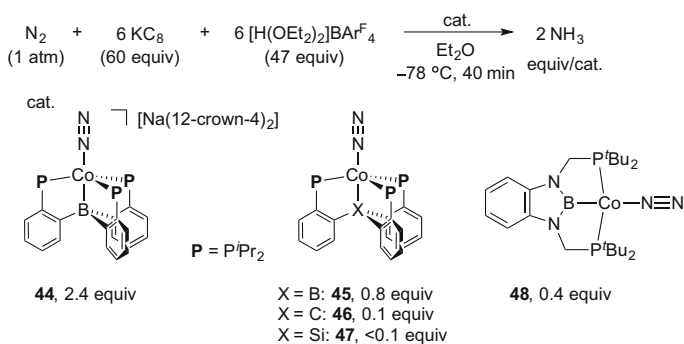


**Fig. 27** Formation of ammonia from molecular dinitrogen using cobalt–dinitrogen complexes as catalysts

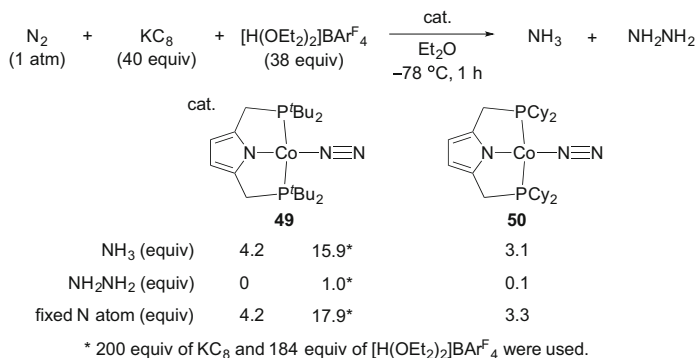


**Fig. 28** Reduction of molecular dinitrogen into ammonia and hydrazine using cobalt–dinitrogen complexes bearing pincer ligands as catalysts

ligand **44** as a catalyst afforded 2.4 equiv. of ammonia based on the cobalt atom in the catalyst under the conditions shown in Fig. 27. Neutral cobalt–dinitrogen complexes bearing TPB, TPC, TPSi, and PBP-type pincer ligands **45–48** did not work as catalysts effectively.

In 2016, Nishibayashi and co-workers reported the first successful example of the cobalt-catalyzed reduction of nitrogen gas into ammonia under ambient reaction conditions [42]. In this reaction system, cobalt–dinitrogen complexes bearing the pyrrole-based PNP-pincer ligand worked as effective catalysts. The reaction using cobalt–dinitrogen complexes **49** and **50** as catalysts afforded 4.2 equiv. and 3.1 equiv. of ammonia based on the catalyst, respectively, under the conditions shown in Fig. 28. When larger amounts of KC<sub>8</sub> and [H(OEt<sub>2</sub>)<sub>2</sub>]BAr<sup>F</sup><sub>4</sub> were employed, the amounts of nitrogenous products much improved; ammonia (15.9 equiv.) and hydrazine (1.0 equiv.) (Fig. 28). The detailed reaction pathway has not yet been clarified, but some cobalt–hydrazine complexes may work as key reactive intermediates in these reactions.

## 4 Summary

Iron and cobalt–dinitrogen complexes are capable of reducing nitrogen gas into not only N(SiMe<sub>3</sub>)<sub>3</sub> but also ammonia and hydrazine in a catalytic manner. The newly disclosed unique catalytic activity of some iron–dinitrogen complexes as catalysts may provide important information for the elucidation of biological nitrogen fixation by the nitrogenase [43, 44]. In addition, new recent findings of the catalytic activity of cobalt–dinitrogen complexes toward the direct reduction of nitrogen gas into ammonia opened an avenue to develop a novel nitrogen fixation system using transition metal–dinitrogen complexes as catalysts. In both cases, however, a low reaction temperature such as  $-78^\circ\text{C}$  is required to promote the catalytic reaction. The development of catalytic nitrogen fixation under ambient reaction conditions

using iron and cobalt–dinitrogen complexes as catalysts remains to be challenged in this research area.

## References

1. Liu H (2013) Ammonia synthesis catalysts. Chemical Industry Press & World Scientific, Singapore & Beijing
2. Hoffman BM, Lukoyanov D, Yang ZH, Dean DR, Seefeldt LC (2014) *Chem Rev* 114:4041
3. Spatzal T, Aksoyoglu M, Zhang L, Andrade SLA, Schleicher E, Weber S, Rees DC, Einsle O (2011) *Science* 334:940
4. Lancaster KM, Roemelt M, Ettenhuber P, Hu Y, Ribbe MW, Neese F, Bergmann U, DeBeer S (2011) *Science* 334:974
5. Lancaster KM, Hu Y, Bergmann U, Ribbe MW, DeBeer S (2013) *J Am Chem Soc* 135:610
6. Wiig JA, Hu Y, Lee CC, Ribbe MW (2012) *Science* 337:1672
7. Köthe C, Limberg C (2015) *Z Anorg Allg Chem* 641:18
8. Khoenkhoen N, de Bruin B, Reek JNH, Dzik WI (2015) *Eur J Inorg Chem* 567
9. Nishibayashi Y (2015) *Inorg Chem* 54:9234
10. Tanabe Y, Nishibayashi Y (2016) *Chem Rec* 16:1549
11. Crossland JL, Tyler DR (2010) *Coord Chem Rev* 254:1883
12. Hazari N (2010) *Chem Soc Rev* 39:4044
13. MacLeod KC, Holland PL (2013) *Nat Chem* 5:559
14. Fryzuk MD (2013) *Chem Commun* 49:4866
15. Yamamoto A, Kitazume S, Pu LS, Ikeda S (1967) *Chem Commun* 79
16. Sacco A, Aresta M (1968) *Chem Commun* 1223
17. Tyler DR (2015) *Z Anorg Allg Chem* 641:31
18. Shiina K (1972) *J Am Chem Soc* 94:9266
19. Kawaguchi M, Hamaoka S, Mori M (1993) *Tetrahedron Lett* 34:6907
20. Mori M (2004) *J Organomet Chem* 689:4210
21. Komori K, Oshita H, Mizobe Y, Hidai M (1989) *J Am Chem Soc* 111:1939
22. Komori K, Sugiura S, Mizobe Y, Yamada M, Hidai M (1989) *Bull Chem Soc Jpn* 62:2953
23. Oshita H, Mizobe Y, Hidai M (1993) *J Organomet Chem* 456:213
24. Tanaka H, Sasada A, Kouno T, Yuki M, Miyake Y, Nakanishi H, Nishibayashi Y, Yoshizawa K (2011) *J Am Chem Soc* 133:3498
25. Yuki M, Tanaka H, Sasaki K, Miyake Y, Yoshizawa K, Nishibayashi Y (2012) *Nat Commun* 3:1254
26. Ung G, Peters JC (2015) *Angew Chem Int Ed* 2015:532
27. Moret ME, Peters JC (2011) *Angew Chem Int Ed* 50:2063
28. Anderson JS, Rittle J, Peters JC (2013) *Nature* 501:84
29. Del Castillo TJ, Thompson NB, Peters JC (2016) *J Am Chem Soc* 138:5341
30. Creutz SE, Peters JC (2014) *J Am Chem Soc* 136:1105
31. Lee Y, Mankad NP, Peres JC (2010) *Nat Chem* 2:558
32. Rittle J, McCrory CCL, Peters JC (2014) *J Am Chem Soc* 136:13853
33. Creutz SE, Peters JC (2015) *J Am Chem Soc* 137:7310
34. Anderson JS, Moret ME, Peters JC (2013) *J Am Chem Soc* 135:534
35. Anderson JS, Cutsail III GE, Rittle J, Connor BA, Gunderson WA, Zhang L, Hoffman BM, Peters JC (2015) *J Am Chem Soc* 137:7803
36. Rittle J, Peters JC (2016) *J Am Chem Soc* 138:4243
37. Kuriyama S, Arashiba K, Nakajima K, Matsuo Y, Tanaka H, Ishii K, Yoshizawa K, Nishibayashi Y (2016) *Nat Commun* 7:12181

38. Yamamoto A, Miura Y, Ito T, Chen HL, Iri K, Ozawa F, Miki K, Sei T, Tanaka N, Kasai N (1983) *Organometallics* 2:1429
39. Siedschlag RB, Bernales V, Vogiatzis KD, Planas N, Clouston LJ, Bill E, Gagliardi L, Lu CC (2015) *J Am Chem Soc* 137:4638
40. Imayoshi R, Tanaka H, Matsuo Y, Yuki M, Nakajima K, Yoshizawa K, Nishibayashi Y (2015) *Chem Eur J* 21:8905
41. Del Castillo TJ, Thompson NB, Suess DLM, Ung G, Peters JC (2015) *Inorg Chem* 54:9256
42. Kuriyama S, Arashiba K, Tanaka H, Matsuo Y, Nakajima K, Yoshizawa K, Nishibayashi Y (2016) *Angew Chem Int Ed* 55:14291
43. Hill PJ, Doyle LR, Crawford AD, Myers WK, Ashley AE (2016) *J Am Chem Soc* 138: 13521
44. Imayoshi R, Nakajima K, Nishibayashi Y (2017) *Chem Lett* 46:466

# Index

## A

Amides, 4, 14  
Ammines, 15, 175  
Ammonia, 1, 24, 153, 216  
    cobalt catalysts, 230  
    iron catalysts, 219  
Aryloxide ligands, 62  
*Azotobacter vinelandii*, 198

## B

Badger's rule, 73  
Benzenesulfonic acid hydrazide, 206  
1,3-Bis(2-(di-*tert*-butylphosphino)ethyl)  
    imidazol-2-ylidene (Im-PCP[2]), 185  
Bis(di-*tert*-butylphosphinoethyl)  
    phenylphosphine) pincer ligand  
    (PPP), 165  
1,3-Bis((di-*tert*-butylphosphino)methyl)  
    benzimidazol-2-ylidene (Bim-PCP[1]),  
    185  
1,3-Bis(2-diphenylphosphanylethyl)imidazol-  
    2-ylidene (PCP), 125  
Bis(3-(diphenylphosphino)propyl)phosphine  
    (prPPHP), 144  
Bis(phosphine) molybdenum diazenides, 11  
Bond dissociation enthalpies (BDEs), 7, 186  
Bond dissociation free energies (BDFEs), 1, 7  
Bonding, 71  
Borohydride-hydride complex, 221

## C

Calix[4]arene, 63  
Carbodiimides, 95

Catalysis, mechanism, 171  
Catalysts, 153, 215  
Chatt cycle, 3, 9, 115, 225  
Chromium, 86, 155, 159, 217  
Cobalt–dinitrogen complexes, 25, 215, 229  
Cobalt hydrazine complexes, 232  
Cobalt hydride complexes, 34  
Copper dinitrogen complex, 33  
Cumulenes, 60, 81  
Cyclopentadienides, 78, 89, 100

## D

Decamethylchromocene, 3, 174, 185  
Decamethylcobaltocene, 165  
DFT calculations, 5, 10, 113, 140, 173, 180,  
    186, 201, 218, 228  
Diarylhydrazines, 208  
Diazenides, 1, 4, 9, 73  
Diketiminates, 33, 92, 205  
Dimethylurea, 95  
Dimolybdenum complexes, 90, 161, 171, 175,  
    183, 192  
Dinitrogen, 153, 197, 215  
    activation, 45  
    cleavage, 23  
    complexes, 45  
    fixation, 23  
    splitting, 71  
Dithiolates, 54

## E

Electron-nuclear double resonance (ENDOR),  
    175, 199, 206

End-on bridging, 74  
Ethyl-bis(3-(diphenylphosphino)propyl)phosphinate, 118

**F**

FeMoco, 114, 198–210  
FeMo-nitrogenase, 198, 216  
Fenske-Hall computations, 74  
Ferrocenyldiphosphines, 90

**G**

Group 4 elements, 31, 81  
Group 5 elements, 30, 45, 76, 95, 97  
Group 6 elements, 29, 81, 85, 89, 92  
Group 7 elements, 28, 85, 91, 102  
Group 8 elements, 26, 91, 101

**H**

Haber-Bosch ammonia synthesis, 2, 24, 72, 91, 172, 216  
Heterocumulenes, 95  
*N*-Heterocyclic carbene (NHC), 185  
Hydrazides, 4, 9, 73  
Hydrazine, cleavage, 208  
Hydrides, multimetallic, 23  
Hydrogenation, 23  
Hydrogen atom transfer (HAT), 5, 8  
Hydrosilylation, 59, 87

**I**

Imidazolylidene/phosphanyl hybrid ligands, 119  
Imides, 4, 12  
Iron, 197, 215  
  catalysts, 2  
Iron–dinitrogen complexes, 217  
  S ligands, 201  
Iron hydride complexes, 27  
Iron-imide-sulfide heterocubanes, 208  
Iron–sulfide clusters, 204  
Isocyanates, 72, 95, 98

**L**

LANL2DZ, 177  
Lowe–Thorneley model, 199  
[LutH]OTf, 185  
2,6-Lutidinium tetrakis[3,5-bis(trifluoromethyl)phenyl]borate, 174

**M**

Manganese hydride complexes, 28, 29  
Molybdenum, 113, 153, 171  
Molybdenum–bis(silyl)hydrazido(2–) complexes, 155  
Molybdenum–dinitrogen complexes, 30, 113, 171  
Molybdenum hydride complexes, 30  
Molybdenum–iron (MoFe) protein, 114  
Molybdenum(0)phosphine complexes, 113  
Molybdenum triamides, 48, 81, 86  
Molybdenum(III)tris(amido)amine, 3

**N**

Nickel hydride complexes, 34  
Niobium, 45  
Niobium aryloxide complexes, dinitrogen cleavage, 62  
Niobium–dinitrogen complexes, 53  
Niobium tetrahydride complexes, 36  
Niobium tris(amide) complexes, 66  
Nitrides, 23, 45, 71, 81, 94  
  N<sub>2</sub>-derived, 45  
Nitriles, 38, 66, 72, 98  
Nitrogenase, 2, 24, 46, 72, 81, 114, 172, 197, 216  
Nitrogen atom transfer, 45  
Nitrogen fixation, 1, 71, 113, 153, 171, 216

**O**

Octamethylzirconocene, 80  
Osmium, 91, 92

**P**

PCP ligands, 113, 120, 149, 185  
  pincer ligands, 185, 194  
PEP ligands, 115, 130, 149  
Phenylhydrazido species, 206  
Phosphanyl hybrid ligands, 119  
Phosphine/carbene ligands, 113, 119  
Phosphine ligands, multidentate, 113  
PNP pincer ligand, 13, 27, 88, 114, 173, 226  
Potassium azodicarboxylate, 206  
Proton coupled electron transfer (PCET), 4, 17  
Protonolysis, 3, 93

**R**

Reduction, 153, 215  
Rhenium, 28, 88, 98, 101

- Rhenium–dinitrogen complexes, 28  
Rhenium hydride complexes, 29  
Rhodium, 17  
Rhodium–dinitrogen complexes, 26  
Ruthenium, catalysts, 2  
Ruthenium dihydrogen complex, 30  
Ruthenium–dinitrogen complexes, 27
- S**  
Side-on bridging, 77  
Silylamine, 153, 155, 215, 230  
Silylation, 87, 98, 153–157  
    catalytic, 217, 230  
Silylhydride, 54  
Sodium amalgam, 137  
Stuttgart-Dresden pseudopotentials (SDD), 177  
Sulfides, 197, 206  
Sulfur, 24, 114, 172, 197
- T**  
Tantalum, 45  
Tantalum–dinitrogen complexes, 53  
Tantalum tetrahydride complexes, 36  
Tetrahydrothiophene (THT), 202  
Thioether, 201, 202  
Thiolates, 197, 203, 222  
Titanium, 16, 50, 76, 98, 217  
Titanium dinitrogen, 46  
Titanium heptahydride complexes, 37  
Titanium hydrides, 37, 101
- Titanium trialkyl complexes, 37  
Titanocenes, 31  
Transition metals, 45  
    hydride complexes, 23, 25, 45  
    nitrides, 71  
Triamides, 81, 86  
Triamidoamine, 83  
Trimethylpyridinium  
    trifluoromethanesulfonate, 165  
(Triphosphine)alkyl (TPC), 221  
Triphosphineborane (TPB), 219  
(Triphosphine)silyl (TPSi), 221  
Trisanilide molybdenum(VI) nitrides, 98  
Tungsten, 159  
Tungsten–dinitrogen complexes, 30
- V**  
Vanadium, 14, 45, 76, 95, 159, 205, 216  
Vanadium–dinitrogen complexes, 46  
Vanadium(III) isocyanate, 95  
Vanadium nitride complexes, 50
- Y**  
Yandulov–Schrock cycle, 174
- Z**  
Zirconium–dinitrogen complex, 35  
Zirconocene hydride complexes, 32, 60  
Zirconocenes, 32, 80